

# Optical Chemical Sensors

Edited by

F. Baldini, A.N. Chester,  
J. Homola and S. Martellucci

NATO Science Series

II. Mathematics, Physics and Chemistry – Vol. 224

# Optical Chemical Sensors

## NATO Science Series

*A Series presenting the results of scientific meetings supported under the NATO Science Programme.*

The Series is published by IOS Press, Amsterdam, and Springer in conjunction with the NATO Public Diplomacy Division.

### *Sub-Series*

<b>I. Life and Behavioural Sciences</b>	IOS Press
<b>II. Mathematics, Physics and Chemistry</b>	Springer
<b>III. Computer and Systems Science</b>	IOS Press
<b>IV. Earth and Environmental Sciences</b>	Springer

The NATO Science Series continues the series of books published formerly as the NATO ASI Series.

The NATO Science Programme offers support for collaboration in civil science between scientists of countries of the Euro-Atlantic Partnership Council. The types of scientific meeting generally supported are "Advanced Study Institutes" and "Advanced Research Workshops", and the NATO Science Series collects together the results of these meetings. The meetings are co-organized by scientists from NATO countries and scientists from NATO's Partner countries — countries of the CIS and Central and Eastern Europe.

**Advanced Study Institutes** are high-level tutorial courses offering in-depth study of latest advances in a field.

**Advanced Research Workshops** are expert meetings aimed at critical assessment of a field, and identification of directions for future action.

As a consequence of the restructuring of the NATO Science Programme in 1999, the NATO Science Series was re-organized to the four sub-series noted above. Please consult the following web sites for information on previous volumes published in the Series.

<http://www.nato.int/science>

<http://www.springer.com>

<http://www.iospress.nl>



**Series II: Mathematics, Physics and Chemistry – Vol. 224**

# Optical Chemical Sensors

edited by

**F. Baldini**

IFAC-CNR,  
Florence, Italy

**A.N. Chester**

Hughes Research Laboratories, Inc.,  
Malibu, California, U.S.A.

**J. Homola**

IREE-Academy of Sciences,  
Prague, Czech Republic

and

**S. Martellucci**

The University of Rome "Tor Vergata",  
Rome, Italy



Published in cooperation with NATO Public Diplomacy Division

Proceedings of the NATO Advanced Study Institute on  
Optical Chemical Sensors  
Erice, Italy  
29 July-10 August 2004

A C.I.P. Catalogue record for this book is available from the Library of Congress.

ISBN-10 1-4020-4610-3 (PB)  
ISBN-13 978-1-4020-4610-0 (PB)  
ISBN-10 1-4020-4609-X (HB)  
ISBN-13 978-1-4020-4609-4 (HB)  
ISBN-10 1-4020-4611-1 (e-book)  
ISBN-13 978-1-4020-4611-7 (e-book)

---

Published by Springer,  
P.O. Box 17, 3300 AA Dordrecht, The Netherlands.

*www.springer.com*

*Printed on acid-free paper*

---

All Rights Reserved  
© 2006 Springer

No part of this work may be reproduced, stored in a retrieval system, or transmitted in any form or by any means, electronic, mechanical, photocopying, microfilming, recording or otherwise, without written permission from the Publisher, with the exception of any material supplied specifically for the purpose of being entered and executed on a computer system, for exclusive use by the purchaser of the work.

Printed in the Netherlands.

## Table of Contents

Preface.....	ix
List of contributors.....	xi
Directors’s list of participants.....	xvii
Editorial.....	xxv
List of ISQE courses.....	xxvii
1 Birth of the maser and laser C.H. Townes.....	1
2 Fiber optic chemical sensors and biosensors: a view back O.S. Wolfbeis and B.M. Weidgans.....	17
<b>Fundamentals of optical chemical sensing</b>	
3 Fundamentals of optoelectronics A. Dybko.....	47
4 Optical fibres for optical sensing I. Kasik, V. Matejec, M. Chomat, M. Hayer and D. Berkova.....	59
5 Absorption-based sensors A. Lobnik.....	77

6	Fluorescence-based sensors	
	G. Orellana.....	99
7	Vibrational spectroscopic sensors	
	M. Kraft.....	117
8	Chemiluminescence-based sensors	
	L.J. Blum and C.A. Marquette.....	157
9	Sensors based on spectroscopy of guided waves	
	J. Homola.....	179
10	Planar optical sensors and evanescent wave effects	
	C.S. Burke, O. Stránik, H.M. McEvoy and B.D. MacCraith.....	193
11	Interferometry in bio- and chemosensing	
	G. Gauglitz.....	217
12	Surface-enhanced Raman scattering	
	T. Vo-Dinh and F. Yan.....	239
13	Planar waveguiding systems for optical sensing	
	P.V. Lambeck and H.J.W.M. Hoekstra.....	261
14	Ultracompact optical sensors based on high index-contrast photonic structures	
	A. Driessen, H.J.W.M. Hoekstra, W. Hopman, H. Kelderman, P.V. Lambeck, J. van Lith, D.J.W. Klunder, R.M. de Ridder, E. Krioukov and C. Otto.....	281

<i>Table of Contents</i>	vii
15 Polymers in optical sensors	
G.J. Mohr.....	297
16 Fundamentals of enzyme-based sensors	
M.C. Moreno-Bondi and E. Benito-Peña.....	323
17 Sol-gels for optical sensors	
H. Podbielska, A. Ulatowska-Jarza, G. Müller and H.J. Eichler.....	353
18 Methods for attachment of antibodies onto optical biosensors	
E. Brynda.....	387
<b>Applications of optical chemical sensing</b>	
19 The optical nose	
D.R. Walt and T. Sternfeld.....	405
20 Invasive sensors in medicine	
F. Baldini.....	417
21 Biosensors for detection of bioterrorist threats	
F.S. Ligler.....	437
22 Review of methods of optical gas	
J.P. Dakin and P. Chambers.....	457
23 DNA and protein sensor arrays	
C. Preininger.....	479



## 24 Sensors for food safety and security

D.B. Papkovsky.....501

## 25 Optical chemical sensors for cultural heritage

G. Cristoforetti, S. Legnaioli, V. Palleschi, A. Salvetti, E. Tognoni.....515

Index..... 527

## PREFACE

Chemical sensing using optics is under extensive research all over the world and many optical chemical sensors are finding increasing application in industry, environmental monitoring, medicine, biomedicine and chemical analysis. This is evidenced by an annual growth in the number of international scientific conferences in which advances in the field of optical chemical sensors are reported. These conferences, are, however, focused on disseminating the latest scientific results rather than providing in-depth education in the field of optical chemical sensors. In addition, the topic of optical chemical sensors is only just beginning to find its way into the curricula of universities and colleges in Europe and in the US. Due to the prominence that optical sensors are assuming, it has become more and more important to establish a framework for discussion and interchange, in addition to traditional conferences, to aid research and education in this important field.

In the summer of 2004, the NATO A.S.I. on the subject “Optical Chemical Sensors” was organised in Erice, Sicily. This NATO A.S.I. was the 40<sup>th</sup> Course of the International School of Quantum Electronics, under the auspices of the “Ettore Majorana Foundation and Center for Scientific Culture” and was directed by Dr. J. Homola of the Institute of Radio Engineering and Electronic (IREE) of the Academy of Sciences in Prague and by Dr. F. Baldini of the “Nello Carrara Institute of Applied Physics” (IFAC-CNR). It is also the fourth course in the framework of the ASCOS (Advanced Study Course on Optical Chemical Sensors) series, founded in 1999 by Prof. Otto Wolfbeis. This book presents the Proceedings of this advanced course providing a deep overview of both the fundamentals of optical chemical sensing and the applications of chemical sensors.

The objective of the NATO A.S.I. was to bring together bright young (future) scientists, coming from all imaginable fields of expertise related to optical chemical sensors, to learn from selected researchers and from each other in an appropriate atmosphere. The course covered all the principal optical chemical sensor technologies and related fields and provided a platform to exchange ideas and experience. The objective was accomplished through teaching theory and basics on a level every participant could follow and then giving the participant an opportunity to apply the gained knowledge.

The quality of the course was assured by the presence of 27 lecturers, key specialists for each topic, coming from 13 different countries (12 European countries plus the USA).

An outstanding presence was assured by Prof. Charles Townes, one of the inventors of the laser, who was invited in occasion of the forty-year celebration of the Nobel Prize award in Physics for the discovery of the laser. His lecture during the ceremony was one of the most exciting moments

of the Course; it was focused on an historical re-examination of the invention of the laser and a discussion of the bases and principles which can guide additional research activity.

The chapters in these Proceedings follow for the most part the chronology of the NATO A.S.I.. The first section is devoted to the fundamental aspects of optical chemical sensing. All the spectroscopic techniques utilised in chemical sensing are described (absorption, fluorescence, chemiluminescence, Raman spectroscopy, surface plasmon resonance) as well as the main chemical aspects concerning the sensing mechanism and/or the identification of the proper chemical transducer (enzyme-based reactions, antibody/antigen interaction,) and its immobilisation on the most suitable support (polymers, sol-gel, covalent bond). After this first section, attention is given to sensor applications with chapters focused on the different areas in which optical sensors find their utilisation (detection of bioterrorist threats, food safety, invasive applications in medicine, cultural heritage, gas sensing, the optical nose, DNA protein and sensor arrays, etc.). On this basis we grouped the chapters in two main topics: fundamentals of optical chemical sensing and applications of optical chemical sensing.

By way of introduction, these two sections are preceded by the lecture of Prof. Townes on the birth of laser and maser and by a retrospective vision of optical chemical sensors of Prof. Wolfbeis.

We greatly acknowledge the invaluable help of Dr. Ambra Giannetti from IFAC-CNR, scientific secretariat of the NATO A.S.I.. We also greatly appreciate the help from Dr. Alessandro Schena for much of the computer processing work. We acknowledge with gratitude the generous financial support of the NATO A.S.I. Programme Committee and also the support received from the Sicilian Regional Parliament, the National Research Council (CNR), the University of Rome "Tor Vergata" and the Italian Society for Optics and Photonics (SIOF).

The Editors

S.Martellucci and J.Homola  
Directors of the NATO ASI

A.N.Chester  
Co-director of the ISQE

F.Baldini  
Co-director of the 40<sup>th</sup> ISQE Course

July 2005

## LIST OF CONTRIBUTORS

- C.H. TOWNES** Senior Author  
*Department of Physics, University of California  
557 Bridge  
Berkeley, CA 94720-7300, USA*
- O.S. WOLFBEIS** Senior Author  
*Institute of Analytical Chemistry, University of Regensburg  
Universitätstraße 31  
Regensburg, Germany*
- B.M. WEIDGANS**  
*Institute of Analytical Chemistry, University of Regensburg  
Universitätstraße 31  
Regensburg, Germany*
- A. DYBKO** Senior Author  
*Department of Analytical Chemistry, Warsaw Univ. Technology  
Noakowskiego 3  
Warsaw, Poland*
- I. KASIK** Senior Author  
*Institute Radio of Engineering and Electronic, Academy of Sciences  
Chaberskà 57  
Prague 8, Czech Republic*
- V. MATEJEC**  
*Institute Radio of Engineering and Electronic, Academy of Sciences  
Chaberskà 57  
Prague 8, Czech Republic*
- M. CHOMAT**  
*Institute Radio of Engineering and Electronic, Academy of Sciences  
Chaberskà 57  
Prague 8, Czech Republic*
- M. HAYER**  
*Institute Radio of Engineering and Electronic, Academy of Sciences  
Chaberskà 57  
Prague 8, Czech Republic*
- D. BERKOVA**  
*Institute Radio of Engineering and Electronic, Academy of Sciences  
Chaberskà 57  
Prague 8, Czech Republic*

**A. LOBNIK**

*Faculty of Mechanical Engineering, University of Maribor  
Smetanova 17  
Maribor, Slovenia*

Senior Author

**G. ORELLANA**

*Department of Organic Chemistry  
Universidad Complutense de Madrid  
Madrid, Spain*

Senior Author

**M. KRAFT**

*CTR - Carinthian Tech Research AG, Centre for Sensors and Actuators  
Europastraße 4  
Villach/St. Magdalen, Austria*

Senior Author

**L.J. BLUM**

*Laboratoire de Génie Enzymatique et Biomoléculaire  
Université Claude Bernard Lyon 1  
Villeurbanne Cedex, France*

Senior Author

**C.A. MARQUETTE**

*Laboratoire de Génie Enzymatique et Biomoléculaire  
Université Claude Bernard Lyon 1  
Villeurbanne Cedex, France*

**J. HOMOLA**

*Institute Radio of Engineering and Electronic, Academy of Sciences  
Chaberská 57  
Prague 8, Czech Republic*

Senior Author

**C.S. BURKE**

*National Centre for Sensor Research, Dublin City University  
Glasnevin, Dublin 9, Ireland*

**O. STRÁNIK**

*National Centre for Sensor Research, Dublin City University  
Glasnevin, Dublin 9, Ireland*

**H. MCEVOY**

*National Centre for Sensor Research, Dublin City University  
Glasnevin, Dublin 9, Ireland*

**B.D. MACCRAITH**

*National Centre for Sensor Research, Dublin City University  
Glasnevin, Dublin 9, Ireland*

Senior Author

**G. GAUGLITZ**

*Institut für Physikalische und Theoretische Chemie  
Auf der Morgenstelle 8  
Tübingen, Germany*

Senior Author

*List of Contributors*

xiii

**T. VO-DINH**

Senior Author

*Advanced Biomedical Science and Technology Group  
Life Sciences Division, Oak Ridge National Laboratory  
Oak Ridge, Tennessee, USA*

**F. YAN**

*Advanced Biomedical Science and Technology Group  
Life Sciences Division, Oak Ridge National Laboratory  
Oak Ridge, Tennessee, USA*

**P.V. LAMBECK**

Senior Author

*MESA<sup>+</sup> Institute, University of Twente  
Enschede, The Netherlands*

**H.J.W.M. HOEKSTRA**

*MESA<sup>+</sup> Institute, University of Twente  
P.O. Box 217  
Enschede, The Netherlands*

**A. DRIESSEN**

Senior Author

*Integrated Optics MicroSystems, MESA<sup>+</sup>  
University of Twente  
P.O. Box 217  
Enschede, The Netherlands*

**W. HOPMAN**

*Integrated Optics MicroSystems, MESA<sup>+</sup>  
University of Twente  
P.O. Box 217  
Enschede, The Netherlands*

**H. KELDERMAN**

*Integrated Optics MicroSystems, MESA<sup>+</sup>  
University of Twente  
P.O. Box 217  
Enschede, The Netherlands*

**J. VAN LITH**

*Integrated Optics MicroSystems, MESA<sup>+</sup>  
University of Twente  
P.O. Box 217  
Enschede, The Netherlands*

**D.J.W. KLUNDER**

*Integrated Optics MicroSystems, MESA<sup>+</sup>  
University of Twente  
P.O. Box 217  
Enschede, The Netherlands*

**R. DE RIDDER**

*Integrated Optics MicroSystems, MESA<sup>+</sup>  
University of Twente  
P.O. Box 217  
Enschede, The Netherlands*

**E. KRIOUKOV**

*Biophysical Techniques Group, MESA<sup>+</sup>  
University of Twente  
P.O. Box 217  
Enschede, The Netherlands*

**C. OTTO**

*Biophysical Techniques Group, MESA<sup>+</sup>  
University of Twente  
P.O. Box 217  
Enschede, The Netherlands*

**G.J. MOHR**

*Institute of Physical Chemistry, Friedrich-Schiller University Jena  
Lessingstrasse 10  
Jena, Germany*

Senior Author

**M.C. MORENO-BONDI**

*Department of Analytical Chemistry  
Universidad Complutense  
Madrid, Spain*

Senior Author

**E. BENITO-PEÑA**

*Department of Analytical Chemistry  
Universidad Complutense  
Madrid, Spain*

**H. PODBIELSKA**

*Wroclaw Univ. Technology, Institute of Physics  
Wybrzeze Wyspianskiego 27  
Wroclaw, Poland*

Senior Author

**A. ULATOWSKA-JARŻA**

*Wroclaw Univ. Technology, Institute of Physics  
Wybrzeze Wyspianskiego 27  
Wroclaw, Poland*

**G. MÜLLER**

*Wroclaw Univ. Technology, Institute of Physics  
Wybrzeze Wyspianskiego 27  
Wroclaw, Poland*

*List of Contributors*

XV

**H.J. EICHLER**

*Wroclaw Univ. Technology, Institute of Physics  
Wybrzeze Wyspianskiego 27  
Wroclaw, Poland*

**E. BRYNDA**

*Institute of Macromolecular Chemistry, Academy of Sciences  
Heyrovsky sq.2  
Prague 6, Czech Republic*

Senior Author

**D.R. WALT**

*Department of Chemistry  
Tufts University  
Medford Massachusetts, USA*

Senior Author

**T. STERNFELD**

*Department of Chemistry  
Tufts University  
Medford Massachusetts, USA*

**F. BALDINI**

*Institute of Applied Physics  
National Council of Research  
Via Madonna del Piano10  
50019 Sesto Fiorentino (Fi), Italy*

Senior Author

**F.S. LIGLER**

*Center for Bio/Molecular Science & Engineering  
Naval Research Laboratory  
Washington, DC, USA*

Senior Author

**J.P. DAKIN**

*Optoelectronics Research Centre  
University of Southampton  
Southampton, U.K*

Senior Author

**P. CHAMBERS**

*Optoelectronics Research Centre  
University of Southampton  
Southampton, U.K*

**C. PREININGER**

*Austrian Research Centers – ARC  
A-2444 Seibersdorf, Austria*

Senior Author

**D.B. PAPKOVSKY**

*Laboratory of Biophysics and Bioanalysis  
Dept. of Biochemistry, University College Cork  
Lee Maltings  
Cork, Ireland*

Senior Author



**G. CRISTOFORETTI**

*Istituto per i Processi Chimico Fisici del CNR  
Area di Ricerca di Pisa, Via G.Moruzzi, 1  
Pisa, ITALY*

**S. LEGNAIOLI**

*Istituto per i Processi Chimico Fisici del CNR  
Area di Ricerca di Pisa, Via G.Moruzzi, 1  
Pisa, ITALY*

**V. PALLESCHI**

*Istituto per i Processi Chimico Fisici del CNR  
Area di Ricerca di Pisa, Via G.Moruzzi, 1  
Pisa, ITALY*

Senior Author

**A. SALVETTI**

*Istituto per i Processi Chimico Fisici del CNR  
Area di Ricerca di Pisa, Via G.Moruzzi, 1  
Pisa, ITALY*

**E. TOGNONI**

*Istituto per i Processi Chimico Fisici del CNR  
Area di Ricerca di Pisa, Via G.Moruzzi, 1  
Pisa, ITALY*

## DIRECTORS'S LIST OF PARTICIPANTS

### a) DIRECTORS

Sergio MARTELLUCCI  
Engineering Faculty  
University of Rome "Tor Vergata"  
Via del Politecnico 1  
00133 Rome  
Italy

Jiri HOMOLA  
Institute of Radio Engineering and  
Electronic  
Academy of Sciences  
Chaberská 57  
18251 Prague 8  
Czech Republic

### b1) LECTURERS from NATO Countries

Eduard BRYNDA  
Institute of Macromolecular Chemistry  
Academy of Sciences  
Heyrovsky sq.2  
16206 Prague 6  
Czech Republic

Universitätstraße 31  
D-93040 Regensburg  
Germany

Ivan KASIK  
Institute of Radio Engineering and  
Electronic  
Academy of Sciences  
Chaberská 57  
18251 Prague 8  
Czech Republic

Barna KOVACS  
Dept. General and Physical Chemistry  
University of Pecs  
Ifjusag str.6  
7624 Pecs  
Hungary

Loic BLUM  
Laboratoire de Génie Enzymatique et  
Biomoléculaire  
Univ. Claude Bernard  
Lyon  
France

Francesco BALDINI  
Institute of Applied Physics  
National Council of Research  
Via Madonna del Piano 10  
50019 Sesto Fiorentino (Fi)  
Italy

Guenther GAUGLITZ  
Institut für Physikalische und  
Theoretische Chemie  
Auf der Morgenstelle 8  
D-72076 Tübingen  
Germany

Vincenzo PALLESCI  
Applied Laser Spectroscopy  
IPCF/ CNR  
Via G. Moruzzi 1  
56124 Pisa  
Italy

Gerhard MOHR  
Institute of Physical Chemistry  
Friedrich-Schiller University Jena  
Lessingstrasse 10  
D-07743 Jena  
Germany

Alfred DRIESSEN  
University of Twente  
MESA+ Research Institute  
P.O. Box 217  
7500 AE Enschede  
Netherlands

Otto WOLFBEIS  
Institute of Analytical Chemistry  
University of Regensburg

Paul V. LAMBECK  
Lightwave Devices Group  
MESA+ University of Twente  
P.O. Box 217  
7500 AE Enschede  
Netherlands

Artur DYBKO  
 Dept. of Analytical Chemistry  
 Warsaw Univ. Technology  
 Noakowskiego 3  
 PL-00-664 Warsaw  
 Poland

Halina PODBIELSKA  
 Wroclaw Univ. Technology  
 Institute of Physics  
 Wybrzeze Wyspianskiego 27  
 50-370 Wroclaw  
 Poland

Aleksandra LOBNIK  
 Faculty of Mechanical Engineering  
 Centre of Sensor Technology  
 University of Maribor  
 Smetanova 17  
 SI-2000 Maribor  
 Slovenia

Maria Cruz MORENO-BONDI  
 Dept. Analytical Chemistry  
 Universidad Complutense de Madrid  
 E-28040 Madrid  
 Spain

Guillermo ORELLANA  
 Dept. Organic Chemistry  
 Universidad Complutense de Madrid  
 E-28040 Madrid  
 Spain

John DAKIN  
 Optoelectronic Research Centre  
 Univ. Southampton  
 Highfield  
 SO171BJ Southampton  
 UK

Robert LIEBERMAN  
 Intelligent Optical Systems  
 2520 W. 237th Street  
 Torrance, CA 90505  
 USA

Frances LIGLER  
 Center for Bio/Molecular Science and  
 Engineering  
 Naval Research Laboratory  
 Code 6900, 4555 Overlook Av., SW  
 Washington, DC 20375  
 USA

Charles H. TOWNES  
 Physics Dept  
 University of California  
 557 Bridge, Berkeley  
 CA 94720-7300  
 USA

David WALT  
 Dept. Chemistry  
 Tufts University  
 Medford, MA 02155  
 USA

## **b2) LECTURERS from non-NATO partner Countries**

Martin KRAFT  
 CTR - Carinthian Tech Research AG  
 Centre for Sensors and Actuators  
 Europastraße 4  
 A-9524 Villach/St. Magdalen  
 Austria

Claudia PREININGER  
 Austrian Research Centers – ARC  
 A-2444 Seibersdorf  
 Austria

Brian MAC CRAITH  
 Optical Sensors Laboratory  
 School of Physical Sciences  
 National Centre for Sensor Research  
 Dublin City University  
 Glasnevin, Dublin 9  
 Ireland

Dmitri PAPKOVSKY  
 Laboratory of Biophysics and  
 Bioanalysis, Dept. of Biochemistry  
 University College Cork  
 Lee Maltings, Cork  
 Ireland

**c1) ASI Students from NATO countries**

Charles JOACHAIN  
Universite Libre de Bruxelles  
Department of Physics  
Campus Plaine  
C.P. 227  
B-1050 Brussels  
Belgium

Pavel ADAM  
Institute of Radio Engineering and  
Electronics  
Academy of Sciences  
Chaberská 57  
18251 Prague 8  
Czech Republic

Martin DVORAK  
Institute Radio Engineering and  
Electronics  
Academy of Sciences  
Chaberská 57  
18251 Prague 8  
Czech Republic

Pavla GAVLASOVA  
Institute of Chemical Process  
Fundamentals  
Academy of Sciences  
Rozvojová 135  
16502, Prague 6  
Czech Republic

Olga TELEZHNIKOVA  
Institute of Radio Engineering and  
Electronics, Academy of Sciences  
Chaberská 57  
18251 Prague 8  
Czech Republic

Hana VAISOCHEROVA  
Institute of Physics  
Charles University  
Ke Karlovu 5  
121 16 Prague 2  
Czech Republic

Joanna KONAT-STEPOWICZ  
Institute of Optics  
Technische Univ. Berlin Sekr. PN 0-1  
Hardenbergstrasse 36  
D-10623 Berlin  
Germany

Michael KUMPF  
Institut für Physik. und Theor. Chemie  
Auf der Morgenstelle 8  
D-72076 Tübingen  
Germany

Martin MAIWALD  
Institute of Optics  
Technische Univ. Berlin, Sekr. PN 0-1  
Hardenbergstrasse 36  
D-10623 Berlin  
Germany

Bernd Peter MOEHRLE  
Institut für Physik. und Theor. Chemie  
Auf der Morgenstelle 8  
D-72076 Tübingen  
Germany

Anna TSIGARA  
NTUA National Technical Univ. Athens  
Vasileos Konstantinou Ave. 48  
116 35 Athens  
Greece

Akos MARKOVICS  
Dept. General and Physical Chemistry  
University of Pecs  
Ifjusag str.6  
7624 Pecs  
Hungary

Zsolt PUSKAS  
Microvacuum Ltd  
Kerekgyarto U. 10  
H-1147 Budapest  
Hungary

Monika SZILI  
University of Pecs  
Faculty of Natural Sciences  
Dept. General and Physical Chemistry  
Ifjúság útja 6  
7624 Pécs  
Hungary

Damir TESANOVIC  
University of Pecs  
Dept. General and Physical Chemistry  
Ifjúság útja 6  
7624 Pécs  
Hungary

Mahmoud ABURISH HMIDAT  
SCIMEX (Scientific Materials Europe)  
Zona Ind. Loc. Boccasara  
08048 Tortoli' (NU)  
Italia

Enrico ALLARIA  
Università di Firenze  
Istituto Nazionale di Ottica Applicata  
Largo E. Fermi 6  
50125 Firenze  
Italia

Fortunato Tito ARECCHI  
Phys. Dept. University of Firenze  
Istituto Nazionale di Ottica Applicata  
L.go E. Fermi 6  
50125 Firenze  
Italy

Mario BERTOLOTTI  
Università di Roma "La Sapienza"  
Dipartimento di Energetica  
Via Antonio Scarpa 16  
00161 Roma  
Italy

Barbara BRUNETTI  
Di.Pro.Ve, Università di Milano  
Via Celoria 2  
I-20133 Milano  
Italia

Nunzio CENNAMO  
Dip. Ingegneria dell'Informazione  
Seconda Università di Napoli  
Via Roma 25  
81031 Aversa (CE)  
Italia

Ambra GIANNETTI  
Institute of Applied Physics  
National Council of Research  
Via Madonna del Piano 10  
50019 Sesto Fiorentino (Fi)  
Italy

Vincenzo ITALIA  
Università del Sannio  
Dipartimento di Ingegneria  
Palazzo Bosco Lucarelli  
Corso Garibaldi 107  
82100 Benevento  
Italia

Elisabetta MACIS  
DIBE – Dept. Biophysical and  
Electronic Engineering  
University of Genoa  
Via Opera Pia 11/A  
16145 Genova  
Italia

Maria Grazia MANERA  
IMM-CNR  
Lecce University Campus  
Via Arnesano  
73100 Lecce  
Italia

Massimo PALMA  
Dip. Tecnologie dell'Informazione  
University of Milan  
Via Bramante 65  
26013 Crema (CR)  
Italy

Lucia ROTIROTI  
IMM-CNR  
Via Pietro Castellino 111  
80131, Napoli  
Italia

Marco RUGGERI  
INFN – Unità di Modena  
Via Campi 213  
41100 Modena  
Italia

Alex RYDZY  
Engineering Faculty  
University of Rome "Tor Vergata"  
Via del Politecnico 1  
00133 Rome  
Italy

Alessandro SCHENA  
Institute of Applied Physics  
National Council of Research  
Via Madonna del Piano 10  
50019 Sesto Fiorentino (Fi)  
Italy

Walter VASTARELLA  
ENEA C.R: CASACCIA  
Via Anguillarese 301  
I-00060 S. Maria di Galeria (Roma)  
Italia

*Directors's List of Participants*

xxi

Vykintas TAMULIS  
Institute of Theoretical Physics and  
Astronomy  
Vilnius University  
A.Gostauto 12  
Vilnius 2600  
Lithuania

Joris BOKKES  
University of Twente  
Witbreuksweg 395-105  
7522 ZA Enschede  
Netherlands

Joris VAN LITH  
IOMS, University of Twente  
Faculty of Electrical Engineering  
P.O. Box 217  
7500AE Enschede  
Netherlands

Leszek ADAMOWICZ  
Warsaw University of Technology  
Faculty of Physics  
Koszykowa 75  
PL-00-662 Warsaw  
Poland

Iwona HOLOWACZ  
Wroclaw Univ. Technology  
Institute of Physics  
Wybrzeze Wyspianskiego 27  
50-370 Wroclaw  
Poland

Zdzisław MACZENSKI  
Warsaw University of Technology  
Faculty of Electronics and Information  
Technology  
Nowowiejska St. 15/19  
00-665 Warsaw  
Poland

Danuta SLAWINSKA  
Department of Physics  
August Cieszkowski Agricultural  
University of Poznan  
Wojska Polskiego 38/42  
60-637 Poznan  
Poland

Dorota STADNIK  
Dept. of Analytical Chemistry  
Warsaw Univ. Technology

Noakowskiego 3  
PL-00-664 Warsaw  
Poland

Andrzej TADEUSIAK  
Warsaw University of Technology  
Faculty of Physics  
Koszykowa 75  
PL-00-662 Warsaw  
Poland

Michał WIERZBICKI  
Warsaw University of Technology  
Faculty of Physics  
Koszykowa 75  
PL-00-662, Warsaw  
Poland

Paulo CALDAS  
Unidade de Optoelectronica e  
Sistemas Electronicos  
INESC Porto and Dept Physics  
University of Porto  
Rua do Campo Alegre 687  
4169-007 Porto  
Portugal

Pedro JORGE  
Unidade de Optoelectronica e  
Sistemas Electronicos  
INESC Porto and Dept Physics  
University of Porto  
Rua do Campo Alegre 687  
4169-007 Porto  
Portugal

Simona Larisa APOSTOL  
Valahia Univerity  
Physics Department  
24 Bd Unirii  
0200 Targoviste  
Romania

Irina DUMITRIU  
National Institute of Materials Physics  
105bis Atomistilor Street  
077125 Bucharest-Magurele  
Romania

Ravan ROESCU  
National Institute of Materials Physics  
105bis Atomistilor Street  
77125 Bucharest-Magurele  
Romania

Spela-Mojca KORENT  
Faculty of Mechanical Engineering  
University of Maribor  
Smetanova 17  
SI-2000 Maribor  
Slovenia

Ozlem GUMRAH  
Hacettepe University  
Department of Chemistry  
06532 Beytepe, Ankara  
Turkey

Mete TAYANC  
Dept of Environmental Engineering  
Marmara University  
Goztepe Campus, Kadikoy  
81040 Istanbul  
Turkey

Gokhan UMAROGULLARI  
Trakya Universitesi  
Muhendislik Mimarlik Fakultesi  
Mimarlik Bolumu  
22030 Edirne  
Turkey

Christina BOOZER  
Department of Chemical Engineering  
University of Washington  
Box 351750  
98195, Seattle - WA  
USA

Matt MARTIN  
Oak Ridge National Lab  
One Bethel Valley Road  
Oak Ridge, TN 37831  
USA

## **c2) ASI students from non-NATO partner Countries**

Hektor PREZA  
University of Tirana  
Chemistry Department  
Boulevardi 206 I  
Tirana  
Albania

Ilir VULLKAJ  
Polytechnic University  
Department of Physics  
Sheshi Nene Tereza, No. 4  
335 Tirana  
Albania

Katarzyna DERWINSKA  
ARC Seibersdorf research GmbH  
Dept Biotechnology  
A-2444 Seibersdorf  
Austria

Alina HUSCHYNCKAIA  
Ministry of Education and Science  
9 Sovetskaya St.  
220010 Minsk  
Belarus

Snezana MILJANIC  
Department of Chemistry  
Faculty of Science  
Strossmayerov trg 14  
HR-10000 Zagreb  
Croatia

Clare HIGGINS  
Optical Sensors Laboratory  
School of Physical Sciences  
National Centre for Sensor Research  
Dublin City University  
Glasnevin, Dublin 9  
Ireland

Ondrej STRANIK  
Optical Sensors Laboratory  
School of Physical Sciences  
National Centre for Sensor Research  
Dublin City University  
Glasnevin, Dublin 9  
Ireland

Abutrab ALIVERDIEV  
Russian Academy of the Science  
Institute of Physics of Daghestan  
Scientific Centre  
94 M. Yaragskogo Street  
367003 Makhachkala  
Russia

Alexandre MAJOUGA  
Moscow State University  
Department of Chemistry  
Vorobjovy Gory  
119899 Moscow  
Russia

*Directors's List of Participants*

xxiii

Ekaterina OBRAZTSOVA  
Physics Department  
M.V. Lomonosov Moscow State  
University  
Leninsky Gory  
1198992 Moscow  
Russia

Lydia SOKOLOVSKAYA  
M.V. Lomonosov Moscow State  
University  
Department of Chemistry  
Leninskie Gory 1 bldg. 73  
119992 Moscow  
Russia

Andrei VARLAMOV  
Moscow Technological University  
Institute of Steel and Alloys  
Leninski prospect 4  
117936 Moscow  
Russia

Nicolas LEDERMANN  
Hach Ultra Analytics  
rte de Compois 6  
1222 Vesenz  
Switzerland

Eric STUDEMANN  
Hach Ultra Analytics  
rte de Compois 6  
1222 Vesenz  
Switzerland

Andrij SAVCHENKO  
Institute of Semiconductor Physics  
National Academy of Sciences of  
Ukraine  
Nauki prospect 45  
03028 Kiev  
Ukraine

Zulfiya BAKAEVA  
Heat Physics Department  
Uzbekistan Academy of Sciences  
Katartal street 28  
700135 Tashkent  
Uzbekistan

Oksana ISMAILOVA  
Heat Physics Department  
Uzbekistan Academy of Sciences  
Katartal street 28  
700135 Tashkent  
Uzbekistan



## EDITORIAL

The present Proceedings mark a milestone in the history of the laser as well as a milestone in the International School of Quantum Electronics.

2004 marks the 40th anniversary of the award of the 1964 Nobel Prize in Physics "for fundamental work in the field of quantum electronics, which has led to the construction of oscillators and amplifiers based on the maser-laser principle." This award, given to Profs. Charles H. Townes, Nicolay G. Basov and Aleksandr M. Prokhorov, acknowledged the discovery and early development of masers and lasers, which have so richly benefited both scientific research and practical applications.

2004 also commemorates the 40<sup>th</sup> Course of ISQE, which has presented workshops and short courses on almost every aspect of lasers from 1971 through the present Course on "Optical Chemical Sensors." A list of the courses and workshops is appended to these remarks for reference.

Because of this fortuitous coincidence, we decided early in the planning of the 2004 Course to set aside time in the program for a ceremony to commemorate the "birthday" of the laser, with the participation if possible of those who contributed to its initial discovery and development. Unfortunately, Profs. Basov and Prokhorov are no longer living; however, Prof. Andrei Varlamov, on behalf of the Russian Academy of Sciences, agreed to attend the ceremony and give his recollections of these gentlemen and their early years of laser research.

Prof. Townes, who is presently with the University of California, Berkeley, California, kindly consented to not only attend the ceremony, but also to give the keynote address. His remarks capture the excitement and energy of the early days of maser and laser research, and also touch on the breadth of applications today. He also points out that 2004 is also the 50<sup>th</sup> year of the operation of the first maser, making this a threefold anniversary. Prof. Townes' talk is included in these Proceedings under the title "Birth of the Maser and Laser".

The ceremony was held on August 1, 2004, hosted by Prof. Sergio Martellucci, Co-Director of the International School of Quantum Electronics. A number of distinguished scientists and national leaders participated in the ceremony representing the Italian institutions (Universities, Research and Industry) operating in the field of laser. At the end of the Ceremony Prof. Townes has been awarded by the Galileo Galilei medal of the Italian Optics and Photonics Society (S.I.O.F.).

It is especially fitting that this Course on Optical Chemical Sensors should be the occasion to recollect the early days of the laser and honor those whose vision and brilliance opened up such a rich and productive area of science. Laser-based chemical sensors serve as valuable research tools while at the same time they have found many practical applications – in this sense, they offer a representative snapshot of the entire field of masers and

lasers. Moreover, these sensors reach across the boundaries from physics and engineering to chemistry and biology, and thus they epitomize the inherent interdisciplinary characteristics of the laser itself.

Directors of the International School of Quantum Electronics:

Arthur N. Chester  
Hughes Electronics Corp. &  
HRL Laboratories (Retired),  
Malibu, California, USA

Sergio Martellucci  
Engineering Faculty  
University of Rome "Tor Vergata"  
Rome, Italy

## LIST OF ISQE COURSES

INTERNATIONAL SCHOOL OF QUANTUM ELECTRONICS - Ettore Majorana Foundation and Centre for Scientific Culture

INTERNATIONAL SCHOOL OF QUANTUM ELECTRONICS - Directors: F.T. ARECCHI - D. ROESS

1st Course: *Physical and Technical Measurements with Lasers* - Director: A. SONA  
8 - 21 May 1971

INTERNATIONAL SCHOOL OF QUANTUM ELECTRONICS - Directors: F.T. ARECCHI - D. ROESS

2nd Course: *Nonlinear Optics and Short Laser Pulses* - Directors: W. KAISER - O. SVELTO  
16 - 29 April 1972

INTERNATIONAL SCHOOL OF QUANTUM ELECTRONICS - Directors: F.T. ARECCHI - D. ROESS

3rd Course: *Laser Frontiers: Short Wavelengths and High Powers* - Directors: P. CALDIROLA - S. RAMSDEN  
3 - 16 June 1973

INTERNATIONAL SCHOOL OF QUANTUM ELECTRONICS - Directors: F.T. ARECCHI - D. ROESS

4th Course: *Co-operative Phenomena in Multi-component Systems* - Directors: R. BONIFACIO - H. HAKEN  
21 May - 5 June 1974

Proceedings: *Cooperative Effects: Progress in Synergetics*  
Editor: H. Haken. Publisher: North-Holland Publishing Company (1974)

INTERNATIONAL SCHOOL OF QUANTUM ELECTRONICS - Directors: F.T. ARECCHI - D. ROESS

5th Course: *Molecular Spectroscopy and Photo-chemistry with Lasers* - Directors: F.P. SCHAEFER - A. SONA  
25 June - 10 July 1975

INTERNATIONAL SCHOOL OF QUANTUM ELECTRONICS - Directors: F.T. ARECCHI - D. ROESS

6th Course: *Coherent Optical Engineering*  
1 - 15 September 1976

Proceedings: *Coherent Optical Engineering*  
Editors: F.T. Arecchi and V. Degiorgio. Publisher: North-Holland Publishing Company (1977)

INTERNATIONAL SCHOOL OF QUANTUM ELECTRONICS - Directors: A.N. CHESTER - S. MARTELLUCCI

7th Course: *Physics and Technology of Free Electron Lasers*  
17 - 29 August 1980

Proceedings: *Free Electron Lasers*  
Editors: S. Martellucci and A.N. Chester. Publisher: Plenum Press (1983)

INTERNATIONAL SCHOOL OF QUANTUM ELECTRONICS - Directors: A.N. CHESTER - S. MARTELLUCCI

8th Course: *Integrated Optics: Physics and Applications*. NATO A.S.I.

17 - 29 August 1981

Proceedings: Integrated Optics: Physics and Applications

Editors: S. Martellucci and A.N. Chester. Publisher: Plenum Press (1983)

INTERNATIONAL SCHOOL OF QUANTUM ELECTRONICS - Directors: A.N. CHESTER - S. MARTELLUCCI

9th Course: *Analytical Laser Spectroscopy*. NATO A.S.I.

23 September - 3 October 1982

Proceedings: Analytical Laser Spectroscopy

Editors: S. Martellucci and A.N. Chester. Publisher: Plenum Press (1985)

INTERNATIONAL SCHOOL OF QUANTUM ELECTRONICS - Directors: A.N. CHESTER - S. MARTELLUCCI

Workshop on: *Hybrid Ray Mode Formulation of Wave Propagation*

25 - 27 September 1982

INTERNATIONAL SCHOOL OF QUANTUM ELECTRONICS - Directors: A.N. CHESTER - S. MARTELLUCCI

10th Course: *Laser Applications to Medicine and Biology*

4 - 16 September 1983

Proceedings: Laser Photobiology and Photomedicine

Editors: S. Martellucci and A.N. Chester. Publisher: Plenum Press (1985)

INTERNATIONAL SCHOOL OF QUANTUM ELECTRONICS - Directors: A. CHESTER - S. MARTELLUCCI

Workshop on: *Optical Phase Conjugation*

24 - 30 March 1984

INTERNATIONAL SCHOOL OF QUANTUM ELECTRONICS - Directors: A.N. CHESTER - S. MARTELLUCCI

Workshop: *Progress in Microemulsions*

26 October - 1 November 1985

Proceedings: Progress in Microemulsions

Editors: S. Martellucci and A.N. Chester. Publisher: Plenum Press (1989)

INTERNATIONAL SCHOOL OF QUANTUM ELECTRONICS - Directors: A.N. CHESTER - S. MARTELLUCCI

11th Workshop: *Optical Fiber Sensors*. NATO A.S.I.

2 - 10 May 1986

Proceedings: Optical Fiber Sensors

Editors: A.N. Chester, S. Martellucci and A.M. Verga Scheggi. Publisher: Martinus Nijhoff Publishers (1987)

INTERNATIONAL SCHOOL OF QUANTUM ELECTRONICS - Directors: A.N. CHESTER - S. MARTELLUCCI

12th Course: *Laser Science and Technology*

11 - 19 May 1987

Proceedings: Laser Science and Technology

Editors: A.N. Chester, V.S. Letokhov and S. Martellucci. Publisher: Plenum Press (1988)

INTERNATIONAL SCHOOL OF QUANTUM ELECTRONICS - Directors: A.N. CHESTER - S. MARTELLUCCI

13th Course: *Non Linear Optics and Optical Computing*

11 - 19 May 1988

Proceedings: Nonlinear Optics and Optical Computing

Editors: S. Martellucci and A.N. Chester. Publisher: Plenum Press (1990)

INTERNATIONAL SCHOOL OF QUANTUM ELECTRONICS - Directors: A.N. CHESTER - S. MARTELLUCCI

14th Course: *Optoelectronics for Environmental Science* – Directors: V.S. LETOKHOV - A.M. SCHEGGI

3 - 12 September 1989

Proceedings: Optoelectronics for Environmental Sciences

Editors: S. Martellucci and A.N. Chester. Publisher: Plenum Press (1991)

INTERNATIONAL SCHOOL OF QUANTUM ELECTRONICS - Directors: A. CHESTER - S. MARTELLUCCI

15th Course: *Laser Systems for Photobiology and Photomedicine*. NATO A.S.I.

11 - 20 May 1990

Proceedings: Laser Systems for Photobiology and Photomedicine

Editors: S. Martellucci, A.N. Chester and A.M. Scheggi. Publisher: Plenum Press (1991)

INTERNATIONAL SCHOOL OF QUANTUM ELECTRONICS - Directors: A.N. CHESTER - S. MARTELLUCCI

16th Course: *Phase Transitions in Liquid Crystals*

2- 12 May 1991

Proceedings: Phase Transitions in Liquid Crystals

Editors: S. Martellucci and A.N. Chester. Publisher: Plenum Press (1992)

INTERNATIONAL SCHOOL OF QUANTUM ELECTRONICS - Directors: A.N. CHESTER - S. MARTELLUCCI

17th Course: *Laser Applications for Mechanical Industry*. NATO A.S.I. - Directors: L. PERA - A.M. SCHEGGI

4 - 16 April 1992

Proceedings: Laser Applications for Mechanical Industry

Editors: S. Martellucci, A.N. Chester and A.M. Scheggi. Publisher: Kluwer Academic Publishers (1993)

INTERNATIONAL SCHOOL OF QUANTUM ELECTRONICS - Directors: A.S. CHESTER - S. MARTELLUCCI

18th Course: *Advances in Integrated Optics* - Directors: M. BERTOLOTTI - G.C. RIGHINI

1 - 9 June 1993

Proceedings: Advances in Integrated Optics

Editors: S. Martellucci, A.N. Chester and M. Bertolotti. Publisher: Plenum Press (1994)

INTERNATIONAL SCHOOL OF QUANTUM ELECTRONICS - Directors: A. CHESTER - S. MARTELLUCCI

19th Course: *Biomedical Optical Instrumentation and Laser-assisted Biotechnology*. NATO A.S.I. - Directors: R. PRATESI - A.M. SCHEGGI

10 - 22 November 1995

Proceedings: Biomedical Optical Instrumentation and Laser-Assisted Biotechnology

Editors: A.M. Verga Scheggi, S. Martellucci, A.N. Chester and R. Pratesi. Publisher: Kluwer Academic (1996)

INTERNATIONAL SCHOOL OF QUANTUM ELECTRONICS - Director: S. MARTELLUCCI

20th Course: *Diffraction Optics and Optical Microsystems* - Directors: F. GORI - G.C. RIGHINI

14 - 24 November 1996

Proceedings: Diffractive Optics and Optical Microsystems

Editors: S. Martellucci and A.N. Chester. Publisher: Plenum Press (1997)

INTERNATIONAL SCHOOL OF QUANTUM ELECTRONICS - Directors: A.N. CHESTER - S. MARTELLUCCI

21st Course: *Global Automotive Technology. Senior Management Briefing* - Director: M. NASIM UDDIN

27 - 31 July 1997

INTERNATIONAL SCHOOL OF QUANTUM ELECTRONICS - Directors: A.N. CHESTER - S. MARTELLUCCI

22nd Course: *Optical Sensors and Microsystems: New Concepts, Materials Technologies* - Directors: A. DOMANSKY - A.G. MIGNANI

27 November - 2 December 1997

Proceedings: *Optical Sensors and Microsystems: New Concepts, Materials Technologies*

Editors: S. Martellucci, A.N. Chester and A.G. Mignani. Publisher: Plenum Press (2000)

INTERNATIONAL SCHOOL OF QUANTUM ELECTRONICS - Directors: A.N. CHESTER - S. MARTELLUCCI

23rd Workshop: *Excimer Lasers for Fusion and Industrial Application* - Director: M.J. SHAW

29 November - 4 December 1997

Proceedings: *Excimer Lasers for Fusion and Industrial Applications (Abstracts Collection)*

Editors: L. Cemoli and S. Martellucci. Publisher: University of Rome "Tor Vergata" (to be reproduced upon request)

INTERNATIONAL SCHOOL OF QUANTUM ELECTRONICS - Directors: A.N. CHESTER - S. MARTELLUCCI

24th Course: *Advances in Optoelectronics for Environmental Monitoring* - Director: C. BELLECCI

16 - 22 November 1998

INTERNATIONAL SCHOOL OF QUANTUM ELECTRONICS - Directors: A.N. CHESTER - S. MARTELLUCCI

25th Course: *Observational Data Base and Mechanisms of Climate* - Director: G.P. GREGORI

21 - 27 November 1998

INTERNATIONAL SCHOOL OF QUANTUM ELECTRONICS - Directors: A.N. CHESTER - S. MARTELLUCCI

26th Course: *Monitoring Black Sea Environmental Conditions* - Directors: R.C. RAGAINI - S. MARTELLUCCI

27 February - 3 March 1999

Proceedings: *Monitoring Black Sea Environmental Conditions*

Editor: L. Krueger. Publisher: The World Federation of Scientists (1999)

INTERNATIONAL SCHOOL OF QUANTUM ELECTRONICS - Directors: A.N. CHESTER - S. MARTELLUCCI

27th Course: *Bose-Einstein Condensates and Atom Lasers* - Directors: A. ASPECT - M. INGUSCIO

19 - 28 October 1999

Proceedings: *Bose-Einstein Condensates and Atom Lasers*

Editors: S. Martellucci, A.N. Chester, A. Aspect and M. Inguscio. Publisher: Kluwer Academic/Plenum (2000)

*List of ISQE Courses*

xxxii

INTERNATIONAL SCHOOL OF QUANTUM ELECTRONICS - Directors: A.N. CHESTER - S. MARTELLUCCI

28th Course: *Laser Beam and Optics Characterization (LBOC5)* - Directors: N. RENG - H. WEBER

20 - 25 March 2000

Proceedings: The 5<sup>th</sup> International Workshop on Laser Beam and Optics Characterization

Editors: H. Laabs and H. Weber. Publisher: Technische Universität Berlin – Optical Institute (2000)

INTERNATIONAL SCHOOL OF QUANTUM ELECTRONICS - Directors: A.N. CHESTER - S. MARTELLUCCI

29th Course: *Nanoscale Linear and Non-linear Optics* - Directors: M. BERTOLOTTI - C.M. BOWDEN - R. HORAK

2 - 14 July 2000

Proceedings: Nanoscale Linear and Nonlinear Optics

Editors: M. Bertolotti, C.M. Bowden and C. Sibilìa. Publisher: American Institute of Physics (2001)

INTERNATIONAL SCHOOL OF QUANTUM ELECTRONICS - Directors: A.N. CHESTER - S. MARTELLUCCI

30th Course: *Atoms, Solids and Plasmas in Super-Intense Laser Fields* - Directors: D. BATANI - C.J. JOACHAIN

8 - 14 July 2000

Proceedings: Atoms, Solids and Plasmas in Super-Intense Laser Fields

Editors: D. Batani, C. Joachain, S. Martellucci and A.N. Chester. Publisher: Kluwer Academic/Plenum (2001)

INTERNATIONAL SCHOOL OF QUANTUM ELECTRONICS - Directors: A.N. CHESTER - S. MARTELLUCCI

31st Course: *Global Automotive Laser Applications* - Directors: F.A. DI PIETRO - J. MAZUMDER

1 - 7 August 2001

INTERNATIONAL SCHOOL OF QUANTUM ELECTRONICS - Directors: A.N. CHESTER - S. MARTELLUCCI

32nd Course: *Optical Coatings: Theory, Production and Characterization* - Directors: E. MASETTI - D. RISTAU

22 - 28 September 2001

Proceedings: Optical Coatings: Theory, Production and Characterization

Editors: E. Masetti, D. Ristau and A. Krasilnikova. Publisher: ENEA, Unità Comunicazione (2003)

INTERNATIONAL SCHOOL OF QUANTUM ELECTRONICS - Directors: A.N. CHESTER - S. MARTELLUCCI

34th Course: *Laser Spectroscopy* - Directors: G. FERRANTE - S. MARTELLUCCI

6 - 13 July 2002

INTERNATIONAL SCHOOL OF QUANTUM ELECTRONICS - Directors: A.N. CHESTER - S. MARTELLUCCI

35th Course: *Free and Guided Optical Beams* - Directors: M. SANTARSIERO - J. TURUNEN

20 - 27 November 2002

Proceedings: Free and Guided Optical Beams

Editors: S. Martellucci and M. Santarsiero. Publisher: World Scientific (2004)

INTERNATIONAL SCHOOL OF QUANTUM ELECTRONICS – Directors: A.N. CHESTER – S. MARTELLUCCI

36th Course: *Advances in Quantum Information Processing: from Theory to Experiments*

Directors: S.F. HUELGA – C. MACCHIAVELLO – G.M. PALMA – M.B. PLENIO

15 – 22 March 2003

INTERNATIONAL SCHOOL OF QUANTUM ELECTRONICS - Directors: A.N. CHESTER - S. MARTELLUCCI

37th Course: *Atoms, Solids and Plasmas in Super-Intense Laser Fields* - Directors: D. BATANI - C.J. JOACHAIN

5 - 15 July 2003

Proceedings: Atoms and Plasmas in Super-Intense Laser Fields

Editors: D. Batani, C. Joachain and S. Martellucci. Publisher: Editrice Compositori, Bologna (2004)

INTERNATIONAL SCHOOL OF QUANTUM ELECTRONICS - Directors: A.N. CHESTER - S. MARTELLUCCI

38th Course: *Spectroscopic Techniques for Materials, Environment and Cultural Heritage*

Directors: N. OMENETTO - V. PALLESCHI

5 - 15 July 2003

INTERNATIONAL SCHOOL OF QUANTUM ELECTRONICS - Directors: A.N. CHESTER - S. MARTELLUCCI

39th Course: *Microresonators as Building Blocks for VLSI Photonics*

Directors: M. BERTOLOTTI – A. DRIESSEN – F. MICHELOTTI

18 - 25 October 2003

Proceedings: Microresonators as Building Blocks for VLSI Photonics

Editors: F. Michelotti, A. Driessen and M. Bertolotti. Publisher: American Institute of Physics (2004)

INTERNATIONAL SCHOOL OF QUANTUM ELECTRONICS - Directors: A.N. CHESTER - S. MARTELLUCCI

40th Course: *Optical Chemical Sensors*. NATO A.S.I. Directors: F. BALDINI – J. HOMOLA

29 July – 10 August 2004

Proceedings: Optica Chemical Sensors

Editors: F. Baldini, A.N. Chester, J. Homola and S. Martellucci. Publisher: Kluwer Academic NATO A.S.I. series (2006)



# Chapter 1

## BIRTH OF THE MASER AND LASER

Charles H. Townes  
*University of California*  
*Physics Department*  
*Berkeley, CA 94720-7300*  
*USA*

### 1. THE LECTURE

Thank you. I'm enormously pleased to be here. I know that this School in Erice was formed some time ago, but this is my first opportunity to be here. Erice is a wonderful city. In addition, I think very highly of the Ettore Majorana Foundation, the Schools, and the Courses here.

You will see from my talk about the laser how important I feel it is for scientists to interact, to bring people together, to talk with each other, to exchange ideas, and also for different fields to interact, so that one can pick up some idea from another field, and so on. That's a very important part of the progress of science and the progress of scientists.

I certainly appreciate what Professor Martellucci is doing in this wonderful School, and I appreciate the opportunity to be here. And I thank you for the honor that you are bestowing on me.

Now, I want to talk about the laser. It's a personal history in part, but also I think a very important illustration of how new science and new technology develop. It's simply one of many examples, but one I happen to know personally, so that's the one I will talk about.

First, let's look at what current lasers and masers do. Lasers vary in size from single atoms, or submicroscopic size, to lasers as big as tall buildings. Well, the single atoms in small lasers produce fantastically small amounts of power – let's say,  $10^{-16}$  watts. The big ones have produced as much as  $10^{+16}$  watts – that is, ten million billion watts, more than we have from any other kind of source. Now, that lasts for a short time, because it would be too expensive to have it on all the time, of course. Nevertheless, it's very powerful, and that great power produces an intensity which allows us to study and to understand new states of matter with very high energy concentration.

Energy concentration is even more important than power. With a laser,  $10^{+15}$  or  $10^{+16}$  watts can be concentrated in an area about the size of one wavelength, so we have maybe  $10^{+23}$  watts per square centimeter. That's a fantastic concentration of power, which produces new kinds of conditions and opens up some new science.

But in addition to producing very high temperatures and fantastic power, the laser also has produced the coldest things we have ever known. It has produced new forms of matter that have temperatures below one millionth of one degree Absolute. And new forms of matter produce new effects and new applications. So the laser gives us these new areas of science: very high energy intensity, very low energy intensity, and new forms of matter.

Also, the laser or maser measures time very precisely. The hydrogen maser, for example, can measure times with a precision of about  $10^{-15}$ . It can also measure short times – as short as  $10^{-15}$  seconds. So we can see atomic and molecular phenomena occurring on very short time scales.

Lasers also measure length very accurately. In fact, the standard of length has been changed – it's no longer the standard meter in Paris, but it's the wavelength of a particular form of light. We can send a laser beam to the moon and measure the time that it takes for its reflection to return, and we can determine the distance to the moon to one or two centimeters. So the laser enables all kinds of high precision measurements, in time, in space, in size, and so on.

Amplifiers. The maser produced a new kind of amplifier, which was about a hundred times more sensitive than the amplifiers we had at the time. The maser had a so-called "noise temperature" of about one degree Absolute – you can get down to about that amount of noise. However, other amplifiers at that time were a hundred times more noisy. Thus the maser allowed us to measure more sensitively.

Well, those are some of the kinds of things that masers and lasers have made possible.

The maser and the laser, I'm delighted to say, have been very useful scientific tools. And that was my primary interest, to get a good scientific tool to do new things. Since the Nobel Prize in 1954 there have been twelve other Nobel Prizes that used masers or lasers as tools. That doesn't mean that the masers and lasers produced the Nobel Prize, but the person who did the Nobel Prize work was able to do things that he couldn't do otherwise, using masers and lasers as tools.

Now let me mention some of the commercial applications, because of course it has had an enormous commercial impact. When the laser first came along, and we were talking about it, some of my friends said, "Well, that's a nice idea, but what good is it? What can it do?" Today, it's fantastic to think that anybody would even ask that question. Look at all the uses! Well, I could foresee some of the uses, certainly in communications and so on, and in heat. The laser marries optics and electronics, and those two touch on

many different fields. Initially, we couldn't even imagine all of the uses that it would have, and in fact those uses have appeared and been developed with the contributions of many different scientists and engineers.

But communications is one of the most important commercial applications, because a beam of light gives us an enormously wide bandwidth. Bandwidths have been produced up to about 100 gigabytes, in other words, a hundred billion pieces of information per second, in one light beam. Now actually, in principle, the bandwidth could be one hundred times more than that. As we develop the technology, we can transfer a million billion pieces of information per second, and that will be more than all of the radio, TV and telephones all over the world, put on one light beam. So the laser has an enormous potential for communications, and it's already being used in this way.

But there are other applications as well, such as recording and reading information. We see this at a grocery store, scanning bar codes on products. You also see laser pointers, which are used here in some of the lectures. All kinds of very simple things as well as very complex things.

One of the first applications I pointed out was that you can produce a straight line – a surveyor can use a laser beam to define a straight line, and by getting the reflection back he can also measure the exact distance to within a millimeter. Just simple surveying, producing a straight line. Now the GPI, Global Positioning Indicator, this uses a maser clock, that's another application.

Cutting and welding, and heavy manufacturing. Lasers are now being used in making automobiles. Lasers can burn and cut very fast, and they can also make very precise cuts. They can also cut things without heating up the rest of the material. Or, they can evaporate and clean a surface by a spurt of energy without overheating the underlying material. There are already many laser applications in manufacturing and I'm sure there will be many more, particularly in nanotechnology – because although lasers can be enormously powerful, they can also be weak and precise. With laser tweezers we can pick up an individual molecule or an individual living cell without injuring it, and move it to another place. In this way, we can construct and manufacture extremely small things.

I'm particularly pleased with the use of the laser for medicine. Now, just as an illustration of the difficulty of predicting the future development of science and technology, shortly after the laser came along, a medical doctor came to me and said that he was very interested in possible medical uses of the lasers. Would I be willing to help him write a paper on medical uses of lasers? I said, of course, I'd be delighted, and so we wrote an article covering as many ideas as we could. However, we missed some of the most important medical applications. Perhaps the first very important medical use for the laser was re-attaching detached retinas. If the retina comes loose, you can use a very precise burst of light to re-attach it – it's very simple. And I'm

just delighted that lasers have saved the eyes of some of my friends. Emotionally, that affects me more than almost any other application. But at the time the doctor asked me to write about medical uses, I'd never heard of detached retinas, and he didn't mention it, and so we missed this application. But nevertheless, that was one of the first very important medical uses of the laser. And of course, since then the laser has been used for many other kinds of operations as well.

Now, what more? I would say at present that lasers are still in a preliminary stage of development – perhaps what I would call late adolescence in a human. When a child grows up, by the time they get into adolescence we can sort of see their potentiality, we can see how smart they are, or what they might do, and how much energy they have. Similarly, today we can visualize how important the field of lasers is, and we can see how active it is, and what it's likely to do, but we can't predict everything that it is going to do in the future. And so I would say the field of lasers is in its adolescence. We can see pretty well that it's got lots of potential, but we can't predict its entire future, and we expect other scientists and engineers to still find many more applications.

Now, I like to make an analogy to describe this situation. The analogy is with a beaver. As you know, a beaver builds a dam in a stream by bringing little branches and putting them together. Well, my story is about the beaver and his friend the rabbit. They are both looking up at Hoover Dam in the United States, which is a wonderful big concrete dam in an enormous canyon, one of the most beautiful and biggest dams we have. And the beaver looks up at this dam and says to his friend the rabbit, "No, I didn't really build that dam, but it's based on an idea of mine!" My point is that it's very important to recognize that science grows as a result of a community, a community of scientists and engineers who add further ideas. Science grows like a tree, as people keep adding on more and more new things. So the success of the laser has arisen because of the scientific community, with contributions from many different people. Not only the scientific work, but also the commercial applications of lasers have depended upon the contributions of such a community.

The question has already been asked, well, why wasn't the laser discovered earlier? In fact, there's no single idea involved in the maser or the laser that somebody didn't already know – but no one put them all together. For example, Einstein pointed out that stimulated emission occurs when light passes near an excited atom or molecule. The light can induce the excited atom or molecule to give up its energy to the light, and that's a very critical part of masers and lasers. Now, did Einstein think about amplification? No. Did he say anything about the coherence of this induced emission? No, he didn't say that.

However, in 1924, [Richard C.] Tolman, a theoretical physicist who studied thermodynamics and light interacting with molecules, described how

light gets absorbed by molecules and how some molecules in a lower state will absorb, and some in an upper state will emit. And he said, well, of course, if there were more molecules in the upper state than in the lower state, you'd have negative absorption, that is, amplification. But he said, it would probably be very weak. That's all he said about it, and nobody paid any attention to it.

Tolman also said that no one has proved that the light induced this way, the light produced by the molecule, is the exact same frequency and phase as the inducing light, but it probably is. However, nobody had proved it mathematically. As a matter of fact, in some of my early work on the maser, people challenged me on this point, and I went back to the notes I had taken in quantum mechanics courses I had taken back in 1937 – I pulled out these notes, I could see the equations there, and I could see that the emitted light has to be coherent. But not everybody recognized that, although certainly some people knew it.

So, you see the field is in fact a very old one, and so why wasn't it put together? Well, this is another example of how science and technology advance. Different scientific fields have to interact – people have to be interested enough to do some new work, and talk to each other, and new ideas grow out of fields which had seemed not to be relevant at all. The laser, an intense light, came out of the study of the microwave spectra of molecules. The microwave spectra of molecules – now, what would motivate someone to say, I want a very bright light, so I will hire somebody to study the microwave spectra of molecules? He wouldn't do that, he couldn't possibly think of that. No, he would go to some company that's making bright lights now, and ask them to make it a little bit brighter. They might double the intensity. But microwave spectra of molecules produced lasers with billions of times more intensity.

Now, how can I say that masers and lasers grew out of the field of microwave spectroscopy? Well, of course, that was my own field, from which I got my ideas. It was also the field of [Nicolay G.] Basov and [Aleksandr M.] Prokhorov – they were working in microwave spectra of molecules, and there was a third separate idea, from [Joseph] Weber at the University of Maryland – he had some ideas on masers, and talked about them. He didn't have a very practical system, and never tried to make a maser, but he recognized this possibility, and he was also in the field of microwave spectroscopy. So there were three separate ideas which came out of that field. And this happened because that field married engineering and quantum mechanics, in just the right way. Now at that time, most physicists didn't know much about engineering, and most engineers didn't know much about quantum mechanics, and bringing those concepts together was not so obvious.

Microwave spectroscopy grew out of the radar of World War II. Working with those radars taught many physicists a good deal about engineering. And

it taught me. I worked on radar during World War II. After World War II, I recognized, as did some other physicists, “Hey, this new radar and the technology we have can do spectroscopy of a new kind.” In fact, some radars had unexpectedly run into trouble – they didn’t work very well, because of the absorption of a particular wavelength by water in the atmosphere. And since I was in that field, I knew that we could do a new kind of spectroscopy.

And now, I’ll be talking about the interaction between basic science and applied science, or, you might say, university science and industrial science.

I was working at Bell Telephone Laboratories at that time. Much of the radar development came out of applied work in industrial laboratories, and so did microwave spectroscopy. I persuaded the Bell Laboratories to let me do microwave spectroscopy, and so it started at Bell Labs, but it also started at General Electric, where a friend of mine began it. He did a little bit of work, but then the General Electric people said, no, you must stop, it’s not going to have any use for us, we have no applications. So this work had to stop at General Electric. At RCA, another important electrical company, a friend of mine started it there, and he worked on it for a while, and the company said, no, that’s of no value to us, we won’t pay you anything for it, you must stop.

Microwave spectroscopy also started at Westinghouse, again, an industrial company. It was done by a friend of mine, and he did some nice microwave spectroscopy, but the company said no, shut it down, we can’t pay for that.

Bell Telephone Laboratories asked me to stop, because they said, look, there are some engineering things that we’d like you to do that would be much more important to us. But I didn’t want to do that, and I said, look, I really want to do some physics, and they let me do it. And I continued to do microwave spectroscopy, and pretty soon microwave spectroscopy was interesting enough to other physicists that I got a job at Columbia University. And so I moved to academia because industry wasn’t all that interested in the field.

Now, we recognized that by using radar technology, klystrons and magnetrons, we could do this wonderful new spectroscopy at very high resolution, but we wanted to get to shorter wavelengths. Those electronic devices could produce radar wavelengths as short as a couple of millimeters, but not much shorter. However, I wanted to get on into the far infrared, below a millimeter. And I kept working on this. My students and I tried several methods, and they worked a little bit, but they didn’t work very well. At one point the Navy asked me to head a national committee to try to examine how we could get down to shorter wavelengths – they wanted shorter wavelengths for radar, to get down into the far infrared. They asked me to organize a committee and examine the subject, and we traveled all over Europe and the United States, to many laboratories, trying to see, does anybody have any ideas? And we discovered nothing. The last meeting was

to be in Washington. I chaired the meeting, and I woke up early in the morning, worrying about, now, why haven't we been able to find a good way to get to short wavelengths?

Now, this is one way that new ideas come up. I sat in the park in the early morning thinking, I haven't been able to do this, and I went through all the ideas that I had tried and had looked at. I said, now of course molecules can make short waves, but thermodynamics says you can't get more than a certain amount of energy from them, unless you heat them up very very hot. And then the molecules would fall apart. I had used that argument before, I was proud of myself for knowing enough thermodynamics to know that you can't get much energy out of the molecules.

But then I said, wait a minute, wait a minute! The molecules don't have to be described by a temperature. We could have more molecules in the upper state than in the lower state, and then thermodynamics doesn't have to apply. Aha, wait a minute.

And now, fortunately, here came a particular experience which contributed in the right way. I had just heard a German physicist, Wolfgang Paul, speak at a seminar at Columbia about how to get a very intense beam of molecules using quadrupole focusing magnets, that is, four rods with electrical fields on them, and sending the molecules through between them, and this could select molecules in an excited state with a high intensity. I had just heard his talk about a month earlier and now I thought, well, that's how to get a high intensity of selected molecules in the upper state. I was very familiar with ammonia, I'd been working on ammonia spectroscopy, and I knew about molecular beams because I was at Columbia where [Isidor Isaac] Rabi and [Polycarp] Kusch and others had done famous work on molecular beams. So, I quickly took out a piece of paper and put down the numbers. I knew enough of the numbers and yes, I could make a cavity, I knew what the Q of the cavity resonance would be, and how long the radiation would be sustained by the cavity, and I put down the numbers, and I said, hey, looks like it will work!

I went on to the committee meeting, and we concluded that we had not been able to find any good ideas to go to shorter wavelengths. And so we disbanded the committee. Of course, I had just had what seemed like a new idea, but it was brand new, and I wasn't yet sure of it – I thought that I should think about it some more and did not try to mention it to the Committee.

So, I went back to Columbia. I got my best graduate student Jim [James P.] Gordon to work on it as a thesis. I told him, if we can't make it work, you can still do some nice research, and get a thesis. So he worked on it for about two years, along with a post-doc, Herbert Zeiger. Jim Gordon and Herbert Zeiger both worked on it, and they were very good scientists.

Now, Professor L. H. [Llewellyn Hilleth] Thomas was in the department – he was a good theorist, known for the Thomas effect in electron precession

– he would run into me in the hallway and say, “Charlie, that’s not going to work.” I said, “Why?” But I couldn’t get him to tell me – all he would say was, “I don’t understand how it’s going to work.” So, I went back to my notebooks and I checked over everything. Sure, I took him seriously, but as far as I could see, it was going to work.

Well, we’d been working on this for two years and we hadn’t made a maser yet; we had to get a cavity with a high enough resonance, and do just the right things, getting enough excited molecules. At that time, the chairman of the department was Professor Kusch, who had a Nobel Prize, and Professor Rabi was the previous chairman, he had a Nobel Prize – I’m sure you know who he is, a famous physicist, and Kusch is an excellent physicist. They came into my office, the chairman and the previous chairman, and they said, “Charlie, you’ve got to stop. That’s not going to work. We know it’s not going to work, you know it’s not going to work, you’re wasting the department’s money. You’ve got to stop.”

Now, that’s not so uncommon, for other physicists to disagree with you, but fortunately, I was a Professor then, and American universities have a general rule that if you’re a Professor, you can’t be fired unless you do something morally wrong. That’s what’s called *tenure*. Well, I knew I couldn’t be fired, and I said, “No, I’m going to continue, I think it has a reasonable chance of working.” So they marched out of my office, because they thought I was wasting money. Well, about two months later, Jim Gordon dashed into my classroom and said, “It’s working! It’s working!” So all of us, the whole class, went up to the laboratory to see the maser working, and sure enough, it was oscillating, and that was just great.

Now, Kusch and Rabi weren’t against me, they just didn’t agree with me, and Kusch later said, “Well, I guess I should always recognize that you probably know more about what you’re doing than I do.” And so it was just a real, genuine difference of opinion.

Now I might mention also that Aage Bohr was at Columbia as a post-doc, and I knew Aage well. I was visiting Aage Bohr, and I had a chance to talk with his father Niels Bohr. He and I were walking along the street, and he asked me what I was doing, and I told him, well, we had this maser, which was producing very pure frequencies from molecules. And Niels Bohr looked at me and said, “Oh no, it can’t do that. You must misunderstand something. It can’t do that. Oh, no.” I said, “Well, yes it is,” and I explained. “Well, no, no, that’s not possible.” And finally he said, “Well, maybe you’re right,” but I’m not sure he really understood.

Around the same time, I was at a cocktail party at Princeton University with John von Neumann, whom you probably know, a very famous scientist. John von Neumann and I were talking, and he said, “What are you doing,” and I said, “Well, we’ve got this maser, with very pure frequency.” Von Neumann says, “Oh, no, no, no, that’s just not possible, you’ve got something wrong. Something wrong there, you don’t understand. No, it’s not



possible.” I said, “Yes, it is, and we’re doing it.” “Oh, no, no.” So, he went off to get another cocktail, and in about fifteen minutes he came back, and said, “You’re right! You’re right! Have you tried, could you do this with a semiconductor?” I said, “Well, yes, you might do it with a semiconductor, I’d like to do that, but I don’t know any good semiconductor to try.”

Later, after von Neumann died, I saw his memoirs, and he had written a long series of discussions about putting a semiconductor near an atomic pile, producing neutrons which would excite the electrons in the semiconductor. He hoped to get very intense light out of the excited electrons, and he talked about stimulated emission. Apparently, he had sent this proposal to Edward Teller saying, “Don’t you think we should try this?” Edward Teller never bothered to answer. And so von Neumann dropped it. But he did not mention a resonant cavity for feedback, and he didn’t mention coherence. He was just getting an intense light.

One of the problems that all these scientists had at the time was understanding how one can get a very sharp frequency, a very narrow frequency. You see, in using a beam of excited molecules the molecules pass through a cavity, but they’re only in the cavity for a short time. With a short time duration, you can’t define frequency very precisely. Scientists just weren’t accustomed to feedback. However, if you ask an electrical engineer about feedback in a cavity, he would say, of course, any time you can get feedback, you’ll get a very pure frequency. The molecules pass through the cavity in a short time, so frequency can’t be defined in that way, but people didn’t consider the fact that the cavity maintains the frequency and phase as many molecules continue to pass through. So, you see, we all get fixed in our ideas, because we spend our time looking in a particular direction, and because of this we can overlook a lot of other important things.

Now, shortly after the first maser was working, I went to a conference on spectroscopy in Cambridge, England and I gave a talk. I told them I might talk about this new maser we had, but they wanted a talk about spectral measurements, and so I gave them that kind of a talk instead.

Basov and Prokhorov came over, and it was not common in those days to be able to meet with Russian scientists. They came over, to this Cambridge meeting. And they didn’t announce what they were going to talk about. But what did they talk about? They talked about a possible maser. They were using a beam of excited molecules – ammonia molecules, also – passing through a cavity. They hadn’t made a maser work yet, but they had the ideas, and we walked along the streets of Cambridge and talking, and oh, it was a great pleasure for me to talk with them. Now, I told them about the maser that we had working, and that we used quadrupole focusing, so then they went back and used quadrupole focusing and made it work. But in addition to that, they improved it by using an octupole system. Now I hadn’t thought about that, but the octupoles – eight poles – are still better. So, we had an exchange of ideas, and they made a further improvement.

Well, the maser became very exciting to everybody. Before that, many people had come and visited my laboratory. I told them what we were doing, and they were polite, but nobody was really interested. Nobody except Basov and Prokhorov. Nobody thought it was worthwhile – well, OK, well, that’s an idea, but why would you do it? But once the maser was going, then everybody was excited. There was a lot of competition, a lot of people wanted to work on it.

Now, I went on sabbatical shortly after that. I went to Paris, and there I ran into a former student of mine, who was at the École Normale Supérieure, Arnold Honig. He had been working with a French person, [Jean] Combrisson, and they had studied electron spins in a solid. The electron spin could be pointed up in a magnetic field and it stayed there for a many seconds before it would decay. I said, that’s what we want for a tunable maser – if we vary the magnetic field, it changes the energy levels, and if we can get electron spins that will stay up there a long time, we can make a tunable maser. Now, can we really do this? I was there for about three months and we almost made one work, we got a little bit of amplification, but not much, using electron spins.

Now, back at Cambridge, Massachusetts, Woody Strandberg had thought about using electron spins for a maser. He hadn’t made them work, but he gave a talk about it. And in the back of the room was Nico [Nicolaas] Bloembergen from Harvard, who heard him talking about using electron spins to make masers, and Nico asked, “Why would you want to do that?” And Woody said, “Oh, it will make the most sensitive amplifier we’ve ever had.” “Oh,” said Nico, “Aha!” Now, Nico had been working on electron spins in crystals, with three energy levels not equally spaced. I wasn’t accustomed to that, I hadn’t worked with electron spins much. With a three level system, you can excite the electrons from the bottom energy state to the top state, and then they can fall back to the middle state, and that allows amplification. So the idea of the three level maser, that came from Bloembergen. This shows once again how ideas can get traded back and forth.

After three months in Paris I went to Tokyo, and there I ran into a former post-doc, [K.] Shimoda, who had worked with me as a post-doc at Columbia University, and we talked some about masers. But perhaps most importantly, on the street I met a biologist that I knew, an American biologist, who was on leave then, and I said, “What are you doing?” He said, “Oh, I’m reading a very interesting paper written by an English chemist on the fluctuations in microbial numbers.” A microbe can die or it can divide and make two microbes, and this man had worked out the equations describing the statistics of how the microbe colony grows when some are dying, and some are splitting and multiplying. I said, “Hey, wait a minute, that’s just what we need, to understand the noise fluctuations in a maser.”

We only had to add one more term – spontaneous emission – to the equation. Well, we did that, and then I had a hard time solving the equation, but a mathematician, Dr. [G.] Takahashi solved it. So Takahashi, Shimoda and I then wrote a paper on the maser amplifier, what the noise had to be, the theory of the noise fluctuations, and so on. Again, just trading ideas back and forth.

Well, now, the maser became very very popular, there were lots of people working on it. It was so popular, and so many papers were submitted to Physical Review Letters that the editor of that journal said, I'm not going to take any more papers on masers, we've got too many, we've got to have some space for other things. And so the Physical Review Letters has no papers on masers.

In addition, many people said, "Oh, yeah, that's a good idea, I had that idea, I thought about it, my professor mentioned something like that, oh, yes." Well, very little was written down, but in fact a number of other people had kind of thought about it. But they didn't think of using it, and making it really work.

This reminds me, that I recently saw an article by Arthur Clarke who talked about how changes occur. Arthur Clarke said, "People go through four states before any revolutionary development. First they say, 'It's nonsense, don't waste my time.' Secondly, 'Well, it's interesting, but not important.' Third, 'I always said, this is a very good idea.' Fourth, 'I thought of it first.'" Well, that's not too far wrong, and something we must think about.

Well, at that time, my primary purpose was to try to get to shorter wavelengths. I built the maser first in the microwave region, because I wanted to try the idea, and that was the easiest way to make it work. But I wanted to get into the far infrared. The maser had first operated in 1954 – and so, by the way, this is the fiftieth anniversary of the maser, as well as the fortieth anniversary of the Nobel Prize. Well, three years later, in 1957, I just wanted to get to shorter wavelengths. I said, well, I haven't had any good ideas, I'm just going to sit down and work out what I think is the best way of trying do it. And I wrote down the equations about what was needed, and I said, it looks like it would be very practical to get right on down to optical wavelengths.

I talked with one or two of my students about it. Also, I was consulting at that time with Bell Laboratories, and I had a very good, very happy consulting job. Bell Labs said, just come here one day every two weeks and talk with people here, you know, talk with them about what they're doing. We just want you to interact. That was a good idea from Bell Labs' point of view, I guess, and it was a happy idea for me. So my brother-in-law Arthur Schawlow was there at the time and I went around and talked with him, of course – I got paid for talking with my brother-in-law about science – wow! And I told him about this optical maser idea that I'd had. He said, well, you

know, I think it's a good idea too, and I said, why don't we work on this together. So now Arthur Schawlow came up with the idea of having two mirrors as a resonator for optical waves. I had been using a resonator, but it was a big microwave cavity with some holes in it. I couldn't build an optical oscillator right away, because lots of people would know I was making it, and I would have lots of competition. So we decided that we probably ought to write a theoretical paper first, just showing that this might be done. But we shouldn't write the paper until the patent was filed.

So, as it turned out, we'd have to wait nine months, keeping it somewhat secret. We wrote the paper, but we showed it only to Bell Labs people until the patent was filed, about nine months later. Now again, it's interesting, you see, the preconceived ideas that people have – no one wrote anything during that nine months about the possibility of making shorter waves. They were interested in masers, they were working on masers, but no one thought short waves were possible. Most physicists said, oh, well, you can't do short waves with this, it's a nice idea, but you can't get short waves. I had thought it was pretty hard, too, until I wrote down the equations and recognized it would not be difficult to get down to the short wavelengths of optical light.

And so during that nine months, nothing was written, excepting by one student, Gordon Gould, whom I had talked with. In fact, I talked with him about a month after I had written down the possibilities, and he then wrote some things in his own notebook – he didn't publish it, but just wrote some things in his notebook. That was the only written thing about it, until we published the paper. Now, once the paper was released, it began to be distributed, and by then, everybody got interested and they were all trying to build a laser. I was trying to build a laser, but I had to work in Washington at that time, so I didn't have lots of time. My students were trying. With what time I had I tried with them, but it wasn't much.

At this time, the Navy asked me, would I organize a meeting so we can discuss this field, and what might be its potential. And they could pay for it. So I consulted a lot of different people, in different associated fields, and we talked about whom to invite. We also talked over what to call this new field, and that's how we invented the name *quantum electronics*.

We had this meeting in 1959. Basov and Prokhorov were invited, of course, and they came over. We were just delighted, this was the first time they had come over – getting Russians to come to America was very rare at that time. So they came over. I had a chance to have them in my home, and they were able to visit my laboratory. They talked about their ideas, and what they were doing. A number of people talked about making an optical system, but it hadn't yet been done.

But the next year, in 1960, Ted Maiman built the first laser, the ruby laser. He did that work at Hughes, and I'll ask you to note, now, as we moved from the ideas to its being a hot field with everybody interested, that

it was in Industry that got it done. Ted Maiman was in industry at Hughes. He had been a student of Willis Lamb doing radio spectroscopy. Hughes had hired him, and he built the first laser.

The second kind of laser was built by one of my former students, Mirek Stevenson, and one of Bloembergen's former students, [Peter] Sorokin, at General Electric. The third kind of laser was built at Bell Laboratories by one of my students in microwave spectroscopy, Ali Javan. He worked with Bill Bennett [William R. Bennett, Jr.], one of Kusch's students, who had been working in microwave spectroscopy at Columbia. This new laser was the helium-neon gas laser, built by Javan, Bennett and [Donald R.] Herriott, who was an optical guy. The next type was a semiconductor laser, which was built at General Electric by [Robert N.] Hall.

So all the new lasers were coming from industry. They had originated from basic research in universities, but once industry got really interested, they could work faster and harder than we could in the universities. So once industry got interested, they were the ones who were the most productive and generated all the first lasers. My own students didn't work fast enough, I guess. But as soon as Ted Maiman's laser came out, I said to my students, let's now use it, let's not worry about building new kinds of lasers, but let's use them to do new kinds of physics. So the students began to do a lot of new kinds of physics, including nonlinear optics, another new physics field, one field that I haven't mentioned before.

Nonlinear optics. Well, again, why wasn't this already discovered? Well, you see, we have particular paths of thought which are very important to us, but they can keep us from considering other paths. In addition, engineering and science had to come together so that ideas such as frequency multiplication and mixing seemed natural.

Now in addition to this research, I went out to the University of California a little later, wanting to do astrophysics. I thought that there might be molecules in interstellar space, but the very famous theoretical astrophysicist George Field told me, absolutely not, there won't be molecules. Molecules will get torn apart by the ultraviolet light, I can prove that, he said, You can't have any complex molecules there. And I said, well, no, I think there are some dark areas where people don't see anything except dust, and there might be something there. No, oh no, that's crazy, you're wasting your time.

However, one of the electrical engineers at the University of California, Jack Welch, was willing to work with me, and I could use his radio antenna. So I had a student, Albert Cheung, take a look, and he looked at these dark clouds in space, and sure enough, there was ammonia. Well, since we found ammonia, we thought, we ought to look for water too, just to try this out. So the student looked, and there was water radiation. In fact it was very intense – hey, it had to be a maser, maser amplification in interstellar space! And OH had already seemed to indicate something similar.

Now today, we have found about a hundred different masers in space and some lasers. The difference between a maser and a laser is of course only in the wavelength. But there are some astronomical systems where infrared is getting amplified. Now as has been pointed out, amplification in interstellar space doesn't involve resonances, but it does involve stimulated emission. You know, somebody could have seen these interstellar masers in the radio regions of the spectrum many years ago. Anybody who used the radio technology of 1936, and looked up into the sky, could have detected this water frequency. They didn't bother to look, but it was there all the time. So now we know, lasers have been there for billions of years. Masers have been there billions of years. So that's another way we might have discovered them, but we didn't. Now I emphasize this to indicate that we need to search, we mustn't be too confined by what we think is going to work, we've got to explore.

I'm going to conclude now with just a few summary observations.

Scientific work should not be supported simply for the technological contributions which can be envisioned, but rather as exploration which has the possibility of making completely unexpected contributions. We don't know what applied fields might be developed from a given research project. Here again, if you consider microwave spectroscopy of molecules, why would that have produced intense light? That was quite unpredictable, and that's not atypical for basic science. If you explore new ideas, you get new thoughts and new results, and out of those come applications.

Now, second, interdisciplinary interaction can be very fruitful in generating innovative ideas and discoveries. I might say interdisciplinary interaction also reminds me of Erice, this very important place where you bring people together, and I think we have to be very thankful for what Professor Martellucci is doing in running this place, in organizing it, in bringing people together in different fields, getting scientists from many different countries together. You can see from my illustrations how important that is, in fact.

Third, we must be open to viewpoints, ideas and experiments which do not fit accepted scientific thinking and trends. Perhaps, we even need to encourage challenges to standard paradigms. In particular, I think that we've got to be very careful about overusing committees, which we frequently do. We appoint a committee of important scientists to decide whether certain kinds of science should be pursued, or certain kinds of experiments should be supported. We have these committees, generally composed of senior scientists, and they're very knowledgeable, excellent people, but maybe somewhat fixed in their ideas. We have to listen to them, but I think we've got to be careful not to let senior people completely control the plans for research – we've got to try new and different things.

Finally, there are discussions and interactions between scientists, within the community of scientists, and of applied scientists. These interactions are

very critical in the development of a new field, and of course that's what allowed lasers to grow so rapidly. The development of any new field needs a community – a community of scientists, talking, interacting, each adding their own ideas to it. It's this exciting and productive interaction that we can be thankful for today.

Thank you.

## Chapter 2

# FIBER OPTIC CHEMICAL SENSORS AND BIOSENSORS: A VIEW BACK

Otto S. Wolfbeis and Bernhard M. Weidgans  
*University of Regensburg*  
*Institute of Analytical Chemistry, Chemo- & Biosensors,*  
*D-93040 Regensburg, Germany*

### 1. INTRODUCTION

The past 30 years have seen enormous progress in opto-electronics, information technology and biotechnology, and fiber optic chemical sensors (FOCS) as well as fiber optic biosensors (FOBS) are one of the outcomes. Chemical sensors have been defined as follows<sup>1</sup>: *Chemical sensors are miniaturized analytical devices that can deliver real-time and on-line information on the presence of specific compounds or ions in complex samples.* In the easiest and simplest case, a sensor probe is inserted into the sample of interest to obtain an analytical signal that can be converted into a concentration unit. Chemical sensors ideally act fully reversibly, as do physical sensors for temperature, pressure, and the like. This has been achieved in few cases of FOCS only, and hardly in FOBS (except for some enzyme-based systems). However, despite the fact that most biosensors respond irreversibly or need to be regenerated, clinicians often refer to such single-shot detection elements as biosensors, provided a "reagent" or a "biology" is immobilized on a solid support. True sensors are expected to be small and to work even in complex samples, ideally without sample treatment.

Both FOCS and FOBS rely on optical fiber waveguides which have become available in adequate quality in the late 1970s. In fact, they are so good now that sensing without intermittent amplification has become possible over distances as large as 10 km. Clearly, this was only possible once the respective laser sources have become available.



## 2. THE EARLY HISTORY (UP TO ~1980)

Most probably, the first – but non-fiberoptic – sensors for continuous use where those for pH and for oxygen. It has been known for decades that cellulosic paper can be soaked with pH indicator dyes to give pH indicator strips which, however, leached and thus were of the "single-use" type. The respective research and development is not easily traced back since it is not well documented in the public literature. However, in the 1970s, indicator strips became available where they pH indicator dye was covalently linked to the cellulose matrix, usually via vinylsulfonyl groups. These "non-bleeding" test strips allowed a distinctly improved and continuous pH measurement, initially by visual inspection. In the late 1980's instruments were made available that enabled the color (more precisely the reflectance) of such sensor strips to be quantified and related to pH. Respective instruments are based on the use of LEDs and are small enough to be useful for field tests in that they can be even hand-held. This simple and low cost detection system is still superior to many of the complicated, if not expensive optical pH sensors that have been described in the past 20 years.

In 1975, the immobilization of pH indicator dyes on glass was reported by Harper<sup>2</sup>. Azo dyes were linked to the surface of silicate glass (said to be more stable than cellulosic supports) that was rendered reactive by treatment with the reagent aminopropyl-triethoxysilane. In the early 1980s, Hirschfeld started to use pH-sensitive dyes to monitor pH via fiber optics<sup>3-5</sup>. His early work is difficult to trace back since it is partially hidden in hardly accessible conference proceedings. Fiber optic light guides also were used in order to monitor (by either absorbance or fluorescence) the concentration of chemical species such as uranium ion which in phosphoric acid solution displays intense fluorescence if excited by the 488-nm line of the argon laser. The method was mainly applied to nuclear power stations and research stations, and to monitor groundwater contaminants<sup>4-8</sup>.

Other very early work includes that of Boisdè at the CEA<sup>9, 10</sup>. A scheme of the experimental set-up used by his group is given in Fig. 1. The fiber optic pH sensor described by Peterson et al.<sup>11</sup> in 1980 was another milestone. A 2-volume book that appeared in 1991 gives an account of the early work on fiber optic chemical sensors and biosensors<sup>12</sup> up to about 1989. Earlier reviews include those of Kirkbright et al.<sup>13</sup>, Borman<sup>14</sup>, and Hirschfeld et al.<sup>15</sup>.

Optical sensing of oxygen started with the work of Kautsky and Hirsch in the 1930's. They reported<sup>16</sup> that the easily visible room-temperature phosphorescence of certain dyes adsorbed on silica gel supports is strong only in the complete absence of oxygen. Traces of oxygen were found to quench the phosphorescence of such dyes. Specifically, silica beads were soaked with a solution of a dye such as tryptaflavine or fluorescein, dried, and placed in a flow-through cell schematically shown in Fig. 2. The room temperature phosphorescence was monitored using a fluorometer. It was

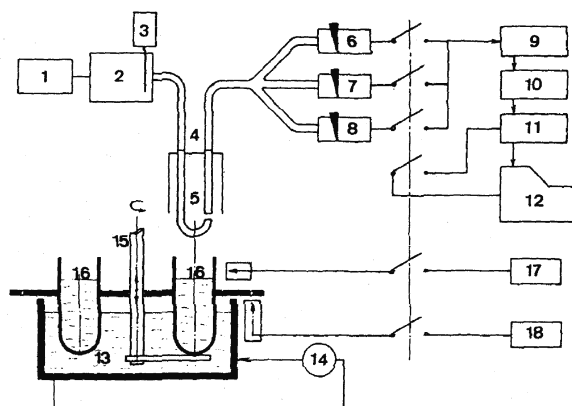


Figure 1. Fiber optic system comprising a light source (1), optical filters (2, 3) for measurement of the concentration of a reagent solution. The fiber bundle (4), after passing the solution (16), is divided into three bundles (6-8) and light intensity is measured at three wavelengths in order to enable spectral correlation at different wavelengths.

found that even ppm quantities of oxygen gas (equivalent to a  $pO_2$  of  $0.5 \cdot 10^{-3}$  torr) were capable of quenching phosphorescence. The effect is fully reversible within 1 – 2 s. The device assisted in the discovery of the Kautsky effect, i. e. the delay in the production of oxygen following illumination of a leaf.

In 1974, Hesse<sup>17</sup> described a fiber optic chemical sensor for oxygen and this appears to have been the first FOCS at all. An oxygen-sensitive chemistry was placed in front of a fiber optic light guide through which exciting light was guided. The fluorescence emitted is guided back through either the same fiber, or through the other fibers of a bundle. The system is based on measurement of either fluorescence intensity or fluorescence decay time, both of which are affected by oxygen. A schematic of the design is shown in Fig. 3.

We believe that the paper on optical affinity sensors for individual metabolites by Schultz & Sims<sup>18</sup> was a milestone paper in optical waveguide

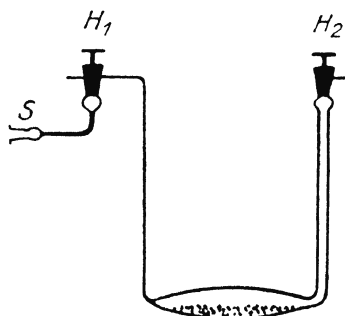


Figure 2. Configuration of Kautsky's flow cell. S, gas sample, containing traces of oxygen;  $H_1$  and  $H_2$ , valves; the sensor material is contained in the cavity on the bottom.

biosensing in that the fundamental principles of affinity sensors were outlined for the first time and in that optical affinity sensing was recognized as a viable alternative to radioisotope techniques. The determination of glucose via concanavalin served as an example.

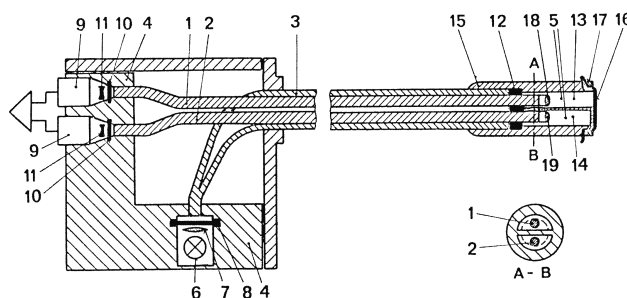


Figure 3. First fiber optic chemical sensor (from ref. [17]; used for sensing oxygen). Also shown is a cross-section of the fiber bundle used. 6: light source; 9: photodetectors; 16: chemically sensitive layer.

### 3. DIRECT (PLAIN) FIBER SENSORS

In these sensors, the intrinsic absorption of the analyte is measured directly. No indicator chemistry is involved. Thus, it is more a kind of remote spectroscopy, except that "the instrument comes to the sample" (rather than the sample to the instrument or cuvette). Numerous geometries have been designed for plain fiber chemical sensors, all kinds of spectroscopies (from IR to mid-IR and visible to the UV; from Raman to light scatter, and from fluorescence and phosphorescence intensity to the respective decay times) have been exploited, and more sophisticated methods including evanescent wave spectroscopy and surface plasmon resonance have been applied.

In the late 1980s, as sensing method known as distributed sensing became known<sup>19, 20</sup>. This enabled chemical analyses to be performed along the distance of an optical fiber and has meanwhile been applied to monitor the quality of river water along a fiber cable and to detect gas and oil leakage along oil and gas pipelines, to mention only two examples.

#### 3.1 Direct Sensors Based on Absorption or Fluorescence

Fiber optics have been used mainly to remotely sense chemical species via their intrinsic absorption or fluorescence. Methane and other hydrocarbons were a target analyte from the beginning. They can be detected by infrared spectroscopy in the gas phase, as impressively shown by the

group of Inaba, for the first time<sup>21</sup> in 1983 using low-loss optical fibers and a light-emitting diode operated at 1.33- $\mu\text{m}$ . Low-level methane was monitored over 2 km using a low-loss silica fiber link and a compact absorption cell ( a so-called White cell). The detection limit was 2000 ppm, which is 4 % of the lower explosion limit of methane, thereby demonstrating that fully remote sensing is possible and can be used for the surveillance of flammable and explosive gases in industrial and mining complexes as well as in residential areas. In subsequent work, differential absorption spectroscopy was applied<sup>22</sup>. This 2-wavelength approach enables direct detection of differential absorption signals of specific overtone bands of methane.

Later on, a 10-km long fiber cable was described that permits remote sensing of methane gas by near infrared absorption<sup>23</sup>. An ultralow-loss silica optical fiber and a compact absorption cell in conjunction with highly radiant light emitting diodes in the near IR region. The bands at around 1.33 and 1.66  $\mu\text{m}$  were analyzed. Finally, an all-optical remote gas sensor system was reported for methane and propane that works over a 20-km range<sup>24</sup>.

In context with methane detection during offshore oil drilling, another infrared fiber optic methane sensor was reported<sup>25</sup>. The detector comprises 3 main units: a microcomputer-based signal processing and control unit, a non-conducting fiber optic gas sensor, and an optical fiber cable module. The system operates at an absorption line of methane where silica fibers have very low losses.

Unlike methane and the other alkanes, aromatic hydrocarbons have absorptions in the UV part of the spectrum, and thus may be detected through UV spectrometry using silica fibers. This scheme is useful for "aromatic" water pollutants such as toluenes and xylenes with their absorption bands between 250 and 300 nm. Similarly, nitrate anion can be monitored (albeit with low sensitivity) in water via its UV absorption at 250 nm.

In principle, any chemical species that absorbs UV-Vis light can be "sensed" by fiber optic ("remote") absorption spectrometry which is interfered by any other species that absorbs at the same wavelength. A fiber optic absorption cell was described for remote determination of the blue copper ion in industrial electroplating baths<sup>26</sup>. The sensor consist of an absorption cell which resides in the plating bath, and utilizes fiber optics to direct light into and out of the cell. The sensor can be placed in strong sulfuric acid for weeks to years. The light source and detection electronics can be maintained in a controlled environment and can be multiplexed to several sensors of similar design, if desired. The sensor operates by measuring the blue-green absorbance of  $\text{Cu}^{2+}$  ion with a near-IR light-emitting diode (820 nm) as the light source. The device is capable of measuring copper(II) ion concentrations from 50 mM to 500 mM with relative standard deviations of less than 1%.

The feasibility of an optical fiber system was demonstrated for the differential absorption analysis of the car pollutant nitrogen dioxide. It absorbs in the visible and can be "sensed" using an Ar-ion laser<sup>27</sup>. The yellow metabolite bilirubin has been monitored in blood via fiber optic spectrometry in serum<sup>28</sup>. The tip of a fiber optic cable was inserted into a injection needle so to reach the blood sample, and absorbance (and later fluorescence) was acquired of a sample contained in the cavity at the tip of the fiber or needle.

Another milestone paper was the one by Newby et al. on remote spectroscopic sensing of chemical adsorption via evanescent wave spectroscopy using a single multimode optical fiber<sup>29</sup>. Decad single fibers were developed for collecting evanescently excited fluorescent signals from solutions. It was shown that the sensor is particularly useful for studying species adsorbed onto the sensor surface, for example dye-labeled proteins. Also, Raman data from benzene were collected to indicate its sensitivity in the bulk mode.

### **3.2 Early Refractometric Sensors**

Refractometry is as unspecific as is absorption spectrometry, but has its merits if applied under well-characterized conditions. In 1984, Haubenreisser et al.<sup>30</sup> reported on (a) the relation between transmission and refractive index characteristics, (b) the sensitivity, and (c) the working range of a fiber optic refractometer of mixtures of fluids. The U-shaped fiber refractometer was shown to be useful for various physical quantities that vary with refractive index.

Another early fiber optic refractive "sensor" was the one for measurement of temperature and salinity variations of sea water<sup>31</sup>. The sensing region consisted of a partly uncovered light guide. It detects salinity variations in water of known temperature, and temperature variations in water of known salinity with an accuracy of +/- 2 g/L and 1 °C, respectively, at NaCl concentrations of 300 g/L.

Resonant photoacoustic gas spectrometry was adapted to fiber optic sensor technology<sup>32</sup> as early as in 1984. A Mach-Zehnder arrangement was combined with a resonant photoacoustic cell for gap analysis. The pollutant gas NO<sub>2</sub> was detectable in a concentration of 0.5 ppm. In a smart optical fiber hydrogen sensor, the fiber is coated with palladium metal which expands on exposure to hydrogen. This changes the effective optical path length of the fiber, which is detected by interferometry<sup>33</sup>.

## 4. INDIRECT FIBER OPTIC CHEMICAL SENSORS

This section covers early indirect fiber optic chemical sensors (FOCS) for species that cannot be sensed directly but require the use of indicators, probes, labeled biomolecules, or color-forming reactions.

### 4.1 Sensors for (Dissolved) Gases, Vapors and Humidity

#### 4.1.1 Sensors for Oxygen

A sterilizable oxygen sensor for use in bioreactors and using a rod-like fiber waveguide<sup>34</sup> was reported in 1983. Microsensors (with diameters of 0.2-1.0 mm) for oxygen, pH and CO<sub>2</sub> were described first<sup>35, 36</sup> in 1984. True microsensors, with diameters of <50 μm were first reported<sup>37, 38</sup> in 1995 and enabled sub-millimeter resolution studies in marine microbiology. Optical fiber oxygen sensors are commercially available now and have found widespread application in biological and marine research. A fiber optic moisture sensor reported in 1985 relies on the long-known color change of cobalt chloride (from pink to blue) if exposed to a humid atmosphere<sup>39</sup>. The salt (in gelatin) was cast on the surface of 600-μm optical fibers. The absorption at 680 nm is measured through the fiber by internal reflection spectroscopy to detect the relative humidity of air between 40 % and 80 %.

Oxygen sensing has very much attracted researchers. The method of Kautsky and Hirsch was modified (in non-fiber-optic systems) by Pringsheim et al.<sup>40</sup> and Zakharov et al.<sup>41</sup>. Complete optical sensor systems and devices were reported by Bergman<sup>42</sup> and Stevens<sup>43</sup>. Hendricks<sup>44</sup> described a method for detection of oxygen by contacting a film comprising poly(ethylene naphthalenedicarboxylate) with oxygen and exposing this film to ultraviolet light. On subsequent heating, the presence of oxygen is indicated by thermoluminescence.

In 1975 and 1976 Lübbers & Opitz described instruments capable of online monitoring of oxygen and carbon dioxide, respectively<sup>45-47</sup>. Oxygen may also be monitored via the chemiluminescence produced by oxygen on reaction with an amino-ethylene<sup>48</sup>. Marsoner<sup>49</sup> dissolved pyrenebutyric acid in poly(vinyl chloride) containing a plasticizer. In 1984, Wolfbeis covalently immobilized pyrene-butyrac acid on porous glass to obtain a breath gas sensor<sup>50</sup>. In order to eliminate ambient light, the sensor layer was covered with a solution of particles of ferric oxide in silicone. This layer was referred to as an optical isolation that also can prevent interferences by the intrinsic fluorescence of fluid samples. Cox and Dunn in 1985 used a fluorophore-polymer composite matrix consisting of poly(dimethylsiloxane) coupled to 9,10-diphenyl anthracene and deposited on an optical fiber<sup>51</sup>.

Peterson et al.<sup>52</sup> were the first to demonstrate sensing of oxygen *in-vivo*. The FOCS for measuring pO<sub>2</sub> consisted of two 250-μm strands of plastic

optical fiber ending in a section of porous polymer tubing (3 mm long and 0.6 mm in diameter). The tubing was packed with dye on an adsorptive support. The general construction is similar to the pH probe reported earlier<sup>11</sup>. The development required the solution of 3 problems not encountered before in application of this principle: (1) a dye was needed with the combined properties of suitable sensitivity to oxygen, excitation by visible light, and resistance to fading; perylene dibutyrate (solvent green 5, CI 59075) was selected; (2) a hydrophobic, oxygen-permeable polypropylene envelope was necessary; and (3) an adsorptive support (Amberlite XAD 4) was required which activated the dye without sensitivity to humidity. This design provided a small-size, low-cost probe suitable for tissue and blood vessel implantation.

In 1988, the first dual sensor material was described. It responds to both, oxygen and carbon dioxide by giving two spectrally independent signals<sup>53</sup>. Two materials were placed into one sensor layer. The first consisted of an oxygen-sensitive fluorescent probes (a ruthenium dye) that gives a red fluorescence with a peak at 620 nm. The second consists of a material sensitive to CO<sub>2</sub> (the dye HPTS in bicarbonate buffer and this solution soaked into a polyacrylamide layer) that gives a green fluorescence peaking at 520 nm. This, 2 signals are obtained from one sensor. Fluorescence energy transfer is not observed because the dyes are spatially separated.

The utility of phosphorescent ruthenium ligand complexes for use in optical oxygen sensing was recognized<sup>54</sup> in 1986. Ruthenium tris(bipyridyl) was adsorbed onto silica gel and placed in a silicone membrane. The material can be excited with a blue LED and displays a red emission that is strongly quenched by oxygen. Better quenchable ruthenium dyes were reported by Demas<sup>55</sup> and coworkers in 1987. Since the ruthenium polypyridyl complexes have decay times in the order of a few microseconds, they are ideally suited for sensing based on measurement of decay time. The first article on luminescence decay time-based sensors<sup>56</sup> using appeared in 1988.

Following the discovery that the fluorescence of metalloporphyrins is strongly quenched by oxygen<sup>57</sup>, optical sensor membranes were developed that are suitable for phosphorescent sensing of oxygen<sup>58</sup>. Table 1 summarizes fundamental articles on optical sensors for oxygen until the year 2000.

#### **4.1.2 Sensors for Carbon Dioxide**

Carbon dioxide is another clinically important analyte, but also of highest interest in marine sciences and in context with the greenhouse effect. While “sensible”, in principle, by IR absorptiometry, this is difficult in case of fluid samples. An indicator-based fiber optic device for CO<sub>2</sub> was described

Table 1. Fundamental Contributions to Optical Oxygen Sensor Technology up to the Year 2000 (only main author/s given).

<i>Author</i>	<i>Year</i>	<i>Remarks</i>
Kautsky	1931	first oxygen sensor (non-fiber optic); based on dynamic quenching of the phosphorescence of adsorbed dyes
Hesse	1974	first fiber optic sensor; also measures decay time
Lübbbers / Opitz	1975	quenching of pyrenebutyric acid in teflon-covered solution; applied to blood gas sensing
Lübbbers / Opitz	1981	glucose biosensor (via GOx)
Kroneis / Marsoner	1983	sterilizable fiber optic oxygen probe for bioreactors (1 cm i.d.)
Wolfbeis	1984	glass-immobilized oxygen probes (breath gas sensor)
Peterson / Goldstein	1984	fiber optic oxygen in vivo sensor (1 mm i.d.)
Wolfbeis / Leiner	1986	ruthenium dyes in fiber optic oxygen sensors
Demas / Bacon	1987	ruthenium dyes in oxygen sensors
Lippitsch / Wolfbeis	1987	decay time based sensor (Ru)
Wolfbeis	1988	first dual sensor using one matrix (oxygen and CO <sub>2</sub> )
Okazaki	1988	frequency doubled diode laser (390 nm) used to excite the oxygen probe benzoperylene
Trettnak / Wolfbeis	1988	dual glucose sensor with compensation for oxygen supply
Nyberg	1988	metal oxide sensor layer whose reflectivity reversibly changes with pO <sub>2</sub>
Butler	1989	oxygen sensing via reflectivity of nickel film
Moreno-Bondi	1990	fiber optic glucose biosensor (via oxygen)
MacCraith	1992	evanescent wave sensing using sol-gel
Baldini / Scheggi	1992	absorption-based fiber sensor (cobalt dye)
Charlesworth	1993	oxygen via RTP phosphorescence of camphorquinone
Sanz-Medel / Diaz-Garcia	1994	oxygen via RTP phosphorescence quenching of ferrone chelates
Preininger/Wolfbeis	1994	bacterial sensor (for BOD)
Klimant	1995	microsensors (20 μm tips)

by Vurek et al.<sup>59</sup> in 1982. The sensing scheme is derived from previously developed pH schemes and functions like the Severinghouse-type CO<sub>2</sub> electrodes in that CO<sub>2</sub> diffuses into a small cavity where it changes the pH according to the chemical reaction  $\text{CO}_2 + \text{OH}^- \rightleftharpoons \text{HCO}_3^-$  by consuming the hydroxide anion. The resulting decrease in pH is indicated by a pH indicator and measured by reflectometry.

Zhang and Seitz somewhat later described a sensor for carbon dioxide that is based on measurement of fluorescence<sup>60</sup>. It was prepared by covering a pH sensor based on fluorescence with a CO<sub>2</sub>-permeable membrane and contacting the pH-sensitive membrane with a reservoir of hydrogen carbonate. As CO<sub>2</sub> diffuses across the membrane it causes a change in pH which is measured via the change in fluorescence from the base form of the



pH-sensitive fluorescent dye. The usable range of response depends on the concentration of hydrogen carbonate in contact with the membrane. The sensor also responds to sulfide and sulfite. Munkholm et al. also used a fiber optic system with covalently immobilized pH probes<sup>61</sup>.

The "plastic type" CO<sub>2</sub>-sensor is different from the above Severinghouse-type sensor in that it does not require the presence of a carbonate buffer. Kawabata et al. described the first type of such a sensor<sup>62</sup>. Raemer and coworkers, in a patent<sup>63</sup>, described a similar system, this time based on an ion pair and the addition of a lipophilic base, both contained in a plastic matrix. This scheme was later widely extended by Mills et al.<sup>64</sup>. The first "capillary" waveguide sensor<sup>65</sup> was published in 1994. Carbon dioxide was sensed by using a capillary (that also may serve as a sampling device) whose inner surface was covered with a CO<sub>2</sub>-sensitive layer. The fluorescence of the layer was excited through the capillary waveguide, and fluorescence was collected at the distal end of the capillary.

#### 4.1.3 Sensors for Other Gases

Numerous other chemistries for specific gases have been described. Butler<sup>33</sup> designed a hydrogen sensor based on the capability of palladium metal (Pd) to absorb hydrogen gas, thereby undergoing an expansion. If the Pd forms the coating of an optical fiber, the effect changes – through bending – the effective path length of the fiber, and this is detected by interferometry. Later, the Pd/WO<sub>3</sub> chemistry for hydrogen gas was applied to hydrogen sensing<sup>66</sup>. Exposure of this material (a Pd film on MoO<sub>3</sub>) to hydrogen results in the appearance of the deep blue color (possibly the Mo<sup>5+</sup> ion) that can be monitored at 780 nm via waveguide optics. The same effect is shown by MoO<sub>3</sub> sputtered onto glass supports and covered with a thin layer of Pd.

The poorly reproducible Fujiwara reaction may be used for quasi-continuous monitoring of chlorinated hydrocarbons as they can occur in drinking water<sup>67</sup>. Following Hirschfeld's reservoir sensor for uranium (using phosphoric acid reagent) this appears to have been the second reservoir type of sensor. A fiber optic fluorosensor for determination of both halothane and/or oxygen appears to have been the first dual sensor based on a single sensor matrix<sup>68</sup>. Its chemistry consists of a highly halothane-sensitive indicator layer exposed to the sample. Interferences by oxygen are taken into account by a second, poly(tetrafluoroethylene)-covered fluorescent indicator layer highly sensitive toward oxygen. Halothane concentrations can be calculated with the help of an extended Stern-Volmer relation.

Like carbon dioxide, (dissolved) ammonia can be sensed via the pH changes it induces when diffusing into a small cavity containing an internal buffer<sup>69, 70</sup>. The same is true for sulfur dioxide<sup>71</sup>. Selectivity for one of these

gases can be governed to some extent by proper choice of internal buffer. Gaseous sulfur dioxide may also be sensed via the quenching effect it exerts on certain fluorophores<sup>72</sup>.

Kopelman et al.<sup>73</sup> have prepared fiber optic sensors that are selective for nitric oxide and do not respond to most potential interferents. Both micro- and nanosensors have been prepared, and their response is fast (<1 s), reversible, and linear up to 1 mM concentrations of nitric oxide. The respective "chemistry" at the fiber tip was contacted with the sample, light was guided to the sample through the microfiber, and emitted light was collected by a microscope (without the use of fibers, however).

## 4.2 pH Sensors

As stated above, the beginning of optical pH sensor technology remains hidden. What is nowadays referred to as a sensor layer was formerly mostly referred to as a test strip, a dry reagent chemistry, or an immobilized reagent.

A general logic that is based on the immobilization chemistry of commercial reflectometric test strips was presented and extended to various pH ranges<sup>74</sup>. Such sensing "chemistries" are easily produced and can be coupled to fiber optics. This enabled sensing to be performed at formerly inaccessible sites. Peterson et al. were the first to report on a fiber optic pH sensor<sup>52</sup>. The system comprised plastic fibers, a pH chemistry at their end (composed of a cellulosic dialysis tubing filled with a mixture of polystyrene particles and polyacrylamide beads dyed with phenol red), LED light sources, and photodiodes. The system is operated at two wavelengths. Fig. 4 gives a schematic of the fiber tip.

As the potential of optical fiber probes for pH measurements was rapidly recognized, several other articles appeared within a few years<sup>75-83</sup>. Most were reflectance-based, and Seitz reported the first fluorescent pH sensors<sup>84, 78</sup>. The article by Janata<sup>85</sup> on whether pH optical sensors can really measure pH is another "must" in the early literature since it points to aspects hardly addressed in pH sensor work.

The dependence on ionic strength is an intrinsic limitation of pH sensors using indicator dyes. Opitz and Lübbers<sup>86</sup> and Offenbacher et al.<sup>87</sup> have presented solutions to this by making use of two indicators whose dependency of their  $pK_a$  on ionic strength is different, so that two independent signals are obtained from two dyes or sensors. Given the advantages of diode lasers operated at wavelengths of above 600 nm,

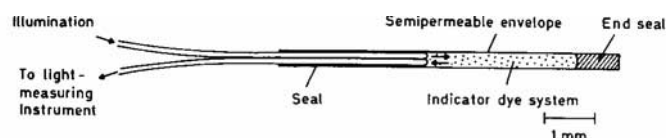


Figure 4. First fiber optic pH sensor for in vivo use.

respective pH probes were used<sup>88</sup>. Abraham et al.<sup>89</sup> applied the probe of Peterson et al. successfully to monitoring intra-arterial pH in dogs even under extremes of physiological conditions. The difference between fiber optic and electrode pH gave a maximal difference of 0.12 pH units.

Peterson's pH probe also was modified in order to give a miniature fiber optic sensor potentially suitable for glucose measurements<sup>90</sup>. Kopelman et al.<sup>91</sup> developed a fiber-optic pH nanosensor for physiological measurements using a dual-emission sensitive dye. The performance of a pH sensor was reported<sup>92</sup>. An unclad fiber was dip-coated with a thin layer of porous cladding within which a pH-sensitive dye was entrapped. The fundamental

Table 2. Fundamental Work on pH Optical Sensors until the Year 2000.

<i>Author</i>	<i>Year</i>	<i>Remarks</i>
G.B. Harper	1975	Re-usable glass-bound indicators
J.I. Peterson et al.	1980	First fiber optic pH probe
S. Goldstein et al.	1980	Miniature fiber optic pH sensor for blood
Tait et al.	1982	fiber optic in vivo pH sensor
L.A. Saari, W.R. Seitz	1982	pH sensor based on immobilized fluorescein
J.S. Suidan et al.	1983	Fiber optic pH sensor for blood monitoring
G.F. Kirkbright et al.	1984	pH indicators on ion exchange polymers (XAD)
Z. Zhujun, W.R. Seitz	1984	First fluorescent pH sensor (HPTS)
Abraham et al.	1985/6	Fiber optic in-vivo pH probe
H. Offenbacher et al.	1984	Optical sensors for pH and ionic strength
D. Walt, F. Milanovich, S. Klainer	1986	Polymer modification of a fluorescent fiber optic pH sensor
A. Scheggi, F. Baldini	1986	Comparison of absorption, reflection, and fluorescence
J.L. Gehrich et al.	1986	Intravascular blood pH monitoring system
J. Janata	1987	accuracy and precision of optical pH sensors
E. Grattan et al.	1987	2-wavelength optical fiber pH sensor
Y. Kawabata et al.	1987	Fiber optic pH sensor with monolayer indicator
B. Boisdé, J.J. Pérez	1987	Miniature pH sensor (1 mm fibers)
M. Monici et al.	1987	pH sensor for seawater monitoring
J.W. Attridge et al.	1987	pH sensing via refractive index
E.T. Knobbe et al.	1988	Immobilization of pH probes in sol-gels
H.E. Posch et al.	1989	Gastric pH sensor (pH 0 – 7)
M.E. Lippitsch et al.	1992	First time domain fluorescent pH sensor
W. Tan et al.	1992	Sub-micrometer intracellular pH sensor
Z. Ge et al.	1993	Fiber optic evanescent wave sensor using polyaniline
K.S. Bronk, D.R. Walt	1994	pH sensor array using fiber bundles
W.C. Michie et al.	1995	Distributed fiber sensors using swellable polymers
Z. Zhang et al.	1995	pH sensor based on reflectance of swelling polymer
M.N. Taib et al.	1996	pH sensor range extended via artificial neural network

work on optical pH sensors before the year 2000 is summarized in Table 2. A good review has been presented by Lin<sup>93</sup>.

### 4.3 Sensors for Cations

#### 4.3.1 Alkali and Earth Alkali Ions

It appears that Charlton et al.<sup>94, 95</sup> have discovered the first methods for reversible and continuous optical measurement of the clinically highly important alkali and earth alkali ions. In one approach<sup>94</sup> they use plasticized poly(vinyl chloride) along with valinomycin as the ion carrier, and a detection scheme that was later referred to as co-extraction. In their system, potassium ion is extracted into plasticized PVC, and the same quantity of the anionic red dye erythrosine is co-extracted into it. The extracted erythrosine is quantified via absorbance or reflectance.

Charlton also discovered the ion exchange principle<sup>95</sup>. Again they used a plasticized PVC film containing valinomycin and - in addition - a deprotonable dye (MEDPIN; a lipophilic 2,6-dichlorophenol-indophenol). On extraction of potassium from the sample into the sensor membrane a proton is released from MEDPIN which then turns blue. The sensor layer measures potassium over the clinical range with excellent performance<sup>96-98</sup>. This scheme proved to be highly flexible. The dye used in the commercial system is superior (in terms of stability) to other dyes such as Nile Blue that later have been applied in the ion exchange detection scheme.

While heavy metals can be easily detected by making use of known indicator dyes or quenchable probes, the alkali and earth alkaline elements are not easily recognized by conventional dyes at neutral pH and room temperature, and without addition of reagent. Therefore the molecular recognition properties of crown ethers and cyclic peptides have been widely used. The first studies were made by co-extraction of ions from water into chlorinated hydrocarbons, but later on the reagents were dissolved in plasticized PVC<sup>99</sup>. The amberlite ion exchanger (of the XAD type) is another widely used matrix for immobilizing indicator probes<sup>100</sup>.

Crown ethers have excellent recognition properties and can recognize numerous ions including alkali ions. Unfortunately, those synthesizing new crown ethers tend to investigate their properties in organic solutions such as acetonitrile and then claim that the findings may be useful for sensing alkali ions, thus ignoring the fact that alkali ions usually are sensed in aqueous solutions (including blood) where binding constants are very different. An interesting scheme for an optical sensor for sodium and based on ion-pair extraction and fluorescence was introduced by the Seitz group<sup>101</sup>.

The chromo- and fluoro-ionophores form a particularly interesting class of probes since they can combine recognition properties with optical

transduction such as changes in color or fluorescence. Chromo-ionophores are being used in clinical test strips for  $K^+$  since 1985 and based on the work of Voegtle<sup>102</sup> and others. The fluorescence of many fluorophores is particularly sensitive to perturbations of its microenvironment. For example, the photo-induced electron transfer (PET) can be suppressed on binding alkali ions. This has been demonstrated in impressive work by the groups of Valeur<sup>103</sup> and DeSilva<sup>104</sup>. Most noteworthy, the fluoro-ionophores are contained in a hydrophilic rather than hydrophobic matrix. The fluoro-ionophores are used in Roche's and Osmetech's Opti-1 clinical electrolyte analyzer<sup>105</sup>.

A novel approach for ion sensing is based on the use of potential-sensitive or polarity-sensitive dyes (PSDs) and was presented first<sup>106</sup> in 1987. PSDs are charge dyes and typically located at the interface between a lipophilic sensor phase and a hydrophilic sample phase. The transport of an ion into the lipophilic sensor layer causes the PSD to be displaced from the hydrophilic/hydrophobic interface into the interior of the respective phase (or vice versa), thereby undergoing a significant change in its fluorescence properties<sup>107-110</sup>.

#### **4.3.2 Heavy Metal Ions**

It has been known for many years that metal ions can be detected qualitatively by immobilizing indicator dyes on solid supports such as cellulose. In fact, this approach forms the basis for the widely used test strips for heavy metals. Again, Zhujun and Seitz<sup>111</sup> appear to have been the first to exploit this scheme to FOCS. The sensor described responds to  $Al^{3+}$ ,  $Mg^{2+}$ ,  $Zn^{2+}$ , and  $Cd^{2+}$  and was prepared by immobilizing quinolin-8-ol-5-sulfonate (QS) on an ion-exchange resin and attaching the resin to the end of a trifurcated fiber-optic bundle. The weak fluorescence of QS is strongly enhanced on complexation of metal ions. Detection limits for the metal ions are all  $<1 \cdot 10^{-6}$  M. Immobilized and dissolved QS behave similarly with respect to pH and interferences. Other metal ion sensing schemes were reported by the same group<sup>112</sup>.

Numerous other FOCS schemes have been described for heavy metals in the past 20 years (for reviews, see 113-115). In looking at the more recent literature one may state, however, that some of the newly described "chemistries" perform hardly better than the rather old commercial systems based on the use of dry reagent chemistries, with the additional advantage that they are compatible with a single instrument for read-out. In fact, some of the newer systems involve rather extensive chemistry and – worst of all – seem to strongly differ in terms of spectroscopy and analytical wavelengths so that they all require their own opto-electronic platform. On the other hand, there is substantial need for (low-cost) sensors for less common

species, and those<sup>116</sup> for  $\text{Al}^{3+}$  and certain heavy metals<sup>111</sup> are typical examples.

#### 4.4 Sensors for Anions

Nitrate has an intrinsic absorption at around 250 nm that may be used for sensing it in drinking water. However, practically all other matrices have such a strong background absorption in the UV that sensing of nitrate (and of any other UV absorbing species) is impossible. Other schemes are therefore needed. Anions such as chloride, nitrate, but also salicylate and penicillinate can be detected by the co-extraction method ("anion in – proton in") using phase transfer agents such as tetralkylammonium salts<sup>117-120</sup>. In contrast to extraction processes on electrodes, those occurring in optical sensor membranes require complete mass transfer. The scheme can be made pH-independent<sup>121</sup>. The fact that halides and pseudohalides quench the fluorescence of certain dyes as reported by Stokes<sup>122</sup> in 1869 was used to optically sense halides<sup>123</sup>. It displays selectivity due to the use of an enantio-selective carrier.

The ion sensing scheme based on the use of potential-sensitive or polarity-sensitive dyes (PSDs) was extended to other anions. Both the clinically significant chloride ion<sup>124</sup> and the environmentally important nitrate anion<sup>125</sup> can be sensed in the desired concentration ranges. Such sensors have the unique advantage of having a virtually pH-insensitive response.

### 5. BIOSENSORS

#### 5.1 Early Enzyme-Based and Cell-Based Biosensors

The chemical sensors described so far, and also those for ammonium ion, ammonia, or hydrogen peroxide may be used to monitor enzymatic reactions. The first (albeit not fiber optic) enzyme-based fiber optic biosensor (FOBS) was described by the Lübbers group<sup>126-128</sup> and made use of an oxygen transducer and glucose oxidase. In another type of FOBS, the enzyme alkaline phosphatase was immobilized at the surface of a bifurcated optical fiber bundle, and p-nitrophenyl phosphate acted as the chromogenic substrate which gives yellow p-nitrophenoxide as the detectable species<sup>129</sup>. Numerous kinds of optical sensor membranes have been designed later on for monitoring reactions that are accompanied by the production of low molecular species such as  $\text{H}^+$ ,  $\text{CO}_2$ ,  $\text{NH}_3/\text{NH}_4^+$ , NADH, or  $\text{H}_2\text{O}_2$ , and by the year 1991 an impressive variety of detections schemes was available for enzyme substrates<sup>12, 130, 131</sup>. These are summarized in Table 3. Many more have become known thereafter but are not included in this Table.

Table 3. Early optical enzyme-based biosensors, and respective transducers (work published until 1992). Data on work by Schaffar & Wolfbeis from ref. 130. For a recent review see ref. (131).

<i>Analyte (Substrate)</i>	<i>Enzyme</i>	<i>Via</i>	<i>Reference</i>
alcohols	LADH	NADH	Walters et al., 1988
alcohols	alcohol oxidase	O <sub>2</sub>	Völkl et al., 1980; Wolfbeis & Posch, 1988
glucose	glucose dehydrogenase	NADH	Narayanaswamy & Sevilla, 1988
glucose	glucose oxidase (GOx)	PH	Goldfinch & Lowe, 1984; Trettnak et al., 1989; Kulp et al., 1988
glucose	GOx	O <sub>2</sub>	Völkl et al., 1980; Trettnak et al., 1988; Kroneis et al., 1987; Schaffar & Wolfbeis, 1990; Moreno-Bondi et al., 1990
glucose	GOx	fluorescence of GOx	Trettnak & Wolfbeis, 1989
lactate, pyruvate	lactate dehydrogenase	NADH	Wangsa & Arnold, 1988
lactate	lactate oxygenase	O <sub>2</sub>	Dremel et al., 1989
lactate	lactate mono-oxygenase	fluorescence of enzyme	Trettnak & Wolfbeis, 1989
lactate	lactate mono-oxygenase	O <sub>2</sub> , CO <sub>2</sub>	Lübbbers et al., 1981; Trettnak & Wolfbeis, 1989
creatinine	creatinine iminohydrolase	NH <sub>4</sub> <sup>+</sup>	Wolfbeis & Li, 1991
esters	esterases	pH	Luo & Walt, 1989
urea	urease	NH <sub>3</sub> /NH <sub>4</sub> <sup>+</sup>	Rhines & Arnold, 1989; Wolfbeis & Li, 1991
urea	urease	pH	Goldfinch & Lowe, 1984; Luo & Walt, 1989; Yerian et al., 1986
glutamate	glutamate oxidase (GLOx)	O <sub>2</sub>	Dremel et al., 1991
glutamate	GLOx	CO <sub>2</sub>	Dremel et al., 1991
oxalate	oxalate decarboxylase	CO <sub>2</sub>	Schaffar & Wolfbeis, 1991
phenols	phenolase	O <sub>2</sub>	Schaffar & Wolfbeis, 1991
sulfite	sulfite oxidase	O <sub>2</sub>	Schaffar & Wolfbeis, 1991
penicillin	penicillinase	pH	Goldfinch & Lowe, 1984; Kulp et al., 1987
bilirubin	bilirubin oxidase	O <sub>2</sub>	Schaffar, 1988; Trettnak, 1989
ascorbate	ascorbate oxidase	O <sub>2</sub>	Schaffar, 1988
uric acid	uricase	O <sub>2</sub>	Schaffar & Wolfbeis, 1991
xanthine	xanthine oxidase	O <sub>2</sub>	Völkl et al., 1980
cholesterol	cholesterol oxidase	O <sub>2</sub>	Trettnak & Wolfbeis, 1990

Sensors for glucose are most important and have received most attention. The preferred format still is based on the use of glucose oxidase (GOx). Other glucose biosensors using immobilized glucose oxidase<sup>132-134</sup> or a pH sensor<sup>137</sup> or O<sub>2</sub> sensor<sup>135, 136</sup> acting as transducer were reported.

Later, it was discovered<sup>138</sup> that the FAD coenzymes of certain oxidases display large changes in their fluorescence if exposed to their substrates. Thus, the fluorescence of the FAD unit of lactate mono-oxygenase changes substantially on loading with lactate, and this can serve as the analytical information in an optical sensor.

Subsequent work showed<sup>139, 140</sup> that not only enzyme substrates, but also enzyme activity may be detected via fiber optics if they contain a nonfluorescent enzyme substrate at the tip. On exposure to an enzyme, the nonfluorescent substrate is converted into the fluorescent product, and this is "seen" by the fiber optic system. Inversely, a chromogenic substrate may be assayed via immobilized alkaline phosphatase<sup>141</sup>. Finally, the inhibition of enzymes by pesticides and warfare agents can be detected using fiber optics<sup>142</sup>. In an extension of this scheme, the biochemical oxygen demand has been determined by coupling coating an oxygen-sensitive membrane with a layer of immobilized bacteria<sup>143</sup>.

## 5.2 Fiber Optic Affinity Sensors, Immunosensors and Gene Sensors

An implantable sensor for glucose and other metabolites was described by Schultz<sup>144, 145</sup>. The principle of detection is similar to that used in radioimmunoassays and is based on the competitive binding of a particular metabolite and a fluorescein-labeled analog, with receptor sites specific for the metabolite and the labeled ligand. This concept was directed toward the development of an affinity sensor for glucose. Concanavalin A, a protein with specific binding character for glucose, was immobilized on the inside surface of a hollow dialysis fiber. Fluorescein-labeled (FITC) dextrane was selected as the competitive labeled ligand. The cutoff of the dialysis fiber is low enough to completely retain the dextrane within the fiber lumen while glucose can freely pass through the dialysis membrane. The sensor is completed by inserting a single optical fiber in the lumen of the dialysis fiber, thus allowing measurement of the unbound FITC-dextrane.

A novel fiber optic sensor concept using antibody-antigen reactions at a glass-liquid interface was reported by Daehne<sup>146</sup>. The reaction of antibodies immobilized onto the surface of fused silica fiber optic or planar waveguides with antigens in solution was detected by interaction with the evanescent wave. By detecting in-line fluorescence, the measurement of human IgG is described.

Fiber-optic biosensors based on luminescence and immobilized enzymes for the detection of NADH and ATP can be found in ref. (147-152).



## 6. EARLY REVIEWS

It is appropriate to make reference to early reviews where the state of the art at the time they were written are summarized. Reviews have appeared on remote UV-VIS-NIR spectroscopy using fiber optic chemical sensing<sup>153</sup>; on remote and in-situ analysis<sup>154</sup>; on optical fiber sensors in chemical analysis<sup>155</sup>; on fluorescent probes for optical sensors<sup>156</sup>; on biomedical sensing using optical fibers<sup>157</sup>; on low-cost fiber optic chemical sensors<sup>158</sup>; on the application of single optical fibers to remote absorption measurements<sup>159</sup>; on spectral filtering optical fiber sensors<sup>160</sup>; on chemical and biological sensors<sup>161</sup>; on optical fiber sensors for industrial applications<sup>162</sup>; on in-vivo optical chemical sensors<sup>163</sup>; on the feasibility of using fiber optics for monitoring groundwater contaminants<sup>164</sup>; on instrumentation for remote sensing over fiber optics<sup>165</sup>; on chemical sensors based on fiber optics<sup>166</sup>; on optical fiber sensor technology in general including chemical and biosensors<sup>167, 168</sup>; and on optical fiber sensors in medicine<sup>169</sup> and biomedical applications<sup>170</sup>.

## 7. COMMERCIAL INSTRUMENTATION

Many of those working on optical sensors have been overoptimistic. While many chemical sensors and biosensor have found applications in the laboratory and in research, they are much less often applied than physical sensors, e.g. those for temperature, pressure, velocity, or strain. This may be due to several factors, of which the following are considered to be most significant:

- (a) most chemical sensors suffer from poor selectivity; therefore, they can only be applied to rather specific matrices;
- (b) most chemical sensors and biosensors suffer from inadequate stability (both storage stability and operational stability); in fact, the significance of material sciences is heavily underestimated in sensor research; in our opinion, too many researcher focus on sensing schemes, but not enough on sensor materials;
- (c) most sensors are too expensive; this not only is true for the costs for product development, but also for the instrument itself and the sensor materials used; the market size for such devices is too small and it is quite unrealistic to assume that an investment into development of a commercial sensor for, e.g. copper(II) ion, may ever produce adequate return, unless the same instrument can sense several other species as well.

While several optical chemical sensors and biosensors in use that do not rely on fiber optics, the commercialization of FOCS technology started slowly, probably because of the limitations imparted to optical sensing if

combined with fiber optics. In 1984, CDI (later 3M) introduced their critical care monitoring system (GasStat 300) for oxygen, pH and CO<sub>2</sub> for cardiopulmonary monitoring (see Fig. 5). The sensors employed are based on the work (papers and patents) of D. W. Lübbers et al., O. S. Wolfbeis et al., M. Yafuso, W. W. Miller and J. Tusa. The sensor head consists of a flow-through cell containing sensor spots and fiber optic cables attached to the cell in order to optically interrogate the sensor spots. The sensor exhibits excellent performance if properly calibrated.

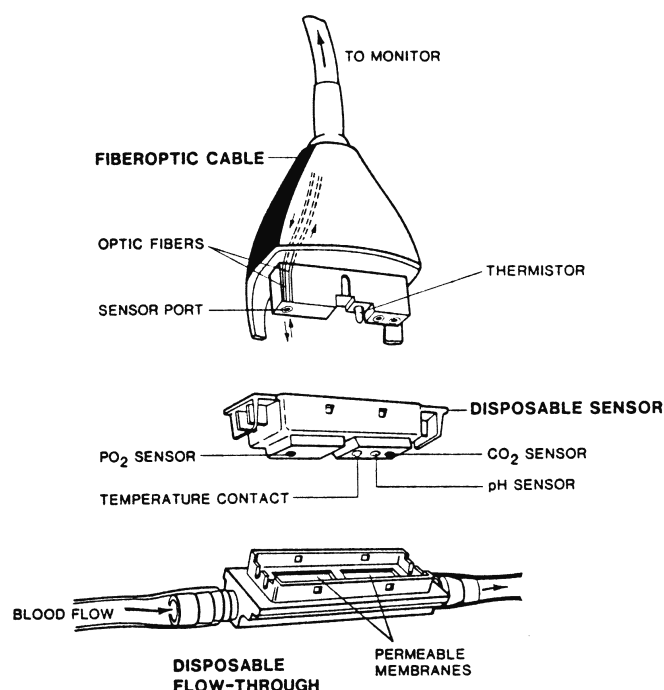


Figure 5. Triple sensor for pH, oxygen and CO<sub>2</sub> for monitoring the blood status during cardiopulmonary bypass (CDI Inc., 1986).

Fig. 5 shows the instrumental arrangement of the commercially most successful optical chemical sensor between 1984 and 2000. It is used in about 70% of all critical care operations in the US to monitor pH, pCO<sub>2</sub> and pO<sub>2</sub> in the cardiopulmonary bypass operations<sup>35</sup>. It contains 3 fluorescent spots, each sensitive for one parameter, in contact with blood. Fluorescence intensity is measured at two wavelengths and the signals are then submitted to internal referencing and data processing.

Other medical products based on optical sensor technology include those of Cardiomed (System 4000), Puritan-Bennett, and one of Radiometer (Copenhagen) which has been withdrawn meanwhile. Optical (but non-fiber) sensors for oxygen and for CO<sub>2</sub> also are widely used for the determination of bacteria in blood. In 1986, Gehrich et al.<sup>36</sup> described an optical fluorescence

sensing system for intravascular blood gas monitoring, and Miller et al.<sup>35</sup> reported on an in-vivo catheter for blood gas monitoring. While announced, the systems were never commercialized.

Among the non-medical sensors, those for oil contamination and for oxygen are predominant. Fig. 6 shows the tip of the fiber optic oxygen microsensor of Presens.

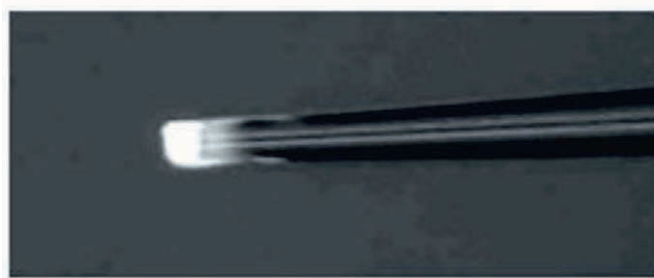


Figure 6. Tip of the 20- $\mu\text{m}$  tip of a fiber optic oxygen microsensor. The tip is coated with a ormosil-type of sol-gel doped with a ruthenium indicator for oxygen that display red luminescence. The sensor measures its decay time as a function of oxygen partial pressure.

A smart sensor chip was presented by Texas Instruments<sup>171</sup>. It includes an LED light source, a photodiode, a chemically sensitive waveguide and an inert reference waveguide. It is schematically shown in Figure 7.

Table 4 below summarizes the commercial fiber optical sensors that have come to our attention.

In conclusion, it can be said that the past 20 years have seen a tremendous leap forward in the technologies leading to FOCS and FOBS.

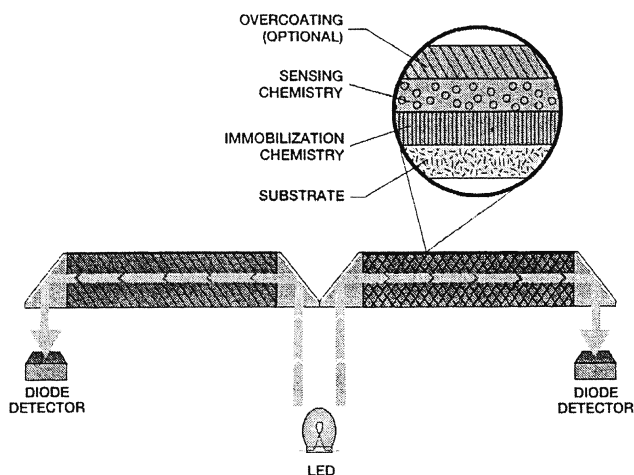


Figure 7. Waveguide chip package of Texas Instruments.

Sensing schemes have become reliable enough to be of practical utility, instrumentation has become available at costs that make this sensor technology competitive to established sensors, and numerous other sensors schemes have been presented that are of interest, at least from an academic point of view.

Table 4. Selection of Commercial Fiber Optic Chemical Sensors.

<i>Product</i>	<i>Manufacturer</i>	<i>Analytes</i>	<i>Remarks</i>	<i>Internet address</i>
GeoSensor	GeoCenters	pH 3-8	+/- 0.1 units; robust	unknown
PetroSense	FiberChem	hydrocarbons gasoline	1-mm fibers, robust	www.decisionlinkinc.com
MicrOx	Presens	O <sub>2</sub>	30 µm tip; via decay time, autoclavable	www.presens.de
FibOx	Presens	O <sub>2</sub>	2-mm fibers, DLR based, autoclavable	www.presens.de
NTH microsensor	Presens	pH 5-9	140 µm tip; DLR based	www.presens.de
pH Finger	Presens	pH 5-9	2.8-mm fibers, DLR based	www.presens.de
YSI 8500	Yellow Springs	CO <sub>2</sub>	for bioprocess control; autoclavable	www.yxi.com
FiberDek	Soundek	oil on water	reflectance based; 2 LEDs, hand-held	http://www.otech.fi/
TP300	Ocean Optics	pH (wide range)	reflectance based, fiber bundles	www.oceanoptics.com
FOXY	Ocean Optics	O <sub>2</sub>	1-mm fibers, intensity based	www.oceanoptics.com
Oxygen Sensor	SMSI	O <sub>2</sub>	solid-state transducer	www.s4ms.com
Oxygen Sensor	Photosense LLC	O <sub>2</sub>	1-mm fibers, via decay time	www.photosense.com

## REFERENCES

1. The *Cambridge Definition of Chemical Sensors*, by Cammann K., Hall E.A.H., Kellner R., Schmidt H.L., Wolfbeis O.S., 1995.
2. Harper G.B., Glass-immobilized pH indicators, *Anal. Chem.* 1975; 47: 348.
3. Milanovich F.P., Hirschfeld T., Process, product, and waste stream monitoring with fiber optics. *Adv. Instrum.* 1983; 38: 407.
4. Hirschfeld T., Deaton T., Milanovich F.P., Klainer S.M., Feasibility of using fiber optics for monitoring groundwater contaminants, *Opt. Eng.* 1983; 22: 27.
5. Miller H.H., Hirschfeld T.B., Fiber optic chemical sensors for industrial and process control, *Proc. SPIE-Int. Soc. Opt. Eng.* 1987; 718: 39.

6. Perry D.F., Klainer S.L., *Report* 1984.
7. Jia W.J., He A.D., Wang Z.L., Chin C.T., Application of laser-induced optical fiber fluorimetry to the analysis of ultralow level of uranium, *J. Radioanal Nucl. Ch.* 1987; 108: 33.
8. Boisdé G., Guillot P., Monier J., Perez J. J., *Report* 1983.
9. Boisdé G., Perez J.J., Fr. Pat. 2.317.638 (1975).
10. Perez J.J., Boisdé G., Automation of plutonium spectrophotometry, *Analysis* 1980; 8: 344.
11. Peterson J.I., Goldstein S.R., Fitzgerald R.V., Buckhold R.V., Fiber optic pH probe for physiological use, *Anal. Chem.* 1980; 52: 864.
12. Wolfbeis O.S. (ed.), *Fiber Optic Chemical Sensors and Biosensors*, CRC Press, Boca Raton, Florida, 1991.
13. Kirkbright G.F., Narayanaswamy R., Welti N.A., Studies with immobilized chemical reagents using a flow-cell for the development of chemically sensitive fiber-optic devices. *Analyst* 1984; 109: 15.
14. Borman S., Voyager infrared spectromete, *Anal. Chem.* 1981; 53: 1616A.
15. Hirschfeld T., Callis J.B., Kowalski B.R., Chemical sensing in process analysis, *Science* 1984; 226: 312.
16. Kautsky H., Hirsch A. Energy transformations on boundary surfaces. IV. Interaction of excited dyestuff molecules and oxygen. *Chem. Ber.* 1931; 64, 2677. For a review, see: Kautsky H., Quenching of luminescence by oxygen, *Trans. Faraday Soc.* 1939; 35: 216.
17. Hesse H.H., East Ger. Pat. 106086 (1974).
18. Schultz J.S., Sims G., Affinity sensors for individual metabolites, *Biotechnol. Bioeng. Symp.* 1979; 9: 65.
19. Rogers A.J., Distributed optical-fiber sensors, *J. Phys. D: Appl. Phys.* 1986; 19: 2237.
20. Kvasnik F., McGrath A.D., Distributed chemical sensing utilizing evanescent wave interactions, *Proc. SPIE-Int. Soc. Opt. Eng.* 1990; 1172: 75.
21. Chan K., Ito H., Inaba H., Optical remote monitoring of methane gas using low-loss optical fiber link and indium gallium arsenide phosphide light-emitting diode in 1.33-mm region, *Appl. Phys. Lett.* 1983; 43: 634.
22. Chan K., Ito H., Inaba H., Humio H., Remote sensing system for near-infrared differential absorption of methane gas using low-loss optical fiber link. *Appl. Optics* 1984; 23: 3415.
23. Chan K., Ito H., Inaba H., Furuya T., Ten-kilometer long fiber-optic remote sensing of methane gas by near infrared absorption, *Appl. Phys. B* 1985; 38: 11.
24. Inaba H., Chan K., Ito H., All-optical remote gas sensor system over a 20 km range based on low-loss optical fibers in the near infrared region, *Proc. SPIE-Int. Soc. Opt. Eng.* 1984; 514: 211.
25. Stueflotten S., Christensen T., Iversen S., Hellvik J.O., Almas K., Wien T., Graav A., An infrared fiber optic gas detection system, *Proc. SPIE-Int. Soc. Opt. Eng.* 1984; 514: 87.
26. Freeman J.E., Childers A.G., Steele A.W., Hieftje G.M., A fiber-optic absorption cell for remote determination of copper in industrial electroplating baths, *Anal. Chim. Acta* 1985; 177: 21.
27. Kobayasi T., Hirama M., Inaba H., Remote monitoring of monomeric nitrogen dioxide molecules by differential absorption using optical fiber link, *Appl. Optics* 1981; 20: 3279.
28. Coleman J.T., Eastham J.F., Sepaniak M.J., Fiber optic based sensor for bioanalytical absorbance measurements, *Anal. Chem.* 1984; 56: 2246.
29. Newby K., Reichert W.M., Andrade J.D., Benner R.E., Remote spectroscopic sensing of chemical adsorption using a single multimode optical fiber, *Appl. Optics* 1984; 23: 1812.

30. Haubenreisser W., Lehmann J., Perthel R., Willsch R., Fiber optic refractometry, *Experimentelle Technik der Physik* 1984; 32: 519.
31. Ivanov V.N., Ivanov S.V., Kel'balikhanov B.F., Klimova L.G., Trubnikov B.N., Chernyi V.V., Elisashvili D.T., Measurement of temperature and salinity variations of water with a fiber-optical sensor, *Fizika Atmosfery i Okeana* 1985; 21: 555.
32. Munir Q., Weber H.P., Battig R., Resonant photoacoustic gas spectrometer fiber sensor, *Proc. SPIE-Int. Soc. Opt. Eng.* 1984; 514: 81.
33. Butler M.A., Optical fiber hydrogen sensor, *Appl. Phys. Lett.* 1984; 45: 1007.
34. Kroneis H.W., Marsoner H.J., A fluorescence-based sterilizable oxygen probe for use in bioreactors, *Sensor Actuat B-Chem* 1983; 4: 587.
35. Miller W.W., Yafuso M., Yan C., Hui H.K., Arick S., Performance of an in vivo, continuous blood-gas monitor with disposable probe, *Clin. Chem.* 1987; 33: 1538.
36. Gehrich J.L., Lübbers D.W., Opitz N., Hansmann D.R., Miller W.W., Tusa J.K., Yafuso M., Optical fluorescence and its application to an intravascular blood gas monitoring system, *IEEE Trans. Biomed. Eng.* 1986; 33: 117.
37. Klimant I., Meyer V., Kuhl M., Fiber-optic oxygen microsensors, a new tool in aquatic biology, *Limnol. Oceanography* 1995; 40: 1159.
38. Holst G., Glud R. N., Kuehl M., Klimant I., A micro-optode array for fine-scale measurement of oxygen distribution, *Sensor Actuat B-Chem* 1997; B38: 122, and refs. cited.
39. Russell A.P., Fletcher K.S., Optical sensor for the determination of moisture, *Anal. Chim. Acta* 1985; 170: 209.
40. Pollack M., Pringsheim P., Terwood D., Method for determining small quantities of O, *J. Chem. Phys.* 1944; 12: 295.
41. Zakharov I.A., Grishaeva T.I., Determination of microconcentrations of water-dissolved oxygen by quenching of the adsorbate afterglow, *Zh. Anal. Khim.* 1980; 35: 481; and refs. cited.
42. Bergman I., Rapid-response atmospheric oxygen monitor based on fluorescence quenching, *Nature* 1968; 218: 396.
43. Stevens P.R., *US Pat.* 3.612.866 (1982).
44. Hendricks H.D, Method for determination of oxygen, *Mol. Phys.* 1971; 20: 189 (US Pat. 3.709.663).
45. Lübbers D.W., Opitz N., The pCO<sub>2</sub>-/pO<sub>2</sub> optode, a new probe for measurement of partial pressure of carbon dioxide or partial pressure of oxygen in fluids and gases, *Z. Naturforsch.* 1975; 30C: 532.
46. Opitz N., Lübbers D.W., A new fast-responding optical method to measure pCO<sub>2</sub> in gases and solutions, *Eur. J. Physiol.* 1975; 355: R120.
47. Lübbers D.W., Opitz N., Quantitative fluorescence photometry with biological fluids and gases, *Adv. Exptl. Biol.* 1976; 75: 65.
48. Freeman T.F., Seitz W.R., Oxygen probe based on tetrakis(alkylamino)ethylene chemiluminescence, *Anal. Chem.* 1981; 53: 98.
49. Marsoner H., Kroneis H., *Eur. Pat. Appl.* 109958 & 109959 (1984); US Pat. 4.587.101
50. Wolfbeis O.S., Offenbacher H., Kroneis H., Marsoner H. A fast responding fluorescence sensor for oxygen. *Mikrochim. Acta* 1984; I: 153.
51. Cox M.E., Dunn B., The use of fluorescence quenching to measure oxygen concentration, *Proc. SPIE-Int. Soc. Opt. Eng.* 576: 60 (1985).
52. Peterson J.I., Fitzgerald R.V., Buckhold D.K., Fiber-optic probe for in vivo measurement of oxygen partial pressure, *Anal. Chem.* 1984; 56: 62.
53. Wolfbeis O.S., Weis L., Leiner M.J.P., Ziegler W.E., Fiber optic fluorosensor for oxygen and carbon Dioxide, *Anal.Chem.* 1988; 60: 2028.
54. Wolfbeis O.S., Leiner M.J.P., Posch H.E., A new sensing material for optical oxygen measurement, *Mikrochim. Acta (Vienna)* 1986; III: 359.

55. Bacon J.R., Demas J.N., Determination of oxygen concentrations by luminescence quenching of a polymer-immobilized transition-metal complex, *Anal. Chem.* 1987; 59: 2780.
56. Lippitsch M.E., Pusterhofer J., Leiner M.J.P., Wolfbeis O.S., Fibre optic oxygen sensor with the fluorescence decay time as information carrier. *Anal. Chim. Acta* 1988; 205: 1.
57. Vanderkooi J.M., Maniara G., Green T.J., Wilson D.F., An optical method for measurement of dioxygen concentration based upon quenching of phosphorescence, *J. Biol. Chem.* 1987; 262: 5476.
58. Kahil H.E., Gouterman M.P., Green E., PCT Appl. WO 87.00023 (1987).
59. Vurek G.G., Feustel P.J., Severinghaus J.W., A fiber optic pCO<sub>2</sub> sensor, *Ann. Biomed. Eng.* 1983; 11: 499.
60. Zhang Z., Seitz W.R., A carbon dioxide sensor based on fluorescence, *Anal. Chim. Acta* 1984; 160: 305.
61. Munkholm C., Walt D.R., Milanovich F.P., A fiber-optic sensor for carbon dioxide measurement, *Talanta* 1988; 35, 109.
62. Kawabata Y., Kamichika T., Imasaka T., Ishibashi N., Fiber-optic sensor for carbon dioxide with a pH indicator dispersed in a poly(ethylene glycol) membrane, *Anal. Chim. Acta* 1989; 219: 223.
63. Raemer D.B., Walt D.R., Munkholm C., US Pat. 5.005.572 (1991).
64. Mills A., Chang Q., McMurray N., Equilibrium studies on colorimetric plastic film sensors for carbon dioxide, *Anal. Chem.* 1992; 64, 1383.
65. Weigl B.H., Wolfbeis O.S., Capillary optical sensors, *Anal. Chem.* 1994; 66: 3323.
66. Nishizawa K., Yamazaki T., Jap. Kokai 60.209.149 (1986).
67. Klainer S.M., Goswami K., Nelson N.R., Simon S.J., Eccles L.A., US Pat. 4.892.383 (1990).
68. Wolfbeis O.S., Posch H.E., Kroneis H., Fiber optical fluorosensor for determination of halothane and/or oxygen, *Anal. Chem.* 1985; 57: 2556.
69. Arnold M.A., Ostler T.J., Fiber optic ammonia gas sensing probe, *Anal. Chem.* 1986; 58: 1137.
70. Wolfbeis O.S., Posch H.E., Fiber optic fluorescing sensor for ammonia, *Anal. Chim. Acta* 1986; 185: 321.
71. Stangelmayer A., Klimant I., Wolfbeis O.S., Optical sensors for dissolved sulfur dioxide, *Fresenius J. Anal. Chem.* 1998; 362: 73.
72. Wolfbeis O.S., Sharma A., Fibre-optic fluorosensor for sulphur dioxide, *Anal. Chim. Acta* 1988; 208: 53.
73. Barker S.L., Kopelman R., Meyer T.E., Cusanovich M.A., Fiber-Optic Nitric Oxide-Selective Biosensors, *Anal. Chem.* 1998; 70: 971.
74. Mohr G.J., Wolfbeis O.S., Optical sensors for a wide range of pH based on azo dyes immobilized on a novel support, *Anal. Chim. Acta* 1994; 292: 41.
75. Edmonds T.E., Ross I.D., Low-cost fiber optic chemical sensors, *Anal. Proceed.* 1985; 22: 206.
76. Kirkbright G.F., Narayanaswamy R., Welti N.A., Fiber-optic pH probe based on the use of an immobilized colorimetric indicator, *Analyst* 1984; 109: 1052.
77. Boisdé G., Perez J.J., Miniature chemical optical fiber sensors for pH measurements, *Proc. SPIE-Int. Soc. Opt. Eng.* 1987; 798: 238.
78. Saari L.A., Seitz W.R., pH sensor based on immobilized fluoresceinamine, *Anal. Chim. Acta* 1982; 54: 821.
79. Bacci M., Baldini F., Scheggi A.M., Spectrophotometric investigations on immobilized acid-base indicators, *Anal. Chim. Acta* 1988; 207: 343.
80. Tait G.A., Young R.B., Wilson G.J., Steward D.J., MacGregor D.C., Myocardial pH during regional ischemia: evaluation of a fiber-optic photometric probe, *Am J. Physiol. Heart Circ. Physiol.* 1982; 243: H1027.
81. Suidan J.S., Young B.K., Hetzel F.W., Seal H.R., pH Measurement with a fiber-optic tissue-pH monitor and a standard blood-pH meter, *Clin. Chem.* 1983; 29: 1566.

82. Grattan K.T.V., Mouaziz Z., Selli R.K., A pH sensor using a LED source in a fiber optic device, *Proc. SPIE-Int. Soc. Opt. Eng.* 1987; 798: 230.
83. Offenbacher H., Wolfbeis O.S., Furlinger E., Fluorescence optical sensors for continuous determination of near-neutral pH values, *Sensors Actuat.* 1986; 9: 73.
84. Heitzmann H., Kroneis N., US Pat. 4.557.900 (1985).
85. Janata J., Do optical sensors really measure pH, *Anal. Chem.* 1987; 59: 1351.
86. Opitz N., Lübbers D.W., New fluorescence photometrical techniques for simultaneous and continuous measurements of ionic strength and hydrogen ion activities, *Sensor Actuat.* 1983; 4: 473.
87. Wolfbeis O.S., Offenbacher H., Fluorescence sensor for monitoring ionic strength and physiological pH values, *Sensor Actuat.* 1986; 9: 85.
88. Wolfbeis O.S., Werner T., Rodriguez N.V., Kessler M.A., LED-compatible fluorosensor for measurement of near-neutral pH values, *Mikrochim. Acta* 1994; 108, 133.
89. Abraham E., Markle D.R., Fink S., Ehrlich H., Tsang M., Smith M., Meyer A., Continuous measurement of intravascular pH with a fiberoptic sensor, *Anesth. Analg.* 1985; 64: 731.
90. Peterson J.L., Goldstein S.R., A miniature fiberoptic pH sensor potentially suitable for glucose measurements, *Diabetes Care* 1982; 5, 272.
91. Song A., Parus S., Kopelman R., High-performance fiber-optic pH microsensors for practical physiological measurements using a dual-emission sensitive dye, *Anal. Chem.* 1997; 69: 863.
92. MacCraith B.D., Ruddy V., Potter C., O'Kelly B., McGilp J.F., Optical waveguide sensor using evanescent wave excitation of fluorescent dye in sol-gel glass. *Electron. Lett.* 1991; 27: 1247.
93. Lin J., Recent development and applications of optical and fiber-optic pH sensors, *Trends Anal.Chem.* 2000; 19: 541-551.
94. Charlton S.C., Fleming R.L., Zipp A., Solid-phase colorimetric determination of potassium, *Clin. Chem.* 1982; 28, 1857.
95. Charlton S.C., US Pat. 4.645.744 (1987)
96. Gibb I., Evaluation and assessment of new disposable strip for determination of plasma potassium concentration, *J. Clin. Pathol.* 1987; 40, 298.
97. Ng R.H., Sparks K.M., Statland B.E., Colorimetric determination of potassium in plasma and serum by reflectance photometry with a dry-chemistry reagent, *Clin. Chem.* 1992; 38: 1371.
98. Zipp A., Hornby W.B., Solid-phase chemistry: its principles and applications in clinical analysis, *Talanta* 1984; 31: 863.
99. Nakamura H., Takagi M., Ueno K., Complexation and extraction of alkali metal ions by 4'-picrylamino-18-crown-6 derivatives, *Anal. Chem.* 1980; 52: 1668.
100. Alder J.F., Ashworth D.C., Narayanaswamy R., Moss R.E., Sutherland I.O., An optical potassium ion sensor, *Analyst* 1987; 112: 1191.
101. Zhujun Z., Mullin J.L., Seitz W.R., Optical sensor for sodium based on ion-pair extraction and fluorescence, *Anal. Chim. Acta* 1986; 184: 251.
102. Voegtle F., (ed.) *Comprehensive Supramolecular Chemistry*, Volume 2: Molecular Recognition: Receptors for Molecular Guests, Pergamon Press, Oxford, UK, 1996.
103. Valeur B., Leray I., Design principles of fluorescent molecular sensors for cation recognition, *Coord. Chem. Rev.* 2000; 205: 3.
104. Prasanna de Silva A, Gunaratne H.Q.N., Gunnlaugsson T., Huxley A.J.M., McCoy C.P., Rademacher J.T., Rice T.E., Signaling Recognition Events with Fluorescent Sensors and Switches, *Chem. Rev.* 1997; 97: 1515 (review).
105. He H., Leiner M.J.P., Tusa J., *Proc. Europt(r)ode 2000* (Lyon, Fr.), Book of Abstracts, P. Coulet (ed.), p. 49-50.
106. Wolfbeis O.S., Schaffar B.P.H., An ion-selective optrode for potassium, *Anal. Chim. Acta* 1987; 198: 1.



107. Wolfbeis O.S., Fluorescence-based ion sensing using potential-sensitive dyes, *Sensor Actuat B-Chem* 1995; 29: 140.
108. Krause C., Werner T., Huber C., Wolfbeis O.S., Emulsion-based fluorosensors for potassium featuring improved stability and signal change, *Anal. Chem.* 1999; 71: 5304.
109. Kawabata Y., Tahara R., Imasaka T., Ishibashi N., Fiber-optic potassium ion sensor using alkyl-acridine orange in plasticized poly(vinyl chloride) membrane, *Anal. Chem.* 1990; 62: 1528.
110. Murkovic I., Lobnik A., Mohr G.J., Wolfbeis O.S., Fluorescent potential-sensitive dyes for use in solid-state sensors for potassium ion, *Anal. Chim. Acta*, 1996; 334: 125.
111. Zhujun Z., Seitz W.R., A fluorescent sensor for aluminum(III), magnesium(II), zinc(II) and cadmium(II) based on electrostatically immobilized quinolin-8-ol sulfonate, *Anal. Chim. Acta* 1985; 171, 251.
112. Seitz W.R., Saari L.A., Zhang Z., Pokornicki S., Hudson R.D., Sieber S.C., Ditzler M.A., Metal ion sensors based on immobilized fluorogenic ligands, *ASTM Special Techn. Publ.* 1985; 863: 63.
113. Narayanaswamy R., Sevilla F., Optical fiber sensors for chemical species, *J. Phys. E: Sci. Instrum.* 1988; 21: 10.
114. Seitz W.R., Chemical sensors based on immobilized indicators and fiber optics, *CRC Crit. Rev. Anal. Chem.* 1988; 19: 135.
115. Oehme I., Wolfbeis O.S., Fundamental Review: Optical Sensors for Determination of Heavy Metal Ions, *Mikrochim. Acta* 1997; 126: 177.
116. Saari L.A., Seitz W.R., Immobilized morin as fluorescence sensor for determination of aluminum(III), *Anal. Chem.* 1983; 55: 667.
117. Tan S.S.S., Hauser P.C., Chaniotakis N.A., Suter G., Simon W., Anion-selective optical sensors based on a coextraction of anion-proton pairs into a solvent-polymeric membrane, *Chimia* 1989; 43: 257.
118. Morf W.E., Seiler K., Lehmann B., Behringer C., Hartman K., Simon W., Carriers for chemical sensors: design features of optical sensors (optodes) based on selective chromoionophores, *Pure Appl. Chem.* 1989; 61: 1613.
119. Seiler K. and Simon W., Theoretical aspects of bulk optode membranes, *Anal. Chim. Acta* 1992, 266: 73.
120. Wang E., Meyerhoff M.E., Anion selective optical sensing with metalloporphyrin-doped polymeric films, *Anal. Chim. Acta* 1993, 283: 673.
121. Huber C., Werner T., Krause C., Wolfbeis O.S., Leiner M.J.P., Overcoming the pH-Dependency of Optical Sensors: a pH-Independent Chloride Sensor Based on Co-Extraction, *Anal. Chim. Acta* 1999, 398: 137.
122. Stokes G.G., Studies on luminescence, *J. Chem. Soc.* 1869; 22: 174.
123. Urbano E., Offenbacher H., Wolfbeis O.S., Optical Sensor for Continuous Determination of Halides, *Anal. Chem.* 1984; 56: 427.
124. Huber Ch., Werner T., Krause Ch., Wolfbeis O.S., Novel Chloride-Selective Optode Based on Polymer-Stabilized Emulsions Doped with a Lipophilic Fluorescent Polarity-Sensitive Dye, *Analyst* 1999; 124: 1617.
125. Mohr G.J., Wolfbeis O.S., Application of Potential-Sensitive Fluorescent Dyes in Anion-Sensitive and Cation-Sensitive Polymer Membranes, *Sensor Actuat B-Chem.* 1997; 37: 103.
126. Völkl K.P., Opitz N., Lübbers D.W., Continuous measurement of concentrations of alcohol using a fluorescence-photometric enzymic method, *Fresenius J. Anal. Chem.* 1980; 301: 162.
127. Völkl K.P., Grossmann U., Opitz N., Lübbers D.W., The enzyme optode, *Adv. Physiol. Sci.* 1981; 25: 99.
128. Lübbers D.W., Opitz N., Optical fluorescence sensors for continuous measurement of chemical concentrations in biological systems, *Sensors Actuat.* 1983; 3: 641.
129. Arnold M.A., Enzyme-based fiber optic sensor, *Anal. Chem.* 1985; 57 (2): 565.

130. Schaffar B.P.H., Wolfbeis O.S., *Chemically Mediated Fiber Optic Biosensors*, chapter 8 in: *Biosensors Principles and Applications*, L.J. Blum, P.R. Coulet (eds.), M. Dekker, New York, chapter 8, pp. 163-194 (1991).
131. Marazuela M.D., Moreno-Bondi M.C., Fiber-optic biosensors - an overview, *Anal. Bioanal. Chem.* 2002; 372: 664.
132. Trettnak W., Wolfbeis O.S., A fully reversible fibre optic glucose biosensor based on the intrinsic fluorescence of glucose oxidase, *Anal. Chim. Acta* 1989; 221: 195.
133. Dremel B.A., Schaffar B.P., Schmid R.D., Determination of glucose in wine and fruit juice based on a fiber-optic glucose biosensor and flow-injection analysis, *Anal. Chim. Acta* 1989; 225: 293.
134. Narayanaswamy R., Sevilla F., An optical fiber probe for the determination of glucose based on immobilized glucose dehydrogenase, *Anal. Lett.* 1988; 21: 1165.
135. Moreno-Bondi M.C., Wolfbeis O.S., Leiner M.J.P., Schaffar B.P.H., Oxygen optrode for use in a fiber optic glucose biosensor, *Anal. Chem.* 1990; 62: 2377.
136. Trettnak W., Wolfbeis O.S., Fiber optic cholesterol biosensor with an oxygen optrode as the transducer; *Anal. Biochem.* 1990; 184: 124.
137. Trettnak W., Leiner M.J.P., Wolfbeis O.S., Fibre-optic glucose sensor with a pH optrode as a transducer, *Biosensors* 1988; 4: 15.
138. W. Trettnak, O.S. Wolfbeis, A fully reversible fiber optic lactate biosensor based on the intrinsic fluorescence of lactate monoxygenase, *Fresenius Z. Anal. Chem.* 1989, 334, 427.
139. Wolfbeis O.S., Fiberoptic probe for kinetic determination of enzyme activities, *Anal. Chem.* 1986, 58, 2874.
140. Zhang Z., Seitz W.R., O'Connell K., Amylase substrate based on fluorescence energy transfer, *Anal. Chim. Acta* 1990; 236: 251.
141. Freeman M.K., Bachas L., Fiber-optic biosensor with fluorescence detection based on immobilized alkaline phosphatase, *Biosensors Bioelectron.* 1992; 7: 49.
142. Trettnak W., Reiningger F., Zinterl E., Wolfbeis O.S., Fiber Optic Remote Detection of Pesticides and Related Inhibitors of the Enzyme Acetylcholine Esterase, *Sensor Actuat B-Chem* 1993; 11: 87.
143. Preininger C., Klimant I., Wolfbeis O.S., Optical fiber sensor for biochemical oxygen demand (BOD), *Anal. Chem.* 1994; 66: 1841.
144. Mansouri S., Schultz J., A miniature optical glucose sensor based on affinity binding, *Bio/Technology* 1984; 2: 885.
145. Schultz J.S., Medical applications of fiberoptic sensors, *Med. Instrum.* 1985; 19: 158.
146. Daehne C., Sutherland R.M., Place J.F., Ringrose A.S., Detection of antibody-antigen reactions at a glass-liquid interface: a novel fiber-optic sensor concept, *Proc. SPIE-Int. Soc. Opt. Eng.* 1984; 514: 75.
147. Gautier S., Blum L.J., Coulet P.R., Alternate determination of ATP and NADH with a single bioluminescence-based fiber-optic sensor, *Sensor Actuat B-Chem* 1990; 1: 580.
148. Gautier S.M., Blum L.J., Coulet P.R., Multifunction fiber-optic sensor for the bioluminescent flow determination of ATP or NADH, *Anal. Chim. Acta* 1990; 235: 243.
149. Scheper T., Bueckmann A.F., A fiber optic biosensor based on fluorometric detection using confined macromolecular nicotinamide adenine dinucleotide derivatives, *Biosens. Bioelectron.* 1990; 5: 125.
150. Blum L.J., Gautier S.M., Coulet P.R., Continuous-flow bioluminescent assay of NADH using a fiber-optic sensor, *Anal. Chim. Acta* 1989; 226: 331.
151. Gautier S.M., Blum L.J., Coulet P.R., Fiber-optic sensor with co-immobilized bacterial bioluminescence enzymes, *Biosensors* 1989; 4: 181.
152. Blum L.J., Gautier S.M., Coulet P.R., Luminescence fiber-optic biosensor, *Anal. Lett.* 1988; 21: 717.
153. Fitch P., Gargus A.G., Remote UV-VIS-NIR spectroscopy using fiber optic chemical sensing, *Am. Lab.* 1985; 17: 64.
154. Hirschfeld T., Remote and in-situ analysis, *Adv. Instrum.* 1985; 40: 305.

155. Narayanaswamy R., Optical fiber sensors in chemical analysis, *Anal. Proceed.* 1985; 22: 204.
156. Wolfbeis O.S., From fluorescent probes to optical sensors, *Anal. Proceed.* 1991; 28: 357.
157. Smith A.M., Biomedical sensing using optical fibers, *Anal. Proceed.* 1985; 22: 212.
158. Edmonds T.E., Ross I.D., Low-cost fiber optic chemical sensors, *Anal. Proceed.* 1985; 22: 206.
159. Hilliard L.A., Application of single optical fibers to remote absorption measurements, *Anal. Proceed.* 1985; 22: 210.
160. Dakin J.P., Spectral filtering optical fiber sensors, *Anal. Proceed.* 1985; 22: 214.
161. Nylander C., Chemical and biological sensors, *J. Phys. E* 1985; 18: 736.
162. Harmer A.L., Optical fiber sensors for industrial applications, *Proc. SPIE-Int. Soc. Opt. Eng.* 1984; 514: 17.
163. Vurek G.G., In vivo optical chemical sensors, *Proc. SPIE-Int. Soc. Opt. Eng.* 1984; 494: 2.
164. Hirschfeld T., Deaton T., Milanovich F., Klainer S.M., Feasibility of using fiber optics for monitoring groundwater contaminants, *Gov. Report Announce. Index* 1984; 84: 153.
165. Hirschfeld T., Haugen G., Milanovich F., Instrumentation for remote sensing over fiber optics, *Analytical Chemistry Symposia Series* 1984; 19: 13.
166. Seitz W.R., Chemical sensors based on fiber optics, *Anal. Chem.* 1984; 56: 16A.
167. Giallorenzi T.G., Bucaro J.A., Dandridge A., Sigel G.H., Cole J.H., Rashleigh S.C., Priest R.G., Optical fiber sensor technology, *IEEE J. Quant. Elect.* 1982; QE18: 626.
168. Turner A.P.F., Karube I., Wilson G.S., *Biosensors: Fundamentals and Application*, Oxford University Press, 1989.
169. Scheggi A.M., Optical fiber sensors in medicine, *Proc. SPIE-Int. Soc. Opt. Eng.* 1984; 514: 93.
170. Peterson J.I., Vurek G.G., Fiber-optic sensors for biomedical applications, *Science* 1984; 224: 123.
171. Polina R.J., Klainer S.M., A field-hardened, optical waveguide hybrid integrated-circuit, multi-sensor chemical probe and its chemistry, *Proc. SPIE-Int. Soc. Opt. Eng.* 1997; 3105: 71

# **FUNDAMENTALS OF OPTICAL CHEMICAL SENSING**

## Chapter 3

# FUNDAMENTALS OF OPTOELECTRONICS

Artur Dybko

*Warsaw University of Technology*

*Department of Analytical Chemistry*

*Noakowskiego 3, 00-664 Warsaw, Poland*

### 1. INTRODUCTION

Fibre optic sensors and systems are finding increasing number of applications in industry, environmental monitoring, medicine and chemical analysis. Optical sensors can measure physical or chemical quantities. Their development has been stimulated by advances in optoelectronic technology mainly for applications in telecommunication. Light sources (light emitting diodes, laser diodes, lamps etc.), photodetectors (photodiodes, photomultiplier tubes etc.), connectors and optical fibres can easily be adapted for sensing purposes. However, in some cases special optoelectronic elements should be used.

The signal conversion, occurring in the fibre optic chemical sensors (FOCS), proceeds in several steps, which are shown in Figure 1.

Since the number of analytes exhibiting their own spectral changes is very limited, it is necessary to match an appropriate reagent. The reagent should recognise the analyte and convert the information on its concentration into changes of optical properties<sup>1-5</sup> (e.g. absorbance, fluorescence, reflectance). The reagent is immobilised in the chemooptical interface, which is in contact with a sample under the test. The principle of operation and the performances (sensitivity, selectivity etc.) of an optical sensor depend on the chemooptical interface. This interface can be designed as a

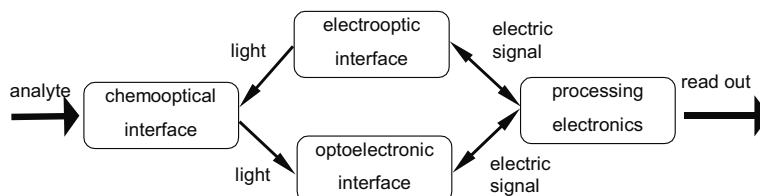


Figure 1. Signal conversion in fibre optic chemical sensor.

separate layer - membrane, which contains reagent molecules, held against the end of a single fibre optic or bundle<sup>1</sup> (so-called extrinsic sensor). In the second group of the sensors, the reagent phase is directly incorporated into the structure of fibre optic e.g. it replaces the removed cladding<sup>1</sup> (so-called intrinsic sensors) or it is immobilised in the porous sol-gel cladding. The exciting beam of light is delivered by the electrooptic interface (there is no such an interface in the case of a chemiluminescent sensor). Its main part is an appropriate light source, which is matched to the maximum of absorbance or excitation of the reagent. After having interacted with the chemo-optical interface, this light is converted into an electrical signal by the optoelectronic interface, which contains a photodetector (e.g. photodiode) and an amplifier. Both optoelectronic and electrooptic interfaces can be driven by the processing electronics. Contemporary measuring systems are based on the use of microprocessors (microcomputers) and they give a direct read out after applying a calibration of the sensor and/or additional signal processing.

The aim of this tutorial is to present briefly some of the optoelectronic elements, which can be used for designing of the interfaces for FOCS. More details on optoelectronic devices can be found in the references<sup>6-8</sup>. Special attention is placed on the appropriate spectral matching of these elements in order to obtain a sensor exhibiting optimal measuring properties such as dynamic range, sensitivity etc.

## 2. OPTICAL FIBRES

The main requirement of the fibre used in a sensor is to guide the light to and from an optrode. Multimode fibres are the most frequently used in chemical sensors (according to ref.<sup>4</sup> around 70 %). Single-mode fibres are used only in 5% of sensors whereas planar waveguides are applied in 25 % of constructions. The practical dominance of multimode fibres is due to the wide range of optoelectronic devices available on the market and their capability to transmit light over short and medium distances. In chemical sensors, standard telecommunication fibres can be used, with typical diameter of 125  $\mu\text{m}$  (50  $\mu\text{m}$  core), as well as large size fibres up to 1.5 mm. Bundles of the multimode fibres are assembled from fibres of diameter approx. 40-50  $\mu\text{m}$  with very thin cladding. The diameters of plastic fibres vary from 0.25 to 1.5 mm.

The attenuation of an optical fibre results from physical phenomena either occurring within the fibre or coming from the environment. This is the sum of light lost by scattering in the fibre, absorption by the fibre materials, leakage of light out of the core due to environmental factors (e.g. microbends). Scattering and absorption losses dominate in every fibre.

Standard silica telecommunication fibre exhibits several minima of the attenuation (so-called transmission windows): 0.8, 1.3 and 1.55  $\mu\text{m}$ . Special

attention should be paid in the systems utilising UV radiation. Typical silica fibres exhibit quite a high attenuation at this region and quartz optical fibres should be used in this case. Plastic fibres have much higher losses comparing to the silica fibres. Nevertheless, plastic fibres are much more elastic and are frequently used in the medical sensors. Their high acceptance angle (NA) allows to couple relatively high optical power. Additional advantage is the low weight, low cost and flexible choice of refractive index (1.35 – 1.6). Due to their high attenuation only a short optical links are made, mainly in visible range. A sensor designed for the application in infrared radiation should be based on special fibres e.g. fluoride, chalcogenide. Such fibres are used, for example, in gas sensors.

## **2.1 Connectors**

The attenuation of a light transmitted in a sensor system is caused not only by the fibre. Very important are also interconnections: component (e.g. light source) to fibre, fibre to fibre, and fibre to component (e.g. photodetector). The connectors can be made in various forms depending on specific requirements. They can be grouped into three main classes:

- (a) demountable connectors: fibre to fibre, fibre to light source, fibre to photodetector;
- (b) splices – permanent joints between two fibres;
- (c) couplers for distribution of the light between fibres.

The primary requirement for making any connection is to minimise the optical power that is lost in it. Intrinsic losses result from technological variations of the fibres to be connected i.e. core area mismatch, numerical aperture mismatch, and profile mismatch. These obvious errors can only be omitted by proper matching of connected fibres or additional optical elements should be used. Contrary to the intrinsic losses, extrinsic ones can be corrected by a mechanical alignment. Extrinsic losses are caused if ends of the fibres are in some distance and the light from the input fibre cannot be collected by the sink fibre. A similar situation with power losses occurs in lateral displacement and angular misalignment.

In connectors light source to optical fibre, power losses result from different space characteristics of the light source and the fibre. Each light source emits a beam in its typical shape whereas a fibre can accept only these rays within the acceptance cone. Some typical losses are presented in Figure 2.

The incoming light reflects from the end surface of a fibre, which is caused by the difference in refractive indexes of a fibre, a light source and a gap between them. Such losses are usually small as compared with other losses occurring in the system. The losses caused by different numerical apertures cannot be avoided. As higher NA of the fibre, as lower losses of

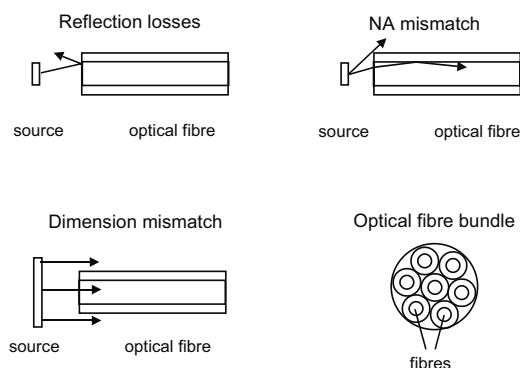


Figure 2. Different sources of optical power losses in source to fibre connectors.

the connection. A serious problem arises from the dimensions of the light source and the fibre. Usually dimensions of the source are much higher than the fibre and it becomes necessary to use transforming optics.

When the fibres are assembled into a bundle, another type of losses occurs. Each fibre consists of the core and the cladding and the latter should be kept as thin as possible so as much light as possible can be transmitted by the light-carrying cores. The fraction of the core surface per unit area is called packing factor and it depends on diameter of core, cladding and gaps between the fibres.

A fusion splice is a connection in which minimal losses can be obtained. Such a connection is made in a fibre optic splicer (usually controlled by a computer). Two fibres are put into an electric arc where they melt and create a low-loss splice. The splice obtained must be covered with a protective layer in order to prevent the junction from the damage and from the influence by the environment.

In fibre optic systems, it is often necessary to divide the light emitted by a light source or to use some part of the light as a reference channel for monitoring of possible fluctuations of the source. This can be done by means of traditional optics such as mirrors, prisms, lenses etc., and precise micropositioners should be used for adjustment. The alternative solution is an optical fibre coupler. The primary requirement is to put two or more fibres close together in order to allow exchange of optical power between the fibres. There are several ways to fabricate such a device: by polishing the fibres up to a half and joining them or by etching fibres. The most efficient method is based on melting of the fibres. The optical fibres, with removed claddings, are twisted and heated over a gas flame. During this process, the fibres melt to finally form a common region where optical signal is split into separate fibres.



### 3. LIGHT SOURCES

An integral part of a fibre optic sensor is the light source. Its primary task is to deliver an appropriate light, which possesses such features as: an optical power suitable to interact with an analyte or an indicator from the optrode, a wavelength matched to the spectral properties of the sensors in order to obtain the highest sensitivity, and, in dependence on the construction of the sensor, polarisation, short pulse etc. There are many various light sources utilised in the fibre optic chemical sensors. They differ in spectral properties, generated optical power and coherence.

Considering the spectral bandwidth of the light sources, they can be classified into three main groups:

- a) monochromatic (lasers, laser diodes);
- b) pseudomonochromatic (light emitting diodes);
- c) continuous (incandescent lamps, arc lamps).

The comparison of spectral properties of typical continuous light sources is presented in Figure 3.

Incandescent and gas discharge lamps are called white light sources because they emit light in a very broad spectral range. Figure 3 shows three of them, which are the most frequently used in the chemical sensors. A xenon arc lamp seems to be the universal light source. It emits radiation starting from UV up to infrared but it is expensive and the optical power is not very stable. If a sensor needs to be excited only in the UV range, a deuterium lamp can give better results. This is a relatively short-lived lamp (1000-2000 h) and quite expensive. Tungsten halogen lamps are much cheaper than the previously mentioned types. Powered by a relatively simple power supply, they emit stable optical signal and have long lifetime.

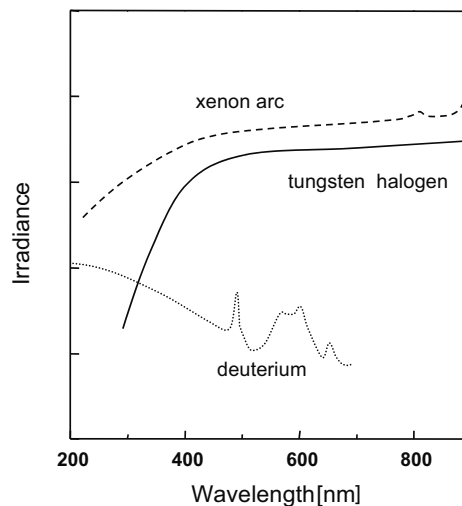


Figure 3. Emission spectra of continuous light sources used in sensors.

One of common disadvantages of these light sources is the necessity of using a wavelength-selecting device. Absorption filters, interference filters or monochromators are utilised to match the light to the sensor requirements. Absorption filters can filter out a wavelength with spectral bandwidth of the order of 50 nm, whereas interference filters produce much more monochromatic light (1 nm) but they introduce quite a high attenuation to the system. The necessity of using filters limits the application of the whole sensor system. When a sensor with a different analytical wavelength should be designed, the filter must be replaced. The application of a monochromator is more flexible. With its use, any wavelength can be selected very smoothly to match exactly the analytical radiation, but they are quite expensive.

Frequently a modulation of light is introduced to the system in order to increase the signal to noise ratio. Flash lamps by their construction give pulses of light with repetition, which can be controlled by the user. Other lamps cannot be modulated through their driving current because the emitted radiation would be unstable over time. In this case, the application of an external modulator, e.g. a mechanical chopper, is the only solution. In both cases, the frequency of modulation is rather low – up to kilohertz.

Light emitted by an LED is nearly monochromatic (pseudomonochromatic). LEDs are robust and their lifetimes are more than 100 000 hours. Spectral characteristics of exemplary LEDs in comparison with laser diodes (LD) are shown in Figure 4.

A typical spectral bandwidth of LED is within the range of 20-50 nm (it varies from type to type and is the lowest for superluminescent diodes - 5 nm). LEDs cover the whole visible range starting from 370 nm up to infra red radiation. The radiation emitted by an LED depends on the

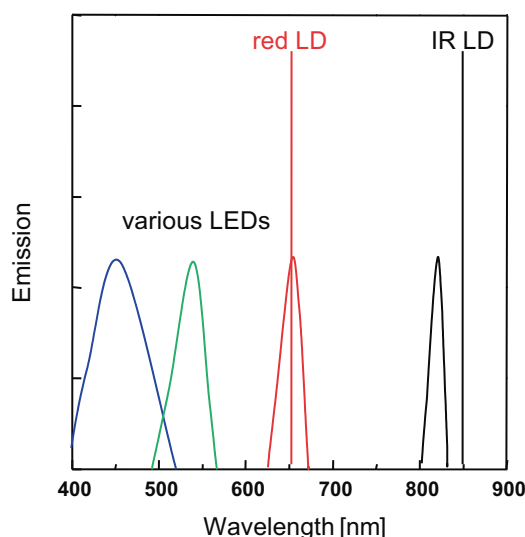


Figure 4. Emission spectra of LEDs and laser diodes.

semiconductor used for its fabrication. III-V compounds from periodic system are used in LEDs fabrication. Their band-gap can be changed depending on the composition of the compound. Various compounds of gallium, arsenic and phosphorus with zinc, oxygen or nitrogen dopands produce radiation in the visible range, whereas gallium arsenide doped with either silicon or zinc gives infrared wavelengths (900-1020 nm). The emitted optical power can be stabilised or LED can operate in a pulse mode. Their long lifetime, low cost and small dimensions are additional advantages in designing the sensor.

Semiconductor laser diodes are widely used in CD players, DVDs, printers, telecommunication or laser pointers. In the structure, they are similar to LEDs but they have a resonant cavity where laser amplification takes place. A Fabry-Perot cavity is established by polishing the end facets of the junction diode (so that they act as mirrors) and also by roughening the side edges to prevent leakage of light from the sides of the device. This structure is known as a homojunction laser and is a very basic one. Contemporary laser diodes are manufactured as double heterojunction structures.

The laser radiation produced by an LD can be modulated by the driving current and allows a very simple instrumentation. The emitted light beam is coherent and highly monochromatic. Usually, during manufacturing process, additional optical elements are introduced into a laser diode structure or case. For example, a grating can be imposed on the laser cavity or used as the rear mirror to make a wavelength favoured over the others. A photodiode placed in the case behind the structure gives a feedback signal for optical power stabilisation.

Monochromatic light can also be obtained from other types of lasers: solid state, gas, ion, dye. Among them argon ion laser with its many lines is an especially valuable light source used in many sensors. However, these types of lasers are expensive, the modulation of the light cannot be done internally and external modulators (e.g. choppers) should be used. Wavelengths emitted by some exemplary lasers are presented in Table 1.

Table 1. Various types of lasers.

<i>Laser</i>	<i>Emitted wavelength [nm]</i>		<i>Comments</i>
solid state	ruby	694.3	harmonic generation based on NL materials
	Nd:YAG	1064	
gas	atomic HeNe	633	many lines possible
	Ar-ion	275-514	many lines possible
liquid dye	Rhodamine 6G	546-640	many lines possible depending on pump source
	Coumarin 102	453-520	

#### 4. PHOTODETECTORS

The primary task of a photodetector in any fibre optic sensor is to convert the light carrying the information about the measurand into an electrical signal. The light, having interacted with the analyte or indicator, carries the information about the presence or concentration of the analyte. In fact, the process of conversion takes place in an optoelectronic interface as a whole optoelectronic system, because the photodetector is usually combined with optical elements (lenses, filters) and amplifiers. The work of optoelectronic interface can be synchronised by a modulation wave driving the light source. Key considerations in selecting a detector are the required sensitivity, the level of noise inherent in the detector (and thus the signal to noise ratio), spectral sensitivity, linearity, response time etc.

Photomultiplier tube (PMT) being the most sensitive device is capable to detect single photons. The photon of incident light produces on the photocathode an electron, which is then accelerated towards first dynode where secondary electrons are generated. The process of electron generation and their acceleration continues up to the anode resulting in a huge number of electrons. In this way, a single photon, generating a single photoelectron at the first stage, is multiplied by a given factor. One of the major parameters of PMT is its quantum efficiency (QE). The QE shows the ratio of photons incident on the PMT to electrons emitted from the photocathode and can be considered as the intrinsic sensitivity of a PMT to light.

The material used for manufacture of photocathode governs both the sensitivity and the spectral range of the PMT. The spectral characteristics of PMTs are presented in Figure 5.

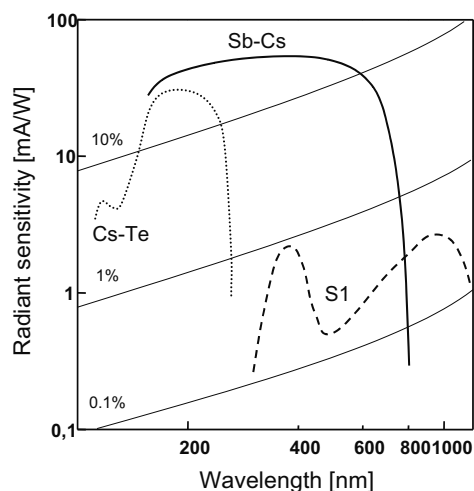


Figure 5. Spectral characteristics of different PMTs (solid thin lines mark quantum efficiency).

Typical PMTs are made in a form of glass tube, which make them mechanically fragile and relatively bulky (although there are some miniaturised versions). The linear response range of a typical PMT is up to about four orders of magnitude.

Quantum photodetectors are based on the use of a semiconductor. Upon the light interaction, changes in conductivity or changes in generated voltage are observed. The most popular quantum device is a photodiode. The incident light generates additional carrier pairs (hole and electron) in the p-n junction causing the increase of the current, which rises in proportion to the intensity of the light. The pin photodiode is a compact, monolithic device, which is many times smaller than the PMT. Although there are some constructions of photodiodes integrated with an operational amplifier in one case they are rather suitable for medium to high level light measurements. A serious limitation of pin photodiodes is their noise base that is typically three orders of magnitude higher than that of a PMT.

Avalanche photodiode (APD) was a response of the producers in competition between PMTs and semiconductor devices. It combines the benefits of both pin photodiodes and PMT, exhibiting the internal gain. A strong internal electrical field is created inside the APD by connecting it to a high reverse bias voltage. This field accelerates the electrons through the diode structure and thus secondary electrons are produced by impact ionisation. A special avalanching region can cause the increase of the gain factor up to several hundred.

The spectral properties of a photodiode depend on the material used for its fabrication. Typical characteristics are presented in Figure 6.

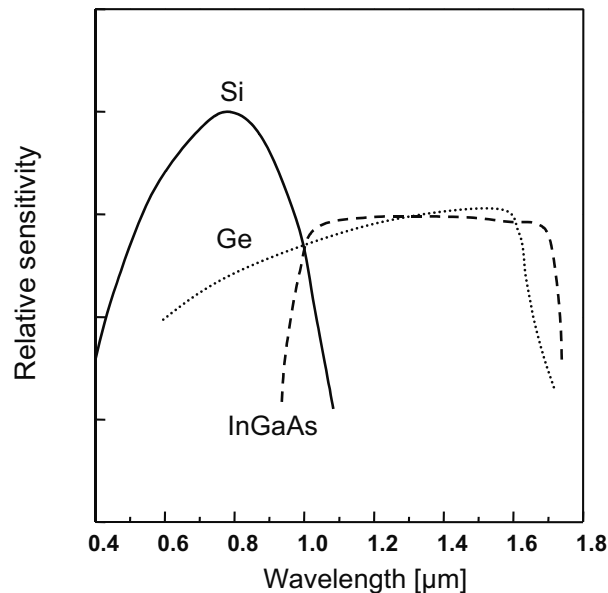


Figure 6. Spectral characteristics of photodiodes made from various semiconductors.

Silicon photodiodes exhibit maximum sensitivity at about 800 nm and they can be used in the whole visible range however their sensitivity drops by several times at the blue region. Special structures can be made with enhanced blue sensitivity (so-called blue or UV diodes). Germanium photodiodes are capable to detect radiation from 600 nm up to 1700 nm. In telecommunication applications InGaAs elements are widely used.

Charged coupling devices (CCD) made in a form of linear array are applied in multiwavelength detection or made as a matrix (e.g. 1024x1024 pixels) are used in cameras. A single CCD pixel is a metal-oxide-silicon capacitor. A p-type silicon substrate has an insulating silicon dioxide layer, on the top of which there is a metal electrode (gate). After connecting a bias voltage, holes move away from the depletion region and thus a potential energy well is created. The incident light generates electrons, which are next accumulated in this well. The charge accumulated is proportional to the light detected. The single CCDs are connected in an array or matrix and varying the bias voltage the charge is shifted to the next pixel resulting in a read-out signal. Such devices are used in miniature fibre optic spectrometers offered by various manufacturers.

## **5. SPECTRAL MATCHING OF OPTOELECTRONIC DEVICES**

The first step in the design of the chemical sensor is the chemical matching of the reagent molecules to the analyte to be measured (or determination of spectral properties of the analyte in case of a reagent-less sensor). The following step includes the attachment of the reagent phase to the optical fibre by producing a chemooptical interface. After having immobilised the indicator, it is necessary to determine the spectral properties of the optrode, and to choose the wavelengths, that should be used in the system. For the sensors based on the absorbance indicators, these are the analytical and the reference wavelengths i.e. where no absorbance changes occur, for the fluorescence sensors – the excitation and the emission wavelengths. These investigations allow to match an appropriate light source and a photodetector. The choice of an optical fibre is more flexible. The essential factor in matching the fibre is the attenuation at a given wavelength.

The whole measuring system is constructed in stages, with strong feedback between specialists from various science disciplines. The work of a contemporary system is governed by a personal computer where software is a very important component. User-friendly software should allow modifications during the measurements (voltage ranges, sampling frequency etc.) as well as a calibration process of the sensor. An additional advantage

of the system will be a computer controlled chemical equipment (e.g. a burette, a pump, a stirrer, valves etc.) for sample dosing and the sensor calibration.

## 5.1 Design Example

The selection of a light source, a photodetector and an optical fibre should be compatible with spectral properties of the indicator used. A typical spectrum of a pH indicator is presented in Figure 7-left.

There are several characteristic wavelengths on the graph. At the wavelengths denoted  $\lambda_1$  and  $\lambda_3$  two tautomeric forms of the indicator absorb the light. The application of  $\lambda_3=522$  nm allows to construct a sensor of the highest sensitivity. If the  $\lambda_1=410$  nm would be chosen, the dynamic range of the sensor would be smaller (compare appropriate calibration curves in Figure 7-right). Two others wavelengths,  $\lambda_2$  and  $\lambda_4$ , can be chosen as reference ones since no absorbance changes are observed. The first one results from the isosbetic point of the indicator (approx. 470 nm). However, the temperature influences on this point and it is safer to choose the reference wavelength from the infrared region. The indicator presented in Figure 7 is very compatible with LEDs. To obtain any of the mentioned wavelengths, an LED can be selected from a variety of commercially available elements. This will reduce the total cost of the system and will make it more portable. If another indicator would be used, the situation may be not so lucky. Then an LED emitting radiation close to the analytical wavelength has to be used. In such a case, we utilise the fact that LEDs do not emit strictly monochromatic radiation. As a consequence of the LED-indicator mismatch, a decrease of dynamic range will be observed.

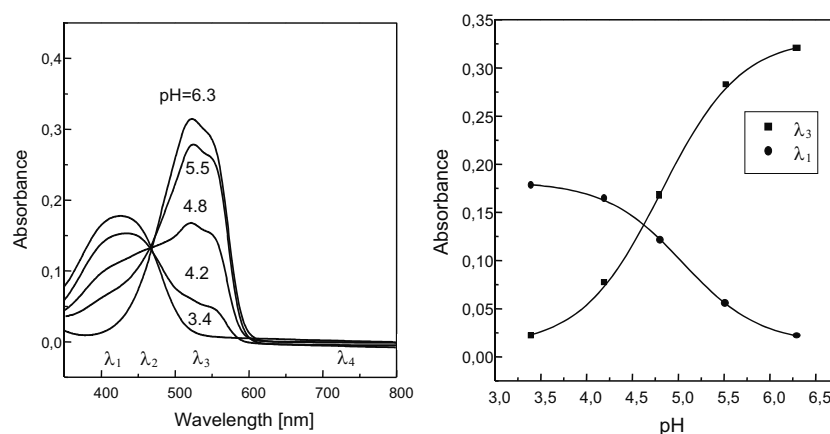


Figure 7. Left: absorbance spectra of pH indicator as a function of pH; right: calibration curves of the sensor obtained at different wavelengths.

The construction of the optoelectronic interface can be based on a silicon photodiode since analytical and reference wavelengths are from the visible and the IR regions, respectively. The signals can be filtered out by optical filters (then two photodiodes are required) or one photodiode can be synchronised with modulation waves of the LEDs used. Finally, silica optical fibres can be used as light waveguides. The choice between single fibre or bundle is determined by the application of the sensor.

## 6. CONCLUSIONS

Having constructed the optrode, it is very important to match the optoelectronic devices with respect to their essential parameters: light source (wavelength range, optical power, stability), photodetector (spectral response, sensitivity, noise) and optical fibres (attenuation as a function of wavelength). All these components and the indicator used should be compatible spectrally. Sometimes a compromise should be reached e.g. when there is no commercially available light source emitting the given analytical wavelength.

Successful development of fibre optic chemical sensors requires the co-operation of many specialists in various fields of science. Scientists in analytical chemistry, polymer science, material science, optoelectronics and electronics etc. can be involved in this multidisciplinary task. Depending on the application of the sensor biologists, medical doctors or environmentalists can also be incorporated to the working group. Although, the contribution of all specialists cannot be classified by the importance, analytical chemistry and material science seem to be the key to the success.

## REFERENCES

1. Seitz W.R., *Crit. Rev. in Anal. Chem.* 1988; 19: 135.
2. Wolfbeis O.S., *Fibre optic chemical sensors and biosensors*, Vol. 1 and 2. Boca Raton FL: CRC, 1991.
3. Wis D., Wingard L.B., *Biosensors with fibreoptics*. Clifton, New Jersey: Humana Press, 1991.
4. Boide G., Harmer A., *Chemical and biochemical sensing with optical fibres and waveguides*, Boston – London: Artech House, 1996.
5. Spichiger-Keller U.E., *Chemical Sensors and Biosensors for Medical and Biological Applications*, Weinheim: Willey-VCH, 1998.
6. B.Culshaw and J.Dakin (ed.), *Optical fiber sensors: Components and subsystems*, Vol.3, Artech House, Boston – London, 1996.
7. Culshaw B and Dakin J., *Optical fiber sensors: Applications, analysis, and future trends*, Vol.4, Boston – London: Artech House, 1997.
8. Hecht J., *Understanding fiber optics*, Upper Side River, N.J.: Prentice Hall, 1999.



## Chapter 4

# OPTICAL FIBRES FOR OPTICAL SENSING

Ivan Kasik, Vlastimil Matejec, Miroslav Chomat, Milos Hayer  
and Daniela Berkova

*Institute of Radio Engineering and Electronics  
Academy of Sciences of the Czech Republic  
Chaberska 57, 182 51 Prague 8, Czech Republic*

### 1. INTRODUCTION – FIBRE-OPTIC SENSORS

Optical sensors (Figure 1) can be defined as devices for optical monitoring of physical parameters (pressure<sup>1</sup>, temperature<sup>2</sup>, etc.) or (bio)chemical properties of a medium by means of optical elements (planar optical waveguides or optical fibres). Chemical or biochemical fibre-optic sensors<sup>3</sup> are small devices capable of continuously and reversibly recording the concentration of a (bio)chemical species constructed by means of optical fibres.

The capability of remote sensing, high sensitivity in a wide dynamic range, on-line performance, immunity to electromagnetic interference, possibility of internal reference<sup>4</sup> and potential of fully distributed sensing along the fibre length as well as the possibility of point or multipoint detection belong undoubtedly to advantages of fibre-optic chemical sensors. The geometry and material properties of optical fibres make them

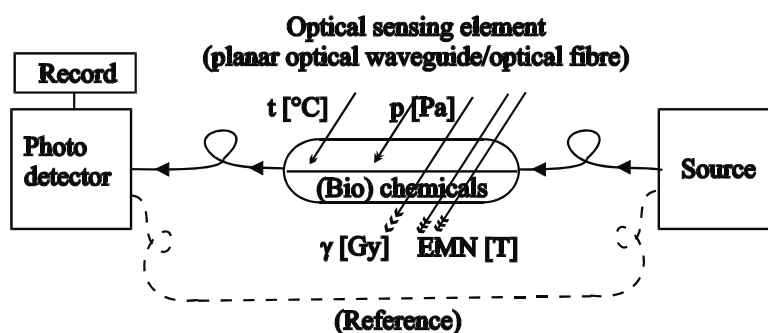


Figure 1. Principal arrangement of fibre-optic sensors.

indispensable tools for sensing in medicine<sup>5-7</sup> (see chapter 20), because they can be applied in all parts of the human body, for the detection of explosives or easily flammable substances (like hydrogen, petrol etc.)<sup>8</sup> as fibre probes eliminate the risks of overheating or sparking, and for operating in high-voltage facilities due to their dielectric character. On the other hand, certain limitations as e.g. contingent photodegradation of samples, limited performance in harsh (e.g. dusty, suspension) environments, effects of parasitic signals occurring due to light scattering in the medium, unwanted background fluorescence etc. should also be mentioned.

Optical information (signal) about the fibre surroundings can be obtained as intensity changes<sup>4</sup> (based on the number of photons transmitted after absorption or emitted by luminescence, scattering or refractive-index changes) (see chapters 5, 6 and 9), wavelength changes (based on spectral-dependent variations of absorption or fluorescence), phase changes (based on the interference of light waves between separate paths in interferometry) (see chapter 11), changes of the state of polarisation and changes in the time domain (lifetime, decay of fluorescence). Despite the diversity of the mentioned principles, each fibre-optic sensor employs the same fundamental parts: a source (see chapter 3), an optical sensing element (fibre) and a photodetector together with recording device (Figure 1). These components form the “optical hardware” of the sensor. By a proper choice of the optical hardware, the selectivity, sensitivity and time response of the sensor can be tailored. In cases when the chemical changes are accompanied by a strong optical response (e.g. a spectral or refractive-index change), the optical information can easily be obtained directly. In cases when the optical responses are too weak, opto-chemical transducers<sup>9</sup> can be applied to enhance the sensor response. The transducers are materials that change optical properties of the fibre (optical absorption in the case of using indicators or dyes, emission in the case of using fluorescent dopants) in dependence on the character of the analyte or its concentration. In this sense (i.e. the choice of analytical principle or of opto-chemical transducers) we can speak about the “chemical software” of the sensor. By a proper choice of the chemical software, the selectivity and sensitivity of the sensor can be tailored.

The place, where the surroundings (analyte) interacts with the guided light, is called the detection site. The sensors, in which the detection site is outside the fibre and the fibre is used only passively to lead the light to and from the sensing element, are denoted as extrinsic. When the fibre itself acts as an active sensing element and the detection site is inside the fibre, we speak about intrinsic sensors. Optical information can be obtained either from the light transmitted through the fibre (Figure 1) or from the reflected light (Figure 2).

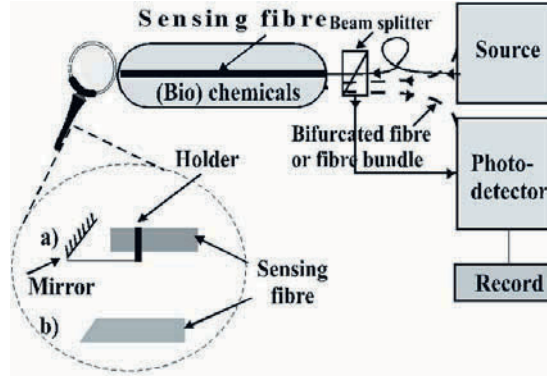


Figure 2. Arrangement for reflection sensing.

## 2. OPTICAL HARDWARE

### 2.1 Optical Fibres

Optical fibres (Figure 3) are dielectric, in most cases cylindrical structures, whose diameters are much smaller than their lengths, composed of an optical core ( $n_1$ ) surrounded by an optical cladding with a refractive index ( $n_2, n_3$ ) lower than that of the core<sup>6</sup>. The light is guided through the fibre as a result of total reflections on the core/cladding boundary. The claddings, having no optical but merely mechanical protective function, are denoted as jackets ( $n_4$ ).

Important parameters, characterizing fibre properties, are the attenuation  $\alpha$  and numerical aperture NA. The attenuation (Equation 1) represents optical losses caused by absorption or scattering of the light guided through the unit fibre length. It is given by:

$$\alpha = 10/L * \log (P_0/P) \quad (\text{Eq.1})$$

where  $P_0, P$  are the input and output optical powers and  $L$  is the fibre length.

The meaning of the numerical aperture (given in Equation 2) can be seen from Figure 4.

$$NA = (n_1^2 - n_2^2)^{1/2} = \sin (\beta/2) \quad (\text{Eq.2})$$

Optical fibres were originally studied and developed for the transmission of information in telecommunications and have been used for building of long-haul as well as local networks for years. Such kinds of optical fibres have to be of ultra-low optical losses, standard size, resisting to temperature changes in a large interval or to chemical influence of their surroundings, etc. In contrast to these “standard” widely used fibres, the “special” ones are

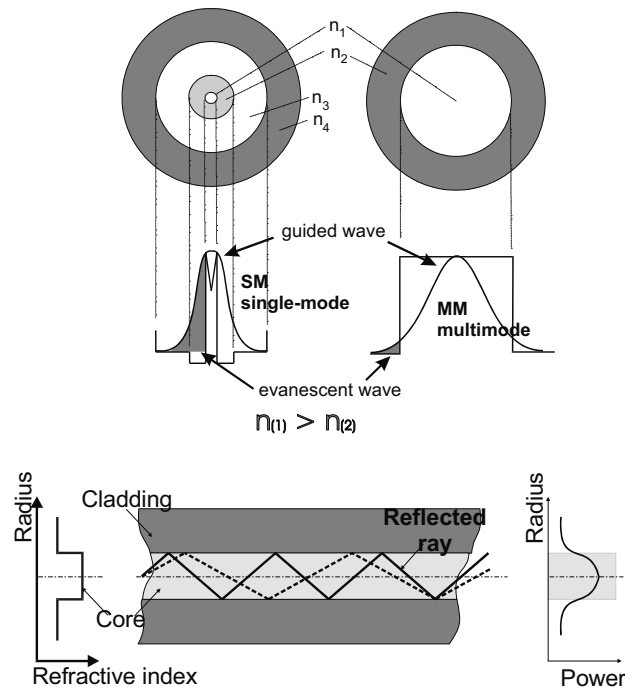


Figure 3. Principle of optical fibre.

employed not only for passive transmission of signals but also for the generation or processing of information, as in the case of fibre-optic sensors.

So the function of special optical fibres for sensing is to produce a sensitive response to changes in the fibre surroundings. Such requirements on optical hardware as durability to the analyte, transparency (i.e. minimum optical losses) in a wide spectral range and common availability should be pointed out. Related to these requirements, the choice of the fibre material as well as of the fibre coating and fibre structure belong to fundamental tasks in the design of fibre-optic sensors.

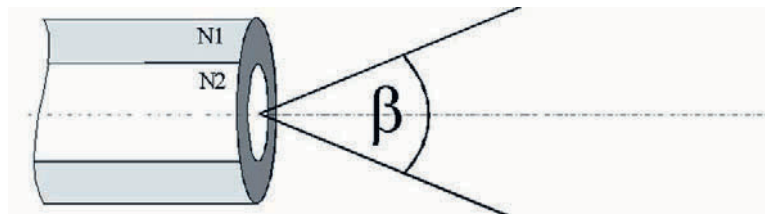


Figure 4. Illustration of the fibre numerical aperture.

## 2.2 Optical Fibre Technology

Optical fibres can be prepared from different materials in a variety of structures – circularly symmetric of different diameters, non-circularly symmetric, with different coatings. Optical fibres can be drawn or extruded from melts (crucible, double crucible techniques) or drawn from preforms (rods). The former technique is frequently applied for preparation of plastic fibres or fibres from soft glasses. The latter one is suitable for the preparation of silica-based optical fibres as it allows to save structures (e.g. graded-index profiles) previously tailored in rods-preforms by Chemical Vapour Deposition (CVD) technologies, e.g. MCVD<sup>10</sup>. This approach makes possible to prepare materials of ultra-high purity (as the starting materials are in the liquid or gaseous state and so they can be effectively purified) and multilayered structures (as the glass volume is formed via the deposition of a number of thin layers). In contrast to CVD technologies, melts are prepared from starting materials mainly in the solid state and so the level of purity of fibres drawn from them is by several orders worse. To reach suitable mechanical properties and to prevent effects of ageing, the fibres are immediately (in-line) coated with a protective polymer coating (section 2.5).

## 2.3 Optical Fibre Materials

Changes of fibre optical properties and thus changes of the analyte can be detected in the ultraviolet (UV), visible (VIS), near infrared (NIR) and middle/far infrared (IR) regions. There are only a few materials sufficiently transparent in the UV region, and among them, the pure silica is uniquely suitable for fibre drawing. From Figure 5 it can be seen that the UV

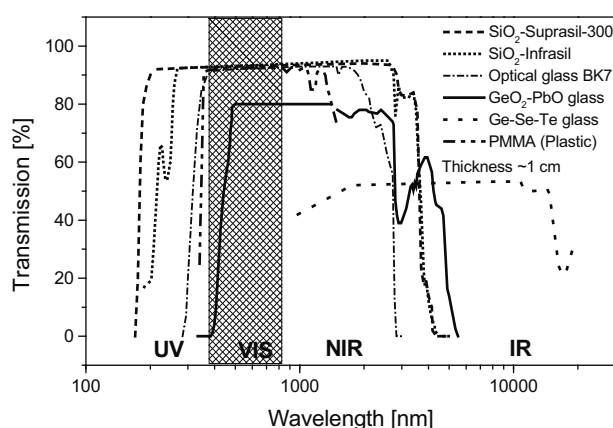


Figure 5. Spectral transmission of several kinds of materials.

absorption edge depends on the kind of silica and varies from approximately 170 to 260 nm.

From the spectral attenuation curve of an optical fibre drawn from Optran-UV (Figure 6) it can be seen that the losses are relatively high, but still acceptable (of the order of dB/m in the UV) for practical sensing. Refractive index of silica is 1.457 at 633 nm and falls down with increasing wavelength.

Most of optical fibres are transparent in the visible and NIR spectral regions. Among them, silica fibres are of extremely low losses (minimum of 0.2 - 20 dB/km, depending on the wavelength and structure). They are nearly ideal candidates for sensing as it is possible to prepare a variety of fibre sensing structures (section 2.4) via CVD technologies of preform preparation. The comparison of spectral transmission of bulk silica and other kinds of glasses can be seen from Figure 5. The spectral attenuation of a simple step-index fibre structure made from such bulk silica can be seen from Figure 6. The minimum optical losses at 850 nm ( $\sim 10$  dB/km) can be considered as suitable for sensing. Silica fibres are applicable in a spectral region up to 2  $\mu\text{m}$ . The refractive index of doped silica varies from 1.45 to 1.50 (at 633 nm) depending on the doping. Silica fibres are chemically and mechanically stable (tensile strength  $\sim 6$  GPa).

Close to silica fibres are silicate fibres drawn from optical glasses. Silicate fibres are typically applicable in the visible spectral region. Their optical losses in the visible region usually reach much higher values than silica fibres - at least  $10^2$  dB/km. On the other hand, the refractive index can be tailored in a large interval (from 1.5 for the BK-class to 1.95 for the

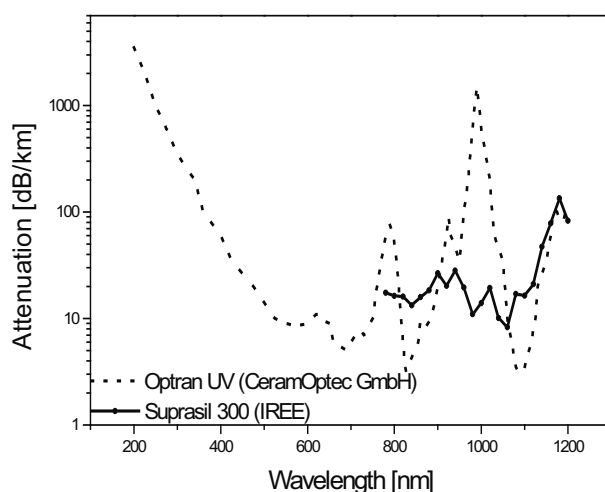


Figure 6. Spectral attenuation of PCS fibres drawn from silica (Optran UV and Suprasil 300).

SF-class<sup>11</sup>) by a proper choice of glass composition. This point is important for evanescent-wave sensing (see chapter 10) in cases when the refractive index of the analyte reaches higher values. Fibres from non-silicate oxide-based glasses such as germanate ones<sup>12</sup> are transparent further to mid-IR region but they are of lower chemical resistance and thermal stability.

Optical fibres composed of plastics are also transparent in the visible spectral region but optical losses reach  $10^2 - 10^3$  dB/km<sup>13</sup>. Their refractive index varies from 1.35 to 1.6 depending on the kind of polymer used (e.g. polymethylmethacrylate PMMA  $\sim 1.49$ ). The chemical resistance is much worse than that of silica fibres and thermal stability is incomparable. On the other hand, low temperature processes of plastic fibre preparation allow us mix the starting polymer with organic dyes which enables the production of luminescent fibres suitable e.g. for fluorescence-based sensing<sup>13</sup>.

Materials suitable for sensing in the IR region are fluoride glasses such as ZBLAN, ZBG or ZBLA, chalcogenide, or chalcogen-halide glasses such as pure glassy Se, As<sub>2</sub>S<sub>3</sub>, As<sub>2</sub>Se<sub>3</sub>, Ge-Se, Ge-S, Ge-Se-Te, Ge-As-Se systems<sup>14-16</sup>. A number of these materials are transparent up to 20  $\mu\text{m}$  and the theoretical losses of the fibres are even lower than those of silica fibres. But the lowest losses achieved in practice vary from 0.01 dB/m<sup>17</sup> to 4 dB/m<sup>18</sup> in dependence on wavelength. The fibre technology is rather complicated and maybe that for this reason these fibres are not so widely available as the silica ones. A certain exception among the glassy fibres represents silver-halide<sup>19</sup> or sapphire crystalline fibres that have recently been successfully employed for IR fibre sensing<sup>20</sup>. The refractive indices of glassy materials are usually high (e.g. from 2 to 2.5 for chalcogenides). Excluding fluoride glasses, these materials are chemically stable enough but their thermal stability is often low due to low  $T_g$ .

The availability and prices of sensor components (fibres as well as sources and photodetectors) can be considered key parameters for the sensor design. With some simplification it can be stated: the further from the VIS-NIR spectral region, where the technological basis is anchored in large-scale production for telecommunications, the higher the prices of all components. However, valuable results have been obtained in the IR region<sup>21</sup> (see chapter 7).

## 2.4 Optical Fibre Structures

The simplest case of fibre structure is the step-index one, characterized by a constant circular refractive index profile in the core and polymer cladding of lower refractive index (Figure 3). The refractive indexes of the core and cladding depend on the materials used. The cores of these structures can be prepared from melts as well as from preforms without radial and azimuthal variations of the refractive index. To obtain suitable mechanical

properties, the diameter of the fibre core should be 70-80  $\mu\text{m}$  at least. Due to this large value many modes can be guided through such a fibre and so the structure is called multimode (MM). The typical diameter of such fibres varies in a range from 200 to 1000  $\mu\text{m}$ .

Most of fibre-optic sensor applications (around 70% estimated<sup>22</sup>) are based on multimode structures, particularly on PCS (polymer-clad-silica) fibres, suitable for both passive and active applications in the visible and NIR regions. The PCS fibres consist of a high-quality silica core (produced e.g. by Heraeus, Corning Glass, Schott or Quartz et Silice etc.) with the refractive index of 1.457 (at 633 nm) and a thermally curable polysiloxane cladding with the refractive index of around 1.41 (at 633 nm). The PCS fibres have been successfully used for a variety of applications because of their common availability, low cost and good mechanical properties. Their experimental sensitivity<sup>23</sup> to the analyte refractive-index changes can be seen from Figure 7. The sensing principle based on the detection of refractive-index changes of an analyte can be applied only for the analytes whose refractive index is below that of silica, otherwise the fibre cannot act as a waveguide (Figure 3). For the detection of substances of higher values of the refractive index performed in this way it is necessary to use a step-index structure drawn from highly doped silica or from soft optical glass (PCG - polymer-clad-glass) of proper refractive index. In the second case the applicability of such fibres is limited to the visible spectral region. As an example, monitoring of the epoxide curing process (refractive index up to 1.58) sensed by a declad step-index fibre (drawn from optical glass SF2 with a refractive index of 1.62) inserted into the epoxy resin, can be given<sup>27</sup>.

From Figure 3 (distribution of the light power) it can also be seen that the largest part of the light in multimode structures is concentrated inside the fibre core and only a small part of it is in the region outside the fibre core,

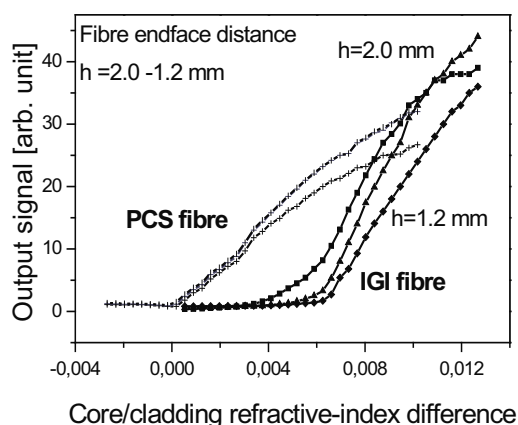


Figure 7. Experimentally determined sensitivity curves for IGI and reference PCS fibres.



where it can interact with the analyte. So the sensitivity of MM structures in the case of evanescent-wave sensing (see chapter 10) cannot be very high. To increase this sensitivity, novel multimode structures like inverted graded-index (IGI) fibres<sup>25-27</sup> have been designed and tested. The refractive-index profile of this kind of such structures is inverted with respect to the conventional ones (Figure 8). The development of the MCVD technology (section 2.2) has made it possible experimental preparation of such fibres. Comparison of the sensitivity of a conventional PCS fibre and IGI one excited under optimum conditions can be seen from the Figure 7. The concept of IGI fibres can be exploited for sensitive detection of hydrocarbons dissolved in water in ppm concentrations<sup>28</sup>.

When the core diameter is inside several microns, only one (or several) modes can be guided in the fibre core and so these structures are called single-mode or few-mode ones. Single-mode (SM) silica fibres have a typical outer diameter of 125  $\mu\text{m}$  with a 5-8- $\mu\text{m}$  diameter of the core and a

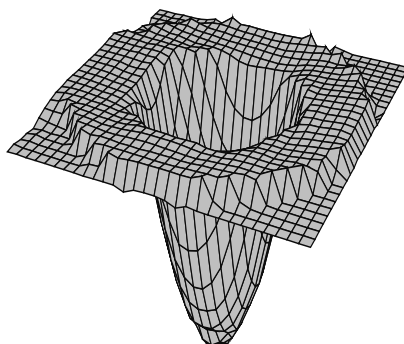


Figure 8. Refractive-index profile of the IGI structure.

refractive index difference between the core and cladding of 0.005-0.010. Few-mode fibres are of slightly larger core diameter. In single-mode structures the light power distribution (Figure 3) can significantly extend beyond the core area, however, mostly into the region with no direct contact of the light with the analyte (compact glass optical cladding). So, standard types of these fibres cannot be directly used for sensing purposes.

A possible solution to this problem is based on removing part of the glass cladding, which enables the interaction between the analyte, penetrating through the cladding, and the fibre core, while a large and robust part of the fibre is preserved. Such an approach is applied in the “D-shaped” fibres<sup>29</sup>. This type of structure makes possible the access of the analyte, which penetrates through the cladding to the fibre core of single-mode or few-mode structures, while their mechanical properties remain essentially unchanged. However, the detection site is limited to a longitudinal spot along the fibre length.

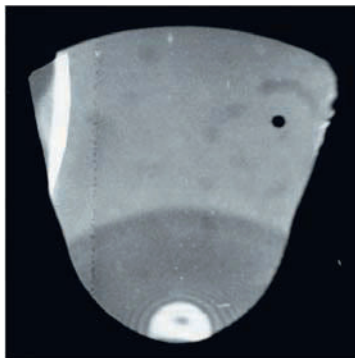


Figure 9. Sectorial S-fibre structure (microphoto), core diameter  $\sim 30 \mu\text{m}$ .

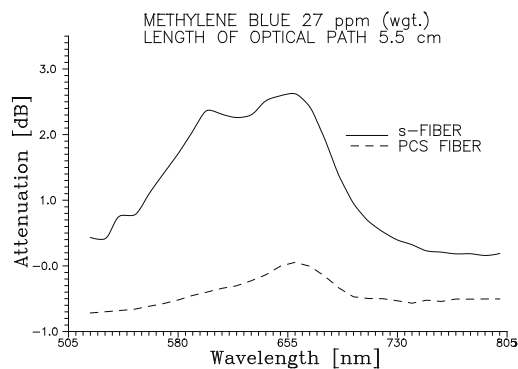


Figure 10. Spectral dependence of the attenuation of the s-fibre and PCS fibre in solution of methylene blue.

To enlarge the detection site and to improve the fibre sensitivity without using a longer active fibre length, the “S-fibre” structure (Figure 9) has been designed<sup>30</sup>. In this case a large part of the core is declad and can interact with the surroundings while the fibre remains robust enough and mechanically stable (in comparison with extremely brittle single-mode or few-mode PCS step-index fibres with a core diameter comparable with the size of the excitation beam, i.e. several microns). From Figure 10 it can be seen the comparison of spectral responses of PCS and S-fibres immersed into an immersion coloured with an indicator. But a drawback for practical use of these fibres should be noticed. After coating this structure with a circularly symmetric cladding, the position of the core becomes eccentric which makes splicing or connecting these fibres with the standard ones difficult.

To overcome this drawback, “capillary sectorial fibres” (Figure 11) were fabricated<sup>31</sup>. In this case part of the preform ground to the designed shape was inserted into a circularly symmetric silica tube and drawn. The active length of the sensor is defined by the distance between the input and output of the analyte produced in the capillary wall by special diamond tools. Despite promising results achieved, difficulties in the application of sensitive layers on the core surface remain a drawback of this kind of fibres and the

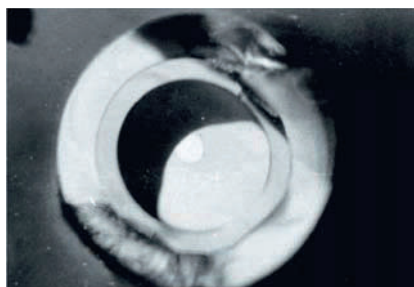


Figure 11. Structure of capillary sectorial fibre (microphoto).

necessity the sampling of analyte under overpressure represents certain complication.

Although single-mode or few-mode fibres represent useful “optical hardware” for chemical sensing, in practise there are only around 5% of sensor applications based on them<sup>22</sup>. It can be caused by complicated handling (coupling the light) due to a small core size or by slightly higher costs for the instrumentation in comparison with multimode structures.

At this point, hollow fibres should also be noticed as a special case of optical fibre structures<sup>32-33</sup> (compare Figure 3 with Figure 12). In the case when the hollow part is filled with an analyte of higher refractive index than that of the coated or uncoated inner surface of the capillary ( $n_1 > n_3, n_2$ ) the structure operates as a standard waveguide. This is the case of a sensor where the detection site is inside the core area. So the optical information is obtained from the guided wave that is much more intensive and sensitive to changes in comparison with the weak evanescent wave (see chapters 9 and 10). In the case when the inner surface of the substrate capillary ( $n_3$ ) is coated with a layer of higher refractive index ( $n_2$ ) than that of the flowing analyte ( $n_1$ ) as well as of the substrate ( $n_3$ ), the light is guided inside this circular ring ( $n_2$ ) and the structure is operated as a special kind of the evanescent-wave sensor<sup>34</sup>. Such fibres are drawn from substrate tubes of proper refractive index or from tubes with a specially coated inner surface by some (e.g. sol-gel) layer. There are also materials (sapphire, special oxide glasses, alumina), whose refractive index drops below the value of 1.0 in the far IR region (7-17  $\mu\text{m}$ ). Using these materials as claddings ( $n_2$ ) in the IR region, the hollow waveguide acts as a special kind of optical fibre with the

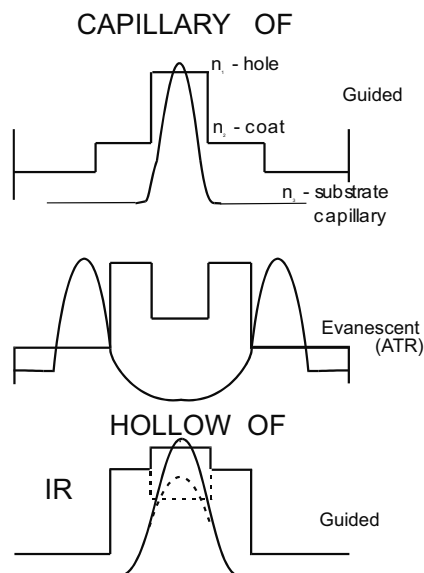


Figure 12. Capillary and hollow optical fibres.

detection site in the core. Such fibres were successfully applied e.g. for trace-level detection of halogenated hydrocarbons in the infrared region<sup>35</sup>.

## 2.5 Optical Fibre Coatings – Requirements

Optical fibre coatings represent an integral part of “optical hardware” as they make possible to tailor the access of the analyte to the detection site and to immobilize opto-chemical transducers in the detection site. The choice of suitable coating (and suitable transducer) is important task of sensor designing. The coating of standard SM fibres by hard UV-curable acrylates with a refractive index of around 1.65 or of PCS fibres by soft polysiloxane polymers can be considered a standard procedure, while the coating of fibres with PTFE ( $n_D=1.29$ ) primary coating is not so usual. Only several items of requirements important for optical fibre technology will be noticed here as the attention to this issue is given elsewhere (see chapter 15).

Transducers have to be miscible with starting materials for coating (monomers etc.), should be stable (especially during the curing process) and have a strong and selective colour or absorption response to the detected substance. Starting materials for coatings can be characterized as liquids with good adhesion to the substrate fibre surface, stable enough before curing, of proper viscosity and easily curable (thermally, by UV irradiation etc.) The cured coatings should be porous to a certain controllable degree to make possible penetration of analytes to the fibre core, adhesive with the fibre, stable and hydrophobic. Refractive index of the coating should be lower than that of the core, nevertheless special coatings of higher refractive

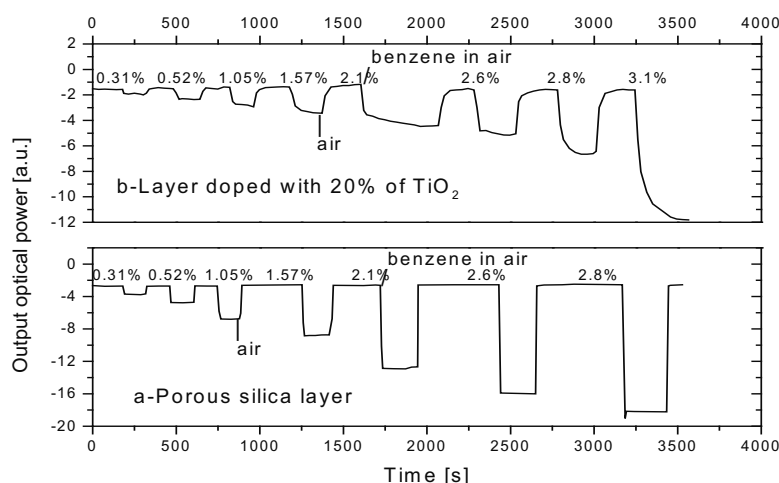


Figure 13. Influence of  $\text{TiO}_2$  doping of the coating on the time response of the sensing fibre.

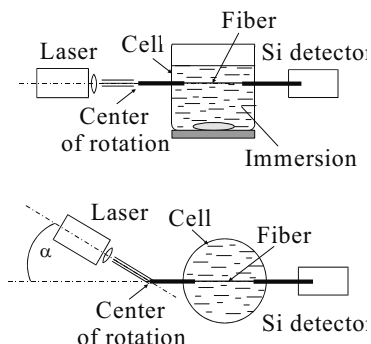


Figure 14. Comparison of arrangements for selective (left) and axial (right) excitation introducing an increase of sensitivity for several times in comparison.

index have been applied, too<sup>36</sup>. In such a case the coated layer can be considered part of a multilayer core and the fibre can be used for core-based detection, but it is a very tricky matter. Coatings can be applied continuously (directly) in the process of fibre drawing (section 2.2) or short pieces of fibres can be coated additionally by the dip-coating method.

From Figure 13 it can be seen a typical example demonstrating the influence of the properties of the fibre coating on fibre sensing properties.

Apart from the optimisation of properties of sensing fibres themselves, the arrangement of optical hardware, i.e. the conditions of excitation and detection, play an important role influencing the selectivity and sensitivity of the sensor. As examples, the selective excitation (Figure 14) with the axial excitation or the detection with an output mode filter<sup>30</sup> can be presented (Figure 15, Figure 16).

## 2.6 Optical Fibre Processing and Accessories

The preparation of a coated special fibre from a suitable material in a proper structure and the source and detector choice are not the final list of problems to be solved in the framework of sensor design. From Figure 3 it

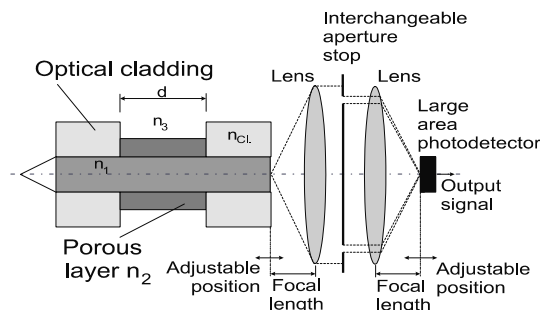


Figure 15. Arrangement of output mode filter.

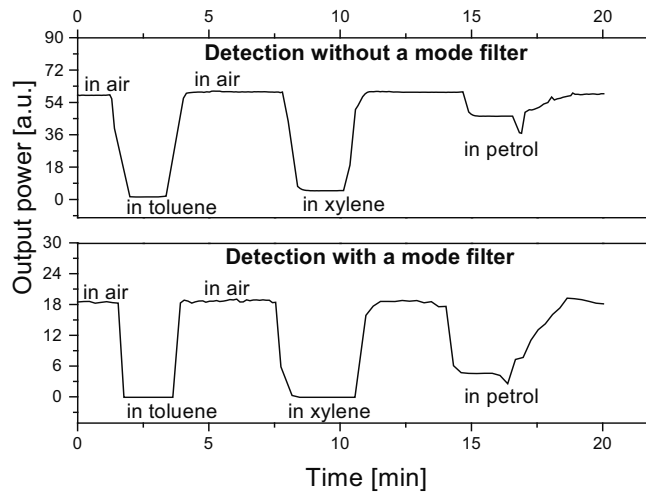


Figure 16. Time response of a bent PCS fibre to liquid hydrocarbons and petrol with and without the output mode filter.

can be seen optional loops of passive optical fibres coupling light from the source into the active fibre and guiding the obtained signal to the detector. In a laboratory set-up the connection of fibres can be effectively managed by means of a V-groove and micropositioners but such a solution is not suitable for field applications. In these cases fibres can be connected by splicing (by means of a splicing machine) or by connectors. Number of kinds of connectors for telecommunication fibres (FC, HMS-10, PC, D4, SMA, SC, DIN, ST etc.) is commercially available<sup>37-38</sup>.

Their common function is to hold the fibre and to align it with another identical size fibre with high repeatability in tolerances as close as possible (Figure 17). The main component of the connector is the ferrule made from

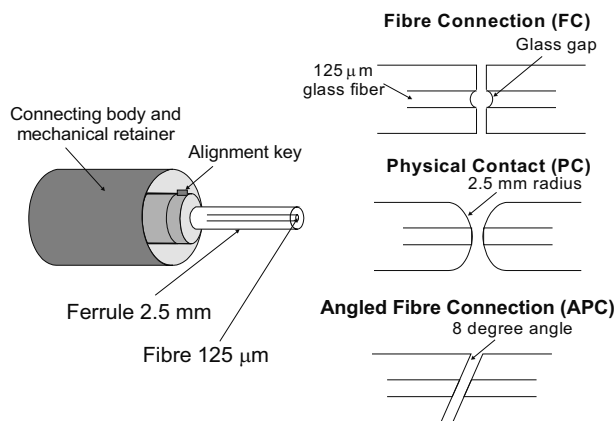


Figure 17. Fibre connector.

metallic or ceramic material (stainless steel,  $\text{Al}_2\text{O}_3$  or  $\text{ZrO}_2$ ). The ferrule holds the glass fibre, precisely centred. The alignment key keeps the fibre from rotating. Smooth end-face of fibre terminating is reached by careful polishing of the holding material of the ferrule together with the fibre end. The dimensions of the connectors have been standardised for fibre diameter of  $125\ \mu\text{m}$  and outside ferrule diameter of  $2.5\ \text{mm}$ . The differences between connector types are mainly differences in the mechanical assembly that hold the ferrule in position against another, identical one. For terminating fibres of larger diameter, usually prepared for sensing to ensure sufficient robustness, special connectors based on the modified parts have to be individually developed. For the case of joining the fibres of diameters different from standard ones, fibre tapers<sup>39</sup> could be also applied, but such solution is quite expensive.

In cases when the fibre ends play only a passive role, the fibre can be terminated for splicing or connecting by cutting, e.g. by means of a cutting knife. In cases when the fibre end plays an active role (Figure 2), the probe has to be carefully processed. The end-face of reasonable quality making an angle of  $90^\circ$  with the fibre axis can be obtained by cutting e.g. by means of a fibre cleaver. For bevelling of the cut fibre end, grinding by means of diamond tools or foils has to be applied. The end-faces obtained in this way (Figure 18) can be further processed by coating with sol-gel layers or layers applied by some PVD techniques. For better fixing of the sensitive layers on the fibre end-face, cavities can be formed. Such an approach can be useful particularly in the case of multianalyte detection or of optical noses (see chapter 19).

A single optical fibre cannot be a suitable tool for the last mentioned application as well as for many others arranged in the reflection layout. For these applications individual optical fibres are collected to sets – bundles. Such optical elements are particularly convenient for image transmission. In chemical sensing, fibre bundles can be employed for remote Raman, fluorescence or absorption spectroscopy<sup>4,40</sup>, for visualisation etc. The

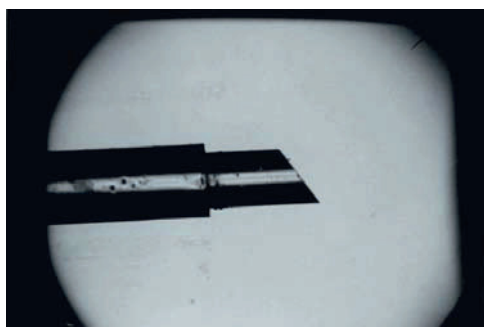


Figure 18. Bevelled fibre tip.

simplest Y-shaped twin fibre components are available as “bifurcated fibre assembly” or “splitter fibre assembly”<sup>37</sup>.

When the fibre cross-section is too large (e.g. for nano-scale applications) or for improving the fibre sensitivity in evanescent-wave sensing<sup>41</sup>, tapering of the fibre end can be used. At the fibre end the polymeric cladding is removed and then the solution of hydrofluoric acid is applied. The fibre is continuously and slowly withdrawn from the acidic bath, and if the etching process is well controlled and smooth enough, a tip of desired shape can be prepared<sup>42</sup>. Another way is to employ controlled elongation of the de-clad fibre end in a flame.

A certain group of optical sensors is based on gratings written into optical fibre structures. The gratings can be of a short period or the order of nanometres (Fibre Bragg Gratings – FBG), or of a long period on the order of tenths of a millimetre (Long Period Gratings – LPG). The gratings are written into the structure by irradiating the fibre by UV lasers (250, 190 or 380 nm) via masks (FBGs), or by scanning a high-power CO<sub>2</sub> laser beam across the fibre (LPG). The induced refractive-index perturbations depend on changes of the fibre internal strain and are related to differences of the expansion coefficients of the core/cladding glass materials and to the thermal shock during the laser exposure. To obtain gratings with strong index modulations, the fibres should be of specially tailored structures containing materials highly doped with germanium oxide.

### 3. FINAL COMMENTS

Special optical fibres have been intensively investigated during recent years because of their potential wide-range use for on-line monitoring of material properties or processes in a number of areas of human activity (environment protection, food industry, medicine etc.) Their technology can be considered an integral part of the team-work on optical fibre sensors development. Despite special optical fibres represent a unique and often indispensable tool for a variety of sensor applications, special fibre production still represents only a small fraction of the market. Probably it is because of their low consumption (in comparison with standard telecommunication fibres), the need for much more advanced know-how and lower reproducibility.

### ACKNOWLEDGEMENT

The authors wish to thank the Grant Agency of the Czech Republic for the financial support (contracts No. 102/02/0780, 102/03/0475, KSK 4074) of this work.



## REFERENCES

1. Mitchell G.L., A review of fabry-perot Interferometric sensors, in Optical Fiber Sensors, Proc.6th Int.Conf. OFS'89 (1989), H.J.Arditty, J.P.Dakin, R.ThKersten eds., Springer-Verlag, pp. 450-478.
2. K.T.V. Grattan, Fibre optic sensor technology, *Sensors & Actuators A* 2000; 82: 40-61.
3. Wolfbeis O.S., Reisfeld R., Oehme I., Sol-gels and chemical sensors, *Structure and Bonding* 1996; 85: 51-98.
4. Boisdé G., Harmer A., *Chemical and biochemical sensing with optical fibres and waveguides*, Artech House, 1996.
5. Baldini F., Bechi P., Bracci S., Cosi F., Pucciani F., In vivo optical-fibre pH sensor for gastro-oesophageal measurements, *Sensors & Actuators* 1995; B29: 164-168.
6. Miller S.E., Chynoweth A.G., *Optical Fiber Telecommunications*, Academic Press (1979), pp.167-226.
7. Bluenstein B., Walczak I., Chen S.Y., Fiber-optic evanescent-wave immunosensors for medical diagnostics, *Trends Biotechnol* 1990: 161-168.
8. Bevenot X., Trouillet A., Veillas C. et.al., Hydrogen leak detection using an optical fibre sensor for aerospace applications, *Sensors & Actuators B* 2000; 67: 57-67.
9. Brecht A., Gauglitz G.: Recent developments in optical transducers for chemical or biochemical applications, *Sensors and Actuators B* 1997; 38:1-7.
10. Nagel S., MacChesney J.B., Walker K., *IEEE J. of Quantum. El.* 1982; QE-18: 459-478.
11. *Optische Glas*, Schott catalogue.
12. Kasik I., Lezal D., Karel M., Zavadil J.: Germanate glasses doped with rare-earth, Proc. 5th ESG Conf. (1999), Prague, p.151.
13. Grattan K.T.V., Meggitt B.T., *Optical fiber sensor technology, Vol.4 Chemical and environmental sensing*, Kluwer Academic Publishers, 1999, pp. 205-248.
14. Hocde S., Pledel-Boussard C., Fonteneau G., Lucas J., TeAsSe glass fibers for evanescent wave spectroscopy, Proc. SPIE 3849 (1999), Boston.
15. Le Sergent C., Chalcogenide glass optical fibers, Proc.SPIE 799 (1987), pp.18-24.
16. Donald I.W., McMillan P.W., Infrared transmitting materials, *J.Mat.Sci.* 1978; 13: 1151-1176.
17. Poulain M., Advances glasses, *Annales de chimie-science des materiaux* 28 (2003) 87-94.
18. Hewak D.W., Taylor E., Payne D.N., Optical amplifiers and lasers in IR fibers, Proc.SPIE 3849 (1999), Boston.
19. Shalem S., German A., Barkay N., Moser F., Katzir A., Mechanical and optical properties of silver-halide infrared transmitting fibres, *Fiber and integrated optics* 1997; 16: 27-54.
20. Hahn P., Tacke M., Jakusch M., Mizaikoff B., Detection of hydrocarbons in water by MIR evanescent-wave spectroscopy with flattened silver halide fibres, *Applied Spectroscopy* 2001; 55: 39-43.
21. Schwotzer G. et. al., Optical sensing of hydrocarbons in air or in water using UV absorption in the evanescent field of fibers, *Sensors & Actuators B* 1997; 38: 150-153.
22. Dybko A., Fundamentals of optoelectronics, Proc. ASCOS 2000.
23. Matejec V., Kasik I., Chomat M., Ctyroky J., Berkova D., Huttel I., Modified inverted graded-index fibers for evanescent-wave chemical sensing, Proc. SPIE 3860 (1999), Boston, pp.443-451.
24. Chailleux E., Salvia M., Jaffrezic-Renault N., Matejec V., Kasik I., A fibre optic sensor for monitoring the polymer cure process, Proc. SPIE 4016 (1999), Prague, pp.136-142.
25. Matejec V., Chomat M., Kasik I., Ctyroky J., Berkova D., Hayer M., Inverted-graded

- index fiber structures for evanescent-wave chemical sensing, *Sensors & Actuators B* 1998, 51: 340-347.
26. Chomat M., Berkova D., Matejec V., Ctyroky J., Kasik I., The detection of refractive-index changes by using a sensing fiber with an inverted parabolic index profile, Proc. SPIE 3860 (1999), Boston.
  27. Bardin F., Kasik I., Trouillet A. et.al., SPR sensor using an optical fiber with IGI profile, *Appl. Opt.* 2002; 41: 2514-2520.
  28. M. Chomát, D. Berková, V. Matějec, I. Kašík, G. Kuncová, The effect of hydrodynamic conditions on the detection of aqueous solutions of toluene by means of an inverted graded-index fiber, *Sensors & Actuators B* 2003; 90: 151-156.
  29. Stewart G., Jin W., Culshaw B., Prospects for fibre-optic evanescent-field gas sensors using absorption in near-infrared, *Sensors and Actuators B* 1997; 38-39: 42-47.
  30. Matejec V., Chomat M., Pospisilova M., Hayer M., Kasik I.: Optical fiber with novel geometry for evanescent-wave sensing, *Sensors & Actuators* (1995) B 29, pp. 416-422.
  31. Matejec V., Chomat M., Hayer M., Berkova D., Pospisilova M., Kasik I., Improvement of the sectorial fiber for evanescent-wave sensing, *Sensors & Actuators B* 1997; 38-39: 334-338.
  32. Wilson S.J., Hollow core glass waveguides, Proc. SPIE 799 (1987), pp.54-60.
  33. Saggese S.J., Harrington J.A., Sigel G.H., Hollow waveguides for sensor applications, Proc. SPIE 1368 (1990), San Jose, pp.2-14.
  34. Doupovec J., Brunner R., Suchy F., Evanescent fiberoptic sensors based on capillary optical fibers, Proc. 3<sup>rd</sup> Europtrode (1996), Zurich, p.150.
  35. Murthy Ch.S., Pustogov V.V., Mizaikoff B., Inberg A., Croitoru N., Trace level gas detection using mid infrared hollow waveguides, Proc. 5<sup>th</sup> Europtrode (2000), Lyon, p.275.
  36. Matejec V., Chomat M., Hayer M., Kasik I., Berkova D., Abdelmalek F., Jaffrezic-Renault N., Development of special optical fibers for evanescent-wave sensing, *Czechoslovak J.of Phys.* 1999; 49: 883-888.
  37. <http://www.OceanOptics.com>.
  38. D. Derickson et. al., *Fiber optic test and measurement*, Prentice Hall PTR, 1998.
  39. <http://www.oxford-electronics.com>.
  40. Wolfbeis O.S., Novel techniques and materials for fiber optic chemical sensing, Proc.6th Int.Conf. OFS'89 (1989), Paris, Springer-Verlag, pp.416-424.
  41. Gupta B.D., Sharma A., Singh C.D., Fiber optic evanescent-wave absorption sensors based on uniform and tapered fibers, Proc. 2<sup>nd</sup> Europtrode (1994), Firenze, p.189.
  42. Shiverlanke L.C., Anderson G.P., Golden J.P., Ligler F.S., The effect of tapering the optical fiber on evanescent-wave measurements, *Analytical Letters* 1992; 25: 1183-1199.

## Chapter 5

# ABSORPTION-BASED SENSORS

Aleksandra Lobnik

Faculty of Mechanical Engineering, Centre of Sensor Technology, University of Maribor  
Smetanova 17, SI-2000 Maribor, Slovenia

### 1. INTRODUCTION

Optical sensors rely on optical detection of a chemical species. Two basic operation principles are known for optically sensing chemical species:

- intrinsic optical property of the analyte is utilized for its detection;
- indicator (or label) based sensing is used when the analyte has no intrinsic optical property. For example, pH is measured optically by immobilizing a pH indicator on a solid support and observing changes in the absorption or fluorescence of the indicator as the pH of the sample varies with time<sup>1-20</sup>.

Fiber-optic chemical sensors (FOCSs) represent a subclass of chemical sensors in which an optical fiber is used as part of the transduction element.

Typically, a chemical sensor consists of a chemical recognition phase coupled with a transduction element (Figure 1).

Some sensors may include a separator which is, for example a membrane. In the receptor part of a sensor the chemical information is transformed into a form of energy which may be measured by the transducer. The transducer part is a device capable of transforming the energy carrying the chemical

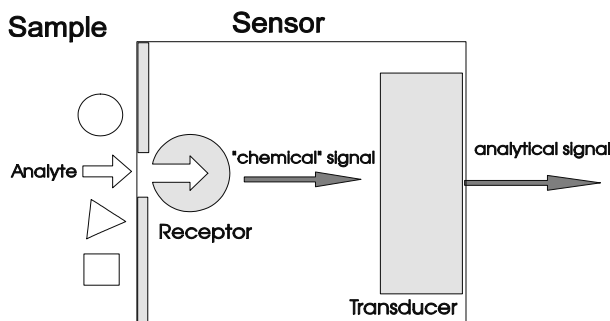


Figure 1. Schematic representation of the composition and function of a chemical sensor.

information about the sample into a useful analytical signal. The transducer does not show selectivity. The receptor part may be based on various principles:

- *physical*, where no chemical reaction takes place. Typical examples are those based on measurement of absorbance, refractive index, conductivity, temperature or mass change;
- *chemical*, in which a chemical reaction with participation of the analyte gives rise to the analytical signal;
- *biochemical*, in which a biochemical process is the source of the analytical signal. They may be regarded as a subgroup of the chemical ones.

Chemical sensors may be classified according to the operating principle of the transducer as optical, electrochemical, electrical, mass sensitive, etc.

## 2. PRINCIPLE OF UV/VIS ABSORPTION SPECTROSCOPY

### 2.1 Introduction

Many molecules absorb ultraviolet or visible light. The absorbance of a solution increases as attenuation of the beam increases. Absorbance is

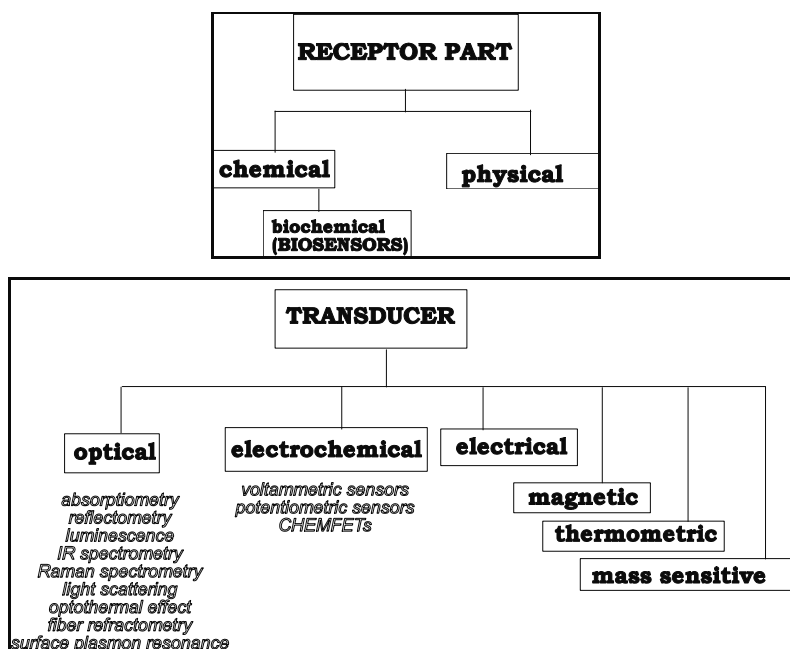


Figure 2. Classification of chemical sensors according to the operating principle of the receptor and transducer.

directly proportional to the path length,  $b$ , and the concentration,  $c$ , of the absorbing species. Beer's Law states that

$$A = \epsilon bc \quad (\text{Eq.1})$$

where  $\epsilon$  is a constant of proportionality, called the absorbtivity.

Different molecules absorb radiation of different wavelengths. An absorption spectrum will show a number of absorption bands corresponding to structural groups within the molecule. For example, the absorption that is observed in the UV region for the carbonyl group in acetone is of the same wavelength as the absorption from the carbonyl group in diethyl ketone.

Ultraviolet-visible spectroscopy (UV = 200 - 400 nm, visible = 400 - 800 nm) corresponds to electronic excitations between the energy levels that correspond to the molecular orbital of the systems. In particular, transitions involving  $\pi$  orbital and ion pairs ( $n$  = non-bonding) are important and so UV/VIS spectroscopy is of most use for identifying conjugated systems which tend to have stronger absorptions<sup>1-3, 18, 21, 22, 24</sup>.

## 2.2 Electronic Transitions

The absorption of UV or visible radiation corresponds to the excitation of outer electrons. There are three types of electronic transition which can be considered:

1. Transitions involving  $\pi$ ,  $\sigma$ , and  $n$  electrons
2. Transitions involving charge-transfer electrons
3. Transitions involving  $d$  and  $f$  electrons (not covered in this Unit)

When an atom or molecule absorbs energy, electrons are promoted from their ground state to an excited state. In a molecule, the atoms can rotate and vibrate with respect to each other. These vibrations and rotations also have discrete energy levels, which can be considered as being packed on top of each electronic level (Figure 3).

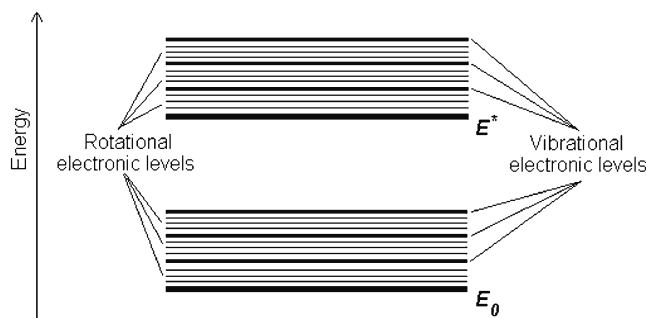


Figure 3. Energy levels.

### 2.2.1 Absorbing Species Containing $\pi$ , $\sigma$ , and $n$ Electrons

Absorption of ultraviolet and visible radiation in organic molecules is restricted to certain functional groups (chromophores) that contain valence electrons of low excitation energy (Figure 4). The spectrum of a molecule containing these chromophores is complex. This is because the superposition of rotational and vibrational transitions on the electronic transitions gives a combination of overlapping lines. This appears as a continuous absorption band.

#### $\sigma \rightarrow \sigma^*$ Transitions

An electron in a bonding  $\sigma$  orbital is excited to the corresponding antibonding orbital. The energy required is large. For example, methane (which has only C–H bonds, and can only undergo  $\sigma \rightarrow \sigma^*$  transitions) shows an absorbance maximum at 125 nm. Absorption maxima due to  $\sigma \rightarrow \sigma^*$  transitions are not seen in typical UV-VIS spectra (200 - 700 nm).

#### $n \rightarrow \sigma^*$ Transitions

Saturated compounds containing atoms with lone pairs (non-bonding electrons) are capable of  $n \rightarrow \sigma^*$  transitions. These transitions usually need less energy than  $n \rightarrow \sigma^*$  transitions. They can be initiated by light whose wavelength is in the range 150 - 250 nm. The number of organic functional groups with  $n \rightarrow \sigma^*$  peaks in the UV region is small.

#### $n \rightarrow \pi^*$ and $\pi \rightarrow \pi^*$ Transitions

Most absorption spectroscopy of organic compounds is based on transitions of  $n$  or  $\pi$  electrons to the  $\pi^*$  excited state. This is because the absorption peaks for these transitions fall in an experimentally convenient region of the spectrum (200 - 700 nm). These transitions need an unsaturated group in the molecule to provide the  $\pi$  electrons.

Molar absorptivities from  $n \rightarrow \pi^*$  transitions are relatively low, and range from 10 to 100  $\text{L mol}^{-1} \text{cm}^{-1}$ .  $\pi \rightarrow \pi^*$  transitions normally give molar absorptivities between 1000 and 10,000  $\text{L mol}^{-1} \text{cm}^{-1}$ .

The solvent in which the absorbing species is dissolved also has an effect on the spectrum of the species. Peaks resulting from  $n \rightarrow \pi^*$  transitions are

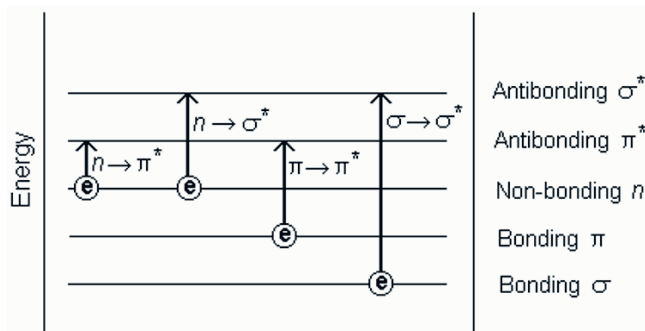


Figure 4. Possible electronic transitions of  $\pi$ ,  $\sigma$ , and  $n$  electrons.

shifted to shorter wavelengths (blue shift) with increasing solvent polarity. This arises from increased solvation of the lone pair, which lowers the energy of the n orbital. Often (but not always), the reverse (i.e. red shift) is seen for  $\pi \rightarrow \pi^*$  transitions. This is caused by attractive polarisation forces between the solvent and the absorber, which lower the energy levels of both the excited and unexcited states. This effect is greater for the excited state, and so the energy difference between the excited and unexcited states is slightly reduced - resulting in a small red shift. This effect also influences  $n \rightarrow \pi^*$  transitions but is overshadowed by the blue shift resulting from solvation of ion pairs.

### 2.2.2 Charge-Transfer Absorption

Many inorganic species show charge-transfer absorption and are called charge-transfer complexes. For a complex to demonstrate charge-transfer behavior one of its components must have electron donating properties and another component must be able to accept electrons. Absorption of radiation then involves the transfer of an electron from the donor to an orbital associated with the acceptor<sup>1-3, 23, 24</sup>.

Molar absorptivities from charge-transfer absorption are large (greater than  $10,000 \text{ Lmol}^{-1}\text{cm}^{-1}$ ).

## 2.3 Beer-Lambert Law

The Beer-Lambert law (also called the Beer-Lambert-Bouguer law or simply Beer's law) is the linear relationship between absorbance and concentration of an absorber of electromagnetic radiation. The general Beer-Lambert law is usually written as<sup>1-3, 22, 24</sup>:

$$A = a_{\lambda} \cdot b \cdot c \quad (\text{Eq.2})$$

where  $A$  is the measured absorbance,  $a_{\lambda}$  is a wavelength-dependent absorptivity coefficient,  $b$  is the path length, and  $c$  is the analyte concentration. When working in concentration units of molarities, the Beer-Lambert law is written as:

$$A = \varepsilon_{\lambda} \cdot b \cdot c \quad (\text{Eq.3})$$

where  $\varepsilon_{\lambda}$  is the wavelength-dependent molar absorptivity coefficient with units of  $\text{M}^{-1}\text{cm}^{-1}$ . The  $\lambda$  subscript is often dropped with the understanding that a value for  $\varepsilon$  is for a specific wavelength. If multiple species that absorb light at a given wavelength are present in a sample, the total absorbance at that wavelength is the sum due to all absorbers:

$$A = (\varepsilon_1 \cdot b \cdot c_1) + (\varepsilon_2 \cdot b \cdot c_2) + \dots \quad (\text{Eq.4})$$

where the subscripts refer to the molar absorptivity and concentration of the different absorbing species that are present.

Experimental measurements are usually made in terms of transmittance ( $T$ ), which is defined as:

$$T = \frac{P}{P_0} \quad (\text{Eq.5})$$

where  $P$  is the power of light after it passes through the sample and  $P_0$  is the initial light power. The relation between  $A$  and  $T$  is:

$$A = -\log(T) = -\log\left(\frac{P}{P_0}\right) \quad (\text{Eq.6})$$

The Figure 5 shows the case of absorption of light through an optical filter and includes other processes that decrease the transmittance such as surface reflectance and scattering.

In analytical applications we often want to measure the concentration of an analyte independent of the effects of reflection, solvent absorption, or other interferences. The next figure shows the two transmittance measurements that are necessary to use absorption to determine the concentration of an analyte in solution (Figure 6). The top diagram is for solvent only and the bottom is for an absorbing sample in the same solvent. In this example,  $P_s$  is the source light power that is incident on a sample,  $P$  is the measured light power after passing through the analyte, solvent, and sample holder, and  $P_0$  is the measured light power after passing through only the solvent and sample holder. The measured transmittance in this case is attributed to only the analyte.

Depending on the type of instrument, the reference measurement (top diagram) might be made simultaneously with the sample measurement (bottom diagram) or a reference measurement might be saved on computer to generate the full spectrum.

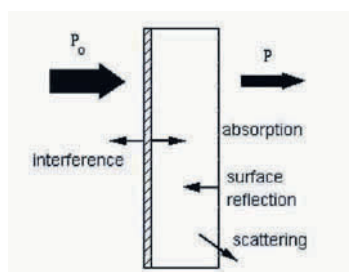


Figure 5. Case of absorption of light through an optical filter.



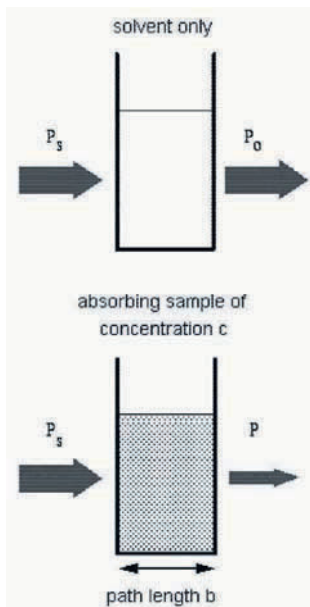


Figure 6. Two transmittance measurements that are necessary to use absorption to determine the concentration of an analyte in solution.

Modern absorption instruments can usually display the data as transmittance, %-transmittance, or absorbance. An unknown concentration of an analyte can be determined by measuring the amount of light that a sample absorbs and applying Beer's law. If the absorptivity coefficient is not known, the unknown concentration can be determined using a working curve of absorbance versus concentration derived from standards.

## 2.4 Instrumentation

The light source is usually a hydrogen or deuterium lamp for UV measurements and a tungsten lamp for visible measurements. The wavelengths of these continuous light sources are selected with a wavelength separator such as a prism or grating monochromator. Spectra are obtained by scanning the wavelength separator and quantitative measurements can be made from a spectrum or at a single wavelength<sup>24</sup>.

## 3. EXAMPLES OF ABSORPTION-BASED SENSORS

An indicator acts as a transducer for the chemical species that cannot be determined directly by optical means. Consequently, it is the concentration

of the indicator species that is determined rather than the analyte itself. The chemistry of indicators is fairly established but not optimized for chemical sensing purposes. Many indicators cannot be used because of unfavorable analytical wavelengths, poor photostability, low molar absorbance, additional reagents.

Most absorbance-based indicators undergo a color change (with one band appearing as the other disappears) rather than an intensity change of one band only. Usually, both the complexed and uncomplexed species have an absorption of comparable intensity in the visible. These are referred to as two-color indicators and are mostly compatible with LED or filament lamp light source.

Absorbance based indicators are known to undergo either ion combination reactions (such as with protons, cations, or anions) or oxidation-reduction reactions<sup>31-43</sup>.

### 3.1 pH Optical Sensors

Among the great variety of organic chromophores such as azo dyes, nitrophenols, phthaleins, sulfophthaleins, aniline-sulfophthaleins, triphenylmethane dyes, polymethines, and others, only a few have so far been considered to be useful and applied to sensor technology (Table 1)<sup>25-34</sup>.

Important characterization parameter of pH indicator is its pKa value:



$$K_a = [\text{Ind}^-][\text{H}^+] / [\text{H-Ind}] \quad (\text{Eq.8})$$

$$\text{pKa} = -\log ([\text{Ind}^-][\text{H}^+]/[\text{H-Ind}]) \quad (\text{Eq.9})$$

where [H-Ind] is the concentration of the pH indicator, [Ind<sup>-</sup>] is the anion concentration and [H<sup>+</sup>] is the proton concentration.

Connection between pH, pKa and absorbance is given by Henderson Hasselbach equation:

$$\text{pH} = \text{pKa} + \log [\text{Ind}^-]/[\text{H-Ind}] \quad (\text{Eq.10})$$

and we can determinate the pKa value spectrophotometrically from the titration plot:

$$\text{pKa} = \text{pH} - \log (\text{Ex} - \text{EA})/(\text{EB} - \text{Ex}) \quad (\text{Eq.11})$$

where Ex is the absorbance by the given wavelength and determinate pH; EA, EB are the absorbance by the wavelength typical for acid and basic form of the indicator.

Table 1. Selected absorption indicators for measurements of acidic or basic pHs, and respective  $pK_a$  values at room temperatures<sup>1</sup>.

<i>Indicator</i>	<i>Absorbance maximum or color of acid/base forms</i>	<i>or <math>pK_a</math> value or pH range</i>
ACIDIC RANGE		
N-Benzylaniline sulfophthalein	Yellow/blue	0,30
Methyl violet	Yellow/blue	0.0-1.6
Methyl green	Yellow/blue	0.2-1.8
Crystal violet	Yellow/blue	0.2-2.0
Ethyl violet	Yellow/blue	0.2-2.4
Malachite green	Yellow/blue-green	0.2-1.8
Cresol red	Red/yellow	1.0-2.0
Thymol blue	Red/yellow	1.2-2.8
Meta cresol purple	Red/yellow	1.2-2.8
Orange IV	Orange/red	1.4-2.8
Bromophenol blue	Yellow/blue	2.8-4.8
Methyl orange	Orange/yellow	3.0-4.4
Congo red	Blue/red	3.0-5.0
Bromocresol green	Yellow/blue	4.6
Methyl red	Red/yellow	4.6-6.0
Alizarin red	Yellow/red	4.6-6.0
Bromocresol purple	Yellow/purple	6.3
ALKALINE RANGE		
Brilliant yellow	Yellow/orange	7.0-8.8
Cresol red	Yellow/red	7.0-8.8
Meta-cresol purple	Yellow/purple	7.4-9.0
Thymol blue	Yellow/blue	8.0-9.6
Cresolphthalein	Colorless/red	8.2-9.8
Naphtholbenzein	Orange/blue	8.2-10.0
Phenolphthalein	Colorless/purple	8.4-10.0

There is some need for new pH indicators with improved characteristics which allow also covalent binding. P. Makedonski report about new kind of reactive azo dyes and their application as reversible pH sensors<sup>35</sup>. They prepare a new pH indicating sensors based on thin films prepared from azo dyes that are covalently bonded by an acetal linkage to a vinylalcohol ethylene copolymer (Figure 7). The absorption spectra of the polymer bond

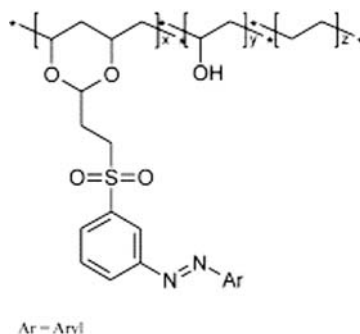


Figure 7. General formula of the dye-polymer composites.

dye (Figure 8) recorded for different pH values show a considerable shift with respect to the ones observed for the free dye. The authors consider, that the polymeric environment renders deprotonation of the dye more difficult and therefore requires higher pH values.

Optical chemical pH sensors are often used in narrow pH range. We can overcome this problem by using several pH indicators with different  $pK_a$ 's. J. Lin and G. Liu<sup>36</sup> developed a method to produce a linear response over a broad pH range by using multiple pH indicators for development of optical pH sensors. The  $pK_a$  between the indicators, the colors and concentrations of the indicators must be considered in deriving such a linear response to pH. A sol-gel glass pH sensor was developed by co-entrapping four sulphonephthalein indicators (bromocresol green, bromocresol purple, phenol red, thymol blue) which produced a linear response over 3.5 pH units from pH 6.3 to 9.8. Although the colors of their base forms are not the same, their absorption bands are close, as shown in Figure 9.

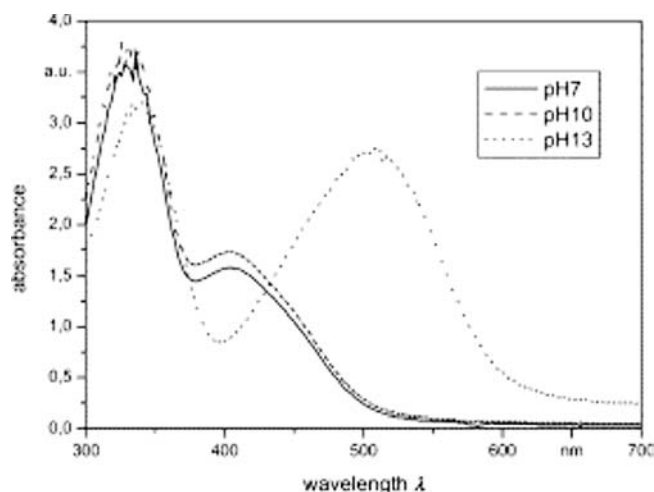


Figure 8. UV/VIS spectra of polymer bonded phenol azo dye at different pH-values.

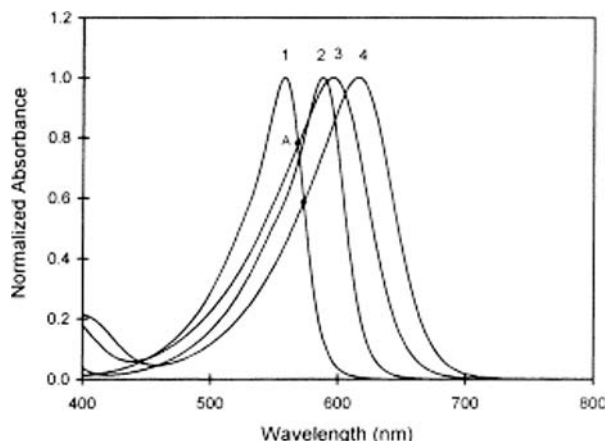


Figure 9. Normalized spectra of the base form of four indicators (1 – phenol red, 2 – bromocresol purple, 3 – thymol blue, and 4 – bromocresol green).

Figure 10 shows the absorbance response of an indicator to pH change. As can be seen, with the use of an indicator, the pH measurements can be made only over a range of about two pH units, i.e.  $pK_a \pm 1$ . Beyond this range, the change in absorbance with pH becomes small and the error in pH measurements will be large.

Various polymer matrices can be used as solid support into which pH indicator dye can be immobilized (cellulose, PVA, PVC). R. Makote and M.M. Collinson shows that also organically modified silicate films can be used for stable pH sensors<sup>37</sup>.

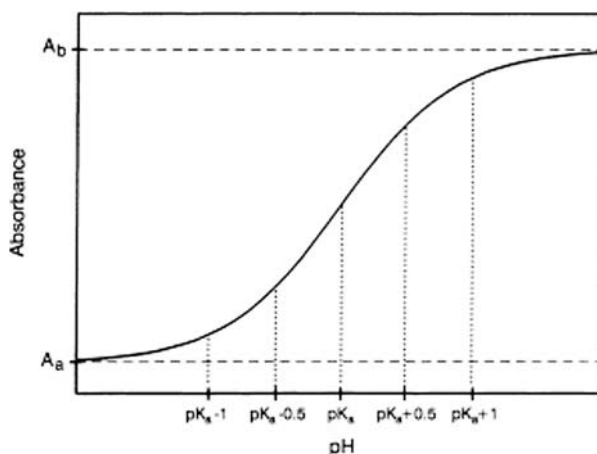


Figure 10. Absorbance response of an indicator to pH change. (The calculations were made for the absorbance measured at a wavelength where the absorptivity of the base form of the indicator is larger than that of the acid form so that  $A_b > A_a$ .  $A_b$  is the absorbance at a high pH when all the indicator is in its base form and  $A_a$  is the absorbance at a low pH when all the indicator is in its acid form).

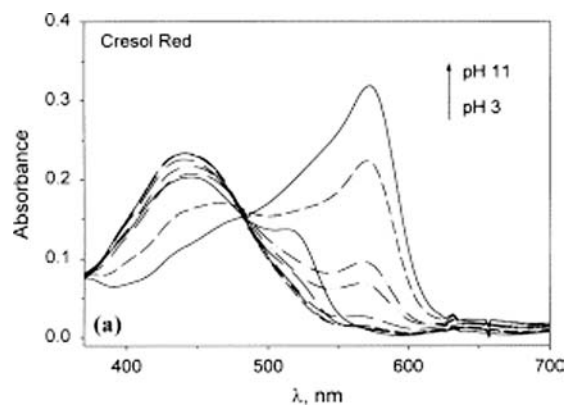


Figure 11. Absorption spectra of gel-immobilized cresol red after immersion in different pH buffer solutions (3, 4, 5, 6, 7, 8, 9, 10) for 1 min. Films prepared from TEOS:MTMOS (2:1) sol.

Representative absorption spectra for cresol red in a 2:1 tetraethoxysilane (TEOS): methyltrimethoxysilane (MTMOS) film after immersion in buffer solutions of varying pH can be seen in Figure 11. The absorbance for gel-immobilized cresol red at 570 nm increases with increasing pH. Isosbestic points can be observed at ca. 480 nm for gel-immobilized cresol red.

The sol-gel co-immobilization of a non-fluorescent blue indicator bromothymol blue (BTB) with an europium (III)-complex intense antenna mediated lanthanide dye represents a new scheme for the fluorescence analysis<sup>38</sup>. Luminescence spectra of europium (III)-complex shown in Figure 12 were found to be independent of pH changes in the range 1-10. Therefore, BTB, a non-fluorescent pH indicator with alkaline absorption maximum close to main europium emission band was added to the sol-gel mixture to shield reversibly the emission of the europium (III)-complex at different pH's without quenching of the antenna function.

Figure 13 shows pH response of bromothymol blue (BTB) as co-immobilized non fluorescent pH indicator detect by fluorescence.

There are several works published on pH sensors based on energy transfer. Jordan and Walt developed a single-fiber optic sensor based on

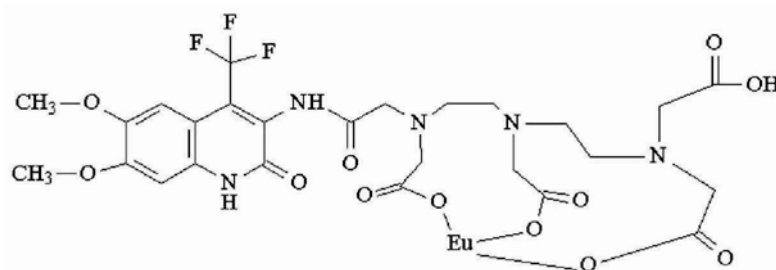


Figure 12. Europium (III) complex.

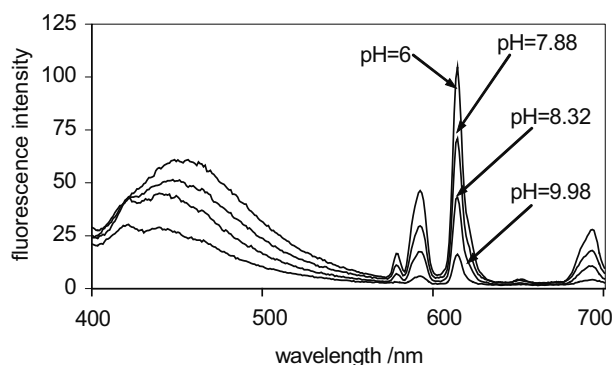


Figure 13. pH response of bromothymol blue as co-immobilized non-fluorescent indicator detect by fluorescence.

energy transfer from a pH insensitive fluorophore, eosin (the donor), to a pH sensitive absorber, phenol red (the acceptor). The dyes were co-immobilized with acrylamide. The fluorescence spectrum overlaps with the absorption spectrum of the base form of phenol red<sup>39</sup>.

As the pH increases, the concentration of the base form of phenol red increases, resulting in increased energy transfer from eosin to phenol red and in a diminished fluorescence intensity of eosin. Thus, changes in the absorption of phenol red as a function of pH are detected as a change in the fluorescence signal of eosin.

Similarly, all pH indicators mentioned can be used for measurement of acidic and basic gases. Figure 14 shows the example of deprotonated bromophenol blue when dissolved in silicone and upon exposure to ammonia when the color of bromophenol blue changed from yellow to blue<sup>40, 41</sup>.

### 3.2 Redox Indicators

The classes of indicators to be described are all organic dyestuffs, exhibiting reversible redox reactions. If a redox half reaction is represented by

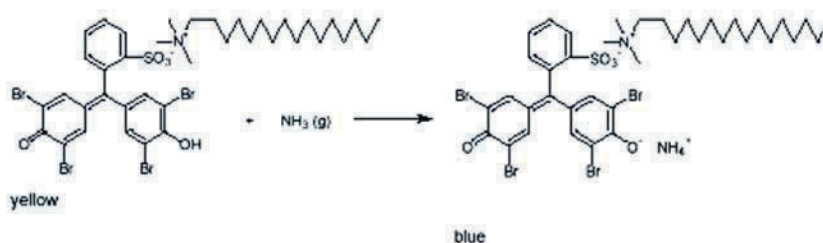


Figure 14. Bromophenol blue in yellow and blue form.

Table 2. Selected absorption redox indicators<sup>1</sup>.

Indicator/(color change)	Redox potential $E_o$ (at pH 0 and 20 °C)	$E_m$ (at pH 7 and 30 °C)
Amidoblack/yellow-blue	+0.57	+0.84
Anilic acid/purple-colorless	+0.89	-
Diphenylamine/colorless-purple	+0.7	-
Eriogreen B/orange-yellow	+1.01	-
m-cresol-indophenol/blue-colorless	+0.21	-
Methylen blue/blue-colorless	0.53	-
Neutral red/purple-colorless	-	-0.45
Nile blue/blue-colorless	+0.24	-0.29
Toluylene blue(violet-colorless)	+0.6	+0.11



where  $O_x$  as usual represents the oxidized species and  $Red$  the reduced species, and  $n$  is the number of electrons,  $e$ , transferred, then the electrode potential of the redox couple will be given by the Nernst equation<sup>1</sup>.

An optical sensor highly sensitive to hydrogen peroxide has been prepared by incorporating the indicator dye Meldola blue (MB) into sol-gel layers, prepared from (a) pure tetramethoxysilane (TMOS) and (b) variation of TMOS and methyltrimethoxysilane (Me-TriMOS) (Figure 15). Sensor layers based on TMOS doped with MB were found to be most appropriate for purposes of sensing hydrogen peroxide in giving large signal changes and displaying rapid response times over the wide concentration range of  $10^{-8}$  –  $10^{-1}$  M (Figure 16)<sup>42</sup>.

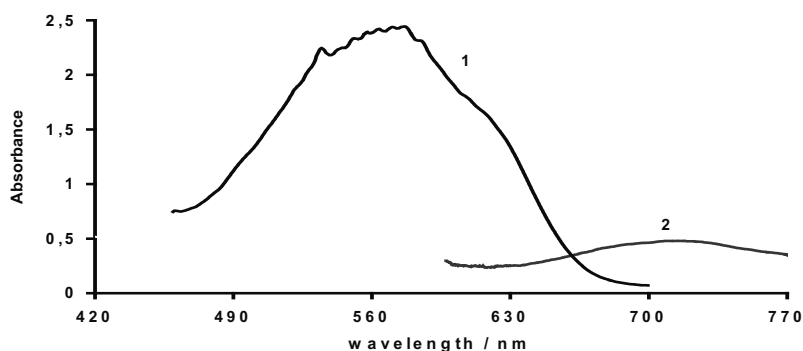


Figure 15. Absorbance spectra of dissolved oxidized form of MB (1) and immobilized MB in poly-TMOS sensor layer L1 (2).



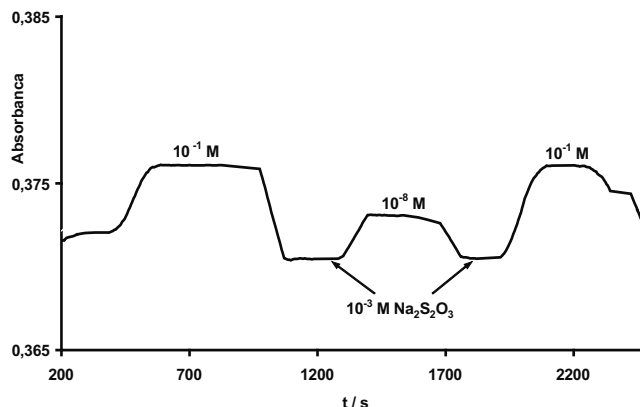
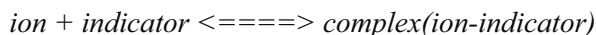


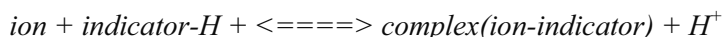
Figure 16. Response of sensor layer L1 to dissolved hydrogen peroxide at pH 7 and its reversibility by exposing to  $\text{Na}_2\text{S}_2\text{O}_5$  measured at 720 nm.

### 3.3 Ion Sensing Using Metal Indicators (Chelators)

There are many types of compounds that form colored complexes with metal ions. The color reaction must be sufficiently selective and the value of the stability constant of the complex formed should be such as to make the reaction reversible in order to make the device a sensor rather than a single-shot probe<sup>1,3,18,43-50</sup>.



If however, the ion binding process involves the displacement of protons according to:



then the process is cross-sensitive to pH. In order to provide a rather natural aqueous environment for the indicator dyes, they should be embedded in hydrophilic rather than in lipophilic polymers. This, however, requires significant synthetic effort because the indicator should be covalently linked to the polymer in order to prevent leaching.

#### 3.3.1 Ionophore-Based Cation Detection

The term ionophore is used to describe ligands that selectively bind ions. Typically ionophores are macrocyclic molecules with an ion binding cavity. Crown ether dyes have found particular attention and they are best known class of ionophores. Chromogenic ionophores are designed to bring about specific color change on the interaction with metal cations such as alkali and alkaline earth metals, thus serving as probes or photometric reagents selective for these metal ions.

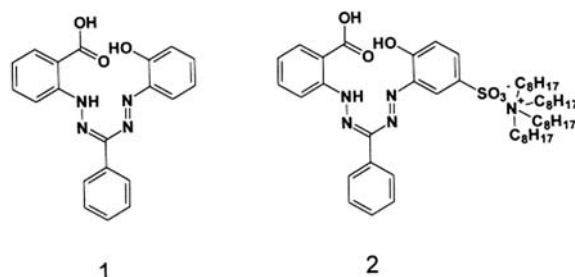


Figure 17. Chemical structure of 2-carboxy-2'-hydroxy-formazylbenzene (1) and the Zirconium-tetraoctylammonium ion pair (2).

### 3.3.2 Chromo-Ionophore-Based Cation Detection

The *chromophoric* groups can bear one or more dissociable protons or can be nonionic. In the former, the ion exchange between the proton and appropriate metal cations causes the color change, while in the latter the coordination of the metal ion to the chromophoric donor or acceptor of the dye molecule induces a change of the charge transfer band of the dye.

Another approach for ion-sensing (here: copper and zinc) is based on the water-soluble ligand zincon and the ion pair with quaternary ammonium halides shown in Figure 17 which can be homogeneously dissolved in polymers such as plasticized poly(vinyl acetate), ethyl cellulose, and polyurethane.

As can be seen in Figure 18, the slopes of the response curves are concentration dependent and, therefore, can be used as the analytical information. Notwithstanding the differences in the slopes, all curves finally end up at the same absorbance.

The selective determination of Cu(II) was accomplished by making use of pyrocatechol violet indicator, dissolved in plasticized PVC membrane as a

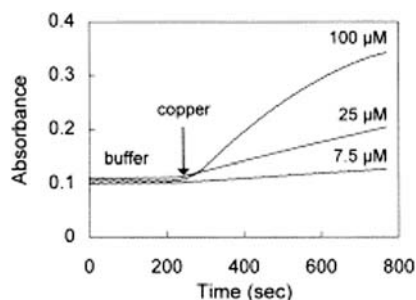


Figure 18. Kinetics of the increase in absorbance at 620 nm as a result of exposure of membrane to different concentrations of copper(II).

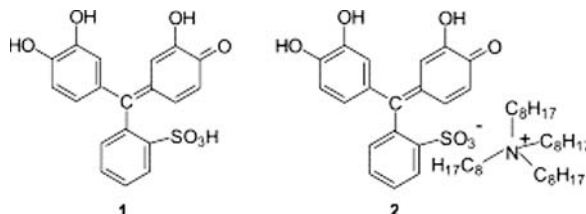


Figure 19. Chemical structure of pyrocatechol violet (1) and the pyrocatechol violet-tetraoctylammonium ion pair (2).

lipophilic ion pair with tetraoctylammonium cation. The membrane response to Cu(II) by changing colour irreversibly from yellow to green (740 nm)<sup>52</sup>.

The chemical structure of pyrocatechol violet and the pyrocatechol violet-tetraoctylammonium ion pair are shown in Figure 19.

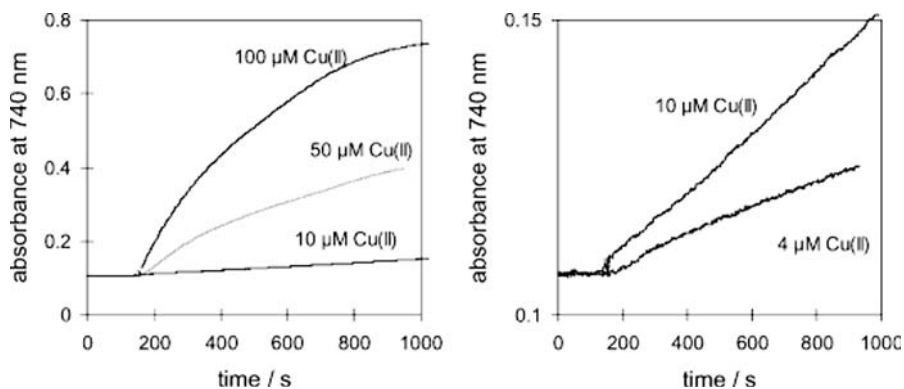


Figure 20. Typical dynamic response curves of membrane recorded at 740 nm as a result of exposure to different concentrations of Cu(II).

The dynamic response to Cu(II) was monitored as a change in absorbance at 740 nm as the membrane was exposed to a buffer solution containing copper ions. Characteristic response curves obtained for different concentrations of Cu(II) are shown in Figure 20.

A new Ni(II) optical chemical sensor based on immobilizing of 2-amino-1cyclopentene-1dithiocarboxylic acid (ACDA) (Figure 21), to transparent acetyl cellulose films was developed<sup>52</sup>.

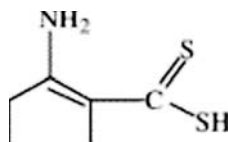


Figure 21. Structure of the ACDA.

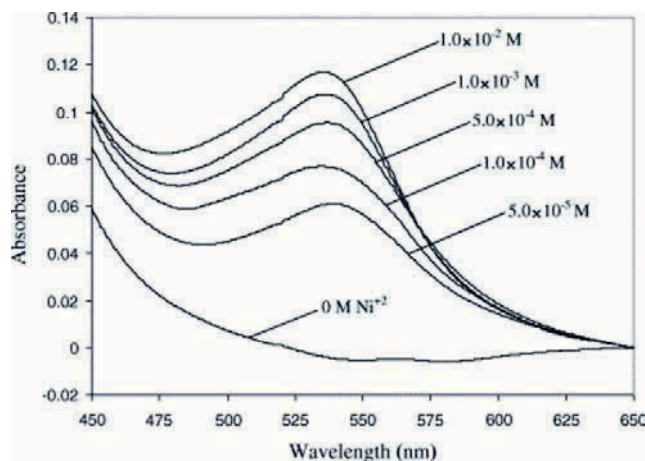


Figure 22. Absorption spectra for ACDA in membrane at different Ni(II) concentration at pH 6.5

Figure 22 shows typical absorbance of the membrane sensors at different Ni(II) concentrations at the optimized conditions.

Two new chromogenic crown ether derivatives based on an identical design principle have been synthesized. The lipophilic KBC-002 shown in Figure 23 is a useful new chromo- ionophor for the highly selective calcium determination with cation exchange type optode<sup>53</sup>.

The absorption maximum for the  $\text{Ca}^{2+}$ -complexed form of KBC-002 is observed at 550 nm (Figure 24a). When  $\text{Ca}^{2+}$  measurements were performed at a pH of 9.0 using the optode membrane, a dynamic response range between 10  $\mu\text{M}$  and 10 mM was observed for the sensors as illustrated by the calibration function shown in Figure 24b.

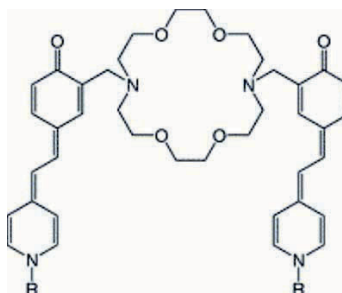


Figure 23. Chemical structures of the novel betaine lariat ethers KBC-001 ( $\text{R}=\text{CH}_3$ ) and KBC-002 ( $\text{R}=\text{C}_{12}\text{H}_{25}$ ).

#### 4. CONCLUSIONS

The interdisciplinary nature of optical chemical sensors opens a variety of new directions in sensor development. The issue of chemical selectivity is

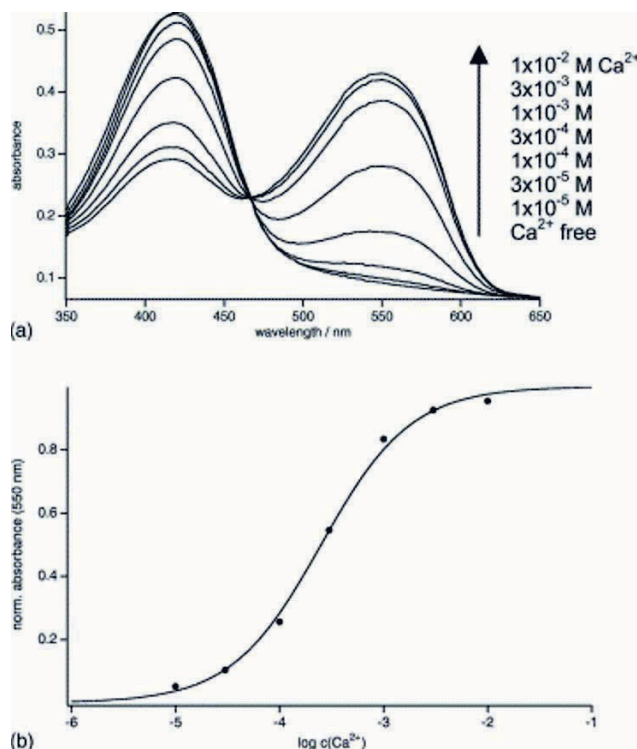


Figure 24. (a) Absorption spectra of a calcium-selective optode membrane (DOS/PVC) based on KBC-002 after equilibration with pH-buffered (0.1 M boric acid/0.1 M TMACl; pH 9.0) calcium solutions and (b) calibration curve for the optode at 550 nm for  $\text{Ca}^{2+}$  (•).

still the most challenging. There are several on-going directions for improving the selectivity of optical chemical sensors. One way is certainly in the field of supramolecular organic chemistry, and in the synthesis of the highly selective receptor molecules which will possess a chromogenic part. In addition, the investigations of the mechanisms by which naturally occurring carriers and ionophores act within a living organism can provide new ideas for sensing schemes. The most interesting promoters for environmental analysis are found in bacteria that survive in environments contaminated by, for example heavy metals or organic compounds. The ability of the bacteria to survive in a contaminated environment is usually based on a genetically encoded resistance system, the expression of which is regulated very precisely. Although the reported sensing scheme is relatively complex, and is not yet transformed to a solid-state, it represents a novel and promising approach which is especially advantageous in terms of sensitivity and selectivity.

Furthermore, biomonitoring, as already a well-established field of environmental analysis (especially for monitoring of pollution caused by heavy metals), can serve as a basis and the first step towards the development of "living sensors".

A second approach of improving selectivity is based on the use of absorption based sensor arrays combined with chemometrics, as well as the use of "higher order sensors". On the basis of the second-order approach, optical sensors for determination of heavy metals and chlorinated hydrocarbons have been developed. This opens a new and challenging field to sensor researchers and chemometricians, particularly in developing complicated calibration algorithms which are needed to deconvolute the often collinear or nonlinear signal brought by the second-order sensors. Although it could seem to be an expensive and complicated approach, the growing field of micromachining makes it more and more cost-effective.

In addition, the integration of modern optical technology and electrochemical techniques for sensing applications appears to be a powerful new approach. A new type of optoelectrochemical sensor for chlorine, based on an electrochromic thin-film sensing layer placed on top of a planar waveguide, has demonstrated the applicability of this combined approach.

The development in field of optoelectronics, digital components and light emitting diodes and laser diodes is of particular importance in manufacturing commercially attractive instruments.

In addition, the development in sensor materials opens a number of new possibilities, such as incorporation of organic and biochemical specific sites into inorganic matrices prepared by the sol-gel process.

The recent progress in miniaturized integrated optical sensors offer several advantages, such as a possibility of mass-producing, low-cost sensor chips. Furthermore, by placing multiple sensing regions (sensing pads) on a single chip, the multicomponent sensing with on-chip referencing becomes possible.

## REFERENCES

1. Wolfbeis O.S. (ed.), *Fiber Optic Chemical Sensors and Biosensors*, Vols. I and II, CRC Press, Boca Raton, 1991.
2. Göpel W., Hesse J., Zemel J.N. (eds.), *Sensors - A Comprehensive Survey*, VCH, Weinheim, 1991-1993.
3. Janata J., *Principles of Chemical Sensors*, Plenum Press, New York 1989.
4. Wolfbeis O.S., Chemical sensors-survey and trends, *Fresenius J. Anal. Chem.* 1990; 337: 522-527.
5. Hulanicki A., Glab S., Ingman F., Chemical sensors: definitions and classification. Commission on General Aspects of Analytical Chemistry, *Pure & Appl. Chem.* 1991; 63: 1247.
6. Coon D.R., Babb C.W., Rechnitz G.A., Biomagnetic Neurosensors. 2. Magnetically Stimulated Sensors, *Anal. Chem.* 1994; 66: 3193.
7. Seitz W.R., Chemical sensors based on fibre optics, *Anal. Chem.* 1984; 56: 16A-34A.
8. Arnold M.A., Fiber-optic chemical sensors, *Anal. Chem.* 1992; 64: 1015A-1025A.
9. Clement R.E., Eiceman G.A., Koester C.J., Environmental Analysis, *Anal. Chem.* 1995; 67: 221R-255R.

10. Heitzer A., Malachowsky K., Thonnard J.E., Bienkowski P.R., White D.C., Saylor G.S., Optical biosensor for environmental on-line monitoring of naphthalene and salicylate bioavailability with an immobilized bioluminescent catabolic reporter bacterium, *Appl. Environ. Microbiol.* 1994; 60: 1487-1494.
11. Selifonova O., Burlage R., Barkay T., Bioluminescent sensors for detection of bioavailable Hg(II) in the environment, *Appl. Environ. Microbiol.* 1993; 59: 3083-3090.
12. Barrero J.M., Moreno-Bondi M.C., Perez-Conde M.C., Camara C., *Talanta* 1993; 40: 1619.
13. Klainer S.M., Thomas J.R., Francis J.C., Fibre-optical. sensors offer a realistic solution to environmental monitoring needs, *Sensors Actuators B* 1993; 11: 81-86.
14. Kuselman I., Lev O., Organically-doped sol-gel-based tube detectors: determination of iron (II) in aqueous solutions, *Talanta* 1993; 40: 749-75.
15. Ahmad M., Narayanaswamy R., Fibre Optic Reflectance Sensor for the Determination of Aluminium (III) in Aqueous Environment, *Anal. Chim. Acta* 1994; 291: 255-260.
16. Goebel R., Krska R., Kellner R., Katzir A., Development of Protective Polymer-Coatings for Silver-Halide Fibers and Their Application as Threshold Level Sensors for Chlorinated Hydrocarbons in Sea-Water, *Fresenius J. Anal. Chem.* 1994; 348: 780-781.
17. Mohr G.J., Werner T., Oehme I., Preininger C., Klimant I., Kovacs B., Wolfbeis O.S., Novel optical sensor materials based on solubilization of polar dyes in apolar polymers, *Advanced materials* 1997; 14: 1108-1113.
18. Seitz W.R., Optical ion sensing, in: *Fiber optic chemical sensors and biosensors II* (Wolfbeis O.S., ed.), CRC Press, Boca Raton, Florida, 1991.
19. Mohr G., Materials and Polymers in *Optical sensing*, ASCOS 2000, Workshop on Optical chemical Sensors & Biosensors, 2000.
20. Lobnik A., Sensor Coatings, Workshop on Optical Chemical sensors & Biosensors, 1999.
21. MacCraith B.D., O'Keeffe G., McEvoy A.K., McDonagh C.M., McGilp J.F., O'Kelly B., O'Mahony J.D., Cavanagh M., LED-based oxygen sensing using evanescent wave excitation of a dye-doped sol-gel coating, *Journal of Optical Engineering* 1994; 33: 3861-3866.
22. Wong J., Angell C.A., *Glass Structure by Spectroscopy*, Marcel Dekker, New York, 1977.
23. Kunz R.E., Totally integrated optical measuring sensors, Proc. SPIE, Vol. 1587: 98-113. (1992).
24. Skoog D.A., West D.M., Holler F.J., *Analytical Chemistry*, Saunders College Publishing, 1994.
25. Seiler K., Simon W., Theoretical aspects of bulk optode membranes, *Anal. Chim. Acta* 1992; 266: 73
26. Wolfbeis O.S., Fluorescence-based ion sensing using potential-sensitive dyes, *Sensors Actuators B* 1995; 29: 140.
27. Huber C., Werner T., Krause C., Wolfbeis O.S., *Analyst* 1999; 124: 1617.
28. Shortreed M., Kopelman R., Kuhn M., Hoyland B., Fluorescent Fiber-Optic Calcium Sensor for Physiological Measurements, *Anal. Chem.* 1996; 68: 1414-1418.
29. Oehme I., Prokes B., Murkovic I., Werner T., Klimant I. Wolfbeis O.S., LED-compatible copper(II)-selective optrode membrane based on lipophilized Zincon, *Fresenius J. Anal. Chem.* 1994; 350: 563-567.
30. Weigl B.H. et. al., *J. Biotechnol.* 1994; 32: 127.
31. Mohr G. Citterio D., Demuth C., Fehlmann M., Luzi J., Lohse C., Moradian A., Nezel T., Rothmaier M. Spichiger U.E., Reversible chemical reactions as the basis for optical sensors used to detect amines, alcohols and humidity, *Journal of Materials Chemistry* 1999; 9: 2259.
32. Ozawa S., Hauser P.C., Seiler K., Tan S.S., Morf W.E., Simon W., Ammonia-gas-selective optical sensors based on neutral ionophores, *Anal. Chem.* 1991; 63: 640.
33. Dinten O., Spichiger U.E., Chaniotakis N., Gehrig P., Rusterholz B., Morf W.E., Simon

- W., Lifetime of neutral-carrier-based liquid membranes in aqueous samples and blood and the lipophilicity of membrane components, *Anal. Chem.* 1991; 63: 596-603.
34. Ditzler M.A. et al., *Anal. Chim. Acta* 1982; 142: 305.
  35. Makedonski P., Brandesa M., Grahn W., Kowalsky W., Wichern J., Wiese S., Johannes H., Synthesis of new kinds of reactive azo dyes and their application for fibre-optical pH-measurements, *Dyes and Pigments* 2004; 61: 109-119.
  36. Lin J., Liu D., An optical pH sensor with a linear response over a broad range, *Analytica Chimica Acta* 2000; 408: 49-55.
  37. Makote R., Collinson M.M., Organically modified silicate films for stable pH sensors, *Analytica Chimica Acta* 1999; 394: 195-200.
  38. Lobnik A., Majcen N., Niederreiter K., Uray G., Optical pH sensor based on the absorption of antenna generated europium luminescence by bromothymolblue in a sol-gel membrane, *Sensors and Actuators B* 2001; 74: 200-206.
  39. Jordan D.M., Walt D.R., Milanovich F.P., Physiological pH fiber-optic chemical sensor based on energy transfer, *Anal. Chem.* 1987; 59: 437-439.
  40. Mohr G.J., Citterio D., Demuth C., Fehlmann M., Luzi J., Lohse C., Moradian A., Nezel T., Rothmaier M. Spichiger U.E., Reversible chemical reactions as the basis for optical sensors used to detect amines, alcohols and humidity., *Journal of Materials Chemistry* 1999; 9: 2259.
  41. Ozawa S., Hauser P.C., Seiler K., Tan S.S., Morf W.E., Simon W., Ammonia-gas-selective optical sensors based on neutral ionophores, *Anal. Chem.* 1991; 63: 640.
  42. Lobnik A., Čajlaković M., Sol-gel based optical sensor for continuous determination of dissolved hydrogen peroxide, *Sensors Actuators B* 2001; 74: 194-199.
  43. Merian E. (ed.), *Metals and Their Compounds in the Environment* VCH, Weinheim, 1991.
  44. Schneider H.J., Dürr H. (eds.), *Frontiers in Supramolecular Organic Chemistry and Photochemistry*, VCH, Weinheim, 1991.
  45. Virta M., Lampinen J., Karp M., A Luminescence-Based Mercury Biosensor, *Anal. Chem.* 1995; 67: 667.
  46. Hertz J., Bioindicators for Monitoring Heavy Metals in the Environment 221-233, in *Optical sensing*, ASCOS 2000, Workshop on Optical chemical Sensors & Biosensors, 2000.
  47. Lin Z., Booksh K.S., Burgess L.W., Kowalski B.R., A Second-Order Fiber Optic Heavy Metal Sensor Employing Second-Order Tensorial Calibration, *Anal. Chem.* 1994; 66: 2552-2560.
  48. Tauler R., Smilde A.K., Hernshaw J.M., Burgess L.W., Kowalski B.R., Multicomponent Determination of Chlorinated Hydrocarbons Using a Reaction-based Chemical Sensor. Part 2. Chemical Speciation Using Multivariate Curve Resolution, *Anal. Chem.* 1994; 66: 3337-3344.
  49. Piraud C., Mwarania E., Wylangowski G., Wilkinson J., O' Dwyer K., Schiffrin J., An optoelectrochemical thin-film chlorine sensor employing evanescent fields on planar optical waveguides, *Anal. Chem.* 1992; 64: 651.
  50. Lev O., Tsionsky M., Rabinovich L., Glezer V., Sampath S., Pankratov I., Gun J., Organically modified sol-gel sensors, *Anal. Chem.* 1995; 67: 22A-30A.
  51. Oehme I., Prokes B., Murkovic I., Werner T., Klimant I., Wolfbeis O.S., LED-compatible copper(II)-selective optrode membrane based on lipophilized Zincon, *Fresenius J. Anal. Chem.* 1994, 350: 563.
  52. Murković Steinberg I., Lobnik A., Wolfbeis O.S., Characterisation of an optical sensor membrane based on the metal ion indicator Pyrocatechol Violet, *Sensors Actuators B.* 2003; 90 (1-3): 230-235.
  53. Citterio D., Omagari M., Kawada T., Sasaki S., Suzuki Y., Suzuki K., Chromogenic betaine lariates for highly selective calcium ion sensing in aqueous environment, *Anal. Chim. Acta* 2004; 504 (2): 227-234.



## Chapter 6

# FLUORESCENCE-BASED SENSORS

Guillermo Orellana

*Laboratory of Applied Photochemistry  
Department of Organic Chemistry, Faculty of Chemistry  
Universidad Complutense de Madrid  
E-28040 Madrid, Spain*

### 1. INTRODUCTION

The natural luminescent phenomena (from the Latin words “lumen” and “essentia”, i.e., “made of light”) such as northern lights (aurora borealis), marine brightness, glow-worms, shining putrid fish scales, “bluish”-appearing water when contained in certain wooden cups (quinine fluorescence), some stones heated at high temperatures with reducing agents (BaS phosphorescence), or light emitted while crushing sugar (triboluminescence) already fascinated our ancestors<sup>1</sup>. Nowadays we understand that ultraviolet and visible emission of light originates from a competitive deactivation pathway of the lowest electronic excited state of atoms and molecules that produces the so called *luminescence* (the sub-terms *fluorescence* and *phosphorescence* just designate whether the return of the excited to the ground state is an “allowed” or “forbidden” process, namely it is fast or slow, the loosely-defined border between them being a  $1\text{-}\mu\text{s}^{-1}$  rate constant)<sup>2</sup>. Actually, luminescence is the only method to generate light in the known Universe regardless it is powered by the nuclear reactions in the stars, the ohmical heating in bulbs, an electric discharge, the absorption of light or a (bio)chemical reaction (chemiluminescence).

However, the widespread analytical application of fluorescence had to wait until the middle of the XX century, much longer than that of absorption spectroscopy<sup>3</sup>. The latter was a general feature of materials and chemicals compared to the very small number of light-emitting species. Moreover, in past times the high sensitivity of fluorescence was a disadvantage rather than a bonus, since many impurities were an important source of interference. The strong effect of the light source intensity, the optical layout and the photon detector on the measured luminescence (in addition to the luminophore nature and concentration), combined with the lack of robust

and stable standards, were an additional burden to the adoption of luminescent analytical methods. The advent of powerful light sources, particularly the laser beam, cheaper sensitive photosensors (photomultiplier tubes, photodiodes, avalanche photodiodes) with ns time resolution capability, computers, two-dimensional detectors (diode arrays, CMOS, CCDs), optical fibers, confocal microscopes and flow cytometers have put an end to that situation. Luminescence is currently one of the most popular techniques for chemical and biochemical analysis and optical sensing<sup>4</sup>.

Sensors are regarded as the “*senses of electronics*”<sup>5</sup> eyes and ears capable of seeing and hearing beyond the human perception; electronic noses and tongues that can recognize odors and flavors without a lifetime training; touches that are able not only to feel the surface roughness and temperature but even to discern its chemical composition. Among the world of *chemical* sensors, *optical* devices (sometimes termed “optodes”, from the Greek “the optical way”) have reached a prominent position in those areas where the features of light and of the light-matter interaction show their advantage<sup>6,7</sup> contactless and/or long distance monitoring, detection sensitivity, wavelength selectivity, absence of electrical interference or risks, lack of analyte consumption and so on, to name a few. The introduction of optical fibers and integrated optics has added more value to such sensing since now light can be confined and readily carried to difficult-to-reach locations, higher information density can be transported, indicator dyes can be immobilized at the distal end or the evanescent field for unique chemical and biochemical sensing (including multiplexed and distributed measurements), optical sensors can be subject to mass production and novel optosensing schemes have been established (interferometric, surface plasmon resonance, energy transfer, supramolecular recognition...).

## 2. LUMINESCENCE AND CHEMICAL SENSING

*Fluorescent* chemical sensors occupy nowadays a prominent place among the optical devices due to its superb *sensitivity* (just a *single* photon sometimes suffices for quantifying luminescence compared to detecting the intensity difference between two beams of light in absorption techniques), combined with the required *selectivity* that photo- or chemi-luminescence impart to the electronic excitation. This is due to the fact that the excitation and emission wavelengths can be selected from those of the absorption and luminescence bands of the luminophore molecule; in addition, the emission kinetics and anisotropy features of the latter add specificity to luminescent measurements<sup>8-10</sup>.

We can just measure the *intrinsic* fluorescence of the target analyte or design sensors based on the variation of the fluorescence of an *indicator* dye, with the determinand concentration. In the latter case, the probe molecule

can be immobilized onto a (thin) polymer support (sometimes even the waveguide surface itself) and placed at the distal end or in the evanescent field of an optical fiber or integrated optics sensor. Some examples of (non-photochemical) fluorescence *intensity*-based sensors that are now commercially available from the many schemes developed in laboratories worldwide include the chlorophyll meters for natural water (thanks to the strong emission of this pigment), the NO<sub>x</sub> chemiluminescence monitors, and the fluorescent thermometers based on materials such as Cr-doped yttrium gallium garnet or Mn(IV)-activated magnesium fluorogermanate<sup>11</sup>.

Provided it is optically diluted, the relationship between a luminophore (= “luminescence bearer”) concentration and the intensity of its emission is a linear one:

$$I_L = \Phi_L I_0 \kappa \varepsilon_\lambda l c \quad (\text{Eq.1})$$

where  $\Phi_L$  is the luminescence quantum yield (i.e. the ratio of emitted to absorbed photons per unit of time, an intrinsic feature of the luminophore),  $I_0$  is the intensity of the excitation light,  $\kappa$  is an instrumental parameter (related to the geometry of the luminescent sample, the source and the detector, i.e. the emission collection efficiency),  $\varepsilon_\lambda$  is the luminophore absorption coefficient at the excitation wavelength (in  $\text{dm}^3 \text{mol}^{-1} \text{cm}^{-1}$ ),  $l$  is the optical pathlength (in cm) and  $c$  is the luminophore concentration (in  $\text{mol dm}^{-3}$ ). Such relationship helps to understand potential problems that may arise when designing and operating optical sensors based on polymer-supported luminescent probes<sup>12</sup>.

In order to speed up the sensor response when an analyte transfer step from the sample bulk into the indicator phase is required for measuring, the fluorescent probe is immobilized into a very thin polymer film (typically a few micrometers thick). The small  $l$  determines a low  $I_L$  but it can be enhanced using highly luminescent probes ( $\Phi_L$  as close as possible to 1) featuring a strong absorption of light (high  $\varepsilon_\lambda$ ). Since these two parameters are intrinsic to the luminophore, they are not always selectable by the user; therefore, a high indicator loading and a powerful light source are often used. However, a high excitation intensity focused onto a small sensitive tip (particularly when using optical fibers to carry the light to and from the distal end) causes photobleaching of the indicator dye and, consequently, noticeable signal drift. The problem worsens if we take into account that solid supports provide significant scattering of the incident light (compared to luminescence measurements at right angle in solution). The closer the emission wavelength to the excitation wavelength (Stokes shift), the higher the contribution of the scattered light to the fluorescence signal background, so that the sensor dynamic range narrows. Consequently, researchers strive to design photostable luminescent indicators with a large Stokes shift<sup>13</sup>.

Interestingly, the vast majority of luminescent molecules that fulfil the latter condition are those displaying an *intramolecular charge transfer* (ICT)

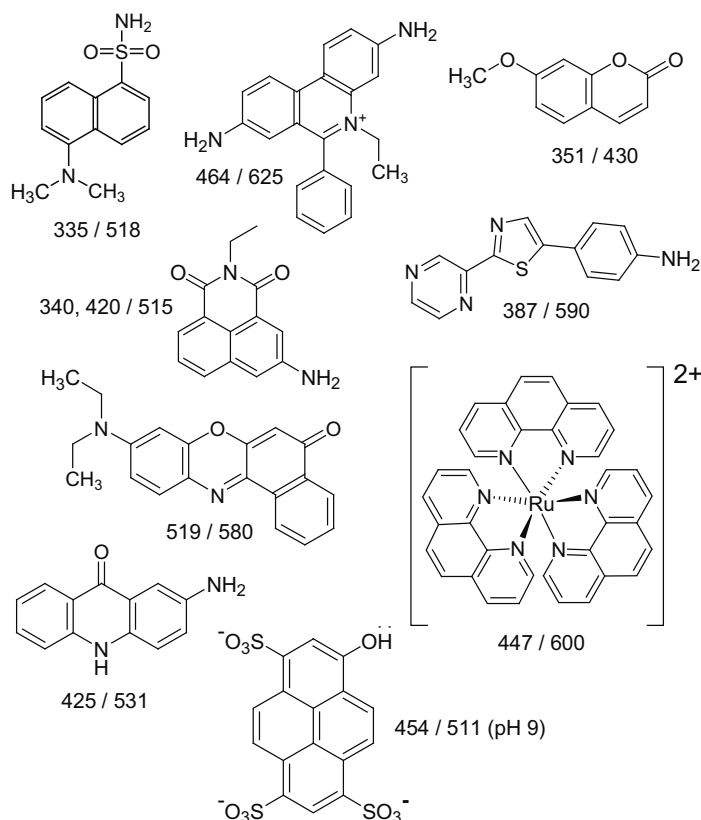


Figure 1. Some examples of luminescent probes with intramolecular charge transfer (ICT) electronic excited states. The numbers in parenthesis indicate the typical wavelengths of the excitation/emission maximums for each of them in polar media; however, introduction of chemical groups in the unsubstituted molecular frame or attachment to a solid support may shift those values.

excited state (Figure 1)<sup>14</sup>. This is due to the large difference in the electronic features of the excited state compared to those of the ground state as a consequence of the ICT process<sup>15</sup>.

The luminescence intensity of the indicator dye may decrease (so that the emission decay kinetics speeds up, see below) in the presence of a particular analyte species due to the so called *quenching* process. A competitive deactivation path for the excited state opens by way of *electron, proton or energy transfer* to/from the analyte (Figure 2)<sup>16</sup>. The new photochemical process, which was nonexistent in the absence of the quencher species, is selected to be reversible in order to allow for continuous monitoring of the latter: photoredox bimolecular deactivation ultimately renders the original reagents due to the fast back electron transfer; photoinduced energy transfer returns the fluorophore ground state and the (short-lived) electronically excited quencher; photoacidic or photobasic indicator dyes transfer hydrogen ions to/from Brønsted bases/acids present in solution (including the solvent

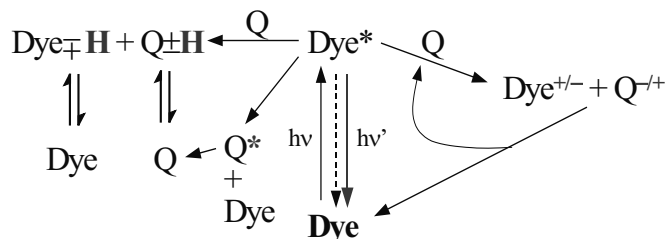


Figure 2. Principles of reversible luminescence sensing using photochemical quenching processes (electron, energy or proton transfer). Dye = luminescent indicator; Q = quencher species; dotted arrow: non-radiative deactivation processes. The luminescence intensity (and excited state lifetime) of the indicator dye decreases in the presence of the quencher. The indicator dye is typically supported onto a polymer material in contact with the sample. The quencher may be the analyte itself or a third partner species that interacts with the analyte (see text).

molecules). Of course, not every luminescent indicator molecule undergoes *all* of the above mentioned excited state deactivation pathways. Molecular engineering allows preparation of dyes with the appropriate redox potential (in the excited state), luminescence spectrum, or pH-sensitive functional groups to sense the target determinand using a particular quenching process. Properly calibrated, the luminescence intensity from the sensitive tip informs on the analyte concentration.

For instance, based on energy transfer quenching, luminescent fiber-optic sensors have been developed and commercialized for O<sub>2</sub> monitoring in natural waters, marine sediments, lichen colonies, whole blood, fermenters and process control in flammable environments. In all these cases, luminescent O<sub>2</sub> sensors show definite advantages due to their inherent features of minute size (down to micrometer), safety, accuracy (indicator-tunable dynamic range), lack of analyte consumption, independence of the sample flow, immunity to poisoning by hydrogen sulfide, resistance to biofouling and cost effectiveness compared to competing techniques such as electrochemical, paramagnetic or solid state sensors<sup>17</sup>. Optical waveguides are not essential: luminescent oxygen sensing layers have been stuck to the inner side of transparent plastic envelopes for non-intrusive monitoring of packaged foods<sup>18</sup> and to the bottom of 96-well microplates for cell growth assays<sup>19</sup>.

Fluorescence quenching may be *dynamic*, if the photochemical process is the result of a collision between the photoexcited indicator dye and the quencher species, or *static*, when the luminophore and the quencher are pre-associated before photoexcitation of the former<sup>20</sup>. It may be easily demonstrated that dynamic quenching in isotropic 3-D medium obeys the so-called Stern-Volmer equation (2)<sup>21</sup>:

$$\frac{I_0}{I} = 1 + K_{SV} [Q] \quad (\text{Eq.2})$$

where  $I_0$  and  $I$  stand for the fluorescence intensity in the absence and in the presence of the quencher ( $Q$ ), respectively,  $[Q]$  is the quencher concentration, and the ‘‘Stern-Volmer’’ constant ( $K_{SV}$ ) is actually the product of the unquenched excited state lifetime ( $\tau_0$ , see below) times the bimolecular quenching rate constant ( $k_q$ ). Therefore, a long-lived excited state and a fast photochemical process (i.e. diffusion- and not chemically-controlled) provide the highest analytical sensitivity.

It may also happen that an association equilibrium exists between the luminescent indicator and the quencher. Non-associated indicator molecules will be quenched by a dynamic process; however, the paired indicator dye will be instantaneously deactivated after absorption of light (static quenching). Equation 2 still holds provided static quenching is the only luminescence deactivation mechanism (i.e. no simultaneous dynamic quenching occurs) but, in this case,  $K_{SV}$  equals their association constant ( $K_{as}$ ). However, if both mechanisms operate simultaneously (a common situation), the Stern-Volmer equation adopts more complicated forms, depending on the stoichiometry of the fluorophore:quencher adduct, the occurrence of different complexes, and their different association constants. For instance, if the adduct has a 1:1 composition (the simplest case), the Stern-Volmer equation is given by equation 3:

$$\frac{I_0}{I} = 1 + (K_{SV} + K_{as})[Q] + K_{SV}K_{as}[Q]^2 \quad (\text{Eq.3})$$

where  $K_{SV}$  and  $K_{as}$  have the same meaning than those defined above.

The Stern-Volmer equations discussed so far apply to solutions of the luminophore and the quencher, where both species are homogeneously distributed and Fick diffusion laws in a 3-D space apply. Nevertheless, this is a quite unusual situation in fluorescent dye-based chemical sensors where a number of factors provoke strong departure from the linearity given by equation 2. A detailed discussion of such situations is beyond the scope of this chapter; however, the optosensor researcher must take into account the following effects (where applicable):

- (i) the possible contribution of *scattered light* from the powerful excitation source (at the monitored emission wavelength) that reaches the detector, even using wavelength-selecting devices; this effect is particularly dramatic for opaque sensitive layers containing the immobilized fluorophore and provides a constant signal background on top of the luminescence quenching phenomenon that is not considered in equation 2 or the like<sup>12</sup>;
- (ii) the intrinsic *heterogeneity* of the dyed *polymer* film at the microscopic or nanoscopic level; immobilization of the fluorophore onto a solid

- support yields species located in different microenvironments, each of them displaying a different Stern-Volmer constant (possibly including also  $K_{SV} = 0$ ) due to restricted accessibility of the quencher species; variation in the radiative and/or non-radiative deactivation constants are also possible. Incomplete solubilization of the dye in the polymer film also needs to be considered<sup>22</sup>; different multi-site models have been developed to account for typical downward curved Stern-Volmer plots observed for the oxygen quenching of solid-supported luminophores<sup>23</sup>;
- (iii) the effect of reduced or fractal *dimensionality* (i.e. <3D) on the quenching reaction space. fluorescence deactivation upon adsorption of the quencher onto a polymer material may take place by diffusion of the species within a 2-D surface, or even a confined monodimensional space (e.g. the narrow channels within a zeolite)<sup>24</sup>;
  - (iv) the possibility of *acid/base reactions* in the excited state that yield the fluorophore in different protonation states, each of them displaying distinct emission features<sup>25</sup>.

In any case, all those effects as well as others not discussed above are unfavorable for routine calibration purposes (yet some of them enhance the sensitivity of fluorescence-based optochemical sensors!). Therefore, numerous attempts to linearize the observed dose-response quenching plots have been described. Although frequently devoid of physical meaning, the most used method is the one assuming that a fraction of the measured luminescence signal is not quenchable ( $K_{SV} = 0$ ) while the remaining part follows a Stern-Volmer behavior characterized by a single  $K_{SV}$  constant. In this case the Stern-Volmer equation takes the form of equation 4:

$$I = I_{NQ} + \frac{(I_0 - I_{NQ})}{(1 + K_{SV}[Q])} \quad (\text{Eq.4})$$

where  $I_{NQ}$  is an empirical parameter that accounts for the part of the measured emission signal that can not be deactivated. This parameter is just chosen to yield the best fit of the  $I$  vs.  $[Q]$  plot.

### 3. LUMINESCENCE: A MULTI-FACETED OPTICAL PROPERTY

More fluorescence features than just the emission *intensity* can be used to develop luminescent optosensors with enhanced selectivity and longer operational lifetime. The *wavelength* dependence of the luminescence (emission spectrum) and of the luminophore absorption (excitation spectrum) is a source of specificity. For instance, the excitation-emission matrix has shown to be a powerful tool to analyze complex mixtures of fluorescent species and fiber-optic devices for in-situ measurements (e.g.

hydrocarbons, fermentation broths,...) are already in the market<sup>26</sup>. In these cases chemometrics (particularly principal components analysis and artificial neural networks) becomes an essential tool to extract quantitative information for simultaneous analysis of luminophores with partially overlapping spectra and different emission quantum yields.

*Ratiometric* luminescent probes make a smart use of the excitation wavelength effect on the emission intensity for extended optosensor performance. For example, the fluorescence from 8-hydroxy-1,3,5-pyrenetrisulfonate (HPTS) and other pH-sensitive dyes in water comes only from its (photo)excited basic form, but the absorption spectra of HPTS and  $\text{PTS}^-$  ( $\text{p}K_a$  7.3) differ considerably (Figure 3).

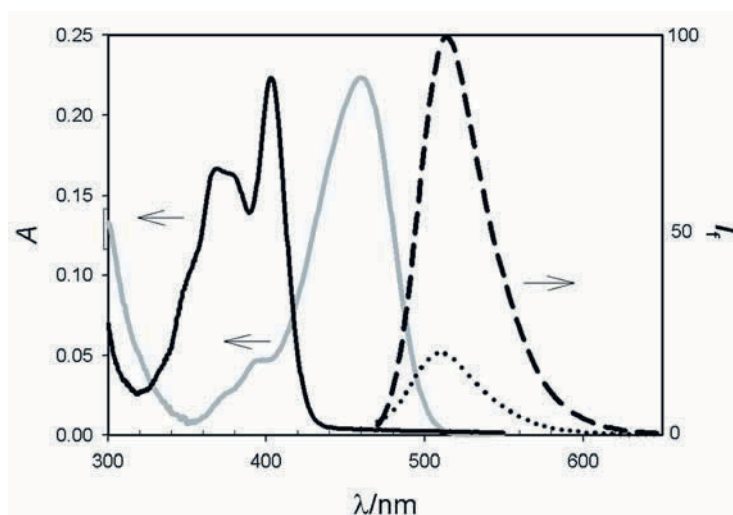


Figure 3. Absorption/fluorescence features of 8-hydroxy-1,3,5-pyrenetrisulfonate (HPTS) in water at different pH values (dark solid line: absorption at pH 2; light solid line: absorption at pH 11; dashed line: emission at pH 11; dotted line: emission at pH 2).

By measuring the ratio of fluorescence intensities upon excitation at two wavelengths (corresponding to HPTS and  $\text{PTS}^-$ , respectively), the sample pH can be accurately monitored in the 6–8 pH range provided HPTS is attached to a hydrophilic support. This proton-transfer photochemistry of HPTS and related dyes (e.g. rhodamines, coumarines,...) has been used in various miniature clinical optosensors targeted to in situ blood analysis of patients in critical condition. If a gas-permeable membrane separates the fluorophore-containing hydrogel from the sample, then carbon dioxide optosensors can also be fabricated since the incoming  $\text{CO}_2$  will undergo hydration and a pH decrease in the sensitive layer will follow. Such fluorescent fiber-optic  $\text{CO}_2$  monitors are currently marketed for fermentation control and biotechnology. Other acidic/basic gases (e.g.  $\text{NH}_3$  or  $\text{H}_2\text{S}$ ) can be sensed in the same way.



#### 4. LUMINESCENCE LIFETIME SENSORS

Fluorescence intensity has the disadvantage of being dependent on the excitation source output, the amount of indicator dye immobilized at the sensor tip, the detector sensitivity and the possible sneaking of ambient light on it. Therefore, intensity-based optosensors are prone to drift due to aging of the light source and detector, interference from ambient light, fluorophore leaching and photodegradation. These drawbacks are eliminated if the luminescence *lifetime* ( $\tau$ ) is used instead. The parameter  $\tau$  represents the reciprocal of the rate constant of the (first order) emission decay that follows an “instantaneous” excitation of the luminophore by a flash of light (Figure 4). The fluorescence lifetime is usually calculated by fitting the digitized emission decay profile to equation 5, where  $I_0$  is the amplitude (fluorescence intensity at the end of the “instantaneous” excitation flash)<sup>28</sup>. Alternative, it can be demonstrated by integration that  $\tau$  may also be calculated from the area under the decay curve ( $S$ ) and  $I_0$  (equation 6) without having recourse to data fitting or even a particular function to model the decay profile:

$$I_t = I_0 e^{-t/\tau} \quad (\text{Eq.5})$$

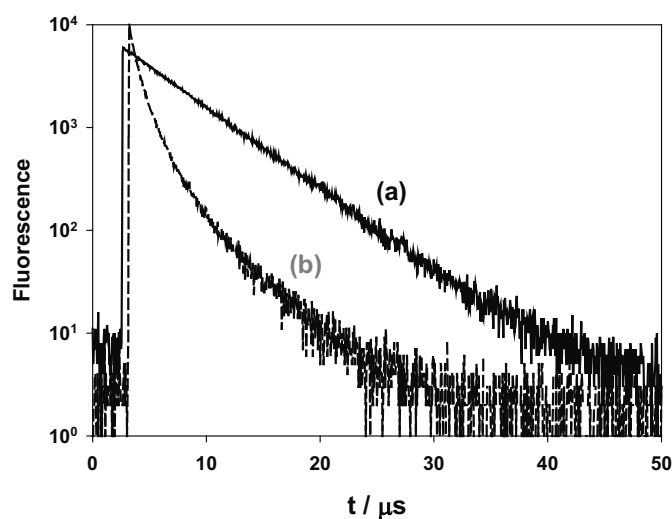


*Figure 4.* Luminescence decay profile of an oxygen indicator dye excited by a short flash of light, in (a) solution and (b) embedded into a gas-permeable film used to fabricate fiber-optic sensors for such species. The logarithmic scale of the Y-axis allows to compare the exponential emission decay in homogeneous solution and the strongly non-exponential profile of the photoexcited dye after immobilization in a polymer matrix.

$$\tau = S / I_0 \quad (\text{Eq.6})$$

When the fluorophore is immobilized on a solid support, the decay profile usually departs from the exponential kinetics predicted by equation 5 and verified in homogeneous media (e.g. solution, Figure 4). In this case, it is customary to fit the kinetic data to a sum of exponentials (equation 7) and mean lifetime values are used to characterize the return of the photoexcited molecule to the ground state<sup>28</sup>. If the so called pre-exponential weighted mean lifetime ( $\tau_M$ ) is used, equation 6 may still be used (equation 8):

$$I_t = \sum_i I_i e^{-t/\tau_i} \quad (\text{Eq.7})$$

$$\tau_M = \frac{\sum_i I_i \tau_i}{\sum_i I_i} = S / I_{max} \quad (\text{Eq.8})$$

where  $I_{max}$  is the maximum intensity of the fluorescence decay curve (zero or negligible signal background is assumed throughout the above equations).

The luminescence lifetime may also be extracted from *phase-sensitive detection* of the modulated emission that originates from modulated continuous excitation of the indicator dye (equation 9)<sup>2</sup>:

$$\tan \varphi = 2\pi f \tau \quad (\text{Eq.9})$$

where  $\varphi$  is the measured phase shift between the excitation and emission sinusoidal signals and  $f$  is the excitation modulation frequency (in Hz).

The commercialization of inexpensive robust LED and laser diode sources down to the uv region (370 nm) and cheaper fast electronics has boosted the application of luminescence lifetime-based sensors, using both the pump-and-probe and phase-sensitive techniques. The latter has found wider application in marketed optosensors since cheaper and more simple acquisition and data processing electronics are required due to the limited bandwidth of the sinusoidal tone(s) used for the luminophore excitation. Advantages of luminescence lifetime sensing also include the linearity of the Stern-Volmer plot, regardless the static or dynamic nature of the quenching mechanism (equation 10):

$$\frac{\tau_0}{\tau} = 1 + K_{SV} [Q] \quad (\text{Eq.10})$$

Nevertheless, the same factors described above may yield heavily non-linear quenching plots, which sometimes may be linearized with the “false light” strategy.

It is even possible to convert changes of the fluorophore emission *intensity* as a function of the analyte level into *lifetime*-based sensing devices using phase-sensitive detection. The technique is called “dual lifetime

referencing" (DLR)<sup>29</sup> and is based on the perturbation of the modulated luminescence signal (e.g. the  $\mu\text{s}$  emission of a Ru(II) polypyridyl complex) by a short lived fluorophore that emits (and absorbs) in the same region than the former. The composition of the phase-shifted long-lived emission with the perturbing zero-shifted fluorescence depends not only on their respective luminescence lifetimes but also on their relative emission intensities. Therefore variations of the fluorescence intensity of the indicator dye produce a change in the measured apparent emission lifetime.

## 5. FLUORESCENCE QUENCHING AND CHEMICAL SENSING

Regardless the static or dynamic nature of the quenching process (see above), quenching of the indicator dye fluorescence by the analyte itself or by an analyte-sensitive third party is one of the most widespread methods to develop chemical optosensors. Excited state *proton transfer* photochemistry<sup>25,30</sup> lies behind many pH sensors. It is not unusual that acids and bases increase dramatically their proton-releasing or proton-accepting features in their electronic excited state, compared to their acidity constants in the ground state, as a consequence of the charge redistribution they undergo upon absorption of light. However, care should be exercised when designing pH sensors based on fluorescence quenching when either the emission arises exclusively from the acid (or base) form of the photoexcited indicator due to "instantaneous" proton transfer, or the excited state proton transfer is an *non-equilibrium* process. In the first case (e.g. the HPTS indicator dye, see above) we can not use emission lifetime measurements to measure the sample pH since it would not change as a function of this parameter (only the fluorescence intensity would be modified). If the proton transfer photochemistry to/from the excited state is an irreversible process we will certainly observe both intensity and lifetime quenching as a function of the solution acidity<sup>31</sup>; however, the degree of quenching (Stern-Volmer plot, equation 2) will be a function of the acid/base strength of the quencher ( $k_q$ ) so that a universal calibration curve for the pH optosensor will be unattainable.

It is also possible to fabricate fluorescent sensors based on excited state *energy transfer* quenching. Efficient deactivation of both singlet and triplet electronic excited states by molecular oxygen is the base of the first fiber-optic fluorosensors. Typically,  $\text{O}_2$  quenches the fluorescence of most aromatic fluorophores at diffusion-controlled rates by enhancing intersystem crossing to the triplet state, frequently producing "singlet" molecular oxygen<sup>32</sup>. The longer lived phosphorescence of some indicator dyes in their triplet excited state is also quenched effectively by  $\text{O}_2$  via an energy transfer mechanism by electron exchange. Since the triplet state lifetime is much

longer than the singlet state lifetime, highly sensitive O<sub>2</sub> sensors based on phosphorescence (porphyrins<sup>33</sup>, Ru(II) polypyridyls,<sup>17,34</sup> metal-Ferron complexes<sup>35</sup>) have been developed (see above). Photosensitized production of singlet molecular oxygen as a consequence of the triplet excited state quenching may have a quantum yield as high as unity; therefore, photooxidation (with concomitant bleaching) of the indicator dye is not an unusual side effect in luminescent oxygen sensors.

Fluorescence resonance energy transfer (FRET) has also been used very often to design optical sensors. In this case, the sensitive layer contains the fluorophore and an analyte-sensitive dye, the absorption band of which overlaps significantly with the emission of the former. Reversible interaction of the absorber with the analyte species (e.g. the sample acidity, chloride, cations, anions,...) leads to a variation of the absorption band so that the efficiency of energy transfer from the fluorophore changes<sup>36</sup>. In this way, both emission intensity- and lifetime-based sensors may be fabricated.

Photoinduced *electron transfer* (PET) quenching processes can also be employed to develop fluorescence optosensors<sup>37</sup>. Due to the electron promotion upon absorption of light, every electronic excited state is both a better oxidant and a better reducing agent than its corresponding ground state. Therefore, the analyte will undergo a photoredox reaction with the appropriate (luminescent) indicator dye (intermolecular quenching) or will interfere with an existing intramolecular PET quenching. For instance, halide anions deactivate the fluorescence of acridinium and quinolinium cations via PET so that sensors for such species have been developed<sup>38</sup>. The strongly fluorescent naphthalimides undergo an intramolecular PET when an amino group is introduced in their structure at the end of a flexible spacer chain. The PET almost completely switches off their emission. However, attachment of a sodium ion-selective crown ether that also contains the quencher nitrogen atom has allowed fabrication of a smart Na<sup>+</sup> optosensor for physiological use because (reversible) complexation with the cation makes the indicator dye glow due to disappearance of the intramolecular PET process<sup>39</sup>. Similar schemes can be used to detect anions via molecular recognition coupled to interference with PET quenching of fluorescence<sup>40</sup>. The excited state redox reaction is normally reversible due to very fast back electron transfer (particularly in the solvent-caged encounter complex formed by reagents in condensed media), so that no net chemical change occurs.

## 6. APPLICATIONS AND NOVEL AREAS OF RESEARCH

As it has been discussed above, fluorescent-based sensors have found application to the analysis of every possible species: from gases (O<sub>2</sub>, CO<sub>2</sub>,

NH<sub>3</sub>, SO<sub>2</sub>, anesthetics, N<sub>2</sub>O,...) to cations, anions and neutral species (water, H<sub>2</sub>O<sub>2</sub>, hydrocarbons, nitroaromatics, glucose,...). It would be impossible to summarize here all the optical fluorosensors and their applications reported so far. Many more examples and details are given in other chapters of this book. In the following paragraphs we will just mention a few current areas of research in the field and future trends.

The versatility of luminescence goes beyond intensity-, wavelength- and kinetic-based measurements. Fluorescence *polarization* (or anisotropy) is an additional parameter still largely unexplored for optical sensing yet widely used in Biochemistry to study the interaction of proteins, the microfluidity of cell membranes and in fluorescence immunoassays. Although only a few optosensors based on luminescence polarization measurements can be found in the literature, elegant devices have recently been reported to measure chemical parameters such as pH or O<sub>2</sub> even with the bare eye<sup>41</sup>.

Since there are hundreds of sensing principles and fluorophores with many different excitation/emission wavelengths, emission yields and excited state lifetimes, significant efforts are currently being made towards the *molecular engineering* of indicator dyes<sup>42</sup>. Luminescent sensors will be cost-effective if the sensitive tips can be interrogated with a single light source and the emission analyzed with the same filter/detector combination. Such versatility requires careful design and preparation of a family of tailored fluorophores and tuned optoelectronics, so that multichannel multi-analyte fiberoptic monitors are possible<sup>43</sup>. Investigations have also been carried out to minimize or suppress the *biofouling* that produces significant signal drift in long term monitoring with luminescent sensors, particularly in the environmental and medical fields. For instance, nanometrical-thick polyacrylic coatings with pendant phosphoryl choline groups have shown to be very effective to that aim: more than 90% reduction of the adhesion of marine bacteria or platelets to the sensitive tip of luminescent O<sub>2</sub> sensors has been achieved<sup>44</sup>.

Near-infrared fluorophores (i.e. those emitting beyond 700 nm) and novel materials for fluorescent sensing is another area of active research. The former allow excitation with inexpensive powerful laser diodes currently used for telecommunications. Moreover, parasitic light scattering that normally perturbs the weak fluorescence measurements (see above) decreases as the detection wavelength increases following a  $\lambda^{-4}$  relationship. Unique emission features can be obtained from organic *nanoparticles*<sup>45</sup> and the so called semiconductor “*quantum dots*”<sup>46</sup>. While the former have been shown to entrap or covalently hold on its surface thousands of indicator dye molecules, chemical surface modification of the dots has still to be perfected to profit from the tunability and narrow width of their fluorescence. However, FRET quenching has recently been reported between CdSe/ZnS quantum dots and dye-labeled protein acceptors bound to their surface<sup>47</sup>. Novel organic (e.g. cyclosiloxanes)<sup>48</sup> and inorganic (e.g. organically

modified sol-gel)<sup>49</sup> polymers for increased analyte permeability and indicator accessibility are also giving birth to new generations of fluorescent sensors. Fluorescent dye-loaded polymer nanoparticles make it possible even to peer into single living cells<sup>50</sup>.

Bidimensional fluorescent sensors rather than point-sensing devices are bound to take over in clinical (bio)chemistry and biology. Fluorescence-based fiberoptic arrays comprised of thousands of fused waveguides (3–10  $\mu\text{m}$  diameter each) provide an individually addressable parallel sensing platform (ca.  $2 \times 10^7$  sensors  $\text{cm}^{-2}$ )<sup>51</sup>. The individual fiber cores can also be etched to form a high-density microwell array capable of housing analyte-sensitive microspheres. Such devices, together with chemometrics, have been applied to odor recognition, simultaneous chemical measurements (e.g.  $\text{O}_2/\text{pH}/\text{CO}_2$ ), oligonucleotide recognition and whole cell-based screening. The possibility of monitoring simultaneously an entire surface for a particular analyte (e.g. molecular oxygen, pH,...), using fluorescence intensity or lifetime, decreases dramatically the analysis throughput time and allows real-time monitoring of phenomena in living organisms, tissues and microwell plates<sup>52</sup>. Pressure-sensitive paints for prototype development in wind tunnels, based on imaging of the fluorescence quenching by  $\text{O}_2$  as a function of its partial pressure, have been introduced too.

## 7. FLUORESCENT BIOSENSORS

Analyte-selective *biosensors* can be manufactured by coupling a recognition element of biological origin (ionophore, enzyme, antibody, or even a whole living cell) and a fluorescent indicator layer. The interaction between the analyte and the recognition element must elicit some response (e.g. production or consumption of a chemical, very often  $\text{O}_2$  or  $\text{H}^+$ ) that is monitored by the luminescent indicator dye. For instance, glucose, lactate, cholesterol, ascorbic acid, glutamate, ethanol, tyrosine and other metabolites can be measured using the corresponding oxidase or oxygenase enzyme and a luminescent  $\text{O}_2$  transducer<sup>53</sup>. The biochemical oxygen demand (BOD) of waters, a measurement of their organic matter contents, can be monitored with optosensors based on bacteria and an  $\text{O}_2$ -sensitive photoluminescent dye<sup>54</sup>. Biosensors are thoroughly discussed in other chapters of this book.

In order to avoid the inherent fragility of enzymes and antibodies, fully synthetic receptors called *molecularly imprinted polymers* (MIP) have been developed for chemical recognition in fluorescence sensing<sup>55</sup>. Such insoluble materials contain acrylic networks that are formed by copolymerization in the presence of the analyte (template). The latter is subsequently eliminated leaving behind specific cavities and binding groups capable of re-binding the analyte species. The binding process must be coupled to a fluorescence tag (e.g. the fluorescent-labeled target analyte in competition assays or

fluorescent monomers) if MIPs are to be used for optical chemosensor development.

Although we currently master the principles underlying spontaneous emission of light from electronic excited states, fluorescence will continue by helping chemical and biochemical sensing due to its many advantages and applications. Among them fluorescent sensors will certainly monitor our environment, our industrial processes and our health.

## REFERENCES

1. Harvey E.N., *A History of Luminescence*, The American Philosophical Society, Philadelphia, 1957.
2. Lakowicz J.R., *Principles of Fluorescence Spectroscopy*, 2<sup>nd</sup> ed., Kluwer Academic/Plenum Publishers, New York, 1999.
3. Nevertheless, the first specific application of fluorescence to chemical analysis is probably the Al(III) determination using its morin chelate: Goppelsröder G. *J. Prakt. Chem.* 1867, 101, 408–415.
4. Valeur B., *Molecular Fluorescence*, Wiley-VCH, Weinheim, Germany, 2001.
5. Göpel W., Hesse J., Zemel J.N. (Eds.), *Sensors: A Comprehensive Survey*, Vol. 1: Fundamentals and General Aspects, VCH, Weinheim, Germany, 1991.
6. López-Higuera J.M., *Encyclopedia of Optical Sensors*, CRC Press, Boca Raton, Fla., 2003.
7. Narayanaswamy R., Wolfbeis O.S. (Eds.), *Optical Sensors: Industrial, Environmental and Diagnostic Applications*, Springer Series on Chemical Sensors and Biosensors Vol. 1, Springer, Berlin-Heidelberg, Germany, 2004.
8. Wolfbeis O.S. (Ed.), *Fiber-Optic Chemical Sensors*, Vol. 1 and 2, CRC Press, Boca Raton, Fla., 1991.
9. Cámara C., Moreno M.C., Orellana G., *Chemical Sensing with Fiberoptic Devices*, in: *Biosensors with Fiberoptics*, Wise D.L., Wingard Jr. L.B. (Eds.), Humana Press, Clifton, NJ, 1991, pp. 29–84.
10. Lübbers D.W., *Fluorescence Based Chemical Sensors*, in: *Advances in Biosensors*, Vol. 2, JAI Press, New York, 1992, pp. 215–260.
11. Further cases of *non-photochemical* fluorescent sensors include those where the luminophore undergoes a variation in the originally populated electronic excited state due to temperature or environmental changes (solvent, viscosity, ionic strength,...).
12. Strictly speaking, eq. 1 only holds for luminophores in solution (liquid or *transparent* solids). If the luminescent indicator dye is adsorbed onto an opaque support, which is a very common situation in optical sensing, eq. 1 holds only if the background absorption at the excitation wavelength is much higher than that of the supported luminophore. On the other limiting situation, the emission intensity is proportional to the square root of the luminophore concentration provided the background absorption is negligible and the dye absorption is low enough compared to the scattering coefficient of the supporting material (see, Oelkrug D., Mammel U., Brun M., Günther R., Uhl S., *Fluorescence Spectroscopy of Light Scattering Materials*, in *Fluorescence Spectroscopy: New Methods and Applications*, Wolfbeis O.S. (Ed.), Springer, Berlin-Heidelberg, Germany, 1993; pp 65–78).
13. Lakowicz J.R. (Ed.), *Topics in Fluorescence Spectroscopy, Vol. 4: Probe Design and Chemical Sensing*, Plenum, New York, 1994.
14. Rettig W., Kinetic Studies on Fluorescent Probes Using Synchrotron Radiation, in: *Fluorescence Spectroscopy: New Methods and Applications*, Wolfbeis O.S. (Ed.), Springer, Berlin-Heidelberg, Germany, 1993; pp 13–24.

15. See, for instance, Orellana G., Gómez-Carneros A.M., de Dios C., García-Martínez A.A., Moreno-Bondi M. C., Reversible Fiber-Optic Fluorosensing of Lower Alcohols, *Anal. Chem.* 1995; 67: 2231–2238.
16. Sometimes the quencher species is not the analyte itself, but a *third* (non-luminescent) *partner*, the concentration of which is set by the analyte level. For instance, the pH value (analyte) determines the amount of energy accepting dye that quenches the luminescence from the indicator by an energy transfer process.
17. a) Demas J.N., DeGraff B.A., Coleman P.B., Oxygen Sensors Based on Luminescence Quenching, *Anal. Chem.* 1999; 71: 793A–800A; b) Klimant I., Meyer V., Kühl M., Fiber-optic Oxygen Microsensors, a New Tool in Aquatic Biology, *Limnol. Oceanogr.* 1995; 40: 1159–1165. c) Leiner M.J.P., Optical Sensors for In-Vitro Blood-Gas Analysis, *Sens. Actuat. B: Chem.* 1995; 29: 169–173.
18. Papkovsky D.B., Smiddy M.A., Papkovskaia N.Y., Kerry J.P., Nondestructive Measurement Of Oxygen In Modified Atmosphere Packaged Hams Using A Phase-Fluorimetric Sensor System, *J. Food Sci.* 2002; 67: 3164–3169.
19. Wodnicka M., Guarino R.D., Hemperly J.J., Timmins M.R., Stitt D., Pitner J.B., Novel Fluorescent Technology Platform For High Throughput Cytotoxicity And Proliferation Assays, *J. Biomol. Screening* 2000; 5: 141–152.
20. While both photoinduced electron transfer and photoinduced energy transfer by the electron exchange (Dexter) mechanism require indeed a collision between the electronically excited luminophore and the quencher species, photoinduced energy transfer by the so-called dipole-dipole (Förster) mechanism may occur without collision between partners (yet its efficiency still depends on the donor-acceptor distance). Moreover, many proton-transfer reactions are known to take place by a long-range hydrogen ion exchange mechanism involving solvent molecules. Anyhow, all of the above mentioned quenching processes are included within the *dynamic* quenching category.
21. Gilbert A., Baggott J., *Essentials of Molecular Photochemistry*, Blackwell Scientific, Oxford, UK, 1991.
22. Bowman R.D., Kneas K.A., Demas J.N., Periasamy A., Conventional, Confocal And Two-Photon Fluorescence Microscopy Investigations of Polymer-Supported Oxygen Sensors, *J. Microscopy* 2003; 211: 112–120.
23. Demas J.N., DeGraff B.A., Xu W., Modeling of Luminescence Quenching-Based Sensors: Comparison of Multisite And Nonlinear Gas Solubility Models, *Anal. Chem.* 1995; 67: 1377–1380.
24. a) Klafter J., Drake J.M. (Eds.), *Molecular Dynamics in Restricted Geometries*, Wiley, New York, 1989; b) Berg H.C., *Random Walks in Biology*, Princeton University Press, Princeton, NJ, 1983.
25. Nelly R.N., Schulman S.G., Proton-Transfer Kinetics of Electronically Excited Acids and Bases, in: *Molecular Luminescence Spectroscopy: Methods and Applications*, part 2, Schulman S.G. (ed.), Wiley-Interscience, New York, 1988; pp 461–510.
26. Marose S., Lindemann C., Scheper T., Two-Dimensional Fluorescence Spectroscopy: A New Tool for On-Line Bioprocess Monitoring, *Biotechnol. Prog.*, 1998; 14: 63–74.
27. If the width of the excitation flash (nowadays typically from a pulsed LED or laser diode) is not shorter than approximately 1/3 of the fluorescence lifetime to be measured, signal deconvolution should be used to extract meaningful values from the kinetic data fit.
28. (a) Carraway E.R., Demas J.N., DeGraff B.A., Luminescence Quenching Mechanism for Microheterogeneous Systems, *Anal. Chem.* 1991; 63: 332–336; (b) Carraway, E.R., Demas, J.N., DeGraff, B.A., Bacon J.R., Photophysics and Photochemistry of Oxygen Sensors Based on Luminescent Transition-Metal Complexes, *Anal. Chem.* 1991; 63: 337–342.
29. Klimant I., Huber C., Liebsch G., Neurauder G., Stangelmayer A., Wolfbeis O.S., Dual Lifetime Referencing (DLR) – a New Scheme for Converting Fluorescence Intensity



- into a Frequency-Domain or Time-Domain Information, in Valeur, B.; Brochon, J.-C. (Eds.), *New Trends in Fluorescence Spectroscopy. Applications to Chemical and Life Sciences*, Springer, Berlin-Heidelberg, Germany, 2001; pp. 257–274.
30. (a) Vos J.G., Excited-State Acid-Base Properties of Inorganic Compounds, *Polyhedron* 1992; 11: 2285–2299; (b) Lasser, N., Feitelson, J., Excited State pK Values from Fluorescence Measurements, *J. Phys. Chem.* 1973; 77: 1011–1016.
  31. (a) Orellana G., Moreno-Bondi M.C., Segovia E., Marazuela M.D., Fiber-Optic Sensing of Carbon Dioxide Based on Excited-State Proton Transfer to a Luminescent Ruthenium(II) Complex, *Anal. Chem.* 1992; 64: 2210–2215; (b) Marazuela M.D., Moreno-Bondi M.C., Orellana G., Luminescence Lifetime Quenching of a Ruthenium(II) Polypyridyl Dye for Optical Sensing of Carbon Dioxide, *Appl. Spectrosc.* 1998; 52(10): 1314–1320; (c) Xavier M.P., Orellana G., Moreno-Bondi M.C., Díaz-Puente J., Carbon Dioxide Monitoring in Compost Processes Using Fibre-Optic Sensors Based on a Luminescent Ruthenium(II) Indicator, *Quim. Anal.* 2000; 19: 118–126.
  32. Schweitzer C., Schmidt R., Physical Mechanisms Of Generation And Deactivation Of Singlet Oxygen, *Chem. Rev.* 2003; 103: 1685–1757.
  33. Papkovsky D.B., Ponomarev G.V., Trettnak W., O'Leary P., Phosphorescent Complexes of Porphyrin Ketones – Optical Properties And Application to Oxygen Sensing, *Anal. Chem.* 1995; 67: 4112–4117.
  34. (a) Xavier M.P., García-Fresnadillo D., Moreno-Bondi M.C., Orellana G., Oxygen Sensing in Nonaqueous Media Using Porous Glass with Covalently Bound Luminescent Ru(II) Complexes, *Anal. Chem.* 1998; 70(24): 5184–5189; (b) García-Fresnadillo D., Marazuela M.D., Moreno-Bondi M.C., Orellana G., Luminescent Nafion Membranes Dyed with Ruthenium(II) Complexes as Sensing Materials for Dissolved Oxygen, *Langmuir* 1999; 15(19): 6451–6459.
  35. Díaz-García J., Costa-Fernández J.M., Bordel-García N., Sanz-Medel A., Room-Temperature Phosphorescence Fiber-Optic Instrumentation for Simultaneous Multiposition Analysis of Dissolved Oxygen, *Anal. Chim. Acta* 2001; 429: 55–64.
  36. Kosch U., Klimant I., Werner T., Wolfbeis O.S., Strategies To Design pH Optodes With Luminescence Decay Times In The Microsecond Time Regime, *Anal. Chem.* 1998; 70: 3892–3897.
  37. De Silva, A.P., Gunaratne, H.Q.N., Gunlaugsson, T., Huxley, A.J.M., McCoy, C.P., Rademacher, J.T., Rice, T.E. Signaling Recognition Events with Fluorescent Sensors and Switches, *Chem. Rev.* 1997; 97: 1515–1567.
  38. Urbano E., Offenbacher H., Wolfbeis O.S., Optical Sensor for Continuous Determination of Halides, *Anal. Chem.* 1984; 56: 427–429.
  39. He H., Mortellaro M.A., Leiner M.J.P., Young S.T., Fraatz R.J., Tusa J.K., A Fluorescent Chemosensor for Sodium Based on Photoinduced Electron Transfer, *Anal. Chem.* 2003; 75: 549–555.
  40. Fabbri L., Licchelli M., Taglietti A., The Design of Fluorescent Sensors for Anions: Taking Profit from the Metal-Ligand Interaction and Exploiting Two Distinct Paradigms, *J. Chem. Soc., Dalton Trans.* 2003; 3471–3479.
  41. Gryczynski I., Gryczynski Z., Lakowicz J.R., Polarization Sensing with Visual Detection, *Anal. Chem.* 1999; 71: 1241–1251.
  42. Orellana G., García-Fresnadillo D., Environmental And Industrial Optosensing With Tailored Luminescent Ru(II) Polypyridyl Complexes, in Narayanaswamy R., Wolfbeis O.S. (Eds.) *Optical Sensors: Industrial, Environmental and Diagnostic Applications*, Springer Series on Chemical Sensors and Biosensors Vol. 1, Springer, Berlin-Heidelberg, Germany, 2004; pp 309–357.
  43. Orellana G., Moreno-Bondi M.C., From Molecular Engineering of Luminescent Indicators to Environmental Analytical Chemistry in the Field with Fiber-Optic (Bio)sensors, in 15th Optical Fiber Sensors Conference Technical Digest (OFS-2002), IEEE, Piscataway, NJ, 2002; pp. 115–118 (ISBN 0-7803-7289-1).

44. Navarro-Villoslada F., Orellana G., Moreno-Bondi M.C., Vick T., Driver M., Hildebrand G., Liefelth K., Fiber-Optic Luminescent Sensors with Composite Oxygen-Sensitive layers and Anti-Biofouling Coatings, *Anal. Chem.* 2001; 73: 5150–5156.
45. Kuerner J.M., Wolfbeis O.S., Klimant I., Homogeneous Luminescence Decay Time-Based Assay Using Energy Transfer from Nanospheres, *Anal. Chem.* 2002; 74: 2151–2156.
46. Gaponenko S.V. *Optical Properties of Semiconductor Nanocrystals*, Cambridge University Press, Cambridge, UK, 1998.
47. Clapp A.R., Mendintz I.L., Mauro J.M., Fisher B.R., Bawendi M.G., Mattoussi H. Fluorescence Resonance Energy Transfer Between Quantum Dot Donors and Dye-Labeled Protein Acceptors, *J. Am. Chem. Soc.* 2004; 126: 301–310.
48. Xu W., Schmidt R., Whaley M., Demas J.N., DeGraff B.A., Karikari E.K., Famer B.L., Oxygen Sensor Based on Luminescence Quenching: Interactions of Pyrene with the Polymer Supports, *Anal. Chem.* 1995; 67: 3172–3180.
49. McDonagh C., MacCraith B.D., McEvoy A.K., Tailoring of Sol-Gel Films for Optical Sensing of Oxygen in Gas and Aqueous Phase, *Anal. Chem.* 1998; 70: 45–50.
50. Clark H.A., Kopelman R., Tjalkens R., Philbert M.A., Optical Nanosensors for Chemical Analysis inside Single Living Cells. 1. Fabrication, Characterization, and Methods for Intracellular Delivery of PEBBLE Sensors, *Anal. Chem.* 1999; 71: 4831–4836.
51. Epstein J.R., Walt D.R., Fluorescence-Based Fibre Optic Arrays: A Universal Platform For Sensing, *Chem. Soc. Rev.* 2003; 32: 203–214.
52. Mayr T., Igel C., Liebsch G., Klimant I., Wolfbeis O.S., Cross-Reactive Metal Ion Sensor Array in a Micro Titer Plate Format, *Anal. Chem.* 2003; 75: 4389–4396.
53. See, for instance: Moreno-Bondi M.C., Wolfbeis O.S., Leiner M.J.P., Schaffar B.P.H., Oxygen Optrode for Use in a Fiber-Optic Glucose Biosensor, *Anal. Chem.* 1990, 62: 2377–2380.
54. Preininger C., Klimant I., Wolfbeis O.S., Optical-Fiber Sensor For Biological Oxygen-Demand, *Anal. Chem.* 1994; 66: 1841–1846.
55. Díez-García M.E., Badía R., Molecularly Imprinted Polymers for Optical Sensing Devices, in Narayanaswamy R., Wolfbeis O.S. (Eds.) *Optical Sensors: Industrial, Environmental and Diagnostic Applications*, Springer Series on Chemical Sensors and Biosensors Vol. 1, Springer, Berlin-Heidelberg, Germany, 2004; pp 35–5.

## Chapter 7

# VIBRATIONAL SPECTROSCOPIC SENSORS

## Fundamentals, Instrumentation and Applications

Martin Kraft  
CTR - Carinthian Tech Research AG  
A-9524 Villach/St. Magdalen, Austria

### 1. INTRODUCTION

In textbook descriptions of chemical sensors, almost invariably a chemical sensor is described as a combination of a (dumb) transducer and a (smart) recognition layer. The reason for this is that most transducers, while (reasonably) sensitive, have limited analyte specificity. This is in particular true for non-optical, e.g. mass-sensitive or electrochemical systems, but also many optical transducers are as such incapable of distinguishing between different substances. Consequently, to build sensors operational in multi-component environments, such transducers must be combined with physico-chemical, chemical or biochemical recognition systems providing the required analyte specificity. Although advancements have been made in this field over the last years, selective layers are frequently not (yet) up to the demands set by industrial or environmental applications, in particular when operated over prolonged periods of time. Another significant obstacle are cross-sensitivities that may interfere with the analytical accuracy. Together, these limitations restrict the real-world applicability of many otherwise promising chemical sensors.

To reduce the dependence on potentially error-prone recognition systems, the use of smart transducers with possibly high intrinsic analyte specificity would be an obvious escape route. This leads directly to spectroscopic sensors. With spectroscopic transducers, the signal measured is a, more or less specific, spectral “fingerprint” rather than a change of some non-specific parameter like adsorbed mass or refractive index. Hence, it is possible to realise directly measuring sensors, capable of working either entirely independent of recognition systems or in combination with comparatively simple layers, e.g. for trace component enrichment. The degree of achievable specificity is very much dependent on the chosen wavelength range. While generally moderate in the electron excitation domain (UV/VIS), analyte

selectivity increases significantly when entering the range of vibrational spectroscopy. The two common vibrational spectroscopic methods, Infrared (IR) and Raman spectroscopy, both have proven their worth as substance-specific, reliable transducer principles for chemical sensing. Together, IR and Raman allow quantitative and qualitative detection of practically any molecule consisting of more than one atom. Thus, it is possible to detect almost any substance, in solid, liquid or gaseous form using vibrational spectroscopic sensors, even labile compounds and transient intermediates. As an added bonus, the individual spectral signatures of different compounds allow to simultaneously detect and quantify multiple analytes with one sensor, giving IR and Raman transducers a key advantage over sensors with pure mono-analyte capability.

Recent advances in instrumentation range from novel (laser) sources and highly compact spectrometers over waveguide technology to sensitive detectors and detector arrays. This, in combination with the progress in electronics, computer technology and chemometrics, makes it possible to realise compact, robust vibrational spectroscopic sensor devices that are capable of reliable real-world operation. A point that also has to be taken into account, at least when aiming at commercialisation, is the price. Vibrational spectroscopic systems are usually more expensive than most other transducers. Hence, it depends very much on the application whether it makes sense to implement IR or Raman sensors or if less powerful but cheaper alternatives could be used.

## **2. FUNDAMENTALS OF VIBRATIONAL SPECTROSCOPY**

Vibrational spectroscopy measures and evaluates the characteristic energy transitions between vibrational or vibrational-rotational states of molecules and crystals. The measurements provide information about nature, amount and interactions of the molecules present in the probed substances. Different methods and measurement principles have been developed to record this vibrational information, amongst which IR and Raman spectroscopy are the most prominent. The following focuses on these two techniques, the corresponding instrumentation and selected applications.

As this chapter aims at explaining the basics, operational principles, advantages and pitfalls of vibrational spectroscopic sensors, some topics have been simplified or omitted altogether, especially when involving abstract theoretical or complex mathematical models. The same applies to methods having no direct impact on sensor applications. For a deeper introduction into theory, instrumentation and related experimental methods, comprehensive surveys can be found in any good textbook on vibrational spectroscopy or instrumental analytical chemistry<sup>1-4</sup>.

## 2.1 Molecular Vibrations

The theory behind molecular vibrations is a science of its own, involving highly complex mathematical models and abstract theories and literally fills books. In practice, almost none of that is needed for building or using vibration spectroscopic sensors. The simple, classical mechanical analogue of mass points connected by springs is more than adequate.

Any molecule consisting of more than one atom can be described as a group of mass points (*atoms*) arranged in a geometrical pattern (*molecular structure*) and held in position by springs (*chemical bonds*). Due to the flexible nature of the connections, the mass points are able to respond to an impulse (*energy*) by vibrating around their equilibrium positions. For the simplest structure, two masses connected by one spring, this vibration results in a periodic elongation and shortening of the interatomic bond. The resonance frequency of this vibration is dependent on the masses of the two mass points and the force constant of the spring, according to Hooke's law. On the molecular scale, both the mass of the involved atoms and the bond strengths influence the vibration frequencies. Consequently, IR and Raman can distinguish between different isotopes and/or bond-types in a molecule.

Systems involving more mass points are capable of more complex vibrations, since the vibrational modes may involve several to many atoms and all three dimensions are available for vibrational movements. Vibrations where primarily the distances along the bond axis between the involved atoms change during the vibration are called *valence vibrations*. Vibrations causing a deformation of a bond angle are referred to as *deformation vibrations*. Deformation movements can also "rock", "wag" or "twist" a molecular (sub-) structure (Figure 1).

Altogether, molecular vibrations are highly substance specific. Ring structures for example are accompanied by ring vibrations that are usually not only characteristic for the presence and the size of a ring but also for the kind, number and position of groups attached. Additionally, the selectivity of vibrational spectroscopic systems is not restricted to actual changes of the molecular structure but includes any influence affecting the vibrational properties. Such effects can be *intermolecular interactions*, e.g. solvation effects, *intramolecular interactions* or the *chemical* (pH, ...) and *physical conditions* (temperature, ...). Occasionally, such correlations make it possible to detect even monoatomic molecules, which are not directly detectable by vibrational methods due to the lack of bonds that could vibrate. In any case, the proper control of measurement conditions and environmental parameters is crucial. While IR or Raman sensors can e.g. be used to detect differences in the secondary structures of proteins with identical primary structure, if wrongly applied they may also function as (rather expensive) pH-optodes or thermometers.

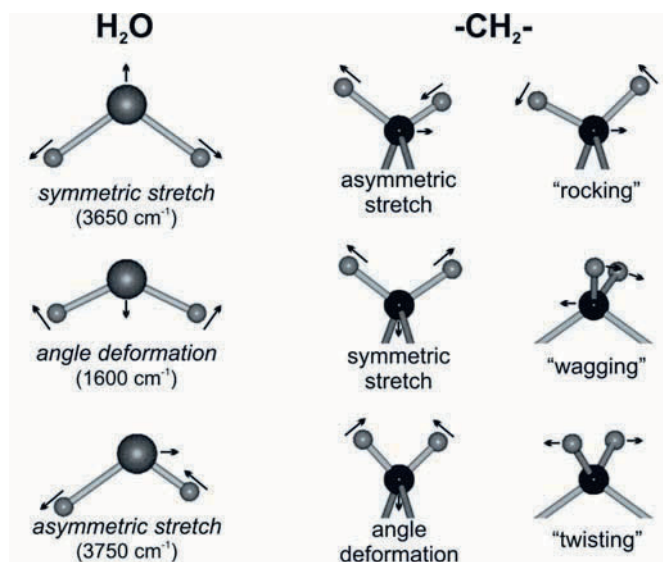


Figure 1. Vibrational modes of water and a methylene group.

The one crucial deviation from the mechanical model is the nature of the vibrational oscillation. In the classical model, the vibrational modes correspond to harmonic oscillators and the potential energy can be mathematically described by a parabolic function with the equilibrium position as energy minimum. Following this model, the vibrational energy levels would be equidistant, transitions are only allowed from a vibrational level to one level higher or one level lower and one energy quantum can excite one transition only. In reality, molecular vibrations behave like *inhomogeneous oscillators*. In the compressed state of the vibration, the mutual repulsion of the electron clouds of the two atoms leads to a steep increase in energy, while during the expansion movement the energy potential curve flattens out at increased interatomic distances towards a limit value representing the chemical bond dissociation energy (Figure 2).

As a direct consequence of the asymmetrically distorted energy potential, the actual properties of vibrational states and their transitions differ significantly from the behaviour predicted for harmonic vibrations. First, the energy gaps between the different vibrational states decrease with increasing excitation order instead of being equidistant. From this it follows that the transition rule “vibrational level  $\pm 1$  level only” is no longer strictly observed. It is now possible for a single photon to excite a molecule from its ground state directly to its second (or higher) vibrational state (Figure 3-b) or to excite two vibrations at once (combination vibrations). Together, these transition types are the backbone of the most widespread IR sensing method, near-IR spectroscopy.

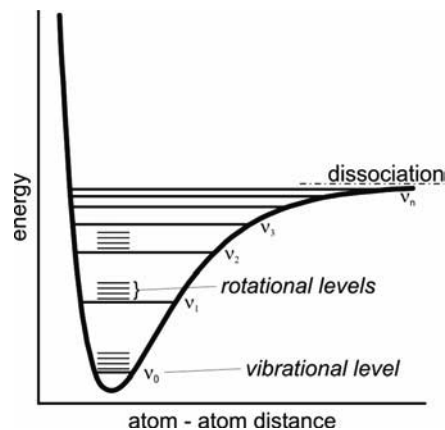


Figure 2. Vibrational and vibrational-rotational energy levels for a two-atomic molecule.

Apart from molecular vibrations, also *rotational states* bear a significant influence on the appearance of vibrational spectra. Similar to electronic transitions that are influenced by the vibrational states of the molecules (e.g. fluorescence, Figure 3-f), vibrational transitions involve the rotational state of a molecule. In the gas phase the rotational states may superimpose a rotational fine structure on the (mid-)IR bands, like the multitude of narrow water vapour absorption bands. In condensed phases, intermolecular interactions blur the rotational states, resulting in band broadening and band shifting effects rather than isolated bands.

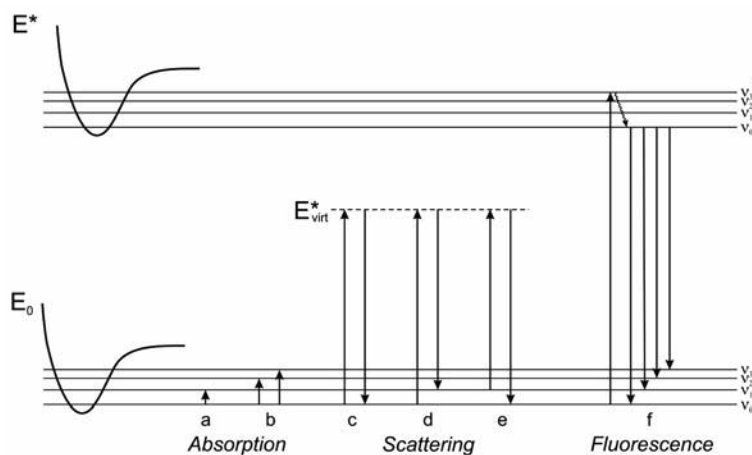


Figure 3. Energy schemata of transitions involving vibrational states (a: excitation of 1<sup>st</sup> vibrational state - mid-IR absorption; b: excitation of overtone vibrations - near-IR absorptions; c: elastic scattering - Rayleigh lines; d: Raman scattering - Stokes lines; e: Raman scattering - Anti-Stokes lines; f: fluorescence).

## 2.2 Infrared Spectroscopy

Usually, when referring to infrared spectroscopy, *IR absorption spectroscopy* is meant. Although this is the dominant method, occasionally it can be useful for sensing applications to also use *IR emission spectroscopy*.

### 2.2.1 IR Absorption Spectroscopy

IR absorption spectroscopy follows the principles of classical absorption spectroscopy. A sample is irradiated with electromagnetic radiation and the transmitted or reflected radiation is (spectrally) analysed. In IR spectroscopy, the wavelengths used are in the  $\mu\text{m}$ -range.

In contrast to UV/VIS radiation, IR photons have insufficient energy to excite electronic transitions ( $E \rightarrow E^*$ , Figure 3). Instead, the electric vector of the incident IR radiation couples to electric dipoles present in a molecule, causing the dipoles to reorient themselves after the external field. As the field oscillates, the molecular dipoles attempt to reorient over time to follow the changes in field polarity. If a net dipole in the molecule is now capable of oscillating at a frequency matching the interacting photon, an energy transfer from the photon to the molecule occurs and the molecule is excited to an excited vibrational state. Concurrently, the transmitted IR radiation is attenuated at the absorption wavelength(s) in comparison to wavelengths where no corresponding vibrations can be excited in the sample. Together, the different vibrations of a molecule, with different vibrational energies and hence frequencies, form a highly characteristic absorption spectrum.

From the energy interaction principle, the rules for IR absorption can be deduced. First, the overall dipole must change during the corresponding vibrational movement. If the dipole moment does not change, the molecule cannot interact with the external electromagnetic field and the vibration is IR inactive. This is condensed into the *IR selection rule*, stating that, *for a vibrational mode to be IR active, the overall dipole moment must change during the vibration* (compare Figure 4). The second point is that the resonance criterion must be fulfilled, in other words that the molecule must be able to vibrate at a frequency corresponding to the energy of the absorbed photon. In practice, the IR is segmented into three ranges based on the different kinds of vibrational transitions. Each range has its own particular instrumentation, applications, advantages and limitations.

#### 2.2.1.1 Mid-Infrared

In the mid-IR region of the spectrum, the incident radiation excites the *fundamental transitions* between the ground state of a vibrational mode and its first excited state (Figure 3-a). The corresponding wavelengths are



between  $4000\text{ cm}^{-1}$  ( $2,5\ \mu\text{m}$ ) and  $400\text{ cm}^{-1}$  ( $25\ \mu\text{m}$ ). Mid-IR bands are generally well structured and several orders of magnitude stronger than near-IR absorptions, giving the mid-IR an advantage in sensitivity and selectivity.

For sensing applications, one obstacle is the strong absorption of mid-IR radiation by water. The average achievable transmission pathlength in water is a few ten micrometers, in contrast to some millimetres in the near-IR. This renders classical transmission probes useless and reduces the sensitivity advantage by diminishing the permissible absorption pathlength. To measure in aqueous or other strongly absorbing environments, special techniques, like attenuated total reflection, have to be applied. Another problem is the limited availability of affordable instrumentation and suitable waveguides. Although some optical fibres and also hollow waveguides for this wavelength range are nowadays commercially available, many of these suffer from poor mechanical or chemical properties and/or limited long-term stability. This makes an implementation in sensors for practical use at least difficult.

#### 2.2.1.2 Near-Infrared

In the near-IR, *overtone vibrations* (transitions between the ground state of a vibrational mode and its second or higher excited state; Figure 3-b) and *combination vibrations* (excitation of two separate vibrational modes by one photon) are excited. The wavelengths corresponding to these transitions range from  $12800\text{ cm}^{-1}$  ( $780\text{ nm}$ ) to  $4000\text{ cm}^{-1}$  ( $2,5\ \mu\text{m}$ ). As such transitions are quantum-mechanically less likely than fundamental transitions band intensities are significantly weaker. This results in a reduced sensitivity in comparison to the mid-IR. On top, NIR bands are broader and generally less structured than mid-IR or Raman bands, resulting in a reduced capability to distinguish different analytes exclusively by their spectral characteristics.

Nonetheless, near-IR is the most widely used IR technique. Less intense water absorptions permit to increase the sampling volume to compensate, to some extent, for the lower near-IR absorption coefficients and the inferior specificity of the absorption bands can for many applications be overcome by application of advanced chemometric methods. Miniaturised light sources, various sensor probes, in particular based on transmission or transreflectance layouts, and detectors for this spectral range are available at competitive prices, as are (telecommunications) glass or quartz fibres.

While the field of near-IR sensing is frequently regarded as having reached its (scientific) limits, with advances restricted to minor progress in instrumentation and data evaluation procedures, interesting developments are reported in particular in the field of near-IR spectral imaging.

#### 2.2.1.3 Far-Infrared

Energy absorptions in the far-IR correspond to *rotational* and *translational movement states*, overlying *lattice vibrations* and *differential*

*transitions* (transitions between two different excited states). Until recently, the far-IR has been regarded as of purely academic interest. This changed over the last few years, when, under the name “THz Spectroscopy”, this spectral range has transformed into one of the hottest research fields in optical spectroscopy. However, though essentially of interest also for sensor applications, with the available instrumentation it seems currently out of question to set up practically applicable, affordable chemical THz-sensors.

### 2.2.2 IR Emission Spectroscopy

IR emission spectroscopy makes use of the reciprocal effect of IR absorption spectroscopy. At temperatures above 0 °K, molecules undergo a number of vibrational, vibrational-rotational or purely rotational movements. The relaxation of these excited states leads to the emission of thermal radiation, primarily in the IR region.

Thermal radiation emitted by an object can be continuous, discontinuous or, in most cases, a mixture. A continuous radiation profile corresponds to an ideal black body, where only the temperature of the emitting object determines the emission profile. Discontinuous thermal emission spectra are caused by photons emitted during the relaxation of excited vibrational states. Since vibrational states are quantised, this results in emission bands at the wavelengths of the corresponding IR absorption bands.

Consequently, any (non black-body) object broadcasts a characteristic thermal signature. When attempting a metrological detection of these emissions, a number of complications occur. For a significant flux of emission radiation the involved vibrations must be sufficiently excited. Also, since the warmer an object the more thermal radiation it emits, the sample must be the hottest spot of the entire measuring arrangement or its spectral signature will be covered by background emissions. Together, these two requirements ask for a possibly hot sample. A further limitation is the re-absorption of emitted radiation by molecules in their ground state. As, according to the Boltzmann distribution, there are always more molecules in the ground state than in an excited state, the molecules surrounding the emitting moiety will effectively absorb the emitted radiation. This limits the information depth for liquid or solid phases to just a few  $\mu\text{m}$ . While in a laboratory it is possible to adapt the experimental conditions accordingly, e.g. by cooling the entire spectrometer, for chemical sensing IR emission spectroscopy is limited to samples of at least 100 °C, preferably in gaseous form or as thin films on substrates with low broadband emissivity. While the number of emission IR sensor applications is small, the method is especially useful for remotely analysing hot samples that are not well accessible.

## 2.3 Raman Spectroscopy

Raman spectroscopy comprises a family of spectral measurements based on inelastic optical scattering of photons at molecules or crystals. It involves vibrational measurements as well as rotational or electronic studies and non-linear effects. Following, “Raman” will be used in the established but slightly inaccurate way as a synonym for the most important and most common technique of the family, linear vibrational Raman scattering.

The advantage of Raman over IR is that vibrational spectra ranging from  $\sim 4000 \text{ cm}^{-1}$  to  $\sim 30 \text{ cm}^{-1}$  can be obtained using standard UV, VIS or NIR sources, optics and detectors. Basically any optically accessible sample can be measured, even aqueous or other strongly IR-absorbing systems. The disadvantage that prevented the more widespread use for a long time is the inferior sensitivity due to low Raman scattering cross sections. As the Raman intensity increases linearly with the intensity of excitation radiation, this intensity problem could be resolved to a large extent by the introduction of laser sources, which are nowadays invariably used. Another problem is related to the wavelength of the excitation radiation. The intensity of Raman lines exhibits a fourth order dependence on the frequency of the excitation radiation. Shorter excitation wavelengths are hence preferable when aiming at high sensitivity. At the same time, the shorter the wavelength of the excitation radiation, the more likely is the excitation of sample fluorescence. As fluorescence is approximately three orders of magnitude stronger than Raman scattering and hence will cover the Raman scattering lines, it must be avoided. While in laboratory set-ups the two effects can be separated using ultra-fast time-gated arrangements, this is not practicable in sensing. As NIR radiation is usually too low in energy to excite fluorescence, near-IR lasers have gained substantial importance for Raman measurements of fluorescing samples. Yet, since Raman intensities in the NIR are even lower the detection power of such sensors will be further compromised.

### 2.3.1 Vibrational Raman Effect

The signal generation principle of Raman is inelastic molecular light scattering, in contrast to resonant energy absorption/emission in IR spectroscopy. During the measurement, the sample is irradiated with intense monochromatic radiation. While most of this radiation is transmitted, refracted or reflected, a small amount is scattered at the molecules.

During scattering, the involved molecule is excited to a virtual electronic excitation state. This quantum-mechanically forbidden and consequently instable excited state  $E^*_{\text{virt}}$  decays practically instantaneously ( $< 10^{-14} \text{ s}$ ) and the “stored” energy is reemitted as a photon in a random direction. For the majority of scattering events, the molecules relax back to their initial

vibrational states (Figure 3-c) and photons of the same wavelength as the excitation radiation are emitted. This elastic process is known as *Rayleigh scattering*. Provided that excitable vibrational states are present in a molecule, the excited molecule may, during the course of the relaxation, also return to a vibrationally excited level of its electronic ground state (Figure 3-d). A part of the photonic energy is used to excite vibrational levels in the target molecules, while the remaining energy is emitted from the scattering target as a photon with a slightly longer wavelength. These emissions on the low-energy side of the Rayleigh line are called *Stokes lines*. A second set of lines occurs if the excitation radiation interacts with already vibrationally excited molecules. This happens with a certain likelihood since a significant amount of vibrationally excited states are populated at temperatures above 0 °K. During the subsequent relaxation, the molecule can add its stored vibrational energy to the energy of the excitation photon while returning to its electronic and vibrational ground state (Figure 3-e). The energy transfer results in the emission of photons with higher energies and hence shorter wavelengths than the excitation radiation, the so-called *Anti-Stokes lines*. As significantly more molecules are in the ground state than in vibrational excited states, Anti-Stokes events are less likely than Stokes Raman scattering. Depending on the sample temperature, Anti-Stokes lines are typically about one order of magnitude weaker than Stokes lines.

In either case, the information on the vibrational transition is contained in the energy difference between the excitation radiation and the inelastically scattered Raman photons. Consequently, the parameters of interest are the intensities of the lines and their position relative to the Rayleigh line, usually expressed in wavenumbers ( $\text{cm}^{-1}$ ). As the actually recorded emissions all are in the spectral range determined by the excitation radiation, Raman spectroscopy facilitates the acquisition of vibrational spectra through standard VIS and/or NIR spectroscopy.

When looking at the principles behind the energy transfer, it must be taken into account that inelastic photon scattering is a vibronic interaction. At the wavelengths used, the excitation radiation has sufficient energy to interact with the molecular electron cloud, thus exciting the molecule to a (virtual) excited electronic state. On the particle scale, the electrons in the molecular orbital react to the electric field vector of the photon, bringing about a shift in local electron density and thus a polarisation of the molecular orbitals. The degree of polarisation is determined by the external field strength and the electronic polarisability. The electronic polarisability is the measure for the ease with which the electron cloud of a molecule responds to an external electromagnetic field. As long as the polarisability is constant, the electron cloud oscillates without coupling to the molecular vibrations. If, conversely, during the vibrational movement of a molecule the overall polarisability changes, the variation in the resistance against the change of polarisation couples the energy available in the oscillating electron cloud to

the vibrational states, facilitating a transfer of the amount of energy required to excite the matching vibration. This interaction is the physical background for the *Raman activity rule: vibrations are Raman active if the polarisability changes during the vibration*, a concept that is otherwise a bit hard to understand without going into mathematics.

The differences in the selection rules of IR and Raman become obvious when looking at a simple example, like carbon dioxide (Figure 4). The CO<sub>2</sub> molecule is capable of three energetically different vibrations and has negative partial charges ( $\Delta^-$ ) at the oxygen atoms and the corresponding positive charge ( $\Delta^+$ ) at the carbon atom. As it is fully symmetric, there is no net dipole moment in the equilibrium state.

During the symmetric stretching vibration ( $\nu_s$ ) both bonds stretch or contract symmetrically. As no overall change of dipole moment (+/-) occurs, the vibration is IR inactive. At the same time, the polarisability of the electron clouds of the bonds changes due to the oscillating bond lengths. The vibration is therefore Raman active. In the asymmetrical stretching vibration ( $\nu_{as}$ ), during the vibration one bond shortens while the other elongates. Thus, the polarisability increases in one bond but decreases in the other, resulting in a net change of polarisability of zero. Hence, this vibration is Raman inactive. At the same time, the asymmetric vibration causes a charge shift in the molecule, resulting in a dipole moment changing over time - the vibration is IR active. The same applies to the deformation vibration ( $\delta$ ). This vibration causes a change of bond angle, resulting again in an oscillating dipole. As at the same time the bond lengths are not affected, the polarisability remains constant over the vibration cycle. The vibration is IR active but Raman inactive.

The different interaction principles also explain why strongly IR-active vibrations typically exhibit weak Raman bands and vice versa, even if the selection rules would allow a vibration. If a strong dipole exists in a molecule, the electron cloud is strongly polarised. A change of polarisation in response to the electric field of a photon is therefore not very likely.

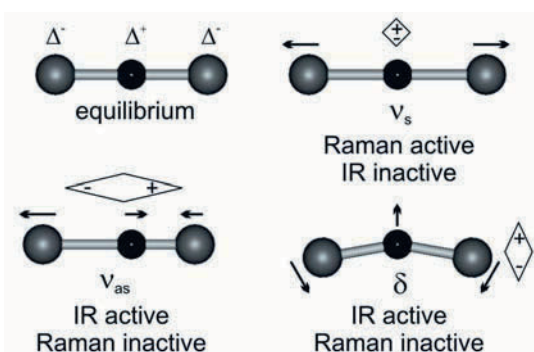


Figure 4. Vibrational modes of CO<sub>2</sub> ( $\nu_s$ : symmetric stretch;  $\nu_{as}$ : asymmetric stretch;  $\delta$ : deformation) and their respective IR and Raman activity.

Although the polarisation level is high, the polarisability is low, as subsequently is the energy coupling efficiency. If the dipole moment is low, the electrons in the cloud can move more easily and the coupling is more efficient. This results in stronger Raman bands, while due to the less pronounced molecular dipole little or no IR-activity can be observed.

### 2.3.2 Surface Enhanced Raman (SERS)

As the Raman scattering cross sections are low, Raman as such is not suitable for the detection of analytes at low concentrations. A popular way to resolve this problem is to add finely disperse (noble) metal particles or roughened surfaces, with particle sizes in the 100 nm - 10  $\mu$ m range to the sample or the sample/sensor interface. In such an environment, Raman line intensities can be enhanced by up to seven orders of magnitude, an effect known as Surface-Enhanced Raman Scattering (SERS) (see chapter 12). Thus, quantitative and qualitative analysis can be performed down to trace level concentrations. The application of VIS lasers gives significantly higher enhancement factors than NIR sources, but, especially when measuring labile compounds, strong photodegradation of the analytes at the rough surface will complicate the measurements.

A related effect has been described for IR spectroscopy - Surface Enhanced Infrared Absorption spectroscopy (SEIRA). However, as the enhancement factors are significantly lower than for SERS and both the required metal particle size and the activation distance between the target molecule and the particle are more than one order of magnitude smaller, no practically applicable SEIRA sensors have been demonstrated up to now.

## 3. INFRARED SENSORS

Applications of infrared sensors have been reported in the fields of biology/biochemistry, medical diagnostics, environmental monitoring and process control. IR sensors can measure analytes in solid, liquid or gaseous form using one of several different transducer layouts.

The majority of currently deployed IR sensors operate in the near-IR. Although near-IR sensors suffer from limited selectivity and sensitivity due to the relatively unstructured broadband absorptions in this frequency range, the easy availability of waveguides and other instrumentation give this spectral range a significant advantage over the mid-IR. Main application areas involve substance identification and process control.

The mid-IR range is attractive for optical sensing as highly molecule-specific information is provided, but difficult to access with standard sensor instrumentation. The application of mid-IR sensors is in particular of interest

when the required limits of detection can not be met with NIR systems, if spectral interferences have to be resolved or for the detection of substances that are inactive in the near-IR. Advances in IR fibre optics, mid-IR laser technology, spectrometer miniaturisation and novel coating materials open a wide range of application perspectives for mid-IR sensors.

### 3.1 Sensor Layouts

For IR sensing, three transducer principles are standard: classical *transmission* for (sufficiently) transparent samples, (diffuse) *reflection* for opaque samples, in particular solids and strongly turbid liquids and *attenuated total reflection (ATR)*, in particular for strongly absorbing samples and fluids with varying amounts of suspended solids or gas bubbles.

Apart from the sampling principle, sensor layouts can also be subdivided into *point-probe sensors*, giving averaged information about the analytes within the sensitive field, and *imaging sensors*, delivering a spatially as well as spectrally resolved image of the investigated area.

#### 3.1.1 Transmission

Transmission sensors have the advantages of being comparatively simple in design and well comparable to transmission laboratory experiments. The transmission pathlength and with it the probed volume is exactly defined and the sensitivity of the sensor can be adjusted by choosing a probe with a suitable transmission length. Most commercially available near-IR sensor devices for liquid samples are based on a transmission layout, as are some mid-IR sensors for operation in organic liquids. The exact design depends on the manufacturer and the application. The sensing area can e.g. be in the front (Figure 5-a) or the side part of the sensor head, with transmission lengths ranging from less than one mm to several cm. Also fibre-optically connected probes or probes with variable optical pathlengths are available.

For *liquid samples*, practical applications are restricted to qualitative and quantitative detection of main and minor components in clear, sufficiently transparent media. The sensing area is usually designed as a flow channel optimised on fast exchange of material for given flow conditions. Thus, transmission sensors can quickly detect changes in analyte concentrations. In samples with strongly absorbing backgrounds, e.g. aqueous solutions in the mid-IR, the permissible transmission pathlength may be less than 100  $\mu\text{m}$ . Such transmission sensors can be built, but their hydrodynamic properties would be unacceptable for most applications. Another problem is turbidity, either due to suspended solids or gas bubbles. The scattering at these particles, more than the actual absorptions, attenuate the transmitted light

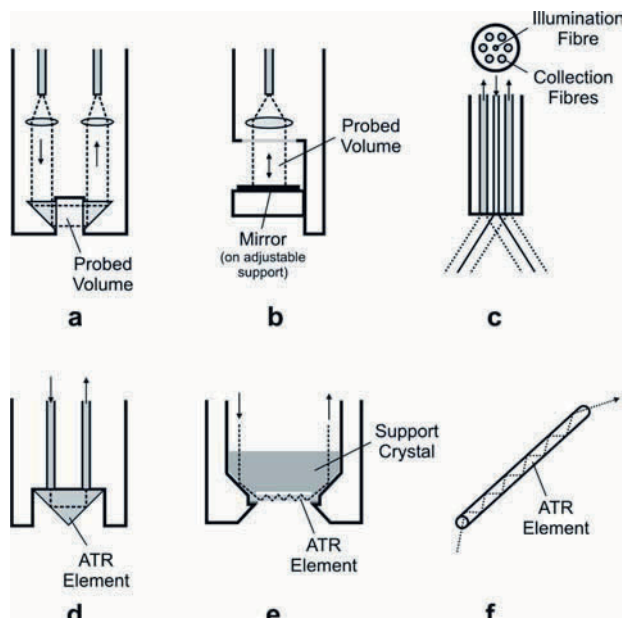


Figure 5. Single-point IR sensor head layouts a: transmission probe with fibre coupling; b: transflectance probe with variable pathlength and single fibre coupling; c: (diffuse) reflection probe with single illumination fibre and collection fibre bundle; d: two-reflection ATR probe with fibre-optic coupling; e: multi-reflection ATR probe (DiComp<sup>®</sup>-type); f: ATR fibre (“fibre evanescent wave” sensor).

and thus worsen the signal to noise ratio. Gas bubbles present even more of a problem in case the flow dynamics change over time, as the size distribution of the gas bubbles may change as well, thus causing a non-linear offset of the baseline. Finally, sensor modifications, e.g. to reduce the background or enrich specific analytes, are hardly possible.

*Solid samples* can also be measured in transmission, although reflection or transflection measurements are more common. Open arrangements with the source on one side of the sample and the spectral analyser on the other side are prevalently used, e.g. in industrial process control. For absolute quantitative analysis the thickness of the object must either be constant or be measured.

An entirely different kind of transmission cells is used for *gaseous samples*. Due to the lower density in the gas phase, a significantly higher pathlength is required to achieve acceptable limits of detection. While for higher analyte concentrations single-pass transmission cells can be used, for trace analysis high pathlengths are required. As multi-pass White cells can hardly be regarded as sensors, an alternative is the use of hollow waveguides as gas transmission cells. Such layouts look similar to the ATR fibre in Figure 5-f, with the exception that the light propagates in the waveguide not



by total reflection but by mirror reflection and that the sample would not be around the waveguide but be flushed through its hollow core.

### 3.1.2 Reflection

For some applications, especially such involving solid samples or fluids containing suspended particles, reflection spectroscopic systems are better suitable than transmission sensors. Apart from specular reflection, which provides comparatively little information and is of hardly any practical importance for IR sensing, two reflectometric methods can be used to gain spectroscopic information about a sample: *diffuse reflection* and *transflection*, a combination of transmission and diffuse reflection.

#### 3.1.2.1 Diffuse Reflection

In addition to the specular reflection at the immediate surface, a part of the illumination radiation may penetrate into the bulk of a sample. This penetration involves multiple reflection, refraction and diffraction events before parts of the radiation will eventually make it back to the surface. Due to the multitude of radiation - sample interactions, the diffusely reflected radiation has now a significantly higher information content about the sample than the specularly reflected light. The information depth is very much dependent on the wavelength and the sample, in particular its (optical) density, and can range from a few microns to tens of millimetres, thus allowing even bulk analysis for certain samples. As the reflected radiation comes off not only in the specular direction but in all other directions as well, diffusely reflected radiation can be separated from the (sensor-blinding) specularly reflected component e.g. by off-angle positioning of the sensor in respect to the position of the illumination source.

In IR sensing, open diffuse reflection (DR) layouts are most common for imaging systems, with the light source separated from the sensor unit. Also fibre optic probes (Figure 5-c) are available, usually in form of a single illumination fibre and a bundle of collection fibres. These can be used both for solid samples, e.g. powders, and for liquids containing a sufficiently high amount of scattering particles. Problematic with this kind of transducers is an absolute quantification, in particular if the density of scattering centres is not constant.

#### 3.1.2.2 Transflection

Transflection is essentially a cross between transmission and mirror reflection. When light is shined onto a reflective surface covered by an optically clear sample, either in liquid or in solid form, two processes occur -

reflection off the top surface of the sample and transmission and reflection off the mirror, followed by a second transmission. As for most materials the surface reflection is low in comparison to the reflection off the mirror, the total collected radiation corresponds to a transmission measurement with double pathlength. Due to the transmission doubling, this principle is popular when building compact sensor heads with yet large optical pathlengths. Also, this principle is more suitable to build probes with variable optical pathlength (Figure 5-b) than standard transmission layouts.

Transflection layouts are used in process analysis e.g. for the control of a (thin organic) coating on a reflecting metal substrate. For such applications, usually open layouts are used, with a directed light source shining IR radiation onto the sample and a detector positioned at the reflection angle. More common than open layouts are fibre-optic probes, as exemplarily shown in Figure 2-b, that are especially used for liquid samples. Again, various designs are available, as transfectance probes have the advantage of being highly versatile. Apart from the, in comparison to transmission probes of the same size, increased transmission pathlengths and the possibility to easily change the pathlength, transfectance probes can also be operated as diffuse reflection probes if the turbidity in the sample increases. Thus, DR probes can be used also in processes where the samples may vary from optically clear (suitable for transmission probes, not suitable for DR probes) to optically opaque, e.g. due to high amounts of suspended solids (suitable for DR probes, but not for transmission units). An important practical limitation for this case is that calibration curves for the transmission case and the diffuse reflection domain are not identical and in the mixed domain also not linear, which makes an absolute calibration of such principle-crossing sensors difficult.

### 3.1.3 Attenuated Total Reflection

For strongly absorbing matrices or samples that are otherwise unsuitable for transmission probes, e.g. due to variable amounts of suspended solids or gas bubbles, transducers based on *Attenuated Total Reflection* (ATR) are the method of choice. ATR makes use of the phenomenon of total internal reflection<sup>5,6</sup>. Radiation striking the interface of two dielectric media from the optically denser medium at an angle of incidence larger than the critical angle is totally reflected back into the optically denser medium. The reflectivity at the interface is a function also of the wavelength dependent optical properties of the optically rarer medium. Thus, the totally reflected radiation may pick up information from the medium adjacent to the waveguide. If an absorbing sample is placed in contact with the surface, the reflectance for total internal reflection is attenuated at the absorption wavelengths of the sample. Effectively, all molecules within a certain

distance (“information depth”) from the interface absorb energy from the evanescent field at their specific absorption wavelengths and the radiation transmitted through an ATR element shows an absorption pattern similar to standard absorption spectra derived from transmission experiments (see chapter 10).

As a rule of thumb, each attenuated total reflection provides the same information as a transmission cell with an optical pathlength equalling the wavelength of the totally reflected photon. Consequently, it is possible to build sensor heads with “transmission pathlengths” of just a few  $\mu\text{m}$  to some hundred  $\mu\text{m}$  without encountering the hydrodynamic problems occurring when a fluid has to be flushed through what essentially is a capillary. Instead, a crystal surface has to be brought in close contact with the sample, something that for fluids can easily be achieved by suitable positioning of the ATR probe or e.g. by adding flow deflectors. Also, as most liquids wet the ATR surface, on a submerged ATR probe a thin, stable liquid film forms across the sensitive area. Gas bubbles present e.g. in a reactor and suspended solids can not disrupt this film and hence cause significantly less problems than with other optical probes. Solids, in particular powders, can also be measured using ATR sensors, although for absolute quantification considerable care must be taken that the density in the probed volume remains constant.

One restriction of ATR sensors is their limited sensitivity. Typically, concentrations down to the 0,1 g/L range can be measured, depending also on the sample matrix. This can be compensated when modifying the sensor surface to exclude strongly absorbing backgrounds and/or enrich the analytes of interest. In contrast to transmission layouts, with ATR transducers this is easily possible by coating the sensitive area with a thin layer of a suitable, e.g. hydrophobic material. ATR sensors modified in such a way are capable even of trace component detection, but the specific pitfalls connected to modification layers must be observed when aiming at a practical application. Another point is the comparatively complex design and the significantly higher costs of such tools. Also, the total transmission through ATR elements is comparatively low, requiring sensitive detectors.

A few ATR probes are commercially available. In the near-IR ATR probes are mostly used as easy-to-use sticking probes for liquids and solids. As the aim is primarily to identify a material, not to measure low concentrations, probes with typically one or two reflections (Figure 5-d) are used. In the mid-IR, similar layouts can be found, using e.g. zinc selenide, germanium or silicon crystals as sensing elements. More sensitive and generally better suited for industrial process control DiComp<sup>®</sup>-type probes (Figure 5-e). The actual ATR element is in this case a thin diamond disc supported by a suitably shaped ZnSe crystal. ATR probes of that type are available off the shelf with between one and nine reflections. If more

reflections are required, it is either possible to take a longer ATR element or to resort to (bare) optical fibres.

### *3.1.3.1 Fibre Evanescent Wave Spectroscopy*

Fibre Evanescent Wave Spectroscopy (FEWS) is based on the same principle as conventional ATR, but uses an optical fibre as a waveguide (Figure 5-f). Fibres allow to increase the number of total internal reflections, which in turn increases the sensitivity of the sensor. This is of particular interest for trace analysis in non-absorbing matrices, but also for strongly absorbing media where the matrix component(s) can be excluded from the detection volume, e.g. by sensor surface modifications. Additionally, entirely fibre-optic systems are generally more flexible and, both optically and mechanically, easier to design and align than systems involving rigid optics. Finally, fibre-optic sensors are, at least theoretically, significantly cheaper.

A couple of complications limit the real-world applicability of optical fibres as sensing elements, in particular in the mid-IR. The first obstacle is the high attenuation of many (mid-)IR waveguides (see Table 1). This limits the permissible fibre length, as increased noise levels will soon neutralise the increase in signal. A second snag are the often inadequate chemical and/or mechanical properties of many (bare) fibres. In particular when using laser sources also the modal distribution of the light transport in an optical fibre may become a problem. Low order modes contribute less to the sensor response, while high order modes have a higher number of reflections and incidence angles closer to the critical angle and thus contribute more strongly. As the modal distribution is dependent on the coupling conditions and the arrangement of the fibre, changes of the sensor geometry, e.g. due to a collision with some solid object, may influence the sensor calibration.

In practice, very few applications of FEWS sensors can be found outside laboratory applications and demonstration systems. In the near-IR, suitable fibres are readily available but usually there is no real necessity to use them. Possible transmission pathlengths are sufficiently large to allow using standard transmission probes, while turbid samples can be measured using transfection or diffuse reflection probes. In the mid-IR, high intrinsic losses, difficulties in fibres handling and limited chemical and mechanical stability limit the applicability of optical fibres as sensor elements.

### **3.1.4 Emission**

Emission sensing arrangements are usually quite simple, provided the sample is significantly warmer than its surroundings, including all parts of the sensing unit in contact with the radiation. The hot sample acts as the source. The emitted light is collected by suitable optics, usually mirror

(telescope) optics and transferred into a spectral analyser, in most cases an FT-spectrometer with a cryostatic detector.

Applications of emission sensors can be found in remote sensing of hot, gaseous samples, in particular (industrial) exhaust gases.

### 3.1.5 Imaging Sensors

As most sensors are limited to single point probing, their application is confined to samples where the investigated point(s) are representative for the sample. Though this is the case for the majority of fluid samples, solid objects may not fulfil this requirement. This is true for high-tech products containing a wide range of different materials as well as e.g. in the food industry, where an item that is analysed as edible at one spot may very well be rotten at a different one.

A solution to this problem is the application of optical sensors with application-matched imaging capabilities<sup>7-9</sup>. To obtain such “spectral images”, three fundamental approaches in instrumentation and acquisition are available. The classical scheme of *sample scanning with a single point probe* is flexible in methodology and resolution, but the prohibitively high time consumption renders this approach useless for most practical applications. The second method is *wavelength scanning SI*. This technique is based on acquiring a number of 2D-images of a sample at different wavelengths. The wavelength selection can be achieved either by (i) a number of discrete filters<sup>10</sup>, e.g. on a filter wheel, (ii) tuneable filters<sup>11, 12</sup> or (iii) by illumination of the sample at selected discrete wavelengths<sup>13</sup>. In either case, the images recorded for the different wavelengths are combined by a computer and spectra are calculated for each pixel. The drawback of this method is that the sample must be kept stationary under the SI unit during image acquisition for all wavelengths of interest. This may prove a technical and process-logistical problem when acquiring images at more than just a few different wavelengths. Also, the spectra are available for further processing, e.g. classification, only after the last spectrally encoded image has been recorded. In contrast, *spatial scanning SI*, also known as “push-broom scanning SI”, records the spatial information line-wise, with the spectrum for each pixel along the sampling line being projected along the second axis of the two-dimensional detector chip. By combining the slices, the second spatial axis can be derived, resulting in a full image. The spectral encoding can be provided either by linearly variable filters<sup>14</sup> or by dispersive optics forming an imaging spectrograph<sup>15, 16</sup>. This method is preferable for many industrial applications, as it allows analysing the samples without disrupting the process. As the spectra for the single points are immediately available, a classification can be performed in real-time.

## 3.2 Instrumentation

In recent years, the evolution of the technological components required for IR sensor systems has been denoted by a significant miniaturisation of light sources, optics and detectors. Essentially, an IR sensor consists of (i) a polychromatic or monochromatic radiation source, (ii) a sensor head and (iii) a spectral analyser with a detector. As sensors where all optical elements can be included in the sensor head are the exception rather than the rule, also various optics, waveguides and filters may form essential parts of IR-optical chemical sensors. Another important building block, in particular when aiming at sensors capable of detecting trace levels, are modifications of the sensor element itself.

### 3.2.1 Radiation Source

Two types of radiation sources are used in IR sensing. Common sources are *thermal broadband emitters*. The second type are *laser sources*, mostly semiconductor lasers. The application of (monochromatic) laser sources trades the ability of multi-component detection against higher sensitivity for pre-defined target analytes. Hence, laser sources are primarily suitable for sensitive sensing in well-defined, stable systems, also because spectrally interfering substances can neither be detected as such nor compensated.

Thermal broadband sources are essentially black bodies heated to a certain temperature and hence emitting a defined spectral profile. In the mid-IR, commonly SiC (Glowbar<sup>®</sup>, ~ 1500 °K), ZrYTh-oxides (Nernst glower, ~ 1700 K) and carbon (micro)filaments are used. While glowbars and Nernst glowers have a substantial thermal mass and are best operated under constant conditions, the newly developed carbon filament sources<sup>17, 18</sup> have a much lower thermal mass and can be modulated at frequencies up to ~ 10 Hz, which can be useful for some applications. In the near-IR, mainly tungsten halogen lamps (~ 3000 °K) are used.

In the near-IR, in particular below 1,5 μm, also *light emitting diodes* are obtainable for many different wavelengths. These are supplemented by near-IR laser sources, available both as laser tubes and as diode lasers. A limitation of these sources is that, since they originate from telecommunications technology, laser sources are commercially available (at sensible prices) only for a few selected wavelengths, in particular in the shortwave near-IR. In the mid-IR, laser sources have been even rarer until recently. Existing *gas lasers*, e.g. the CO<sub>2</sub>-laser, are inconveniently large and much too high in power demand for sensing applications. Mid-IR diode lasers, usually *lead salt lasers*, have been introduced as an alternative to conventional IR light sources<sup>19, 20</sup>. The high energy density at the emission wavelength results in significantly better limits of detection compared to

conventional systems and the high possible pulse rates allow measuring at high time resolution. Still, lead salt lasers operate at cryostatic temperatures and it is usually necessary to have a monochromator to select the preferred laser mode, which makes the application of these sources rather inconvenient. The most recent development in the area of IR lasers are *quantum cascade lasers*<sup>21, 22</sup>. These lasers are compact and very stable, have a higher energy density than lead salt lasers and do not require cryo-cooling. QCL's are based on semi-conductor layer structures, forming a cascade of quantum wells. Each injected electron generates multiple photons due to a cascaded active region, resulting in output powers up to 200 mW. The emission characteristics are controlled by the layer thickness rather than material composition<sup>23</sup> allowing to design lasers with emission wavelengths up into the far-IR<sup>24</sup>. Also two-colour QCLs have been reported<sup>25</sup>.

### 3.2.2 Optical Elements

A number of different materials are available as lens or window materials for the near-IR as well as the mid-IR range. In the near-IR, mainly quartz is used, but also CaF<sub>2</sub> or sapphire optics can occasionally be useful. In the mid-IR, common materials are chalcogenide glasses, ZnSe, CaF<sub>2</sub> and KBr. Common to refractive elements in both wavelength ranges is the problem of chromatic aberration. Due to the wavelength dependence of the effective refractive index, the refractive properties and with it e.g. the focal lengths depends on the wavelength. This results in blurred focal points and similar optical aberrations when handling broadband radiation. While in the visible this problem can be resolved using achromatic lens arrangements, such optical designs are prohibitively expensive (if available at all) in the near-IR and (currently) not available in the mid-IR.

Consequently, *mirror optics* are more common, in particular in the mid-IR. The mirrors used are usually aluminium- or gold-coated flat or curved substrates. While near-IR mirrors are usually protected by thin SiO<sub>2</sub>-layers, in the mid-IR unprotected mirrors have to be used. Disadvantages of mirror optics are the elevated space consumption and the higher prices in comparison to refractive optics, especially comparing non-standard mirrors against non-standard lens. In total, mirror optics are so preferable to fibres and refractive optics, at least in the mid-IR, that in some technical applications they are used to replace waveguides to transport IR radiation between source, sensor head and spectrometer.

### 3.2.3 Waveguides

In the majority of applications, radiation source and/or spectral analyser are spatially separated from the actual sensing element. This has a number of

advantages, but necessarily requires some kind of waveguide to transport the radiation from the source to the sensor head and the optical signal from the sensor head to the analyser. The distances bridged can range from a few cm to several tens of meters, e.g. in distributed sensing or analytical observation of remote and/or (potentially) hazardous locations.

The prevalently used waveguides are *optical fibres*. Fibre technology is standard in the UV to near-IR, but also some fibres for light transport in the mid-IR have been developed. An overview of different IR fibre materials and their characteristic performance parameters is given in Table 1. More details can be found in a number of reviews focused on the material properties of IR transmitting optical fibres<sup>26-31</sup>. For some applications, as an alternative to optical fibres also *hollow waveguides* may be used.

Table 1. Material properties of common IR waveguides.

Material	Transmission range [ $\mu\text{m}$ ]	Attenuation [db/km] @ [ $\mu\text{m}$ ]	N.A.	max. operating temperature [ $^{\circ}\text{C}$ ]
SiO <sub>2</sub>	0.35 – 1.4	0.4 @ 1.32	0.16	300
SiO <sub>2</sub> , low OH	0.35 – 2.5	12 @ 0.82	0.16	300
Sapphire	0.5 – 3.0	2000 @ 2.90	1.42	1800
Fluoride	0.4 – 5.5	15 @ 2.5	0.21	200
Chalcogenide	1 – 12	250 @ 6	0.4	150
Tellurium halides	3 – 13	1000 @ 9	-	250
Silver halides	4 – 18	500 @ 11	0.5	300
Hollow waveguides	3 – 17	500 – 1500 @ 10.6	0.05	500 – 1800

### 3.2.3.1 Optical Fibres

In the near-IR, sensors almost exclusively rely on *silica fibres* (standard or low-OH) as they are accepted as industrially fully applicable<sup>32, 33</sup>. Silica-based glass fibres are chemically and mechanically robust, easy to handle, inexpensive, available with various core and outer diameters, a core-clad transfer fibres or bare sensing fibres, and have successfully been optimised to their theoretical attenuation limit<sup>34</sup>. The spectral window allows application up to 2,5  $\mu\text{m}$ .

*Sapphire fibres* have a slightly wider spectral range. The main argument for their application is their outstanding thermal stability, up to 2000 K. Also, their chemical stability is superior to most other waveguide materials.

Towards longer wavelengths, *chalcogenides* (AsSeTe - composites) are the technically most evolved and most commonly applied fibre materials in the mid-IR. If mid-IR fibres are used in practical applications, chalcogenides are usually the material of choice. Chalcogenides are chemically reasonable



stable but susceptible to crack propagation and generally fragile. Another problem are ageing effects. The temperature range is limited by a glass transfer temperature around 270 °C.

*Silver halide fibres* ( $\text{AgCl}_x\text{Br}_{1-x}$ ) have the widest spectral range in the mid-IR, well into the fingerprint range. Due to their crystalline nature, they have a superior flexibility. Problematic is their tendency to decompose upon contact with UV radiation or base metals. Also sulphides will chemically destroy the fibre material. Other points against are the high intrinsic attenuation due to absorption by impurities or scattering at inclusions or micro-crystals and the non-availability of (applicable) core-clad fibres.

### 3.2.3.2 Hollow Waveguides

A hollow waveguide (HWG) is essentially a hollow tube that transports light from one end to the other either by multiple mirror reflection or by total internal reflection. The hollow structure gives them several advantages: (i) a high power threshold, (ii) low insertion losses, (iii) no end reflections, (iv) a small beam divergence, (v) robustness and - especially important for sensor applications - (vi) a wide spectral transmission range.

Depending on the radiation propagation principle, the waveguides are grouped into “leaky guides” and “ATR fibres”. *Leaky guides* consist of a structural tube, a thin reflective layer covering the inner wall of the tube and a thin dielectric layer deposited onto the reflective layer for reflectivity enhancement and protection against corrosive substances. The waveguiding principle is reflection at a reflective surface. By using different materials for the structural tube, the reflective layer and the dielectric layer, it is possible to optimise HWGs for different wavelength ranges and applications<sup>35-37</sup>. *ATR fibres* are made from some dielectric material with refractive indices less than one for the wavelengths of interest. The waveguiding principle in this instance is total reflection at the inner surface of the waveguide. Although some applications have been described for ATR fibre hollow waveguides, leaky guide systems are much more common.

For sensing applications, high bending losses restrict the applicability as (flexible) light pipes. Practical applications are mostly restricted to gas cells, where the hollow waveguide acts as a compact multi-reflection cell to increase the sensitivity in comparison to single-pass cells.

### 3.2.4 Sensor Surface Modification

As vibrational spectroscopic sensors have a high inherent specificity, selective layers are usually not necessary. Still, sensor modifications can strongly enhance the sensitivity. At the same time, in particular for complex multi-component samples with spectrally interfering analytes, also the sensor

selectivity can be enhanced further by application of carefully selected and optimised sensor surface coatings. Another function of sensor coatings is protection of the transducer against mechanical, chemical and biological damage, e.g. due to corrosive components in the sample or biofouling.

In practice, surface modifications are restricted to sensors of the ATR- or FEWS-type. For other transducer layouts, the sample - radiation interaction is less localised, making a modification difficult to impossible. Depending on the analytes and the environment of the sensor, two basic surface modification strategies can be used to enhance the function of vibrational spectroscopic optical chemical sensors. The functional layers can either be (i) more or less sophisticated physico-chemical analyte extraction layers or (ii) chemo-reactive layers.

In the first strategy, the sensor surface is modified by coating with an in-situ solid-phase micro-extraction (SPME) layer. Determined by the partition coefficients for the system coating / sample matrix, the analytes are either enriched in the coating or excluded from the layer volume. If the layer thickness is matched to the information depth of the transducer, by selecting a suitable layer material the analytes are enriched in the probed volume while interferences can be excluded and hence effectively suppressed. The classical example is the enrichment of hydrophobic analytes in a thin hydrophobic layer, while the (strongly broad-band absorbing) water and other highly polar and/or hydrophilic substances are poorly or not enriched in the coating. These two effects - enrichment of the analytes and the exclusion of the, mostly aqueous, background - allow to enhance the sensor sensitivity by several orders of magnitude (% -> ppb) in comparison to a non-coated sensor of the same type. Layer materials encompass a range of synthetic polymers of varying hydrophobicity as well as sol-gel layers<sup>38</sup>. In either case, it is important for sensor applications for the analytes to diffuse into and out of the solid-phase extraction layers as quickly as possible to enable fast reaction of the sensor to changing analyte concentrations. In practice, this means that the layers must be possibly thin and homogenous.

If a sensor requires a higher selectivity than a vibrational spectroscopic sensor plus a moderately selective layer can provide, it is also possible to use highly selective systems as used for many other sensors. As one example, the combination of vibrational spectroscopic transducers with molecularly imprinted polymer or sol-gel layers opens a range of potential applications. The basic principle of molecular imprinting is to form specific recognition sites in an appropriate polymer matrix by polymerising a polymer around target analyte molecules (template) and washing them out after the polymerisation. By using monomers able to interact with this so-called "template", and with a high degree of cross-linking, "imprinted" recognition sites are formed, which are complementary to the template in terms of the shape and the positioning of the functional groups<sup>39, 40</sup>. Due to the general applicability of this procedure, molecularly imprints against a large variety

of template substances and for various applications are possible<sup>41</sup>. MIPs can effectively mimic the recognition properties of antibodies<sup>42</sup> while exhibiting much better chemical and physical stability (see also chapter of G.Mohr and chapter of H.Podbielska).

Another possibility is to immobilise enzymes either on the sensor element itself or in the vicinity of the sensing element. The operation principle is in most cases a semi-continuous spectral difference measurement in combination with a kinetic data evaluation. A sample containing the analyte of interest is recorded by the sensor immediately after contact with the sample and again after a certain time. Provided that no other changes in the composition of the sample occur over time, the spectral differences between the two measurements are characteristic for the analyte (and the metabolic products of the enzymatic reaction) and can quantitatively be evaluated. Provided that suitable enzymes are available that can be immobilised, this may be a viable option to build a sensor, in particular when the enzymatic reaction can not (easily) be monitored otherwise, e.g. by production or consumption of oxygen or a change of pH. In any case, the specific properties and stumbling blocks related to enzymatic systems must be observed (see chapter 16).

### **3.2.5 Spectral Analyser**

The simplest IR sensor would consist of a source, a sample interface and a detector. Although quite sensitive, such an arrangement would have no selectivity as any IR absorbing substance would cause an attenuation of the detected radiation. To get the selectivity that is a main driving force behind the application of IR systems, the radiation has to be spectrally analysed. This can be accomplished either by measurement at discrete wavelengths or, for multi-component sensors or samples containing (potentially) interfering substances, by full spectral analysis of the collected radiation.

#### *3.2.5.1 Discrete Wavelength Analysers*

When wishing to avoid a spectrometer, e.g. because the sensor has to be possibly cheap and only one analyte with characteristic absorption bands that do not overlap with other absorptions is of interest, a broadband light source can be equipped with a static wavelength selector, e.g. a narrow bandpass filter. Such filters are commercially available for the whole near-IR and wide ranges of the mid-IR. Alternatively, a number of narrow-band infrared light sources are available. The central disadvantage of all of these systems is the fact that only a transmission reading at a fixed single wavelength - or a narrow band - is obtained from the instrument. Consequently, such systems

are restricted to target analysis and are generally less flexible than spectroscopic instruments.

For multi-wavelength measurements, two technologies based on discrete wavelength analysis are available. One option is to take a number of single-wavelength sources to form a source array. This is not very economic for the VIS and NIR, where reliable dispersive spectrometers are available cheaply, but in the mid-IR QCL-arrays might replace existing spectrometers in the future. Alternatively, some laser sources can be tuned within a certain range. The second option is to take a broadband light source and a set of filters – or alternatively a gradient filter. The problem here is the high cost of such filters together with a severely limited spectral resolution.

### 3.2.5.2 Spectrometers

For environmental analysis or other fields where flexibility in analyte detection and/or the possibility to record whole spectra is essential, the use of spectrometers is inevitable. Recording full spectra also allows using chemometric methods to extract information from these spectra for multi-component analysis<sup>43</sup>.

In the near-IR, small, reliable spectrometers, consisting of a combination of a static (blazed) grating and a detector array, usually an InGaAs line array, are commercially available at competitive prices. These spectrometers can be reduced to a size that fits e.g. on a standard computer PCI card. An alternative is the use of a Carpenter's prism (grating prism) as dispersive element and a spectrally matched 2D camera as detector<sup>44</sup>. The main disadvantage is the low energy density at a specific wavelength, resulting in a reduced sensitivity when compared to single-wavelength systems.

When detector arrays are not available or too expensive, spectrometers with moving gratings can be used. The limitation of such systems is that the moving gratings necessarily involve moving parts, which complicates the design and has a negative influence on the sensor stability, and that gratings are generally useful only over a limited wavelength range around the design wavelength of that particular grating. Also, for compact systems the achievable resolution is severely limited. Nevertheless, occasionally such systems are used, both in the near-IR or the mid-IR.

In the mid-IR, routine infrared spectroscopy nowadays almost exclusively uses Fourier-transform (FT) spectrometers. This principle is a standard method in modern analytical chemistry<sup>45</sup>. Although some efforts have been made to design ultra-compact FT-IR spectrometers for use under real-world conditions, standard systems are still too bulky for many applications. A new approach is the use of micro-fabrication techniques. As an example for this technology, a miniature single-pass Fourier transform spectrometer integrated on a 10 x 5 cm optical bench has been demonstrated to be feasible. Based upon a classical Michelson interferometer design, all

components are micro-fabricated from silicon, including dovetailed bearing surfaces for precise translation of the moving mirror<sup>46, 47</sup>. Thus, a spectral resolution of  $0.1 \text{ cm}^{-1}$  is achievable. Considering that for many sensor applications a spectral resolution of  $4 \text{ cm}^{-1}$  is more than sufficient – especially in the liquid phase –, the reduction of the interferometer size to hand-held instruments is a viable option. Combining such miniaturised interferometers with MIR fibre-optic sensor technology may very well lead to a new generation of multi-component analyser systems, applicable in environmental monitoring as well as process control. Other developments in the field of micromechanical components concerning e.g. miniaturised translation mirrors with electrostatic actuation, are currently also under research. By using MEMS components, in the future FT-spectrometers with tolerable resolution and sensitivity could be reduced to the size of a few  $\text{cm}^3$ , with the actual detector being easily the biggest part of the layout.

Some developments are also going on towards building grating spectrometers with fixed gratings and detector arrays. These efforts are limited by the limited spectral range of a single diffraction grating and the availability of mid-IR detector arrays. The driving force behind these is military surveillance, which puts some restrictions of the availability. Also, mid-IR arrays and cameras are currently in a price range that is effectively prohibiting a mass application.

### 3.2.6 Detector

IR detectors convert (thermal) radiation energy into electrical signals. Two classes of such detectors exist: *thermal detectors* and *quantum detectors*.

Thermal detectors are based on the change of a material property due to the IR radiation. This material property is then transformed into an electric signal. Used effects include the Seebeck effect (thermocouples, thermopiles), the change of the resistance due to warming of the detector element (bolometers) and pyroelectricity (spontaneous electrical polarisation and hence charge separation due to a change in surface temperature; e.g. in DTGS detectors). All these detectors can be used over a wide spectral range and possess an (almost) uniform detectivity, provided the response is not influenced e.g. by windows protecting the actual detector element. Most common are pyroelectric detectors, in particular DTGS (deuterated triglycine sulphate) detectors, as they can be operated at room temperature. A problem is the high time constant in comparison to quantum detectors and the inferior detectivity (Figure 6).

Quantum detectors are based on semiconductors. The absorption of a photon excites an electron from the valence band into the conduction band. This can be measured either through a change in resistance (photoconductive

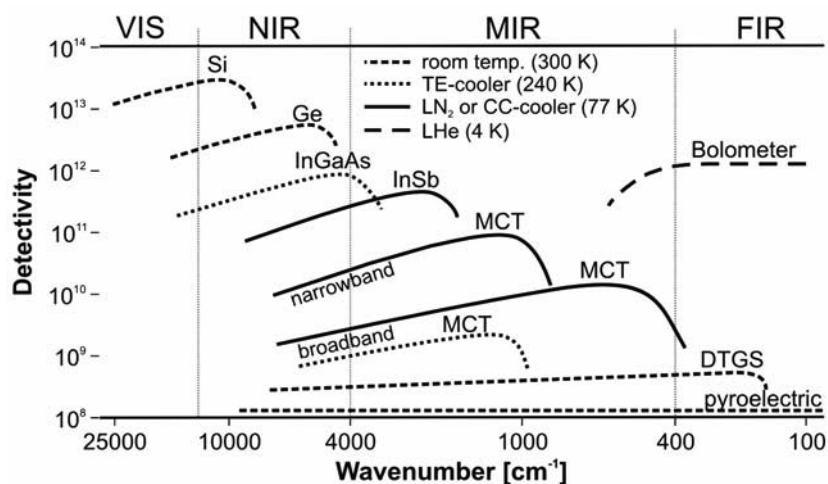


Figure 6. Typical detectivity curves and application ranges for selected IR detectors.

detectors) or by measuring the voltage that is induced during the process (photovoltaic detectors). Quantum detectors are significantly more sensitive, especially when cooled to cryo-temperatures to reduce the inherent noise, but require a certain minimum energy (“cut-off wavelength”) to excite the electrons over the band-gap and the detectivity decreases with increasing frequency (decreasing wavelength) of the detected radiation.

In the near-IR, InGaAs and InSb detectors are most common. InGaAs detectors are available also as line and 2D arrays. In the mid-IR, these photodiodes cover only the low-wavelength range. For the fingerprint region, which is of more interest for sensing applications, MCT (mercury cadmium telluride) detectors are prevalent. MCT detectors have short rise times and good sensitivity, but have to be operated at cryo-temperatures. For sensor applications, systems equipped with thermoelectric (Peltier) coolers ( $\sim 240$  °K) or Stirling (closed-circle, CC; 77 °K) coolers are commercially available, although especially CC-coolers are rather costly.

A new type of high sensitivity mid-IR detector for single wavelengths is based on an inverted QCL-principle (QCD, quantum cascade detector), but these are still under development and not yet commercially available.

### 3.3 Applications

With regard to the development of infrared sensors during the last decade, some major fields of application can be identified, covering *biological, biochemical or medical applications, environmental monitoring* and *process monitoring*, with the latter being considered as the area closest to a widespread application of IR optical sensor systems.

Since in many applications minor absorption changes have to be detected against strong, interfering background absorptions of the matrix, advanced chemometric data treatment, involving techniques such as wavelet analysis, principle component analysis (PCA), partial least square (PLS) methods and artificial neural networks (ANN), is a prerequisite.

### 3.3.1 Biological, Biochemical or Medical Applications

Due to usually complex sample matrices, only few applications of IR sensors dedicated to medical diagnostics or biological monitoring have been reported. The most advanced medical IR sensors, which are currently in clinical testing, are diffuse reflectance NIR spectral imaging systems. They are currently applied for detection of malignant growth, in particular on the skin. Characteristic spectral features can be identified to distinguish healthy skin tissue from cancerous areas, enabling also the determination of the stage of the skin disease, especially in combination with the imaging information. Generally, the combination of spectral and spatial data, often complemented by spectrally resolved VIS images, provides a wealth of information that can be correlated with superior accuracy to certain forms of cancer.

Also (non-imaging) mid-IR studies on human skin and tissue have been performed, e.g. by fibre-optic evanescent wave sensing. These experiments aim at the direct surface analysis of suspiciously looking spots on human skin and skin tissues for the discrimination of normal, pre-cancerous and cancerous states<sup>48</sup>. This, like many other applications are still in the laboratory phase, while others have proven inferior to competing sensing methods. As an example, it has been shown that blood glucose can be measured, either directly or through enzymes immobilised on a chalcogenide fibre, but the performance of the IR sensors did not merit a practical application, in particular in view of the strong competition in particular in this field.

### 3.3.2 Environmental Monitoring

The continuous determination of compounds, which may adversely affect ecosystems and/or human health, is a major regulative and legislative goal of environmental protection nowadays. Considering the costs and efforts related to this task corroborates a clear demand for portable, real-time, in-situ, field applicable and cost-effective monitoring techniques. Due to their inherent properties, vibrational spectroscopic sensors, in particular fibre-optic sensors show a high potential to contribute to these applications.

One example are fibre-optic chemical sensor systems for volatile organic pollutants in water<sup>49-53</sup>. These sensors are based on coupling the IR radiation

of a FT-spectrometer into an IR-transmitting fibre acting both as transfer waveguide and sensor element. The actual sensing area is coated with a thin hydrophobic polymer layer serving both as an extractor phase enriching the hydrophobic analytes in close vicinity to the sensor surface and as protection against water. In combination with a broadband IR light source and an FTIR spectrometer, simultaneous qualitative and quantitative detection of various organic pollutants is possible. A similar system is based on a compact turning grating spectrometer and an ATR crystal as sensor element<sup>54</sup>. In this example, the entire system, including the spectrometer, is designed to fit into a 2" cylinder to be used for application in groundwater probing wells.

Other environmental monitoring applications have been described for the measurement of environmentally relevant gases, either using hollow waveguide transmission cells combined with a spectrometer for multi-component analyses or compact, dedicated single-analyte gas cells based on integrated semiconductor structures<sup>55</sup>. Also IR emission-based remote sensors have successfully been used to analyse e.g. exhausts of passing cars or from (distant) industrial flue gases.

### 3.3.3 Process Monitoring

Process monitoring, in particular in-situ and in real time, is certainly the biggest application area of IR sensors. In particular near-IR probes for standard applications, like product identification and quality control, are widely used, but also process surveillance and process control can be coupled to near-IR sensors. Mid-IR sensors have roughly the same applications, but are practically used only if near-IR sensors fail to perform satisfactorily. In-situ mid-IR process sensors have been used for composition control of well-defined organic reaction mixtures, e.g. melamine formation, as well as for e.g. broth monitoring in bio-fermentations<sup>56, 57</sup>. Also solids, in particular powders can be analysed, even highly abrasive substances when using diamond optics.

Gas sensing applications, with special emphasis on fast response times and small sample volumes, have been realised based on hollow waveguides acting as capillary flow cells for gases such as ethylene<sup>58, 59</sup>, methane, butane<sup>60</sup> and CO<sub>2</sub><sup>61</sup>. The ATR fibre type has been used to measure NO<sub>2</sub> and SO<sub>2</sub><sup>60</sup>, utilising the high chemical inertness of this type of waveguides. The gaseous sample is pumped through the hollow waveguide core while the IR radiation is coupled into the waveguide by a focusing mirror or a suitable lens. Due to the internal reflections the waveguide acts as a low-volume multi-pass gas cell. Consequently, such a system shows a high sample exchange rate and an increased sensitivity compared to a conventional single-pass gas cells.



For solid samples, *spectral imaging sensors* are frequently the method of choice. The task here is rarely to detect trace amounts, but rather main and minor components and their distribution on the surface. The investigable sample size is determined by the optics and the resolution of the detector element. Practically, it can range from kilometres to millimetres, with spatial resolutions in the range of one hundredth to one ten thousandth of the overview area. In the near-IR, the material of the investigated samples or the type of a surface contamination can be determined. Applications range from the quick investigation of jewels over contamination detection on food<sup>62, 63</sup> to real-time sensors for the on-line identification and classification of e.g. polymer parts for an automated waste sorter<sup>64</sup>.

## 4. RAMAN SENSORS

Raman sensors can be used for all three physical states. It is possible to measure gases, though at the expense of sensitivity due to the lower sample density, liquids and solids of different forms and shapes. Basically any Raman active substance could be detected, also in aqueous solution, provided substance and the sample matrix permit Raman measurements (fluorescence problem, absorption, ...) and the analyte concentrations are sufficiently high.

In the majority of sensor applications, the motivation behind using Raman is to measure the selective features available through vibrational spectroscopy without having to deal with the problems coming with infrared measurements. The two related top advantages are the applicability of inexpensive standard fibres for light transfer and the capability of measuring in water. Applications encompass environmental monitoring in groundwater wells as well as process control. A second incentive is the ability to measure vibrational states that are not IR-active or occur at wavenumbers belonging to the far-IR. Raman sensors allow e.g. to detect molecular hydrogen or to distinguish between different crystalline formations of one substance during a manufacturing process. The third reasoning is the application as trace amount sensor using surface enhancement effects, e.g. in environmental in-situ monitoring.

### 4.1 Sensor Layouts

The basic layout of Raman sensors is similar to fluorescence probes. The common sensor form is that of a fibre optic probe, with excitation and collection fibres. As the excitation light comes from a monochromatic source no excitation filter is required, but a spectrally matched emission notch filter blocking the excitation wavelength is almost always part of the sensor head.

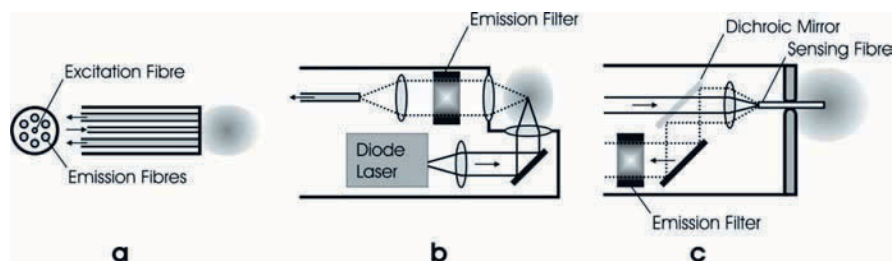


Figure 7. Exemplary Raman sensor layouts; a: reflection-type probe with single excitation fibre and collection fibre bundle; b: angular probe with internal laser diode; c: sensing fibre probe.

The actual sensor head geometry can be adapted to the respective application. Common layouts follow the classical backscattering geometry (Figure 7-a), with coaxially arranged excitation and the collection fibres and angular layouts (Figure 7-b), where the excitation and the collection fibres are spatially separated. Both varieties can be found with or without windows, depending on the intended application, and are commercially available from various suppliers.

Occasionally, arrangements with a fibre as sensing element (Figure 7-c) are used, in particular for SERS measurements (the fibre is then coated with the SERS substrate). When using such a layout, it must be taken into account that also the Raman scattering caused by the waveguide material is recorded and must be filtered out. The same applies to arrangements where a window or any other optical element illuminated by the excitation radiation is in the field of view of the collection optics.

#### 4.1.1 SERS

For trace analysis in fluids, some Raman sensors (try to) make use of the SERS effect to increase their sensitivity. While the basic sensor layout for SERS sensors is similar to non-enhanced Raman sensors, somehow the metal particles have to be added. Other than in the laboratory, where the necessary metal particles can be added as colloidal solution to the sample, for sensor applications the particles must be suitably immobilised. In most cases, this is achieved by depositing the metal particles onto the surfaces of the excitation waveguide or the interface window and covering them with a suitable protection layer. The additional layer is required as otherwise wash-out effects or chemical reactions between e.g. sulphur-compounds and the particles reduce the enhancement effect. Alternatively, it is also possible to disperse the metal particles in the layer material before coating and apply them in one step with the coating. Suitable protection or matrix materials for SERS substrates could be e.g. sol-gel layers or polymer coatings. In either

case, the material must be as freely permeable for the intended target molecules as possible.

A general problem with SERS measurements is the quantification. First, some modes will be strongly enhanced, some weaker and some not at all. A second problem is that the enhancement factors strongly depend on the particle surface, size, etc. In practice, this means not only that each SERS sensor has to be calibrated individually but also that the sensor response will drift if the particles change, e.g. due to aging. Reliable, stable quantification is most easily obtained by measuring a ratio against an internal standard, something that is not always easy to realise in real-world sensing. For more information on sensors based on surface enhanced Raman spectroscopy sensors and active substrates, please see chapter 12.

## **4.2 Instrumentation**

Similar to IR sensors, Raman sensors have profited from miniaturisation and improvement of light sources and optics. Essentially, a Raman sensor consists of (i) a monochromatic source, a (ii) sensor head, a (iii) filter separating the Raman lines from the excitation radiation and Rayleigh scattering and a (iv) spectral analyser.

In most arrangements, the source and the spectrometer are outside the actual sensor head, either in separate or in a common housing, while the optical connection to the actual sensor head is achieved by optical fibres or fibre bundles. The emission filter is integrated either in the sensor head or in the entrance part of the spectrometer. Such arrangements are especially advantageous for sensors operating in harsh environments, like elevated temperature, strong electric or magnetic fields or radioactive hazard zones. In other designs, the laser source and occasionally even the spectrometer are also integrated into the sensing unit to keep the optical distances short and thus optimise the sensitivity.

### **4.2.1 Source**

In practical application, Raman sensors exclusively use frequency-stabilised laser sources to compensate for the low intensity of the Raman radiation. For Raman sensors, prevalently compact high-intensity external cavity laser diodes are used, operated in CW (continuous wave) mode. These diode lasers combine high intensity with the spectral stability required for Raman applications and are commercially available at various wavelengths.

The wavelength selection depends very much on the samples to be investigated and is influenced by three main considerations. First, the sample must not (strongly) absorb at the excitation wavelength. Otherwise, the

sample will heat up, at the best influencing the vibrational states and at the worst burning or photo-bleaching the sample. For excitation in the VIS, this means the samples should not be coloured, while in the NIR in particular the water absorptions may be a serious problem. Second, as the Raman intensities have a forth-order relationship to the excitation frequency, possibly short excitation wavelengths should be used, but without exciting fluorescence in the sample. A third factor is the wavelength dependent sensitivity of the chosen/available detector or detector array.

For sensing, excitation wavelengths are typically between 400 nm and 1  $\mu\text{m}$ . For non-fluorescing samples, a possibly short excitation wavelength should be selected. Mostly blue or green laser sources are used. For samples (potentially) containing fluorophores, a good compromise is to use sources operating in the red (600 - 700 nm) or the short-wave near-IR around 800 - 900 nm. At these wavelengths, the fluorescence problem is generally low, the intensities of the Raman lines are for many analytes still acceptable and water absorption bands do not interfere.

#### 4.2.2 Waveguides and Optical Elements

In Raman sensing, waveguides are usually used only for light transfer, taking the excitation radiation from the source to the sensor head and the scattered light from the sensor head to the spectral analyser. The selection of a suitable waveguide depends on the excitation wavelength. Usually core-clad high-quality standard quartz or low-OH quartz fibres are used. Excitation fibres can be multi-mode or mono-mode, as collection fibres always multi-mode fibres are used. The excitation light is usually delivered by one fibre, often pig-tailed into the laser diode, while the emission is collected by a fibre bundle to increase the overall sensitivity. All these waveguides are easily available at low prices, both as naked fibres or assembled fibre-optic cables. For special applications, in particular at high temperatures or in chemical environments incompatible to quartz, also sapphire fibres or other suitable materials can be used.

Similar to the choice of waveguides, standard optics suitable for the respective excitation wavelengths can be used. Obviously, high quality optics should be used, in particular in the collection light path to achieve optimal system performance. The one thing that has to be taken into account during the optical layout is that virtually any optical element in contact with the excitation radiations will produce its own Raman scattering radiation. This is irrelevant if the excitation and the collection light paths are entirely separated. If common optical elements are used, e.g. a window or lenses, Raman peaks originating from the optics will occur in the recorded spectra. This may be of advantage, as these signals can be used as internal reference

signals, but the signals might as well interfere with the sample spectra and thus complicate the signal evaluation.

#### 4.2.3 Emission Filter

Independent of the geometry, the collected light contains large amounts of reflected excitation radiation and Rayleigh scattering. Since this radiation is several orders of magnitudes stronger than the Raman signals, it must be filtered out before detecting the Raman lines. To block Rayleigh scattering and reflected excitation light, nowadays primarily volume holographic filters (“notch filters”) are used. Although more expensive than classical dielectric filters, the high transmittance in the range of the Raman signals together with a high optical density in the blocking range and the narrow achievable bandwidths well merit the extra expense. Notch filters are nowadays commercially available in various sizes for practically any wavelength in the UV to shortwave NIR.

The implementation of notch filters makes the application of compact single-stage spectrographs, as used for chemical sensors, possible in the first place. Additionally, it permits to detect Raman lines much closer to the Rayleigh wavelength than previously possible.

#### 4.2.4 Spectral Analyser

As a rule of thumb, a difference of  $4\text{ cm}^{-1}$  in the Raman spectrum corresponds to a wavelength shift of  $\sim 0,1\text{ nm}$  in the measured spectrum. To distinguish two spectral features  $50\text{ cm}^{-1}$  apart, full spectral separation must be achieved over an interval of less than  $2\text{ nm}$ . This effectively excludes filter solutions. Therefore, Raman arrangements practically always rely on spectrometers for spectral analysis.

While essentially any spectrometer suitable for the spectral range around the excitation wavelength can be used, spectrometers used for Raman sensors are almost exclusively based on a static grating in combination with an array detector. The spectrometers are typically tied to a fixed excitation wavelength and optimised on possibly high resolution over a narrow wavelength range ( $\sim 100\text{ nm}$ ). High-resolution grating spectrometers for sensor applications (Raman resolution  $< 4\text{ cm}^{-1}$ ) employ possibly sensitive detector arrays, but are rather expensive. Alternatively, low-resolution systems (Raman resolution  $\sim 16\text{ cm}^{-1}$ ) are available at significantly lower prices, but also at the cost of a reduced sensitivity. Grating spectrometers are available for excitation wavelengths up to around  $1\text{ }\mu\text{m}$ . Above that, grating spectrometers are usually too insensitive, also because of the lower

sensitivity of the available detectors (Figure 6), while FT-Raman spectrometers are not very well compatible with sensor applications.

### 4.3 Applications

Similar to IR sensors, process analysis is the prevalent application area. Due to the applicability of standard VIS instrumentation, Raman probes have been used for more than two decades<sup>65, 66</sup>. Typically, Raman probes are applied where near-IR probes fail and hence are in direct competition to mid-IR probes.

Practical applications have been reported e.g. to distinguish between different crystalline forms of TiO<sub>2</sub> in a titanium oxide factory, based on the characteristic lattice vibrations<sup>67</sup>, but also to analyse the composition in the highly radioactive environment of a nuclear waste cooling tank<sup>68</sup>. A different application, that is exclusively available through Raman sensing, is the isotope selective detection of hydrogen and deuterium<sup>69</sup>, e.g. for fusion reactors.

Some standard Raman sensors aim also at other applications, e.g. groundwater monitoring. However, the majority of such applications, where high sensitivity is significantly more important than for process control, use the SERS approach. While SERS sensors are currently under development, some interesting results have already been published, dealing with biochemical and biological analysis<sup>70, 71</sup> or with environmental pollution monitoring, e.g. in the marine environment<sup>72</sup>.

## REFERENCES

1. Schrader B., (Ed.), *Infrared and Raman spectroscopy*, VCH-Verl.-Ges., 1995.
2. Chalmers J. M. (Ed.), *Handbook of vibrational spectroscopy*, Wiley, 2002.
3. Meyers R.A. (Ed.), *Encyclopedia of analytical chemistry*, Vol. 12 & 15, Wiley & Sons, 2000.
4. Lindon J. C. (Ed.), *Encyclopedia of spectroscopy and spectrometry*, Acad. Press, 2000.
5. Harrick N.; *Internal Reflection Spectroscopy*, 3<sup>rd</sup> Ed., Harrick Scientific Corp., 1987.
6. Klein M., Furtak T.; *Optik*, 2<sup>nd</sup> Ed., Springer Verlag, 1988.
7. van der Meer F., De John S.M. (Eds.); *Imaging Spectrometry*, Kluwer Acad. Publ., 2002.
8. Bearman G.H., Levenson R.M., Cabib D. (Eds); *Spectral Imaging: Instrumentation, Applications, and Analysis*, SPIE Publications, 2000.
9. Smith R.D., Nelson M.P., Treado P.J., *Proc. SPIE*, 2000; 3920: 14.
10. Hopkins M.F., Four-color pyrometry for metal emissivity characterization, *Proc. SPIE*, 1995; 2599: 294.
11. Eisenreich N., Rohe T., *Encyclopedia of Analytical Chemistry*, Wiley & Sons, 2000, 7623 – 7644.
12. Gat N., Imaging Spectroscopy Using Tunable Filters: A Review, *Proc. SPIE*, 2000; 4056: 50-64.

13. Carstensen J.M., European Patent *EP 1051660 B1*, 1999.
14. Gat N., US Patent *US 5166755*, 1992.
15. Fately W.G., Hammaker R.M., DeVerse R.A., Coifman R.R., Geshwind F.B., The other spectroscopy: demonstration of a new de-dispersion imaging spectrograph, *Vib. Spec.*, 2002; 29: 163-170.
16. Aikio M., European Patent *EP 0635138 B1*, 1993.
17. Johnson E.A., US-Patent *US 6249005*, 2001.
18. Daley J.T., Wollam J.S., Bodkin W.A., Johnson E.A., European Patent Application *EP 1101391 A1*, 2000.
19. Kastner J., Tacke M., Katzir A., Edl-Mizaikoff B., Göbel R. and Kellner R., Optimizing the modulation for evanescent-wave analysis with laser diodes (EWALD) for monitoring chlorinated hydrocarbons in wat, *Sensors Actuators B* 1997; 38: 163-170.
20. Krska R., Kellner R., Schiessl U., Tacke M. and Katzir, Fiber optic sensor for chlorinated hydrocarbons in water based on infrared fibers and tunable diode lasers, *Appl. Phys. Lett.*, 1993; 63 (14), 1868-1871 A.
21. Faist J., Capasso F., Sivco D., Sirtori C., Hutchinson A. and Cho A., Quantum cascade laser, *Science*, 1994; 264: 553-556.
22. Strasser G., Gianordoli S., Hvozdar L., Bichl H., Unterrainer K., Gornik E., Kruck P., Helm M., Heyman J., GaAs/AlGaAs intersubband mid-infrared emitter, *Mat. Res. Soc. Symp. Proc.*, 1998; 484: 165-170.
23. Capasso F., Band-Gap Engineering : From Physics and Materials to New emiconductor Devices, *Science*, 1987; 235: 172-176.
24. Capasso F., Gmachl C., Sivco D.L., Cho A.Y., Quantum cascade lasers, *Phys. World*, 1999; 12: 27.
25. Gmachl C., Tredicucci A., Sivco D.L., Hutchinson A.L., Capasso F., Cho A.Y., Bidirectional Semiconductor Laser, *Science*, 1999; 286: 749.
26. Savage J.A. in Almeida R.M. (Ed.), *Halide Glasses for Infrared Fiber Optics*, NATO ASI Series E. 123, Martin Nijhoff Publishers, 1987.
27. Harrington J.A. and Katzir A.(Eds.), *Infrared Fiber Optics Proc. SPIE*, 1989; Vol. 1048.
28. Harrington J.A. and Katzir A.(Eds.), *Infrared Fiber Optics II Proc. SPIE*, 1990; Vol. 1228.
29. Harrington J.A. and Katzir A.(Eds.), *Infrared Fiber Optics III Proc. SPIE*, 1991; Vol. 1591.
30. Drexhage M.G., Moynihan C.T., *Scientific American*, 1988; 110-115.
31. Sanghera J.S., Aggarwal I.D.(Eds.), *Infrared Fiber Optics*, CRC Press, 1998.
32. Arditty H.J., Dakin J.P., Kersten R.T. (Ed.), *Optical Fibre Sensors*, Springer, 1989.
33. Wolfbeis O.S.(Editor), *Fiber Optic Chemical Sensors and Biosensors*, CRC Press, 1991.
34. Miya T., Terunuma Y., Hosaka T., Myashita T., *Electron. Lett.*, 1979; 15: 106.
35. Croitoru N., Inberg A., Dahan R. and Ben David M., Scattering and beam profile measurements of plastic, silica, and metal radiation waveguides, *J. Biomedical Optics*, 1997; 2 (2): 235-242.
36. Alaluf M., Dror J., Dahan R. and Croitoru N., Plastic hollow fibers as a selective infrared radiation transmitting medium, *J. Appl. Phys.*, 1992; 72 (9): 3878-3883.
37. Alaluf M., Dror J. and Croitoru N., Plastic hollow waveguides as transmitters and filters in mid-IR radiation, *Proc. SPIE*, 1991; 1591: 146-149.
38. Han L., Niemczyk T.M., Lu Y., Lopez G.P., Chemical Sensors Based on Surface-Modified Sol-Gel-Coated Infrared Waveguides, *Appl. Spectrosc.*, 1998; 52(1): 119-122.
39. Wulff G., *Angew.Chem.*, 1995; 107: 1958-1979.
40. Mosbach K., *Trends Biochem. Sci.*, 1994; 19: 9-14.
41. Mosbach K., Ramström O., *Biotechnology*, 1996; 14: 163-170.
42. Haupt K., Mosbach K., *TIBTECH*, 1998; 16: 468-475.
43. Martens H. and Naes T., *Multivariate Calibration*, Wiley & Sons, 1989.

44. LeHaitre M., Leclercq M., Lepère D., *Proc. OCEANS '98 Conference*, Nice/France, IEEE Press, 1998.
45. Ferraro J. and Krishnan K.(Eds.), *Practical Fourier Transform Infrared Spectroscopy*, Academic Press, 1990.
46. González C., Collins S.D., Magnetically actuated fiber-optic switch with micromachined positioning stages, *Optics Lett.*, 1997; 22(10): 709-711.
47. Collins S.D., Smith R.L., González C., Stewart K.P., Hagopian J.G., Sirota J.M., Fourier-transform opticalmicrosystems, *Optics Lett.*, 1999; 24(12): 844-846.
48. Brooks A.L., Afanasyeva N.I., Makhine V., Bruch R.F., McGregor B., FEW-FTIR Spectroscopy Applications and Computer Data Processing for Noninvasive Skin Tissue Diagnostics In Vivo, *SPIE*, 1999; 3596: 140-151.
49. Bürck J., Mayer J., Zimmermann B., Aache H.-J., Integrated optical sensor for chemical analysis based on near-infrared evanescent wave absorbance measurements, *SPIE*, 1995; 2508: 243-252.
50. Walsh J.E., MacCraith B.D., Meany M., Vos J.G., Regan F., Lancia A., Artjushenko S., Midinfrared fiber sensor for the in-situ detection of chlorinated hydrocarbons, *SPIE*, 1995; 2508: 233-242.
51. Walsh J.E., MacCraith B.D., Meany M., Vos J.G., Regan F., Lancia A., Artjushenko S., Sensing of chlorinated hydrocarbons and pesticides in water using polymer coated mid-infrared optical fibres, *Analyst*, 1996; 121: 789-792.
52. Regan F., Meaney M., Vos J. G., MacCraith B.D., Walsh J.E., Determination of pesticides in water using ATR-FTIR spectroscopy on PVC/chloroparaffin coatings, *Anal. Chim. Acta*, 1996; 334: 85-92.
53. Regan F., MacCraith B.D., Walsh J.E., O'Dwyer K., Vos J.G., Meaney M., Novel teflon-coated optical fibres for TCE determination using FTIR spectroscopy, *Vib. Spec.*, 1997; 14: 239-246.
54. Beyer T., Hahn P., Hartwig S., Konz W., Scharring S., Katzir A., Steiner H., Jakusch M., Kraft M., Mizaikoff B., , Mini spectrometer with silver halide sensor fiber for in situ detection of chlorinated hydrocarbons, *Sensors Actuators B*, 2003; 90: 319 - 323.
55. Bodkin W.A., Johnson E.A., US-Patent *US 6528792 B2*, 2003.
56. Kornmann H., Rhiel M., Cannizzaro C., Marison I., Stockar U. V., *Biotechn. & Bioeng.*, 2003; 82 (6): 702-709.
57. Doak D.L., Phillips J.A., *Biotechnol. Prog.*, 1999; 15: 529-539.
58. Worrell C., Giles I. and Adatia N., Remote gas sensing with mid-infra-red hollow waveguide, *Electr. Lett.*, 28 (7): 615-617.
59. Worrell C. and Gallen N., Trace-level detection of gases and vapours with mid-infra-red hollow waveguides, *J. Phys. D: Appl. Phys.*, 1997; 30: 1984-1995.
60. Sato S., Saito M. and Miyagi M., Infrared Hollow Waveguides for Capillary Flow Cells, *Appl. Spectrosc.*, 1993; 47 (10): 1665-1669.
61. Kozodoy R., Micheels R. and Harrington J., Small-Bore Hollow Waveguide Infrared Absorption Cells for Gas Sensing, *Appl. Spectrosc.*, 1996; 50 (3): 415-417.
62. Lawrence K.C., Windham W.R., Park B., Buhr R.J., Hyperspectral imaging for poultry contaminant detection, *NIR News*, 2001; 12(5) :3-6.
63. Windham W.R, Lawrence K.C., et.al., International Patent Application *WO 02063939 A2*, 2001.
64. Gurschler C., Kulcke A., Leitner R., Scherf W., European Patent Application *EP 1421999 A2*, 2004.
65. McCreery R.L., Fleischmann M., Hendra P., Fiber Optic Probe for Remote Raman Spectroscopy *Anal. Chem.*, 1983; 55: 146 – 148.
66. Lewis I.R., Griffiths P.R., Raman Spectrometry with Fiber-Optic Sampling, *Appl. Spectrosc.*, 1996; 50 (10): 12A – 30A.
67. Besson J.P., King P.W.B., Williams T.A., McIvor M., Everall N., European Patent *EP 0767222 B1*, 2001.



68. *Integrated Raman Sensor for In-Tank Corrosion Chemistry Monitoring*, US Department of Energy Report DOE/EM-0631, 2002.
69. Zeigler K.E., Lascola R.J., Tovo L.L., US Department of Energy Report WSRC-TR-2003-00284, 2001.
70. Narayanan V., Begun G., Stokes D., Sutherland W., Vo-Dinh T., Normal Raman and surface-enhanced Raman scattering (SERS) spectra of some fungicides and related chemical compounds, *J. Raman Spectrosc.*, 1992; 23: 281-286.
71. Vo-Dinh T., SERS chemical sensors and biosensors: New tools for environmental and biological analysis, *Sensors Actuators B*, 1995; B 29: 183-189.
72. Murphy T., Schmidt H., Kronfeldt H., Use of sol-gel techniques in the development of surface-enhanced Raman scattering (SERS) substrates suitable for in situ detection of chemicals in sea-water, *Appl. Phys. B*, 1999; 69(2): 147-150.

## Chapter 8

# CHEMILUMINESCENCE-BASED SENSORS

Loïc J. Blum and Christophe A. Marquette  
*Laboratoire de Génie Enzymatique et Biomoléculaire*  
*Enzymes Membranes Biologiques et Biomimétiques (EMB2)*  
*UMR 5013 CNRS-Université Claude Bernard Lyon 1*  
*Bâtiment CPE - 43, Bd du 11 novembre 1918*  
*69622 Villeurbanne Cedex, France*

### 1. INTRODUCTION

Luminescence is the emission of light from an electronically excited compound returning to the ground state. The source of excitation energy serves as a basis for a classification of the various types of luminescence. Chemiluminescence occurs in the course of some chemical reactions when an electronically excited state is generated. Bioluminescence is a special case of chemiluminescence occurring in some living organisms and involves a protein, generally an enzyme.

Bio- or chemiluminescence measurements consist in monitoring the rate of production of photons and thus, the light intensity depends on the rate of the luminescent reaction. Consequently, light intensity is directly proportional to the concentration of a limiting reactant involved in a luminescence reaction. With modern instrumentation, light can be measured at a very low level, and this allows the development of very sensitive analytical methods based on these light-emitting reactions. Bioluminescence-based and chemiluminescence-based sensors have been then developed with the aim of combining the sensitivity of light-emitting reactions with the convenience of sensors. Optical fibres associated with a sensitive light detector appeared to be convenient transducers for designing biosensors involving these kind of luminescent reactions. In addition to these optical fibre-based sensors several luminescence analytical systems including immobilized reagents but not optical fibres have been described. More recently, chemi- and electrochemiluminescence detections have been also used instead of fluorescence for the development of biochips and microarrays.

## 2. LIGHT-EMITTING REACTIONS

### 2.1 Chemiluminescence

Chemiluminescence reactions are currently exploited mainly either for analyte concentration measurements or for immunoanalysis and nucleic acid detection. In the latter case, a compound involved in the light emitting reaction is used as a label for immunoassays or for nucleic acid probes. In the former case, the analyte of interest directly participates in a chemiluminescence reaction or undergoes a chemical or an enzymatic transformation in such a way that one of the reaction products is a coreactant of a chemiluminescence reaction. In this respect, chemiluminescent systems that require  $H_2O_2$  for the light emission are of particular interest in biochemical analysis. Hydrogen peroxide is in fact a product of several enzymatic reactions, which can be then coupled to a chemiluminescent detection.

Among the different synthetic compounds used for hydrogen peroxide determination, only luminol and oxalate esters have found widespread use and were really evaluated for  $H_2O_2$  detection.

#### 2.1.1 Luminol Chemiluminescence Reaction

The chemiluminescent properties of luminol (5-amino-2,3-dihydrophthalazine-1,4-dione) were first reported in 1928 by Albrecht<sup>1</sup>. Since that time, the chemiluminescence of luminol and related hydrazides has been studied extensively.

In aprotic media, the chemiluminescent oxidation of luminol requires only oxygen and a strong base<sup>2-4</sup>.

In protic solvents (*e.g.* water), an oxidation system and an oxidative catalyst are required in addition to alkaline conditions<sup>1</sup> (pH 10-13). Hydrogen peroxide is the most frequently used oxidizing agent. Transition metal cations ( $Cr^{3+}$ ,  $Mn^{4+}$ ,  $Fe^{2+}$ ,  $Fe^{3+}$ ,  $Co^{2+}$ ,  $Ni^{2+}$ ,  $Cu^{2+}$ ,  $Hg^{2+}$ ), either free or complexed to organic or inorganic ligands, catalyze the luminol chemiluminescence oxidation. This is why heme-containing proteins, particularly horseradish peroxidase (EC 1.11.1.7) are able to catalyze the chemiluminescence of luminol in the presence of hydrogen peroxide. The use of this enzyme has the advantage over other catalysts such as ferricyanide in that the chemiluminescent reaction can proceed at near neutral pH values<sup>5</sup> (8-8.5).

Another way to produce light from luminol is electrogenerated chemiluminescence<sup>6, 7</sup>. Luminol is oxidized using a positively biased electrode and in the presence of hydrogen peroxide the light emission occurs.

The overall reaction scheme of the luminol chemiluminescence in an aqueous medium is shown in Figure 1. The luminol oxidation leads to the formation of an aminophthalate ion in an excited state, which then emits light on return to the ground state. The quantum yield of the reaction is low ( $\approx 0.01$ ) compared with bioluminescence reactions and the emission spectrum shows a maximum<sup>1</sup> at 425 nm.

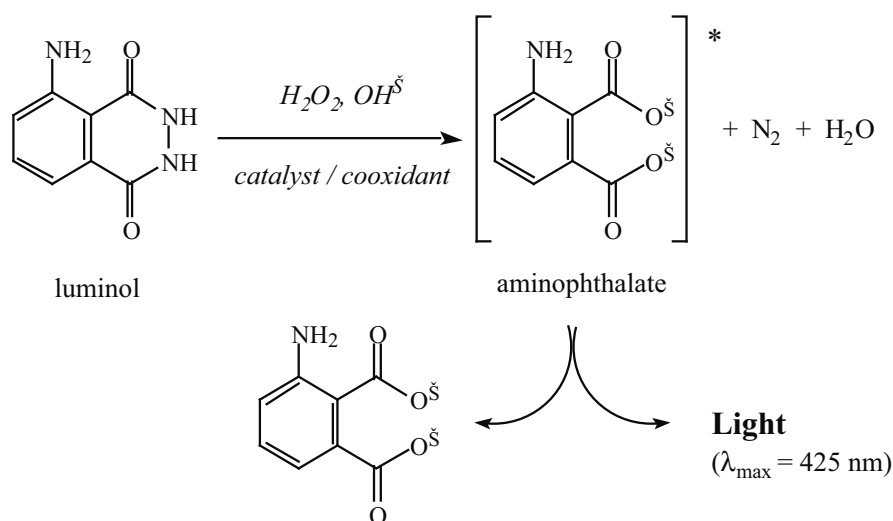


Figure 1. Overall luminol chemiluminescence reaction in aqueous medium.

### 2.1.2 Oxalate Ester Chemiluminescence Reaction

Some esters of oxalic acid, mainly aryl-oxalates, react with the oxidant  $H_2O_2$  in the presence of suitable fluorescers to give rise to light emission. The chemical system is generally known as the peroxyoxalate chemiluminescence system and is an energy transfer system. By reacting with hydrogen peroxide, the oxalic acid ester gives an unstable intermediate of high energy, 1,2-dioxetanedione, which in turn excites the fluorescer. The excited fluorescer returns to the ground state emitting light in a typical fluorescence process<sup>8, 9</sup>. The overall reaction of aryl-oxalate chemiluminescence is shown in Figure 2. In fact, the production of 1,2-dioxetanedione proceeds in two steps with first, the production of one phenol molecule and peroxyoxalic acid which decomposes into a second phenol molecule and 1,2-dioxetanedione intermediate. Then, the intermediate forms a charge-transfer-type complex with the fluorescer. This unstable intermediate releases excited fluorescer and two carbon dioxide molecules.

The best known ester of oxalic acid and probably the more efficient is TCPO (bis-(2,4,6-trichlorophenyl)oxalate). With suitable fluorescers such as

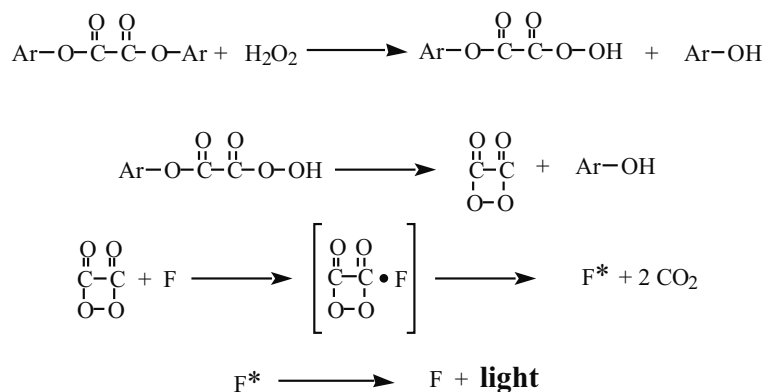


Figure 2. Aryl-oxalate chemiluminescence reaction. F is a fluorescer.

perylene, rubrene or 9,10-diphenylanthracene the quantum yield of the chemiluminescence reaction is of the order of 0.22 - 0.27 and the colour of the emitted light depends on the fluorescer used.

The chemiluminescence reaction of esters of oxalic acid can proceed within a wider pH range than for luminol. However, the most efficient oxalate derivatives are only soluble in organic solvents such as ethyl acetate, acetonitrile, dioxane or dimethoxyethane and dissolution problems of these solvents in aqueous media are encountered. This can limit the use of this chemiluminescence reaction for a direct coupling to an H<sub>2</sub>O<sub>2</sub>-generating enzymatic reaction.

## 2.2 Bioluminescence

Although numerous luminous organisms are known, only a few of them has been studied and really exploited. Analytical applications of bioluminescence concern mainly the detection of ATP with the firefly luciferase and of NADH with some marine bacteria systems. Luciferase from the North American firefly, i.e., *Photinus pyralis*, has been extensively studied<sup>10-12</sup> and afterwards, attention has been paid to the luciferase from *Luciola mingrelica*, i.e., the North Caucasus firefly<sup>13-15</sup>.

In some bioluminescent organisms, light is produced without the intervention of a luciferase, directly from a protein-luciferin complex, called a photoprotein, where the luciferin is tightly or covalently bound to the protein. These systems are able to release energy in the form of light emission, independently of a chemical or enzymatic reaction. This energy "discharge" occurs in the presence of a triggering compound, generally H<sup>+</sup> or Ca<sup>2+</sup> ions depending on the bioluminescent systems.

For example, the jellyfish *Aequorea* contains a photoprotein called aequorin of molecular weight about 20,000 and with a heterocyclic compound called coelenterazine covalently linked to it. The protein contains bound oxygen and three calcium binding sites and upon addition of calcium ions, a blue light is produced<sup>16</sup>. This bioluminescence system can be used for imaging the  $\text{Ca}^{2+}$  content in living cells. However, it has not been exploited for sensor development since the protein does not turnover and consequently is efficient only once for the production of light.

### 2.2.1 Firefly Bioluminescence

The firefly luciferase (EC 1.13.12.7) catalyzes the emission of light in the presence of ATP,  $\text{Mg}^{2+}$ , molecular oxygen and firefly luciferin a specific natural substrate (Figure 3).

The colour of the light emission is yellow-green with a maximum at 560 nm. The quantum yield of the firefly luciferase bioluminescence reaction is close to 1 under optimum conditions of temperature and pH and in the presence of saturating luciferin concentration<sup>17</sup>.

Synthetic luciferin as well as purified preparations of native and recombinant firefly luciferases are now commercially available allowing the bioluminescent determination of ATP to be used as a routine analysis technique in some laboratories.

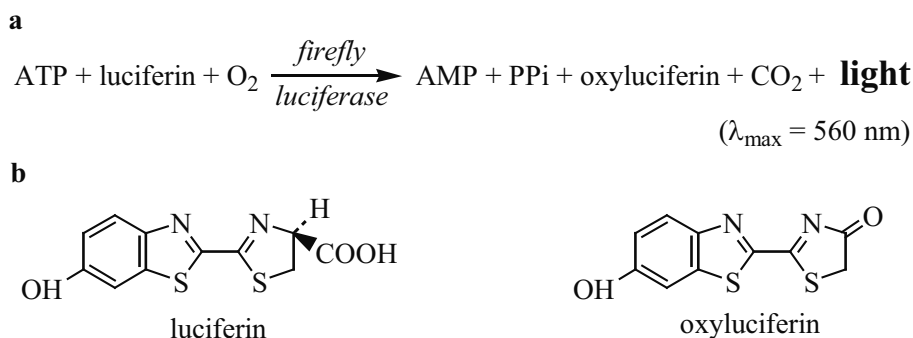


Figure 3. (a) The firefly luciferase bioluminescence reaction. (b) Structure of the specific substrate luciferin and the corresponding reaction product oxyluciferin.

### 2.2.2 Bacterial Bioluminescence

The bacterial bioluminescent reaction is also catalyzed by a luciferase (EC 1.14.14.3) isolated from marine bacteria. The four most studied types are *Vibrio harveyi*, *Vibrio fischeri*, *Photobacterium phosphoreum* and *Photobacterium leiognathi*<sup>18, 19</sup>. In these different luminescent bacteria the

same light emission mechanism is involved and the luciferases are similar<sup>20</sup>. The substrates of the bacterial luciferase reaction include reduced flavin mononucleotide (FMNH<sub>2</sub>), molecular oxygen and a long-chain aldehyde (R-CHO). In vitro, decanal is generally used as the aliphatic aldehyde and light emission occurs with a peak at 490 nm. FMNH<sub>2</sub> is only a transient intermediate and is produced in the course of an oxido-reduction reaction, catalyzed by an oxidoreductase, which involves the oxidation of NADH or NADPH concomitantly with the reduction of FMN.

This reductase was isolated from various strains of bioluminescent bacteria as well as in several species of non-luminous aerobic and anaerobic bacteria<sup>21</sup>. The two most useful light-emitting systems were isolated from *V. harveyi* and *V. fischeri*. Distinct oxidoreductases for NADH and NADPH were identified in extracts of *V. harveyi*<sup>22</sup> whereas *V. fischeri* appears to have only one oxidoreductase acting on both NADH and NADPH. Thus, the bacterial bienzymatic system allows NAD(P)H to be assayed, providing it is the limiting substrate (Figure 4). In addition, the use of coupled reactions makes it easy to determine various substrates and enzymes involved in NAD(P)H producing or consuming reactions.

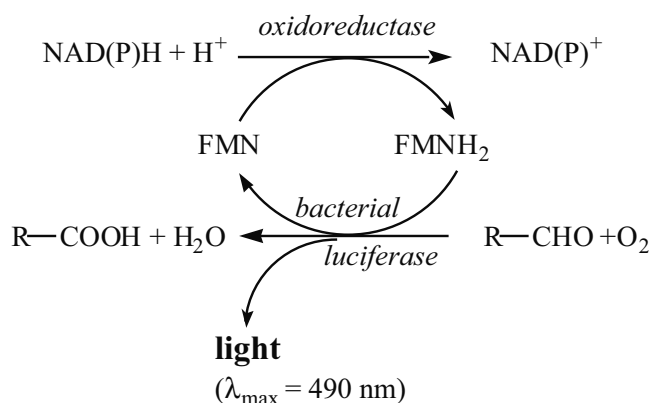


Figure 4. Coupled bacterial bioluminescent reaction allowing the detection of NADH or NADPH.

### 3. COUPLED ENZYMATIC REACTIONS

Bioluminescence and chemiluminescence are very powerful analytical tools, since in addition to the direct measurement of ATP, NAD(P)H or hydrogen peroxide, any compound or enzyme involved in a reaction that generates or consumes these metabolites can be theoretically assayed by one of the appropriate light-emitting reactions. Some of these possibilities have been exploited for the development of optical fibre sensors, mainly with bacterial bioluminescence and with luminol chemiluminescence.

### 3.1 NADH-Dependent Reactions

The bioluminescent determinations of ethanol, sorbitol, L-lactate and oxaloacetate have been performed with coupled enzymatic systems involving the specific suitable enzymes (Figure 5). The ethanol, sorbitol and lactate assays involved the enzymatic oxidation of these substrates with the concomitant reduction of  $\text{NAD}^+$  in NADH, which is in turn reoxidized by the bioluminescence bacterial system. Thus, the assay of these compounds could be performed in a one-step procedure, in the presence of  $\text{NAD}^+$  in excess. Conversely, the oxaloacetate measurement involved the simultaneous consumption of NADH by malate dehydrogenase and bacterial oxidoreductase and was therefore conducted in two steps.

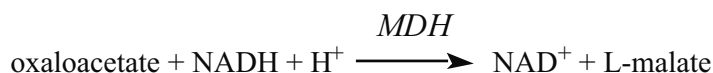
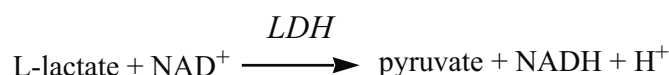
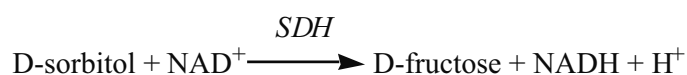
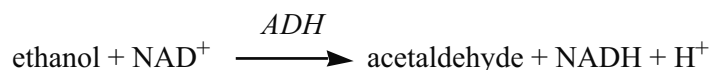


Figure 5. Example of dehydrogenase reactions which can be coupled with the bienzymatic bacterial bioluminescent system. ADH = alcohol dehydrogenase (EC 1.1.1.1), SDH = sorbitol dehydrogenase (EC 1.1.1.14), LDH = lactate dehydrogenase (EC 1.1.1.27), MDH = malate dehydrogenase (EC 1.1.1.37).

### 3.2 $\text{H}_2\text{O}_2$ -Generating Enzymatic Systems

The main interest of luminol chemiluminescence in biochemical and clinical analysis is the possibility of coupling this light-emitting reaction with enzyme-catalyzed reactions generating hydrogen peroxide. Simple auxiliary  $\text{H}_2\text{O}_2$ -generating reactions as well as multi-enzymatic systems leading to the production of hydrogen peroxide can be used for the specific chemiluminescent detection of different metabolites. Some of these systems, used for the design of chemiluminescence-based biosensors, are listed in Table 1.



Table 1. H<sub>2</sub>O<sub>2</sub>-generating enzymatic systems for chemiluminescence-based optical fibre biosensors (Abbreviations: OX = oxidase, PNPase = purine nucleoside phosphorylase).

<i>Metabolite</i>	<i>Enzyme</i>	<i>Enzymatic reaction</i>
Choline	choline OX (EC 1.1.3.17)	choline + 2 O <sub>2</sub> = betaine + 2 H <sub>2</sub> O <sub>2</sub>
Ethanol	alcohol OX (EC 1.1.3.13)	primary alcohol + O <sub>2</sub> = aldehyde + H <sub>2</sub> O <sub>2</sub>
D-Glucose	glucose OX (EC 1.1.3.4)	$\beta$ -D-glucose + O <sub>2</sub> = H <sub>2</sub> O <sub>2</sub> + D-glucono-1,5-lactone
L-Glutamate	L-glutamate OX (EC 1.4.3.11)	2 L-glutamate + O <sub>2</sub> + H <sub>2</sub> O = 2 NH <sub>3</sub> + 2 $\alpha$ -ketoglutarate + H <sub>2</sub> O <sub>2</sub>
L-Glutamine	Glutaminase (EC 3.5.1.2)	L-glutamine + H <sub>2</sub> O = NH <sub>3</sub> + L-glutamate
	L-glutamate OX (EC 1.4.3.11)	2 L-glutamate + O <sub>2</sub> + H <sub>2</sub> O = 2 NH <sub>3</sub> + 2 $\alpha$ -ketoglutarate + H <sub>2</sub> O <sub>2</sub>
Hypoxanthine	xanthine OX (EC 1.1.3.22)	hypoxanthine + O <sub>2</sub> + H <sub>2</sub> O = xanthine + H <sub>2</sub> O <sub>2</sub>
	xanthine OX (EC 1.1.3.22)	xanthine + O <sub>2</sub> + H <sub>2</sub> O = urate + H <sub>2</sub> O <sub>2</sub>
L-Lactate	lactate OX	L-lactate + O <sub>2</sub> = pyruvate + H <sub>2</sub> O <sub>2</sub>
L-Lysine	L-lysine OX (EC1.4.3.14)	L-lysine + O <sub>2</sub> = NH <sub>3</sub> + H <sub>2</sub> O <sub>2</sub> + 6-amino-2-oxo-hexanoate
Phosphate	PNPase (EC 2.4.2.1)	Pi + inosine = ribose-1-phosphate + hypoxanthine
	xanthine OX (EC 1.1.3.22)	hypoxanthine + O <sub>2</sub> + H <sub>2</sub> O = xanthine + H <sub>2</sub> O <sub>2</sub>
	xanthine OX (EC 1.1.3.22)	xanthine + O <sub>2</sub> + H <sub>2</sub> O = urate + H <sub>2</sub> O <sub>2</sub>
Sulphite	sulphite OX (EC 1.8.3.1)	SO <sub>3</sub> <sup>2-</sup> + O <sub>2</sub> + H <sub>2</sub> O = SO <sub>4</sub> <sup>2-</sup> + H <sub>2</sub> O <sub>2</sub>
Xanthine	xanthine OX (EC 1.1.3.22)	xanthine + O <sub>2</sub> + H <sub>2</sub> O = urate + H <sub>2</sub> O <sub>2</sub>

#### 4. DESIGN OF FIBEROPTIC BIOSENSORS

The first biosensor combining an optical fibre and an enzyme-catalyzed light-emitting process was described about twenty-five years ago by Freeman and Seitz<sup>23</sup>. It consisted of a 2 feet-long optical fibre with a 1/8 inch diameter at the tip of which was placed horseradish peroxidase immobilized in a thin layer of polyacrylamide. The other end of the optical fibre was placed in front of a photomultiplier tube. The sensing part of the sensor was immersed in a 10-ml stirred solution of buffer containing luminol. When hydrogen peroxide was injected in this reaction medium, light was emitted at the enzymatic phase and transmitted through the optical fibre to the detector. The first optical fibre biosensor based on bioluminescence reactions was

described in 1988 and consisted of a 1-meter glass fibre bundle of 8 mm in diameter<sup>24</sup>. The bioluminescence enzymes were immobilized on a white polyamide membrane maintained in close contact with the surface of one end of the fibre bundle, the other end being connected to the photomultiplier tube of a luminometer. The sensor was immersed in a 4.5 ml stirred and thermostated reaction medium protected from the ambient light by a polyvinyl chloride jacket.

Finally, all the bio- and chemi-luminescence-based optical fibre biosensors described were designed according to nearly the same principle, that is an optical fibre or a fibre bundle with one end connected to a light detector, generally a photomultiplier tube, and with the other end bearing the immobilized light-emitting enzymes and protected from ambient light to avoid interferences. This basic configuration was used either in batch systems or included in flow injection analysis (FIA) systems. As an example, schematic representations of the devices developed in our laboratory for batch analysis and FIA with luminescence-based optical fibre biosensors are shown in Figures 6 and 7, respectively.

#### 4.1 Sensing Layer Design

Except the physical entrapment of horseradish peroxidase in a polyacrylamide gel used by Freeman and Seitz<sup>23</sup>, immobilization of the

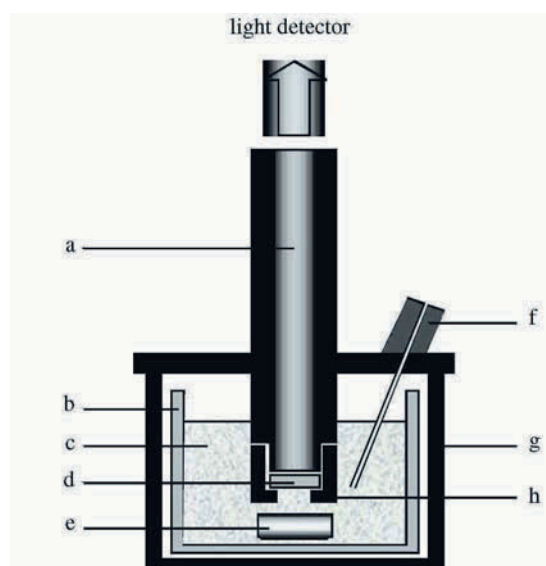


*Figure 6.* Optical fibre biosensor setup. (a) Optical fibre bundle; (b) thermostated reaction vessel; (c) reaction medium; (d) sensing layer; (e) stirring bar; (f) septum and needle guide for sample injection; (g) PVC jacket; (h) screw-cap for securing the sensing layer.

luminescence enzymes was mainly performed *via* a covalent coupling on a synthetic membrane. Commercially available membranes, supplied in a preactivated form, were used by several authors: Immunodyne from Pall, Immobilon-AV from Millipore or UltraBind from Gelman Sciences.

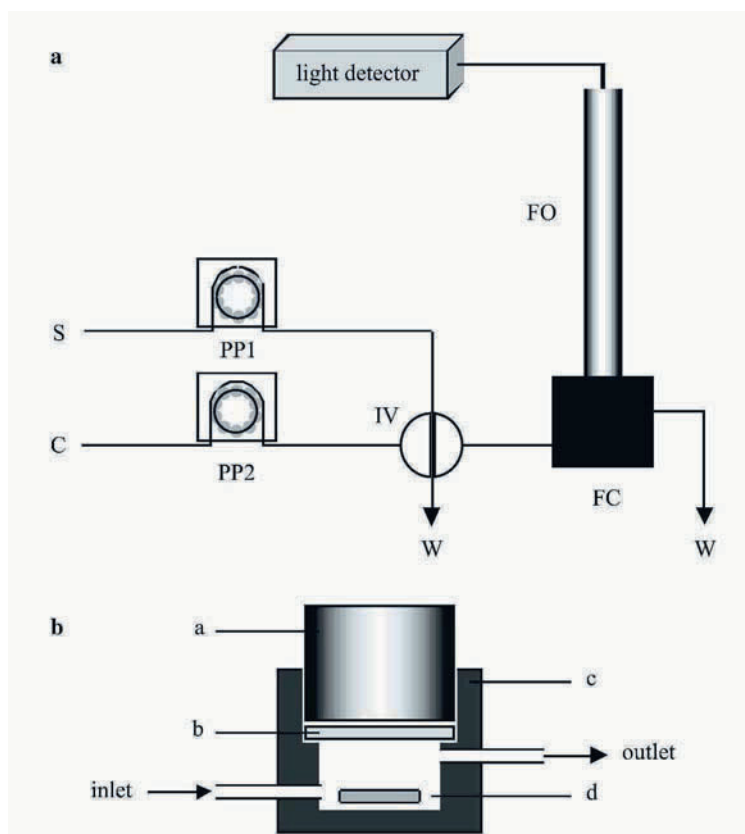


Figure 7. (a) Flow diagram of the optical fibre continuous-flow system for bioluminescence and chemiluminescence measurements: S, sample; C, carrier stream; PP, peristaltic pump; IV, injection valve; W, waste; FO, optical fibre; FC, flow-cell. (b) Details of the optical fibre biosensor/flow-cell interface: a, optical fibre; b, sensing layer; c, light-tight flow-cell; d, stirring bar.

#### 4.1.1 Co-Immobilized Auxiliary Enzymes

As mentioned above, in order to extend the potentialities of the luminescence-based optical fibre biosensors to other analytes, auxiliary enzymes can be used. The classical approaches consist either of the co-immobilization of all the necessary enzymes on the same membrane or of the use of microreactors including immobilized auxiliary enzymes and

placed in a FIA system, upstream from the luminescence-based optical fibre sensor.

#### 4.1.2 Compartmentalized Sensing Layer

Another approach, developed in our laboratory, consists of the compartmentalization of the sensing layer<sup>25-27</sup>. This concept, only applicable for multi-enzyme based sensors, consist in immobilizing the luminescence enzymes and the auxiliary enzymes on different membranes and then in stacking these membranes at the sensing tip of the optical fibre sensor. This configuration results in an enhancement of the sensor response, compared with the case where all the enzymes are co-immobilized on the same membrane. This was due to an hyperconcentration of the common intermediate, i.e. the final product of the auxiliary enzymatic system, which is also the substrate of the luminescence reaction, in the microcompartment existing between the two stacked membranes.

#### 4.1.3 Entrapped Coreactants

Since ideally, a biosensor should be reagentless, that is, should be able to specifically measure the concentration of an analyte without a supply of reactants, attempts to develop such bioluminescence-based optical fibre biosensors were made for the measurements of NADH<sup>28-30</sup>. For this purpose, the coreactants, FMN and decanal, were entrapped either separately or together in a polymeric matrix placed between the optical fibre surface and the bacterial oxidoreductase-luciferase membrane. In the best configuration, the period of autonomy was 1.5 h during which about twenty reliable assays could be performed.

For luciferin, a firefly luciferase cosubstrate, another method of retention has been evaluated which consisted of incorporating the substrate in acrylic microspheres during their formation, these last being then confined in a polymeric matrix<sup>31</sup>. Using the suitable co-immobilized enzymes (adenylate kinase and creatine kinase), the three adenylic nucleotides (ATP, ADP and AMP) could be assayed continuously and reproducibly with a self-containment working time of 3 h.

### 4.2 Characteristics and Performances of Bioluminescence and Chemiluminescence-Based Fiberoptic Sensors

The main performances of batchwise and flow luminescence-based optical fibre sensors are summarized in Tables 2 and 3. As it can be shown

in these tables, the sensitivity achieved is generally better with bioluminescence-based sensors than with chemiluminescence-based sensors. This could be explained by considering the quantum yield of these light-emitting reactions. For the firefly luciferase reaction the quantum yield is closed to 1 and for the bacterial bioluminescence reaction it is about 0.3 whereas it is only 0.01 for the luminol chemiluminescence reaction.

Table 2. Performances of batchwise and flow injection analysis (FIA) bioluminescence-based optical fibre sensors.

Analyte	Linearity or detection limit	Precision	System	Reference
ADP <sup>(a)</sup>	1 x 10 <sup>-11</sup> mol	4.3%	FIA	31
AMP <sup>(a)</sup>	25 x 10 <sup>-11</sup> mol	6%	FIA	31
ATP	2.8 x 10 <sup>-10</sup> - 1.4 x 10 <sup>-6</sup> M	///	batch	24
ATP <sup>(b)</sup>	1 x 10 <sup>-10</sup> - 1 x 10 <sup>-6</sup> M	6% at 9 x 10 <sup>-9</sup> M	batch	32
ATP <sup>(b)</sup>	0.25 x 10 <sup>-12</sup> mol	4-4.5%	FIA	33
ATP <sup>(a)</sup>	2.5 x 10 <sup>-12</sup> mol	4%	FIA	31
Ethanol	4 x 10 <sup>-7</sup> - 7 x 10 <sup>-5</sup> M	5.4% at 5 x 10 <sup>-6</sup> M	batch	34
Lactate <sup>(c)</sup>	2 x 10 <sup>-7</sup> M	5.1%	batch	26
LDH	5 - 250 IU l <sup>-1</sup>		FIA	35
NADH	3 x 10 <sup>-9</sup> - 3 x 10 <sup>-6</sup> M	///	batch	24
NADH	1 x 10 <sup>-9</sup> - 3 x 10 <sup>-6</sup> M	5% at 4 x 10 <sup>-8</sup> M	batch	36
NADH	2 x 10 <sup>-9</sup> M <sup>(d)</sup>	4.2% at 4 x 10 <sup>-8</sup> M	batch	37
NADH	0.3 x 10 <sup>-9</sup> M <sup>(e)</sup>	4.8% at 4 x 10 <sup>-8</sup> M	batch	37
NADH	2 x 10 <sup>-12</sup> - 1 x 10 <sup>-9</sup> mol	3.4% at 1 x 10 <sup>-10</sup> mol	FIA	38
NADH <sup>(a)</sup>	1 x 10 <sup>-9</sup> - 1 x 10 <sup>-6</sup> M	6% at 4 x 10 <sup>-8</sup> M	batch	32
NADH <sup>(a)</sup>	5 x 10 <sup>-12</sup> mol	4-4.5%	FIA	33
NADH <sup>(f)</sup>	5 x 10 <sup>-12</sup> - 5 x 10 <sup>-10</sup> mol	< 3%	FIA	30
oxaloacetate	3 x 10 <sup>-9</sup> - 2 x 10 <sup>-6</sup> M	5.1% at 5.5 x 10 <sup>-8</sup> M	batch	34
sorbitol	2 x 10 <sup>-8</sup> - 2 x 10 <sup>-5</sup> M	6% at 4.4 x 10 <sup>-7</sup> M	batch	34

(LDH) lactate dehydrogenase.

<sup>(a)</sup> reagentless biosensor with luciferin immobilized in microspheres included in a polymeric matrix.

<sup>(b)</sup> firefly luciferase co-immobilized with the bacterial oxidoreductase-luciferase system.

<sup>(c)</sup> compartmentalized system.

<sup>(d)</sup> bacterial oxidoreductase-luciferase system from *V. harveyi*.

<sup>(e)</sup> bacterial oxidoreductase-luciferase system from *V. fischeri*.

<sup>(f)</sup> reagentless biosensor, i.e. with FMN and decanal entrapped in a polymeric matrix.

Table 3. Performances of batchwise and flow injection analysis chemiluminescence-based optical fibre sensors.

Analyte	Linearity or detection limit	Precision	System	Reference
Choline	$1 \times 10^{-6}$ - $1 \times 10^{-3}$ M	///	FIA	39
	$0.5 \times 10^{-12}$ mol	2.6%	FIA	40
Ethanol	$3 \times 10^{-6}$ - $7.5 \times 10^{-4}$ M	2.4% at $3 \times 10^{-4}$ M	FIA	41
D-Glucose	$3 \times 10^{-7}$ - $3 \times 10^{-4}$ M	3.8% at $5 \times 10^{-5}$ M	batch	42
	$2 \times 10^{-3}$ - $1.8 \times 10^{-2}$ M	///	batch	43
	$2.5 \times 10^{-10}$ - $2.5 \times 10^{-7}$ mol	3.8% at $1 \times 10^{-9}$ mol	FIA	44
L-Glutamate	$1 \times 10^{-7}$ - $6 \times 10^{-5}$ M	///	FIA	45
L-Glutamine	$1 \times 10^{-6}$ - $2.5 \times 10^{-3}$ M	///	FIA	45
H <sub>2</sub> O <sub>2</sub>	$1 \times 10^{-6}$ - $1 \times 10^{-4}$ M	5% at $1 \times 10^{-4}$ M	batch	23
	$2 \times 10^{-8}$ - $2 \times 10^{-5}$ M	///	batch	24
	$2.4 \times 10^{-8}$ - $1.2 \times 10^{-4}$ M	2.6% at $2.5 \times 10^{-5}$ M	batch	42
	$2.5 \times 10^{-12}$ - $2.5 \times 10^{-8}$ mol	2.5% at $1 \times 10^{-10}$ mol	FIA	44
	$1 \times 10^{-8}$ - $1 \times 10^{-3}$ M	3%	FIA	46
	$6.25 \times 10^{-12}$ - $2.5 \times 10^{-8}$ mol	3% at $2.5 \times 10^{-10}$ mol	FIA	47
Hypoxanthine	$1 \times 10^{-6}$ - $3.1 \times 10^{-4}$ M	///	batch	48
L-Lactate	$2.5 \times 10^{-10}$ - $1.25 \times 10^{-6}$ mol	1.7% at $6 \times 10^{-9}$ mol	FIA	49
L-Lysine	$1 \times 10^{-5}$ - $1 \times 10^{-3}$ M	///	FIA	50
	$1 \times 10^{-6}$ - $1 \times 10^{-3}$ M	///	FIA	51
Phosphate	$1 \times 10^{-7}$ - $1 \times 10^{-4}$ M	///	FIA	51
Sulphite	$1 \times 10^{-6}$ - $1 \times 10^{-4}$ M	///	batch	52
Xanthine	$3.1 \times 10^{-6}$ - $3.1 \times 10^{-4}$ M	///	batch	48

### 4.3 Electrochemiluminescence-Based Fiberoptic Biosensors

As mentioned above, an original and unusual way to obtain a high sensitive hydrogen peroxide detection is the electrogenerated chemiluminescence of luminol (ECL). Based on this electro-optical process, a flow injection analysis optical fibre H<sub>2</sub>O<sub>2</sub> sensor has been developed<sup>53,54</sup>. The electrochemiluminescence was generated using glassy carbon electrode polarized vs a platinum pseudo-reference electrode and integrated in a flow injection analysis system (Figure 8).

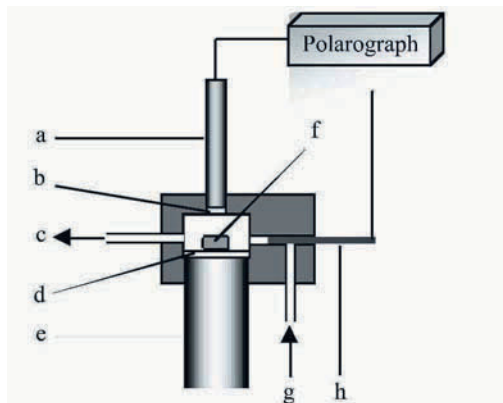


Figure 8. Flow cell for electrochemiluminescence measurements: (a) glassy carbon electrode; (b) sensing layer; (c) reagent solution outlet; (d) Plexiglas window; (e) liquid core single optical fiber; (f) stirring bar; (g) reagent solution inlet; (h) platinum electrode.

The optimization of the reaction conditions showed that an applied potential of + 425 mV vs a platinum pseudo-reference electrode enabled the realization of a sensitive  $\text{H}_2\text{O}_2$  sensor while avoiding passivation of the working electrode. An optimum pH measurement of 9 was found and moreover, the pH dependence of the ECL sensor appeared less pronounced than when using immobilized HRP as the sensing layer. Under optimum conditions, hydrogen peroxide measurements could be performed in the range 1.5 pmol - 30 nmol. This ECL  $\text{H}_2\text{O}_2$  sensor then exhibited slightly higher performances than membrane-based horseradish peroxidase chemiluminescent FIA biosensors (see <sup>44</sup>, Table 3).

#### 4.3.1 Glucose and Lactate Electrochemiluminescent Biosensor

For the development of glucose and lactate ECL FIA biosensors<sup>53</sup>, the hydrogen peroxide ECL sensor was associated with the catalytic action of glucose oxidase and lactate oxidase. The oxidases were immobilized on synthetic preactivated membranes brought into contact with the glassy carbon electrode. The glucose or lactate electro-optical biosensor was then able to detect the target analyte with detection limits of 150 pmol and 60 pmol, respectively. In each case, glucose and lactate measurements could be performed over 4 decades.

These biosensors were tested for glucose and lactate measurements in sera, and for lactate measurements in whey solutions. Good agreements were obtained between the present method and reference methods. For glucose analysis in serum, the coefficient of variation for 53 repeated measurements performed over a 10 h period was 4.8% while for lactate analysis, 80 assays performed over a 15 h period gave a coefficient of variation of 6.7%. Thus,

the ECL-based biosensors gave the possibility to sensitively detect glucose and lactate in complex matrices without pre-treatment of the samples.

#### 4.3.2 Choline Electrochemiluminescent Biosensor

A flow injection optical fibre biosensor for choline was also developed<sup>55</sup>. Choline oxidase (ChOX) was immobilized by physical entrapment in a photo-cross-linkable poly(vinyl alcohol) polymer (PVA-SbQ) after adsorption on weak anion-exchanger beads (DEAE-Sepharose). In this way, the sensing layer was directly created at the surface of the working glassy carbon electrode. The optimization of the reaction conditions and of the physicochemical parameters influencing the FIA biosensor response allows the measurement of choline concentration with a detection limit of 10 pmol. The DEAE-based system also exhibited a good operational stability since 160 repeated measurements of 3 nmol of choline could be performed with a variation coefficient of 4.5%.

#### 4.3.3 Cholesterol Electrochemiluminescent Biosensor

A new cholesterol flow injection analysis biosensor has also been described as an application of the H<sub>2</sub>O<sub>2</sub> ECL sensor<sup>56</sup>. In that work, the luminol electrochemiluminescence, previously studied in aqueous media, was implemented in Veronal buffer added of 0.3% triton X-100 (v/v), 0.3% PEG and 0.4% cholate to enable the solubilisation of the cholesterol and then its efficient oxidation catalyzed by the immobilized cholesterol oxidase. The ECL reaction occurred thus in a micellar medium and the performances of the H<sub>2</sub>O<sub>2</sub> ECL sensor were investigated.

The calibration curve obtained for hydrogen peroxide exhibited a detection limit of 30 pmol and ranged over three decades at least. These performances compared well with those previously obtained in non-micellar media<sup>54</sup>. The presence of surfactant compounds in the ECL measurement buffer appeared thus to have little effect on the H<sub>2</sub>O<sub>2</sub> ECL sensor performances. In optimized conditions, the determination of free cholesterol could be performed with a detection limit of 0.6 nmol and a calibration curve ranging over two decades at least.

## 5. BIOCHIPS AND MICROARRAYS

The chemiluminescence and electrochemiluminescence of luminol have been also exploited for the development of enzyme, DNA and immuno-biochips. Different approaches were studied in our laboratory, in which



bioactive molecules were anchored on microbeads subsequently entrapped in a suitable polymeric structure. Whatever immobilization method of the biological probe and the type of biochip (DNA, enzyme or protein) a unique detection system consisting of a CCD camera was used and both formats, low density arrays and microfluidic biochips were studied.

## 5.1 Composite Sensing Layer on Glassy Carbon Electrode

Beads bearing bioactive molecules have been used to develop generic biochips based on chemi- and electro-chemiluminescent detection. The biochips were composed of arrayed biosensors, including enzyme-charged beads, antigen-charged beads or oligonucleotide-charged beads, entrapped in polyvinyl alcohol (PVA-SbQ) photopolymer. In each case the sensing layers were spotted at the surface of a glassy carbon electrode ( $25 \text{ mm}^2$ ) as  $0.3 \mu\text{l}$  drops, generating  $500\text{-}800 \mu\text{m}$  spots. The luminescent reactions were either catalyzed by the horseradish peroxidase or triggered by the application of a  $+850 \text{ mV}$  potential between the glassy carbon electrode and a platinum pseudo-reference.

Enzyme biochips were designed for the concomitant detection of choline, glucose, glutamate, lactate, lysine and urate, based on the corresponding oxidase-charged beads and the ECL reaction of the produced hydrogen peroxide with luminol-immobilized beads<sup>57, 58</sup>. Limits of detection of  $1 \mu\text{M}$  for glutamate, lysine and uric acid,  $20 \mu\text{M}$  for glucose and  $2 \mu\text{M}$  for choline and lactate were found with detection ranging over three decades at least.

A tri-enzymatic sensing layer based on kinase-oxidase activities for the detection of acetate was also described. A reaction sequence using acetate kinase, pyruvate kinase and pyruvate oxidase enabled the production of  $\text{H}_2\text{O}_2$  in response to acetate injection in the range  $10 \mu\text{M} - 100 \text{ mM}$ <sup>59</sup>.

Based on IgG-bearing beads, a chemiluminescent immuno-biochip has been also realized for the model detection of human IgG. Biotin-labeled anti-human IgG were used in a competitive assay, in conjunction with peroxidase labelled streptavidin<sup>59</sup>. In that case, the planar glassy carbon electrode served only as a support for the sensing layer since the light signal came from the biocatalytic activity of horseradish peroxidase. Free antigen could then be detected with a detection limit of  $25 \text{ pg}$  ( $10^8$  molecules) and up to  $15 \text{ ng}$ .

In a similar way, the use of oligonucleotide-immobilized beads enabled the realization of DNA sensitive biochips that could be used to detect biotin labelled sequence as  $5 \cdot 10^8$  molecules<sup>59</sup>.

## 5.2 Direct Entrapment of Micrometric Beads in PDMS

Poly(dimethylsiloxane) (PDMS) as an immobilization matrix has been successfully used to design multi-purpose biochips i.e., for either nucleic

acids, proteins or enzymes<sup>60</sup>. A new arraying method based on the properties of PDMS polymer to entrap beads bearing biologically active compounds was described. Such beads could be spotted and dried at the surface of a PVC master and subsequently transferred at the PDMS interface by direct moulding of the polymer on the mask (Figure 9). The use of the PDMS-assisted-immobilization enables the development of either a low density array (100 spots) or a micro-channel biochip with a direct incorporation of the sensing element in a fluidic system for the quantitative detection of enzyme substrates, antigens and oligonucleotides, depending on the immobilized sensing element. As a result, arrays of beads bearing active enzymes, antibodies and oligonucleotides were successfully obtained and enabled the achievement of biochips for the chemiluminescent detection of enzyme substrates, protein antigens and oligonucleotides sequence with detection limit of 1  $\mu\text{M}$ ,  $1.5 \times 10^7$  molecules and  $10^8$  molecules, respectively.

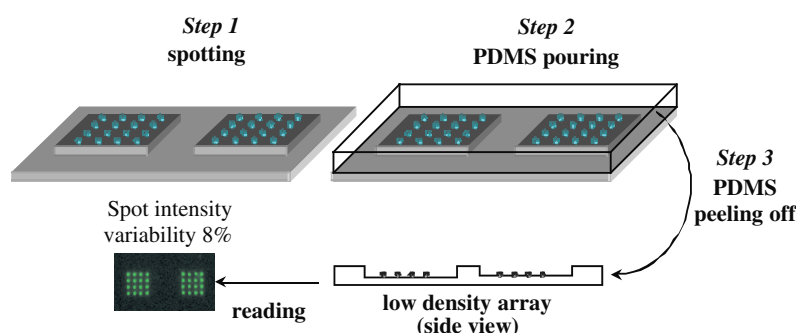


Figure 9. Direct immobilization in PDMS of beads bearing biologically active compounds. Step1: Sepharose beads bearing bioactive compounds are arrayed as 0.3  $\mu\text{l}$  drop onto a flat PVC master; Step 2: a PDMS solution is poured onto the spotted array; Step 3: the PDMS-based array is peeled off from the master and ready to use.

### 5.3 Conducting Elastomer Surface Texturing

A new active support for biochip preparation has been developed based on graphite modified PDMS<sup>61</sup>. The addressed inclusion of Sepharose beads at the surface of the obtained elastomeric electrode generated local high specific surfaces. This electrode structure was characterized by electrochemical and imaging methods and an increase factor of the surface area equal to 50 was found. This was due to the texturing of the surface generated by the presence of the Sepharose beads (Figure 10).

This new material was used to design biochips based on the electrochemiluminescence reaction of luminol in the presence of enzymatically

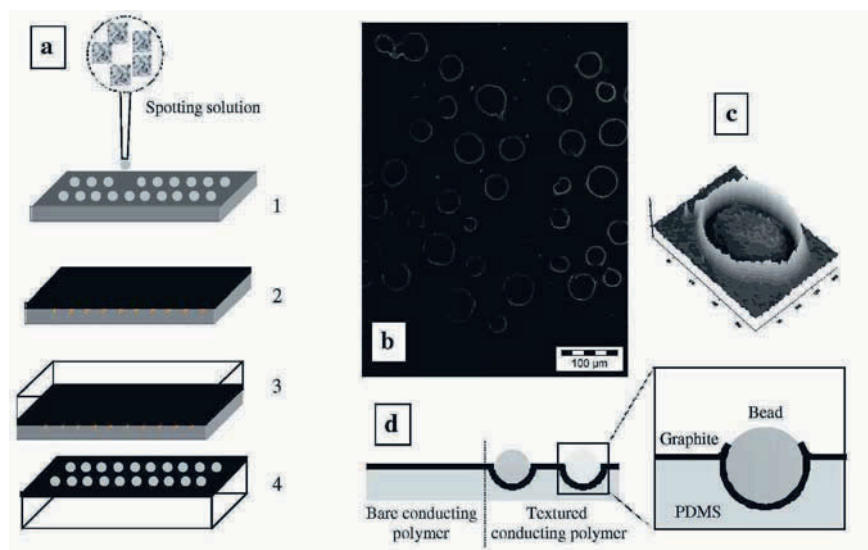


Figure 10. (a) Steps of the preparation of the addressed texturing of the PDMS-graphite conducting elastomer: (1) bead spotting; (2) graphite coating; (3) PDMS molding; (4) PDMS removal. (b) Electron microscopy (15 kV) image of Sepharose bead spots at the surface of the PDMS-graphite elastomer. (c) 3D representation of the scanning electron microscopy image of a Sepharose bead inserted in the the PDMS-graphite elastomer. (d) Schematic representation of the bead-containing layer.

produced  $\text{H}_2\text{O}_2$ . Using beads bearing biomolecules such as oligonucleotides or IgG, in conjunction with glucose oxidase-labelled DNA or antibody, sensitive biochips could be obtained with detection limits of  $10^{11}$  and  $10^{10}$  molecules respectively (Figure 11).

Multi-parameter enzyme-based biochips could also be obtained by locally adsorbing, at the PDMS-graphite surface, several oxidase enzymes.

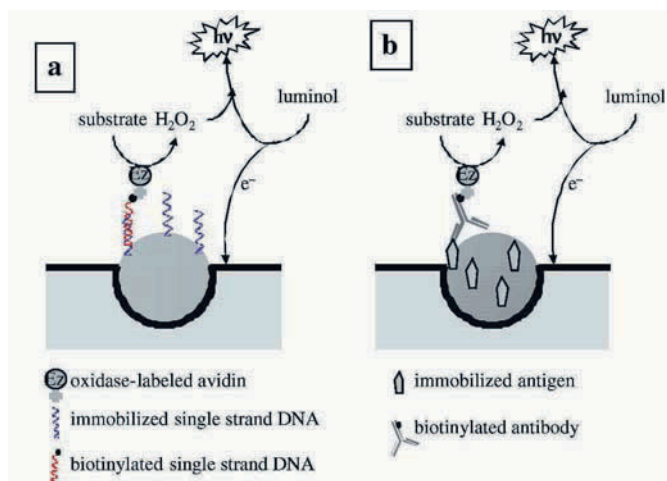


Figure 11. Electrochemiluminescent PDMS-graphite biochip formats: (a) nucleic acid-based biochip; (b) immunoassay (competitive immunoassay).

With the specific suitable oxidases, lactate, choline and glucose could be assayed. Concentration measurements of these metabolites could be performed over at least two decades with a detection limit of 10  $\mu\text{M}$  for lactate and choline and 20  $\mu\text{M}$  for glucose.

## 6. CONCLUSIONS

The field of biosensors is expanding continuously with a constant search for new transducing systems associated with stable biosensing elements. The ultra-sensitivity of bio- and chemiluminescence techniques together with the convenience of immobilized compounds in combination with optical fibres constitutes an attractive opportunity for designing biosensors. In addition to the advantages of optical fibre-based sensors, *i.e.* the possibilities of miniaturization and of remote sensing, bio- and chemiluminescence-based sensors require a simpler instrumentation than those based on other spectroscopic techniques. The coupling of auxiliary enzymes allows to extend the range of compounds that can be monitored at the trace level, including enzyme activities.

The current trends toward miniaturization and the need of massively parallel measurements led to the development of biochips. In this area, biocatalyzed and electrogenerated chemiluminescence reactions appear attractive and represent an alternative to fluorescence detection which is still widespread used despite the numerous problems of quantitative measurements and interference fluorescence emission.

Composite sensing layers, consisting of bioactive molecule-charged beads entrapped in a polymeric structure, have been successfully used to realize multi-purpose biochips for DNA, proteins or enzymes. For all these different biochips, the chemiluminescence and electro-chemiluminescence measurements required only a CCD camera and neither light sources nor optical filters are needed.

## REFERENCES

1. Roswell D.F., White E.H., The chemiluminescence of luminol and related hydrazides, *Methods Enzymol.* 1978; 57: 409-423.
2. White E. H., Zafiriou O., Kägi H. H., Hill J.H.M., Chemiluminescence of luminol: the chemical reaction, *J. Am. Chem. Soc.* 1964; 86: 940-941.
3. White E.H., Bursey M.M., Chemiluminescence of luminol and related hydrazides. The light emission step, *J. Am. Chem. Soc.* 1964; 86: 941-942.
4. Yamazaki I., Yokota K.N., Oxidation states of peroxidase, *Mol. Cell. Biochem.* 1973; 2: 39-52.
5. Cormier M.J., Prichard P.M., An investigation of the mechanism of the luminescent peroxidation of luminol by stopped flow techniques, *J. Biol. Chem.* 1968; 243: 4706-4714.

6. Kuwana T., Electro-oxidation followed by light emission, *J. Electroanal.Chem.* 1963; 6: 164-167.
7. Epstein B., Kuwana T., Electrooxidation of phthalhydrazides, *J. Electroanal. Chem.* 1967; 15: 389-397.
8. Thorpe G.H.G., Kricka L.J., Carter T.J.N., Chemiluminescence, in *Clinical and Biochemical Luminescence*, L. J. Kricka and T.J.N. Carter, eds. Marcel Dekker, New York, 1982, 21-42.
9. Mohan A.G., *Chemi- and Bioluminescence*, J.G. Burr, ed. Marcel Dekker, New York, 1985, 245-258.
10. De Luca M., Firefly luciferase, *Advances Enzymol.* 1976; 44: 37-68.
11. De Luca M., McElroy W. D., Purification and properties of firefly luciferase, *Methods Enzymol.* 1978; 57: 3-15.
12. McElroy W.D., De Luca M., Firefly bioluminescence, in *Chemi- and Bioluminescence*, JG Burr, ed., Marcel Dekker, New York, 1985, 387-399.
13. Ugarova N.N., Luciferase of *Luciola mingrelica* fireflies. Kinetics and regulation mechanism, *J. Biolumin. Chemilumin.* 1989; 4: 406-418.
14. Brovko L.Y., Gandelman O.A., Polenova T.E., Ugarova N.N. Kinetics of bioluminescence in the firefly luciferin-luciferase system. *Biochemistry (Russia)* 1994; 59(2): 195-201.
15. Gandelman O.A., Brovko L.Y., Chikishev A.Y., Shkurinov A.P., Ugarova N.N., Investigation of the interaction between firefly luciferase and oxyluciferin or its analogues by steady state and subnanosecond time-resolved fluorescence, *J. Photochem. Photobiol. B :Biol.* 1994; 22: 203-209.
16. Shimomura O., Johnson F.H., Saiga Y., Extraction, purification and properties of aequorin, a bioluminescent protein from the luminous hydromedusan Aequorea, *J. Cell Comp. Physiol.* 1962; 59: 223-239.
17. Seliger H.H., McElroy W.D., Spectral emission and quantum yield of firefly bioluminescence, *Arch. Biochem. Biophys.* 1960; 88: 136-141.
18. Gonzalus-Miguel A., Meighen E.A., Ziegler M.M., Nicoli M., Neelson K.H., Hastings J.W., Purification and properties of bacterial luciferases, *J. Biol. Chem.* 1972; 247: 398-404.
19. Hastings J.W., Baldwin T.O., Nicoli M.Z., Bacterial luciferase: assay, purification and properties, *Methods Enzymol.* 1978; 57: 135-152.
20. Neelson K.H., Isolation, identification, and manipulation of luminous bacteria, *Methods Enzymol.* 1978; 57: 153-166.
21. Puget K., Michelson A.M., Studies in bioluminescence. VII. bacterial NADH: Flavin mononucleotide oxidoreductase, *Biochimie*, 1972; 54: 1197-1204.
22. Gerlo E., Charlier J., Identification of NADH-specific and NADPH-specific FMN reductase in *Beneckea harveyi*, *Eur. J. Biochem.* 1975; 57: 461-467.
23. Freeman T.M., Seitz W.R., Chemiluminescence fiber optic probe for hydrogen peroxide based on the luminol reaction, *Anal. Chem.* 1978; 50(9): 1242-1246.
24. Blum L.J., Gautier S.M., Coulet P.R., Luminescence fiber-optic biosensor, *Anal. Lett.* 1988; 21(5): 717-726.
25. Berger A., Blum L.J., Enhancement of the response of a lactate oxidase/peroxidase-based fiberoptic sensor by compartmentalization of the enzyme layer, *Enzyme Microb. Technol.*, 1994; 16: 979-984.
26. Michel P.E., Gautier S.M., Blum L.J., Effect of compartmentalization of the sensing layer on the sensitivity of a multienzyme-based bioluminescent sensor for L-lactate, *Anal. Lett.* 1996; 29 (7): 1139-1155.
27. Michel P.E., Gautier S.M., Blum L.J., A high-performance bioluminescent trienzymatic sensor for D-sorbitol based on a novel approach of the sensing layer design". *Enzyme Microb. Technol.* 1997; 21(2): 108-116.

28. Gautier S.M., Blum L.J., Coulet P.R., Bioluminescence-based fiber-optic sensor with entrapped co-reactant: an approach for designing a self-contained biosensor, *Anal. Chim. Acta*, 1991; 243: 149-156.
29. Gautier S.M., Blum L.J., Coulet P.R., Cofactor-containing bioluminescent fiber-optic sensor: new developments with poly(vinyl) alcohol matrices, *Anal. Chim. Acta*, 1991; 255: 253-258.
30. Gautier S.M., Michel P.E., Blum L.J., Reagentless bioluminescent sensor for NADH, *Anal. Lett.*, 1994; 27(11): 2055-2069.
31. Michel P.E., Gautier S.M., Blum L.J., Luciferin incorporation in the structure of acrylic microspheres with subsequent confinement in a polymeric film : a new method to develop a controlled release- based biosensor for ATP, ADP and AMP, *Talanta* 1998; 47: 167-181.
32. Gautier S.M., Blum L.J., Coulet P.R., Alternate determination of ATP and NADH with a single bioluminescence-based fiber-optic sensor, *Sens. Actuators* 1990; B1: 580-584.
33. Gautier S.M., Blum L.J., Coulet P.R., Multifunction fibre-optic sensor for the selected bioluminescent flow determination of ATP or NADH, *Anal. Chim. Acta* 1990; 235: 243-253.
34. Gautier S.M., Blum L.J., Coulet P.R., Fibre-optic biosensor based on luminescence and immobilized enzymes: microdetermination of sorbitol, éthanol and oxaloacetate, *J. Biolumin. Chemilumin.* 1990; 5: 57-63.
35. Gautier S.M., Blum L.J., Coulet P.R., Dehydrogenase activity monitoring by flow injection analysis combined with luminescence based fibre-optic sensors, *Anal. Chim. Acta* 1992; 266: 331-338.
36. Gautier S.M., Blum L.J., Coulet P. R., Fibre-optic sensor with co-immobilised bacterial bioluminescence enzymes, *Biosensors* 1989; 4: 181-194.
37. Blum L.J., Gautier S.M., Coulet P.R., Highly stable bioluminescence-based fiber-optic sensor using immobilized enzymes from *Vibrio harveyi*, *Anal. Lett.* 1989; 22(10): 2211-2222.
38. Blum L.J., Gautier S.M., Coulet P.R., Continuous flow bioluminescent assay of NADH using a fibre-optic sensor, *Anal. Chim. Acta* 1989; 226: 331-336.
39. Lapp H., Spohn U., Janasek D., An enzymatic chemiluminescence optrode for choline detection under flow injection conditions, *Anal. Lett.* 1996; 29: 1-17.
40. Tsafack V.C., Marquette C.A., Pizzolato F., Blum L.J., Chemiluminescent choline biosensor using histidine-modified peroxidase immobilized on metal-chelate substituted beads and choline oxidase immobilized on anion-exchanger beads co-entrapped in a photocrosslinkable polymer, *Biosens. Bioelectron*, 2000; 15: 125-133.
41. Xie X., Suleiman A.A., Guilbault G.G., Yang Z., Sun Z., Flow-injection determination of ethanol by fiber-optic chemiluminescence measurement, *Anal. Chim. Acta* 1992; 266: 325-329.
42. Abdel-Latif M.S., Guilbault G.G., Peroxide optrode based on micellar-mediated chemiluminescence reaction of luminol, *Anal. Chim. Acta* 1989; 221: 11-17.
43. Zhou X., Arnold M.A., Internal enzyme fiber-optic biosensors for hydrogen peroxide and glucose, *Anal. Chim. Acta* 1995; 304: 147-156.
44. Blum L.J., Chemiluminescent flow injection analysis of glucose in drinks with a bi-enzyme fiber optic biosensor, *Enzyme Microb. Technol.* 1993; 15: 407-411.
45. Blankenstein G., Preuschoff F., Spohn U., Mohr K.H., Kula M.R., Determination of L-glutamate and L-glutamine by flow-injection analysis and chemiluminescence detection: comparison of an enzyme column and enzyme membrane sensor, *Anal. Chim. Acta* 1993; 271: 231-237.
46. Preuschoff F., Spohn U., Blankenstein G., Mohr G., Kula M.R., Chemiluminometric hydrogen peroxide sensor for flow injection analysis, *Fresenius J. Anal. Chem.*, 1993; 346: 924-929.
47. Berger-Collaudin A., Blum L. J., Enhanced luminescent response of a fiberoptic sensor for H<sub>2</sub>O<sub>2</sub> by a high-salt concentration medium, *Sens. Actuators B* 1997; 38-39: 189-194.

48. Hlavay J., Haemmerli S.D., Guilbault G.G., Fibre-optic biosensor for hypoxanthine and xanthine based on a chemiluminescence reaction, *Biosens. Bioelectron* 1994; 9: 189-195.
49. Berger A., Blum L. J., Enhancement of the response of a lactate oxidase/peroxidase-based fiberoptic sensor by compartmentalization of the enzyme layer, *Enzyme Microb. Technol.* 1994; 16: 979-984.
50. Preuschoff F., Spohn U., Weber E., Unverhau K., Mohr K.H., Chemiluminometric L-lysine determination with immobilized lysine oxidase by flow-injection analysis, *Anal. Chim. Acta* 1993; 280: 185-189.
51. Spohn U., Preuschoff F., Blankenstein G., Janasek D., Kula M.R., Hacker A., Chemiluminometric enzyme sensors for flow injection analysis, *Anal. Chim. Acta* 1995; 303: 109-120.
52. Hlavay J., Guilbault G.G., Determination of sulphite by use of a fiber-optic biosensor based on a chemiluminescent reaction, *Anal. Chim. Acta* 1994; 299: 91-96.
53. Marquette C.A., Blum L.J., Luminol electrochemiluminescence-based fibre optic biosensors for flow injection analysis of glucose and lactate in natural samples, *Anal. Chim. Acta* 1999; 381: 1-10.
54. Marquette C.A., Blum L.J., Electrochemiluminescence of luminol for 2,4-D optical immunosensing in a flow injection system, *Sens. Actuators B* 1998; 51: 100-106.
55. Tsafack V. C., Marquette C. A., Leca B., Blum L. J., An electrochemiluminescence-based fibre optic biosensor for choline flow injection analysis, *Analyst* 2000; 125: 151-155.
56. Marquette C. A., Raveau S., Blum L. J., Luminol electrochemiluminescence-based biosensor for total cholesterol determination in natural samples, *Anal. Lett.* 2000; 33(9): 1779-1796.
57. Marquette C.A., Blum L.J., Self-containing reactant Biochips for the electrochemiluminescent determination of glucose, lactate and choline, *Sens. Actuators B* 2003; 90: 112-117.
58. Marquette C.A., Degiuli A., Blum L.J., Electrochemiluminescent biosensors array for the concomitant detection of choline, glucose, glutamate, lactate, lysine and urate, *Biosens. Bioelectron.* 2003; 19: 433-439.
59. Marquette C.A., Thomas D., Blum L.J., Design of luminescent biochips based on enzyme, antibody or DNA composite layer, *Anal. Bioanal. Chem.* 2003; 377: 922-928
60. Marquette C.A., Blum L.J., Direct immobilisation in PDMS for DNA, protein and enzyme fluidic biochips, *Anal. Chim. Acta* 2004; 506: 127-132.
61. Marquette C.A., Blum L.J., Conducting elastomer surface texturing: a path to electrode spotting. Application to the biochip production, *Biosens. Bioelectron.*, 2004, 20 (2): 197-203.

## Chapter 9

# **SENSORS BASED ON SPECTROSCOPY OF GUIDED WAVES**

Jiří Homola

*Institute of Radio Engineering and Electronics*

*Academy of Sciences of the Czech Republic*

*Chaberská 57*

*Prague, Czech Republic*

### **1. INTRODUCTION**

The last two decades have witnessed remarkable progress in the development of affinity biosensors and their applications in areas such as environmental protection, biotechnology, medical diagnostics, drug screening, food safety, and security. An affinity biosensor consists of a transducer and a biological recognition element which is able to interact with a selected analyte. Various optical methods have been exploited in biosensors including fluorescence spectroscopy<sup>1</sup>, interferometry (reflectometric white light interferometry<sup>2</sup>, modal interferometry in optical waveguide structures<sup>3</sup>), and spectroscopy of guided modes of optical waveguides. Optical biosensors based on spectroscopy of guided modes of optical waveguides - grating coupler<sup>4</sup>, resonant mirror<sup>5</sup>, and surface plasmon resonance (SPR)<sup>6,7</sup> - rely on the measurement of binding-induced refractive index changes and thus are label-free technologies. This paper reviews fundamentals of optical sensors based on spectroscopy of guided modes of optical waveguides and their applications.

### **2. FUNDAMENTALS OF OPTICAL SENSORS BASED ON SPECTROSCOPY OF GUIDED WAVES**

#### **2.1 Optical Waveguides**

There are several types of optical waveguides – planar waveguides and cylindrical waveguides (optical fibers). Basic optical waveguide geometries are shown in Figure 1.



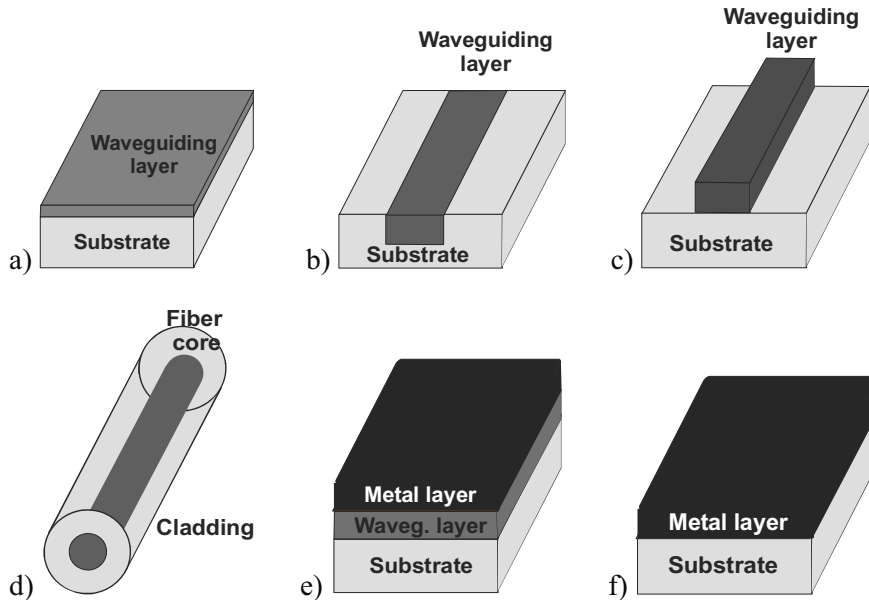


Figure 1. Optical waveguides – a) dielectric slab waveguide, b) dielectric strip waveguide, and c) dielectric channel waveguides, d) optical fiber, e) metal-clad dielectric waveguide, and f) (degenerated) metal-dielectric waveguide.

## 2.2 Light Propagation in Planar Dielectric Waveguides

Let us investigate light propagation in a planar waveguide consisting of three media with the refractive indices  $n_1 < n_2 > n_3$  and a waveguide layer thickness  $d$  (Figure 2).

We shall assume light propagation along  $z$ -axis and electromagnetic field distribution independent of  $y$  coordinate. Solution of Maxwell's equations for such a structure can be assumed in the form:

$$\vec{U}(x, z) = \vec{u}(x) \cdot \exp(i(\alpha x - \beta z)) \tag{Eq.1}$$

where  $\vec{U}(x, z)$  denotes the vector of electric or magnetic field intensity,  $\vec{u}(x)$

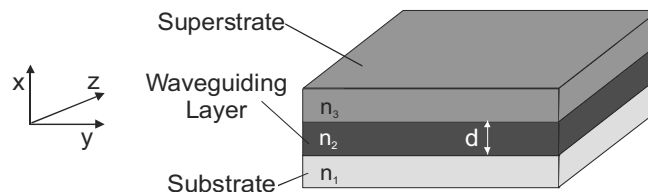


Figure 2. Planar optical waveguide.

field amplitude,  $\omega$  angular frequency,  $t$  time, and  $\beta$  propagation constant. In principle, the solution can be decomposed into two types of waves - transverse electric (TE) modes  $E_z = 0$  and transverse magnetic (TM) modes ( $H_z = 0$ ). For these waves, the wave equations can be written as:

$$\frac{\partial^2 U_y(x)}{\partial x^2} + (\omega^2 \epsilon \mu - \beta^2) U_y(x) = 0 \quad (\text{Eq.2})$$

where  $U_y$  denotes the y-component of the vector of electric (for TE modes) or magnetic (for TM modes) field intensity. In each medium the solution of wave equation can be expressed as a linear combination of  $\exp(ik_i x)$  and  $\exp(-ik_i x)$ , where  $\kappa_i^2 = \omega^2 \mu \epsilon_i - \beta^2$  and  $\epsilon_i$  are dielectric constants of the involved media ( $i = 1, 2, 3$ ).

In order to describe a light wave confined in the vicinity of the waveguide, parameters  $\kappa_1$  and  $\kappa_2$  have to fulfill  $\kappa^2 < 0$  and the electromagnetic field has to exponentially decrease with an increasing distance from the waveguide. Application of boundary conditions requiring continuity of tangential components of electric and magnetic field vectors yields dispersion equations in the form:

$$\text{TE modes:} \quad \tan(\kappa d) = \frac{\gamma_1/\kappa + \gamma_3/\kappa}{1 - (\gamma_1/\kappa)(\gamma_3/\kappa)}, \quad (\text{Eq.3})$$

$$\text{TM modes:} \quad \tan(\kappa d) = \frac{\gamma_1 \epsilon_2 / \kappa \epsilon_1 + \gamma_3 \epsilon_2 / \kappa \epsilon_3}{1 - (\gamma_1 \epsilon_2 / \kappa \epsilon_1)(\gamma_3 \epsilon_2 / \kappa \epsilon_3)}$$

where  $\kappa_2^2 = \omega^2 \mu \epsilon_2 - \beta^2$  and  $\gamma_{1,3}^2 = \beta^2 - \omega^2 \mu \epsilon_{1,3}$ . Solutions of these equations are propagation constants of guided modes of the waveguide. Dependence of the

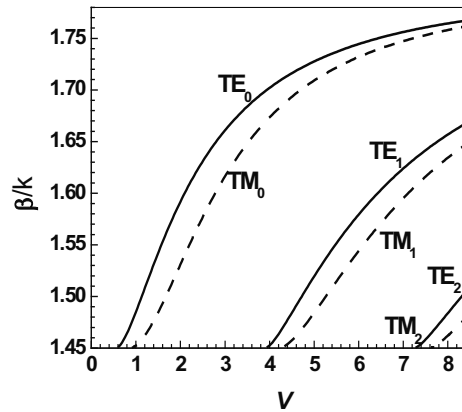


Figure 3. Normalized propagation constant as a function of normalized frequency for three low-order TE and TM modes;  $n_1=1.45$ ,  $n_2=1.8$ ,  $n_3=1.32$ .

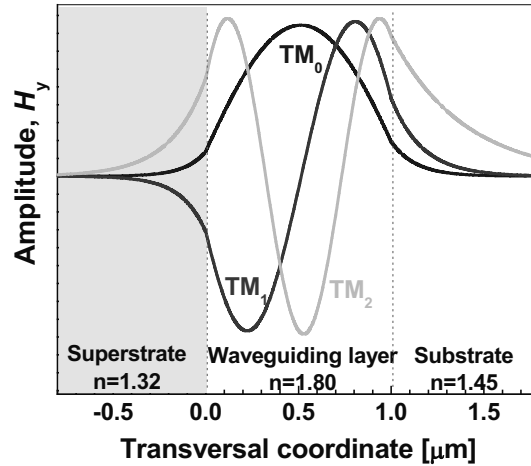


Figure 4. Field distribution for three low-order TM modes;  $n_1 = 1.45$ ,  $n_2 = 1.8$ ,  $n_3 = 1.32$ ,  $\lambda = 830\text{nm}$ .

propagation constant of the first three TE and TM modes as a function of normalized frequency,  $V = kd\sqrt{n_2^2 - n_1^2}$  is shown in Figure 3.

The corresponding mode field distributions are shown in Figure 4.

### 2.3 Surface Plasmons at a Metal-Dielectric Interface

Surface plasmons are special modes of electromagnetic field which can propagate along the boundary between a dielectric and a metal (waveguide geometries *e*) and *f*) in Figure 1), which behaves like nearly-free electron plasma<sup>8, 9</sup>. A surface plasmon is a transverse-magnetic (TM) wave and its (complex) propagation constant is given as:

$$\beta = \frac{\omega}{c} \sqrt{\frac{\epsilon_M \epsilon_D}{\epsilon_M + \epsilon_D}} \quad (\text{Eq.4})$$

where  $\omega$  is the angular frequency,  $c$  is the speed of light in vacuum, and  $\epsilon_D$  and  $\epsilon_M$  are dielectric functions of the dielectric and metal, respectively<sup>8, 9</sup>. This equation describes a true surface plasmon if the real part of  $\epsilon_M$  is negative and its absolute value is smaller than  $\epsilon_D$ . At optical wavelengths, this condition is fulfilled for several metals of which gold is most commonly employed in biosensors due to its chemical stability. The normalized propagation constant of a surface plasmon at a gold-air interface is shown in Figure 5.

Electromagnetic field of a surface plasmon is confined at the metal-dielectric interface and decreases exponentially into both media, Figure 6.

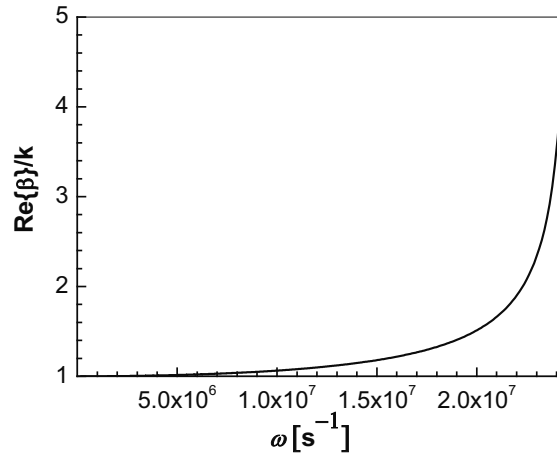


Figure 5. Normalized propagation constant as a function of angular frequency for a surface plasmon propagating along gold-air interface.

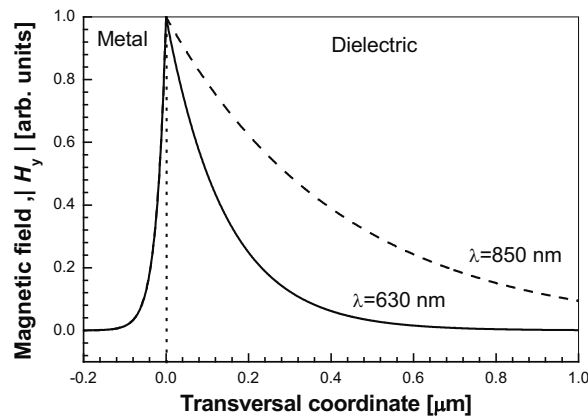


Figure 6. Distribution of the magnetic field intensity for a surface plasmon at the interface between gold and dielectric with a refractive index of 1.32 for two different wavelengths.

## 2.4 Optical Sensors Based on Spectroscopy of Guided Waves

As a portion of electromagnetic field propagates outside the waveguiding layer in the form of an evanescent wave, the propagation constant of a guided mode in the waveguide is sensitive to changes in the refractive index of the medium adjacent to the waveguiding layer. In optical sensors based on spectroscopy of guided waves, changes in the refractive index of sample are determined by measuring propagation constant of a guided mode, Figure 7. It should be noted that propagation constants of different modes are not altered by the same amount as a change in the propagation constant is

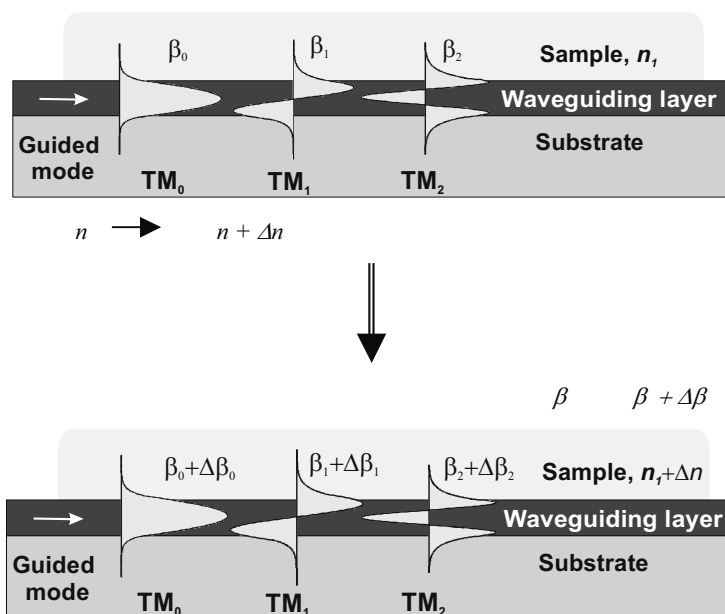


Figure 7. Concept of optical sensor based on spectroscopy of guided modes. A change in the refractive index alters propagation constant of a guided mode.

proportional to a relative concentration of the electromagnetic field of a particular mode in the sample.

## 2.5. Affinity Biosensors Based on Spectroscopy of Guided Waves

In affinity biosensors based on spectroscopy of guided modes, biomolecular recognition elements immobilized on the surface of a waveguiding structure recognize and capture analyte present in a liquid sample producing a local increase in the refractive index at the sensor surface. The refractive index increase gives rise to an increase in the propagation constant of the mode supported by the waveguiding structure (see Figure 8).

Main types of biomolecular recognition elements used in affinity biosensors based on spectroscopy of guided modes include antibodies, nucleic acids and biomimetic materials. Antibodies are used most frequently because of their high affinity, versatility, and commercial availability.

Relying on sensitivity of the propagation to refractive index is strength (no need for labeling) as well as potential weakness of biosensors based on spectroscopy of guided waves. Sensor measurements can be compromised by interfering effects producing refractive index changes such as non-specific interaction between the sensor surface and sample (adsorption of

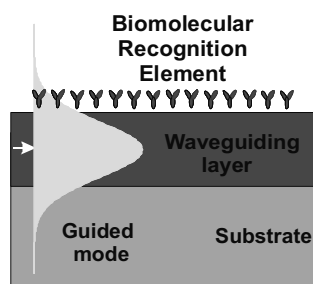
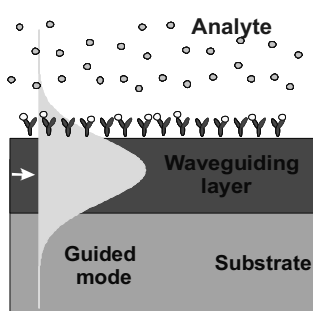
**PRIOR BINDING:**Bilayer refractive index,  $n$ Mode propagation constant,  $\beta$ **ANALYTE BINDING:** $n \rightarrow n + \Delta n$  $\beta \rightarrow \beta + \Delta\beta$ 

Figure 8. Concept of affinity biosensor based on spectroscopy of guided waves.

non-target molecules to the sensor surface), and background refractive index variations (due to sample temperature and composition fluctuations). Therefore, development of sensor platforms providing robust referencing for suppression of bulk refractive index interferences, has been pursued worldwide<sup>10,11</sup>.

### 3. MAIN CONFIGURATIONS OF OPTICAL SENSORS BASED ON SPECTROSCOPY OF GUIDED WAVES

#### 3.1 Surface Plasmon Resonance Sensor

Optical sensors based on spectroscopy of surface plasmons, often referred to as surface plasmon resonance (SPR) sensors, exploit sensitivity of the propagation constant of a surface plasmon to refractive index changes within the evanescent field of the surface plasmon. A change in the refractive index produces a change in the propagation constant of the surface plasmon, which results in a change in the characteristics of the light wave interacting with the surface plasmon<sup>12</sup>. Based on which characteristic of the light wave interacting with the surface plasmon is measured, SPR sensors are classified as sensors with angular, wavelength, intensity, phase and polarization modulations<sup>12</sup>.

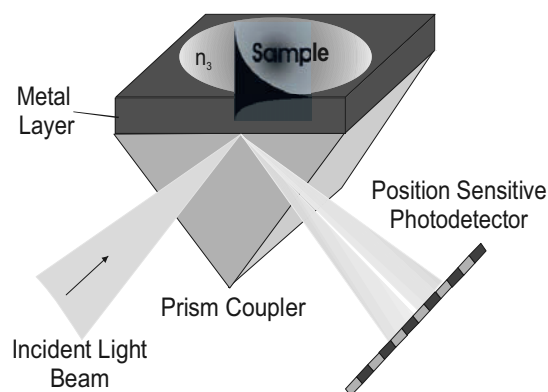


Figure 9. Optical sensor based on spectroscopy of surface plasmons and angular modulation.

The operating principle of optical sensors based on spectroscopy of surface plasmons is illustrated in Figure 9, which shows an SPR sensor with angular modulation. In this geometry, a monochromatic light wave passes through a high refractive index prism and is reflected at the prism-metal layer interface generating an evanescent wave penetrating the metal layer. For a certain angle of incidence, the component of the wave vector of the incident light parallel to the metal surface matches that of the surface plasmon and coupling between the light wave and the surface plasmon occurs. This coupling results in absorption of light and a characteristic dip in the angular spectrum of reflected light, Figure 10.

A change in the refractive index at the surface of the metal film gives rise to a change in the propagation constant of a surface plasmon. This change

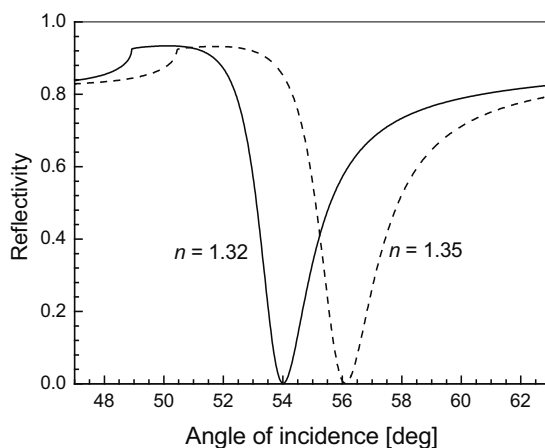


Figure 10. Reflectivity for the geometry consisting of an SF14 glass prism, 50 nm thick gold layer, and a dielectric, as a function of the angle of incidence for two different refractive indices of the dielectric; wavelength = 682 nm.

results in a change in the resonant angle and a shift in the angular position of the SPR dip (see Figure 10).

Surface plasmon resonance sensors can be also constructed using optical fibers<sup>13,14</sup>, integrated optical waveguides<sup>15</sup>, and diffraction gratings<sup>16</sup>.

### 3.2 Resonant Mirror Sensor

Another sensor which exploits a prism for coupling light into a guided mode of an optical waveguide is the resonant mirror sensor, Figure 11. In this sensor, an incident light wave produces an evanescent wave at the prism-buffer layer interface. If the propagation constant of the evanescent wave matches that of a waveguide mode, the coupling of light into the waveguide mode occurs.

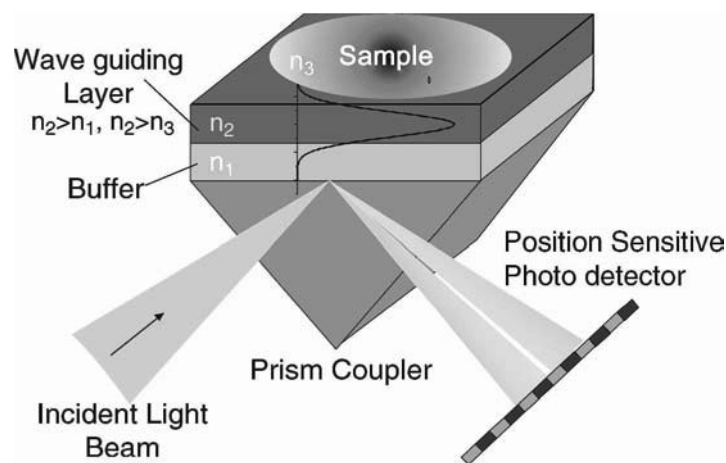


Figure 11. Resonant mirror sensor with angular modulation.

In the angle-modulated version of the sensor, excitation of a mode is manifested as a dip in the angular spectrum of reflected light. Changes in the refractive index at the sensor surface alter the propagation constant of the mode which can be measured by measuring the coupling strength at multiple angles and determining the angle of incidence at which the light intensity minimum occurs. Alternatively, the structure can be illuminated with light containing both TE and TM polarizations and a change in the polarization of output light can be measured<sup>17</sup>.

### 3.3 Grating Coupler Sensor

In grating coupler sensors, a diffraction grating is used to couple light in (Figure 12) or out of (Figure 13) a waveguide<sup>18</sup>. In the input grating coupler



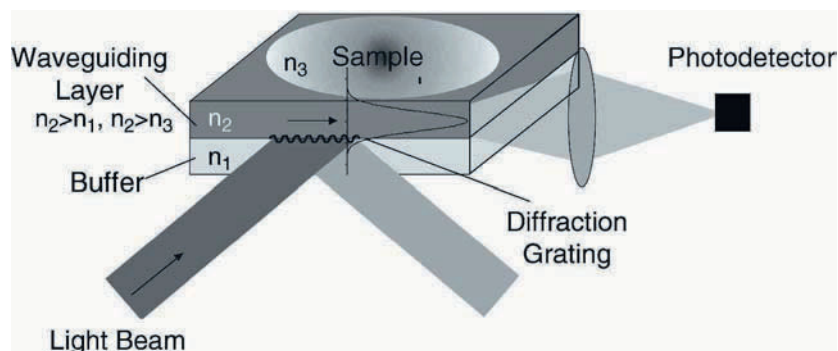


Figure 12. Input grating coupler sensor.

sensor, the momentum of the incident light wave is increased by diffraction on a grating embedded in the waveguide. The angle of incidence is varied and the intensity of light coupled into a waveguide mode is measured. When the diffraction-enhanced momentum of the incident wave matches the propagation constant of a waveguide mode, the detected light intensity reaches its maximum. By tracking the angle of incidence at which the maximum coupling occurs, changes in the refractive index at the sensor surface can be measured.

Optical sensors based on output grating couplers work in the opposite fashion. Light propagating in the waveguide is coupled out of the waveguide by means of a diffraction grating. The outcoupling angle is proportional to the propagation constant of the waveguide mode. Changes in the refractive index at the sensor surface alter the propagation constant of the mode resulting in a change in the outcoupling angle.

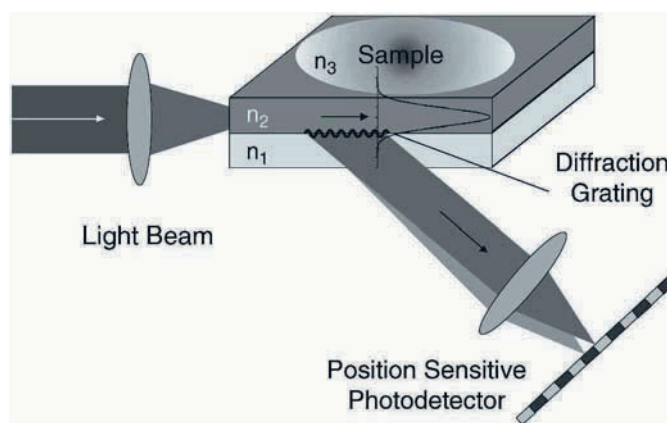


Figure 13. Output grating coupler sensor.

## 4. APPLICATIONS

### 4.1 Detection Formats

Optical sensors based on spectroscopy of guided waves have been demonstrated for detection and identification of numerous chemical and biological analytes. The choice of detection format for a particular application depends on the size of target analyte molecules, binding characteristics of available biomolecular recognition element, and range of analyte's concentrations to be measured.

Direct detection is usually preferred in applications, where direct binding of analyte of concentrations of interest produces a sufficient response. If necessary, the lowest detection limits of the direct biosensors can be improved by using a sandwich assay. Smaller analytes (molecular weight < 10,000) are usually measured using inhibition assay, Figure 14.

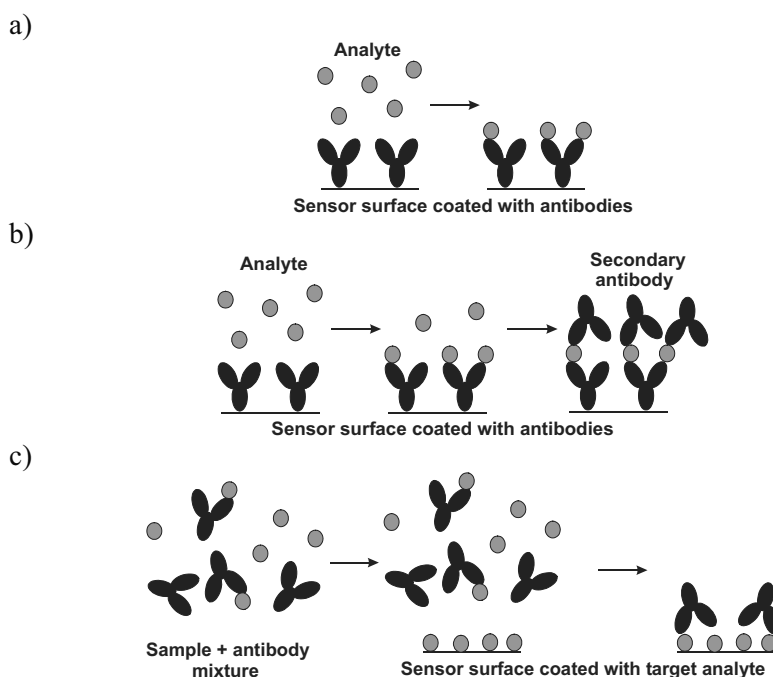


Figure 14. Detection formats used in affinity biosensors based on spectroscopy of guided waves: a) direct detection, b) sandwich assay, and c) competitive inhibition assay.

### 4.2 Detection of Chemical and Biological Analytes

Affinity biosensors based on spectroscopy of guided modes have been used for detection of small analytes such as pesticides and herbicides

(simazine and atrazine), drugs (morphine, methamphetamine and theophylline), and toxins (fumonisin B1). Except for fumonisin B1, which was measured directly<sup>19</sup>, all the analytes were detected using binding inhibition assay<sup>20-22</sup>. The demonstrated detection limits depended on the quality of used antibodies and biosensor instrument and typically ranged from 0.1 to 1 ng/ml.

Representatives of medium-size analytes detected by affinity biosensors based on spectroscopy of guided modes include food-safety related analytes such as staphylococcal enterotoxin B<sup>23, 24</sup>, botulinum toxin<sup>25</sup>, and *E. coli* enterotoxin<sup>26</sup>. These analytes were detected directly or using sandwich assay. The lowest detection limits were mainly dependent on the quality of used antibodies and were 5 ng/ml (direct detection in buffer) and 0.5 ng/ml (sandwich assay in buffer and milk)<sup>24</sup> for staphylococcal enterotoxin B, 2.5 µg/ml for botulinum toxin, and 6 µg/ml for *E. coli* enterotoxin<sup>26</sup>.

Large analytes targeted by affinity biosensor technology include bacterial pathogens such as *Escherichia coli*, *Salmonella enteritidis*, and *Listeria monocytogenes*. *Salmonella enteritidis* and *Listeria monocytogenes* were detected by an SPR sensor at concentrations down to 10<sup>6</sup> cfu/ml<sup>27</sup>.

## 5. SUMMARY

Optical sensors based on spectroscopy of guided waves offer generic label-free technology which in conjunction with appropriate biomolecular recognition elements can be used for rapid detection of a large variety of chemical and biological substances. This technology has been demonstrated to be useful for detection of small and, in particular, medium size analytes. Detection limits for large analytes such as bacterial pathogens still need to be improved to meet today's needs.

Future development of affinity biosensors based on spectroscopy of guided waves will be driven by the needs of the consumer. These biosensor technologies hold potential to benefit important fields including pharmaceutical research, medical diagnostics, environmental monitoring, food safety, and security. Applications in these areas will challenge research and development in the field.

## ACKNOWLEDGEMENT

This work was supported by the Grant Agency of the Czech Republic under contracts 303/03/0249, 203/02/1326 and 102/03/0633.

## REFERENCES

1. Rowe-Taitt C.A., Hazzard J.W., Hoffinan K.E., Cras J.J., Golden J.P., Ligler F.S., Simultaneous detection of six biohazardous agents using a planar waveguide array biosensor, *Biosensors and Bioelectronics* 2000; 15: 579-589.
2. Piehler J., Brecht A., Gauglitz G., Affinity detection of low molecular-weight analytes, *Analytical Chemistry* 1996; 68: 139-143.
3. Heideman R.G., H. Kooyman R. P., Greve J., Performance of a highly sensitive optical waveguide Mach-Zehnder interferometer immunosensor, *Sensors and Actuators B* 1993; 10: 209-217.
4. Clerc D., Lukosz W., Integrated optical output grating coupler as biochemical sensor, *Sensors and Actuators B* 1994; 19: 581-586.
5. Cush R., Cronin J.M., Stewart W.J., Maule C.H., Molloy J., Goddard N. J., The resonant mirror: a novel optical biosensor for direct sensing of biomolecular interactions, Part I: Principle of operation and associated instrumentation, *Biosensors and Bioelectronics* 1993; 8: 347-353.
6. Homola J., Yee S., Gauglitz G., Surface plasmon resonance sensors: review, *Sensors and Actuators B* 1999; 54: 3-15.
7. Homola J., Yee S.S., Myszka D., Surface plasmon biosensors, in F. S. Ligler and C. R. Taitt (editors), *Optical Biosensors: Present and Future*, Elsevier, 2002.
8. Boardman, A.D., editor, 1982, *Electromagnetic Surface Modes*, John Wiley & Sons, Chichester.
9. Reather H., *Surface Plasmons on Smooth and Rough Surfaces and on Gratings*, Springer tracks in modern physics, Vol 111, Springer Verlag, Berlin (1983).
10. Nenninger G.G., Clendenning J.B., Furlong C.E., Yee S.S., Reference-compensated biosensing using a dual-channel surface plasmon resonance sensor system based on a planar lightpipe configuration, *Sensors and Actuators B* 1998; 51: 38-45.
11. Homola J., Lu H.B., Nenninger G.G., Dostálek J., Yee S.S., A novel multichannel surface plasmon resonance biosensor, *Sensors and Actuators B* 2001; 76: 403.
12. Homola J., Yee S.S., Myszka D., Surface plasmon biosensors, in *Optical Biosensors: Present and Future*, editor F. S. Ligler, Elsevier, 2002.
13. Jorgenson R.C., Yee S.S., A fiber-optic chemical sensor based on surface plasmon resonance, *Sensors and Actuators B* 1993; 12: 213-220.
14. Slavík R., Homola J., Čtyroký J., Novel spectral fiber optic sensor based on surface plasmon resonance, *Sensors and Actuators B* 2001; 74: 106 – 111.
15. Dostálek J., Čtyroký J., Homola J., Brynda E., Skalský M., Nekvindová P., Špírková J., Škvor J., Schröfel J., Surface plasmon resonance biosensor based on integrated optical waveguide, *Sensors and Actuators* 2001; 76: 8-12.
16. Hutley M C, *Diffraction Gratings*, Academic Press, London, 1982.
17. Cush R., Cronin J.M., Stewart W.J., Maule C.H., Molloy J., Goddard N.J., *Biosensors and Bioelectronics* 1993; 8: 347-353.
18. Clerc D., Lukosz W., *Sensors and Actuators B* 1994; 19: 581-586.
19. Mullett W., Edward P.C., Yeung M.J., Immunoassay of fumonisins by a surface plasmon resonance biosensor, *Analytical Biochemistry* 1998; 258: 161-167.
20. Minunni M., Mascini M., *Anal. Lett.* 1993; 26: 1441.
21. Miura N., Ogata K., Sakai G., Uda T., Yamazoe N., *Chem. Lett.*, 1997; 8: 713.
22. Sternesjo A., Mellgren C., Björck L., Analysis of Sulfamethazine in Milk by an Immunosensor assay Based on Surface Plasmon Resonance, *Immunoassays For Residue Analysis*, ACS Symposium Series, 621: 463-470 (1996).
23. Rasooly A., Surface plasmon resonance analysis of staphylococcal enterotoxin B in food, *Journal of Food Protection* 2001; 64: 37-43.

24. Homola J., Dostálek J., Chen S., Rasooly A., Jiang S., Yee S.S., Spectral surface plasmon resonance biosensor for detection of staphylococcal enterotoxin B (SEB) in milk, *Intern. J. Food Microbiology* 2002; 75: 61-69.
25. K. Choi, W. Seo, S. Cha, J. Choi, Evaluation of two types of biosensors for immunoassay of botulinum toxin, *J. Biochemistry and Molecular Biology* 1998; 31 (1): 101-105.
26. Spangler B.D., Wilkinson E.A., Murphy J.T., Tyler B.J., Comparison of the Spreeta surface plasmon resonance sensor and a quartz crystal microbalance for detection of *Escherichia coli* heat-labile enterotoxins, *Analytica Chimica Acta* 2001; 444: 149-161.
27. Koubová V., Brynda E., Karasová L., Škvor J., Homola J., Dostálek J., Tobiška P., Rošický J., Detection of foodborne pathogens using surface plasmon resonance biosensors, *Sensors and Actuators B* 2001; 74: 100-105.

## Chapter 10

# PLANAR OPTICAL SENSORS AND EVANESCENT WAVE EFFECTS

Conor S. Burke, Ondrej Stránik, Helen M. McEvoy and Brian D. MacCraith  
*National Centre for Sensor Research  
Dublin City University  
Glasnevin, Dublin 9, Ireland*

### 1. INTRODUCTION

Recent developments in microsystems technology have led to the widespread application of microfabrication techniques for the production of sensor platforms. These techniques have had a major impact on the development of so-called “Lab-on-a-Chip” devices. The major application areas for these devices are biomedical diagnostics, industrial process monitoring, environmental monitoring, drug discovery, and defence. In the context of biomedical diagnostic applications, for example, such devices are intended to provide quantitative chemical or biochemical information on samples such as blood, sweat and saliva while using minimal sample volume.

Specific features of the application contexts listed above have had a major role in dictating current trends in the development of optical sensors, which include miniaturisation, compatibility with mass-production processes, low cost and disposability. The integration of multiple functionalities onto a single platform and multianalyte detection capability are also important goals. Multianalyte detection provides an increased amount of information on the system of interest and, combined with techniques such as chemometrics and multivariate analysis, facilitates the development of devices such as high density biochips and so-called “electronic nose” systems. The advent of high precision microfabrication and micropatterning technologies has also played an essential role in the development of such systems. Disposability of the sensor platform is a significant advantage for a broad range of applications, the nature of which makes the sensing element suitable for single use only. Such applications include those involving irreversible sensing mechanisms, sensing

environments that result in fouling of the platform and medical applications where sterility and hygiene are an issue. Low cost and mass-producibility are, therefore, major driving factors in the development of these platforms.

All of the above trends make a planar platform configuration the ideal choice for the development of such sensors due to the compatibility of this geometry with a range of microfabrication technologies, the availability of low-cost materials for the production of such platforms and the robust nature of planar configurations when compared with alternatives based on optical fibres.

## 1.1 Planar Optical Sensors

The term “planar optical sensor” can refer to a range of sensing configurations, including passive planar substrates onto which discrete sensing spots are deposited along with more complex platforms where the substrate itself offers a degree of functionality, for example, waveguide or microfluidic platforms. Of particular interest here are sensor platforms based on planar waveguides, which exist in a variety of configurations ranging from simple microscope slides, which act as multimode slab waveguides, to ridge and buried waveguides as well as more complex platforms incorporating integrated optical elements. A broad range of planar waveguide-based optical sensors exploit evanescent wave effects in their operation. The evanescent field is generated when light undergoes total internal reflection at the interface between two dielectric materials, as is the case for light propagation within a planar optical waveguide. The nature of this evanescent field along with its applications in optical sensing will be explained in detail in this chapter.

One of the advantages of employing a planar geometry is its compatibility with a variety of deposition techniques for the production of sensing layers. These layers are quite often in the form of thin, porous films into which the analyte of interest is free to diffuse. The use of a thin layer results in reduced sensor response times and, combined with optical techniques such as evanescent wave interrogation, can result in a more efficient sensor platform than that provided by bulk (sensor monolith) systems. Thin film optical sensors are employed in both absorption and fluorescence-based detection platforms and their advantages will become apparent, in particular when combined with dedicated sensor optimisation strategies compatible with planar processing techniques.

## 1.2 Sensor Design Strategies

An essential stage in the production of an effective sensor is an understanding of the device sensitivity with a view to its optimisation.

Sensitivity impacts upon the limit of detection and resolution of the device, making it a key performance parameter. Recently, several strategies have been developed in order to provide sensitivity enhancements for optical sensor platforms based on both optical absorption and fluorescence phenomena. These strategies are the result of rigorous theoretical analyses of the relevant systems and, combined with polymer processing technology and planar fabrication protocols, provide a viable route for the development of low-cost, efficient optical sensor platforms.

## **2. PLANAR OPTICAL SENSOR PLATFORMS**

The key design elements of (non-spectroscopic) optical chemical sensors and biosensors are:

1. the recognition mechanism,
2. the immobilisation method for the chemo / bio recognition elements,
3. the transduction mechanism, and
4. the sensor platform.

The primary focus of this chapter is on the sensor platform and, in particular, on the specific advantages conferred by planar platforms.

The options available for sensor platforms for optical chemical and biosensors are primarily:

- optical fibres, and
- planar platforms.

Optical fibres have formed the basis of a variety of optical sensor systems including distributed sensor networks, sensors possessing high spatial resolution (e.g., tapered tip sensors), remote sensing, spectroscopy and *in-vivo* diagnosis<sup>1-6</sup>. However, these are typically niche applications and there are several disadvantages associated with optical fibres that make them a less attractive candidate for optical sensor platforms in general. The majority of these disadvantages are related to the geometry of the fibres themselves. They are often quite fragile and their inclusion in a sensor head detracts from its robustness and also restricts the possibilities for miniaturisation. The necessity of maintaining effective light coupling to the fibre increases the level of complexity in the sensor head design, as any change in this greatly impairs the efficiency and stability of the device. It is possible to address this issue effectively in a laboratory environment. However, the development of a fibre-based sensor head for field use is far more problematic due to an inability to control the operational environment of the sensor and the resulting impact this could have on the precise alignment required to couple light efficiently to the fibre. The geometry of optical fibres does not lend itself readily to conventional micropatterning techniques, making the incorporation of integrated optical components or microsystems a complex and time consuming task. For evanescent wave sensing applications, the



properties of the cladding are of vital importance as they determine the rate of diffusion of the analyte into the sensing layer, which has a direct impact on the response time of the sensor. This means that in order for commercially available optical fibres to be used for the detection of a particular analyte, they must be de-clad and coated with an analyte-specific sensing layer. This coating step is non-trivial, mainly due to the geometry of optical fibres. For instance, it is not possible to use techniques such as spin-coating or knife-coating to deposit a uniform sensing layer onto an optical fibre. Dip-coating is the only viable method and requires larger volumes of material compared with those mentioned above.

In contrast, planar sensor platforms offer several distinct advantages over fibre-based systems. Their geometry is inherently more robust than that of an optical fibre and, as a result, such platforms can be incorporated into the design of a compact sensor head with relative ease. A planar geometry is compatible with modern microfabrication techniques and facilitates the deposition of uniform sensing layers by a variety of methods including spin-coating and dip-coating. The versatility of this configuration makes it more attractive for the development of practical optical chemical sensors. As mentioned previously, planar sensor platforms exist in a variety of configurations including passive substrates and microfluidic systems. However, it is waveguide-based planar sensor platforms that are of particular interest to this discussion.

## 2.1 Planar Waveguide-Based Optical Sensors

A variety of planar waveguide configurations are currently employed for the development of optical sensor platforms. These include thin film (low-mode) waveguides and ridge waveguides. However, bearing in mind the demand for low-cost sensor platforms, the most practical configuration is that of a multimode slab waveguide, which can take the form of a simple plastic or glass slide. Figure 1 illustrates a typical planar optical sensor platform based on such a waveguide configuration. Light is coupled into the waveguide and propagates along its length where it is then outcoupled to an appropriate detector. The waveguide is coated with an analyte-sensitive layer that exhibits changes in its optical properties in response to the presence of

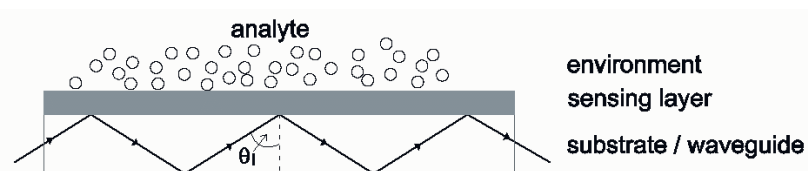


Figure 1. A generalised planar optical waveguide-based sensor.

the analyte. The nature of these changes is dependent on the optical phenomenon employed, e.g., optical absorption or fluorescence effects.

### 2.1.2 Evanescent Wave Interrogation

Figure 2 is a simplified illustration of mode propagation within a planar waveguide.

As the mode propagates within the waveguide by total internal reflection, its exponentially decaying evanescent tail extends into both cover and substrate layers over a distance that is characterised by the penetration depth,  $d_p$ . The extent to which the evanescent field penetrates the cover layer is of vital importance to the operation of evanescent-wave-based sensors. The penetration depth can be calculated from Equation (1) and is typically of the order of the wavelength of the propagating light.

$$d_p = \frac{\lambda_0}{2\pi n \sqrt{(\sin^2 \theta - \sin^2 \theta_c)}} \quad (\text{Eq.1})$$

Here,  $\lambda_0$  is the wavelength of the interrogating light,  $n$  is the refractive index of the waveguide,  $\theta$  is the angle of incidence of the propagating light at the waveguide – cover layer interface and  $\theta_c$  is the critical angle defined by the refractive indices of the waveguide and cover layer. It is clear from the equation that the penetration depth is tuneable and depends on the choice of incident angle, interrogating wavelength and the material refractive indices, which dictate the value of the critical angle,  $\theta_c$ . It will be shown that this characteristic of the evanescent field has major implications for the design of efficient optical biosensors based on fluorescence excitation of surface-bound biomolecules.

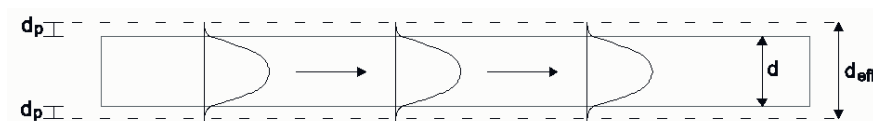


Figure 2. Mode propagation within a planar waveguide.

### 2.1.2 Absorption-Based Optical Sensors

A typical planar platform for absorption-based based optical sensing is depicted in Figure 3. The sensing layer is doped with an analyte-sensitive dye whose absorption properties change upon exposure to the target analyte. The analyte diffuses into the sensing layer where it causes a change in the extinction coefficient,  $\epsilon$ , of the layer. The interrogating light is spectrally

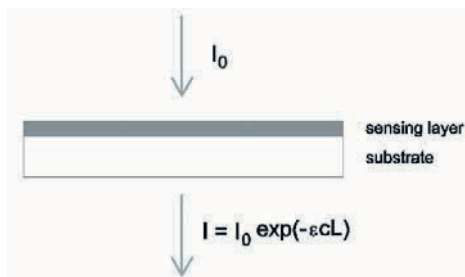


Figure 3. A typical configuration for absorption-based optical sensing.

matched to the absorption band of the sensing layer. Therefore, changes in the optical absorption of the layer result in a modulation of the detected light intensity, which is related to the analyte concentration, thereby providing the basis for the sensor. A number of alternatives for interrogating the sensor layer are available. In the transmittance-based configuration shown in Figure 3, the sensitivity of the platform is proportional to the optical path length ( $L$ ) of the light in the sensing layer, which can, obviously, be increased by employing a thicker sensing film. However, this would lead to an increased response time, adversely affecting sensor performance. It is here that the advantages of a configuration employing evanescent wave interrogation of the sensing layer become apparent.

Figure 4 illustrates such a platform, which consists of a planar waveguide on top of which a thin sensing layer has been deposited. Light propagates along the waveguide by total internal reflection with an incident angle greater than the critical angle determined primarily by the refractive indices of the waveguide and sensing layer. The evanescent field of the propagating light interrogates the sensing layer and the output intensity can be written as

$$I = I_0 \exp(-r \varepsilon C L_{\text{int}}) \quad (\text{Eq.2})$$

where  $L_{\text{int}}$  is the interaction length of the waveguide and  $r$  is the ratio of the optical power present in the evanescent field to the total guided optical power. In this configuration, sensitivity is proportional to the product of  $r$

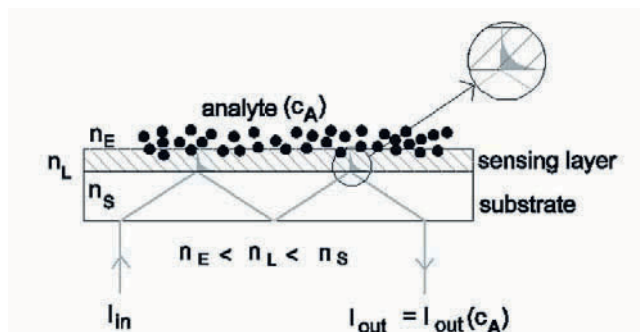


Figure 4. A planar, evanescent-wave absorption-based sensor platform.

and  $L_{\text{int}}$ . Consequently, improved sensitivity can be achieved with an evanescent wave-based platform when compared with a transmittance-based configuration as long as the product,  $rL_{\text{int}}$ , is greater than the optical path length (i.e., sensing layer thickness),  $L$ , in the latter configuration. It is important to note that this improved performance can be achieved while still employing a thin sensing layer, meaning that sensor response time is not adversely affected.

### 2.1.3 Evanescent Wave Effects and Fluorescence-Based Optical Sensors

Perhaps the most effective demonstration of the advantages of evanescent wave interrogation is provided by the optical biosensor platform depicted in Figure 5. The platform consists of a multimode slab waveguide on the upper surface of which antibodies have been immobilised.

These antibodies selectively bind the target analyte, which, in this case, is a specific antigen present in the sample solution that is passed over the platform using the required fluidics. A second solution containing fluorescently labelled antibodies similar to those bound to the surface of the waveguide is subsequently passed over the platform. These antibodies again bind selectively to the surface-bound antigens. Light from a suitable source is coupled to the glass slide and propagates along its length by total internal reflection. The evanescent field of the light extends above the surface of the waveguide where it excites fluorescence from the bound, labelled antibodies. The fluorescence from the upper surface is imaged using an appropriate detector (typically a CCD camera) and the recorded fluorescence is correlated to antigen concentration.

The tuneable nature of the evanescent field penetration depth is critical to the effective operation of this sensor as it facilitates surface-specific excitation of fluorescence. This means that only those fluorophores attached to the surface via the antibody-antigen-labelled antibody recognition event

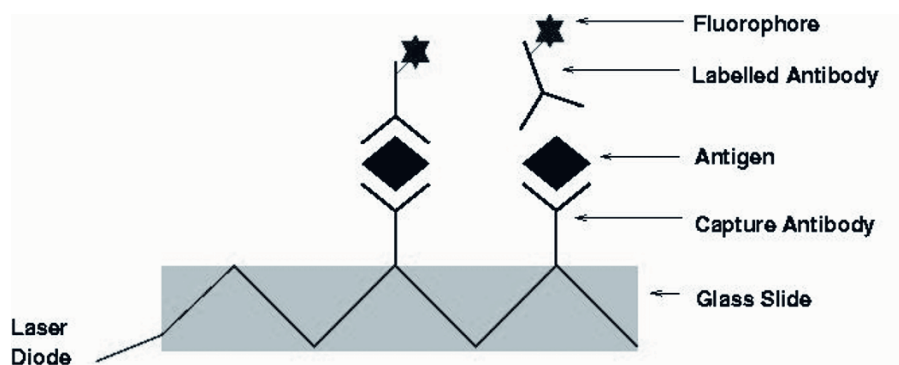


Figure 5. A planar platform for evanescent-wave excitation of fluorescence.

(i.e., those within the distance defined by the penetration depth of the evanescent field) are excited, permitting discrimination between surface binding events and fluorescence from the bulk solution. This property eliminates the need for an additional washing step which would remove unbound fluorophores in the bulk liquid above the waveguide.

The biosensing configuration described above is referred to as a sandwich assay<sup>7</sup> but a similar optical configuration can be used in a variety of other biosensing applications, e.g., monitoring of DNA hybridisation events.

## 2.2 Planar Microfabrication Technologies

Central to the fabrication of low-cost, mass-producible microsystems is the need for high throughput processing technologies that yield potentially disposable platforms. Semiconductor technology, whilst fulfilling the criterion of mass production capability, does not lend itself readily to the production of disposable microsystems as silicon and other semiconductor materials are quite expensive and are often not suited to the operational demands of chemical sensing and biosensing.

Polymer processing technology, on the other hand, provides a route to the fabrication of mass-producible, low-cost microsystems due to the nature of polymers themselves. There are many commercially available polymers providing a range of chemical and physical characteristics that can be used in conjunction with processing technologies such as injection moulding<sup>8,9</sup>, hot embossing<sup>10,11</sup> and laser ablation<sup>12</sup> to produce the required sensor platform. These polymers are cheap, yet capable of fulfilling the physical and chemical requirements placed on them by the target application. Laser ablation can also be used to fabricate the mould or master template for use in the injection moulding or hot embossing stage of the platform fabrication process. Other master fabrication techniques include CNC micromilling and photolithography, which facilitate the production of templates within 24 hours of the initial design concept. In particular, the use of high resolution printing to produce transparency-based photomasks followed by photolithography has been demonstrated as an effective rapid prototyping technique for the production of polymer microfluidic systems<sup>13-15</sup>.

A wide variety of polymer microsystems have been developed to date, ranging from simple mixing chambers to systems incorporating multiple functionalities such as pumping, sorting and analysis on a single chip<sup>16</sup>. The integration of optical elements onto such platforms is also possible due to the ease with which planar elements can be patterned and processed. This facilitates integrated optical interrogation of microfluidic networks, which has applications in cell sorting and optical biosensing<sup>17</sup>.

### 3. SENSOR DESIGN STRATEGIES

#### 3.1 Enhanced Absorption-Based Sensor Platforms

The absorption-based platforms described previously employed evanescent wave interrogation of a thin sensing layer coated onto a planar waveguide. A sensitivity enhancement strategy for optical absorption-based sensors based on planar, multimode waveguides was developed recently by us<sup>18</sup>. The objective was to apply this theory to the development of low-cost, robust and potentially mass-producible sensor platforms and the following section outlines the assumptions and predictions of this theoretical model.

##### 3.1.1 Theoretical Model

Figure 6 illustrates the platform under consideration in this analysis. The principle of sensor operation is as described previously for absorption-based optical sensors employing evanescent wave interrogation of the sensing layer.

For the purposes of the theoretical analysis, the following refractive index condition is assumed:

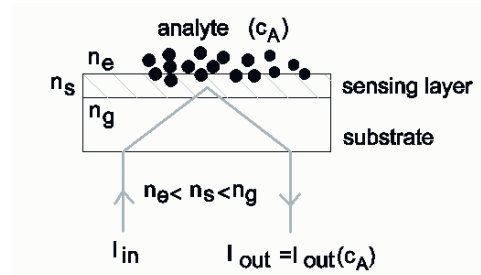


Figure 6. Optical absorption-based sensor platform under consideration for enhancement strategy.

$$n_e < n_s < n_g \quad (\text{Eq.3})$$

where  $n_e$  is the refractive index of the environment,  $n_s$  is the refractive index of the sensing layer and  $n_g$  is the refractive index of the substrate/waveguide. The sensitivity of the device is defined as

$$S(c_A) = \frac{dV}{dc_A} \quad (\text{Eq.4})$$

where  $V$  is the output signal measured by the detector and  $c_A$  is the analyte concentration. It is possible to quantify the variation of output signal with respect to the different optical parameters of the system by analysing the

dependence of reflectivity (R) on these same parameters, and in particular on the angle  $\theta$  at which the light interrogates the sensing layer. Due to the fact that the absorption coefficient of the layer is dependent on analyte concentration, it is possible to examine the sensitivity in terms of the reflectivity and extinction coefficient of the sensing layer, R and  $\gamma_s$ ,

$$\tilde{S}(\gamma_s) \equiv \frac{dR}{d\gamma_s} \quad (\text{Eq.5})$$

where  $\gamma_s$  is related to  $\alpha_s$  by the equation  $\alpha_s = 4\pi\gamma_s/\lambda$ , and  $\lambda$  is the wavelength of the interrogating light.

The results of this theoretical analysis are shown in Figure 7 where the sensitivity is plotted against angle of incidence on the sensing layer with all other optical parameters remaining constant. In order to generate the solid curve, the optical parameters were assumed to be those of a typical sol-gel-derived sensing layer ( $t \approx 400\text{nm}$ ,  $n_s=1.43$ ) coated on a planar glass substrate ( $n_g=1.515$ ) with air as the sensing environment ( $n_e=1.00$ ).

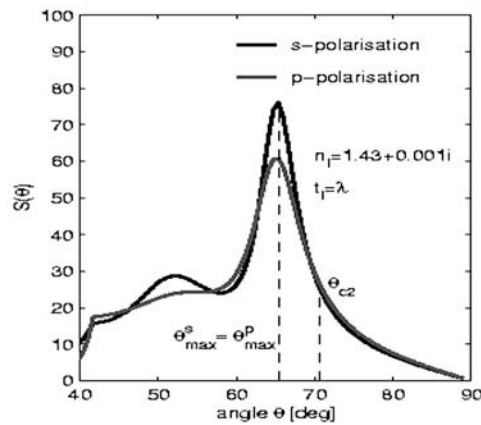


Figure 7. Sensitivity plotted as a function of angle of incidence on the sensing layer.

There is clearly an optimum angle,  $\theta_{opt}$ , at which sensitivity is maximum and, furthermore, this angle does not correspond to the region where the light is evanescent in the sensing layer ( $\theta > 71^\circ$ ). Rather, optimum sensitivity is achieved when the interrogating light is propagating in both the sensing layer and the substrate.

### 3.1.2 Experimental Verification

The results presented in the previous section were verified experimentally using the setup illustrated in Figure 8 to record the reflectivity of a sol-gel sensing layer as a function of incident angle. The results are plotted in Figure

9 where the agreement between the experimental data (circles) and the theoretical predictions (solid line) is clearly evident.

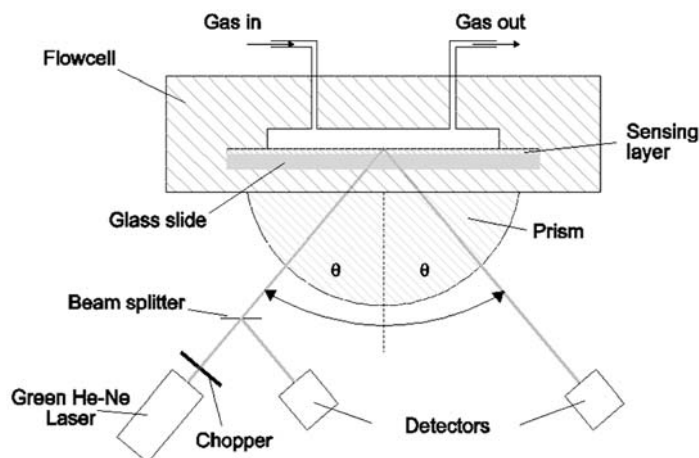


Figure 8. Experimental setup used to investigate  $S(\theta)$ .

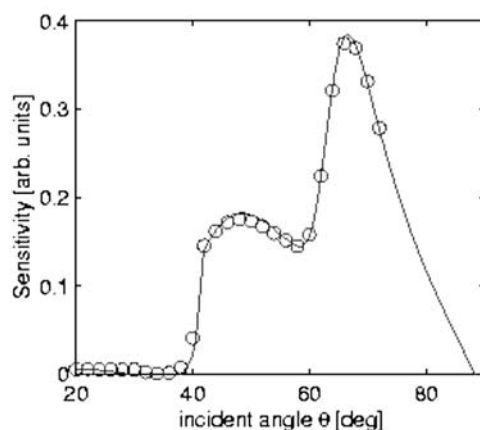


Figure 9. Results of experimental analysis of  $S(\theta)$ .

### 3.1.3 Enhanced Waveguide Platform Development

The next stage in this work was to apply these findings to the development of an optical waveguide platform demonstrating enhanced performance that would also be compatible with planar fabrication technology. To this end, the waveguide platform depicted in Figure 10 was designed. The most important features of this design are the integrated



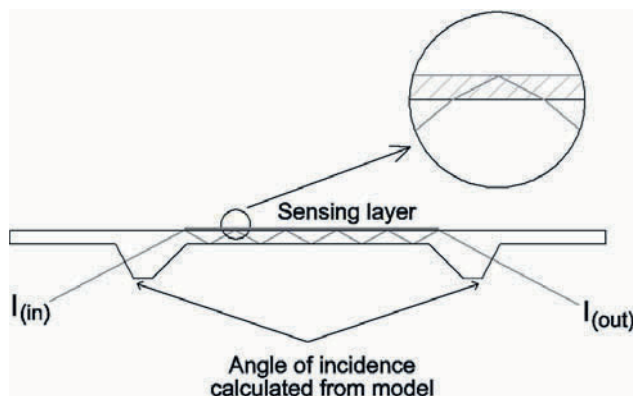


Figure 10. Design for an enhanced waveguide platform.

refractive elements at either end that facilitate coupling of the interrogating light to the waveguide at the optimum angle of incidence on the sensing layer predicted by the model.

Waveguide chips of this design were manufactured from polystyrene using micro-injection moulding, a high-throughput polymer processing technology that permits the fabrication of approximately 200 chips in less than 5 minutes. Sol-gel-derived sensing layers, doped with bromocresol purple, a pH indicator dye, were then deposited on these chips by spin-coating and subsequently applied to the detection of gaseous ammonia using an amber LED ( $\lambda_{\max} = 601\text{nm}$ ) as the light source<sup>19</sup>. A typical sensor response curve is shown in Figure 11. It was possible to achieve a limit of detection (L.O.D.) of 300ppb ammonia in nitrogen using this enhanced sensor platform, which was a greater than ten-fold improvement on previous work where grating couplers were used in conjunction with a planar waveguide<sup>20</sup>. This work illustrates the successful integration of planar

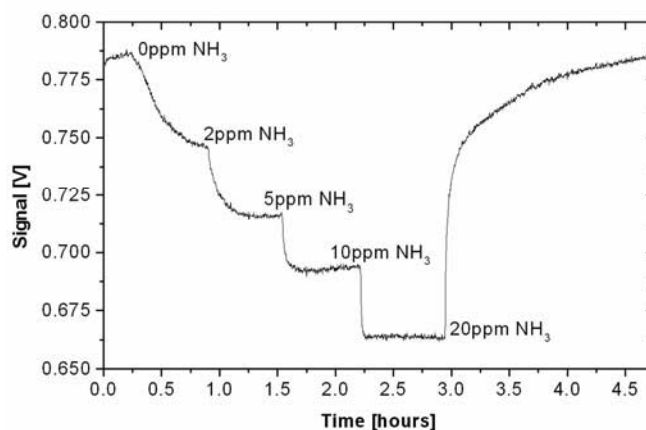


Figure 11. Response of enhanced polymer waveguide platform to gaseous ammonia<sup>26</sup>.

fabrication techniques, polymer processing technology and a dedicated sensor optimisation strategy to yield an effective, low-cost, disposable sensor chip.

## **3.2 Optimisation of Fluorescence Capture Efficiency**

### **3.2.1 Introduction**

Many optical chemical and biological sensors are based on analyte-dependent changes in the fluorescence emitted by a particular fluorophore. Furthermore, many bioassays employ fluorescent labels to yield an optical signal from the binding event. This section details an optimisation strategy for those sensors employing fluorophores that are immobilised on, or close to, a dielectric substrate, such as a glass microscope slide. An example of such a system is the sandwich assay format optical biosensor referred to earlier in the chapter. The optimisation strategy is based on the enhancement of fluorescence capture efficiency. This strategy is based on a detailed electromagnetic wave analysis of the fluorescence emission pattern of a radiating dipole (fluorophore) in such a system. This analysis is then applied to the design of a structure with the purpose of collecting emitted fluorescence more efficiently.

### **3.2.2 Theoretical Background**

The theoretical analysis of a radiating dipole at a dielectric interface is quite involved and its full description is beyond the scope of this chapter. Instead, an outline of the most salient features of the model is presented. The complete analysis can be found in Ref. 25.

Firstly, a point dipole placed at the surface of a glass substrate is considered. The orientation of the dipole is considered to be random. The angular distribution plotted in spherical co-ordinates is shown in Figure 12. The radiation propagating in the positive (down) and negative (up) z-directions corresponds to that radiated into the glass substrate and the environment (air), respectively.

It is well known that when a randomly oriented radiating dipole is located in a free unbound space, its radiation is isotropic<sup>21</sup>. In the representation used in Figure 12, the angular distribution of the radiated intensity would look spherical. As can be seen, however, the angular distribution is significantly altered when the radiating dipole is placed at a dielectric interface. Firstly, it can be noted that the radiation is highly anisotropic. Secondly, a significant part of the luminescence is radiated into the glass substrate, which has a higher refractive index than the environment above it. The angular

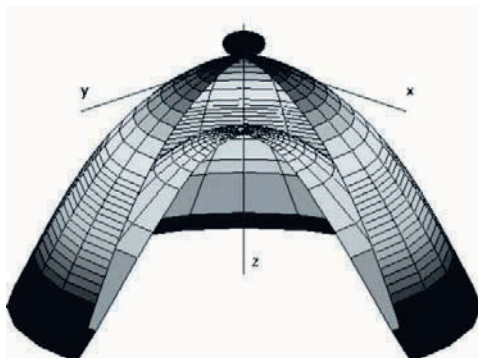


Figure 12. Angular distribution of luminescence radiated by a randomly oriented dipole located at a glass surface.

distribution exhibits a sharp peak, the position of which is in the vicinity of the critical angle corresponding to the environment/substrate interface.

Figures 13(a) and 13(b) illustrate the intensity distributions for two environment/substrate combinations, namely air/glass and water/glass. It can be concluded that the dipole located at a dielectric surface preferably radiates into the higher refractive index substrate at angles close to the critical angle. The intensity radiated into the environment is, on the other hand, relatively small. Yet it is this fraction of the fluorescence intensity that forms the basis of the sensor signal in conventional systems such as the optical biosensor

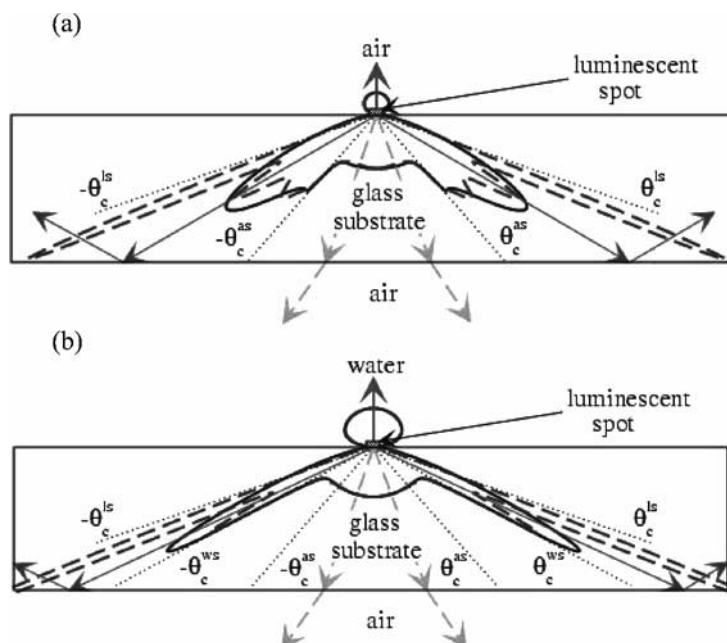


Figure 13. (a): angular intensity distribution of luminescence for an air environment; (b): Angular intensity distribution of luminescence for a water environment.

sandwich assay discussed earlier. Furthermore, such systems lose a substantial portion of the fluorescence radiated into the substrate at angles exceeding the critical angle due to waveguiding and outcoupling of the light at the endfaces of the substrate.

This knowledge of the fluorescence emission pattern and its dependence on the optical parameters of the materials involved allows one to predict the angle at which maximum fluorescence intensity would be recorded for a particular system and to subsequently design a suitably structured platform for enhanced fluorescence capture. The design and implementation of such a platform is described in the following section.

### 3.2.3 Development of an Optical Chip for Enhanced Fluorescence Capture

Figure 14 illustrates an example of a structure that can provide enhanced fluorescence capture. It consists of a truncated cone, on top of which the fluorescent species is deposited. The cone angle,  $\alpha$ , is chosen in order to cause total internal reflection of the emitted fluorescence (the angular distribution of which is calculated from the model) and is therefore dependent on the refractive indices of the cone material and the environment. The emitted fluorescence is reflected onto a detector positioned directly beneath the cone.

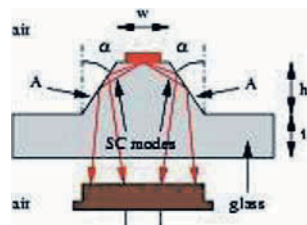


Figure 14. Design of a structure intended to provide enhanced fluorescence capture.

A sensor configuration employing these cones is shown in Figure 15. Fluorescence from the luminescent spots is excited from behind the platform using an appropriate source (LED's in this case), is subsequently emitted via total internal reflection through the sensor chip and is detected by a CMOS camera, which is positioned behind the chip. For the purposes of intensity comparisons, luminescent spots are also deposited directly onto the planar surface of the chip and excited along with those deposited on the cones.

An important aspect of this enhancement strategy is its compatibility with current fabrication techniques, in particular polymer processing technology. The technique of micro-injection moulding was employed to produce polystyrene chips with an integrated array of cone structures intended for use in an aqueous environment.

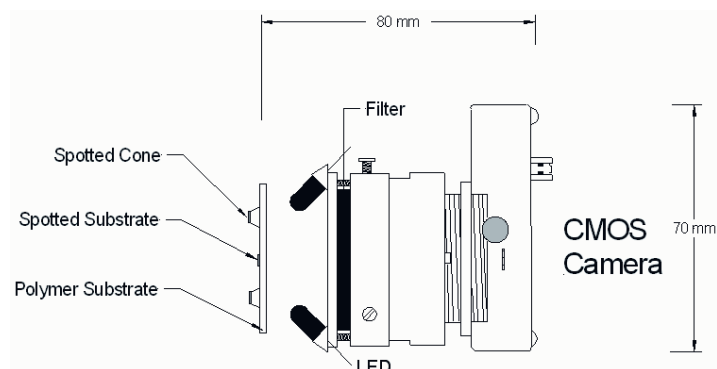


Figure 15. Sensor system employing structures for enhanced fluorescence.

In order to verify the enhancement provided by the cones, a sol-gel layer doped with a fluorescent ruthenium complex was deposited onto a chip in a configuration similar to that shown in Figure 15. Blue LED excitation of the fluorescent sol-gel layers was employed. The resultant fluorescence was recorded using a CMOS camera and the resultant image is shown in Figure 16.

The bright rings surrounding lower intensity spots correspond to the additional fluorescence signal from the sol-gel layer on the surface of the cones. The isolated spots (i.e., those without a surrounding ring) correspond

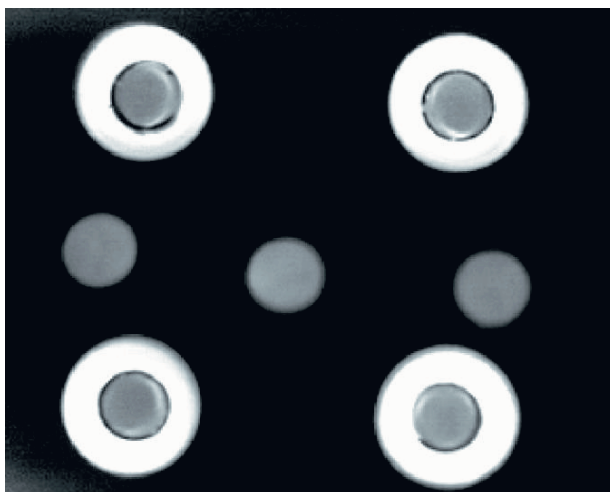


Figure 16. CMOS image of enhanced fluorescence capture provided by frustrated cone structures.

to fluorescence from the sol-gel spots deposited on the planar surface of the chip. The enhanced intensity as a result of the cone is clearly evident. In fact, the cone structures typically provide a 26-fold enhancement in recorded fluorescence over the commonly employed planar substrate. This example illustrates and approach to sensitivity enhancement that is generic and can be applied across a broad range of sensor platforms.

### **3.3 Enhancement of Fluorescence Emission via Plasmonic Interactions**

#### **3.3.1 Introduction**

The presence of metallic surfaces or particles in the vicinity of a fluorophore can dramatically alter the fluorescence emission and absorption properties of the fluorophore. The effect, which is associated with the surface plasmon resonance of the metallic surface, depends on parameters such as metal type, particle size, fluorophore type and fluorophore-particle separation.

In order to investigate this effect, ordered arrays of metallic nano-islands were fabricated on glass substrates by a process of natural lithography using monodisperse polystyrene nanospheres. The metal particle dimensions were tailored in order to tune the plasmon resonance wavelength to match the spectral absorption of the fluorophore. The fluorophore, Cy5 dye, which is widely used in optical immunoassays and has a medium quantum efficiency ( $\sim 0.3$ ), was used in this preliminary study of the plasmonic enhancement effect.

#### **3.3.2 Theoretical Background**

The theory describing the interaction of light, fluorescent dyes and metallic nanoparticles (NP's) is complex and only solved for specific systems. An outline of the theory regarding these interactions will be reported here but a more detailed analysis is presented elsewhere<sup>22, 23</sup>.

It is assumed that the metallic NP consists of an immobile positively charged atom core and negatively charged free conduction electrons. Upon illumination, the displacement of the negative charges by the electric field gives rise to polarisation changes at the NP surface and thus the system acts like an oscillator. When the system is in resonance with the incident electromagnetic (EM) wave the effect is called surface plasmon (polariton) resonance (SPR). A key aspect of the SPR effect is the associated increase in the intensity of the electric field in the proximity of NP's. The E-field decreases with increasing distance from the NP and within a few diameters

of the NP the effect is negligible. It can be shown that the wavelength at which SPR occurs ( $\lambda_{\text{res}}$ ) depends on the shape of the NP, the NP material and the embedded medium.

A fluorophore in the proximity of the NP senses the altered EM-field and its fluorescence properties are consequently modified. There are (at least) two enhancement effects: an increase in the excitation of the fluorophore and an increase in its quantum efficiency (QE). The increased excitation of the fluorophore is directly proportional to the square of the strength of the E-field and is a function of the wavelength and relative position of the NP. The maximum enhancement of this type is achieved if  $\lambda_{\text{res}}$  equals the peak absorption wavelength of the dye.

The unmodified QE of the fluorophore is defined as follows

$$Q_0 = \frac{k_r}{k_r + k_{nr}} \quad (\text{Eq. 6})$$

where  $k_r$  is the radiative decay rate and  $k_{nr}$  is the non-radiative decay rate. In the proximity of the NP a new radiative channel is formed having a corresponding decay rate  $k_m$  and the modified quantum efficiency is given by

$$Q_m = \frac{k_r + k_m}{k_r + k_m + k_{nr}} \quad (\text{Eq. 7})$$

In this case, the maximum enhancement is achieved when  $\lambda_{\text{res}}$  is equal to the peak emission wavelength of the fluorophore. This enhancement is far more significant for fluorophores of low QE than for those of higher QE. An additional effect; namely, a metal-fluorophore quenching can also occur for very small NP-fluorophore separations, typically within 5nm. This has important implications for the fabrication of an enhanced sensor chip, as will be seen in the following section.

### 3.3.3 Preparation of Metallic Nanoislands

One method used to deposit metallic nanoislands onto a glass substrate is known as nanosphere lithography<sup>24</sup>. It involves the use of an ordered monolayer of polystyrene beads (PB's) on a glass surface as a mask for the evaporation of the desired metal onto the glass. A monolayer of PB's having a diameter of 500nm was deposited onto a glass slide by dip-coating at a very low speed ( $< 4\mu\text{m/s}$ ). The slide was then placed in a deposition chamber and a silver layer was deposited. Directly after deposition, the slide was sonicated in ethanol in order to remove the PB's and the resultant nanoisland array is shown in Figure 17. In order to demonstrate enhanced fluorescence emission, it was necessary to evaporate a thin layer of  $\text{SiO}_x$

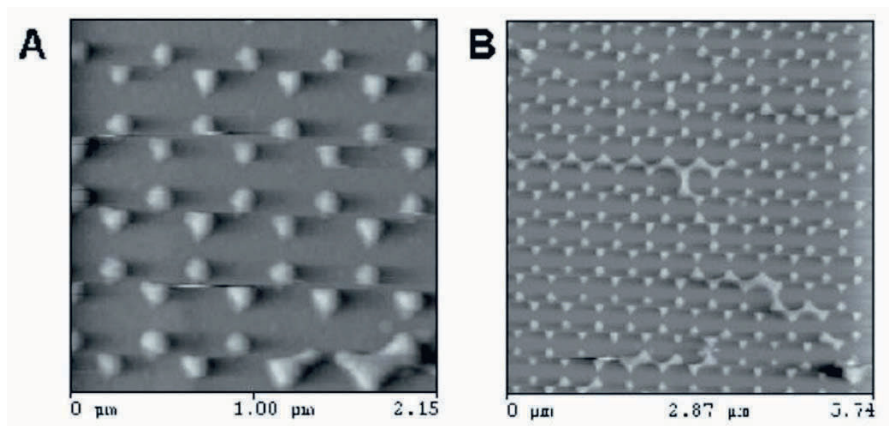


Figure 17. AFM images of nanoisland arrays produced using natural lithography.

(thickness 6 nm) to avoid the metal-fluorophore quenching effect mentioned earlier.

A second set of samples bearing nanoislands of varying geometries was prepared by depositing a silver layer with graduated thickness using an in-built shutter along with PB's of different diameters. The purpose of these samples was to aid in the investigation of the dependence of  $\lambda_{\text{res}}$  on the geometry of the nanoislands. Figure 18 illustrates the range of resonance wavelengths achievable by varying this characteristic. It can be seen from the graph that it was possible to tune the value of  $\lambda_{\text{res}}$  over the most of the visible spectrum.

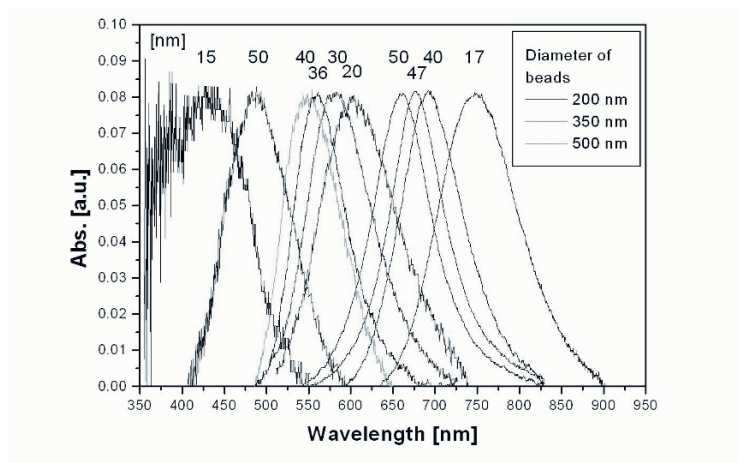


Figure 18. Range of resonance wavelengths achievable by varying nanoisland geometry.



### 3.3.4 Preparation of an Enhanced Chip

Cy5 solution was printed as an array of spots onto a glass slide bearing metallic nanoislands on one section of its surface by pin-printing. The fluorescence from the chip was subsequently recorded at the emission wavelength of Cy5 via a fluorescence laser scanner GMS 418 Array Scanner (Genetic MicroSystems). The resultant, false-colour image is shown in Figure 19. The top two rows of spots correspond to the area of the slide bearing the nanoislands and the enhancement in fluorescence emission compared with the remaining section of the chip (i.e., that section containing Cy5 spots on plain glass) is clear.

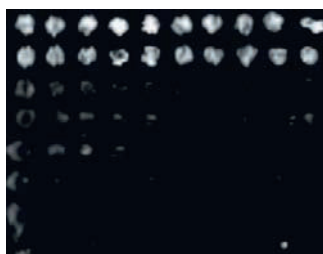


Figure 19. Scanner image of pin-printed Cy5 dye spots on glass chip bearing nanoislands.

In a second experiment, Cy5-labelled antiBSA antibodies were immobilised on a silanised glass slide precoated with metallic nanoislands using a polydimethylsiloxane (PDMS) flow-cell. The antibody solution was left for 1 hour to attach and then the cell was flushed with deionised water. The slide was then dried with N<sub>2</sub>. For this experiment, a portion of the slide was not coated with metallic nanoislands, in order to act as a reference. Figure 20 shows the image recorded using the fluorescence laser scanner mentioned previously. The enhancement in fluorescence emission between those areas with and without nanoislands (B and A, respectively) is again evident. For both chips, an enhancement factor of approximately 8 was recorded. There is considerable interest in the elucidation and exploitation of plasmonic effects for fluorescence-based biosensors and other applications.

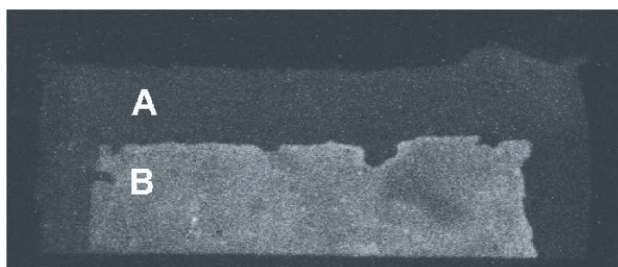


Figure 20. Image of fluorescence recorded from Cy5-labelled antibodies attached to (A) plain glass surface (B) surface containing metallic nanoislands.

The results reported here simply indicate the potential of the technique to provide performance enhancement.

#### **4. CONCLUSIONS**

The demand for mass-producible, low-cost diagnostic chips has had a significant impact on the development trends for optical sensor platforms. Arguably the most important characteristics of recent systems are the integration of multiple functionalities onto a single platform, the ability to perform multianalyte detection and the production of low-cost sensor platforms. These strategies are intended to maximise the viability of a device for development as a commercial product.

The successful realisation of these goals is dependent on current microfabrication technologies and the ease with which they can be integrated into the production of an optical sensor platform. While optical fibre-based systems are well-suited to certain niche applications, their geometry is not compatible with a broad range of microfabrication/deposition technologies nor are they suitable for the production of a robust, disposable commercial product. In contrast, planar configurations are the ideal choice for use with current microfabrication techniques and are also compatible with a range of deposition technologies. A planar geometry is also far more robust than that of an optical fibre and such platforms can be produced from a variety of low-cost materials using high throughput fabrication technologies.

While planar optical sensors exist in various forms, the focus of this chapter has been on planar waveguide-based platforms that employ evanescent wave effects as the basis for sensing. The advantages of evanescent wave interrogation of thin film optical sensors have been discussed for both optical absorption and fluorescence-based sensors. These include the ability to increase device sensitivity without adversely affecting response time in the case of absorption-based platforms and the surface-specific excitation of fluorescence for optical biosensors, the latter being made possible by the tuneable nature of the evanescent field penetration depth.

Recent strategies for sensor enhancements based on rigorous electromagnetic wave analyses of the relevant systems have also been outlined. These strategies are compatible with planar microfabrication techniques and are intended for the production of mass-producible, disposable sensor platforms that operate in a highly efficient manner. It has been shown that enhanced absorption-based polymer waveguide platforms can be easily fabricated and demonstrate a ten-fold improvement in sensitivity compared with previous work. More significant enhancements are possible for fluorescence-based optical sensors. Specifically, by structuring the surface of the optical platform to enhance fluorescence capture efficiency

it is possible to increase the level of detected fluorescence intensity by a factor of 26. Fluorescence emission levels can also be increased significantly via plasmonic interaction effects.

It is important to note that the enhancements mentioned above are achievable using current planar microfabrication techniques and the resultant sensor chips are mass-producible, low-cost and disposable and also have the potential to be integrated into a variety of diagnostic microsystems. This work has significant implications for the production of low-cost, yet efficient measurement platforms for applications in modern society.

## REFERENCES

1. Maughan S.M., Kee H.H., Newson T.P., Simultaneous distributed fibre temperature and strain sensor using microwave coherent detection of spontaneous Brillouin backscatter, *Meas. Sci. Technol.* 2001; 12: 834-842.
2. Ritchie L.J., Ferguson C.P., Bessant C., Saini S., A ten channel fibre-optic device for distributed sensing of underground hydrocarbon leakage, *J. Environ. Monitor.* 2000; 2: 670-673.
3. Scorsone E., Christie S., Persaud K.C., Simon P., Kvasnik F., Fibre-optic evanescent sensing of gaseous ammonia with two forms of a new near-infrared dye in comparison to phenol red, *Sensor. Actuat. B-Chem.* 2003; 90: 37-45.
4. Vo-Dinh T., Cullum B., Kasili P., Development of a multi-spectral imaging system for medical applications, *J. Phys. D-Appl. Phys.* 2003; 36: 1663-1668.
5. Baldini F., In vivo monitoring of the gastrooesophageal system using optical fibre sensors, *Anal. Bioanal. Chem.* 2003; 375: 732-743.
6. Bindig U., Gersonde I., Meinke M., Becker Y., Muller, G., Fibre-optic IR-spectroscopy for biomedical diagnostics, *Spectroscopy-an International Journal* 2003; 17: 323-344.
7. Rowe-Taitt C.A., Golden J.P., Feldstein M.J., Cras J. J., Hoffman K.E., Ligler F.S., Array biosensor for detection of biohazards, *Biosens. Bioelectron.* 2000; 14: 785-794
8. Becker H., Gartner C., Polymer microfabrication methods for microfluidic analytical applications, *Electrophoresis* 2000; 21: 12-26.
9. Malins C., Hulme J., Fielden P.R., Goddard N.J., Grating coupled leaky waveguide micro channel sensor chips for optical analysis, *Sensor. Actuat. B-Chem* 2001; 77: 671-678.
10. Becker H., Heim U., Hot embossing as a method for the fabrication of polymer high aspect ratio structures, *Sensor. Actuat. A-Phys.* 2000; 83: 130-135.
11. Tyrrell É., Gibson C., MacCraith B.D., Gray D., Byrne P., Kent N., Burke C., Paull B., Development of a micro-fluidic manifold for copper monitoring utilising chemiluminescence detection, *Lab on a Chip* 2004; 4: 384-390.
12. Bowden M., Geschke O., Kutter J.P., Diamond D., CO<sub>2</sub> laser microfabrication of an integrated polymer microfluidic manifold for the determination of phosphorus, *Lab On a Chip* 2003; 3: 221-223.
13. Anderson J.R., Chiu D.T., Jackman R.J., Cherniavskaya O., McDonald J.C., Wu H.K., Whitesides S.H., Whitesides G.M., Fabrication of topologically complex three-dimensional microfluidic systems in PDMS by rapid prototyping, *Anal. Chem.* 2000; 72: 3158-3164.
14. Deng T., Wu H.K., Brittain S.T., Whitesides G. M., Prototyping of masks, masters, and stamps/molds for soft lithography using an office printer and photographic reduction, *Anal. Chem.* 2000; 72: 3176-3180.

15. Duffy D.C., McDonald J.C., Schueller O.J.A., Whitesides G.M., Rapid prototyping of microfluidic systems in poly(dimethylsiloxane), *Anal. Chem.* 1998; 70: 4974-4984.
16. Erickson D., Li D., Integrated microfluidic devices, *Anal. Chim. Acta* 2004; 507: 11-26.
17. Chabinye M.L., Chiu D.T., McDonald J.C., Stroock A.D., Christian J.F., Karger A.M., Whitesides G.M., An integrated fluorescence detection system in poly(dimethylsiloxane) for microfluidic applications, *Anal. Chem.* 2001; 73: 4491-4498.
18. Polerecky L., Burke C.S., MacCraith B.D., Optimization of absorption-based optical chemical sensors that employ a single-reflection configuration, *Appl. Opt.* 2002; 41: 2879-2887.
19. Burke C.S., Polerecky L., MacCraith B.D., Enhanced polymer waveguide platforms for absorption-based optical chemical sensors, *Proc. S.P.I.E.*, 2002; 4876: 848-855. Opto-Ireland 2002: Optics and Photonics Technologies and Applications (Galway, Ireland, 2002 ).
20. Malins C., Doyle A., MacCraith B.D., Kvasnik F., Landl M., Simon P., Kalvoda L., Lukas R., Pufler K., Babusik I., Personal ammonia sensor for industrial environments, *J. Environ. Monitor.*, 1999; 1: 417-422.
21. Born M., Wolf E. Principles of Optics (Pergamon, Oxford, 1959).
22. Lakowicz J.R., Radiative decay engineering: Biophysical and biomedical applications, *Anal. Biochem.* 2001; 298: 1-24.
23. Gersten J., Nitzan A., Spectroscopic Properties of Molecules Interacting With Small Dielectric Particles, *J. Chem. Phys.* 1981; 75: 1139-1152.
24. Jensen T.R., Malinsky M.D., Haynes C.L., Van Duyne R.P., Nanosphere lithography: Tunable localized surface plasmon resonance spectra of silver nanoparticles, *J. Phys. Chem. B*, 2000; 104: 10549-10556.
25. Polerecky L., Hamrle J., MacCraith B.D., Theory of the radiation of dipoles placed within a multilayer system, *Appl. Opt.* 2000; 39: 3968-3977.

## Chapter 11

# INTERFEROMETRY IN BIO- AND CHEMOSENSING

Guenter Gauglitz

*University of Tuebingen, Institute of Physical/Theoretical Chemistry  
Auf der Morgenstelle 8  
72076 Tuebingen, Germany*

### 1. INTRODUCTION

Optical methods are a perfect tool to characterize interaction processes between a sensitive chemical or bio polymer layer and analytes<sup>1</sup>. Time-resolved measurements of this interaction process provide kinetic and thermodynamic data. These types of sensors allow the monitoring of production processes, quantification of analytes in mixtures and many applications in the area of diagnostics, biomolecular interaction processes, DNA hybridization studies and even protein/protein interactions<sup>2,3</sup>.

With consideration to the quality of a bio or chemosensor it is therefore necessary to discuss the transduction principle, the quality of the sensitive layer and the data evaluation. These three issues will be discussed in this paper, with the focus on interferometric principles in the area of non-specific measurements using chemosensors and specific interaction processes in the case of biosensing.

In the last years, besides the well-known fibre optic sensors<sup>4</sup>, sensor principles based on reflectometry or refractometry have become more and more interesting for many applications<sup>5</sup>. Both reflectometry and refractometry are based on regular reflection, either in the case of total internal waveguiding or as white light interference at interfaces of thin layers<sup>8</sup>. These layers can be polymer films coated to planar transducers or biomolecular layers with receptor molecules that demonstrate special affinity to specific analytes. It will be discussed that in the case of polymer films the detection of analytes either in gaseous or in liquid phase exhibits selectivity which is mostly rather poor. Therefore in multianalyte measurements in addition to the sensors (mostly organized as sensor arrays with numerous elements) the properties of the elements require a lot of consideration. Chemometrics can overcome the problems using either classical methods

such as principle component analysis or partial least squares, or applying model-free methods such as neural networks or evolutionary approaches.

Since the quality of a sensor and its application depends on all components of the sensor system, optical transduction, sensitive layers and chemometrics will be discussed in more detail in dependence on the different approaches. In the final chapter, quite a few applications will demonstrate the feasibility and the quality of such bio or chemosensors. Since miniaturisation and parallelisation are further essential topics in these applications, these approaches will be included.

## 2. OPTICAL PRINCIPLES

In the field of optical sensing, the measurement of absorption, fluorescence, and reflectance is a very good tool for monitoring any processes happening in the sensitive layers of a bio or chemosensor. In principle, two classes of sensors are distinguished: the first one uses labelled systems, and normally either monitors the colour change of an indicator dye or fluorescence effects. This classification is given in Figure 1 which also demonstrates some possible measurements of fluorescence such as changes in intensity, in anisotropy or using fluorescence correlation spectroscopy.

In addition, typical methods of sensing are total internal reflection fluorescence or monitoring of fluorescence resonance energy transfer<sup>6,7</sup>. The second class is a direct optical detection principle which relies either on reflectometry or refractometry. The latter is connected to evanescent field

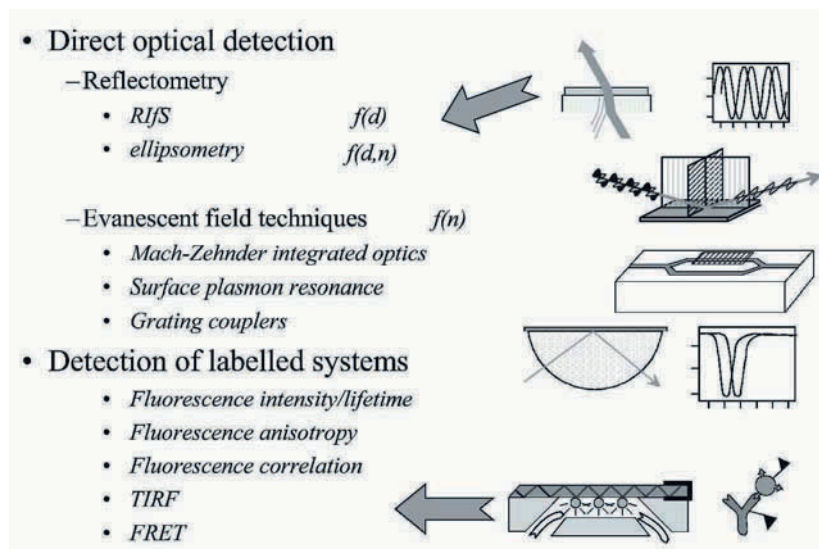


Figure 1. Classification of detection methods using either labelled system or applying direct optical detection.

techniques which are the commercial surface plasmon resonance, grating coupler methods, or Mach-Zehnder interferometry<sup>11</sup>. Reflectometry has been a well-known principle for decades, in the case of ellipsometry<sup>10</sup> applying polarized light and measuring the properties of thin layers with regard to refractive index and physical thickness. A simplified approach is reflectometric interference spectroscopy (RIFS)<sup>9</sup> which cannot separate the refractive index and the physical thickness, but rather measures the product of both, called the optical thickness of a layer.

Figure 2 demonstrates the principles of reflectometry and refractometry by using a waveguide with a refractive index that is higher by  $n_2$  than that of the environment ( $n_1$ ). Radiation incident to an interface between media with different refractive indices is reflected in part; most penetrates the medium. The radiation is reflected and refracted in dependence on the angle of incidence and the ratio of refractive indices in the two media according to Snellius law

$$n_2 \cdot \sin \theta = n_1 \cdot \sin \alpha \quad (\text{Eq. 1})$$

In case of  $n_1 > n_2$ , radiation incident from the medium with  $n_1$  to the interface is refracted to the optical axes; if  $n_1 < n_2$ , it is refracted off the optical axes. In the given case, the waveguide has a refractive index  $n_2$  higher than  $n_1$ ; and there exists a critical angle  $\theta_{\text{crit}}$  for which radiation cannot be refracted beyond the interface but is totally reflected. This, radiation is guided within the waveguide by total internal reflection. However, in contrast to classical concepts some part of the radiation is guided outside as a so-called evanescent field<sup>8</sup>. Quantum dynamics demonstrates that in a semi-conducting waveguide the electric field of the radiation propagating in the waveguide does not drop to zero at the interface. This electric field vector couples to the electric field on the other side of the interface which decreases exponentially into the medium. This evanescent field is considerably influenced in its properties by the refractive index of this medium. Because of this coupling, any change in the refractive index and in the electric field

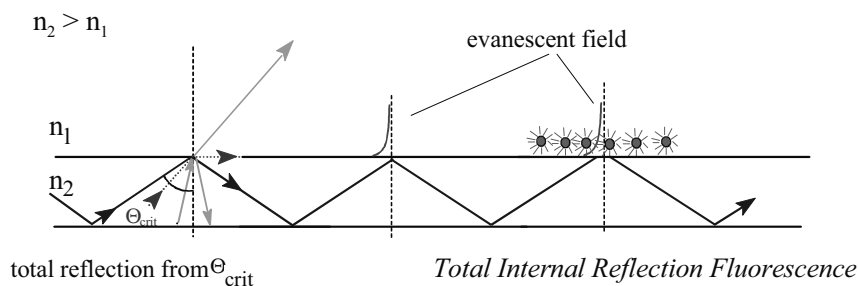


Figure 2. Regular reflectance: Replication of Snellius law for reflected and refracted radiation at interface in dependence on the refractive indices of the media adjacent to this interface, demonstrating total internal reflectance and evanescent field, exciting fluorophores close to the waveguide or even surface plasmon resonance.

vector accordingly at the outside of the waveguide will influence the propagating radiation within the waveguide causing a new effective refractive index. Thus, this waveguide can monitor via its evanescent field any process being close to the waveguide (penetration depth approx. half a wavelength).

One of the possibilities to interrogate the effect of the evanescent field on the propagation of the guided radiation in the waveguide is an interferometric approach. This approach uses so-called Mach-Zehnder interferometers<sup>5, 11</sup> shown in Figure 3.

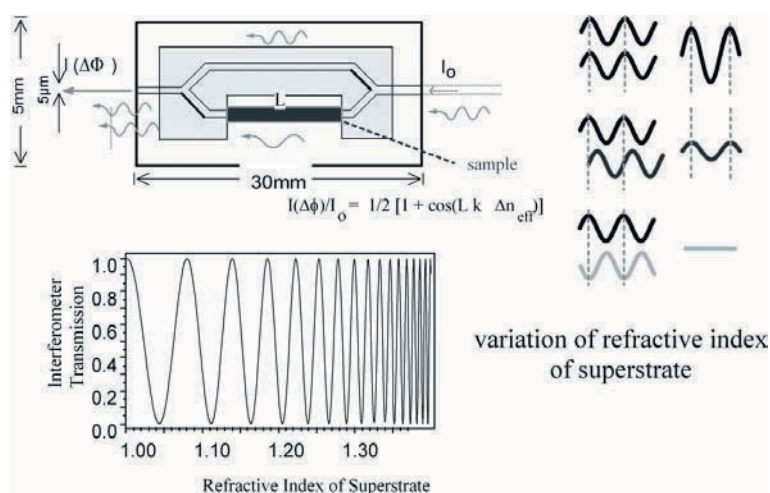


Figure 3. Mach-Zehnder interferometer: One of the arms is covered by inert material (reference arm), the other arm exposes to the sample (measuring arm).

The waveguide is split into two arms; one arm (the reference arm) is shielded and not affected by the environment. At the interface of the other arm, the evanescent field will be influenced by any sensing effect. Thus, the two partial beams will propagate in a different way within the two arms, in dependence on the difference in the refractive indices adjacent to the two arms.

This causes a phase difference which results in a signal in dependence on constructive or destructive interference. A variation of the refractive index close to the measurement arm will modulate the intensity of the measured radiation at the outlet of the Mach-Zehnder interferometer. These chips have to be tailored with respect to waveguide diameter, ratio of refractive indices and wavelength used according to the measurement problem. In most cases, monomode waveguides have the advantage that they result in defined modulations. However, in some cases so-called bulk-waveguide structure in which multimodes are formed are preferable. Modes are transversal stationary oscillations of electromagnetic field within the waveguide.



Thereby monomode explains that just a specific form of the many modes can be excited within the waveguide and propagate within the waveguide<sup>19a, 19b</sup>.

Without discussing in detail the principle of transversal electric and transversal magnetic modes, the modulation depends according to

$$I(\Delta\Phi)/I_0 = \frac{1}{2} \left[ 1 + \cos(L \cdot k \cdot \Delta n_{eff}) \right] \quad (\text{Eq. 2})$$

on the properties of the medium within the evanescent field and on the length of the “interaction window”. This interrogation principle is highly sophisticated, but allows a very sensitive detection of effects on the refractive index in the medium close to the waveguide, which is quite useful in bio and chemo applications.

In contrast to the interference within the two waveguide arms, the above mentioned interference of the two partial beams can also occur at two interfaces of a thin layer. This is a simpler and more robust technique which does not require any considerations regarding the model structure of the waveguide. It is simply based on the path length difference of the second partial beam reflected at the first interface to the second partial beam reflected at the other interface. This is demonstrated<sup>9</sup> in Figure 4. The interference of these two partial beams results in a modulation depending on the physical thickness and the refractive index of this thin layer. It measures the optical thickness of this thin layer and forms also a destructive or constructive interference pattern depending on angle of incidence, wavelength and this layer. Using white light it works as a type of Fabry-Perot interferometer, resulting in an interference spectrum. Any change in the optical thickness of this thin layer will shift this interference pattern with wavelength. The best approach is to graph intensity versus wave number to get the modulation close to a cosine function. At present, changes in the optical thickness below 1 pm can be resolved. This change in the optical thickness can be caused either by swelling of a polymer film, by uptaking analyte molecules, or (in the case of biosensing) by additional molecules binding to the recognition sites of the biomolecular sensitive layer.

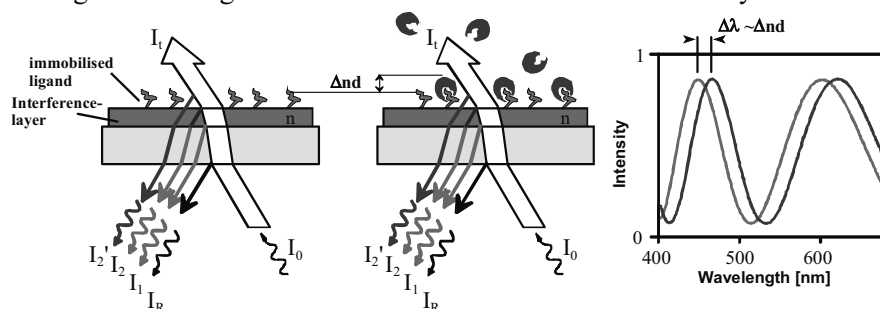


Figure 4. Reflectometric interference spectroscopy (RIS) caused by constructive and destructive superposition of two partial beams being reflected at the two interfaces of a thin layer (300 nm – some  $\mu\text{m}$ ), shift of the interference spectrum caused by a change in the optical thickness.

This is demonstrated in Figure 5.

Whereas the refractive index depends on the temperature, the reflectometric interference spectroscopy using this white light interference at two interfaces is not subject to this dependence. Any reflectometric method using evanescent fields therefore depends rather on temperature in reality. Accordingly, any instrumentation has to be either thermostated very well, even better than 0.01 K, or an instrument with an internal reference measurement has to be set up to eliminate temperature effects. The advantage of reflectometric interference spectroscopy not demonstrating a large temperature dependence results from two opposing effects: on the one side, the volume of this layer will increase by temperature, thus increasing the physical thickness of the layer by a certain amount. On the other hand, the refractive index depends on the number of polarisable molecules within the volume element. This number decreases per volume element with temperature by the expansion. Thus, temperature effects on physical thickness and refractive index compensate to a certain amount. Accordingly, temperature effects measured using reflectometry amount to less than 5% of those measured using refractometry.

After discussing various sensitive layers later, both principles will be applied to monitor effects in biomolecular or chemical sensitive layers. The applications will demonstrate the feasibility of the methods as well as their advantages and their disadvantages. Therefore various applications are given, sometimes even for the same analyte, in order to demonstrate the normal approach in sensor development to select the best transduction principle for a specific application.

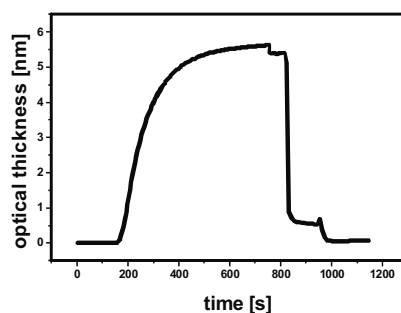


Figure 5. Binding curves: time-resolved measurement of the change in optical thickness during association. The second part of the figure shows the regeneration which returns the signal back to the baseline.

### 3. SENSITIVE LAYER

For the quality of a sensor, not only the transduction is essential but also the sensitive layer. In addition, it determines selectivity sensitivity, stability

and reversibility of the sensor system. This sensitive layer should provide a rather high signal-to-noise ratio, short response times, low limit of detection, and high sensitivity. Furthermore, in many cases the user certainly wants to apply the sensor to real world samples, not just in the lab. Figure 6 shows a variety of layers which exhibit some selectivity whereby simple polymers such as polydimethylsiloxanes are the less selective ones<sup>12, 13</sup>.

Microporous material<sup>20</sup> will demonstrate will show some sieve effects, polymers including some functional groups will also exhibit some selectivity, the best selectivity is exhibited by molecular imprinted polymers<sup>21</sup>. In some cases, the functionality is used to provide biomimetic compounds with certain recognition sites. These will be discussed later in connection with biopolymers.

Figure 7 shows the sensitive processes in case of simple polymers. In a first step, the free analyte in the gaseous phase is sorbed in a first step to the polymer, and will diffuse within the network of the polymer even providing a little selectivity by using functional groups within the polymers. Real selective binding sites can be introduced in form of metal complex compounds or recognition sites as in the case of molecular imprinted polymers. Because of the thermodynamic mass law, high selectivity results in a high binding and equilibrium constant. Thus, the rate of association and interaction will be fast in comparison to the rate of dissociation between analyte and recognition site.

Accordingly, in Figure 8 sensitive layers can demonstrate either a higher reversibility or a higher selectivity. In combination with these properties, polymers usually show a high reversibility since they have poor selectivity and since they are relatively stable in contrast to biomolecular receptor layers where the selectivity and the sensitivity are high, but where the stability is rather poor as is reversibility.

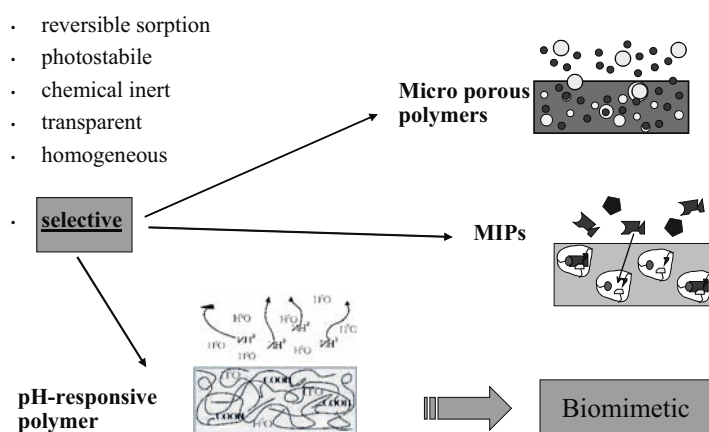


Figure 6. Modified polymers demonstrate various properties and show some kind of selectivity in dependence on the material used.

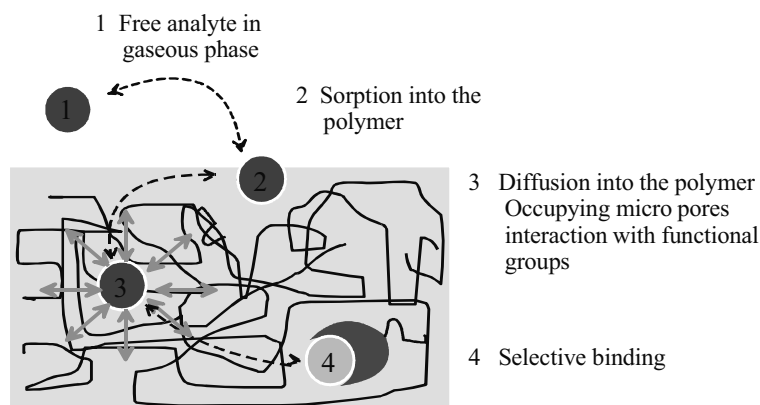


Figure 7. Sorption steps and selective binding; in case of simple polymers sorption processes take place comparable to effects occurring in separation columns. The different steps are demonstrated.

The intended high selectivity of biomolecular recognition sites has the problem that any non-specific binding at this receptor layer has to be avoided. Accordingly, the surface modification on the transducer must supply some additional properties; besides being as stable and inert as possible it must result in a high capacity of binding sites which increase the sensitivity. In addition, this layer must prevent non-specific binding. With regard to this issue, quite a few concepts have been described in literature. These concepts (see Figure 9) either rely on self-assembled layers or, as in the case of polyethylenglycol<sup>16</sup>, on a kind of lawn structure with a high suppression of non-specific binding<sup>17</sup>.

On the other hand, the volume effects provided by e.g. hydrogels such as dextran layers<sup>14, 15</sup> will allow an increased number of binding sites. In addition, Figure 9 shows that biotin streptavidin binding and the use of HIS-

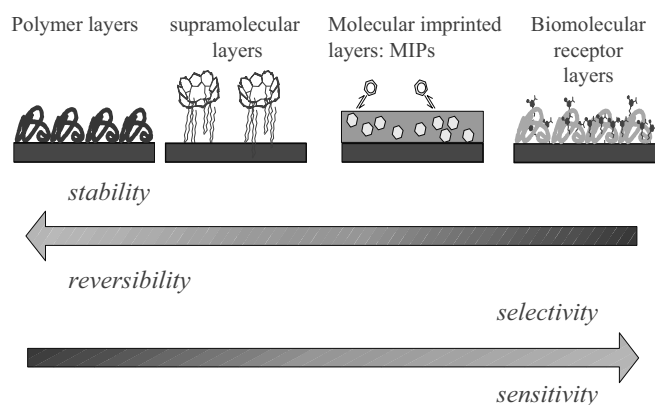


Figure 8. Properties of sensitive material.

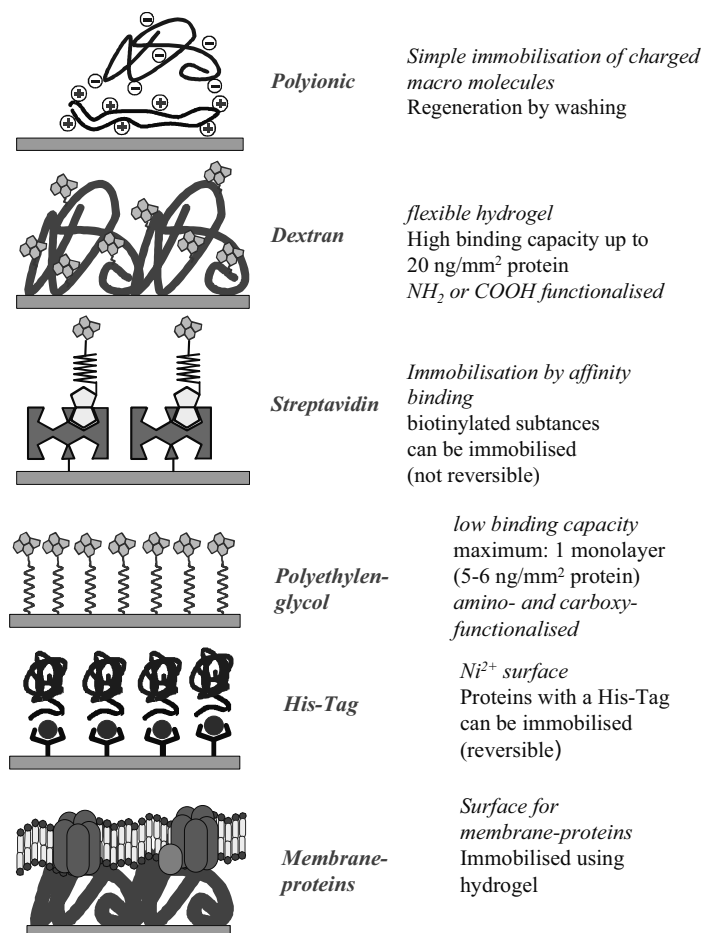


Figure 9. Various biomolecular layers as biopolymeric films allowing immobilisation of recognition sites.

tag<sup>18</sup> or even immobilization of membrane proteins<sup>19</sup> are frequently used methods. In the case of a heterogeneous phase assay it is necessary to discriminate between several processes. At first, in the homogeneous phase, there is an equilibrium between the receptor and the ligand, symbolized in Figure 10, and given by an association rate constant  $k_{\text{ass}}$ . This equilibrium is monitored via the second equilibrium at the transducer where in a biopolymer layer derivatives of the ligand are immobilized. By diffusion, non-blocked receptors can go to the surface immobilized ligands and form a second equilibrium given by an association rate constant  $k_{\text{ass}(\text{het})}$  and  $k_{\text{dis}(\text{het})}$ . This second equilibrium can be used to determine the position of the equilibrium in the homogeneous phase.

In case the number of ligand binding sites at the surface is high, the diffusion will limit the processes on the biopolymer. The mass transport-

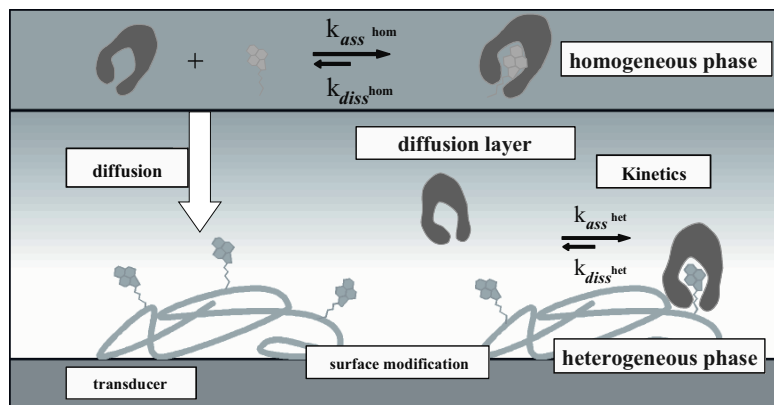


Figure 10. Equilibria between ligand and receptor in the homogeneous phase and at the heterogeneous phase. Non-blocked receptors diffuse by a transport-limited process to the surface and can form a second equilibrium. From this assay type, kinetic as well as thermodynamic constants can be determined.

(diffusion) limited process allows direct determining of the concentration of the non-blocked receptor in the homogeneous phase via the measured signal at the surface. In case the number of binding sites is low, kinetics of this equilibrium at the heterogeneous phase can be determined, allowing to measure  $k_{ass(het)}$  and  $k_{dis(het)}$ . There is even the chance to get information on the kinetics of the equilibrium at the homogeneous phase measuring whiles the equilibrium forms in a pre-incubation phase. This can be achieved by monitoring the process starting as soon as the ligand is added to the receptor (not after the incubation phase) and also indirectly by the measurement of the binding at the surface<sup>22</sup>. However, this method requires quite a lot of mathematics since all processes are superimposed and the different rate constants can only be evaluated by a model fit.

If labelled molecules are used, the binding assay can be varied. It is possible to use either a competitive approach or direct monitoring of even smaller molecules in a binding inhibition assay. These principles are demonstrated in Figure 11; it must be realized that direct optical monitoring of small molecules results either in a large change in the refractive index nor in a large change in the thickness of the physical layer. For this reason, in all these cases inversed binding assays are preferable; this is called a binding inhibition assay. In this, as demonstrated before, small molecules are immobilized to the surface, and during the homogeneous phase interaction between ligand and receptor takes place during the preincubation phase. By this means, the large non-blocked receptors will bind to the surface and increase the signal considerably.

In the following, the application of these concepts is shown both for refractometric and reflectometric measurements using Mach-Zehnder interferometers and reflectometric interference spectroscopy.

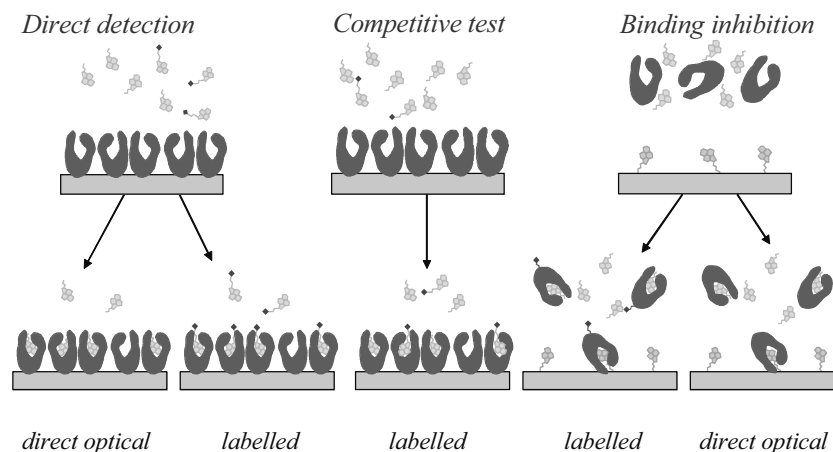


Figure 11. Comparison of different assay types using a direct detection scheme were the receptors immobilized to the surface and the analyte is recognized at the surface (direct optical detection and using labelled systems), a competitive test scheme were labelled analyte molecules compete with the non-labelled sample, and thirdly a binding inhibition assay were analyte derivatives (ligand derivatives) are immobilized at the surface, in a preincubation phase the ligands block receptor molecules, non-blocked receptors go to the surface being either labelled or optically detected.

#### 4.1 Chemosensors

Mach-Zehnder interferometers allow the monitoring of gas concentrations and even the determination of analytes in liquids. Normally one of the measurement arms is covered with a thin polymer film into which the analyte can sorp. According to Nernst's distribution law, we have an equilibrium between the mobile and the stationary phase if a gas or a liquid pass the measurement window<sup>23, 24, 25</sup>. Figure 12 shows a variety of results.

Depending on the changes of the refractive index during the uptake of analytes, the signal is either modulated to a lower or a higher value. For the case of an increase, both modulations are shown on the right hand side of the figure, combining the curve for a concentration uptake with the measured modulated curve and a relation to the change in the refractive index. The left part shows the uptake, the right part the reversible exit of the analyte from the polymer.

Another possibility is to measure the interaction between liquid crystal<sup>26</sup> and two xylene isomers, para- and meta-xylene, which is demonstrated in Figure 13.

Reflectometric interference spectroscopy can also be used to easily determine various interactions between analytes and polymer films<sup>27</sup>. A typical application is given in Figure 14 for a homologous series of alcohols<sup>29</sup>.

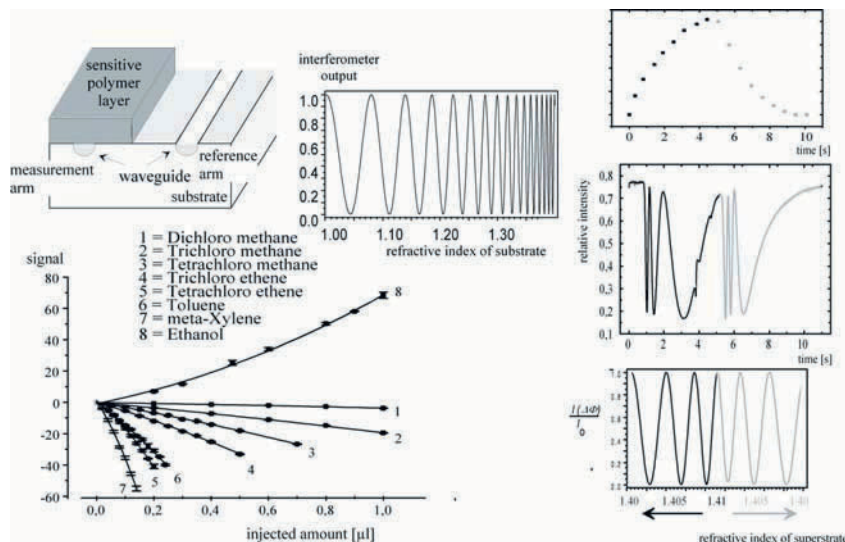


Figure 12. Measurement arm of the Mach-Zehnder interferometer covered by a sensitive polymer layer, resulting in a intensity modulation by a change of the refractive index. This schematic changes are combined with the experimental data on the right side: on top the curve of uptake of analyte, and its diffusion out of the layer (right part), in the middle the experimental modulation, and at the bottom the related changes in refractive index. Bottom left shows the result of intensity signal versus the amount of substance for eight different analytes.

## 4.2 Biosensors

Interferometric sensors frequently have also been applied to biosensor measurements. Thereby, the evanescent field technique (Mach-Zehnder interferometer) has been compared with other optical detection principles regarding information on layer structure and in case of biosensing<sup>30</sup>. The

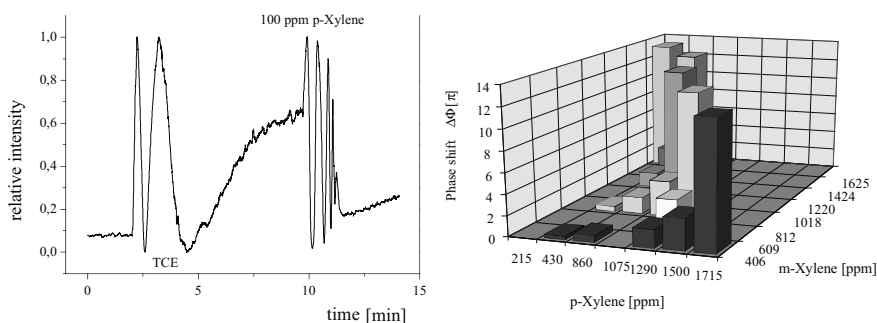


Figure 13. A Mach-Zehnder interferometer used to measure the isomers para- and meta-xylene at various concentrations.



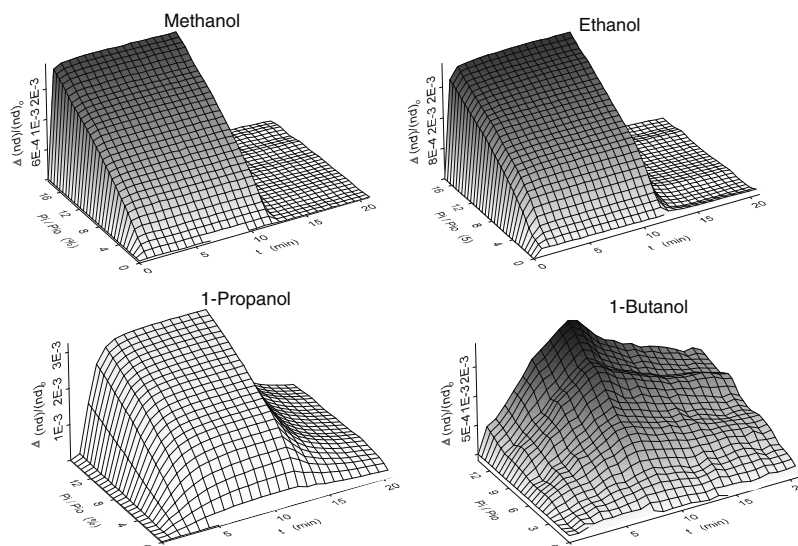


Figure 14. Time-resolved measurements of 4 alcohols with RIFS in an multi-element set-up.

exponentially decreasing evanescent field especially allows to monitor information quite close to the interface to the waveguide. Figure 15 shows the measurement of a multilayer structure of biotin/streptavidin interaction in form of a signal and a calculated physical thickness change. For the first few layers, there is a linear correlation.

In Figure 16, the modulation of the intensity and the calculated concentration graph is given for a measurement of simazine in water<sup>34</sup>. The upper part of the figure shows the signal modulation of the Mach-Zehnder chip obtained for one concentration; the lower part shows the full calibration curve for six different concentrations, demonstrating the sigmoidic plot.

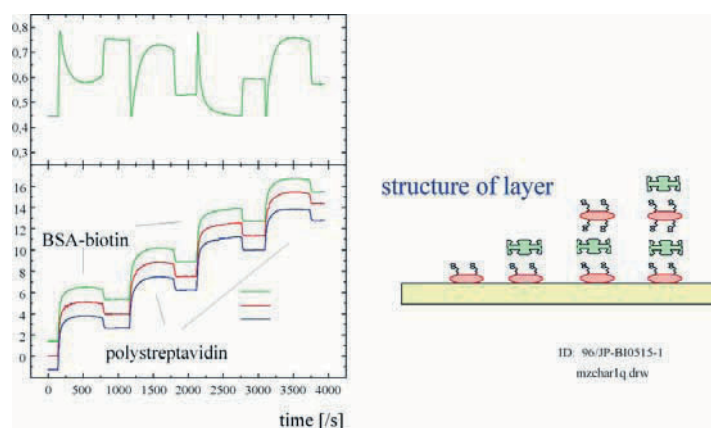


Figure 15. Mach-Zehnder chip used to monitor the growth of a layer structure interchanging streptavidin and avidin molecules. This structure is shown on the right, on the left side, the modulation and the calculated thickness increase is given.

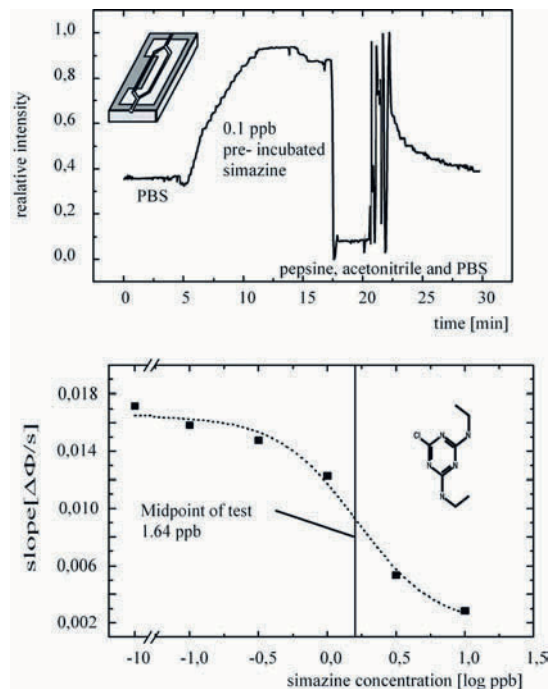


Figure 16. Determination of simazine concentration in water. In the upper part, the modulation of the Mach-Zehnder signal for one concentration, including the regeneration step. The lower part shows the calibration curve for six different simazine concentrations graphed for the slope of this signal versus the simazine concentration in the logarithmic scale.

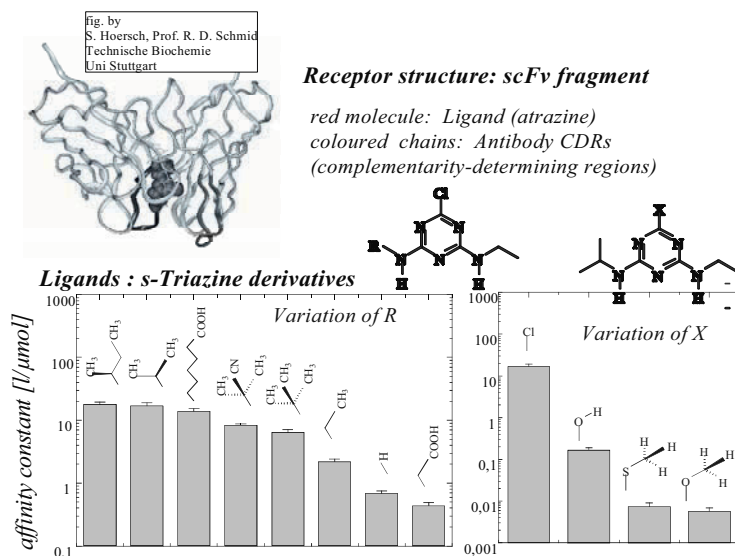


Figure 17. Structure affinity relationship: measurement using reflectometric interference spectroscopy of atrazine versus an antibody in water. A variety of derivatives of triazines are measured at a number of concentrations to obtain affinity constants.

Because of the more simple and robust technique of reflectometric interference spectroscopy, more applications of this method will be given in following.

At the beginning, a variety of triazine derivatives<sup>32, 36</sup> have been examined to find a structure to antibody relationship for a variety of triazine derivatives. For each of these modified triazines compounds, at least eight concentration were measured in water in a binding inhibition test format. The results of the binding constants are shown in Figure 17 in dependence of the two modified functional group. The rather low error bars in the figure demonstrate the high reproducibility of the method.

The interferometric measurements with RIfS can be parallelized as demonstrated in Figure 18. In this case, instead of white light interferometry, only a few wavelengths are used to allow parallel detection of all measurement dots. A filter wheel selects one wavelength at a time from the white light source, while the CCD camera monitors the intensity distribution at the transducer for all spots, in this case in a microtiter plate<sup>35</sup>.

As can be seen in Figure 19, by switching between these filter it is possible to obtain for each wavelength at the same time the information on resulting interference for each well in parallel, and for the different wavelengths one interference signal after the other. Based on this information, interference spectra can be created for all wells, giving in parallel the same information for each wavelength. However, since the switchover between the wavelengths is rather fast (just a few seconds), the binding curves are not influenced too much.

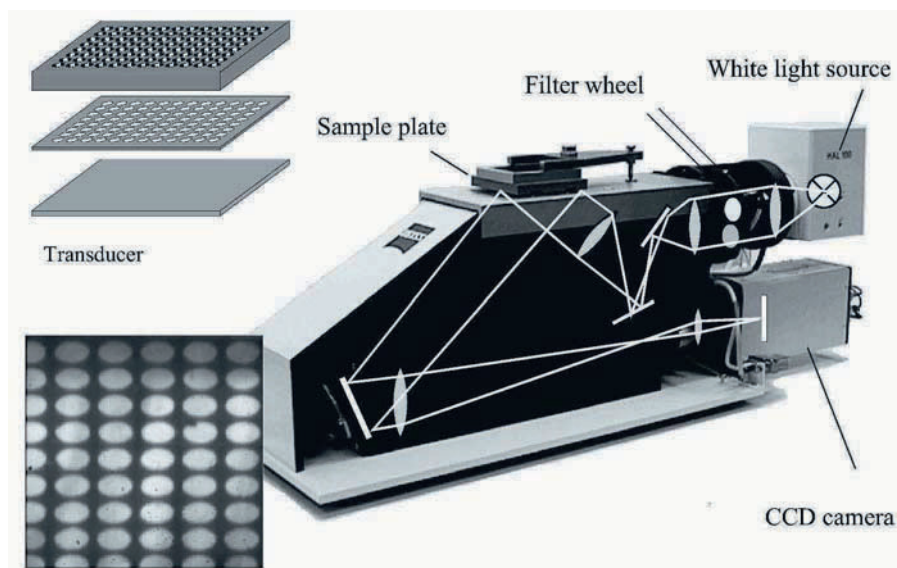


Figure 18. Parallelised set-up for monitoring binding curves in micro titer plate arrays.

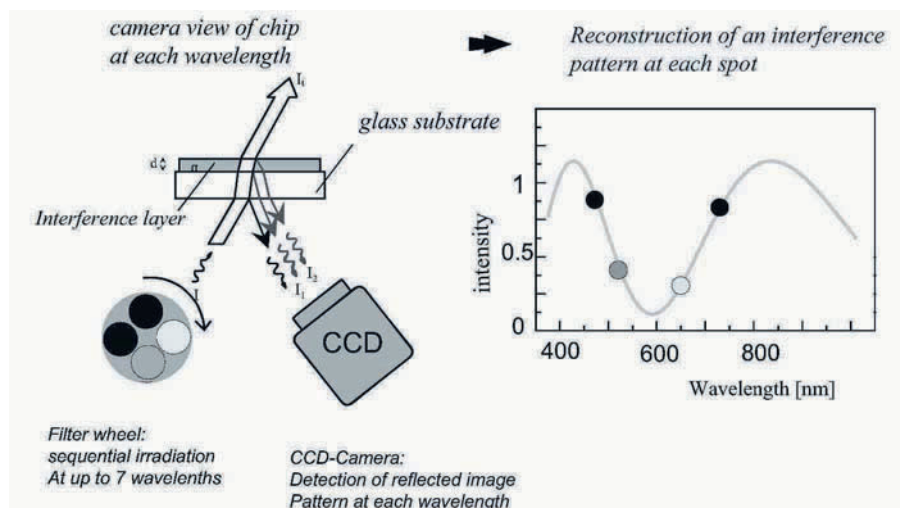


Figure 19. Procedure of measuring reflectometric interference spectroscopy in a parallelized setup. Instead of white light, the wavelength obtained from some filters are used, and the interference spectra is constructed based on these supporting wavelengths. For each wavelength, all the measurement spots are obtained simultaneously, the total time for one wavelength set is less than 10 seconds.

A typical example of such parallelized measurements is given in Figure 20. For a variety of inhibitors, the binding inhibition assay is given for a thrombin inhibition; Figure 20 shows the binding curves obtained in parallel from 96 wells<sup>37</sup>.

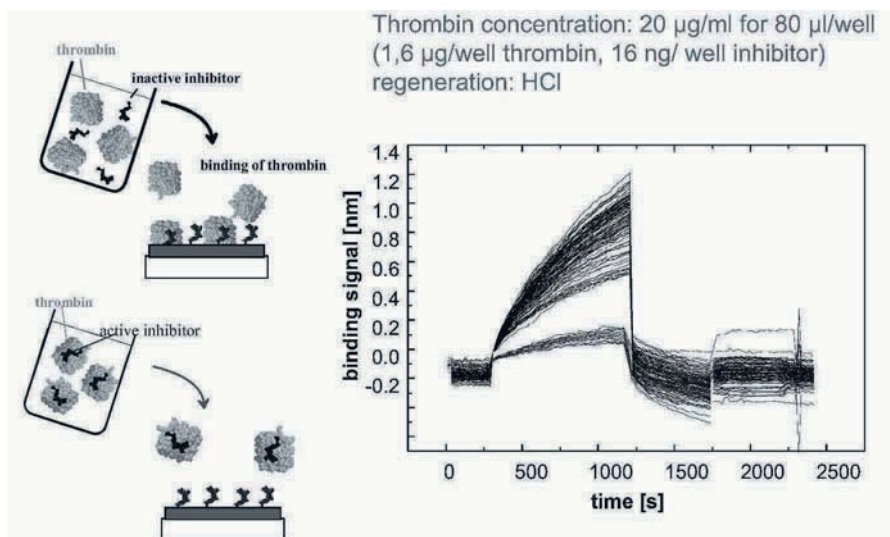


Figure 20. An active inhibitor blocks the thrombin which cannot go to the surface anymore (lower curves), an inactive inhibitor cannot block the thrombin, therefore typical binding signals can be observed depending on the concentration and the activity of the inhibitor.

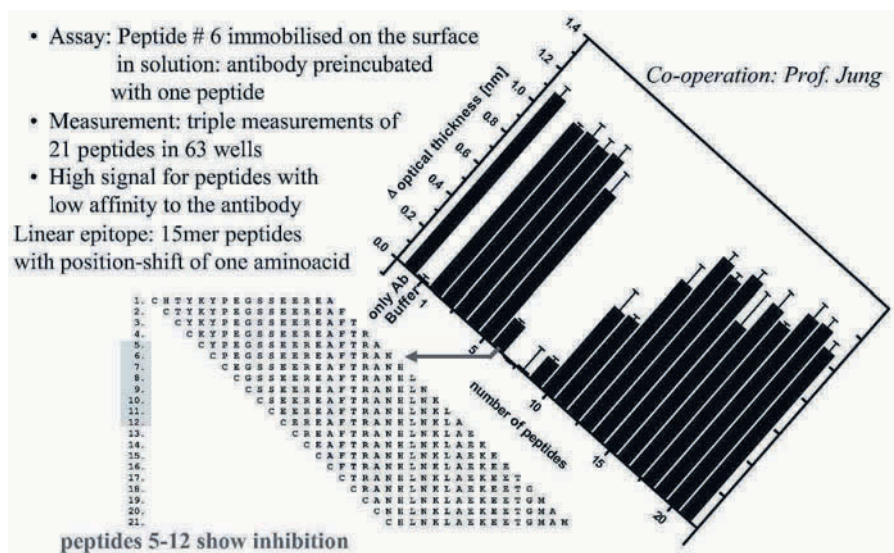


Figure 21. By combinatorial chemistry, 21 15-mer-peptides are synthesized, each shifted by one position of the aminoacid. In binding inhibition assay, an epitope mapping of the antibody is achieved.

Epitope mapping is another example of application of RIfS in parallelized systems. 63 wells of a microtiter plate equivalent format are filled by 21 peptides (three times the same concentration). These 21 peptides are 15-meres and have been synthesized by combinatorial chemistry in cooperation with our colleague, Prof. Jung: A lead structure (peptide # 6) is immobilised to the surface in each well. Adding a buffer, no signal should be detected, adding an antibody with structure complementary to the immobilized sequence results in a high signal<sup>38</sup>.

In a next, in 63 solutions these 21 one sequences are added to the antibody, and the wells are filled with one of the solutions each (three replica). Complementary sequences of the peptides to the antibody will block this antibody and the signal at the surface will decrease accordingly. By these means, the epitope can be mapped and the interesting sequence of an antibody.

As a further example, hybridization studies are given. Reflectometric interference spectroscopy can monitor the hybridization of DNA strands with different sequences, giving matching and mismatching discrimination. The results are shown in Figure 22, demonstrating a binding inhibition assay and documenting the differences in binding curves for 0, 1 and 2 mismatch in case of 23-meres for complementary and non-complementary base pairs<sup>39</sup>.

The possibilities of measuring time-resolved hybridization in this parallel setup are shown in Figure 23, and it even allows to obtain kinetic information for all spots in parallel. Since reflectometric interference

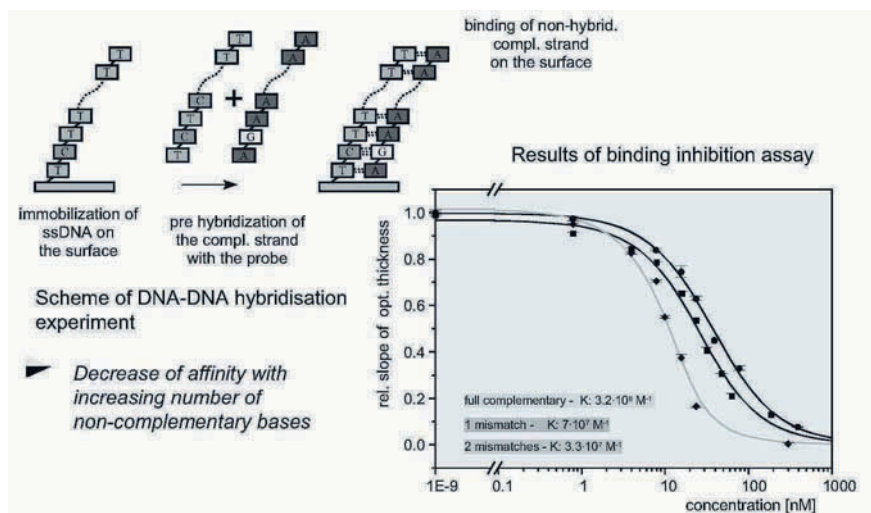


Figure 22. Calibration for the hybridization of various matching and mismatching nucleobase sequences.

spectroscopy does not depend on temperature, it is possible to vary the temperature and thus to determine melting curves.

As a conclusion it has been demonstrated that optical sensors have a wide field of applications in the process control, surveillance and biosciences. They supply the chance to monitor processes an-line and with short time resolution. Interferometric sensors are rather sensitive and applicable in

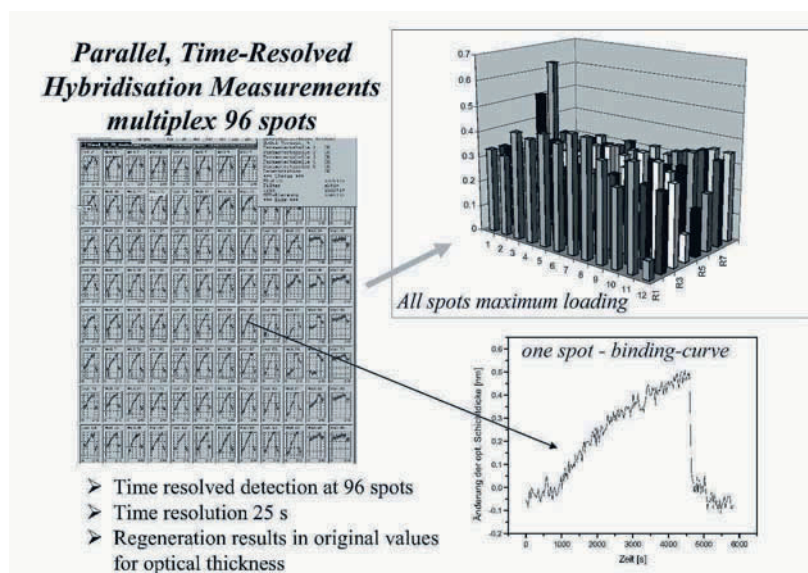


Figure 23. Binding curves in 96 wells in parallel, one well enlarged as a basis for data evaluation of hybridization.

many of these applications. Whereas chemical sensitive layers normally demonstrated reversibility and stability, the biomolecular receptor layers offer more specificity and aim into the area of high throughput screening and biochip technologies. Accordingly down scaling to nanostructures is considered recently.

Optical read out will compete with micro electrode arrays. New developments in array detectors will open new perspectives. Direct optical detection techniques will add new possibilities to bioanalytical applications in addition to fluorescence measurements presently preferred in biochips read out.

Hyphenated techniques like combination of optical detection methods based on reflectometry or refractometry and separation techniques are of future interest. The same is valid for the intention to couple SPR or RfS with mass spectrometry like MALDI<sup>33</sup>.

## REFERENCES

1. Göpel W., Hesse J., Zemel J.N. *Sensors, A Comprehensive Survey*, Vol. I – VIII, VCH Weinheim 1992 ff.
2. *Biosensors in Environmental Monitoring*, Bilitewski U., Turner A. (eds.), Harwood Academic Publishers, Amsterdam 2000.
3. *Frontiers of Biosensors I + II*, Scheller F.W., Schubert F., Fedrowitz J. (eds.), Birkhäuser Verlag, Basel 1996.
4. Wolfbeis O.S., Boisdé G.E. and Gauglitz G., *Sensors Vol. II part I*, ed. H. Baltes, W. Goepel, J. Hesse, Weinheim, 1996, 573.
5. Gauglitz G., *Sensors Update Vol I*, ed. H. Baltes, W. Goepel, J. Hesse, Weinheim, 1996, 1.
6. Lakowicz J.R., *Principles of Fluorescence Spectroscopy*, Kluwer Academic/Plenum Publishers, New York 1999, 298.
7. Weber G., *Fluorescence and Phosphorescence Analysis*, Hercules D.M. (ed.), John Wiley & Sons, New York 1966, 217.
8. Hecht E., Zajec A., *Optics*, Addison-Wesley, Reading, MA.
9. Brecht A., Gauglitz G., Kraus G. and Nahm W., Chemical and biochemical sensors based on interferometry at thin (multi-)layers, *Sensors Actuators B* 1993; 11: 21-27.
10. Azzam R.M.A. and Bahara N.M., *Ellipsometry and polarized light*, North Holland, Amsterdam 1988.
11. Brandenburg A. and Henninger R., Integrated optical Young interferometer, *Appl Optics* 1994; 33: 5941-5947.
12. Baldini F. and Bracci S., *Polymers for optical fiber sensors*, in *Polymer Sensors and Actuators*, Y. Osada, D. E. De Rossi (eds.), Springer Verlag 2000, 91.
13. Rathgeb F. and Gauglitz G., in *Encyclopedia of Analytical Chemistry*, ed. R. A. Meyers, Chichester 2000, John Wiley & Sons Ltd., 2189.
14. Löfas L. and Johnsson B., A novel hydrogel matrix on gold surfaces in surface plasmon resonance sensors for fast and efficient covalent immobilization of ligands, *J Chem Soc Chem Commun* 1990, 1526.
15. Piehler J., Brecht A., Geckeler K.E., Gauglitz G., Surface modification for direct immunoprobes, *Biosens Bioelectron* 1996; 11: 579-590.

16. Feldmann K., Hähner G., Spencer N.D., Harder P. and Grunze M., Probing Resistance to Protein Adsorption of Oligo(ethylene glycol)-Terminated Self-Assembled Monolayers by Scanning Force Microscopy, *J Am Chem Soc* 1999; 121: 10134.
17. Piehler J., Brecht A., Valiokas R., Lidberg B. and Gauglitz G., A high-density poly(ethylene glycol) polymer brush for immobilization on glass-type surfaces, *Biosens Bioelectron* 2000; 15: 473-481.
18. Gershon P.D., Khilko S., Stable chelating linkage for reversible immobilization of oligohistidine tagged proteins in the BIAcore surface plasmon resonance detector, *J Immun Methods* 1995; 183: 65-76.
19. Tien H.T., *Prog Surf Sci* 1985; 19: 169.
20. Park J., Groves W.A. and Zellers E.T., Vapor Recognition with Small Arrays of Polymer-Coated Microsensors. A Comprehensive Analysis, *Anal Chem* 1999; 71: 3877-3886.
21. Haupt K. and Mosbach K., Molecularly Imprinted Polymers and Their Use in Biomimetic Sensors, *Chem Rev* 2000; 100: 2495-2504.
22. Eddowes M.J., Direct immunochemical sensing: basic chemical principles and fundamental limitations, *Biosens* 1987; 3: 1-15.
23. Gauglitz G. and Ingenhoff J., Influence of thin superstrate films on evanescent waves in surface waveguides, *Ber Bunsen Phys Chem* 1991; 95: 1558-1563.
24. Fabricius N., Gauglitz G. and Ingenhoff J., A gas sensor based on an Mach-Zehnder interferometer, *Sensors Actuators B* 1992; 7: 672-676.
25. Gauglitz G. and Ingenhoff J., Integrated optical sensors for halogenated and non-halogenated hydrocarbons, *Sensors Actuator B* 1993; 11: 207-212.
26. Drapp B., Pauluth D., Krause J., Gauglitz G., The application of the phase transition in nematic liquid crystals for the optical detection of volatile organic compounds, *Fresenius J Anal Chem*, 1999, 364, 121-127.
27. Yan H.M., Kraus G., Gauglitz G., Detection of Mixtures of Organic Pollutants in Water by Polymer Film Receptors in Fibre-Optical Sensors Based on the Reflectometric Interference Spectrometry, *Anal Chim Acta* 1995; 312: 1-8.
28. Busche S., Dieterle F., Kieser B. and Gauglitz G., Quantification of binary mixtures of the freones R22 and R134a by surface plasmon resonance, *Sensors Actuators B* 2003; 89: 192-198.
29. Busche S., Kasper M., Belge G., Dieterle F. and Gauglitz G., Quantification of binary mixtures of the freones R22 and R134a by surface plasmon resonance, *Measurement Science and Technology*, 2004 15 (3): 540.
30. Ingenhoff J., Drapp B., Gauglitz G., Biosensors using integrated optical devices, *Fresenius J Anal Chem* 1993; 346: 580-583.
31. Tünnemann R., Mehlmann M., Süßmutz R.D., Bühler B., Pelzer S., Wohlleben W., Fiedler H.-P., Wiesmüller K.-H., Gauglitz G., Jung G., Optical Biosensors. Monitoring Studies of Glycopeptide Antibiotic Fermentation Using White Light Interference, *Anal Chem* 2001; 73: 4313.
32. Lang G., Brecht A., Gauglitz G., Characterisation and Optimisation of an Immunoprobe for Triazines, *Fresenius J Anal Chem* 1996; 354: 857-860.
33. Mehlmann M., Garvin A., Steinwand M., Gauglitz G., Coupling of reflectometric interference spectroscopy with MALDI-MS, in preparation.
34. Drapp B., Piehler J., Brecht A., Gauglitz G., Luff B.J., Wilkinson J.S., Ingenhoff J., Integrated optical Mach-Zehnder interferometers as simazine immunoprobes, *Sensors Actuators B* 1997; 39: 277-282.
35. Rothmund M., Schütz A., Brecht A., Gauglitz G., Berthel G., Graefe D., Label free binding assay with spectroscopic detection for pharmaceutical screening, *Fresenius J Anal Chem* 1997; 359: 15-22.
36. Birkert O., Tünnemann R., Jung G., Gauglitz G., Label-Free Parallel Screening of Combinatorial Triazine Libraries Using Reflectometric Interference Spectroscopy, *Anal Chem* 2002; 74: 834.



37. Birkert O., Gauglitz G., Development of an assay for label-free high-throughput screening of thrombin inhibitors by use of reflectometric interference spectroscopy, *Anal Bioanal Chem* 2002; 372: 141-147.
38. Kröger K., Bauer J., Fleckenstein F., Rademann J., Jung G. and Gauglitz G., Epitope-mapping of transglutaminase with parallel label-free optical detection, *Biosens Bioelectron* 2002; 17: 937-944.
39. Sauer M., Brecht A., Charisse K., Stemmler I., Gauglitz G. and Bayer E., Interaction of Chemically Modified Antisense Oligonucleotides with Sense DNA: A Label-Free Interaction Study with Reflectometric Interference Spectroscopy, *Anal Chem* 1999; 71: 2850.

## Chapter 12

# SURFACE-ENHANCED RAMAN SCATTERING

Tuan Vo-Dinh and Fei Yan  
*Advanced Biomedical Science and Technology Group*  
*Life Sciences Division*  
*Oak Ridge National Laboratory*  
*Oak Ridge, Tennessee 37831-6101, USA*

### 1. INTRODUCTION

In 1928, Sir C.V. Raman documented the phenomenon of inelastic light scattering<sup>1</sup>. Radiation scattered by molecules contains photons with the same frequency as the incident radiation, but may also contain photons with changed or shifted frequency. This effect is very weak - approximately one photon out of a million (0.0001%) will scatter from that sample at a wavelength slightly shifted from the original wavelengths. The process was later named after him, with the shifting of frequency referred to as the Raman effect and the frequently-shifted light as Raman radiation. Raman spectroscopy is based on vibrational transitions that yield very narrow spectral features which are characteristic of the investigated sample. Thus, it has long been regarded as a valuable tool for the identification of chemical and biological samples as well as the elucidation of molecular structure, surface processes, and interface reactions. Despite such advantages, Raman scattering suffers the disadvantage of extremely poor efficiency. Compared to luminescence-based processes Raman spectroscopy has an inherently small cross-section (e.g.  $10^{-30}$  cm<sup>2</sup> per molecule), thus precluding the possibility of analyte detection at low concentration levels without special enhancement processes. Some modes of signal enhancement have included resonance Raman scattering and nonlinear processes such as coherent anti-Stokes Raman scattering. However, the need for high-power, multiple-wavelength excitation sources has limited the widespread use of these techniques.

Nevertheless, there has been a renewed interest in Raman techniques in the past two decades due to the discovery of the surface-enhanced Raman scattering (SERS) effect, which results from the adsorption of molecules on specially textured metallic surfaces. This large enhancement was first

reported in 1974 by Fleischmann and coworkers, who observed the effect for pyridine molecules adsorbed on electrochemically-roughened silver electrodes<sup>2</sup>. It was initially believed that the enhancement resulted from the increased surface area produced by the electrochemical roughening, giving rise to increased probed sample density. The teams of Jeanmaire and Van Duyne<sup>3</sup>, and Albrecht and Creighton<sup>4</sup> later confirmed the enhancement (up to  $10^8$ ) but attributed the effect to more complex surface enhancement processes, which continue to be the subject of intense theoretical studies. Following the first observations of the SERS effect in the 1970's, there have been an extensive amount of fundamental research and theoretical studies on the SERS effect. During a period between the mid-1970s and the early 1980's, this early enthusiasm for SERS decreased and did not lead to practical applications because the Raman enhancement effect had been observed for only a limited number of molecules. Most studies had involved samples at concentrations between  $10^{-1}$  and  $10^{-3}$  M, which are well above the useful concentration ranges for trace analysis. Most fundamental studies were also limited to a few highly polarizable small molecules, such as pyridine, benzoic acid and its derivatives, or some ionic species such as the cyanide radical  $CN^-$  and the anion of dithiozone. It was even thought that the SERS effect occurs only for a few molecules (such as pyridine) only under specific experimental conditions.

The "Renaissance" of SERS started only in the mid-1980's. In 1984, our laboratory first reported the general applicability of SERS as an analytical technique, and the possibility of SERS measurement for a variety of chemicals including several homocyclic and heterocyclic polyaromatic compounds using solid substrates covered with silver-coated nanospheres were first reported<sup>5</sup>. For the following two decades, SERS has been accepted as a general phenomenon and research activities in this field has regained explosive interest. More recent reports have cited SERS enhancements from  $10^{13}$  to  $10^{15}$ , thus demonstrating the potential for single-molecule detection with SERS<sup>6-10</sup>.

Because of the aggressive development of SERS substrates and application to a wide range of chemicals, the potential of SERS as a routine analytical technique was recognized by the mid-1980s. The SERS technique has since continued to receive increased interest, as is evidenced by the large numbers of papers and review articles<sup>11-22</sup>. Furthermore, the scope of SERS has been extended to include other surface-enhanced spectroscopies such as surface-enhanced second-harmonic generation<sup>23</sup> and surface-enhanced hyper-Raman scattering<sup>24</sup>.

A host of biological compounds (e.g., proteins, amino acids, lipids, fats, fatty acids, DNA, RNA, antibodies, enzymes) have been studied via SERS. The extensive progress in the development of dependable SERS substrates over the past few decades has promoted the application of SERS in the rapidly expanding field of biotechnology, as is demonstrated in several

excellent reviews<sup>24-28</sup>. This chapter provides a synopsis of the development and applications of SERS active metallic nanostructures. Some highlights of this chapter include reports of SERS as an immunoassay readout method, SERS gene nanoprobes, near-field scanning optical microscopy SERS probes, SERS as a tool for single-molecule detection, and SERS nanoprobes for cellular studies.

## 2. RAMAN SCATTERING AND SURFACE-ENHANCED RAMAN SCATTERING

The Raman effect arises when a photon is incident on a molecule and interacts with the electric dipole of the molecule. In classical terms, the interaction can be viewed as a perturbation of the molecule's electric field. In quantum mechanics the scattering is described as an excitation to a virtual state lower in energy than a real electronic transition with nearly coincident de-excitation and a change in vibrational energy. The scattering event occurs in  $10^{-14}$  seconds or less. The virtual state description of scattering is shown in Figure 1.

At room temperature the thermal population of vibrational excited states is low, although not zero. Therefore, the initial state is the ground state, and the scattered photon will have lower energy than the exciting photon. This Stokes shifted scatter is what is usually observed in Raman spectroscopy. Figure 1a depicts Raman Stokes scattering.

A small fraction of the molecules are in vibrationally excited states. Raman scattering from vibrationally excited molecules leaves the molecule in the ground state. The scattered photon appears at higher energy, as shown in Figure 1b. This anti-Stokes-shifted Raman spectrum is always weaker than the Stokes-shifted spectrum, but at room temperature it is strong enough to be useful for vibrational frequencies less than about  $1500\text{ cm}^{-1}$ . The Stokes and anti-Stokes spectra contain the same frequency information.

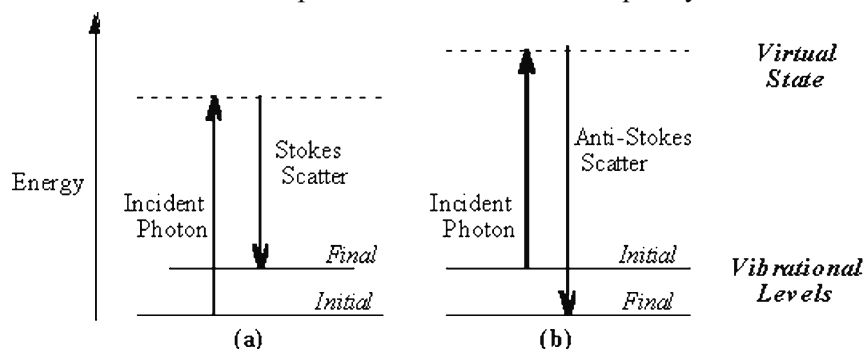


Figure 1. Energy level diagram for Raman scattering. (a) Stokes Raman scattering, and (b) anti-Stokes Raman scattering.

The Raman scattering from a molecule adsorbed on or even within a few Angstroms of a nanostructured metal surface can be  $10^3$ - $10^8$  times greater than in solution. This surface-enhanced Raman scattering is strongest on silver, but is observable on gold and other transition metals as well. Although extensive fundamental studies have been devoted to obtain a better understanding of the sources of enhancement, it is believed that our current understanding of SERS is not complete. Although it is expected that new experimental observations in SERS studies will spur the development of new or refined theoretical models, there are currently two major theoretical models that could explain various experimental observations associated with the SERS effect. The first is an enhanced electromagnetic field produced at the surface of the metal. When the wavelength of the incident light is close to the plasma wavelength of the metal, conduction electrons in the metal surface are excited into an extended surface electronic excited state called a surface plasmon resonance. Molecules adsorbed or in close proximity to the surface experience an exceptionally large electromagnetic field. Vibrational modes normal to the surface are most strongly enhanced. The second mode of enhancement, also known as the chemical enhancement, is due to the formation of a charge-transfer complex between the surface and analyte molecule. The electronic transitions of many charge transfer complexes are in the visible, so that resonance enhancement occurs.

A main difference between the electromagnetic and chemical models is the fact that the chemical effect contribution to SERS is necessarily short-ranged (0.1 to 0.5 nm). This mechanism depends on the adsorption site, the geometry of bonding, and the energy levels of the adsorbate molecule. For specific adsorbate-surface systems, enhancements may be large. The contribution of charge-transfer processes to SERS has been estimated<sup>15</sup> to be approximately  $10$ - $10^3$ . Experimental data have shown that adsorption of molecules to local defect sites on a smooth metal surface results in an approximately 15-65 fold enhancement of the Raman signal for pyridine<sup>2</sup>. Chemical enhancement can provide useful information on chemisorption interactions between metal and adsorbate. However, this enhancement is not a general mechanism and is applicable only to specific adsorbate-metal systems.

### **3. INSTRUMENTATION FOR SERS ANALYSIS**

The SERS spectra can be obtained on a conventional Raman spectrometer (see Figure 2). In this particular system, 632.8 nm radiation from a Helium-Neon laser is used with an excitation power of ~5 mW. Signal collection is performed at  $0^\circ$  with respect to the incident laser beam. This coaxial excitation/collection geometry is achieved with a small prism, which is used to direct the excitation beam to the sample while allowing

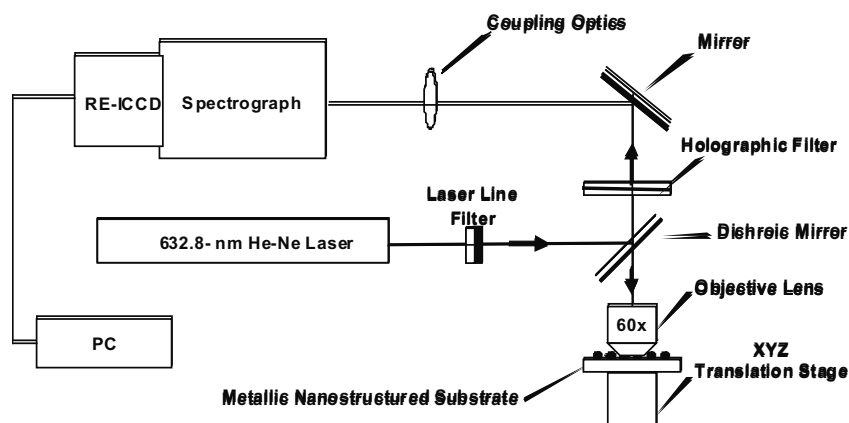


Figure 2. Schematic of the instrument setup used for SERS detection.

most of the collected signal to pass on to the collection fiber. A Raman holographic filter is used to reject the Rayleigh scattered radiation from the collected Raman signal. The Raman signal is focused onto the entrance slit of a spectrograph (ISA, HR-320), which is equipped with a red-enhanced intensified charge-coupled device (CCD) detector (Princeton Instruments, RE-ICCD-576S).

## 4. DEVELOPMENT OF SERS-ACTIVE SUBSTRATES

### 4.1 SERS-Active Metal Electrodes

Electrochemically roughened silver electrodes were the first media with which the SERS effect was observed<sup>2</sup>. The observation of this effect resulted in further inaugural studies to confirm it and to establish enhancement factors<sup>3, 4, 15</sup>. While several metals have been investigated for SERS activity in electrochemical cells<sup>30-34</sup>, silver has been most commonly used. Transition metals such as bare Pt, Ru, Rh, Pd, Fe, Co, and Ni electrodes have also been investigated as SERS substrates<sup>35-37</sup>. It has been found that transition metals exhibit surface enhancement factors ranging from 1 to 4 orders of magnitude, depending on the nature of the metal and the surface morphology. In one study, photoalterations of the copper electrode resulted in a further ten-fold increase in SERS<sup>38</sup>.

### 4.2 SERS-Active Metal Nanoparticle Colloids

SERS-active suspensions of elemental metal colloids or nanoparticles of various sizes can be chemically formed in solution. Silver colloids can easily

be prepared by reducing a solution of  $\text{AgNO}_3$  with ice-cold  $\text{NaBH}_4$ <sup>39-41</sup>, trisodium citrate<sup>42-44</sup>, or hydrogen peroxide under basic conditions<sup>45</sup>. Other more innovative techniques which reduce the need for wet chemistry have been demonstrated. For example, Ahern and Garrell described a unique in situ photoreduction method to produce photocolloids in solutions<sup>46</sup>, while another innovative method involved laser ablation of colloids from silver foils into aqueous solutions<sup>47</sup>. Gold colloids have also been investigated as SERS-active media<sup>42, 48</sup>. Because gold is virtually bioinert, it may prove to be a valuable material for biomedical applications of SERS. Furthermore, gold produces large SERS enhancement factors when near-IR excitation sources are used. Near-IR excitation radiation is particularly useful in biomedical studies because it allows greater penetration depths in tissues while causing less fluorescence background relative to visible radiation.

### 4.3 Solid SERS Substrates Based on Metallic Nanostructures

In addition to immobilized colloids, researchers have developed a variety of solid-surface-based SERS substrates that are produced entirely from solid materials, as depicted schematically in Figure 3. In contrast to immobilized colloids, the solid SERS-based probes described in this section exhibit a high degree of reproducibility. Also, nanoshells with a dielectric core and a metallic shell (e.g.,  $\text{Au/SiO}_2$ ), or a metallic core and a dielectric shell (e.g.,  $\text{SiO}_2@Au$ ), or a metallic core and a metallic shell (e.g.,  $\text{Ag@Au}$ ), provide a tunable geometry in which the magnitude of the local electromagnetic field at the nanoparticle surface can be precisely controlled<sup>49-52</sup>.

#### 4.3.1 Metal Nanoparticle Island Films

Metallic nanostructured SERS substrates based on metal island films (Figure 3a) are among the most easily prepared surface-based media, granted the availability of a vacuum evaporation system. Such systems are commonly equipped with crystal microbalances for monitoring metal film thickness. Metal island films can be produced by depositing a thin (<10 nm) layer of a metal directly onto a smooth solid base support via sputter-deposition<sup>41</sup> or vacuum evaporation. At such a small thickness, the metal layer forms as aggregated, isolated metal islands, the size and shape of which can be influenced largely by the metal thickness, deposition rate, geometry, and temperature, as well as post-deposition annealing<sup>53,54</sup>. Silver island films have been characterized by combining scanning near-field optical microscopy (SNOM) with Raman spectroscopy, thereby achieving <70-nm resolution<sup>55</sup>. A disadvantage of metal island films is that they are

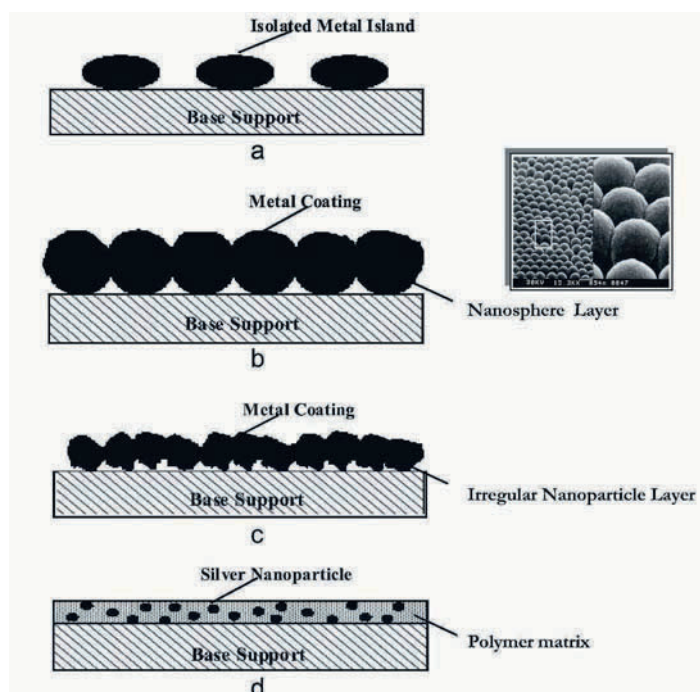


Figure 3. Various type of SERS active metallic nanostructures: (a) metal-island films; (b) metal-coated nanospheres (semi-nanoshells); (c) metal-coated random nanostructures; and (d) polymer coatings embedded with metal nanoparticles. Inset: An SEM image of silver-coated polystyrene spheres.

easily disturbed by solvents encountered in typical biomedical analyses<sup>56, 57</sup>. To minimize this disadvantage, buffer metal layers, (3-mercaptopropyl)-trimethoxysilane (MCTMS) layers, and organometallic paint layers have been applied to glass supports to stabilize gold island films<sup>58</sup>.

#### 4.3.2 Metal-Coated Nanosphere Substrates

In our laboratory, we have developed a very dependable solid-surface-based SERS substrate technology that can be generally described as metal-coated dielectric nanospheres (Figure 3b) supported by various planar support media. Nanospheres within a specific size range (e.g., 50–500 nm) are spin-coated on a solid support in order to produce the roughness required to induce the SERS effect. The resulting nanostructured plate is then coated with a layer of silver (50–150 nm), which provides the conduction electrons required for the surface plasmon mechanisms<sup>59-63</sup>. All factors of surface morphology are easily controlled, enabling high batch-to-batch reproducibility. An additional advantage is that the relatively thick layer of silver is less vulnerable to air oxidation than silver islands. Furthermore, the



surface is highly resistant to disturbance by sample solvents, making this type of SERS substrate very practical for biomedical applications. Teflon and latex are particularly well suited for SERS substrates because they are commercially available in a wide variety of sizes which can be selected for optimal enhancement.

#### 4.3.3 Metal-Coated Nanoparticle Substrates

Nanoparticles with irregular shapes (Figure 3c) can also be used in place of regularly shaped nanospheres in the production of dependable, cost-effective SERS substrates. Dielectric nanoparticle materials investigated in our laboratory have included alumina<sup>64</sup>, titanium dioxide<sup>65</sup>, and fumed silica<sup>66</sup>. The production of irregular nanoparticle-based substrates is achieved with an ease equivalent to that for nanosphere-based substrates described above. Generally, 5–10% (w/v) aqueous suspensions of the nanoparticles are spin-coated onto solid support media, then coated by 75–150 nm of silver via vacuum evaporation. As an alternative to the vacuum evaporation process, other groups have investigated silver coating via chemical processes<sup>67, 68</sup>. Nevertheless, substrates prepared via vacuum evaporation yield exceptional reproducibility<sup>69-77</sup>.

#### 4.3.4 SERS Substrates Based on Metal-Coated Quartz Posts

Silver-coated, regularly-spaced submicron posts formed in quartz substrates have proven to be a dependable, yet labor-intensive SERS substrate. Lithographic techniques have been used to control the surface roughness to a degree suitable for testing the electromagnetic model of SERS<sup>78, 79</sup>. While these surfaces produce a Raman enhancement on the order of  $10^7$ , they are difficult to produce with a large surface area. However, an alternative etching procedure for producing quartz posts overcomes this limitation by using an island film as an etching mask on a  $\text{SiO}_2$ <sup>80-84</sup>. A disadvantage of quartz post-based substrates is the difficult, time-consuming etching procedure required for post fabrication. Nevertheless, optimized quartz posts can serve as the base for a reusable SERS substrate, provided the silver coating is replaced between uses.

#### 4.3.5 SERS Substrates Based on Metal Nanoparticle-Embedded Media

Silver nanoparticles embedded in various solid porous media (Figure 3d) have recently been investigated as stable SERS substrates with the potential for selective detection. The in situ production of these nanoparticles in solid

matrices provides several advantages. For example, a solid matrix not only spatially stabilizes but also physically protects the colloids. In addition, the porosity of such materials as sol-gels, cellulose acetate gels, and polycarbonate films permits interaction of analyte compounds with the embedded metal nanoparticles. Furthermore, control of pore size and matrix polarity through simple chemical means (particularly when using the sol-gel technique) can impart selectivity. Finally, the chemical processes generally used to prepare such substrates make the SERS technique accessible for general analytical laboratories. A silver nanoparticle-embedded sol-gel substrate produced through the chemical reduction of silver halide particles distributed in the sol-gel matrix has been reported for the detection of neurotransmitters and dopamine<sup>85, 86</sup>.

## 4.4 Overcoatings on SERS Substrates

### 4.4.1 Self-Assembled Monolayer (SAM) Overcoatings

SAMs have proven to be a valuable factor in SERS substrate development and theoretical applications of SERS. For example, they have been used to immobilize SERS-active metal colloids on planar supports in a highly ordered fashion<sup>87-92</sup>. In fact, specific colloidal patterns have been prepared by microcontact printing of SAMs on planar surfaces before exposure to SERS-active colloids<sup>89</sup>. SAMs have also been used for the production of UV-induced SERS-active photopatterns on silver films coated with *p*-nitrophenol<sup>103</sup>. In more fundamental studies, the inherent SERS signals of SAMs have been used to evaluate the surface uniformity of SERS probe surfaces, including electrochemically roughened gold electrodes and immobilized gold colloids<sup>92</sup>. The application of SAMs to SERS substrate surfaces also allows selective detection. For example, SAMs of mercaptoalkalinic acids on colloidal silver substrates have been used for the SERS detection of selectively adsorbed cytochrome *c*<sup>93</sup> and have formed the basis for anchoring capture DNA probes for SERS-active hybridization platforms<sup>94</sup>. Monolayers of cysteamine on silver SERS substrates have also been reported<sup>95, 96</sup>. Such monolayers could promote the selective adsorption of proteins.

### 4.4.2 Bioreceptor Monolayer Overcoating

The potential use of SERS in biodiagnostic tests has been demonstrated through the use of immobilized monolayers of bioreceptors, including oligonucleotides and antibodies. The use of surface-enhanced Raman gene

(SERG) probes for medical diagnostics<sup>97-100</sup> is covered in greater detail in following sections.

Antibody monolayers have also been the basis of SERS detection with molecular selectivity<sup>102, 115</sup>, thus demonstrating the potential for SERS in immunoassays. In one study, Nie and coworkers demonstrated the simultaneous detection of two antigens in a single sandwich immunoassay using two reporter molecules<sup>103</sup>. Capture antibodies selective for the target antigens were bound to gold colloids. The capture antibody-coated colloids were then exposed to a mixture of target antigens. Finally reporter antibodies specific to the immobilized target antigens were immobilized on the colloid via interaction with the target antigens. SERS-active markers on the reporter antibodies permitted ultrasensitive detection of the immobilized antigens. Each antigen was assigned a different marker, yet both reporters could be detected in a single measurement because of minimal overlap of the respective Raman spectra. In another study, Dou and coworkers demonstrated the potential for a SERS-based immunoassay with no need for reporter molecules<sup>102</sup>. Instead, they monitored the native SERS signatures of anti-mouse IgG antibodies adsorbed on gold nanoparticles. Because of the structure-specific nature of Raman scattering, they were able to directly confirm conjugation with antigens through the observation of changes in relative intensities of spectral features of the IgG spectrum. Neither reporter probes nor rinsing steps to remove unbound antigens were required in this assay.

## 5. EXAMPLES FOR SERS APPLICATION

### 5.1 SERS as an Immunoassay Readout Method

Immunoassays have also received considerable interest for more than a decade. For example, an early example of a SERS-based immunoassay was reported by Rohr and coworkers in 1989<sup>104</sup>. The same year, Grabbe and Buck reported on SERS studies of native human immunoglobulin-G<sup>117</sup>. More recently, SERS signatures of native antibodies have been the basis for a simplified immunoassay in which conjugation of the antibody with a target antigen was confirmed through observance of alterations of the SERS spectrum for the native antibody<sup>102</sup>.

As an alternative, extremely sensitive detection can be achieved with reporter antibody probes tagged with intensely SERS-active compounds or with enzymes that react with substrates to yield SERS-active products. These methods often involve sandwich immunoassay techniques, which increase the number of required steps but offer the advantages of excellent sensitivity and the potential for “label multiplexing.” For example, Nie and coworkers recently reported the simultaneous detection of two types of antigens in a

single assay by using two reporter antibodies<sup>103</sup>. The labels of the reporter probes yielded SERS spectral features with minimal overlap, permitting exploitation of a label multiplex advantage. In a sandwich assay format, one set of antibodies immobilized the target antigens on gold colloids while the reporter antibody probes were subsequently immobilized at allosteric sites of the target antigens.

In other studies, reporter antibodies have been tagged with the enzyme peroxidase<sup>106, 107</sup>. Once the peroxidase-labeled antigen was immobilized on the target, it could be exposed to the substrates, *o*-phenylenediamine and hydrogen peroxide. A sustained reaction of the enzyme with a multitude of substrate molecules yielded an extremely high yield of the SERS-active product, azoaniline. This method has thus far been limited to sandwich immunoassay formats. For example, in a study to detect membrane-bound enzymes in cells, cells were first exposed to primary antibodies specific to the membrane-bound enzymes, then exposed to a peroxidase-tagged reporter antibody specific to the primary antibody<sup>106</sup>. A format which uses a capture antibody to immobilize a target antigen, and a reporter antibody to bind to a different antigenic site of the immobilized target antigen, has also been reported<sup>107</sup>.

Recently successful detection of immunoglobulins using gold nanoshells was achieved in saline, serum, and whole blood<sup>108</sup>. This system constitutes of a simple immunoassay capable of detecting sub-nanogram-per-milliliter quantities of various analytes in different media within 10-30 min. Innovative results have also been reported by Mulvaney et al<sup>109</sup>, who prepared "glass-coated, analyte-tagged" nanoparticles for use in multiplexed bioassays. Recently Nie et al. reported an improved class of core-shell colloidal nanoparticles that are highly efficient for SERS and are suitable for multiplexed detection and spectroscopy at the single-particle level. The core-shell structure contains a metallic core for optical enhancement, a reporter molecule for spectroscopic signature, and an encapsulating silica shell for protection and conjugation. With nearly optimized gold cores and silica shells, the core-shell nanoparticles are stable in both aqueous electrolytes and organic solvents, yielding intense single-particle SERS spectra<sup>110</sup>.

## 5.2 SERS Gene Probes

Over the last few years, there has been a great deal of interest in the development of optical techniques for genomics analysis such as nonradioactive DNA probes for use in biomedical diagnostics, pathogen detection, gene identification, gene mapping, and DNA sequencing. The hybridization of a nucleic acid probe to DNA biotargets (e.g., gene sequences, bacteria, viral DNA) permits a very high degree of accuracy in identifying DNA sequences complementary to that probe. The possibility of

using SERS for low-level detection of DNA bases and oligonucleotides was demonstrated in several studies in the 1980s<sup>111-114</sup>. More recently, the possibility of using Raman and/or SERS labels for extremely sensitive detection of DNA has been demonstrated. For example, Graham and coworkers have claimed adequate sensitivity for single-molecule DNA detection via surface-enhanced resonance Raman scattering (SERRS)<sup>101</sup>. With the use of labeled DNA as gene probes, the SERS technique has been recently applied to the detection of DNA fragments of the human immunodeficiency virus (HIV)<sup>100</sup> as well as B-cell lymphoma 2 gene<sup>98</sup>.

A critical aspect of sequencing the entire human genome involves defining and identifying large insert clones of DNA corresponding to specific regions of the human genome. An approach that facilitates large-scale genomic sequencing involves developing maps of human chromosomes into maps based on large insert bacterial clones, such as bacterial artificial chromosomes (BACs)<sup>115-116</sup>. In our laboratory, we developed one of its first kind of gene probes based on SERS<sup>97-100</sup>. In the production of SERG probes, SERS-active dye labels can be attached to oligonucleotide primers used in polymerase chain reaction (PCR) amplification of specific target DNA sequences. Following PCR, the resulting labeled amplicons from the targeted DNA region of interest can be denatured, allowing hybridization of specific, single-stranded, labeled DNA to oligonucleotide capture probes, which can be immobilized on solid supports<sup>100</sup>. Contact with SERS-active media permits subsequent detection of the SERG probe. This method combines the high sensitivity of the SERS technique with the inherent molecular specificity offered by DNA sequence hybridization. A time-saving method for detecting multiple BAC-clone-labeled probes simultaneously would be especially appealing for the BAC approach to genome sequencing and mapping. The SERS technique can provide this label-multiplex capability. The SERS gene probes described in this section preclude the need for radioactive labels and have great potential to provide both sensitivity, selectivity, and label multiplexing for DNA sequencing as well as clinical assays (Figure 4).

### 5.3 Near-Field Scanning Optical Microscopy (NSOM) SERS Probes

Near-field scanning optical microscopy (NSOM) is a methodology for obtaining subwavelength resolution (20-200 nm) with the spectroscopic information afforded by conventional optical spectroscopic techniques<sup>131,132</sup>. The high spatial resolution of NSOM permits spectroscopic studies of individual biomolecules in high density systems such as encountered in *in vivo* experiments<sup>9, 121, 122</sup>. In this respect, NSOM combined with a Raman microscope is particularly attractive. So far this novel scanning probe

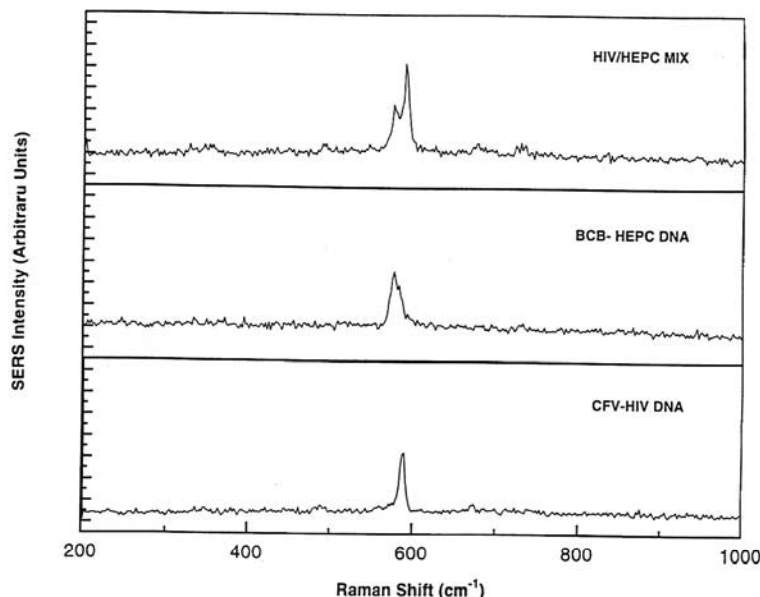


Figure 4. Simultaneous detection of HIV and Hepcidin (HEPC) SERS gene probe hybridizations.

technique has been restricted to fluorescence and luminescence spectroscopy. With the use of SERS and tapered single-mode fiber probes, near-field Raman spectra have been obtained from single silver nanoparticles with excitation intensities as low as 10 nW<sup>123</sup>. Recently, the combination of SNOM and SERS to obtain spectral, spatial, and chemical information of molecular adsorbates with subwavelength lateral resolution was reported<sup>9,10</sup>. Near-field SERS spectra of cresyl fast violet and rhodamine 6G on silver substrates have been obtained. Spectra from as few as 300 molecules or less than 10<sup>-2</sup> monolayers adsorbed on about ten silver nanoparticles can be recorded.

#### 5.4 SERS as a Tool for Single-Molecule Detection

There have been several reports of single-molecule detection using SERS in recent years<sup>6-9, 101, 124, 125</sup>. A critical factor in these milestone studies has been the development of exceptional SERS substrates. Most of the reports of single-molecule SERS detection have involved the use of metal colloids in suspensions. For example, Kneipp and coworkers demonstrated single-molecule detection of crystal violet in both silver<sup>7</sup> and colloid suspensions<sup>8</sup>. In these studies, an effective cross section of approximately 10<sup>-16</sup> cm<sup>2</sup> per molecule was observed, corresponding to a 10<sup>14</sup> enhancement factor. The gold nanoparticles were commercially available, but required proper

agglomeration through the addition of sodium chloride. These results are promising because these cyanine dyes could be used as bioassay markers.

In some cases, bioassay markers can be resonance-enhanced in addition to benefiting from SERS. For example, a DNA marker, 2,5,1',3',7',9'-hexachloro-6-carboxyfluorescein (HEX) has been used to achieve single-molecule detection via surface-enhanced resonance Raman scattering (SERRS) in a silver colloid suspension<sup>101</sup>. The HEX signature was observed for  $8 \times 10^{-13}$  M DNA, which corresponded to less than 1 molecule per probed volume at any time required for measurement. Single-molecule detection has also been demonstrated on planar surface-based substrates. For example, enhancements to factors of  $10^{14}$  to  $10^{15}$  have been observed for rhodamine-6G molecules adsorbed on silver colloids that had been immobilized on a polylysine-coated glass surface.<sup>6</sup> Similarly,  $10^{14}$  to  $10^{15}$  factor enhancements have been reported for hemoglobin molecules adsorbed on silver nanoparticles immobilized on a polymer-coated silicon wafer.<sup>124</sup> Researchers in this study reported, however, that single-molecule detection was observed only for hemoglobin molecules situated between and adsorbed to two silver nanoparticles.

## 5.5 SERS Nanoprobes for Intracellular Analysis

Direct observation of single molecules and single molecular events inside living cells could dramatically improve our understanding of basic cellular processes (e.g., signal transduction and gene transcription) as well as improving our knowledge of the intracellular transport and fate of therapeutic agents (e.g., antisense RNA and gene therapy vectors)<sup>94,126</sup>. Therefore, it is very important to develop techniques to measure the reactions of individual molecules in living cells with spatio-temporal resolution (Kneipp et al. 2002)<sup>127</sup>.

The feasibility of measuring SERS of native constituents with a single viable cell using 60 nm gold particles has been demonstrated recently,<sup>127</sup> where SERS mapping over a cell monolayer with 1  $\mu\text{m}$  lateral resolution shows different Raman spectra at almost all places, reflecting the very inhomogeneous chemical organization of the cells. In order to identify cellular constituents at the single molecule-level within single cells, it is clear that many parameters such as excitation wavelength, nanoparticle size, and state of aggregation still need to be optimized.

## 6. CONCLUSIONS

The development of dependable SERS active metallic nanostructures has spurred renewed interest in Raman scattering as a practical analytical tool in

areas such as medical, environmental, public health, and homeland defense. Both liquid- and solid-based SERS-inducing media are now being used for the detection of important environmental and biological compounds; moreover, innovative SERS-based biomedical applications such as gene probes are being developed. The development of such substrates and their use in practical analytical applications has required a triumph over the daunting challenge of producing nanoscale structures in reproducible and cost-effective ways. A significant portion of recent efforts has been devoted towards investigating SERS coatings to improve selectivity, longevity, and ruggedness. The Raman technique is well known for its high selectivity. With the advances of fiber optic technology, the SERS technique, which amplifies the Raman signal by several orders of magnitude, can provide a remote sensing technique with the added merit of improved sensitivity due to the surface-enhanced scattering effect. It is expected that the current development of SERS-active nanostructures will open new horizons for remote in-situ chemical sensors and biosensors for environmental and biological applications.

## ACKNOWLEDGEMENTS

This work was sponsored by the Federal Bureau of Investigation (Project No. 2051-II18-Y1) and the Office of Biological and Environmental Research, U.S. Department of Energy, under Contract DE-AC05-00OR22725 with UT-Battelle, LLC, and by the Laboratory Directed Research and Development Program (Advanced Plasmonic Sensors Project) at Oak Ridge National Laboratory. Fei Yan is also supported by an appointment to the Oak Ridge National Laboratory Postdoctoral Research Associates Program, administered jointly by the Oak Ridge National Laboratory and Oak Ridge Institute for Science and Education.

## REFERENCES

1. Raman C.V., Krishnan K.S., A new type of secondary radiation, *Nature* 1928; 121: 501-502.
2. Fleischm M., Hendra P. J., McQuilla. A. J., Raman-spectra of pyridine adsorbed at a silver electrode, *Chem. Phys. Lett.* 1974; 26: 163-166.
3. Jeanmaire D.L., Vanduyne R.P., Surface Raman spectro-electrochemistry .I. Heterocyclic, aromatic, and aliphatic-amines adsorbed on anodized silver electrode, *J. Electroanal. Chem.* 1977; 84: 1-20.
4. Albrecht M.G., Creighton J.A., Anomalously intense Raman-spectra of pyridine at a silver electrode, *J. Am. Chem. Soc.* 1977; 99: 5215-5217.
5. Vo-Dinh T., Hiromoto M.Y.K., Begun G.M., Moody R. L., Surface-enhanced Raman spectrometry for trace organic-analysis, *Anal. Chem.* 1984; 56: 1667-1670.



6. Nie S.M., Emory S.R., Probing single molecules and single nanoparticles by surface-enhanced Raman scattering, *Science* 1997; 275: 1102-1106.
7. Kneipp K., Wang Y., Kneipp H., Perelman L.T., Itzkan I., Dasari R., Feld M.S., Single molecule detection using surface-enhanced Raman scattering (SERS), *Phys. Rev. Lett.* 1997; 78: 1667-1670.
8. Kneipp K., Kneipp H., Deinum G., Itzkan I., Dasari R.R., Feld M. S., Single-molecule detection of a cyanine dye in silver colloidal solution using near-infrared surface-enhanced Raman scattering, *Appl. Spectrosc.* 1998; 52: 175-178.
9. Deckert V., Zeisel D., Zenobi R., Vo-Dinh T., Near-field surface enhanced Raman imaging of dye-labeled DNA with 100-nm resolution, *Anal. Chem.* 1998; 70: 2646-2650.
10. Zeisel D., Deckert V., Zenobi R., Vo-Dinh T., Near-field surface-enhanced Raman spectroscopy of dye molecules adsorbed on silver island films, *Chem. Phys. Lett.* 1998; 283: 381-385.
11. Moskovits M., Surface-enhanced spectroscopy, *Reviews of Modern Physics* 1985; 57: 783-826.
12. Wokaun A., Surface-enhanced electromagnetic processes, *Solid State Physics-Advances in Research and Applications* 1984; 38: 223-294.
13. Schatz G.C., Theoretical-Studies of Surface Enhanced Raman-Scattering, *Accounts Chem. Res.* 1984; 17: 370-376.
14. Kerker M., Electromagnetic Model for surface-Enhanced Raman-Scattering (Sers) on Metal Colloids, *Accounts Chem. Res.* 1984; 17: 271-277.
15. Chang R.K., Furtak T.E., *Surface Enhanced Raman Scattering*. Plenum Press, New York, 1982.
16. Garrell R. L., Surface-enhanced Raman-spectroscopy, *Anal. Chem.* 1989; 61: A401-&.
17. Vo-Dinh T., Surface-Enhanced Raman Spectrometry, in *Chemical Analysis of Polycyclic Aromatic Compounds*, Vo-Dinh T. ed., Wiley, New York (1989).
18. Pemberton J.E. in *Electrochemical Interfaces: Modern Techniques for In-Situ Characterization*, Abruna H.D. ed., VCH Verlag Chemi, Berlin, 1991.
19. Cotton T.M., Brandt E.S. in *Physical Methods of Chemistry*, Wiley, New York, 1992.
20. Otto A., Mrozek I., Grabhorn H., Akemann W., Surface-Enhanced Raman-Scattering, *Journal of Physics-Condensed Matter* 1992; 4: 1143-1212.
21. Vo-Dinh T., Surface-Enhanced Raman Spectroscopy, in *Photonic Probes of Surfaces*, Halevi P. ed., Elsevier, New York, 1995.
22. Ruperez A., Laserna J.J. , Surface-Enhanced Raman Spectroscopy, in *Modern techniques in Raman Spectroscopy*, Laserna J.J. ed., Wiley, New York, 1996, pp. 227-264.
23. Haller K.L., Bumm L.A., Altkorn R.I., Zeman E.J., Schatz G.C., Vanduyne R.P., Spatially resolved surface enhanced 2nd harmonic-generation - theoretical and experimental-evidence for electromagnetic enhancement in the near-Infrared on a laser microfabricated Pt surface, *J. Chem. Phys.* 1989; 90: 1237-1252.
24. Golab J.T., Sprague J.R., Carron K.T., Schatz G.C., Vanduyne R.P., A surface enhanced hyper-Raman scattering study of pyridine adsorbed onto silver - experiment and theory, *J. Chem. Phys.* 1988; 88: 7942-7951.
25. Vo-Dinh T., Stokes D.L., Griffin G.D., Volkan M., Kim U.J., Simon M.I., Surface-enhanced Raman scattering (SERS) method and instrumentation for genomics and biomedical analysis, *J. Raman Spectrosc.* 1999; 30: 785-793.
26. Nabiev I., Manfait M., Industrial applications of the surface-enhanced Raman-spectroscopy, *Revue De L Institut Francais Du Petrole* 1993; 48: 261-285.
27. Nabiev, I., Chourpa, I., and Manfait, M. (1994) Applications of Raman and surface-enhanced Raman-scattering spectroscopy in medicine, *J. Raman Spectrosc.* 25, 13-23.
28. Kneipp K., Kneipp H., Itzkan I., Dasari R.R., Feld M.S., Surface-enhanced Raman scattering: A new tool for biomedical spectroscopy, *Curr. Sci.* 1999; 77: 915-924.

29. Koglin E., Sequaris J.M., Surface enhanced Raman-scattering of biomolecules, *Topics Curr. Chem.* 1986; 134: 1-57.
30. Pemberton J.E., Buck R.P., Detection of low concentrations of a colored adsorbate at silver by surface-enhanced and resonance-enhanced Raman spectrometry, *Anal. Chem.* 1981; 53: 2263-2267.
31. Pettinger B., Wenning U., Wetzel H., Surface-plasmon enhanced Raman-scattering frequency and angular resonance of Raman scattered-light from pyridine on Au, Ag and Cu electrodes, *Surf. Sci.* 1980; 101: 409-416.
32. Loo B.H., Surface-enhanced Raman-spectroscopy of platinum .2. Enhanced light-scattering of chlorine adsorbed on platinum, *J. Phys. Chem.* 1983; 87: 3003-3007.
33. Fleischmann M., Graves P.R., Robinson J., The Raman-spectroscopy of the ferricyanide ferrocyanide system at gold, beta-palladium hydride and platinum-electrodes, *J. Electroanal. Chem.* 1985; 182: 87-98.
34. Carrabba M.M., Edmonds R.B., Rauh, R.D., Feasibility studies for the detection of organic-surface and subsurface water contaminants by surface-enhanced Raman-spectroscopy on silver electrodes, *Anal. Chem.* 1987; 59: 2559-2563.
35. Ren B., Lin X.F., Yang Z.L., Liu G.K., Aroca R.F., Mao B.W., Tian, Z.Q., Surface-enhanced Raman scattering in the ultraviolet spectral region: UV-SERS on rhodium and ruthenium electrodes, *J. Am. Chem. Soc.* 2003; 125: 9598-9599.
36. Yang Z.L., Wu D.Y., Yao J.L., Hu J.Q., Ren B., Zhou H.G., Tian, Z.Q., SERS mechanism of nickel electrode, *Chinese Sci. Bull.* 2002; 47: 1983-1986.
37. Tian Z.Q., Ren B., Wu D.Y., Surface-enhanced Raman scattering: From noble to transition metals and from rough surfaces to ordered nanostructures, *J. Phys. Chem. B* 2002; 106: 9463-9483.
38. Thierry D., Leygraf C., The influence of photoalteration on surface-enhanced Raman-scattering from copper electrodes, *Surf. Sci.* 1985; 149: 592-600.
39. Creighton J.A., Blatchford C.B., Albrecht M.C., Plasma resonance enhancement of Raman-scattering by pyridine adsorbed on silver or gold sol particles of size comparable to the excitation wavelength, *J. Chem. Soc. Faraday Trans.* 1979; 2: 790-798.
40. Sheng R.S., Zhu L., Morris, M.D., Sedimentation classification of silver colloids for surface-enhanced Raman-scattering, *Anal. Chem.* 1986; 58: 1116-1119.
41. Ni F., Sheng R.S., Cotton T.M., Flow-injection analysis and real-time detection of RNA bases by surface-enhanced Raman-spectroscopy, *Anal. Chem.* 1990; 62: 1958-1963.
42. Lee P.C., Meisel D., Adsorption and surface-enhanced Raman of dyes on silver and gold sols. *J. Phys. Chem.* 1982; 86: 3391-3395.
43. Munro C.H., Smith W.E., Garner M., Clarkson J., White P.C., Characterization of the surface of a citrate-reduced colloid optimized for use as a substrate for surface-enhanced resonance Raman-scattering, *Langmuir* 1995; 11: 3712-3720.
44. Tarabara V.V., Nabiev I.R., Feofanov A.V., Surface-enhanced Raman scattering (SERS) study of mercaptoethanol monolayer assemblies on silver citrate hydrosol. Preparation and characterization of modified hydrosol as a SERS-active substrate, *Langmuir* 1998; 14: 1092-1098.
45. Li Y.S., Cheng J.C., Coons L.B., A silver solution for surface-enhanced Raman scattering, *Spectrochimica Acta Part A* 1999; 55: 1197-1207.
46. Ahern A.M., Garrell R.L., In situ photoreduced silver-nitrate as a substrate for surface-enhanced Raman-spectroscopy, *Anal. Chem.* 1987; 59: 2813-2816.
47. Prochazka M., Mojzes P., Stepanek J., Vlckova B., Turpin P.Y., Probing applications of laser ablated Ag colloids in SERS spectroscopy: Improvement of ablation procedure and SERS spectral testing, *Anal. Chem.* 1997; 69: 5103-5108.
48. Hildebrandt P., Stockburger M., Surface-enhanced resonance Raman-spectroscopy of rhodamine-6G adsorbed on colloidal silver, *J. Phys. Chem.* 1984; 88: 5935-5944.
49. Cao Y.W., Jin R., Mirkin C.A., DNA-modified core-shell Ag/Au nanoparticles, *J. Am. Chem. Soc.* 2001; 123: 7961-7962.

50. Pham T., Jackson J.B., Halas N.J., Lee T.R., Preparation and characterization of gold nanoshells coated with self-assembled monolayers, *Langmuir* 2002; 18: 4915-4920.
51. Graf C., Van Blaaderen A., Metallodielectric colloidal core-shell particles for photonic applications, *Langmuir* 2002; 18: 524-534.
52. Jackson J.B., Westcott S.L., Hirsch L.R., West J.L., Halas N.J., Controlling the surface enhanced Raman effect via the nanoshell geometry, *Appl. Phys. Lett.* 2003; 82: 257-259.
53. Vanduyne R.P., Hulteen J.C., Treichel D.A., Atomic-force microscopy and surface-enhanced Raman-spectroscopy.1. Ag island films and Ag film over polymer nanosphere surfaces supported on glass, *J. Chem. Phys.* 1993; 99: 2101-211.
54. Semin D.J., Rowlen K.L., Influence of vapor-deposition parameters on SERS active Ag film morphology and optical-properties, *Anal. Chem.* 1994; 66: 4324-4331.
55. Stockle R.M., Deckert V., Fokas C., Zeisel D., Zenobi R., Sub-wavelength Raman spectroscopy on isolated silver islands, *Vibrational Spectrosc.* 2000; 22, 39-48.
56. Roark S.E., Rowlen K.L., Thin Ag Films - influence of substrate and postdeposition treatment on morphology and optical-properties, *Anal. Chem.* 1994; 66: 261-270.
57. Roark S.E., Semin D.J., Lo A., Skodje R.T., Rowlen K.L., Solvent-induced morphology changes in thin silver films, *Anal. Chim. Acta* 1995; 307: 341-353.
58. Mosier-Boss P.A., Lieberman S.H., Comparison of three methods to improve adherence of thin gold films to glass substrates and their effect on the SERS response, *Appl. Spectrosc.* 1999; 53: 862-873.
59. Meier M., Wokaun A., Vo-Dinh T., Silver particles on stochastic quartz substrates providing tenfold increase in Raman enhancement, *J. Phys. Chem.* 1985; 89: 1843-1846.
60. Goudonnet J.P., Begun G.M., Arakawa E.T., Surface-enhanced Raman-scattering on silver-coated Teflon sphere substrates, *Chem. Phys. Lett.* 1982; 92: 197-201.
61. Alak A.M., Vo-Dinh T., Silver-coated fumed silica as a substrate material for surface-enhanced Raman-scattering, *Anal. Chem.* 1989; 61: 656-660.
62. Moody R.L., Vo-Dinh T., Fletcher W.H., Investigation of experimental parameters for surface-enhanced Raman-scattering (SERS) using silver-coated microsphere substrates, *Appl. Spectrosc.* 1987; 41: 966-970.
63. Alak A.M., Vo-Dinh T., Surface-enhanced Raman spectrometry of chlorinated pesticides, *Anal. Chim. Acta* 1988; 206: 333-337.
64. Bello J.M., Stokes D.L., Vo-Dinh T., Silver-coated alumina as a new medium for surface-enhanced Raman-scattering analysis, *Appl. Spectrosc.* 1989; 43: 1325-1330.
65. Bello J.M., Stokes D.L., Vo-Dinh T., Titanium-dioxide based substrate for optical monitors in surface-enhanced Raman-scattering analysis, *Anal. Chem.* 1989; 61: 1779-1783.
66. Alak A.M., Vo-Dinh T., Surface-enhanced Raman-spectrometry of organophosphorus chemical-agents, *Anal. Chem.* 1987; 59: 2149-2153.
67. Li Y.S., Vo-Dinh T., Stokes D.L., Yu W., Surface-enhanced Raman analysis of p-nitroaniline on vacuum evaporation and chemically deposited silver-coated alumina substrates, *Appl. Spectrosc.* 1992; 46: 1354-1357.
68. Li Y.S., Wang Y., Chemically prepared silver alumina substrate for surface- enhanced Raman-scattering, *Appl. Spectrosc.* 1992; 46: 142-146.
69. Helmenstine A.M., Li Y.S., Vo-Dinh T., Surface-enhanced Raman-scattering analysis of etheno adducts of adenine, *Vibrational Spectrosc.* 1993; 4: 359-364.
70. Helmenstine A., Uziel M., Vo-Dinh T., Measurement of DNA-adducts using surface-enhanced Raman- spectroscopy, *J.Toxicol. Environ. Health* 1993; 40: 195-202.
71. Vo-Dinh T., Stokes D.L., Surface-enhanced Raman vapor dosimeter, *Appl. Spectrosc.* 1993; 47: 1728-1732.
72. Alarie J.P., Stokes D.L., Sutherland W.S., Edwards A.C., Vo-Dinh T., Intensified charge coupled device-based fiberoptic monitor for rapid remote surface-enhanced Raman-scattering sensing, *Appl. Spectrosc.* 1992; 46: 1608-1612.

73. Narayanan V.A., Begun G.M., Bello J.M., Stokes D.L., Vo-Dinh T., Analysis of the plant-growth regulator alar (daminozide) and its hydrolysis products using raman-spectroscopy, *Analisis* 1993; 21: 107-112.
74. Narayanan V.A., Begun G.M., Stump N.A., Stokes D.L., Vo-Dinh T., Vibrational-Spectra of Fluvalinate, *J. Raman Spectrosc.* 1993; 24: 123-128.
75. Narayanan V.A., Stokes D.L., Vo-Dihn T., Vibrational spectral-analysis of eosin-y and erythrosin-b - intensity studies for quantitative detection of the dyes, *J. Raman Spectrosc.* 1994; 25: 415-422.
76. Vo-Dinh T., Houck K., Stokes D.L., Surface-enhanced Raman gene probes, *Anal. Chem.* 1994; 66: 3379-3383.
77. Vo-Dinh T., Miller G.H., Bello J., Johnson R., Moody R.L., Alak A., Fletcher W. R., Surface-active substrates for Raman and luminescence analysis, *Talanta* 1989; 36: 227-234.
78. Wachter E.A., Storey J.M.E., Sharp S.L., Carron K.T., Jiang Y., Hybrid substrates for real-time sers-based chemical sensors, *Appl. Spectrosc.* 1995; 49: 193-199.
79. Liao P. F. in *Surface Enhanced Raman Scattering*, Chang R. K., Furtak T.E. eds., Plenum Press, New York, 1982, 379.
80. Vo-Dinh T., Hiromoto M.Y.K., Begun G.M., Moody R.L., Surface-enhanced Raman spectrometry for trace organic-analysis, *Anal. Chem.* 1984; 56: 1667-1670.
81. Meier M., Wokaun A., Vo-Dinh T., Silver particles on stochastic quartz substrates providing tenfold increase in Raman enhancement, *J. Phys. Chem.* 1985; 89: 1843-1846.
82. Vo-Dinh T., Meier M., Wokaun, A., Surface-enhanced Raman-spectrometry with silver particles on stochastic-post substrates. *Anal. Chim. Acta* 1986; 181: 139-148.
83. Liao P.F., Stern M.B., Surface-enhanced Raman-scattering on gold and aluminum particle arrays, *Opt. Lett.* 1982; 7: 483-185.
84. Enlow P.D., Buncick M., Warmack R.J., Vo-Dinh T., Detection of nitro polynuclear aromatic-compounds by surface- enhanced raman-spectrometry, *Anal. Chem.* 1986; 58: 1119-1123.
85. Volkan M., Stokes D.L., Vo-Dinh T., A new surface-enhanced Raman scattering substrate based on silver nanoparticles in sol-gel, *J. Raman Spectrosc.* 1999; 30: 1057-1065.
86. Volkan M., Stokes D.L., Vo-Dihn T., Surface-enhanced Raman of dopamine and neurotransmitters using sol-gel substrates and polymer-coated fiber-optic probes, *Appl. Spectrosc.* 2000; 54: 1842-1848.
87. Fu X.Y., Mu T., Wang J., Zhu T., Liu Z.F., pH-dependent assembling of gold nanoparticles on p- aminothiophenol modified gold substrate, *Acta Physico-Chimica Sinica* 1998; 14: 968-974.
88. Zhu T., Zhang X., Wang J., Fu X.Y., Liu Z.F., Assembling colloidal Au nanoparticles with functionalized self- assembled monolayers. *Thin Solid Films* 1998; 329: 595-598.
89. He H.X., Zhang H., Li Q.G., Zhu T., Li S.F.Y., Liu Z.F., Fabrication of designed architectures of Au nanoparticles on solid substrate with printed self-assembled monolayers as templates, *Langmuir* 2000; 16: 3846-3851.
90. Wang K., Li Y.S., Silver doping of polycarbonate films for surface-enhanced Raman scattering, *Vibrational Spectrosc.* 1997; 14: 183-188.
91. Yang X.M., Tryk D.A., Ajito K., Hashimoto K., Fujishima A., Surface-enhanced Raman scattering imaging of photopatterned self-assembled monolayers, *Langmuir* 1996; 12: 5525-5527.
92. Zhu T., Yu H.Z., Wang J., Wang Y.Q., Cai S.M., Liu Z.F., Two-dimensional surface enhanced Raman mapping of differently prepared gold substrates with an azobenzene self-assembled monolayer, *Chem. Phys. Lett.* 1997; 265: 334-340.
93. Maeda Y., Yamamoto H., Kitano H., Self-assembled monolayers as novel biomembrane mimetics .1. Characterization of cytochrome-c bound to self-assembled monolayers on

- silver by surface-enhanced resonance Raman- spectroscopy, *J. Phys. Chem.* 1995; 99: 4837-4841.
94. Vo-Dinh T., Allain L.R., Stokes D.L., Cancer gene detection using surface-enhanced Raman scattering (SERS), *J. Raman Spectrosc.* 2002; 33: 511-516.
  95. Michota A., Kudelski A., Bukowska J., Chemisorption of cysteamine on silver studied by surface-enhanced Raman scattering, *Langmuir* 2000; 16: 10236-10242.
  96. Michota A., Kudelski A., Bukowska J., Influence of electrolytes on the structure of cysteamine monolayer on silver studied by surface-enhanced Raman scattering, *J. Raman Spectrosc.* 2001; 32: 345-350.
  97. Culha M., Stokes D., Allain L.R., Vo-Dinh T., Surface-enhanced Raman scattering substrate based on a self-assembled monolayer for use in gene diagnostics, *Anal. Chem.* 2003; 75: 6196-6201.
  98. Culha M., Stokes D., Vo-Dinh T., Surface-enhanced Raman scattering for cancer diagnostics: detection of the BCL2 gene, *Expert Rev. Mol. Diagn.* 2003; 3: 669-675.
  99. Vo-Dinh T., Stokes D.L., Griffin G.D., Volkan M., Kim U.J., Simon M.I., Surface-enhanced Raman scattering (SERS) method and instrumentation for genomics and biomedical analysis, *J. Raman Spectrosc.* 1999; 30: 785-793.
  100. Isola N.R., Stokes D.L., Vo-Dinh T., Surface enhanced Raman gene probe for HIV detection, *Anal. Chem.* 1998; 70: 1352-1356.
  101. Graham D., Smith W.E., Linacre A.M.T., Munro C.H., Watson N.D., White P.C., Selective detection of deoxyribonucleic acid at ultralow concentrations by SERRS, *Anal. Chem.* 1997; 69: 4703-4707.
  102. Dou X., Yamaguchi Y., Yamamoto H., Doi S., Ozaki Y., NIR SERS detection of immune reaction on gold colloid particles without bound/free antigen separation, *J. Raman Spectrosc.* 1998; 29: 739-742.
  103. Ni J., Lipert R.J., Dawson G.B., Porter M.D., Immunoassay readout method using extrinsic Raman labels adsorbed on immunogold colloids, *Anal. Chem.* 1999; 71: 4903-4908.
  104. Rohr T.E., Cotton T., Fan N., Tarcha P.J., Immunoassay employing surface-enhanced Raman-spectroscopy, *Anal. Biochem.* 1989; 182: 388-398.
  105. Grabbe E.S., Buck R.P., Surface-enhanced Raman-spectroscopic investigation of human immunoglobulin-g adsorbed on a silver electrode, *J. Am. Chem. Soc.* 1989; 111: 8362-8366.
  106. Hawi S.R., Rochanakij S., Adar F., Campbell W.B., Nithipatikom K., Detection of membrane-bound enzymes in cells using immunoassay and Raman microspectroscopy, *Anal. Biochem.* 1998; 259: 212-217.
  107. Dou X., Takama T., Yamaguchi Y., Yamamoto H., Ozaki Y., Enzyme immunoassay utilizing surface-enhanced Raman scattering of the enzyme reaction product, *Anal. Chem.* 1997; 69: 1492-1495.
  108. Hirsch L.R., Jackson J.B., Lee A., Halas N.J., West J.L., A whole blood immunoassay using gold nanoshells, *Anal. Chem.* 2003; 75: 2377-2381.
  109. Mulvaney S.P., Musick M.D., Keating C.D., Natan M.J., Glass-coated, analyte-tagged nanoparticles: A new tagging system based on detection with surface-enhanced Raman scattering, *Langmuir* 2003; 19: 4784-4790.
  110. Doering W.E., Nie S.M., Spectroscopic tags using dye-embedded nanoparticles and surface-enhanced Raman scattering, *Anal. Chem.* 2003; 75: 6171-6176.
  111. Sequaris J.M.L., Koglin E., Direct analysis of high-performance thin-layer chromatography spots of nucleic purine derivatives by surface-enhanced raman-scattering spectrometry, *Anal. Chem.* 1987; 59: 525-527.
  112. Koglin E., Sequaris J.M., Interaction of proflavine with DNA studied by colloid surface enhanced resonance Raman-spectroscopy, *J. Molecular Struct.* 1986; 141: 405-409.
  113. Koglin E., Sequaris J.M., Valenta P., Surface Raman-spectra of nucleic-acid components adsorbed at a silver electrode, *J. Molecular Struct.* 1980; 60: 421-425.

114. Koglin E., Sequaris J.M., Valenta P., Surface enhanced Raman-spectroscopy of nucleic-acid bases on Ag electrodes, *J. Molecular Struct.* 1982; 79: 185-189.
115. Kim U.J., Shizuya H., Deaven L., Chen X.N., Korenberg J.R., Simon M.I., Selection of a sublibrary enriched for a chromosome from total human bacterial artificial chromosome library using dna from flow-sorted chromosomes as hybridization probes. *Nucl. Acids. Res.* 1995; 23: 1838-1839.
116. Kim U.J., Birren B.W., Slepa, T., Mancino V., Boysen C., Kang H.L., Simon M.I., Shizuya H., Construction and characterization of a human bacterial artificial chromosome library. *Genomics* 1996; 34: 213-218.
117. Kim U.J., Shizuya H., Kang H.L., Choi S.S., Garrett C.L., Smink L.J., Birren B.W., Korenberg J.R., Dunham I., Simon M. I., A bacterial artificial chromosome-based framework contig map of human chromosome 22q, *PNAS* 1996; 93: 6297-6301.
118. Boncheva M., Scheibler L., Lincoln P., Vogel H., Akerman B., Design of oligonucleotide arrays at interfaces. *Langmuir* 1999; 15: 4317-4320.
119. Pohl D.W., Denk W., Lanz M., Optical Stethoscopy - Image Recording with Resolution  $\lambda/20$ , *Appl. Phys. Lett.* 1984; 44: 651-653.
120. Betzig E., Trautman J.K., Harris T.D., Weiner J.S., Kostelak R.L., Breaking the diffraction barrier - optical microscopy on a nanometric scale. *Science* 1991; 251: 1468-1470.
121. Bian R.X., Dunn R.C., Xie X.S., Single molecule emission characteristics in near-field microscopy. *Phys. Rev. Lett.* 1995; 75: 4772-4775.
122. Gresillon S., Aigouy L., Boccara A.C., Rivoal J.C., Quelin X., Desmarest C., Gadenne P., Shubin V.A., Sarychev A.K., Shalaev V.M., Experimental observation of localized optical excitations in random metal-dielectric films. *Phys. Rev. Lett.* 1999; 82: 4520-4523.
123. Emory S.R., Nie S, Surface-enhanced Raman spectroscopy on single silver nanoparticles. *Anal. Chem.* 1997; 69: 2631-2635.
124. Xu H.X., Bjerneld E.J., Kall M., Borjesson L., Spectroscopy of single hemoglobin molecules by surface enhanced Raman scattering, *Phys. Rev. Lett.* 1999; 83: 4357-4360.
125. Bjerneld E.J., Foldes-Papp Z., Kall M., Rigler R., Single-molecule surface-enhanced Raman and fluorescence correlation spectroscopy of horseradish peroxidase, *J. Phys. Chem. B* 2002; 106: 1213-1218.
126. Byassee T.A., Chan W.C.W., Nie S., Probing single molecules in dingle living cells, *Anal. Chem.* 2000; 72: 5606-5611.
127. Kneipp K., Haka A.S., Kneipp H., Badizadegan K., Oshizawa N.Y., Boone C., Shafer-Peltier K.E., Motz J.T., Dasari R.R., Feld M.S., Surface-enhanced Raman spectroscopy in single living cells using gold nanoparticles, *Appl. Spectrosc.* 2002; 56: 150-154.

## Chapter 13

# PLANAR WAVEGUIDING SYSTEMS FOR OPTICAL SENSING

Paul V. Lambeck and Hugo J.W.M. Hoekstra  
MESA+ -institute  
University of Twente  
POB 217, 7500 AE Enschede, The Netherlands

### 1. INTRODUCTION

Driving force of the research in Integrated Optics is the optical (tele-) communication, but in its slipstream a lot of research on Integrated Optical (IO-) sensors has been performed during last decade.

Vast majority of the optical sensing systems are of the modulation type and its functional structure can be sketched as in Figure 1.

In the sensing section a change of the parameter to be measured, the so-called measurand, causes a change of the spatial refractive index distribution inside this section. This may imply a change of the geometry and/or of a change of the optical properties (e.g. the refractive index) of one or more out of the constituting materials (physical cross-effects). As a result at least one out of the characteristics of a light beam which is sent through this section will also change and in the read-out section this change is converted into a

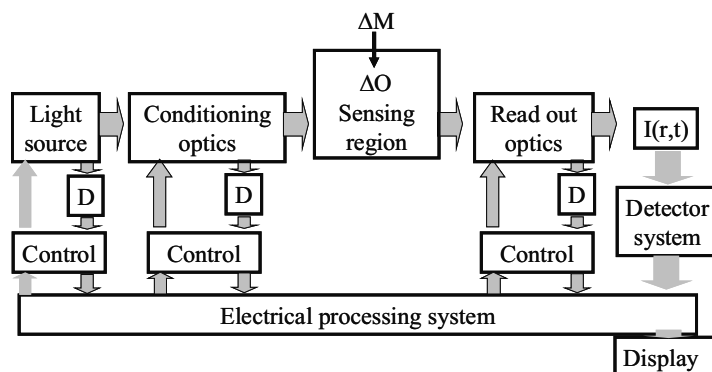


Figure 1. Functional structure of a sensing system of the modulation type.

change of the output power of the system. Opto-electronic detectors transfer the information to the electrical domain, where an electronic sub-system may take care of their proper processing. Electronics can also drive sub-functions of the read-out section or the conditioning section whether for control or for adjustment. In principle all optical sub-systems can be stand alone devices, optically interconnected whether by free space beams or by glass fibers.

For calling a sensor an integrated optical sensor at least the sensing section has to show an integrated optical structure. Often also the conditioning and the read-out sections are integrated optical and are integrated with the sensing section, forming a monolithically integrated optical chip. However in applications wherein a disposable sensing unit is required, the disposable part is held as cheap as possible and then the sensing section will be IO only and preferentially free space beams are used for its optical connection to the other sub-systems.

In some applications it is desired to integrate also light source, detector and sometimes even the electronics into this optical chip. This may be a hybrid integration, in which the individual components are packaged together, but there is a tendency also to consider monolithical integration of the whole sensing system for which generally the use of silicon substrates is required. IO sensors are very appropriate for forming a distributed sensor network consisting of a single light source, a single electronic subsystem and many optical chips which are interconnected by fibers.

Many integrated optical sensing systems have been designed, realized and tested in the laboratories but only a few of them have reached the market.

Development of a certain type of sensor may originate from market pull or from technology push. In case of market pull the sensor description (top-down approach) starts from a set of given specifications as to performance, maintenance, use and price. Requirements to the performance are generally expressed in terms of nature of the measurand, range, sensitivity, resolution, accuracy, selectivity, re-usability, the ability to in situ calibration, operating conditions, reliability, lifetime, etc. In case of technology push one starts (in a bottom-up approach) with a description in terms of principles, materials, technology and physical structures. Both extremes have to be interconnected by design, development, production and testing.

In this paper we approach the integrated optical sensors from the science/technological side. In that way it is avoided to discuss also all kinds of other competing sensing fields, in which the sensors are based on non-optical physical phenomena and are implemented as e.g. electrical, micromechanical or acoustical sensors.

Of course in defining application fields of certain types of IO sensors they have to be compared with competitors in the terms of the market. Strong points of optical sensors are no EMI, potential of high sensitivity and spectral discrimination. The guided mode character adds to these: no need of



adjustment of optical components before use and their smaller dimensions, while their microsystem nature is the source of the large freedom in the choice of materials and geometry, the small dimensions, the simultaneous production of all optical functions of the sensing system in one technological process consisting of a series of individual processing steps, the rigid structure and the prospect of making monolithical multi-sensing arrays.

In this paper we start with a short introduction in Integrated Optics (section 2), continue with an introduction into IO sensors (section 3), while main attention will be paid to treating (the design of) many types of refractive IO sensors (section 4). Finally in section 5 an epilogue is presented.

## 2. INTRODUCTION TO INTEGRATED OPTICS

Just as in glass fibers also in integrated optics<sup>1-3</sup> light is usually propagating as guided modes. Structure and way of production of the light channels in integrated optics however is completely different from those of fibers. In both however the guidance of the light relies on total reflection of light against the boundaries between materials with different index of refraction.

The simplest Integrated Optical structure is the slabguide consisting of three layers of which the middle one has to have the largest refractive index (see Figure 2).

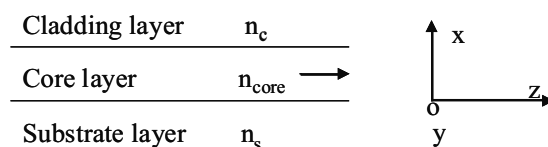


Figure 2. Structure of a three-layer slab guide.

Under certain conditions light propagating through the middle layer is confined in the transverse direction (i.e. perpendicular to the boundary planes) to and hence is guided by this middle layer. Applying the ray picture and the concept of total reflection already many properties of the light propagation through these slabguides can be derived. A complete picture of this propagation and also of the propagation through more complicated IO structures can be obtained by using electro-dynamic theory starting from the Maxwell equations and by applying the appropriate boundary conditions. For the three layer slabguide it appears that light can propagate through these systems as a limited number of mutually independent (assuming that non-linear effects can be neglected) guided modes, each mode being characterized by its specific pattern of the electro-magnetic field (the field

profiles) and its specific propagation speed; both parameters are dependent on the vacuum wavelength  $\lambda_o$  of the applied monochromatic light. Although the electro-magnetic field may contain all the components of the electric field  $E$  and the magnetic field  $H$  these components are mutually dependent, implying for slabguides, that if one of them is known the others can be derived from it straightforwardly. In slabguides two types of mode are possible the TE and TM modes both characterized by the fact that only three of the field components are unequal to zero ( $E_y$ ,  $H_x$  and  $H_z$ ) and ( $H_y$ ,  $E_x$  and  $E_z$ ) respectively. In more complicated structures generally the modes have in good approximation maintained their TE or TM character. The number of modes, which can be supported by a waveguide depends on the geometry of the structure and the refractive indices of the constituent materials. Light guiding structures can be constructed which support one mode (of each polarization) only and these monomodal waveguides are mostly applied in IO sensors. Modes are numbered from 0 to higher integers corresponding to the so-called mode-order, the higher the order the higher its propagation speed.

The propagation of the  $i^{\text{th}}$  TE mode, the  $TE_i$ -mode through a slabguide can be described mathematically by the equation:

$$E_y^i(x, z, \omega, t) = E_y^i(x) \exp j[\omega t - k_0(\omega) N_{eff}(\omega) z] \quad (\text{Eq.1})$$

where  $\omega$  is the angular frequency of the light,  $k_0 = 2\pi/\lambda_o = \omega/c$  the corresponding wavenumber,  $c$  the light velocity in vacuum, while  $N_{eff}(\omega)$  is called the effective refractive index of the mode. Note that the expression denotes a field pattern running into the  $z$ -direction with a phase velocity  $c/N_{eff}$ . For some simple structures the field profile and the  $N_{eff}$ -value can be calculated analytically but a large variety of software programs has been developed for calculating these parameters for more complicated structures. It can be derived that always  $n_{core} > N_{eff} > n_c, n_s$ . Field patterns of the lowest order TE modes are given in Figure 3.

Note that part of the field pattern is propagating (along the  $z$ -direction) outside the core layer and that its magnitude is decaying exponentially with the distance to the corresponding plane boundary. These fields outside the

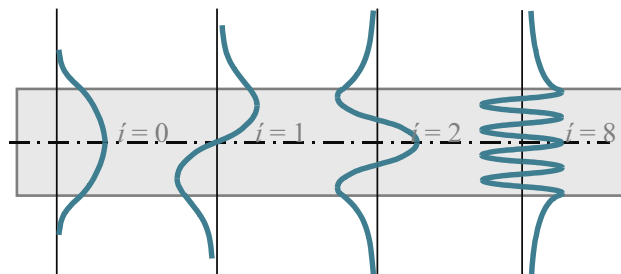


Figure 3. Field profiles ( $E_y$  component) of TE modes.

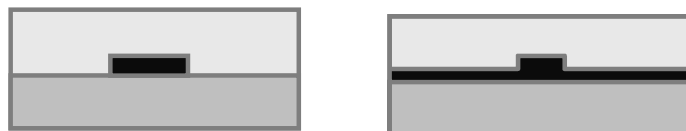


Figure 4. Cross sections of various types of channel guides; on the right the ridge guide; black is core material.

core layer are called the evanescent fields and it will appear later on, that principles of many IO sensors just rely on the presence of these evanescent field tails.

To obtain also guiding along the  $y$ - direction laterally patterning of at least one of these layers is necessary. Some cross sections of channel structures are given in Figure 4. Notice that there are applications of IO, in which the number of layers is larger than 3.

Apart from straight channels (being invariant along the propagation direction of the light) also three other basic structures can be distinguished: tapers, bends and Y-junctions. Top views of these basic structures in which the channels are indicated are given in Figure 5.

From combinations of these three basic structures, nearly all more complicated structures of higher functionality can be built, e.g. sensors (of course), gratings, wavelength filters, modulators, amplifiers etc. Several of these sensing structures will be shown in section 4.

Most integrated optical structures are built by depositing the layer stacks and by laterally patterning them by using photolithography and etching methods. Although in principle a large variety of materials can be used, only a few of them showed to be very useful for integrated optics. Here we can distinguish between the so-called passive, dynamic and active materials. Dynamic materials show strong physical cross effects, like electro-optical, thermo-optical, elasto-optical and chemo-optical ones and locally the refractive index distribution can be varied with time by a physical stimulus (e.g. by applying locally a voltage) enabling dynamic functions such as switches and modulators. Active materials show the property of power conversion from the electrical domain to the optical one or vice versa, useful for building light sources (LEDs or lasers), amplifiers and detectors. The functionality of the IO structure aimed at often determines the materials used. In addition also the control of technology and the costs of technology are important factors in choosing a technology- material combination.

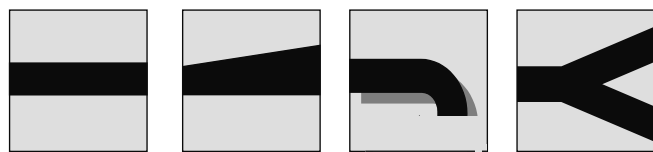


Figure 5. Some basic structures, from the left to the right: straight channel, taper, bend, and Y-junction.

Commonly used material classes are the III-V compounds (especially when dynamic or active functions are needed),  $\text{LiNbO}_3$  (because of its electro-optical properties), the indiffused glasses, the SiON-materials, the polymers and materials obtained from sol-gel technology. Last three will be treated in other chapters of this book. As an example we show the cross section of a simple channel structure based on SiON technology in Figure 6.

The strength of integrated optics is that complicated structures with high functionality can be produced in one technological run. Sub-functions have not to be packaged together but are produced as a complete integrated system, where relative positions are well defined. Also just as in microelectronics many devices can be made from one “wafer”. Compared to fibers IO also shows a much larger flexibility in the choice of materials and geometries. A weak point of IO compared to fiber based optical systems is that mostly light has to be launched into the chips from free space beams or fibers, requiring additional in- and out-coupling functions and leading to additional costs of packaging. There is a trend to integrate also light sources and detectors into the IO circuit.

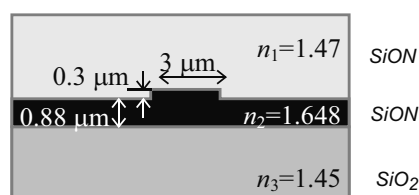


Figure 6. Cross section of a SiON-technology waveguide channel.

### 3. INTRODUCTION TO INTEGRATED OPTICAL SENSORS

Nearly all integrated optical sensors<sup>4-6</sup> rely on evanescent field sensing. This principle can be explained using Figure 7.

On defining the so-called sensing region (alternatively also called detection section or sensing pad) the passive cladding material is locally

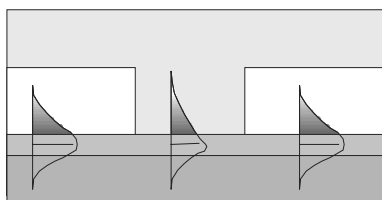


Figure 7. Evanescent field sensing; the black part of the field profile is the operational evanescent field.

substituted by a sensitive material, meaning that one or more of its optical parameters are sensitive to the value of an external parameter. If the value of this parameter, the measurand, changes, also within the sensing region the optical structure changes and this change influences the characteristic parameters of the mode propagating through the sensing region. Notice that the interaction length is given by the length of the sensing window, while in fact the sensitive material is interrogated by the evanescent field, carrying part of the modal power only.

Dependent on the optical parameter of which the change is utilized for sensing we distinguish several classes of sensors: the refractive (the change of the real part of the refractive index is utilized), the absorptive (the imaginary part of the refractive index) and the luminescent (alternatively sometimes called fluorescent) sensors. In refractive sensors the field profiles and the real part of the  $N_{eff}$  value are influenced, the latter implying amongst others, that phase of the light leaving the sensing region becomes dependent on the refractive index of the sensitive material. In absorptive sensors a change of the imaginary part of the refractive index of the sensitive material causes a change of the imaginary part of the  $N_{eff}$  value, which expresses itself as a change of the attenuation of the mode within the sensing region and finally as a change of the transmitted power. Luminescent sensors are in general chemical sensors, meaning that they enable measurement of chemical concentrations. Dependent on the concentration of the measurand luminescence is changing, whether as a result of the generation of luminescent centers or by quenching them. Luminescence can be generated by light transported as a guided mode to the luminescent material, while the emitted luminescent light can be monitored as free space light or as guided modes being trapped again by a waveguide.

Here we will focus on refractive sensors. Both other types will be treated in other chapters of this book. Refractive sensors can be applied for measuring physical parameters by virtue of materials showing cross effects to the optical domain. Most refractive sensors are developed for measuring chemical concentrations. In case we are interested in the concentration of a chemical compound in a solution and if this would be the only solved substance, the refractive index of the solution is a direct measure for the concentration. If the solution contains more substances each with an unknown concentration, one has to introduce the so-called chemo-optical transduction layers also named chemical interfaces. They contain receptor molecules, which can associate only with the chemical entities (molecules or ions) of the substance we are interested in. Notice however that complete selectivity can never be obtained. If association constants are high these entities are concentrated inside the receptors, and partly as a result of replacing at the receptor sites solvent molecules by measurand entities and partly as a result of a change of the electronic structure of the receptor molecules after being filled, the refractive index of a layer containing these

receptors will become concentration dependent. Notice that the filling of the receptors can also result into a change of the absorptive and/ or emission properties of this layer.

Dependent on the thickness of the chemo-optical layer two types of evanescent field sensing one can be distinguished: bulk sensing, also called homogeneous sensing and surface sensing. In the first type the chemo-optical layer is that thick (mostly some micrometers) that in good approximation the whole evanescent tail is confined to that layer. Condition is that the measurand entities can reach the receptors spread over this layer, generally requiring some porosity of the host material.

In surface sensing the receptor molecules are present in a layer with thickness lower than some tens of a nanometer. Often these layers are monomolecular and consist of immobilized receptor molecules only. They are used in case no host materials can be found which allow the diffusion of the measurand entities to the receptor molecules e.g. in case of immunosensing. Compared to bulk sensing surface sensing introduces two complications. Firstly the evanescent field is also probing the solution, hence changes of concentration of other solved substances will also experienced by the modes running through the sensing region. Secondly only a very small part of the evanescent field is probing the thin chemical interface and as a consequence the overall sensitivity will be strongly reduced. Many examples of these chemical interfaces will be given in other chapters.

#### **4. REFRACTIVE INTEGRATED OPTICAL SENSING SYSTEMS**

Principles applied in refractive IO sensors can be divided in two categories:

- 1) principles relying on the measurand induced change of the effective refractive index,  $\Delta N_{eff}$ , within the sensing region; essentially all of them are based on interference phenomena. This is clearly visible in all types of interferometers, such as Mach-Zehnder-, Young-, Michelson-, difference, and Zeeman- interferometers and in resonators such as Fabry-Perot- and ring-resonators, in fact all being implementations of classical principles into integrated optical devices; the interference phenomenon is more hidden in sensors which are based on mode coupling such as the grating couplers, Bragg reflectors and Surface Plasmon Resonance based devices; there has been an extended research on IO sensors based on all these principles, but nevertheless only a few have reached the market.
- 2) principles relying on measurand induced changes of modal field profile,  $\Delta E$ , within the sensing region, such as a bend sensor and sensors in which  $\Delta E$ , manifests itself directly as a modal attenuation; this is a

relatively new area, being in a first stage of exploration only and the limits of performance of this class of sensors are unclear yet.

## 4.1 Interferometers

A strong point of the interferometers is the large resolution that is obtained or is expected to be obtainable. On the one hand the sensitivities to the measurand  $m$ ,  $dP_{out}(r,t)/dm$ , can be large, while on the other hand effects of perturbing parameters  $p$ ,  $dP_{out}(r,t)/dp$ , can be strongly reduced as a direct consequence of the balanced structure of these interferometers, offering a reference in a very effective way. Main driving force behind the large attention to this type of sensors is the prospect of enabling the detection of extremely low concentrations of (bio-)chemical compounds. Here it is hoped, that in some application fields the interferometric sensors will become tough competitors of the fluorescent sensors, with the advantage of offering a label free method. An additional strong point is that all these principles are well suited for developing arrays of sensors on one single optical chip.

Here we will discuss in more detail the IO Mach-Zehnder interferometer<sup>7</sup>. It is a nice vehicle for illustrating in what way the problem of looking for extremely high resolutions can be approached, an approach which appeared to be very successful. We will focus on the MZI used for bulk sensing and we will make some additional remarks on its utilization in surface sensing.

A top view of the basic structure of an IO MZI (for chemical sensing) is given in Figure 8.

All channels are monomodal for the wavelength used. The principle is very simple: monochromatic light is launched into the input channel (on the left), is equally divided over both branches by the first Y-junction and is combined again by the second Y-junction. Here the modes from both branches interfere with each other whether constructively or destructively. In one of the branches a sensing window is applied and over the length of this window, the interaction length  $L$ , the guided mode is experiencing the sensitive ( $\Delta m \rightarrow \Delta n$ ) cladding material.

The principle discharges into the expression:

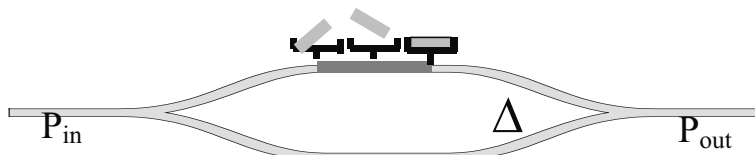


Figure 8. Top view of a chemical IO MZI-sensor.

$$\frac{P_{out}}{P_{in}} = \frac{1}{2} \{1 + \cos(\Delta\varphi_m + \Delta\varphi_0)\} \quad (\text{Eq.2})$$

where the measurand induced phase change  $\Delta\varphi_m$  is given as

$$\Delta\varphi_m = \frac{2\pi}{\lambda_0} \Delta N_{eff} L \quad (\text{Eq.3})$$

and  $\Delta\varphi_0$  is an off-set phase difference as a result of the structure difference of both branches at  $\Delta\varphi_m=0$ .  $\lambda_0$  is the vacuum wavelength of the used light.

For maximizing the sensitivity the transduction chain utilized in the sensor has to be considered. In the MZI this chain is given by  $\Delta m \rightarrow \Delta n \rightarrow \Delta N_{eff} \rightarrow \Delta\varphi \rightarrow \Delta P_{out}$ . If we focus on chemical sensors the measurand  $m$  is the concentration of a specific chemical substance and  $\Delta m$  can be specified as  $\Delta C$ . First step of maximizing the sensitivity now is maximizing the effects of each individual transduction step.

- We leave the first step ( $\Delta C \rightarrow \Delta n$ ) inclusive the selectivity problem to the chemists.
- In literature<sup>8-12</sup> a lot of attention has been paid to maximizing the effect of the second step ( $\Delta n \rightarrow \Delta N_{eff}$ ) implying the maximization of  $\partial N_{eff} / \partial n$ . The value of this derivative depends strongly on the applied materials and the chosen dimensions of the waveguiding channel. For indiffused glasses with their low  $n_{core} - n_s$ -contrast this value is about 0.01, using SiON technology for the most common situation ( $n_c < n_s$ ) a value of about 0.2 can be obtained, but in case of so-called reverse symmetry<sup>11</sup> ( $n_s < n_c$ ) this value can approach 1.0. In very thin freely suspended waveguides surrounded by gases values exceeding 1 can be obtained even<sup>12</sup>.
- The third step ( $\Delta N_{eff} \rightarrow \Delta\varphi$ ) can be optimized by taking a large interaction length and a low wavelength, see (2), but there are trade offs with the desires of limited chip area and limited scattering and absorption losses respectively.
- As to sensitivity last step ( $\Delta\varphi \rightarrow \Delta P_{out}$ ) a high S/N ration favors higher input powers.

Now the influence of perturbations will be analyzed.

Although not the result of a real perturbation the periodical nature of equation (1) leads to some complications: from a measured value of ( $P_{out} / P_{in}$ ) no unambiguous value of  $\Delta\varphi$  can be derived. In fact we can measure changes of  $\Delta\varphi$  only and we have to monitor  $\Delta\varphi$  during the measurement. Also being in an extreme of  $P_{out} / P_{in}$  as a function of  $\Delta\varphi$  the direction of the subsequent change of  $\Delta\varphi$  is not defined (direction ambiguity), while in addition in this state the sensitivity  $\partial P_{out} / \partial \Delta\varphi$  is zero (sensitivity fading).

Imperfect technology also leads to complications: the splitting ratio of the Y-junctions will not be exactly equal to 1:1 and the channel structures of both



branches can be somewhat different, both effects being expressed by the so-called modulation depth  $M$ . Also some scatter light can enter the output. Hence in practice equation (1) has to be rewritten as

$$\frac{P_{out}}{P_{in}} = \frac{1}{2} \{1 + M \cos(\Delta\varphi + \Delta\varphi_0)\} + \frac{P_{scattering}}{P_{in}} \quad (\text{Eq.4})$$

and calibration should be necessary for determining  $M$  and  $P_{scattering}$ .

$P_{out}$  will be decontaminated with noise, mainly arising from the detector + electronic processing unit and from the light source. Effects of varying light source power and specially the drift of the light source power can be reduced by normalizing  $P_{out}$  to the continuously measured light source power and filtering out electronically higher frequency components of the signals.

All these complications can be eliminated by introducing serrodyne modulation<sup>13</sup> in the MZI. What does this mean?

Serrodyne modulation implies the insertion of electro-optical modulators in both branches which are controlled in anti-phase by a triangular ac voltage  $V$  in such a way that the additional phase difference  $\Delta\varphi_{mod}$  which is introduced by the modulator varies linearly with time between 0 and  $2\pi$  exactly. For illustration in Figure 9, the output signal as a function of time is presented for two different values of the sum of the measurand induced and off set phase differences,  $(\Delta\varphi_m + \Delta\varphi_0)$ . After filtering out the dc component a symmetrical ac signal is obtained in which the time difference between  $V=0$  and  $P_{out}=0$  defines the value of  $(\Delta\varphi_m + \Delta\varphi_0 + l 2\pi)$ , where  $l$  is an unknown integer). For reasons of clarity also the signal is digitized, positive and negative values being expressed as 1 and 0 signals respectively.

Which are the results of this serrodyne modulation?

- Increase and decrease of  $(\Delta\varphi_m + \Delta\varphi_0)$  are discriminated from each other by the direction of the movement of the 0-1 transitions. Sudden disappearance of such a moving transition can be electronically monitored and can be used for fringe counting.
- There is no sensitivity fading anymore.
- The zero crossing is independent of the amplitude of the cosine, hence effects of drift of  $P_{in}$  and of (varying) modulation depth  $M$  have been completely eliminated.

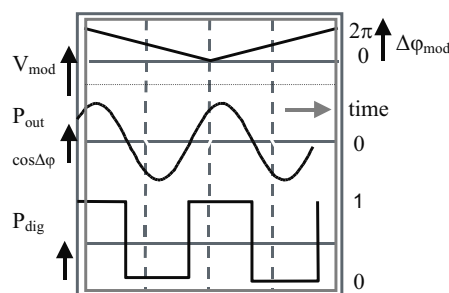


Figure 9. Serrodyne modulation.

- $P_{scattering}$  is removed by removing the DC component.

Note that the appropriated amplitude of the triangular ac voltage (period  $T$ ) can be adjusted using feed back, with e.g. as a criterion that the time difference between both transitions within the same period should be equal to  $T/2$  exactly. Note also, that determination of the zero crossing requires the definition of a certain power window around  $P_{out}=0$  in order that noise should not deteriorate the fringe counting. By averaging the signals obtained from various periods this window size can be decreased. Alternatively however whole the ac component of the  $P_{out}-\Delta\phi$  curve can be registered and by processing these data appropriately the phase can be deduced more accurately.

Temperature variations also have their influence. Effects of a homogeneous change of temperature can be strongly reduced by making both branches as identical as possible. This means that also in the reference branch a sensing window has to be inserted, filled with a non-sensitive cladding material with an identical (temperature coefficient of the) refractive index and thickness as the sensitive cladding. Note that temperature effects of other functions, such as the fiber-to-chip coupling function, are eliminated by the serrodyne modulation. It is preferred to lead the analyte (e.g. a solution containing the measurand) in identical ways to both windows, in order to reduce generation of a temperature difference between both branches. This may require integration with a (simple) microfluidic system. Working in this way also surface sensing can be practised because now the effects of changes of the refractive index of the solution are identical in both branches and hence they are completely eliminated from the device performance. A perfect balance of the MZI-branches also strongly reduces effects of variation of the wavelength of the light source. Using a thermostated solid state laser avoids mode hopping and enhances the wavelength stability.

By using silicon wafers (showing a high value of the thermal conductivity) as a substrate and by taking the distance between both branches as small as possible (of course avoiding interaction of the modes traveling through both branches) temperature differences can be reduced.

For a proper operation of the MZI it is of importance that light of one polarization state only is present. Although the polarization state of the light at the exit of the input fiber will be controlled, it is not excluded that both TE and TM modes are launched. For MZI devices fabricated on top of silicon it is preferred to utilize TE modes in spite of its lower sensitivity compare to TM modes. The reason for this is, that the relatively small power, which might be transferred at the fiber to chip coupling to the TM mode can be strongly attenuated by adjusting the thickness of the buffer layer in such a way, that the TM power leaks strongly into the silicon substrate, while the more confined field profile of the TE mode is not penetrating the silicon.

A well designed bare MZI with a layout<sup>14</sup> as shown in Figure 8 can show a resolution in the refractive index  $\delta n$  down to  $10^{-5}$ , introduction of  $P_{in}$ -measurements ( for monitoring the fluctuations in  $P_{in}$ ) leads to an improvement with about one order of magnitude<sup>14</sup> ( $\delta n \approx 10^{-6}$ ), while use of both serrodyne modulation and optimized structures, realized in SiON-technology, resolutions down to ( $\delta n \approx 10^{-8}$ ), can be obtained<sup>13</sup>. For the latter type of MZI -systems improvements can be envisaged even.

Notice, that with these extremely good resolutions in case of surface sensing contamination of the sensitive layer with solid particles has to be avoided completely, e.g. by an appropriate filtering of the sample solutions. Notice also that the temperature coefficient of the refractive index of water is about  $10^{-4}$  per °C. So if applying the surface sensing mode using watery solutions indeed a perfect balance of both branches and low temperature gradients have to be aimed at.

Similar consideration can be utilized for minimizing the resolution of in other types of interferometers because their principles and structures are very similar.

A Young interferometer<sup>15, 16</sup> (YI) can be seen as a MZI, cut after the windows, where interference between both beams takes place outside the chip and where the resulting spatial interference pattern can be monitored using e.g. a CCD camera.

The analogue between the Young- interferometer (interference pattern in the spatial domain) and the serrodyne modulated MZI (interference pattern in the time domain) is striking. An optimized Young interferometer<sup>17</sup> can also show resolutions down to  $\delta n \approx 10^{-8}$ .

A Michelson interferometer (MI) can be considered as a Young-interferometer with perfect reflectors at the ends of both branches. Compared to the MZI and YI the MI has the advantage that the sensing region is passed twice. Because for monitoring the reflected light a second Y- junction is

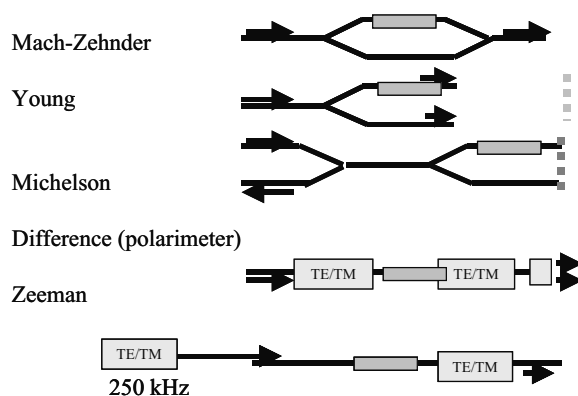


Figure 10. Top view of several types of interferometers: top-down: MZI, YI, MI, Difference interferometer, Zeeman interferometer.

necessary the monitored power is reduced with a factor 4 when compared to the MZI. Problems with implementing perfect reflectors may be hampered application of these MI's for chemical sensing. By introducing a final section with free space beam propagation in one of the branches MI's have been utilized for measuring displacements<sup>18</sup>.

In difference interferometers<sup>19, 20</sup> two modes (generally a TE and a TM mode, defining a polarimeter) are propagating simultaneously through the IO channel of the sensing section. As a result of their difference in mode profile they are experiencing the sensitive cladding layer in a different way. Now the difference of the changes of the effective refractive indices of both modes  $\Delta(N_i - N_j)$  is measured, by making the modes interfering, e.g. in case of a polarimeter by using a 3dB TE/TM coupler. An advantage compared to the other types of interferometers is, that both interfering beams propagate through the same channel, hence e.g. temperature gradients are absent and no "identical" insensitive layer has to be introduced. Not always recognized however are their disadvantages: as a result of measuring  $\Delta(N_i - N_j)$  instead of  $\Delta N_0$  the sensitivity will be lowered, and in addition as a result of the difference of their mode profiles, both modes will experience perturbing factors like a temperature change in a different way.

## 4.2 Resonators

Although theoretically very attractive there are no reports on IO sensors of the Fabry-Perot type. One may assume that this mainly originates from its technological complexity.

The theoretical attraction of these sensors stems from their large sensitivity as a consequence of the fact that the light beam is traversing the sensing section between both reflectors many times. This manifests itself in the transmitted relative power  $P_t$  versus  $N_{eff}$  curves as narrow transmission bands, with at the small  $N_{eff}$  ranges around the inflection points large sensitivities  $(\partial P_t / \partial N_{eff}) \cdot (\partial N_{eff} / \partial n)$ . In theory resonators would be very appropriate for obtaining a high resolution within a small range, hence they would be very suited for measuring extremely small concentrations. However technological imperfectness hampers to produce waveguides with exactly the appropriate values of  $N_{eff}$  at the given wavelength. Tuning whether by wavelength variation (requiring an expensive tunable laser) or by index variation using optical cross effects (requiring a much more complicated device) would be necessary. First papers<sup>21, 22</sup> have been published on micro-ring resonator sensors and a resolution  $\partial n \approx 10^{-8}$  is theoretically predicted.

### 4.3. Devices Based on Mode Coupling

Most famous representatives of this class of sensors are the grating couplers and the Surface Plasmon Resonance (SPR) based devices. In fact in the layouts commonly used in practice, the sensing sections only are supporting guided modes and the change of their  $N_{eff}$  values is derived from the characteristics of the free space beams, which is interrogating the sensing section. From these characteristics the  $N_{eff}$  value of the guided mode can be derived using the so-called coupling condition

$$N_{eff} - n_p \sin \mathcal{G} = m \frac{\lambda_0}{\Lambda} \quad (\text{Eq.5})$$

where  $m=0$  for SPR and an integer  $\neq 0$  for the grating couplers.

- $n_p$  is the refractive index of the substrate material (grating coupler) or the prism material (SPR device).
- $\Lambda$  is the period of the grating.

In a simple implementation of the grating coupling principle<sup>23, 24</sup>, light is launched into a mode of the waveguide and the direction of the out-coupled free space beam, given by the angle  $\mathcal{G}$  is measured. Because all other parameters are known, from (5)  $N_{eff}$  can be derived. Resolution  $\partial n$  obtained by this method is around  $10^{-6}$ . Very elegant implementations do exist, such as the light pointer modification<sup>25</sup>.

In the standard SPR systems (see the chapter of Homola) in fact prism coupling to a special mode is utilized; this mode is a surface plasmon and it can propagate only along the interface of a metal with negative value of the dielectric constant and a dielectric medium. This mode has purely TM character, decays exponentially at both sides of the interface and is heavily attenuated by the metal. Thus its propagation length amounts to some tens of micrometers only. If the incident beam is coupled to the surface plasmon there is a dip in the power of the reflected beam,  $P_{refl}$  because the power coupled into the SP is nearly completely dissipated. The coupling condition can be monitored e.g. by varying the angle of incidence of light beam or by varying its wavelength. Also it is possible to depict immediately the  $P_{refl}$  versus  $\mathcal{G}$  curve by slightly focusing the incident beam and monitoring the angle dependence of the reflected light using a CCD camera. Apart from the amplitude also the phase is changing drastically in passing the resonance condition. Recently first publications<sup>26</sup> appeared in which this phase change is exploited for measuring the shift of  $N_{eff}$ ; resolutions up to  $10^{-8}$  have been obtained.

Strong points of the SPR device are the large  $\partial N_{eff} / \partial n$  – value of the SP, being about 1.2 at maximum and the strong confinement of the field profile, making the SPR method very useful for surface sensing. An excellent review of SPR devices is given in [27].

Both principles can also be implemented in completely integrated optical devices. For the grating device coupling to the reflected guided mode is utilized<sup>28</sup> (Bragg reflection), while in the SPR device the coupling from a guided mode (propagating through a conventional waveguide) to the SP-mode is monitored, the latter propagating through an additional SP mode supporting layer stack which is applied locally on top of that conventional waveguide<sup>29, 30</sup>. In both cases the monitoring is performed by measuring the power transmitted by the conventional waveguide, whether at constant wavelength or (preferentially) as a function of the wavelength.

#### 4.4. Modal Field Change Based Sensors

A third class of refractive sensors, which is in a first stage of exploration yet, is based on measurand induced changes of the modal field. In the waveguides generally applied in the  $\Delta N_{eff}$  based refractive sensors the measurand induced changes of the field profiles are generally very small and in many theoretical treatments of the sensing process they are neglected completely.

However close to the cut off condition, where the difference between  $N_{eff}$  of a mode and the refractive index of (at least) one of the materials (say A) adjacent to the core layer is very small, the modal field is very extended and its penetration depth into material A (related to the decay constant of the evanescent field in material A) is very sensitive to small variations of refractive indices. Field extensions over a given extension length  $L=L_1$  can be monitored e.g if for  $L>L_1$  another material B has been applied with some of its optical properties very different from those of material A. For example if this material B should be strongly absorbing or if it shows a refractive index larger than  $N_{eff}$ , the mode will be the more attenuated, the larger the field penetration into material B. So in these sensors the measurement of a change of refractive index is directly converted into a measurement of the change of the modal attenuation, just as in absorption type sensors. If material B would be fluorescent, the power of the emitted light should be dependent on the penetration depth and the refractive sensor in fact is converted into a luminescent sensor.

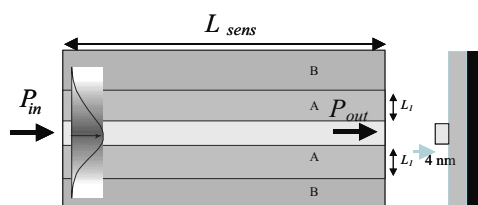


Figure 11. Top view of a top loaded  $\Delta E$  based sensor.

An example of such a sensing system is shown in Figure 11. It shows a monomodal waveguide of the top loaded type, where the load consists of the sensitive material. In case the thickness of the loading layer is very small (e.g. by being a monomolecular antibody layer, with a thickness of about 4 nm) the lateral index contrast (in terms of the so called Effective Index Method) is very low and the mode is laterally close to cut off. More detailed analysis<sup>32</sup> of this type of structures, in which also the properties of the peripheral equipment are taken into account shows, that with waveguide lengths of about 1 cm resolutions in the order of magnitude  $\partial n = 10^{-7}$  should be feasible.

A completely other lay out is given in Figure 12, where a top view of a bend sensor is shown. Tapers and channel off sets have been introduced for reducing the background attenuation.

Here in fact material A and B are identical but in the bend section outside the so-called caustic the material behaves like having a refractive index larger than  $N_{eff}$ , causing power leakage. The lower the lateral refractive index contrast of the mode, the stronger this leakage. In SiON technology a bend sensor has been realized with a resolution<sup>33</sup>  $\partial n \approx 10^{-6}$ . Strong point of these sensors is the relative simplicity of the required technology.

Another way to utilize measurand induced changes of a modal field profile is found in measuring the transmission of a guided mode through a transition of two segments of a monomodal waveguide, one segment containing a sensitive material, the other insensitive materials only. We consider an example in which the difference of the segments arises from the

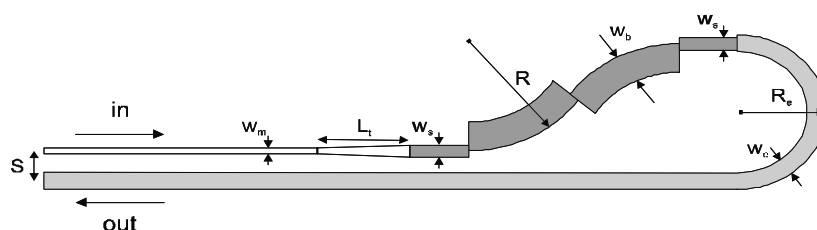


Figure 12. Top view of a bend sensor.

difference in the nature of the cladding materials only. Assume, that at a zero-value of the measurand both cladding materials have identical refractive indices; then the propagating mode does not experience the presence of this transition at all. As soon as both claddings indices are becoming different, also the mode profiles in both segments will become different and as a consequence only part of the power is passing the transition as a guided mode, while the remaining generally very small part has been converted into radiation modes. These modes in principle will be radiated out by the system. At small changes of the refractive index a very small part of the guided power will be lost only. By locating some hundreds of segments in series however, the modal attenuation is strongly enhanced and it becomes

possible to use it as a measure for the refractive index change. A complication arises because part of the power of the radiation modes generated at a transition can be coupled back into the guided mode at next transitions. Segment lengths can be chosen in such a way, that this back coupled light is in anti-phase with the incoming guided mode enhancing the desired effects even.

Such a segmented waveguide sensor has been realized in SiON technology<sup>34</sup> and resolutions in the order of magnitude  $\partial n \approx 10^{-7}$  have been shown.

#### **4.5. Sensor Arrays**

The simplest way to form arrays of integrated optical sensors is to put them all in parallel while all are fed from one input channel the input power being divided over all sensors by using e.g. a star coupler. Every sensor has its own output, detector and electronic processing unit and all sensors can be monitored simultaneously.

More challenging however is to construct a square array, in which the sensors are positioned along a number of parallel waveguides, where each waveguide now contains a series of sensors. The sensors can be individually interrogated using some type of multiplexing/demultiplexing system.

In fact this type of research is in a preliminary stage and only a few of these sensor arrays consisting of Young interferometers have been reported in literature<sup>35 36</sup>. A strongly limiting factor for completely integrated optical sensing arrays is the light confinement within one plane. By lifting this limitation also allowing light propagation in the third dimension can come into play (e.g. grating couplers or SPR-devices) and by monitoring the emitted light by a CCD camera large square integrated optical sensor arrays are forecasted. However in these arrays the IO chip contains the evanescent field sensing sections only. For really large optical sensor arrays non – integrated optical systems such as fiber arrays and methods based on luminescence are much more appropriate.

Note that in future application of photonic bandgap structures may result in very small sensor (-array)s.

### **5. CONCLUSIONS**

Many classical optical sensing principles, which are well known from free space optics can be implemented in integrated optical structures, while integrated optics at its turn can act as source of new principles. Many types of integrated optical sensors have been investigated and demonstrators have been realized, mostly at universities and other research institutes. And also at



present there is a lot of room left for inventing new principles, designing new structures and developing better technologies. However, only a few IO-sensors have reached the market. Apart from the tough competition experienced from sensors based on other physical principles the costs of developing a producible prototype and costs of the production itself are often too high with respect to the expected profits. Factors strongly hampering commercialization are the fragmentation of the sensor market leading to small turnovers and also the absence of foundries, which would enable a cost effective production of small series of sensors. Fortunately during last years some of such foundries have been established. Development of integrated optical sensor platforms enabling tailoring to specific applications in a last process step (e.g. applying a specific chemo-optical interface on top of an IO read out system) may support future commercialization.

Nevertheless consumer applications seem to be far away and at present the only substantial application fields, which can be targeted for application of IO sensors only, are health care, ecology and defense industry.

## REFERENCES

1. Tamir T. (ed), *Integrated optics*, Springer Verlag, Berlin, 1979.
2. Saleh B.E.A., Teich M.C., *Fundamentals of Photonics*, Wiley, New York, 1994.
3. Okamoto K., *Fundamentals of optical waveguides*, Academic Press, 2000.
4. Boisdé G., Harmer A., *Chemical and biochemical sensing with optical fibers and waveguides*, Artech House, Boston-London, 1996.
5. Ligler F.S., Rowe Tait C.A., *Optical biosensors: present and future*, Elsevier, Amsterdam, 2002.
6. Lambeck P.V., Proc. ECIO 01, (2001) 153.
7. Campbell D P., McCloskey C.J., *Interferometric biosensors*, Ch. 9 of [5].
8. Lukosz W., Principles and sensitivities of integrated optical and surface plasmon sensors for direct affinity- and immunosensing, *Biosens. and Bioelectr.* 1991; 6: 215-225.
9. Parriaux O., Veldhuis G.J., Normalized analysis for the sensitivity optimization of integrated optical evanescent-wave sensors, *J of Lightwave Technol.* 1998; 16: 573-582.
10. Cottier K., Wiki M., Voirin G., Gao H., Kunz R.E., Label-free highly sensitive detection of (small) molecules by wavelength interrogation of integrated optical chips, *Sens. and Actuat. B* 2003; 91:241-251.
11. Veldhuis G.J., Parriaux O., Hoekstra H.J.W.M., Lambeck P.V., Sensitivity enhancement in evanescent optical waveguide sensors, *J of Light. Technol.* 2000; 18: 677-682.
12. Horvath R., Pedersen H.C., Demonstration of reverse symmetry waveguide sensing in aqueous solutions, *Appl. Phys. Lett.* 2002; 81: 2166-2168.
13. Heideman R.G., Lambeck P.V., Remote opto-chemical sensing with extreme sensitivity: design, fabrication and performance of a pigtailed integrated optical phase-modulated Mach-Zehnder interferometer system, *Sens. and Actuat. B* 1999; 61: 100-127.
14. Drapp B., Piehler J., Brecht A., Gauglitz G., Luff B.J., Wilkinson J.S., Inghoff J. , Integrated optical Mach-Zehnder interferometers as simazine immunoprobes, *Sens. and Actuat. B* 1997; 39: 277-282.

15. Brandenburg A., Krauter R., Kunzel C., Stefan M., Schulte H., Interferometric sensor for detection of surface-bound bioreactions, *Appl. Opt.* 2000; 39: 6396-6405.
16. Cross G.H., Reeves A.A., Brand A., Popplewell J.F., Peel L.L., Swannand M.J., Freeman N.J. *Biosens.and Bioelectron.* 2003; 19: 383.
17. Ymeti A., Kanger J.S., Wijn R., Lambeck P.V., Greve J., Development of a multi-channel integrated interferometer immunosensor, *Sens. and Actuat. B* 2002; 83: 1-7.
18. Lizet J., Gidon P., Vallette S. *Proc Ecio 87*, Glasgow, 1987, 206.
19. Stamm C., Dangel R., Lukosz W., Biosensing with the integrated-optical difference interferometer: dual-wavelength operation, *Opt.Commun.* 1998; 153: 347-359.
20. Koster T., Lambeck P.V., Fully integrated optical polarimeter, *Sens. and Actuat. B*; 2002; 82: 213-226.
21. Krioukov E., Klunder D.J W., Driessen A., Greve J., Otto C., Sensor based on an integrated optical microcavity, *Opt.Lett.* 2002; 27: 512-514.
22. Krioukov E., Greve J., Otto C., Performance of integrated optical microcavities for refractive index and fluorescence sensing, *Sens. and Actuat. B* 2003; 90: 58-67.
23. Clerc D., Lukosz W., Integrated-optical output grating coupler as bio-chemical sensor, *Sens. and Actuat. B* 1994; 19: 581-586.
24. Piehler J., Brandenburg A., Brecht A., Wagner E., Gauglitz G., Characterization of grating couplers for affinity-based pesticide sensing, *Appl.Opt.* 1997; 36: 6554-6562.
25. Cottier K., Wiki M., Voirin G., Gao H., Kunz R.E., Label-free highly sensitive detection of (small) molecules by wavelength interrogation of integrated optical chips, *Sens and Actuat.B* 2003; 91: 241-251.
26. Nikitin P.I., Grigorenko A.N., Beloglazov A.A., Valeiko M.V., Savchuk A.I., Savchuk O.A., Surface plasmon resonance interferometry for micro-array biosensing, *Sens. and Actuat. A* 2000; 85: 189-193.
27. Homola J., Yee S.S., Gauglitz G., Surface plasmon resonance sensors: review , *Sens and Actuat.* 1999; B54: 3.
28. Veldhuis G.J., Berends J.H., Heideman R.G., Lambeck P.V., An integrated optical Bragg-reflector used as a chemo-optical sensor, *Pure Appl. Opt.* 1998; 7 (1): L23-L26.
29. Kreuwel H.J.M., Lambeck P.V., Beltman J.M.M., Popma T.J.A., Mode coupling in multilayered structures applied to a chemical sensor and a wavelength selective directional coupler,, *Proc ECIO'87*, Glasgow, UK, 1987, 217-220.
30. Lavers C.R., Wilkinson J.S., A waveguide-coupled surface plasmon sensor for an aqueous environment, *Sens. and Actuat. B* 1994; 22: 75-81.
31. Ctyroki J., Homola J., Lambeck P.V., Musa S., Hoekstra H.J.W.M., Harris R.D., Wilinson J.S., Usievich B., Lyndin N.M., Theory and modelling of optical waveguide sensors utilising surface plasmon resonance, *Sens. and Actuat. B* 1999; 54: 66-73.
32. Lambeck P.V., Hoekstra H.J.W.M., VanLith J., Van Elzakker G., Two novel integrated optical sensor types for measuring chemical concentrations, based on chemically induced changes of modal field profiles, *J. Nonlinear Opt Phys. Mat* 2004; 13 (2): 209-217.
33. Veldhuis G.J., VandeVeen L.E.W., Lambeck P.V., Integrated optical refractometer based on waveguide bend loss, *J. Lightwave Technol.* 1999; 17: 857.
34. VanLith J., Lambeck P.V., Hoekstra H.J.W.M., Heidemanand R.G., Wijn R.R., The segmented waveguide sensor: principle and experiments, *J. Lightwave Technol.* 2005; 23 (1): 355-363.
35. Ymeti A., Kanger J.S., Greve J., Lambeck P.V., Wijn R., Heideman R.G., Realisation of a multichannel integrated Young interferometer chemical sensor., *Appl. Opt* 2003; 42:5649-5660.
36. Wikerstal A., PhD thesis, University of Freiburg, Germany, 2001.

## Chapter 14

# ULTRACOMPACT OPTICAL SENSORS BASED ON HIGH INDEX-CONTRAST PHOTONIC STRUCTURES

Alfred Driessen, Hugo J.W.M. Hoekstra, Wico Hopman, Henry Kelderman,  
Paul V. Lambeck, Joris van Lith, Dion J.W. Klunder, René M. de Ridder  
*Integrated Optics MicroSystems, MESA<sup>+</sup>*  
*University of Twente*  
*P.O. Box 217*  
*7500 AE Enschede, The Netherlands*

Evgeni Krioukov and Cees Otto  
*Biophysical Techniques Group, MESA<sup>+</sup>*  
*University of Twente*  
*P.O. Box 217*  
*7500 AE Enschede, The Netherlands*

### 1. INTRODUCTION

There is a strong parallelism between electronic integrated circuits (ICs) and integrated optics. In both cases micro- and increasingly nano-technology is applied resulting in devices for a broad spectrum of applications: communication, data processing, sensing and others. The most striking difference is the maturity and complexity. Electronic ICs have followed Moore's law for about 40 years resulting in the currently more than 100 million transistors in a single chip, whereas in photonic circuitries 10 – 100 functional elements per chip represent state-of-the-art results. Photonics in this respect is clearly lagging behind and will do so also in future, as the minimum dimensions of the functional elements will be always in the order of the wavelength of light, i.e. at least some hundreds of nm. But even then, a density of  $10^3$  to  $10^5$  functional elements per optical chip is feasible, so that the term Very Large Scale Integrated (VLSI) photonics<sup>1</sup> is not an exaggeration.

Optical circuits will not simply mimic electronics, but will exploit in a complementary way the unique phenomena offered by light. For example THz bandwidth amplification is straightforward in optical structures with

gain, e.g. semiconductors or rare-earth doped dielectric waveguides. In electronics this is impossible even in a medium term future. In the case of sensors, optical phenomena can be exploited in highly sensitive and selective devices. In this contribution we will discuss how ultra-compact integrated optics or VLSI photonics could play a role in optical sensing. For this aim we summarize first some basic properties of integrated optics concentrating thereby on optical microresonators and more general on nanophotonics. Thereafter we review some recent results of high index-contrast optical sensors. In the following section we discuss the severe challenges for low-cost mass production of complex nanophotonic sensor systems. Finally some conclusions are presented.

## 2. BASIC PROPERTIES OF HIGH INDEX-CONTRAST WAVEGUIDING STRUCTURES

Optical waveguiding occurs when light is confined in 1 (slab waveguide), 2 (channel waveguide) or 3 (resonator) dimensions. Wave propagation can be understood by the ray-picture, see Figure 1a, or as propagation of modes according to Maxwell's equation, Figure 1b. If two waveguides run parallel with each other at a small distance so that one mode feels the index distortion by the second waveguide, mode coupling can occur with consequently power exchange, Figure 1c. At curved surfaces special modes can occur that reflect only at the outer rim of the waveguiding structure, so called whispering gallery modes, Figure 1d. The confinement originates from total reflection at dielectric interfaces (index guiding) or, in the case of photonic bandgap (PBG) structures, from Bragg reflection at periodic index variations. In both cases, with appropriate high index-contrast materials, the extension of the modal fields can be reduced well below the micrometer range.

Special attention has to be given to low-loss bends, which for decreasing bend radius ask for increasing index contrast  $\Delta n$ . The minimum bend radius

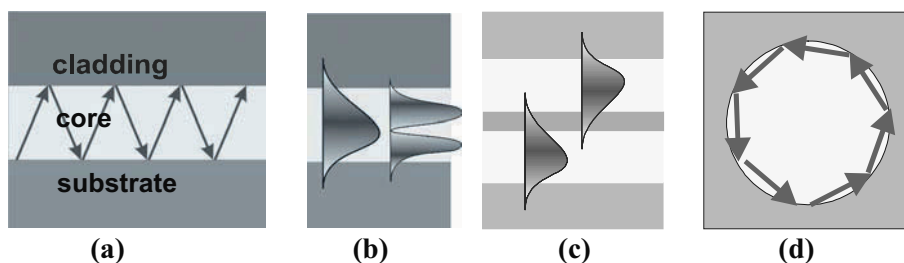


Figure 1. Schematic illustration of waveguiding structures. a: ray-picture; b: modal intensity distribution obtained with the aid of Maxwell's equation; c: mode coupling; d: whispering gallery mode.

for waveguides with modes that are matched to standard single mode fiber ( $\Delta n \sim 0.01$ ), is about 5mm. It is obvious that no complex optical circuitry can be built with such a large radius. For high  $\Delta n$ , the radius can be reduced to a few micrometers. In this way compact structures with optical feedback become possible that allow for a large variety of optical functions. It is interesting to note that increased density and complexity leading eventually to VLSI photonics ask for high index-contrast and consequently submicron waveguides, which can truly be classified as nanophotonics. In both approaches, index guiding or PBG structures, the devices may have the same overall dimensions. Index guiding is an evolutionary approach, as  $\Delta n$  can gradually be increased, whereas the latter is rather revolutionary as the starting point is an ultra-high index contrast  $\Delta n > 1$ .

An optical microresonator<sup>2-4</sup> is an integrated optics structure with optical feedback that allows a variety of functions like wavelength filtering, optical switching or optical sensing. Figure 2a gives a top view of such a device with two adjacent single mode port waveguides. Light enters at  $I_{in}$  and couples in part to the resonator. The rest of the power goes to  $I_{through}$ . Within the ring light propagates in a whispering gallery mode and couples partly to the output waveguide  $I_{drop}$ . After further propagation the light couples partly to  $I_{through}$ . Depending on the phase of the light after a roundtrip, constructive or destructive interference will occur between the just entering and the already present beam within the ring and also between the beam coupled out to  $I_{through}$  and the just transmitted beam. In the case of constructive interference the resonator is on-resonance resulting in a largely enhanced intensity within the ring. In that case the light coupled to  $I_{through}$  has a phase shift of  $180^\circ$  with respect to the just transmitted beam. In this way the transmitted intensity can be largely reduced, in loss-less resonators with symmetric couplers even to zero. Figure 2 b gives schematically the resulting normalized spectral response of such a resonator to a constant power input signal with changing wavelength or alternatively changing

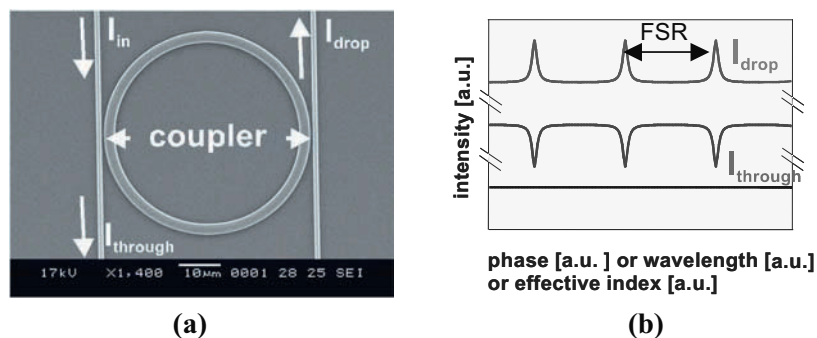


Figure 2. Microresonator with two adjacent waveguides serving as in- and output port; (a): top view; (b): schematic spectral response to a constant input intensity (FSR: free spectral range).

phase in the resonator or changing effective index. The power  $I_{\text{through}}$  is always equal to  $I_{\text{in}}$  with exception near to the resonance, in that case  $I_{\text{drop}} = I_{\text{in}}$ .

The performance of the microresonator is characterized by the free spectral range (FSR) and the 3dB bandwidth  $\Delta\lambda_{3\text{dB}}$  of the resonance peaks. With increasing ring losses, the FSR will decrease and  $\Delta\lambda_{3\text{dB}}$  will increase. A relative measure for the wavelength selectivity of the resonator is the finesse  $F = \text{FSR} / \Delta\lambda_{3\text{dB}}$ . Other parameters are the quality factor  $Q = \lambda / \Delta\lambda_{3\text{dB}}$ , the cavity ring-down time  $\tau_{\text{cav}} = \lambda Q / 2\pi c$  and the average number of roundtrips of photons in a resonator  $m = F / 2\pi$ . For the design of a microresonator the field coupling constant  $\kappa$  between the port waveguides and the ringresonator plays an essential role. In a loss-less resonator with an infinite unloaded finesse the only load is induced by coupling to the port waveguides. Large effective coupling can only be obtained by proper phase matching between the modes in the ring and port waveguides.

There are principally two solutions for the positioning of the adjacent waveguides with respect to the resonator: horizontal or vertical arrangement. Figure 3 gives schematically the geometries. In the vertical arrangement (Figure 3a), a two-step lithographic process is needed. The coupling constant is mainly determined by the thickness and refractive index of the intermediate layer and the relative lateral offset of the underlying waveguide with respect to the ring. This approach provides also design freedom for an independent optimization for ring and port waveguides. Due to the vertical stacking only the resonator itself is exposed to the measurand in the case of sensing applications, the port waveguides are shielded by the separation layer.

In the case of horizontal coupling (Figure 3b), only a single lithographic step with a single mask is needed. The coupling is mainly determined by the width  $w$  of the gap between the straight and bent waveguides and demands nanometer precision in the case of high refractive index contrasts. In addition, there is reduced design flexibility as core layer and core thickness should be identical. In the case of an optical sensor, waveguides as well as resonator are exposed to the measurand. Its refractive index not only

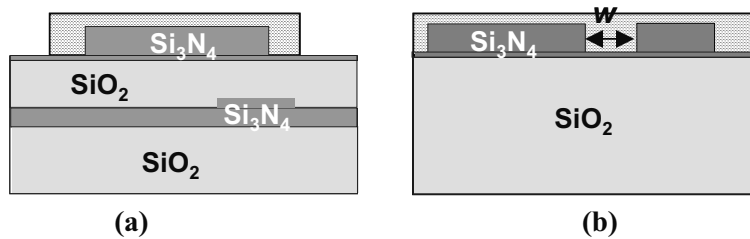


Figure 3. Cross section of the two basic geometries for microresonators with port waveguides; (a) vertical arrangement; (b) lateral arrangement (the dashed region indicates the analyte layer). The structure in this case is fabricated in silicon-based technology, with the index of refraction of  $\text{SiO}_2$  and  $\text{Si}_3\text{N}_4$  1.45 and 2.0 respectively.

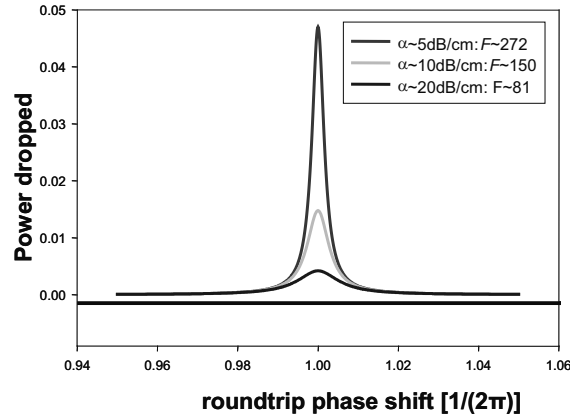


Figure 4. The drop power of a microresonator as a function of phase shift for different values of roundtrip losses  $\alpha$ , c.q. finesse  $F$ .

influences the effective index of the ring and port waveguide modes, but also the coupling constant.

In Figure 2b the spectral response of a microresonator as a function of wavelength has already been given. Just by changing the wavelength, the effective index or the phase light can be directed either to the drop or the through port. When used as a refractive sensor the effective index change of the ring mode is a measure of the concentration or amount of the desired quantity. Small changes near the inversion points of the resonance slopes will lead to large intensity variations at the through as well as drop port. There is another sensing mode. If one considers a single resonance line, the amplitude and width is determined by the roundtrip losses, see Figure 4. By changing the losses and consequently reducing the Q-factor, light can effectively be switched between the two drop ports.

The microresonator therefore can also be used as a sensitive absorption sensor. In both set-ups as refractive or absorption sensor, the ultimate sensitivity is determined by the slope of the resonance peak, which is related to the resonator losses.

In the foregoing the description of microresonators was limited to the index guiding type. Resonators with the same functionality can be implemented in PBG structures<sup>5</sup>. In these cases, with the high index contrast used, the cavity volume is even more reduced resulting in FSRs of 10 - 100 nm.

### 3. EXAMPLES OF ULTRACOMPACT OPTICAL SENSORS

Optical sensing in general is based on changes of the optical properties of materials within the optical circuitry due to changes in the environment.

Except for light generating sensors (e.g. based on luminescence), most optical sensors operate by detecting changes in the refractive index or the absorption at a certain wavelength. Using interferometric sensors, changes as low as  $10^{-8}$  in the index of refraction can be measured<sup>6</sup>. Optical microresonators, based on high index-contrast structures, offer some unique properties for optical sensing as they are very sensitive to small changes in the refractive index. In addition, they are very small (chip area less than  $0.01 \text{ mm}^2$ ) and the measuring volume can be below  $1 \text{ pL}$  ( $10^{-12} \text{ L}$ ). For this reason, they are ideally suited for Lab-on-a-chip applications and sensor arrays that in combination with advanced data read-out could be used as optical nose or tongue.

Krioukov et al.<sup>7</sup> demonstrated the feasibility of optical sensing by measuring the wavelength dependence of the scattered light of a microresonator that is proportional to the light power inside the resonator. For a practical design the change in resonance intensity could much easier be detected by measuring directly the light intensity at the drop port. The device has been realized in  $\text{SiO}_x\text{N}_y$  technology<sup>8</sup> in a vertical coupling geometry. Figure 5 gives a schematic cross-section and top view of the device with a radius of  $15 \text{ }\mu\text{m}$ . Also the approximate mode profile of the whispering gallery mode is given, which extends into the analyte layer.

For a proof of principle they immersed the microresonator in glucose solutions of various concentrations and measured the scattered light when light from a tunable laser was fed to the input waveguide. Figure 6 gives the experimental resonant curves for pure water and a 0.5 and 1% glucose solution. In the not yet optimized set-up refractive index changes well below  $10^{-4}$  could be detected.

Figure 6b gives an overview of the experimental wavelength shift for glucose solutions and ethanol with respect to water, indicating the feasibility of a large measuring range together with high resolution. Large improvements can be obtained by working with even higher finesse resonators and advanced curve fitting. Ultimately a detection limit of index changes as low as  $10^{-8}$  should be feasible.

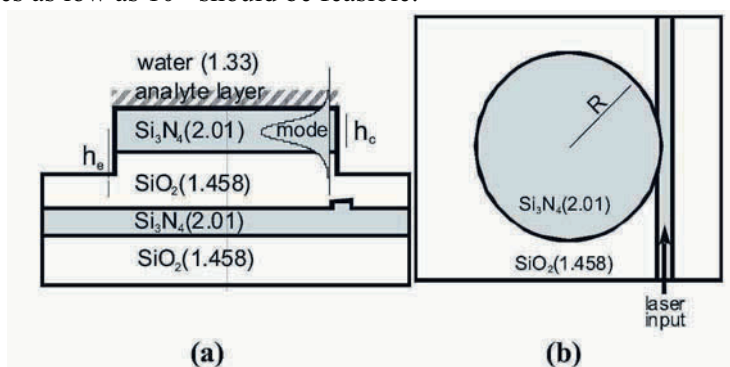


Figure 5. Cross section (a) and top view (b) of an integrated optical microresonator sensor with radius  $R = 15 \text{ }\mu\text{m}$ .



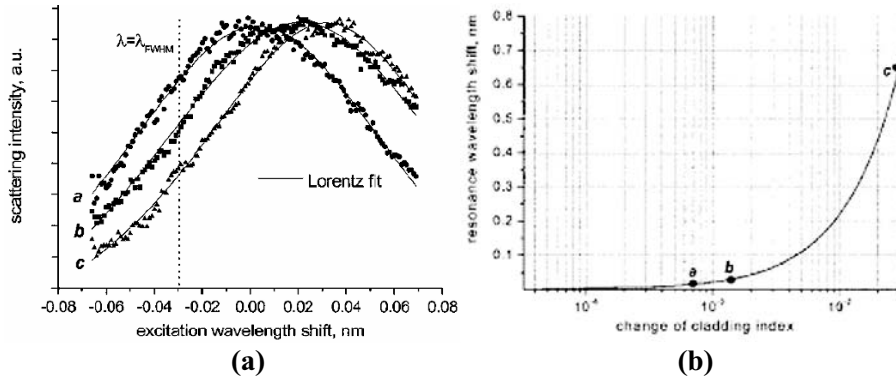


Figure 6. Experimental results of Krioukov et al.<sup>7</sup> of microresonator based optical sensing of glucose; (a) scattering spectra near a resonance recorded by fine laser tuning for "a" water, "b" 0.5% glucose and "c" 1% glucose in the cladding; (c): measured shifts in resonance wavelength for three claddings for "a" 0.5 % glucose, "b" 1% glucose and "c" EtOH ( $n = 1.36$ ).

Recently Chao and Gua<sup>9</sup> employed polymer microrings with sharp asymmetrical resonance for measuring glucose solutions. They found a detection limit of 24 mg/dl corresponding to a  $3 \times 10^{-5}$  index change.

In a second paper Krioukov et al.<sup>10</sup> demonstrated the use of optical microresonators for enhanced optical spectroscopy and sensing. They employed a similar device as depicted in Figure 5, with water as the cladding layer. Measuring the scattering as function of wavelength, a large enhancement of the scattered power at the resonance wavelengths could be observed, see Figure 7. In order to probe more specifically the fluorescence enhancement an Indocyanine Green dye ( $10^{-5}$  M in water) was used as

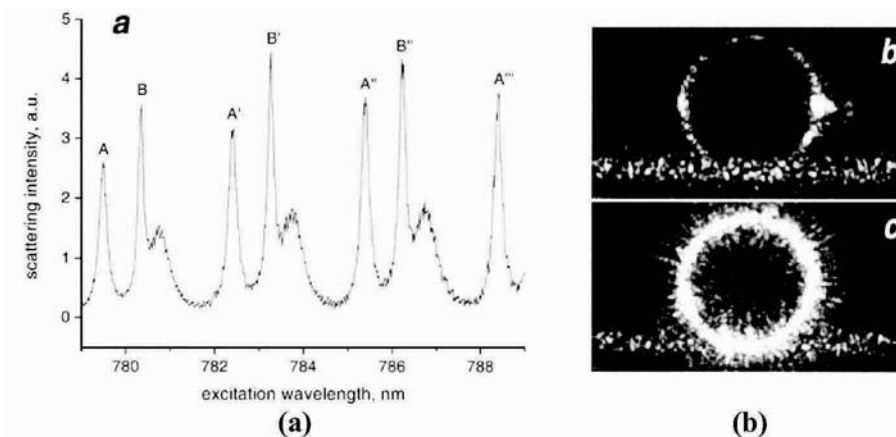


Figure 7. Light scattering of a microresonator with a water cladding; (a) spectra obtained as response to a tunable laser with clearly visible high finesse resonances; (b) CCD camera images of the microresonator obtained off-resonance, (c) idem on-resonance.

analyte. Figure 8a shows the fluorescence spectrum obtained by excitation with laser line around 780 nm. In Figure 8b, the excitation spectrum of the dye solution on top of the microresonator is given. Clearly the enhancement by a factor of 3 can be observed when the exciting laser is operating at a wavelength which is on resonance with the microresonator. With an optimized design for the MR, fluorescence enhancement by a factor of 40 compared with a straight waveguide of the equivalent length becomes feasible.

Also here the small sensing volume makes this kind of sensors attractive devices for high-sensitivity sensing and detection down to the single molecule level.

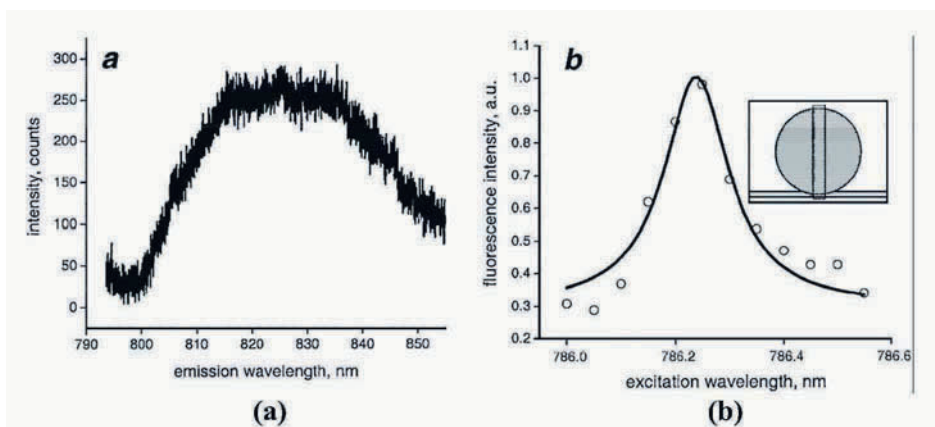


Figure 8. Optical spectroscopy of an indocyanine green dye solution ( $10^{-5}$  M in water); (a): fluorescence spectrum obtained by excitation around 780 nm; (b): excitation spectrum obtained on top of a microresonator; the rectangle in the inset shows the area from which the fluorescence signal is collected.

An alternative approach to ultracompact devices is the use of photonic crystals structures<sup>11</sup>. In a pioneering paper, Holtz and Asher describe polymerized colloidal crystal hydrogel films as intelligent sensing materials<sup>12</sup>. El-Kady and al.<sup>13</sup> used a hexagonal photonic lattice to fabricate tunable narrow-band infrared emitters for gas absorption sensors. These sensors are meanwhile commercially available<sup>14</sup>.

Recently Hopman and al.<sup>15</sup> applied a quasi one-dimensional photonic crystal (length 76  $\mu\text{m}$ ) for optical sensing. They measured the transmission spectrum as a function of the cladding refractive index. The cladding was varied using a liquid flow, of which the index was slowly varied over a small range (Figure 9).

An increase of the cladding refractive index causes a shift of the transmission spectrum of the grating towards longer wavelengths of approximately 23 nm per unit index change (Figure 10). The steep slopes of the photonic band edges (in our case especially the dielectric band edge - at

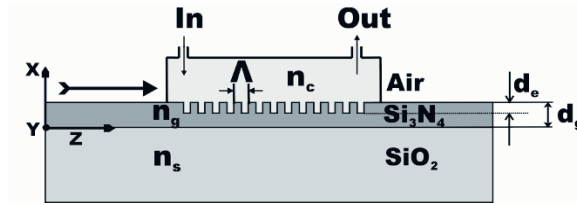


Figure 9. Cross-section of a refractive index sensor based on a quasi one-dimensional photonic crystal with grating period  $\Lambda = 190$  nm. The top cladding over the grating is formed by a fluid contained in a cuvette that is sealed to the sensor chip.

the long-wavelength side of the gap) can be used for increasing the sensitivity of the device.

With a simple photodetector, a variation of  $4 \times 10^{-4}$  in the cladding index could be detected. With some straightforward optimization, an improvement of the resolution by two orders of magnitude may be feasible. A thermally induced spectral shift of approximately 8 pm/K was observed.

#### 4. CHALLENGES FOR NANOPHOTONIC SENSORS

In the previous section first results with promising nanophotonic sensor devices have been demonstrated. It is still some work needed before low-cost, high sensitive and complex optical sensors with a large number of optical functions will be available. For the increase in sensitivity and

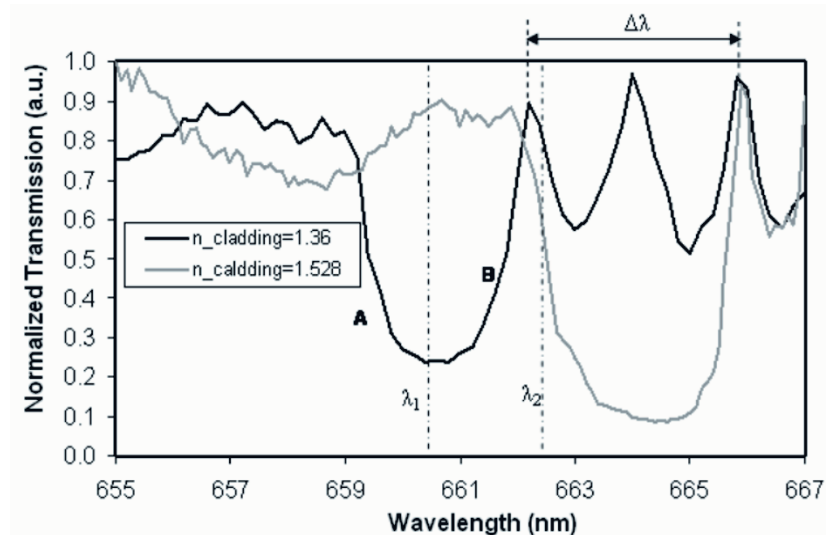


Figure 10. Normalized transmission spectra for two different cladding indices. The air band edge and the dielectric band edge are labeled with the letters A and B.

reduction in size a major challenge are the waveguide losses mainly due to the surface roughness of the interfaces between high index contrast materials. Traditional lithography or etching is not able to provide solutions for an ultimate roughness in the order of only a few nm. Recently surface tension induced smoothening has been demonstrated for silica (Armani et al.<sup>16</sup>) and polymers (Leinse et al.<sup>17</sup>). The latter fabricated PMMA waveguides with dispersive red-1 sidechains by conventional lithography and RIE etching (see Figure 11a). The waveguide losses at 1550 nm were measured by launching a laser in a spiral waveguide of 3.5 cm length and taking an image with an IR- sensitive CCD camera. Heating the waveguide for two hours at 135 °C allowed reflowing of the material and surface smoothening, see Figures 11b and 11c. The effect of the smoothening was a reduction of waveguide losses from 3 dB/cm to 1 dB/cm. Taking into account the materials losses, about 0.8 dB/cm as measured separately in slab waveguides, the scattering losses could be reduced to about 0.2 dB/cm.

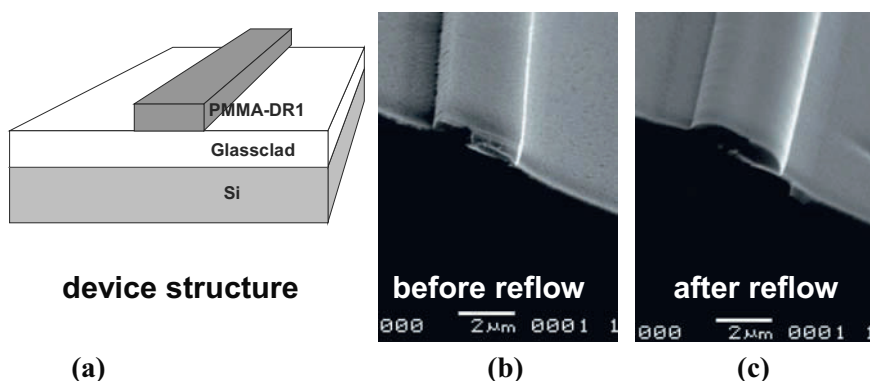


Figure 11. The effect of reflow nearby the glass transition temperature for a PMMA-DR1 waveguide; (a) device structure, (b) SEM picture of waveguide before reflow, (c) idem after reflow.

Once the problem of the scattering losses of the high index-contrast waveguiding structures is solved one should find a route to low-cost mass production. Currently the cost of packaging of integrated optical devices, including fiber-chip coupling, electrical connections and hermetic closure, is 60% to 80% of the total costs. It is evident that only an integral approach to the complete design will result in devices that are reliable, user friendly, low-cost, suitable for automated production, ergonomically and safe without compromises in technical specifications.

Presently integrated optics devices are produced on a small scale by a multi-step clean-room technology involving a large number (>30) of precision steps including repeated deposition of layers, advanced lithography, etching and finally fiber-chip coupling and bonding. To avoid this inherently expensive processing simple fabrication techniques have to be

used like working with photo definable polymers, using high precision molding techniques (like the audio and video CDs) and applying passive alignment for fiber-chip coupling. Another route to low-cost production is further miniaturization resulting in an extreme small chip area that allows integration of thousands or more complete devices on a single wafer. With both approaches a route to low-cost mass production becomes feasible so that on a longer term complex disposable optical sensors will become possible.

Finally there is the challenge of complexity, which enters if one would like to quit from expensive external optical measuring apparatus like tunable light sources, spectrometers and sensitive detector arrays. This is possible if the optical sensor itself incorporates these optical functions. Consider, for example, a sensor chip where microresonators with the typical wavelength response as depicted in Figure 2b are employed as wavelength filter together with a set of microresonators as sensors (see Figure 12). In this case, a cheap broadband light source like a LED could be used together with silicon photodiodes fabricated in CMOS technology. An additional advantage is the inherent possibility for temperature compensation, as only one of the microresonators for each wavelength is exposed to the measurand.

The complexity increases even more if one starts incorporating multisensor functions, Figure 13. Even if for improved performance the filter elements would consist of cascaded microresonators selecting 8 wavelengths, the complete multi-sensor with 96 microresonators could still fit on a few mm<sup>2</sup>. In this way an optical nose or optical tongue with only a modest power supply and without optical peripheral equipment would become feasible.

Increasing complexity of optical sensing circuits is not just doing more of the same. Progress has to be made in several fields. New software tools have to be developed which allow optimization of circuits with a large number of functions. There are commercial software packages available for single

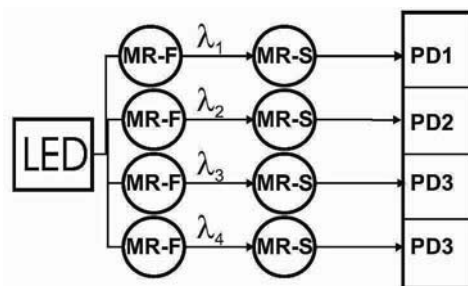


Figure 12. Schematic lay-out of compact optical sensor chip without need of external optical apparatus with identical microresonators as sensors; LED: broad band source, for example Light Emitting Diode, MR-F: microresonator used as optical filter, MR-S: microresonator used as optical sensor, PD: Photo Diode.

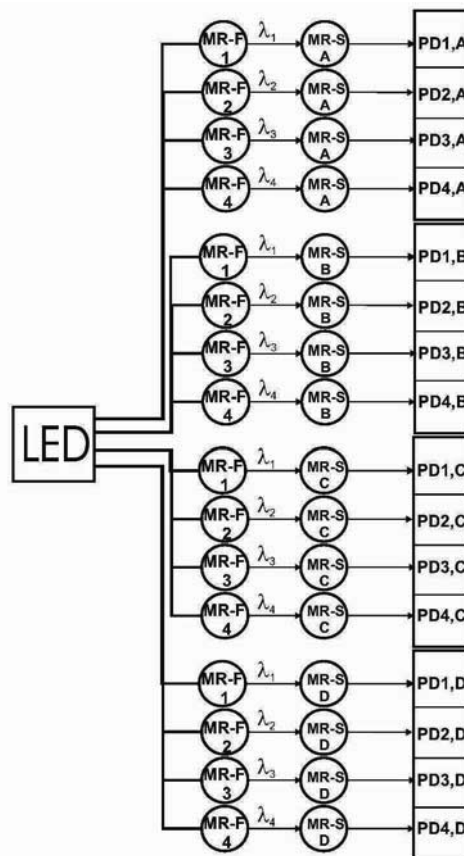


Figure 13. Schematic lay-out of compact optical sensor chip without need of external optical apparatus with 4 different sets of sensing arrays.; LED: broad band source, for example Light Emitting Diode, MR-F: microresonator used as optical filter, MR-S: microresonator used as optical sensor, PD: Photo Diode.

elements, but in contrast to electronic IC design, not for complete integrated optical systems. In addition, the technology has to be improved with respect to accuracy, uniformity, reproducibility and yield. For a single element circuit a yield of 80% is acceptable, for an 8 element circuit this would result in a yield of 17% and for 16 elements in 3%, which is becoming unrealistic small even for just demonstration purposes.

Increasing complexity means also reducing size. The devices described in the previous section had approximately a sensitive area of  $10^2$  to  $10^3 \mu\text{m}^2$ . Assuming an evanescent field penetrating  $1 \mu\text{m}$  into the measurand, the measuring volume is  $10^2$  to  $10^3 \mu\text{m}^3$ , i.e. 0.1 to 1 pL. Increasing the index contrast a measuring volume in the range of fL becomes feasible without loss in sensitivity. In this way the route to highly integrated lab-on-a-chip devices becomes practical. One also can speculate on single molecule detection or single molecule counters.

What would be the target in 10 to 20 years? A recent EC report "Vision 2020 Nanoelectronics at the Centre of Change"<sup>18</sup> identifies 7 items where nanosciences and nano-materials offer breakthrough applications; two of them deal explicitly with sensors:

- nanophotonics - will still increase the speed and lower the cost of data transmission, and also have important applications in sensor technology;
- nano-sensors and nano-actuators - more sensitive and selective sensors and actuators will accommodate voice, vision and tactile senses and stimulation, as well as offering new applications such as biometrics and environmental monitoring.

## **5. CONCLUSIONS**

In the foregoing the potential of integrated optical devices for sensing has been demonstrated and a view of present and future research has been given. A comparison with VLSI electronics has been made, but one has to bear in mind that optical circuitries have a delay of more than 30 years with respect to electronic ICs.

VLSI photonics is feasible by using high index-contrast waveguiding structures in microresonators and other advanced structures. The application fields include optical communication and optical sensing. Two approaches can be followed, index guiding with an evolutionary route to size reduction by increasing gradually the index contrast, and PBG structures, which from the very beginning apply ultra high index-contrast in ultra-compact structures. Both approaches make use of nanophotonic technology.

Severe challenges have to be faced to arrive eventually at low-cost, mass produced VLSI photonic sensors, among others: improved design software, integrated design, improved technology with excellent reproducibility, uniformity and yield with tight specifications and automated production and testing procedures. Once these have been achieved, optical sensors will become consumer photonics devices.

The progress in photonic circuits now and in the near future will be mainly driven by the needs of optical communication. Other application fields, like optical sensing, can take profit of the results obtained there and apply them to the own specific demands.

The introduction of low-cost, mass-produced optical nano-sensors will be based on multidisciplinary research where all aspects - photonics, micro- en nanotechnology, (bio-)chemistry of interfaces and system aspects - are considered. Real breakthrough therefore will be only possible in close cooperations between strong groups active in the different fields.

## ACKNOWLEDGMENTS

The authors would like to thank Mart Diemeer, Anton Hollink, Arne Leinse, Gabriel Sengo, Freddy Tan, Henk van Wolferen and Kerstin Wörhoff for their contribution in the research described in this paper.

Financial support is acknowledged of the Dutch Science Foundations FOM, STW and BTS and the EC project NAIS.

## REFERENCES

1. Little B.E., Chu S.T., Pan W., Kokubun Y., Microring resonator arrays for VLSI photonics, *IEEE Phot. Techn. Letters* 2000; 12: 323-325.
2. Klunder D.J.W., Krioukov E., Tan F.S., van der Veen T., Bulthuis H.F., Sengo G., Otto C., Hoekstra H.J.W.M. and Driessen A., Vertically and laterally waveguide-coupled cylindrical micro resonators in Si<sub>3</sub>N<sub>4</sub> on SiO<sub>2</sub> technology, *Appl. Phys. B* 2001; 73: 603-608.
3. Klunder D.J.W., Photon Physics in Integrated Optics Microresonators, Ph.D. thesis, University of Twente, 135 p (2002).
4. Driessen A., Geuzebroek D.H., Hoekstra H.J.W.M., Kelderman H., Klein E.J., Klunder D.J., Roeloffzen C.H.G., Tan F.S., Krioukov E., Otto C., Gersen H., van Hulst N.F. and Kuipers L., Microresonators as building blocks for VLSI photonics, AIP Conf. Proc. 709, 1-18 (2004).
5. Akahane Y., Asano T., Song B.S. and Noda S., High-Q photonic nanocavity in a two-dimensional photonic crystal, *Nature* 2003; 425: 944-947.
6. Heideman R.G. and Lambeck P.V., Remote opto-chemical sensing with extreme sensitivity: design, fabrication and performance of a pigtailed integrated optical phase-modulated Mach-Zehnder interferometer system, *Sensors and Actuators B* 1999; 61: 100-127.
7. Krioukov E., Klunder D.J.W., Driessen A., Greve J., Otto C., *Optics Letters* 2002; 27: 512-514.
8. Wörhoff K., Hilderink L.T.H., Driessen A., and Lambeck P.V., Silicon oxynitride: a versatile material for integrated optics application, *J. Electrochem. Soc.* 2002; 149: 85-91.
9. Chao C-Y. and Guo L.J., Biochemical sensors based on polymer microrings with sharp asymmetrical resonance, *Appl. Phys. Letters* 2003; 83: 1527-1529.
10. Krioukov E., Klunder D.J.W., Driessen A., Greve J., Otto C., Integrated optical microcavities for enhanced evanescent-wave spectroscopy, *Optics Letters* 2002; 27: 1504-1506.
11. Prasad P.N., *Nanophotonics*, John Wiley, Hoboken, New Jersey (2004), pp 67 ff.
12. Holtz J.H. and Asher S.A., Polymerized colloidal crystal hydrogel films as intelligent chemical sensing materials, *Nature* 1997; 389: 829-832.
13. El-Kady, Biswas R., Ye Y., Su M.F., Puscasu I., Pralle M., Johnson E.A., Daly J. and Greenwald A., Tunable narrow-band infrared emitters from hexagonal lattices, *Photonics and Nanostructures* 2003; 1: 69-77.
14. See <http://www.ion-optics.com/sensorchip.asp>.
15. Hopman W., Pottier P., Yudistira D., van Lith J., Lambeck P.V., de la Rue R., Driessen A., Hoekstra H.J.W.M. and de Ridder R.M., Proc. ICTON 2004, Wroclaw, Poland, pp.342-345 (2004).
16. Armani D.K., Kippenberg T.J., Spillane S.M. and Vahala K.J., Ultra-high-Q toroid microcavity on a chip, *Nature* 2003; 421: 925-928.



17. Leinse A., Diemeer M.B.J. and Driessen A., Scattering loss reduction in polymer waveguides by reflowing, *Electron. Letters* 2004; 40: 992-993.
18. Report of European Nanoelectronics Initiative Advisory Council, Vision 2020 Nanoelectronics at the Centre of Change, June 2004, <http://www.cordis.lu/ist/eniac/>

## Chapter 15

# POLYMERS FOR OPTICAL SENSORS

Gerhard J. Mohr  
*Institute of Physical Chemistry*  
*Friederich-Schiller University Jena*  
*Lessing St. 10*  
*D-07743 Jena, Germany*

### 1. WHY POLYMERS FOR OPTICAL SENSORS?

Polymer materials are frequently used matrices for the indicator chemistry in optical sensors. This is necessary for several reasons: first, the indicator has to be immobilized to an optical waveguide or an optical fibre which is then brought into contact with the analyte solution. If one would pour an aqueous solution of the indicator dye directly into the sample solution, *e.g.* into a bioreactor, then the whole sample solution would be contaminated.

Next, the indicator dye needs a solvent to interact with the analyte. Pure crystalline indicator dyes might react at the surface but not all indicator would react due to hindered diffusion. Therefore, the indicator is dissolved in a polymer which allows free diffusion of the analyte to and from the indicator molecule.

The polymer has the function to retain the indicator in place so that no leaching into *e.g.* aqueous sample solution occurs. This can be achieved by covalently immobilizing the dye to the matrix but also by simply dissolving a hydrophobic and water-insoluble dye in a hydrophobic polymer.

The polymer can also be used to tailor the selectivity and sensitivity of the optical sensor due to enrichment of the analyte by the polymer material. Furthermore, the polymer may be permeable for gases but not by ions again inducing selectivity for certain analytes. Finally, the polymer can provide optical isolation against ambient light and thus prevent bleaching and light interference.

## 2. REQUIREMENTS FOR SENSOR POLYMERS

Polymer materials have to fulfil various requirements to enable optical sensing. First of all, the indicator dye and all additives have to dissolve well in the polymer (and must not be washed out). The analyte also has to be soluble in the polymer and must be able to diffuse fast into the polymer and within the polymer. The polymer material has to be chemically and physically stable in order to achieve good operational lifetime and shelf-life (important for practical applications). Furthermore, no crystallisation/migration/reorientation of the indicator chemistry in the polymer must occur. This can happen even after weeks or months if indicator solubility is not as high as expected. The polymer must be stable even at elevated temperatures (e.g. to be resistant to steam heat sterilization). It should be stable against ambient light, chemicals (acids, bases, oxidants) and it should be non-toxic and biocompatible (especially when used in clinical and biochemical applications). The polymer should not have any intrinsic colour/luminescence, and it should be optically transparent in the spectral range where measurements are being performed. Finally, the material should have good mechanical stability.

## 3. TYPES OF POLYMERS USED IN OPTICAL SENSING

### 3.1 Lipophilic Polymers and Plasticizers

Polymers that have a high glass transition temperature ( $T_g$ ) are brittle. They require plasticizers to make them flexible. Furthermore, the high density/rigidity of the polymer chains (without plasticizers) hinders diffusion of ions and gases in the polymer matrix. Therefore, a plasticizer content of up to 66% is required for the preparation of sensor layers. While poly(vinyl chloride) is soluble in tetrahydrofuran and cyclopentanone, polymers such as poly(methyl methacrylate), polystyrene and poly(vinyl acetate) are also soluble in ethyl acetate, ethylmethyl ketone, or dichloromethane (Table 1). The advantage of plasticized polymers is that their polarity and lipophilicity (and thus selectivity and sensitivity) can be tailored by using different plasticizers with different physical properties. High  $\epsilon$  values indicates strong polarity while high  $\log P$  values indicates high lipophilicity<sup>1</sup> (Tables 2 and 3). A significant disadvantage is that plasticizers may leach out into sample solution or may evaporate on storage. If toxic they must not be used for clinical diagnostics. Immobilization of the indicator chemistry is usually performed by dissolving hydrophobic dyes and ligands in hydrophobic polymers.

Table 1. Lipophilic polymers.

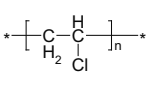
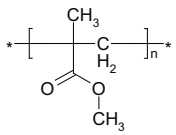
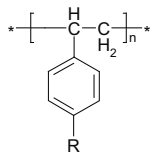
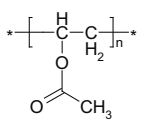
			
poly(vinyl chloride) (T <sub>g</sub> ~90 °C)	poly(methyl methacrylate) (T <sub>g</sub> ~100 °C)	polystyrene-derivatives (T <sub>g</sub> 100-140 °C)	poly(vinyl acetate) (T <sub>g</sub> ~30 °C)

Table 2. Lipophilic plasticizers.

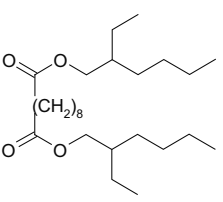
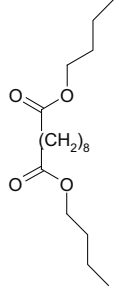
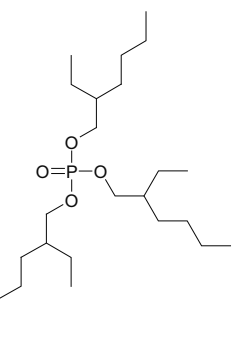
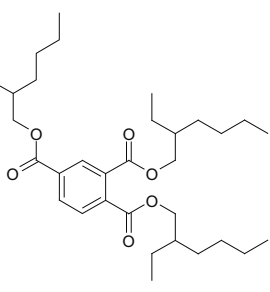
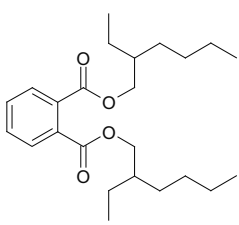
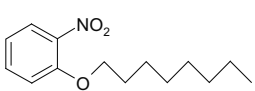
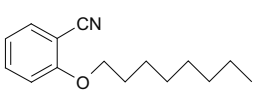
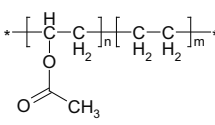
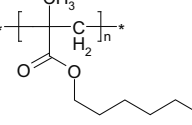
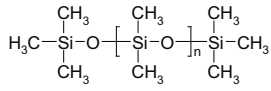
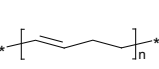
			
bis(2-ethylhexyl) sebacate ( $\epsilon = 3.9$ , log P = 11.0)	dibutyl sebacate ( $\epsilon = 4.4$ , logP = 6.4)	tris(2-ethylhexyl) phosphate ( $\epsilon = 4.8$ , log P = 10.2)	tris(2-ethylhexyl) trimellitate ( $\epsilon = 4.6$ , log P = 17.0)

Table 3. Lipophilic and polar plasticizers.

		
bis(2-ethylhexyl) phthalate ( $\epsilon = 4.9$ , log P = 9.0)	2-nitrophenyloctyl ether ( $\epsilon = 23.9$ , log P = 5.8)	2-cyanophenyloctyl ether ( $\epsilon = 23.0$ , log P = 5.0)

Polymers with low glass transition do not require plasticizers. However, these compounds are often unpolar (Table 4) and, consequently, they are unsatisfactory solvents for polar ligands, ionophores, dyes and analytes.

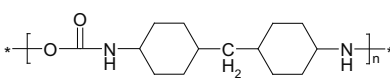
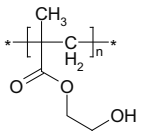
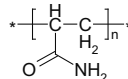
Table 4. Unpolar polymers.

			
poly(ethylene vinyl acetate)	poly(hexylmethacrylate) (T <sub>g</sub> -4 °C)	poly(dimethyl siloxane) (ε ~ 3, T <sub>g</sub> -80 to -40 °C)	cis-polybutadiene (ε ~ 2, T <sub>g</sub> -100°C)

### 3.2 Hydrophilic Polymers

Hydrophilic polymers (Table 5) provide a matrix which is comparable to an aqueous environment. Ions can diffuse quite freely, but the possible water uptake (10-1000%) can cause significant swelling of the polymer. Swelling of the matrix affects the optical properties of the sensors and, consequently, the signal changes. Immobilization of the indicator chemistry usually is achieved via covalent bonding to the polymer.

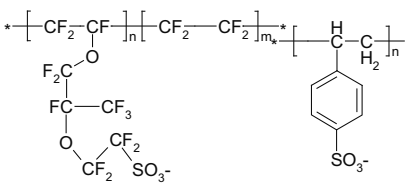
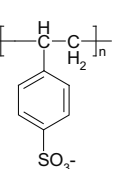
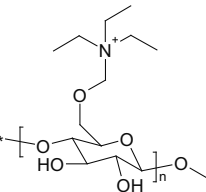
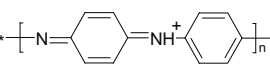
Table 5. Hydrophilic polymers.

		
polyurethane	poly(2-hydroxyethyl methacrylate)	poly(acryl amide)

### 3.3 Ionic Polymers (Polyelectrolytes)

Polyelectrolytes (Table 6) exhibit a large amount of dissociable groups. These compounds are often used for ion-exchange chromatography. They can also be used to exchange their counterions with indicator ions (see section 4).

Table 6. Ionic polymers.

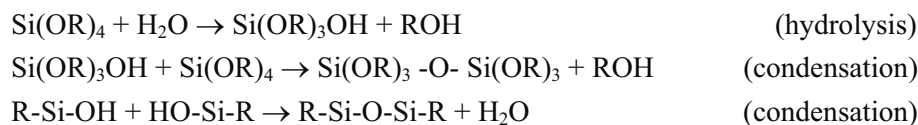
			
Nafion™	polystyrene sulfonates	triethylammonium-methylcellulose	polyaniline

### 3.4 Sol-Gel Glass

The sol-gel process allows the preparation of glass films into which indicator chemistry can be incorporated. The production of ceramic materials and glassy networks is based on the polymerisation of suitable precursors at low temperature. The increasing popularity of sol-gels in sensor applications results from the processing versatility<sup>2</sup>.

There are a number of variables which affect the hydrolysis and condensation rates and hence the microstructure of the sol-gel glass. The detailed microstructure of sol-gel glasses depends on parameters such as nature and concentration of the catalyst, water sol-gel precursor ratio, precursor type, nature of the solvent, ageing time, ageing temperature, drying time and drying temperature. The process can be adapted for formation of thin sensor layers and for nanoparticles. At the sol stage, thin glass films can be formed by dip-coating or spin-coating. These films are porous and are used for sensor applications.

The sol-gel process involves the preparation of inorganic matrices via three steps. Components of the sol-gel cocktail are the sol-gel precursor (e.g. tetramethoxysilane), water, a catalyst (acids or bases), the indicator chemistry and a solvent such as ethanol. Mixing these components causes hydrolysis of the ester, silanol-ester condensation, and silanol-silanol condensation of the precursors:



The first phase in the process is the formation of the “sol”. A sol is a colloidal suspension of solid particles in a liquid. Colloids are solid particles with diameters of 1-100 nm. After a certain period, the colloidal particles and condensed silica species link to form a “gel” - an interconnected, rigid network with pores of submicrometer dimensions and polymeric chains whose average length is greater than one micrometer. After the sol-gel transition, the solvent phase is removed from the interconnected pore network. If removed by conventional drying such as evaporation, so-called “xerogels” are obtained, if removed via supercritical evacuation, the product is an “aerogel”.

“Ageing” is the process that take place after mixing precursor, water, solvent and catalyst to form a sol, but before coating, in the case of coating sols. Ageing or pre-polymerisation of the sol causes aggregation due to hydrolysis and condensation reactions, and consequently an increase in viscosity. During this step, the sol is allowed to stand either at room

temperature or at a higher temperature for a period of time during which hydrolysis and condensation reactions cause aggregation and cross-linking.

The “gel point” is defined as the point at which the entire solid mass becomes interconnected. The physical characteristics of the gel network depends upon the size of particles and extent of cross-linking prior to gelation. Acid-catalysis leads to a more polymeric form of gel with linear chains as intermediates. Base-catalysis yields colloidal gels where gelation occurs by cross-linking of the colloidal particles.

Sol-gel glass is ion-permeable due to its residual hydroxy groups and its porosity, and can be used to optically measure pH by entrapping (caging) conventional pH indicator dyes in the material. Often, water soluble indicator dyes do not have to be chemically modified for immobilisation (see chapter 4) because, due to their size, they are retained in the pores of the sol-gel glass and are not washed out.

Ormosils (organically modified siloxanes) represent hybrid systems in which several precursor types such as organotrialkoxysilanes or diorganodialkoxysilane precursors ( $R'Si(OR)_3$  or  $R'_2Si(OR)_2$ , respectively) are combined in which  $R'$  represents a non-hydrolyzable organic substituent (e.g. methyl, octyl or phenyl). The substituent  $R'$  can also be a reactive aminopropyl group which allows subsequent covalent binding of indicators. Ormosils are not as hydrophilic and brittle as conventional sol-gel glass. If the content of alkyl chains  $R'$  increases, then the material turns hydrophobic and ion-impermeable. Nevertheless, due to its gas-permeability, it can be used for sensing acidic or basic gases which permeate the material and react with indicator dyes (e.g. by protonation/deprotonation of pH indicators).

### 3.5 Molecularly Imprinted Polymers (MIPs)

Molecularly imprinted polymers have recently attracted much attention because they are denoted as artificial antibodies which are made from simple chemical components via polymerization and can be used for the preparation of biomimetic sensors, affinity separation matrices, catalysts, etc. (Figure 1).

Molecular imprinting can be accomplished in two ways: (a), the self assembly approach and (b), the preorganisation approach<sup>3</sup>. The first involves host guest complexes produced from weak intermolecular interactions (such as ionic or hydrophobic interaction, hydrogen bonding) between the analyte molecule and the functional monomers. The self assembled complexes are spontaneously formed in the liquid phase and are sterically fixed by polymerisation. After extraction of the analyte, vacant recognition sites specific for the imprint are established. Monomers used for self assembly are methacrylic acid, vinylpyridine and dimethylamino methacrylate.

The preorganisation approach (b) involves formation of strong reversible covalent arrangements (boronate esters, imines, ketals) of the monomers

with the print molecule before polymerisation. Thus, the print molecule has to be chemically derivatised with the monomers before actual imprinting is performed. After cleaving the covalent bonds and removal of the print molecules, recognition sites complementary to the analyte are obtained again.

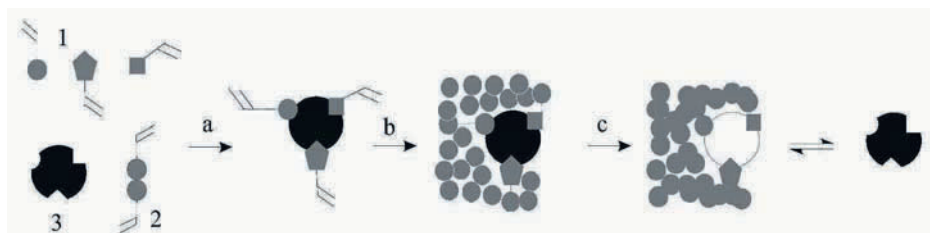


Figure 1. 1, Functional monomers; 2, Cross-linker; 3, Analyte; a, Self-assembly or Pre-organisation; b, Polymerisation; c, Removal of the analyte.

Optical sensors based on molecular imprints can be obtained by copolymerising indicator dyes that respond to the analyte by changing their colour<sup>4</sup> (Figure 2). Another approach is to label the analyte with a small dye molecule, perform imprinting, and then measure the competitive release of the labelled molecule when the MIP is exposed to the actual analyte. Recently, indicator dyes that can perform reversible chemical reactions with the analyte and additionally have functional groups for polymerization have been used for the preparation of MIP-based optical sensor layers<sup>5</sup>. These layers can selectively distinguish between analyte molecules and have detection limits down to the subnanomolar range.

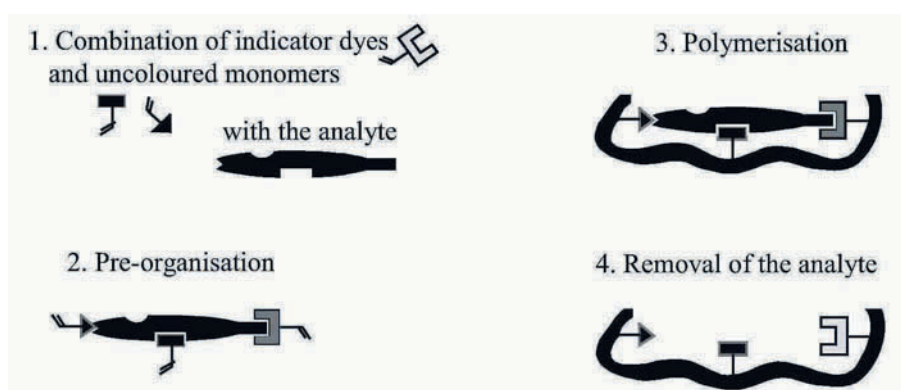


Figure 2. Preparation of coloured molecularly imprinted polymers using analyte sensitive indicator dyes.

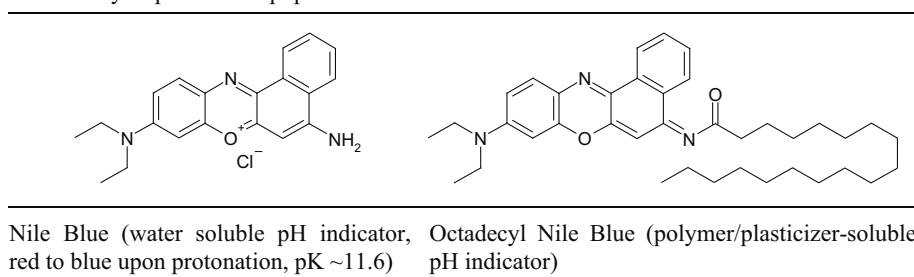


## 4. IMMOBILISATION OF INDICATOR CHEMISTRY IN POLYMERS

### 4.1 Hydrophobic Interactions

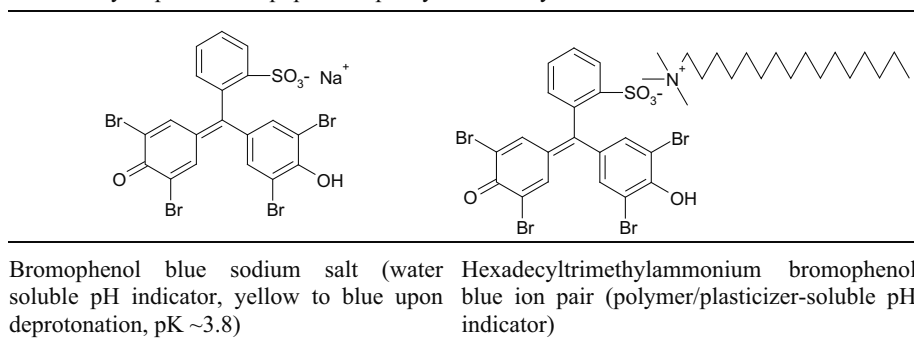
Most indicator chemistry is adapted to aqueous solution (for titration in water). Therefore, the molecules are water-soluble and if dissolved in lipophilic polymers, they are washed out immediately. In order to make dyes, ionophores and ligands soluble in polymers and to avoid leaching of the components into the sample solution, they have to be made lipophilic<sup>6</sup>.

Table 7. Hydrophilic and lipophilic Nile Blue derivatives.



Lipophilic molecules can be obtained by introduction of long alkyl chains (Table 7). However, the chemical synthesis involved can be tedious. Therefore, another possibility is to obtain lipophilic compounds by ion-pairing. Ion pairs are mostly obtained by dissolving both components (water-soluble ionic indicator and water-soluble ionic surfactant of opposite charge) separately in water, pouring both solutions together and filtrating the precipitated product. For example, by mixing aqueous solutions of the sodium salt of bromophenol blue and hexadecyltrimethylammonium chloride a lipophilic polymer-soluble dye is obtained<sup>7</sup> (Table 8).

Table 8. Hydrophilic and lipophilic triphenylmethane dyes.



## 4.2 Ion-Exchange

Positively or negatively charged indicators can be made lipophilic by ion-pairing with surfactants. However, they can also be directly immobilised on the polymer by ion-pairing with ionic polymers (polyelectrolytes) (Table 9). Solutions or suspensions of the polymer are then mixed with aqueous or alcoholic solutions of the dye.

Table 9. Ion pairs of indicator dyes with polyelectrolytes.

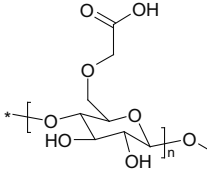
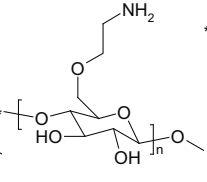
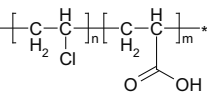
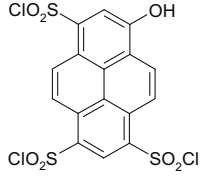
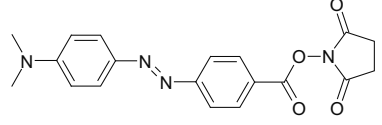
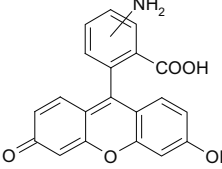
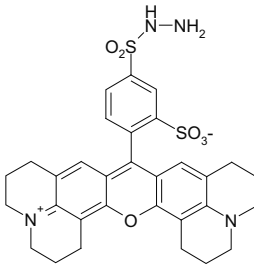
Bromophenol Blue immobilized on triethylammonium methylcellulose	[1,5-Bis(p-dimethylaminophenyl)-2,4-pentadienyl]-carbenium ion immobilised on Nafion <sup>TM</sup>

## 4.3 Covalent Immobilisation

Covalent immobilisation of the indicator chemistry to the polymer matrix is the “Via Regia” of all immobilisation methods. The operational stability and shelf life is superior (no leaching, crystallisation, evaporation of components). However, to obtain indicator chemistry and polymers with functional groups is inevitably linked with significant synthetic effort. Very often, chemical modification of dyes negatively affects their selective and sensitive analyte recognition. In principal two different ways of immobilisation are possible, namely (a) to bind a reactive dye (e.g. fluorescein succinimidyl ester) to a reactive polymer matrix (e.g. aminocellulose), or (b) to polymerise a reactive dye (e.g. a dye with a methacrylate group) with monomers such as methyl methacrylate to give a copolymer<sup>8</sup> (Table 10).

Several indicator dyes are available in a reactive form (primarily for labelling of peptides, proteins or DNA). These reactive molecules with isothiocyanate groups, sulfonyl chloride groups, vinylsulfonyl groups, or succinimidyl groups (fluorescein isothiocyanate, dabcyll succinimidyl ester, hydroxypyrene trisulfonyl chloride) can be covalently attached to aminoethylcellulose or amino-PVC. Indicator dyes with amino or hydrazide groups (aminofluorescein, Texas Red hydrazide) can be coupled to carboxy-PVC or carboxymethylcellulose (Table 10).

Table 10. Polymers and indicator dyes for covalent immobilization of the sensor chemistry.

			
carboxymethyl cellulose	aminoethyl cellulose	carboxy-PVC	8-hydroxypyrene-1,3,6-trisulfonyl chloride
			
DabcyI-N-succinimidyl ester	aminofluorescein	Texas Red hydrazide	

The synthesis of vinylsulfonyl dyes is a good example for a method to obtain pH indicator layers with operational stability of weeks and shelf life of years. Commercial transparencies with a cellulose coating are used as the polymer matrix and the reactive vinylsulfonyl dye is bound to the cellulose

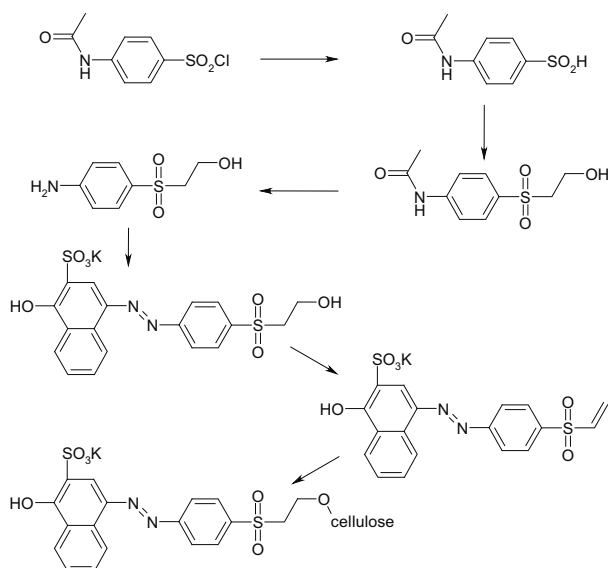


Figure 3. Synthesis of vinylsulfonyl indicator dyes for covalent immobilization to the polymer matrix via Michael addition.

directly from aqueous solution. The cross-sensitivity of the sensor material to changes in ionic strength is low, and the  $pK_a$  of 7.34 matches the physiological range (colour change from yellow to purple). Nevertheless, six synthesis steps have to be performed before obtaining the optical sensor layers<sup>9</sup> (Figure 3).

Another way for covalent immobilisation is to synthesise indicator chemistry with polymerizable entities such as methacrylate groups (Figure 4). These groups can then be copolymerized with monomers such as hydrophobic methyl methacrylate or hydrophilic acryl amide to give sensor copolymers. In order to obtain self-plasticized materials, methacrylate monomers with long alkyl chains (hexyl or dodecyl methacrylate) can be used. Thus, sensor copolymers are obtained which have a  $T_g$  below room temperature. Similarly, ionophores and ionic additives (quaternary ammonium ions and borates) can be derivatised to give methacrylate derivatives.

## 5. POLYMER EFFECT ON INDICATOR CHEMISTRY

The recognition process of the analyte by the indicator chemistry can be completely different, dependent on whether a hydrophilic or a lipophilic polymer matrix is used. In the case of lipophilic polymers, analyte ions can

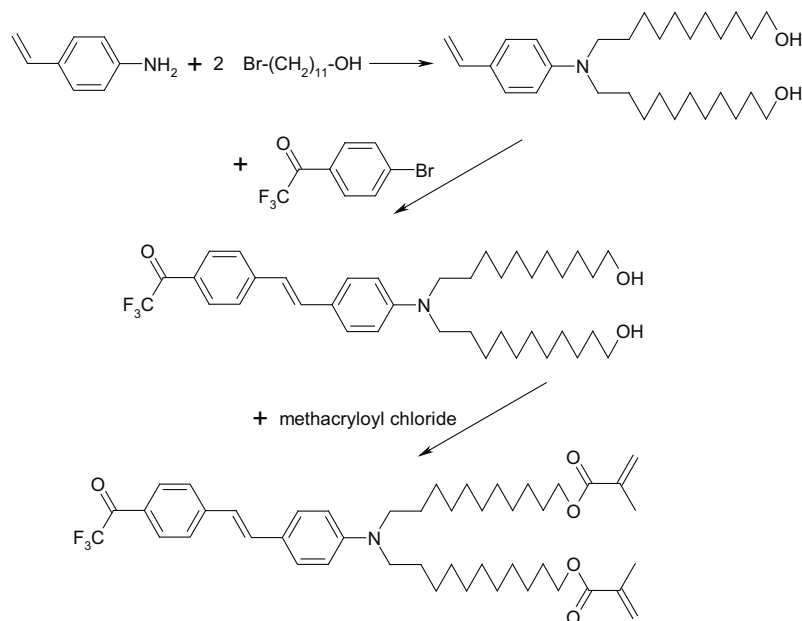


Figure 4. Synthesis of an indicator dye for amines which exhibits methacrylate groups for preparation of copolymers. The dye shows a reversible change in fluorescence from green to blue upon interaction with amphetamine.

only be transported into a polymer layer, if simultaneously another ion is released or co-extracted (see below). This restriction is not valid for hydrophilic polymers, and clearly not for neutral analytes.

## 5.1 Co-Extraction and Ion-Exchange

The optical sensors are composed of ion-selective carriers (ionophores), pH indicator dyes (chromoionophores), and lipophilic ionic additives dissolved in thin layers of plasticized PVC. Ionophores extract the analyte from the sample solution into the polymer membrane. The extraction process is combined with co-extraction or exchange of a proton in order to maintain electroneutrality within the unpolar polymer membrane. This is optically transduced by a pH indicator dye (chromoionophore)<sup>10</sup>.

The preparation of sensor layers is relatively simple. It only requires to dissolve the components (pH-indicator dye, ionophore, ionic additive) together with poly(vinyl chloride) and a plasticizer in tetrahydrofuran (similar to ion-selective electrode membranes). The solutions are then spin-coated on transparent support materials and fixed in flow-through cells, or they are applied onto optical fibres as well as planar wave guides by dip-coating. Since the recognition element (ionophore) and the optical transducer (pH indicator) are different molecules, almost any available ionophore can be combined with one appropriate pH-indicator. Furthermore, it is possible to tailor the properties of the sensor by using plasticizers of different polarity. The mechanism is mathematically well-defined and allows to predict the dynamic range and selectivity of the sensor membrane. A severe disadvantage is the intrinsic cross-sensitivity to pH because sensors based on ion-exchange measure the ratio of activities between analyte ion and the proton, and sensors based on co-extraction measure the product of activities of analyte and protons. In other words, it is not possible to distinguish whether colour changes are due to changes in analyte concentration or due to changes in pH. Consequently, the pH of the sample solution has to be determined or to be adjusted by addition of buffer.

### 5.1.1 Measurement of Cations

In the case of ion-exchange, a selective carrier (e.g. valinomycin for potassium) extracts the cation into the polymer layer (Figure 5 and Table 11).

In order to maintain electroneutrality within the polymer layer, a pH indicator dye (also contained in the layer) releases a proton into aqueous solution. Due to this deprotonation of the dye, a colour change is observed that relates to the concentration of the analyte cation (Table 12).

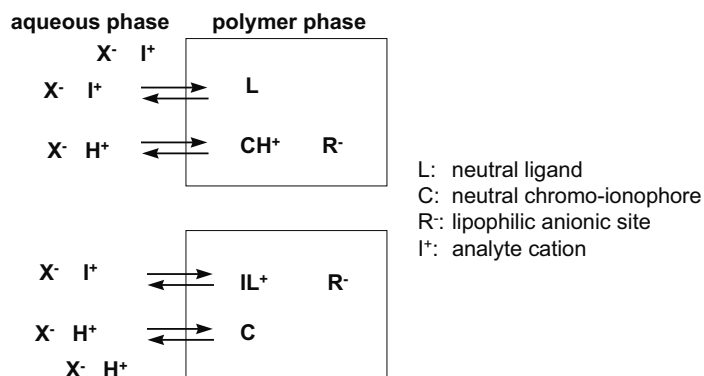


Figure 5. Mechanism of ion-exchange of an analyte ion (I<sup>+</sup>) and a proton (H<sup>+</sup>) between the sensor membrane and the aqueous phase.

Table 11. Selective ligand and ionic additive for ion-exchange sensors.

<p>Calcium-selective ionophore ETH 1001</p>	<p>Lipophilic anionic additive potassium tetrakis(3,5-bis(trifluoromethyl)-phenyl) borate (PTTFPB)</p>

Table 12. Sensor for calcium based on ion-exchange.

<p>pH indicator dye L 109</p>	<p>Decreasing absorbance of a calcium-sensitive ion-exchange membrane at 850 nm (composed of L109, ETH 1001 and PTTFPB in plasticized PVC) upon exposure to increasing concentrations of calcium ion</p>

### 5.1.2 Measurement of Anions

In the case of co-extraction, a selective anion-carrier (ionophore) extracts the analyte anion into the lipophilic sensor membrane. In order to maintain electroneutrality, a proton is co-extracted into the membrane where it protonates a pH indicator dye contained in the polymer membrane. Due to protonation, the dye undergoes a change in either absorption or fluorescence. (Figure 6 and Tables 13 and 14).

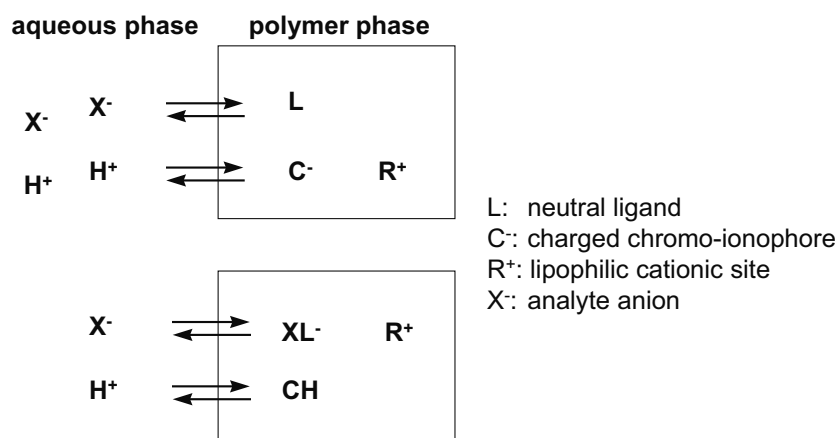
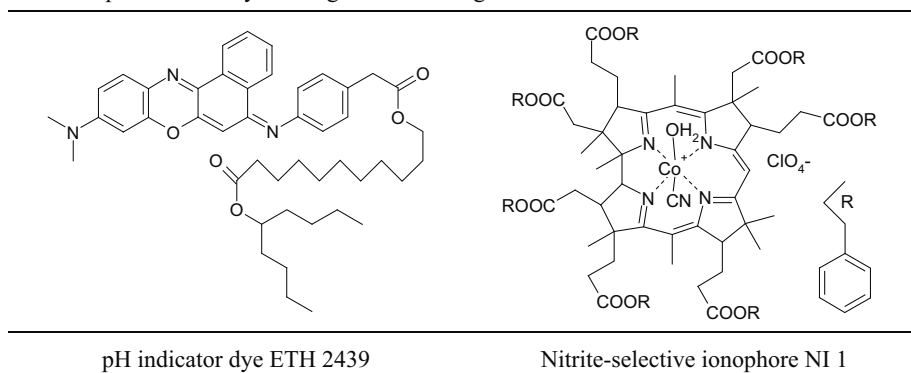


Figure 6. Mechanism of co-extraction of the analyte anion ( $X^-$ ) together with a proton ( $H^+$ ) into the sensor layer.

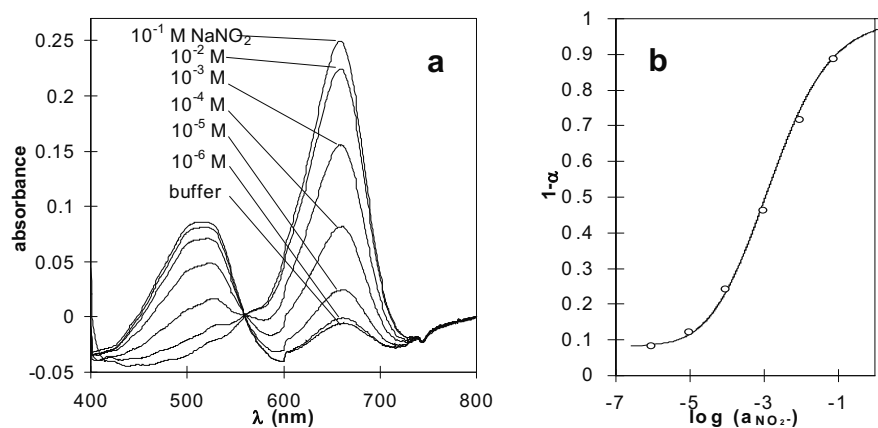
Table 13. pH indicator dye and ligand for sensing nitrite.



## 5.2 Polarity-Sensitive Dyes (PSDs)

Potential-sensitive or polarity-sensitive dyes are known to optically respond to changes in their micro-environment such as changes in polarity or lipophilicity.

Table 14. Optical response of a nitrite sensor layer.



Absorbance of a nitrite selective sensor membrane (composed of ETH 2439, NI 1, and PTTFPB in plasticized PVC) exposed to different concentrations of nitrite

Experimental (o) and theoretical (—) calibration plots

In sensor membranes based on PSDs, these changes are induced by selective carriers, which, similar to the mechanisms of co-extraction and ion exchange, extract analyte ions from the sample solution into the polymer membrane. However, the response to the increase of analyte ions in the polymer phase is different. In the case of ion exchange or co-extraction, electroneutrality in the membrane is maintained via protonation/deprotonation of pH indicator dyes. PSDs usually do not possess functional groups that can be protonated or deprotonated. Therefore, electroneutrality can only be established if the PSD moves between the aqueous and the polymer phase. As a consequence of the motion of the PSD between phases of different polarity, optical signal changes are induced which can result from aggregation, but also from solvatochromism<sup>11</sup>. The sensors exhibit significantly lower cross-sensitivity to pH than optical sensors based on the ion-exchange/co-extraction mechanism using pH indicator dyes.

### 5.2.1 Measurement of Cations

The sensor layer consists of a selective ionophore (e.g. valinomycin for potassium), a lipophilic anionic site (borate) and the cationic PSD. Before interaction with potassium, a lipophilic ion pair between the cationic PSD and borate anion is formed in the polymer layer. When valinomycin (also contained in the layer) selectively extracts potassium into the layer, then the positively charged valinomycin-potassium complex forms an ion pair with



borate. As a consequence, the cationic dye moves into the direction of the aqueous phase to maintain electroneutrality in the layer. However, exposure of the dye to the aqueous phase decreases its solubility and the dye tends to form weakly fluorescent multimers or aggregates. Consequently, a decrease in fluorescence is observed (Figure 7).

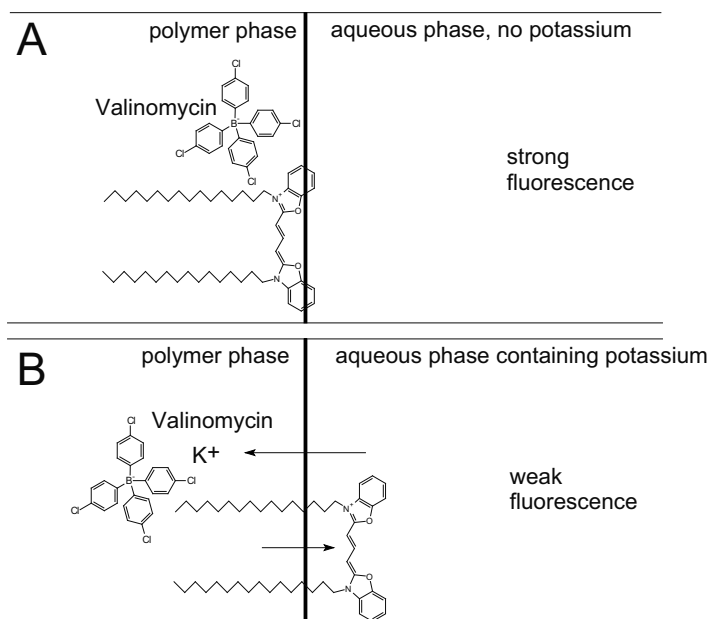


*Figure 7.* Schematic representation of the microenvironment of the cationic PSD diOC16(3) in a potassium sensor before (A) and after (B) extraction of potassium from the aqueous into the lipophilic membrane phase. The sensor membrane is composed of valinomycin, diOC16(3) and a lipophilic borate salt dissolved in plasticized PVC.

### 5.2.2 Measurement of Anions

An anion-selective sensor membrane can be obtained by dissolving a cationic PSD (e.g. rhodamine B octadecylester perchlorate) together with an anion-selective carrier in plasticized PVC. Upon exposure to the analyte, the neutral anion carrier forms a negatively charged complex which can form an ion pair with the cationic PSD. The ion pair is more lipophilic than the PSD alone and a fluorescence increase occurs. The fluorescence changes are caused by a change of the counterion of the PSD which changes the solubility of the PSD in the plasticizer. A different solubility, however, affects the dissociation of dye dimers to monomers. Since the dimers are essentially non-fluorescent, signal changes are observed which correlate with the amount of anion in the sample solution (Figure 8).

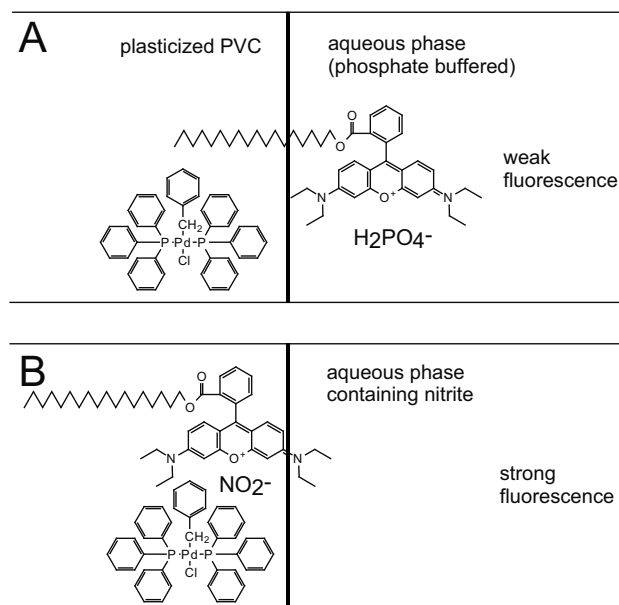


Figure 8. Schematic representation of the micro-environment of a PSD (Rhodamine B octadecyl ester) in an anion sensor before (A) and after (B) extraction of nitrite from the aqueous into the lipophilic membrane phase.

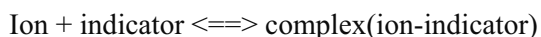
### 5.3 Chromogenic and Fluorogenic Indicators

#### 5.3.1 Measurement of Ions

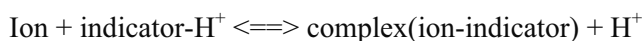
The response of optical sensors based on chromogenic and fluorogenic indicators is completely different to the sensing schemes discussed previously. The above schemes (ion-exchange, coextraction) make use of non-selective pH indicator dyes and selective ionophores. However, chromogenic and fluorogenic ligands are a combination of selective recognition and optical transduction in one molecule. They consist of a chromophoric part directly connected with the recognition moiety. Whereas ion-exchange and coextraction work best in a lipophilic polymer matrix (usually plasticized PVC), indicator dyes should be dissolved in a hydrophilic (aqueous-like) matrix in order to allow rapid diffusion of analyte ions to and from the ligands. Furthermore, due to the facilitated ion diffusion in hydrophilic matrices, no strong pH-cross-sensitivity comparable to the pH-cross-sensitivity of ion-exchange/co-extraction-based sensors is observed.

Generally, sensors based on chromogenic or fluorogenic indicators are advantageous over sensors based on PSDs or ion-exchange/co-extraction. A

specific interaction between a chromophore that already contains the moiety for analyte recognition is simpler than the above mechanisms which require lipophilic ionic sites, specific pH-indicator dyes and selective (uncoloured) ionophores. Furthermore, such ligands are generally less pH-sensitive as long as the recognition process is represented by the equilibrium:



If however, the ion binding process involves the displacement of protons according to:



then the process is cross-sensitive to pH. In order to provide a rather aqueous environment for the indicator dyes, they should be embedded in hydrophilic rather than in lipophilic polymers. This, however, demands a significant synthetic effort because the indicator has to be covalently linked to the polymer in order to prevent leaching.

### 5.3.2 Measurement of Cations

Probably the best optical sensors for pH are based on a pH indicator dye covalently immobilized on transparent cellulose membranes (Table 15). The  $\text{pK}_a$  of the dye is 7.34 and colour changes from yellow to purple are observed upon deprotonation. The cellulose membrane exhibits still more than 50% of the initial colouration after two years of storage in distilled water at ambient light.

Table 15. Vinylsulfonyl indicator dyes for sensing pH and cations.

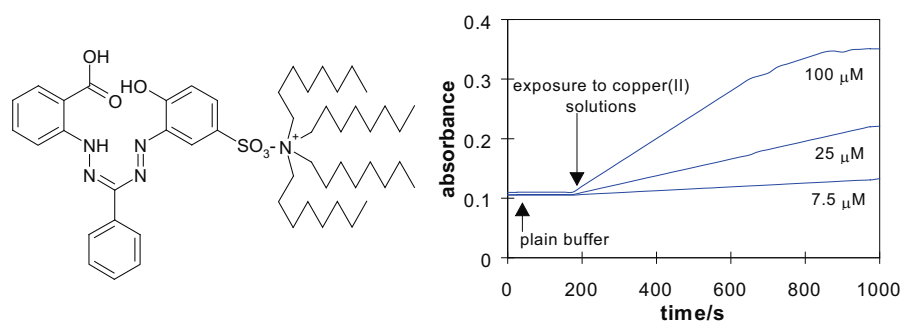
pH indicator dye covalently immobilized on a transparent cellulose membrane via the hydroxy groups of cellulose	Potassium-sensitive dye immobilized on cellulose

This type of chemistry can also be used for measurement of cations using a selective ligand (crown ether) linked to the chromophore. The colour change on complexation of potassium is from red to yellow.

Another approach for ion-sensing (here: copper and zinc) is based on the water-soluble ligand Zincon. Its lipophilic ion pair with quaternary

ammonium halides can be homogeneously dissolved in polymers such as plasticized poly(vinyl acetate), ethyl cellulose, and polyurethane (Table 16).

Table 16. Indicator chemistry for copper ion.



Chemical structure of the Zincon-tetraoctylammonium ion pair

Response of a Zincon-based sensor membrane to different  $\mu\text{M}$  concentrations of copper(II) at pH 6.0 (measured at 620 nm)

When the Zincon ion-pair is exposed to an aqueous sample containing the analyte, the latter diffuses into the sensor membrane to react with the indicator, and gives a colour transition from pink to blue at near neutral pH. The  $\text{pK}_a$  value of Zincon for the color transition from pink to blue is above 13, therefore, the sensor membrane is virtually insensitive to pH changes. However, due to the high complexation constant of Zincon for copper and zinc, the response of sensor membrane is irreversible and must be evaluated kinetically<sup>12</sup>.

### 5.3.3 Measurement of Anions

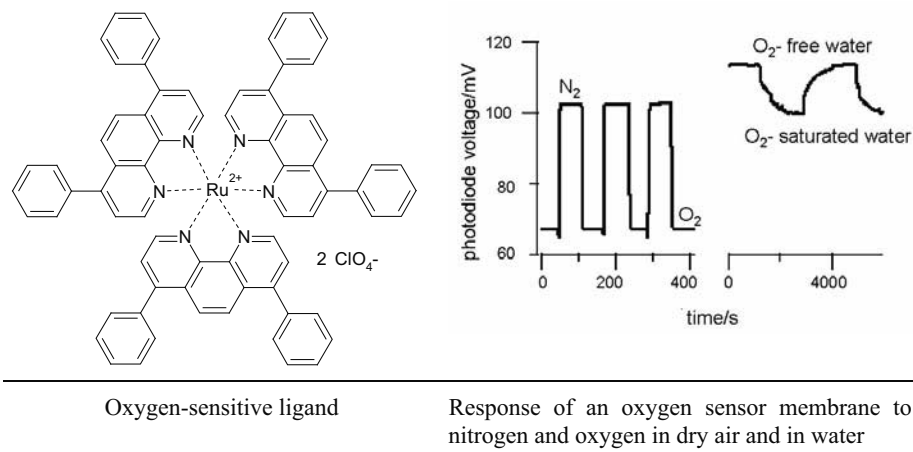
To date, there are only few applications of chromogenic or fluorogenic ligands for anion-sensing. Wolfbeis et al. have presented a sensor for halogenide ions which is based on fluorescence quenching. The indicator is a cationic fluorophore which is covalently immobilized on the polymer matrix<sup>13</sup>. The fluorescence intensity of the fluorophore decreases with increasing halide concentration. The selectivity is governed by the heavy atom effect, therefore, the sensitivity follows the order  $\text{I} > \text{Br} > \text{Cl}$ . Another approach is the chemical reaction of indicator dyes with anions to yield colour changes, e.g. the reaction of coloured aldehydes with bisulfite to form a bisulfite adduct<sup>14</sup>.

### 5.3.4 Measurement of Neutral Analytes

The majority of optical sensors for neutral (uncharged) species is based on indicators which selectively interact with the analyte and additionally give optical signal changes. Since the diffusion of neutral analytes is not as strongly affected by the polymer matrix as it is in the case of ions, all types of polymer matrices can be used.

Optical sensors for oxygen are among the few sensors, which have found practical application for process-monitoring and clinical diagnostics. They are generally based on compounds such as platinum porphyrins or ruthenium phenanthroline derivatives (Table 17) which show a decrease in luminescence upon exposure to molecular oxygen<sup>15</sup>.

Table 17. Sensor chemistry for gaseous and aqueous oxygen.



An alcohol sensor membrane is obtained by dissolving 4-*N,N*-dioctylamino-4'-trifluoroacetylstilbene (ETH<sup>T</sup> 4004) and the catalyst tridodecylmethylammonium chloride in plasticized PVC. On exposure to aqueous ethanol, the orange fluorescence of the reactand (so called because it is a combination of a chemical reagent and a ligand) decreases (Figure 9). This is due to the chemical reaction of the trifluoroacetyl group of the reactand with ethanol to form a hemiacetal. This conversion results in a change of the electron delocalization within the reactand and, consequently, in a change in fluorescence. Reversible chemical reactions of chromo- or fluororeactands with electrically neutral molecules can also be used to detect analytes such as aldehydes, amines, saccharides, carbon dioxide or sulfur dioxide<sup>14</sup>.

Sensors for acidic (HCl, SO<sub>2</sub>, CO<sub>2</sub>, acetic acid) or basic gases (NH<sub>3</sub>, amines) often make use of pH indicator dyes immobilised in polymers. Lipophilic Bromophenol Blue (see section 4.2) dissolved in silicone is

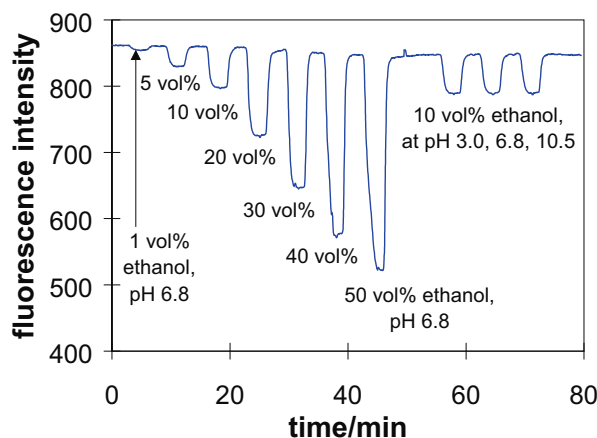
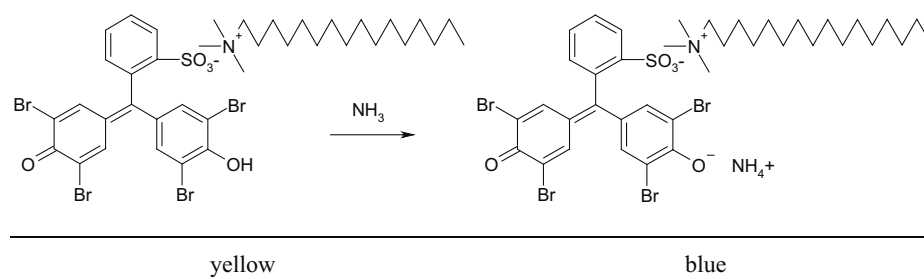


Figure 9. Response of the ethanol sensor layer based on ETH<sup>T</sup> 4004 on exposure to aqueous ethanol solutions.

deprotonated upon exposure to ammonia causing the colour to change from yellow to blue (Table 18).

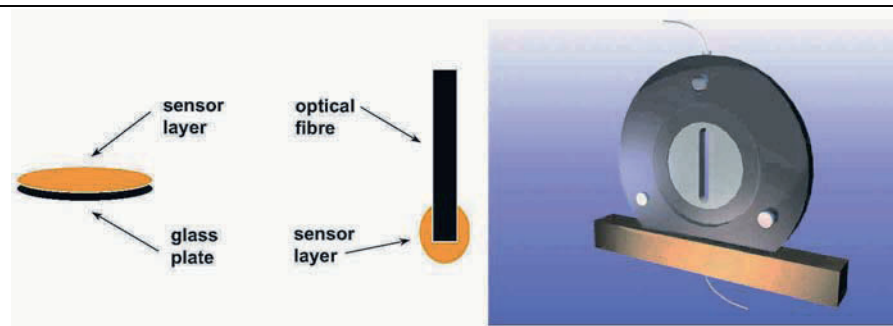
Similarly, all pH indicators mentioned in sections 4.1–4.3 can be used for measurement of acidic and basic gases.

Table 18. Sensor layer for ammonia based on a lipophilic pH indicator dye in silicone.



## 6. COMBINATION OF SENSOR MATERIALS WITH TRANSDUCERS

Sensor layers are mostly attached to a solid support since their mechanical stability is generally quite low. In most cases, all components (polymer, plasticiser, additives and indicator dyes) are dissolved in a common solvent and spin-coated, spray-coated, dip-coated or simply pipetted onto the support material (Figure 10). The solid support can be a glass plate which is mounted in a photometer and exposed to the analyte in a



Deposition of sensor layers is possible on fibre optics, planar waveguides, and test strips

Flow-through cell allowing the simultaneous exposure of the membrane to the analyte and measurement of the optical properties of the sensor layer

Figure 10. Combining sensor chemistry with optical transducers.

flow-through cell but it can as well be a surface plasmon resonance (SPR) cell, an attenuated total reflection (ATR) crystal or an optical fibre known from communication technology. Immobilisation directly on the light source, e.g. a light emitting diode (LED) is possible as well (Figure 10).

Recently, the immobilisation of indicators in tiny beads rather than in polymer layers has provided nanoparticles which can be inserted into cells and allow the measurement of various analytes (oxygen, sodium, potassium) within a living cell<sup>16</sup>.

## 7. POLYMER CHARACTERISATION

### 7.1 Relative Dielectric Constant

Mostly known for plasticizers only (see section 3.1), not for plasticized polymers or commercial polymers. The relative dielectric constant indicates the polarisability of the molecule ( $\epsilon$  of selected solvents for comparison: hexane, 1.9; toluene, 2.4; chloroform, 4.8; ethyl acetate, 6.0; dichloromethane, 9.1; acetone, 20.7; water, 80.2).

### 7.2 Lipophilicity

The logarithm of the 1-octanol - water partition coefficient, denoted  $\log K_{OW}$  or  $\log P$ , indicates the distribution of the compound between the organic and the water phase. For highly lipophilic compounds, the  $\log P$  is determined via reversed-phase thin-layer chromatography, giving the so-called " $\log P_{TLC}$ " value<sup>1</sup>.

Data are available for plasticizers and ionophores, and indicate the operational stability (the higher the  $\log P$  value, the higher the lipophilicity). The minimal lipophilicity  $\log P$  required for membrane components with a lifetime of 30 x 24 h upon exposure to aqueous solution is estimated to be around 10 whereas it has to be as high as 25 for direct measurement in blood, serum and plasma.

### 7.3 Water Uptake

A correlation between the dielectric constant of the plasticizer used in a polymer and its water uptake might be expected. However, according to the table below<sup>17</sup> (Table 19), no predictions can be made.

Table 19. Physical properties of plasticisers and polymers.

Plasticizer	Lipophilicity of plasticizer ( $\log P$ )	Dielectric constant of plasticizer	Water uptake after one week with PVC/plasticizer = 1:2
Dibutyl sebacate	6.4	4.4	0.73%
Bis(2-ethylhexyl) sebacate	11.0	3.9	0.48%
Tris(2-ethylhexyl)-phosphate	10.2	4.8	1.15%
Tris(2-ethylhexyl) trimellitate	17.0	4.6	0.32%
2-Nitrophenyloctyl ether	5.8	23.9	N/A

### 7.4 Average Molecular Weight

Often given for commercial polymers, but usually neglected when sensor performance is discussed.

### 7.5 Solubility of Analyte/Interfering Species

Usually no data available, except for gases such as oxygen, hydrogen or carbon dioxide (Polymer handbook / ed.: J. Brandrup, E. H. Immergut and E. A. Grulke; Wiley cop. 1999).



## 7.6 Glass Transition Temperature ( $T_g$ )

Represents the temperature of the conversion of an amorphous glassy or partially crystalline polymer into a rubbery viscous melt. Important for sensors, because polymers with high  $T_g$  require plasticizers for fast analyte diffusion and response time (see section 3.1).

## 7.7 Solvatochromic Characterization

Polymers can be characterized via the Kamlet-Taft approach which describes the ability of a species to act as a hydrogen bond acid ( $\alpha_1$ ), the ability to act as a hydrogen bond base ( $\beta_1$ ), the dipolarity/polarizability ( $\pi_1^*$ ), and the size of a species. These parameters are obtained by dissolving solvatochromic indicator dyes in the respective polymer and by measuring the shift of their absorbance maxima<sup>18</sup>.

The solvatochromic phenolbetaine “Reichardt’s Dye” (RD) allows to calculate a single parameter that indicates the overall polarity of the polymer. It is obtained by dissolving the dye in the polymer and measuring the absorbance maximum. The molar transition energy ( $E_T(30)$ ) of RD is an empirical parameter to scale solvent polarity and is obtained by calculating<sup>18</sup>  $E_T(30) = hc\nu_{\max}N_A$  or  $2.859\nu_{\max, RD}$ .

Table 20. Kamlet-Taft parameters and corresponding  $E_T(30)$  values.

Polymer (dry)	Hydrogen bond acidity	Hydrogen bond basicity	Polarizability	$E_T(30)$
Polystyrene	0.08	0.06	0.65	42.2
Poly(vinyl chloride)	0.06	0.07	0.87	42.9
Polymethylmethacrylate	0.24	0.38	0.76	44.0
Polyvinyl acetate	0.02	0.44	0.76	40.0
Poly(2-hydroxyethyl methacrylate)	0.67	0.43	0.98	55.0
Poly(isobutylene)	0.33	0.04	0.16	39.8
Poly(vinyl alcohol)	0.29	0.52	1.11	49.3

## REFERENCES

1. Dinten O. et al, Lifetime of neutral carrier based liquid membranes in aqueous samples and blood and the lipophilicity of membrane components, *Analytical Chemistry* 1991; 63: 596.

2. Lobnik A., Wolfbeis O.S., Sol-gel based sensor for dissolved ammonia, *Sensors and Actuators B* 1998; 51: 203.
3. Haupt K., Molecularly imprinted polymers in analytical chemistry, *Analyst* 2001; 126: 747-756.
4. Diaz-Garcia M.E., Badia R., Molecularly imprinted polymers for optical sensing devices" in *Optical Sensors: Industrial, Environmental and Diagnostic Applications*, R. Narayanaswamy, O. S. Wolfbeis, (Eds.), Springer, 2004.
5. Mertz E., Zimmerman S.C., Cross-linked dendrimer hosts containing reporter groups for amine guests, *J. Amer. Chem. Soc.* 2003; 125: 3424-3425.
6. Seiler K., Wang K., Bakker E., Morf W.E., Rusterholz B., Spichiger U.E., Simon W., Characterization of sodium-selective optode membranes based on neutral ionophores and assay of sodium in plasma, *Clinical Chemistry* 1991; 37: 1350-1355.
7. Mohr G.J. et al., Novel optical sensor materials based on solubilization of polar dyes in apolar polymers, *Advanced Materials* 1997; 14: 1108.
8. Munkholm C., Walt D.R., Milanovich F.P., Klainer S.M., Polymer modification of fiber optic chemical sensors as a method of enhancing fluorescence signal for pH measurement, *Analytical Chemistry* 1986; 58: 1427-1430.
9. Mohr G.J. and Wolfbeis O.S., Optical sensors for a wide pH range based on azo dyes immobilized on a novel support, *Analytica Chimica Acta* 1994; 292: 41-48.
10. Seiler K., Simon W., Theoretical aspects of bulk optode membranes, *Analytica Chimica Acta* 1992; 266: 73.
11. Wolfbeis O.S., Fluorescence-based ion sensing using potential-sensitive dyes, *Sensors & Actuators B* 1995; 29: 140.
12. Oehme I. et al., LED-compatible copper(II)-selective optode membrane based on lipophilized Zincon, *Fresenius Journal of Analytical Chemistry* 1994; 350: 563.
13. Huber C., Krause C., Werner T., Wolfbeis O.S., Serum chloride optical sensors based on dynamic quenching of the fluorescence of photo-immobilized lucigenin, *Microchimica Acta* 2003; 142: 245-253.
14. Mohr G.J., Chromo- and fluororeactants: Indicators for detection of neutral analytes using reversible covalent bond chemistry, *Chemistry, A European Journal* 2004; 10: 1083-1090..
15. Klimant I., Wolfbeis O.S., Oxygen-sensitive materials based on silicone-soluble ruthenium complexes, *Anal. Chem.* 1995; 67: 3160-3166.
16. Shortreed M., Kopelman R., Kuhn M., Hoyland B., Fluorescent fiber-optic calcium sensor for physiological measurements, *Analytical Chemistry* 1996; 68: 1414.
17. Dinten O., Experimental and theoretical contributions in order to improve ion-selective electrodes based on PVC liquid membranes in terms of membrane technology, *ETH Ph.D. thesis* No. 8591, 1988.
18. Paley M.S. et al., Solvatochromism. A new method for polymer characterisation, *Macromolecules* 1990; 23: 4557.

## Chapter 16

# FUNDAMENTALS OF ENZYME-BASED SENSORS

María C. Moreno-Bondi and Elena Benito-Peña

*Department of Analytical Chemistry*

*Faculty of Chemistry, Universidad Complutense*

*28040 Madrid, Spain*

### 1. INTRODUCTION

One of the mayor outbreaks in the development of analytical measurement techniques was the introduction, in the mid-twentieth century, of bioprobes for the analysis of chemical and biochemical compounds in real samples. The first devices, developed in the 1950's and 1960's by Clark et al.<sup>1, 2</sup>, were based on electrochemical measurements and allowed the determination of oxygen and glucose in tissues and blood samples. Later on, in the 1970's, optical transduction was coupled to enzymatically-catalyzed reactions<sup>3</sup> and since those early days the field of application of optical biosensors has broaden up considerably. According to the definition proposed by the International Union of Pure and Applied Chemistry (IUPAC)<sup>4</sup>: “*A biosensor is a self-contained integrated device which is capable of providing specific quantitative or semi-quantitative analytical information using a biological recognition element (biochemical receptor) which is in direct spatial contact with a transducer element. A biosensor should be clearly distinguished from a bioanalytical system, which requires additional processing steps, such as reagent addition. Furthermore, a biosensor should be distinguished from a bioprobe which is either disposable after one measurement, i.e. single use, or unable to continuously monitor the analyte concentration*”. The general scheme of a biosensor configuration is shown in Figure 1. Biosensors that include transducers based on integrated circuit microchips are known as biochips<sup>5</sup>.

Biosensors will thus include a recognition element of biological nature, that allows the selective recognition of the analyte in the course of a biochemical reaction (chemical transduction), and an energy transducer (stemming from the latin word *transducere*, to lead across) that transforms

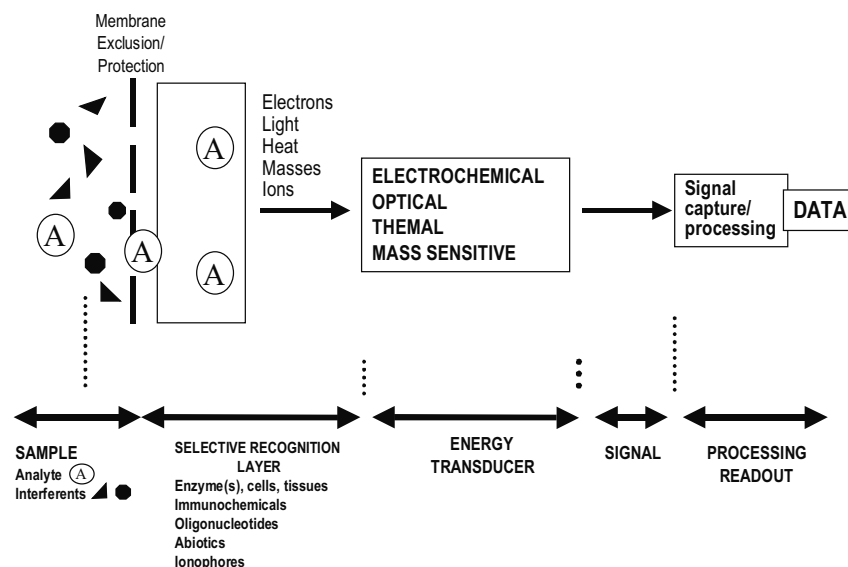


Figure 1. Scheme of the general configuration of biosensors.

the chemical information about the analyte into an electrical signal for data acquisition and interpretation. Based on the nature of the biochemical reaction these devices are usually classified in two main categories<sup>6</sup>:

- biocatalytic sensors, also known as metabolism sensors, that rely on enzymatically catalyzed reactions;
- bioaffinity sensors that are based on ligand-binding interactions, for instance of the antigen-antibody type, or other biological processes that take place without analyte conversion.

Enzyme-based optical fiber sensors belong to the first group. Enzymes are probably the most common biological elements used as specific chemical transducers for the development of biosensors. The broad application of these biocatalysts can be ascribed to several factors: a) the higher catalytic power compared to chemical catalyst; b) a high degree of selectivity for a specific substrate or group of substrates; c) their broad applicability; as a matter of fact, many enzymes display a high specificity for a specific type of reaction while accepting a wide variety of substrate structures, even of non-natural origin; d) some biocatalysts can work even in organic media; e) they can be immobilized and easily applied to biosensor development. Nowadays there are over 3200 enzymes recognized by the International Union of Biochemistry<sup>7</sup>, approximately 10% (~300) of which are commercially available and can be used for preparation of single or multienzyme selective recognition layers.

The biocatalyst is incorporated in different physical forms: as an isolated enzyme, a whole cell, a subcellular organelle or a tissue slice depending on

several factors such as the type of reaction, the need of cofactor recycling and the scale of the biotransformation. The analyte can act as an enzyme substrate, an activator or an inhibitor and will be determined directly or indirectly depending on the optical properties of the compounds that are involved in the enzymatic reaction.

The detection modes commonly applied in enzyme-based optical fiber sensors are based on one of the following principles:

- a) the analyte is assessed directly by monitoring the rate of formation of a product or the disappearance of a reagent with characteristic optical properties (fluorescence, absorbance, etc.) in the course of the enzymatic reaction;
- b) in some cases neither the reagents nor the products (for instance, O<sub>2</sub>, CO<sub>2</sub>, H<sup>+</sup>, etc.) of the biocatalytic process show intrinsic optical properties that can be used with sensing purposes; however, they can interact with the adequate indicator reagent(s) (optochemical transducers) originating optically detectable species, so that the concentration of the analyte will be related indirectly to the generated signal;
- c) alternatively, the variation of the optical properties of the enzyme itself upon interaction with the analyte can be used as the analytical signal.

Optical transduction modes applied in combination with enzyme based fiber-optic sensors include absorbance, reflectance, fluorescence, chemiluminescence, bioluminescence or electrogenerated chemiluminescence. We will describe in this chapter the fundamentals of enzyme-based sensors with special emphasis on the characteristics of the enzymes, the immobilization procedures, the type of biosensor design and measuring methods.

## 2. ENZYMES

The history of enzyme research is a main part of the history of biochemistry. Biological catalysis was first recognized and described in the late 1700s. In 1867 the German physiologist Frederick W. Kühne proposed the term enzyme (from the Greek "in yeast") for the ferments, an old term for yeast, isolated from the viable organisms in which they were formed, rather than being an intrinsic, life-bound part of them.

An *enzyme* is a protein that acts as a catalyst, *i.e.* a compound that increases the rate of a reaction without modifying the overall standard Gibbs-energy change in the reaction. Many different biochemical reactions occur in cells; however, without enzymes they would not happen on a useful time scale to sustain life<sup>8</sup>.

The chemical compound on which an enzyme acts is known as the *substrate*. An *inhibitor* is a substance that diminishes the rate of the

catalyzed reaction and acts by binding to the enzyme in a process called enzyme inhibition. An *activator* is a substance, other than the catalyst or one of the substrates, that increases the rate of the catalyzed reaction. The terms *effector* and *modifier* are general terms that apply to substances that interact with enzymes and either increase or decrease their catalytic action. Enzyme inhibitors and enzyme activators are therefore special cases of effectors and modifiers. The term *effector* is more commonly used when the substance produces effects of physiological significance, whereas the term *modifier* is more appropriate for a substance that is artificially added to an enzyme system being studied *in vitro*. In some cases the added substances increase or decrease the rate of an enzyme-catalyzed reaction upon interaction with substrates, modifiers or effectors that are already present in the system without interacting with the enzyme itself. Such substances may be referred to as *activators* or *inhibitors*, but should not be referred to as enzyme activators, enzyme inhibitors, modifiers or effectors.

In comparison to non-biological catalysts the use of enzymes displays the following *advantages*:

- a) the catalytic power of enzymes is often much greater; they increase the rate of specific reactions in a controlled manner by a factor ranging from  $10^3$  to  $10^{17}$  allowing regulation of pathways at small concentrations of substrate;
- b) they work in aqueous solutions under very mild conditions of temperature (20-40 °C) and pH (5-8) minimizing undesirable side-reactions that occur in traditional methodology;
- c) they are environmentally safe in comparison for instance, to heavy metals;
- d) multienzymatic systems can be applied in order to simplify reaction processes;
- e) they may accept a large variety of man made unnatural substrates and in some cases it is also possible to work in non-aqueous media;
- f) enzymes are chemoselective, *i.e.* they act on a single type of functional group; they are regioselective and diastereoselective, and due to their 3D structure it is possible for them to distinguish between functional groups located in different parts of the molecule; finally, enzymes are enantioselective so they will recognize any type of chirality in the substrate molecule upon formation of the enzyme-substrate complex;
- g) for sensor development, enzymes can be used in combination with different transduction mechanisms<sup>9</sup>.

The main *disadvantages* of enzymes for their application in chemistry are summarized below:

- a) they are provided in nature only in one enantiomeric form so it is not possible to invert the chiral induction of a given enzymatic reaction as in the case of a chiral chemical catalyst;

- b) enzymes require controlled operation parameters although for instance, some of them remain catalytically active even in ice;
- c) many enzymatic processes are prone to substrate or product inhibition limiting the efficiency of the catalytic process;
- d) they show the highest catalytic activity in water and this may become a problem for the analysis of compounds poorly soluble in aqueous media.

## 2.1 Enzyme Structure

With the exception of a small group of catalytic RNA molecules, all the enzymes are proteins. Their molecular weights, as for other proteins, range from about 12,000 to over 1 million Dalton.

Proteins are built up by aminoacids linked by peptide bonds into a polypeptide chain (Figure 2). The sequence of the aminoacids in the chain is known as the *primary structure* of the protein. The primary structure of the protein gives rise to the corresponding three-dimensional structure, and the spatial relationships of the constituents are the key for the peptide function.

The arrangement of the peptide backbone in space (conformation) is known as the secondary structure of the protein. The backbone can form regular, repeating structures held together by the attractions between peptide links along it. Hydrogen bonding is one of the main sources of attraction between the backbone peptide links and depending on the bond angles and the maximum probability of hydrogen bonding, secondary structures can be classified into two groups:  $\alpha$ -helices or  $\beta$ -sheets. In the first arrangement each amino group of the peptide backbone form a hydrogen bond with the carbonyl group of the aminoacid four residues beyond it. Right handed  $\alpha$ -helix are more stable and observed more frequently in proteins than the left handed. The second type of secondary structure is known as  $\beta$ -pleated sheet.

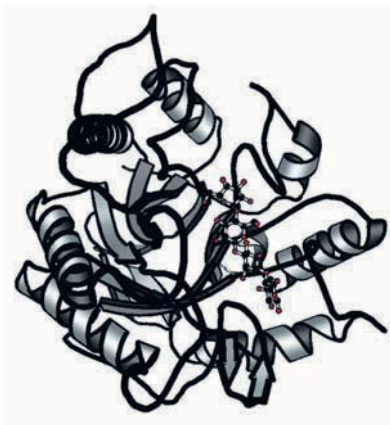


Figure 2. Three dimensional structure of the enzyme cellulase that breaks cellulose into sugar molecules<sup>10</sup>.

The hydrogen bonding is formed, in this case, between parallel sections of peptide chain rather than between the close neighbors as in the  $\alpha$ -helix. The axial distance between adjacent aminoacids is fully extended instead of tightly coiled. The strands of the sheet can be parallel, i.e. the carboxyl terminal ends of the chain would be adjacent to each other, more commonly antiparallel, since the hydrogen bonding angle is  $180^\circ$  when the segments are in opposition.

The tertiary structure of a protein is the arrangement in space of all its atoms and corresponds to the relationships of constituents that are distant in the primary structure. The forces that maintain the tertiary structure are, in principle, the same ones that generate the secondary structure, namely a) hydrogen bonding, quite favored due to the low polarity of the interior of the protein; b) coulombic forces; c) disulfide bonds, formed between cysteine residues and are critical for the maintenance of the tertiary and, sometimes also the quaternary structure of the protein and for the proper biological function; d) hydrophobic bonding that is responsible of the tendency of the non-polar residues to remain in the interior of the structure. The three dimensional shape of the enzyme is a result of the combination of these forces. In the resulting molecule a majority of the polar groups of the side chains of the protein are placed in the outside forming hydrogen bonds with the water molecules, the carboxyl and amino groups of the peptide backbone form interchain hydrogen bonds and the non-polar residues are located in the inside.

Some proteins are formed by a single chain and are called monomeric, but a large number are formed by several polypeptide chains that associate in a multimeric molecule. The relationships of the peptide chains in a multichain protein are known as the quaternary structure. These subunits may work either independently of each other or cooperatively, i.e. the function of one subunit depends on the functional state of the others<sup>11</sup>.

The active site of the enzyme is a specific region that binds the substrate and contains the amino acid residues that directly participate in the formation and breaking of the chemical bonds. These amino acid residues are called "the catalytic groups" and the arrangement of atoms will determine the specificity of the enzyme for a certain substrate(s). The clefts (space between two domains of a globular protein) formed at the active site are surrounded with non-polar amino acid residues that provide a non polar environment, as water is excluded from the active site. This is essential for both binding to the substrate and catalysis (unless water is involved in the reaction) because water disrupts bond breaking and making processes. Only a small portion of the enzyme constitutes its active center, therefore just a small part of the polypeptide chain will be in contact with the substrate. The stability of enzymes in solution is limited and they can be deactivated by denaturalization just due, for instance, to an increase in temperature, the use of extreme pH values or high salt concentration. This may be an important



limitation for sensor development as the enzyme activity may decrease drastically upon immobilization.

The binding of a substrate to its active center was first postulated by E. Fisher in 1894 using the “lock and key” mechanism which states that the enzyme interacts with its substrate like a lock and a key, respectively, *i.e.* the substrate has a matching shape to fit into the active site. This theory assumed that the structure of the catalyst was completely rigid and could not explain why the macromolecule was able to catalyze reactions involving large substrates and not those with small ones, or why they could convert non natural compounds with different structural properties to the substrate.

Later on<sup>12</sup>, Koshland proposed the “induced fit” model of the active site action that considers that during the formation of the enzyme-substrate complex, the enzyme can change its conformation so as to wrap the substrate like it happens when a hand (substrate) fits in a globe (enzyme). This flexing puts the active site and bonds in the substrate under strain, which weakens the bonds and helps to lower the activation energy for the catalyzed reaction.

The binding between the substrate and the enzyme is often provided by relatively weak hydrogen bonds. The E-S complexes have equilibrium constants ranging from one hundredth to one hundred millionth M, which corresponds to interaction free energies of -3 to -12 kcal/mol much lower than the value of -450 kJ/mol characteristic for a covalent bond.

## 2.2 Enzyme Nomenclature and Classification

The responsibility for enzyme nomenclature is supported by the Nomenclature Committee of the International Union of Biochemistry (IUB; now the International Union of Biochemistry and Molecular Biology, IUBMB) and the International Union of Pure and Applied Chemistry (IUPAC). These committees collect information about changes and additions to enzyme nomenclature<sup>13-15</sup>.

Enzymes are usually named in terms of the reaction that is catalyzed, commonly adding the suffix “-ase” to the name of the stoichiometrically converted reactant or substrate. For instance, an enzyme that catalyses the hydrolysis of urea is urease. Enzyme names can only be applied to single enzymes, especially those with termination -ase. For systems that involve the action of two or more enzymes the use of the term should be avoided and the word “system” should be included.

The first Enzyme Commission, in its 1961 report, devised a system for classification of enzymes that also serves as a basis for assigning code numbers to them. Every enzyme has got a 4-digit number EC A.B.C.D. where EC stands for “Enzyme Commission” with the following properties encoded:

Table 1. International classification of enzymes with examples of bioenzymatic sensors for each enzyme main class. 13

No.	Class	TYPE OF CATALYZED REACTION		BIOSENSOR APPLICATION EXAMPLES					Ref
		Action	Subclass examples	Enzyme	Analyte	Transducer	Indicator		
EC1	Oxidoreductases	Enzymes catalysing oxidoreductions (transfer e <sup>-</sup> , H <sup>+</sup> ) <i>dehydrogenase, acceptor reductase, oxidase (O<sub>2</sub> acceptor)</i>	(EC 1.1 – 1.21; 1.97) EC1.1 Acting on the CH-OH ( <i>L-lactate dehydrogenase, alcohol dehydrogenase, etc.</i> ) EC1.3 Acting on the CH-CH ( <i>cholesteronone 5<math>\alpha</math>-reductase, succinate dehydrogenase, etc.</i> ) EC1.6 Acting on NADH or NADPH ( <i>NADPH:quinone reductase, leghaemoglobin reductase, etc.</i> )	Glucose oxidase	glucose	oxygen	Ru(phen) <sub>2</sub> Cl <sub>2</sub>	16	
EC2	Transferases	Enzymes catalysing the transfer of a chemical group. (transfer methyl, acyl, etc.) <i>acceptor transferase, donor transferase</i>	(EC 2.1 – 2.9) EC2.1 Transf. one-carbon groups ( <i>nicotinamide N-methyltransferase, aspartate carbamoyltransferase, etc.</i> ) EC2.3 Acyltransferases ( <i>amino-acid N-acceptiltransferase, ATP citrate synthase, etc.</i> )	Choline oxidase Lactate oxidase /dehydrogenase Adenylate/creatine kinase/firefly luciferase L-lactate dehydrogenase	choline pyruvate AMP, ADP, ATP L-lactate	H <sub>2</sub> O <sub>2</sub> NADH ATP NADH	Luminol - Luciferin / Mg <sup>2+</sup> -	17 18 19 20	
EC3	Hydrolases	Enzymes catalysing the hydrolytic cleavage of groups as C-O, C-N, C-C & transfer. to water <i>donor hydrolase or donor-ase</i>	(EC 3.1 – 3.13) EC3.1 Acting on ester bonds ( <i>acetyl-cholinesterase, cephalosporin-C deacetylase, etc.</i> ) EC3.4 Acting on peptide bonds (peptidases) ( <i>Papain, Streptolysin, etc.</i> ) EC3.5 Acting on carbon-nitrogen bonds, other than peptide bonds ( <i>barbiturase, arginine deiminase, etc.</i> )	Penicillinase Creatinine iminohydrolase acetyl-cholinesterase	penicillin creatinine carbamate	pH pH pH	Aminofluorescein Aminofluorescein Chlorophenol red	21 21 22	
EC4	Lyases	Enzymes catalysing the transfer to or from double bonds. <i>substrate-lyase</i>	(EC 4.1 – 4.6; 4.99) EC4.3 Carbon-Nitrogen Lyases ( <i>phenylalanine ammonia-lyase, carbamoyl-serine ammonia-lyase, ethanolamine ammonia-lyase etc.</i> )	pyruvate decarboxylase	pyruvate	CO <sub>2</sub>	<i>m</i> -1-hydroxypyrene-3,6,8-trisulfonate	23	
EC5	Isomerases	Enzymes catalysing the transfer groups within molecules to yield isomeric forms. <i>substrate-synthetase</i>	(EC 5.1 – 5.5; 5.99) EC5.1 Racemases and Epimerases ( <i>no-cardichin-A epimerase, protein-serine epimerase, etc.</i> )	$\beta$ -fructofuranosidase/aldose 1-epimerase/ glucose oxidase	sucrose	H <sub>2</sub> O <sub>2</sub>	-	24	
EC6	Ligases	Enzymes catalysing the transfer by joining groups as C-C, C-S by ATP cleavage <i>Substrate-ligase</i>	(EC 6.1 – 6.6) EC6.3 Forming Carbon-Nitrogen Bonds ( <i>glutamate-ethyl/amine ligase, etc.</i> ) EC6.5 Forming Phosphoric Ester Bonds ( <i>DNA ligase (ATP), RNA ligase (ATP), etc.</i> )	glutamate-ammonia ligase	L-glutamate	pH	-	25	

- (A) denotes the main type of reaction: (1) oxidation-reduction; (2) functional group transfers; (3) hydrolysis; (4) lysis; (5) isomerisation; and (6) ligation (see Table 1);
- (B) stands for the subtype, indicating the type of substrate or the type of transferred molecule;
- (C) indicates the nature of the co-substrate;
- (D) is the individual enzyme number in its sub-subclass.

For instance, for the enzyme *alcohol dehydrogenase* the formal systematic name would be:

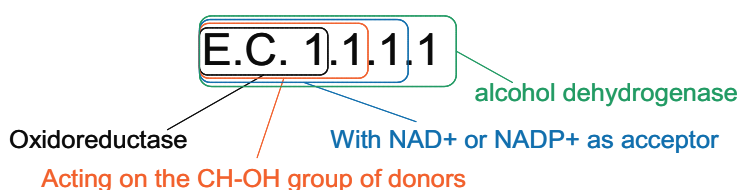


Table 1 summarizes the international classification of enzymes. Classes EC1 and EC3 are the most widely used for the development of optical biosensors. Sometimes different enzymes and transducing schemes can be applied to the analysis of a single analyte and the best combination should be selected depending on the application.

The catalytic activity of some enzymes depends exclusively on the functional groups found in the polypeptide chain and the way it folds into the active protein. Others, known as holoenzymes, require the participation of an "additional reagent" of non-proteic origin, referred to as cofactors, for catalysis. Cofactor is a general term to describe any accessory molecule, from minerals of relatively low molecular weight to larger organic molecules, that is cycled, usually in a metabolic pathway, and is not stoichiometrically consumed *in vivo* as it is the substrate. Nevertheless this definition is not exactly correct for analytical applications since the coenzyme will be stoichiometrically consumed in the measuring process.

In general, cofactors serve as carriers, alternating catalyst that accept and donate chemical groups, hydrogen atoms, or electrons.

Some examples of cofactors are collected in Table 2 and include:

- inorganic ions as iron(II), magnesium(II), calcium(II), zinc(II), etc;
- compounds of high group transfer potential such as ATP and GTP involved in energy coupling with cells;
- compounds derived from vitamins that, while at the active site of the enzyme, react to alter the structure of the substrate to favour the reaction; coenzymes including coenzyme A, which acts as an acyl group carrier in acyl-transfer reactions, pyridoxyl phosphate that takes part in amino group transfers and decarboxylation of amino acids, or vitamin B<sub>12</sub> fall into this group;

- oxidative coenzymes with characteristic redox potential which serve as carriers of hydrogen atoms or electrons, e.g.  $\text{NAD}^+$  (nicotinamide adenine dinucleotide) or FMN (flavine mononucleotide).

Some coenzymes such as  $\text{NAD}^+$  or  $\text{NADP}^+$  can be easily dissociated from proteins and carry hydrogen atoms from one enzyme to another. Other coenzymes such as FAD are more tightly bound to the protein and rarely dissociate from the biocatalyst. The heme groups are covalently bound to the protein, such as the cytochrome c, and only enzyme destruction allows dissociation. Very tightly bound groups are usually known as prosthetic groups and the protein part is called the apoenzyme, although there is not a sharp line dividing the loosely bound coenzymes and the prosthetic groups. Some enzymes require both a coenzyme and one or more metal ions for their activity.

Table 2. Examples of enzyme cofactors.

	<i>Cofactor</i>	<i>Target holoenzyme</i>
Metal ions	$\text{Cu}^{2+}$	Cytochrome oxidase
	$\text{K}^+$	Pyruvate kinase
	$\text{Ni}^{2+}$	Urease
	$\text{Zn}^{2+}$	Carbonic anhydrase, Alcohol dehydrogenase, Carboxypeptidases A and B
Coenzymes	Nicotinamide Adenine Dinucleotide ( $\text{NAD}^+$ )	Alcohol dehydrogenase, Lactate oxidase
	Nicotinamide Adenine Dinucleotide phosphate ( $\text{NADP}^+$ )	Glutamate dehydrogenase, Alcohol dehydrogenase, Aryl-aldehyde dehydrogenase
	Coenzyme A	Benzoyl-coenzyme A reductase, acetyl-coenzyme A carboxylase, 3-methylcrotonyl-coenzyme-A carboxylase
	Prosthetic groups	Flavin Mononucleotide (FMN)
Flavine Adenine Dinucleotide (FAD)		Glycine oxidase, Fumaric hydrogenase, Xanthine oxidase

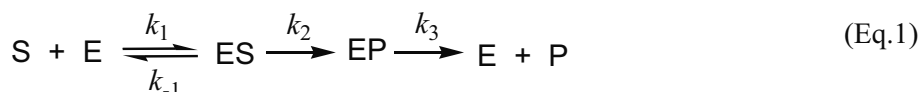
Cofactors are often modified chemically during the enzymatic process and this originates a variation of their optical or electrochemical properties. These changes can be monitored to follow the course of the enzymatic reaction and this approach has been widely used in many enzymatic biosensors<sup>18, 26, 27</sup>.

For example, glutamate analysis has been performed by monitoring the fluorescence of NADH produced during the enzymatic reaction between glutamate and NAD<sup>+</sup>. A detection limit of 0.2  $\mu\text{mol L}^{-1}$  has been achieved within a short response time allowing the determination of this analyte in brain cells<sup>28</sup>. Nevertheless, most enzymes do not show intrinsic optical properties that change upon interaction with the analyte, so the working principle of the biosensor relies normally on a chemical transducer ( $\text{O}_2$ , pH,  $\text{CO}_2$ ,  $\text{NH}_3$ , etc) as it was indicated above<sup>22, 29-30</sup>.

### 2.3 Enzyme Activity: How an Enzyme Works

As it was pointed out above enzymes have a much greater effect on reaction rates than synthetic catalysts. Most importantly, enzymes are specific, that is each enzyme will only catalyze one type of reaction, or a group of closely related reactions, and will show specificity for a particular substrate or group of substrates.

The mode of action of enzymes can be found in detail in many biochemistry and enzymology textbooks<sup>31-33</sup>. The mechanisms of enzyme-catalyzed reactions are complex and all have several steps. The more generally written scheme involves a single substrate and a single intermediate:



where E is the free enzyme that binds the substrate (S). ES and EP correspond to transient complexes of the enzyme with the substrate and the product, respectively, and P is the reaction product. Catalysis does not affect the reaction equilibrium but just the reaction rate. Pauling elaborated the modern theory of enzyme catalysis in 1946.

For enzyme catalysis to occur the biocatalyst must be complementary to the reaction transition state so that weak non-covalent interactions can be formed in the ES complex. These interactions maximize when the substrate reaches the transition state. The binding energy released in the interactions (Figure 3) partially compensates the energy required to reach the top of the energy hill ( $\Delta G^\ddagger_{\text{uncat}}$ ). As a result the net activation energy is lowered

( $\Delta G^\ddagger_{\text{cat}}$ ) and the reaction rate is significantly increased without affecting the reaction thermodynamic equilibrium.

The functional groups of the substrate that are involved in the interaction can be at some distance of the bonds that are broken or changed during the catalysis. The specificity of the enzymatic action, essential for the development of analytical methods that use enzyme biosensors<sup>34</sup> is thus a result of the formation of multiple weak interactions between the enzyme and its specific substrate. In fact, as it was described above, the enzyme itself undergoes a conformational change when interacts with the substrate according to the “induced-fit” model. This change facilitates the right positioning of the functional groups and the formation of additional (weak) bonds in the transition state.

## 2.4 Enzyme Kinetics

The evaluation of the enzymatic reaction rates and how they are affected by the variation of experimental parameters can be of great help in understanding the mechanism of enzyme-catalyzed reactions.

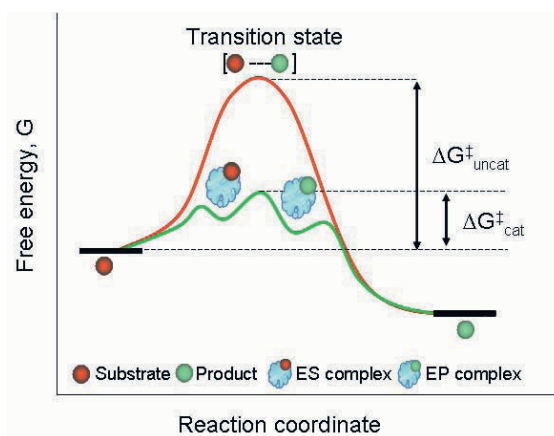


Figure 3. Reaction coordinate diagram comparing enzyme-catalyzed and uncatalyzed reactions.

Let us consider the basic enzyme catalysis mechanism described by the Michaelis-Menten equation (Eq. 2). It includes three elementary steps, namely, the reversible formation and breakdown of the ES complex (which does not mean that it is at equilibrium) and the decomposition of the ES complex into the product and the regenerated enzyme:



The reaction rate can be measured by the product formation rate:

$$v = \frac{d[\text{P}]}{dt} = k_2 [\text{ES}] \quad (\text{Eq.3})$$

At high substrate concentration all the available enzyme will be complexed with the substrate and transformed into the ES complex ( $[\text{E}]_{\text{total}} \approx [\text{ES}]$ ). In this situation the reaction rate is maximal and proportional to the enzyme concentration according to Eq. 3:

$$v_{\text{max}} = k_2 [\text{E}]_{\text{total}} \quad (\text{Eq.4})$$

A plot of the initial reaction rate,  $v$ , as a function of the substrate concentration  $[\text{S}]$ , shows a hyperbolic relationship (Figure 4). As the  $[\text{S}]$  becomes very large and the enzyme is saturated with the substrate, the reaction rate will not increase indefinitely but, for a fixed amount of  $[\text{E}]$ , it reaches a plateau at a limiting value named the maximal velocity ( $v_{\text{max}}$ ). This behavior can be explained using the equilibrium model of Michaelis-Menten (1913) or the steady-state model of Briggs and Haldane (1926). The first one is based on the assumption that the rate of breakdown of the ES complex to yield the product is much slower than the dissociation of ES. This means that  $k_2 \ll k_{-1}$ .

The mass balance for the reaction shown in Eq. 2:

$$[\text{E}]_{\text{total}} = [\text{E}] + [\text{ES}] \quad (\text{Eq.5})$$

$$[\text{S}]_{\text{total}} = [\text{S}] + [\text{ES}] \approx [\text{S}] \quad (\text{Eq.6})$$

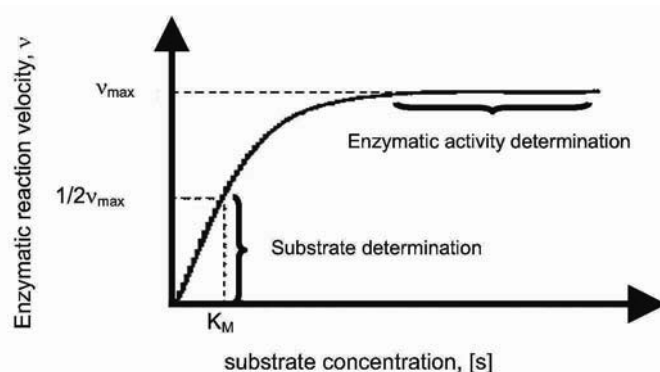


Figure 4. Variation of the reaction rate versus substrate concentration for an enzyme-catalyzed reaction at a constant enzyme concentration.

as the amount of substrate bound to the enzyme is small.

The rate of ES formation will be given by the equation:

$$\text{Rate of formation} = k_1([E]_{\text{total}} - [ES])[S] \quad (\text{Eq.7})$$

ES can break down to yield the product or dissociate back to the substrate, so that the rate of disappearance can be written as:

$$\text{Rate of breakdown} = k_{-1}[ES] + k_2[ES] \quad (\text{Eq.8})$$

The steady-state approach assumes that during most of the reaction ES is produced at the same time it disappears ( $d[ES]/dt = 0$ ), so that:

$$k_1([E]_{\text{total}} - [ES])[S] = k_{-1}[ES] + k_2[ES] \quad (\text{Eq.9})$$

$$k_1[E]_{\text{total}} [S] = (k_{-1} [S] + k_{-1} + k_2)[ES] \quad (\text{Eq.10})$$

$$[ES] = \frac{k_1 [S] [E]_{\text{total}}}{k_{-1} + k_2 + k_1 [S]} \quad (\text{Eq.11})$$

The Michaelis-Menten constant defined by Eq. 11, is the equilibrium constant for the dissociation of the ES complex and is inversely related to the affinity of the enzyme for the substrate, therefore, a low  $K_M$  value reflects high affinity:

$$K_M = \frac{(k_{-1} + k_2)}{k_1} \quad (\text{Eq.12})$$

and Eq. 9 becomes:

$$[ES] = \frac{[S][E]_{\text{total}}}{K_M + [S]} \quad (\text{Eq.13})$$

The rate of product formation is given by the so called Michaelis-Menten equation:

$$v = \frac{d[P]}{dt} = -\frac{d[S]}{dt} = k_2[ES] = \frac{k_2[S][E]_{\text{total}}}{K_M + [S]} \quad (\text{Eq.14})$$

At low substrate concentrations  $[S] \ll K_M$  and the reaction rate is linear with respect to the substrate concentration. The reaction in this region is first



order with respect to substrate concentration, although it is second order overall and finally it also depends on the enzyme concentration. At high substrate concentration,  $[S] \gg K_M$ , the maximum value of the rate constant,  $v_{\max} = k_2[E]_{\text{total}}$ , is achieved. Under these conditions, the reaction is zero order and no longer depends on the substrate concentration but on the enzyme activity. When  $[S] = K_M$ ,  $v = v_{\max}/2$ . From an analytical point of view a decrease in the value of  $K_M$  implies a better sensitivity, although the linear response range will be narrower.

The evaluation of the  $K_M$  and  $v_{\max}$  values for enzymatic reactions is usually carried out using a linear plot of Eq. 14. The Lineweaver-Burke equation is widely used to this aim:

$$\frac{1}{v} = \frac{K_M}{k_2[E]_{\text{total}}[S]} + \frac{1}{v_{\max}} \quad (\text{Eq.15})$$

The Lineweaver-Burke representation is obtained by plotting  $1/v$  against  $1/[S]$ . The value of  $K_M$  can be easily calculated from the slope ( $K_M/v_{\max}$ ) and the intercept ( $1/v_{\max}$ ), respectively.

The one-substrate mechanism is frequently operative in enzyme-based sensors. However, when several substrates or two or more (coupled enzymatic reactions) are required for sensor performance, the derived equations are more complex and usually require simplification for solving<sup>35</sup>.

In addition to  $K_M$  and  $v_{\max}$ , the turnover number (molar activity) and the specific activity are two important parameters in enzyme catalyzed reactions. The turnover number indicates the number of substrate molecules converted per unit time by a single enzyme molecule. The specific activity is given in units and one international unit (i.u.) is the amount of enzyme that consumes or forms 1  $\mu\text{mol}$  of substrate or 1  $\mu\text{mol}$  of product per minute under standard conditions.

Enzymes can be used not only for the determination of substrates but also for the analysis of enzyme inhibitors. In this type of sensors the response of the detectable species will decrease in the presence of the analyte. The inhibitor may affect the  $v_{\max}$  or  $K_M$  values. Competitive inhibitors, which bind to the same active site than the substrate, will increase the  $K_M$  value, reflected by a change on the slope of the Lineweaver-Burke plot but will not change  $v_{\max}$ . Non-competitive inhibitors, *i.e.* those that bind to another site of the protein, do not affect  $K_M$  but produce a decrease in  $v_{\max}$ . For instance, the acetylcholinesterase enzyme is inhibited by carbamate and organophosphate pesticides and has been widely used for the development of optical fiber sensors for these compounds based on different chemical transduction schemes (hydrolysis of a colored substrate, pH changes).

## 2.5 Enzyme Immobilisation

The immobilization of enzymes for sensing purposes frequently provides several important advantages: an increase of its stability, operational reusability and greater efficiency in consecutive multistep reactions. Sometimes immobilization is accompanied by a certain degree of denaturalization; however, the enzyme-matrix interactions may assist in stabilization preventing conformational transitions that favor such process. In some cases excessive bond formation affects the conformation of the active site and the steric hindrances caused by the polymer matrix may render an inactive sensor.

Depending on the immobilization procedure the enzyme micro-environment can also be modified significantly and the biocatalyst properties such as selectivity, pH and temperature dependence may be altered for the better or the worse. Mass-transfer limitations should also be accounted for particularly when the increase in the local concentration of the reaction product can be harmful to the enzyme activity. For instance  $H_2O_2$ , the reaction product of the enzyme glucose oxidase, is able to deactivate it. Operationally, this problem can be overcome sometimes by co-immobilizing a second enzyme able to decompose such product (e.g. catalase to destroy  $H_2O_2$ ).

Methods for enzyme immobilization can be divided into two main classes<sup>36-39</sup>:

1. physical methods that involve localizing an enzyme in any way that is not depending on covalent bond formation:
  - adsorption of the enzyme onto a water-insoluble matrix;
  - entrapment of the enzyme within water-insoluble gel supports (lattice entrapment);
  - entrapment of the enzyme within a semipermeable microcapsule or membrane;
2. chemical methods that involve formation of at least one covalent bond:
  - attachment of the enzyme to water-insoluble functionalized polymers;
  - intermolecular cross-linking of enzyme molecules using multifunctional reagents.

Sometimes the enzyme immobilization may involve both physical and chemical modifications of the protein (“hybrid techniques”).

### 2.5.1 Adsorption

The adsorption of proteins onto surfaces is the oldest and easiest immobilization method. Adsorbing forces can be of different types: Van der Waals interactions, ionic, hydrophobic or hydrogen bonding. The main advantages of this procedure are the simplicity of preparation and the little

enzyme activity losses, so it is usually suggested for short term investigations. However, changes in pH, temperature, ionic strength, concentrations of enzyme or adsorbent can significantly affect the immobilization efficiency. Due to the reversibility of the binding leakage problems may become an important drawback for long-term measurements and have prevented the broad application of this procedure for fabrication of optical fiber enzyme sensors.

The adsorbent should have a high affinity and capacity for the enzyme and it should not absorb the reaction product or enzyme inhibitors. Among the materials used the more popular are cation and anion exchange resins, activated charcoal, silica gel, alumina, control pore glasses and ceramics.

### 2.5.2 Gel Entrapment Techniques

This process involves the suspension of the biocatalyst in a monomer solution which is polymerized, and the enzymes are entrapped within the polymer lattice during the crosslinking process. This method differs from the covalent binding that the enzyme itself does not bind to the gel matrix. Due to the size of the biomolecule it will not diffuse out of the polymer network but small substrate or product molecules can transfer across or within it to ensure the continuous transformation. For sensing purposes, the polymer matrix can be formed directly on the surface of the fiber, or polymerized onto a transparent support (for instance, glass) that is then coupled to the fiber. The most popular matrices include polyacrylamide (Figure 5), silicone rubber, poly(vinyl alcohol), starch and polyurethane.

The advantages of this approach include its experimental simplicity, the mild conditions required for preparation and the possibility of depositing the formed gels on regular or highly irregular surfaces. Among the disadvantages, the need to control the experimental factors and the possible

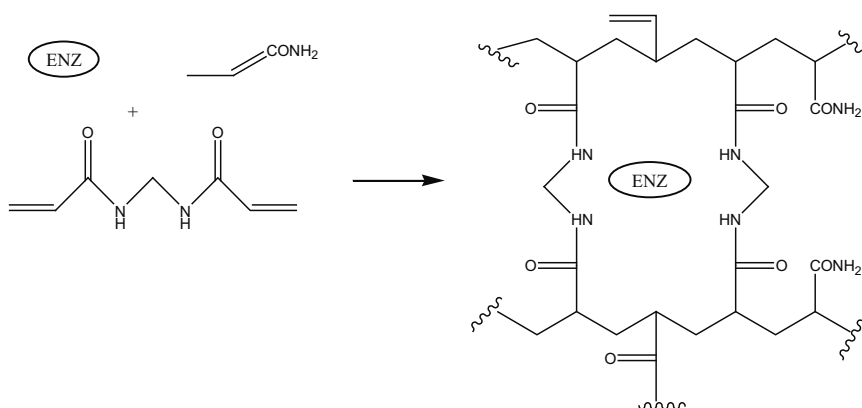


Figure 5. Entrapment of an enzyme by polymerisation of acrylamide.

thermal or chemical enzyme inactivation during gel formation can be found. Other problems are the leakage of enzyme from the polymer network: larger micropores yield higher leakage, and the limitation of the size of the substrate and products as usually lattice-entrapped enzymes show very little activity towards macromolecular substrates.

Sol-gel technology has also been applied to enzyme immobilization. The preparation of the matrix that usually show a good mass transport, is carried out under relatively mild experimental conditions, so the integrity of the biomolecule is preserved.

### **2.5.3 Microencapsulation**

Enzymes can be immobilized by enclosing them within semi-permeable polymer membranes. The preparation of the microcapsules requires extremely well controlled conditions and it is possible to use different procedures for their preparation:

- interfacial polymerization: an aqueous mixture of the enzyme and a hydrophilic monomer are emulsified in a water-immiscible organic solvent; the emulsion is vigorously stirred and the same hydrophilic monomer is added to the organic solvent; polymerization of the monomers then occurs around the emulsified microdroplet at the interface between the aqueous and organic solvent phases; as a result, the enzyme in the aqueous phase will be enclosed in a membrane of polymer;
- liquid drying: a polymer is dissolved in a water-immiscible organic solvent (of lower boiling point than water); an aqueous solution of the enzyme is dispersed in the organic phase forming a water-in-oil type emulsion; the emulsion containing the aqueous micro-droplets is dispersed in an aqueous phase that contains protective colloidal substances such as gelatin, and surfactants, to obtain a secondary emulsion; the organic solvent is then removed by warming the mixture in vacuum and a polymer membrane is thus obtained containing the enzyme micro-capsules.

Polyamide, collodion (cellulose nitrate), ethylcellulose, cellulose acetate butyrate or silicone polymers have been used for preparation of permanent microcapsules. This method offers a double specificity due to the presence of both the enzyme and a semipermeable membrane. Moreover, it allows simultaneous immobilization of many enzymes in a single step and the surface area for contacting the substrate and the catalyst is large. The need of high protein concentration and the restriction to low molecular weight substrates are the main limitations of enzyme microencapsulation.

#### **2.5.4 Containment within Semipermeable Membrane Devices**

For sensing purposes, an aqueous solution of the enzyme together with other indicator or coenzyme reagents can be held at the sensor tip by simple enclosure behind a dialysis or an ultrafiltration membrane. The biocatalyst will be kept in the reaction compartment by the membrane but small substrate/product molecules will diffuse freely through the barrier. The successful operation of the sensor will depend on the permeability characteristics of the membrane barrier and this type of immobilization can be easily used in combination with flow-through cells. The procedure for preparing the sensing layer is simple, since no chemical modification of the enzyme is required, and the biocatalyst will exhibit the same features than in solution. The procedure also allows simultaneous immobilization of many enzymes and mass transfer limitations or alteration of the catalytic properties are largely avoided. Synthetic membranes based on polyamide or polyethersulfone with a broad range of pore sizes are commercially available at low price in various shapes, such as foils or hollow fibers.

#### **2.5.5 Intermolecular Cross-Linking**

This method involves the formation of covalent bonds between multifunctional low molecular weight reagents and the enzyme molecules to produce intermolecular cross-linked species. The enzyme molecules may be cross-linked either with themselves or co-cross-linked with an inactive protein. The second approach is applicable in those cases that extensive modification of the enzyme may lead to deactivation or when the enzyme is expensive and insufficient. Proteins such as albumin, bovine or human, have been used to that aim. This procedure requires a delicate control of the experimental factors, such as the enzyme concentration and the multifunctional agent, the pH, the ionic strength of the solution, the temperature and the reaction time. These factors will also affect the degree of intramolecular crosslinking and the strength of the insoluble derivative although the obtained bio-layers are often of a gelatin type nature that limits their application for sensor development.

Generally, cross-linking is best used together with one of the other methods. In a first approach the enzyme can be adsorbed or entrapped onto silica, cellophane or active carbon, followed by crosslinking with the multifunctional reagent. This procedure has the advantage that essentially a monolayer of enzyme molecules is formed facilitating the catalytic reaction, although the previous enzyme adsorption/entrapment step must be carefully optimized. In some cases multifunctional reagents are used to introduce chemical groups in an insoluble polymer matrix that reacts covalently with the enzyme. Both approaches have been used in sensor development.

The most common reagent used for cross-linking is glutaraldehyde (Figure 6). The reactive groups involved in the cross-linking are not only the free amino but also sulfhydryl- and hydroxy groups.

Cross-linking reactions are carried out under relatively severe conditions. Nevertheless, it must be taken into account that such harsh conditions may alter the conformation of the active center of the enzyme leading to a significant loss of activity.

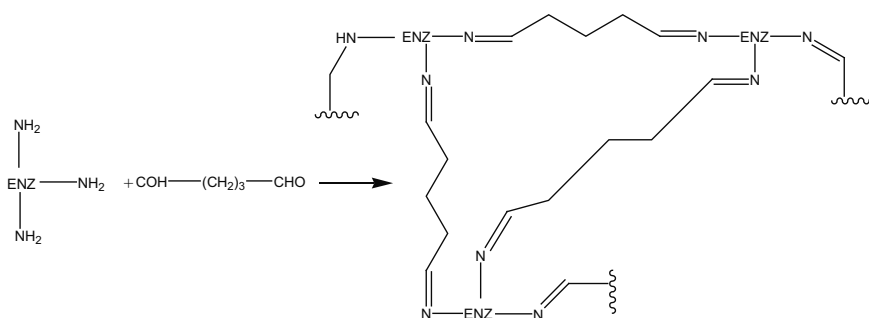


Figure 6. Cross-linking of enzymes with glutaraldehyde.

### 2.5.6 Covalent Attachment

Covalent attachment of the enzyme to water-insoluble carriers is the prevalent method for enzyme immobilization in sensor manufacturing, as it avoids leaking completely. In the selection of the binding procedure several issues must be considered: 1) the loss of enzymatic activity during the binding reaction should be as low as possible; 2) the active site of the enzyme should be unaffected during the reaction and, 3) the active site should not be hindered by the presence of the matrix. Unfortunately, in most cases major activity losses and/or changes on the substrate selectivity are produced during the harsh conditions required for the chemical reaction. In fact, it has been pointed out that the enzyme will decrease its activity approximately one fifth per formed bond<sup>38</sup>.

The functional groups of the enzyme involved in the chemical bonding are the *N*-terminal and  $\epsilon$ -amino groups (from lysine) as well as the carboxy- (aspartic or glutamic acid), sulfhydryl- (cysteine), hydroxyl- (serine, threonine), indole (tryptophan), imidazole (hystidine) and phenolic (tyrosine) functions.

The supports employed for covalent attachment of enzymes can be classified into two groups: a) natural (agarose, dextran, cellulose, porous glass, silica, the optical fiber itself or alumina) and b) synthetic (acrylamide-

based polymers, methacrylic acid-based polymers, maleic anhydride-based polymers, styrene-based polymers or nylon, to name a few).

Some important factors that must be considered in the selection of the support for covalent binding are: its capacity to bind the enzyme, as the linearity and the limit of detection of the sensing layers will be influenced by this value; the mechanical and chemical stability of the support; the efficiency of interaction with the analyte or the sample matrix; the ease of preparation and the cost, regenerability and availability of the material.

Fabrication of immobilized supports can be carried out in different ways and some examples are summarized in Table 3<sup>36-40</sup>:

- reaction of the enzyme with a reactive polymer such as, maleic anhydride-based copolymers or methacrylic acid anhydride-based copolymers;
- activation of the polymer through chemical conversion of its functional groups followed by reaction with the enzyme. One example is diazotization of aminoaryl polymers and the activation of hydroxyl-containing polymers with cyanogen bromide;
- activation of the polymer through chemical conversion of its functional groups in the presence of the enzyme. For instance the activation of carboxyl-containing polymers with carbodiimides;
- activation of the polymer by chemical conversion of a functionalized group with a multifunctional low molecular weight reagent followed by addition of the enzyme. One part of the reagent binds to the matrix and the other binds to the enzyme. For example, aminoethylcellulose or polyacrylamide treated with glutaraldehyde before enzyme coupling (Figure 7).

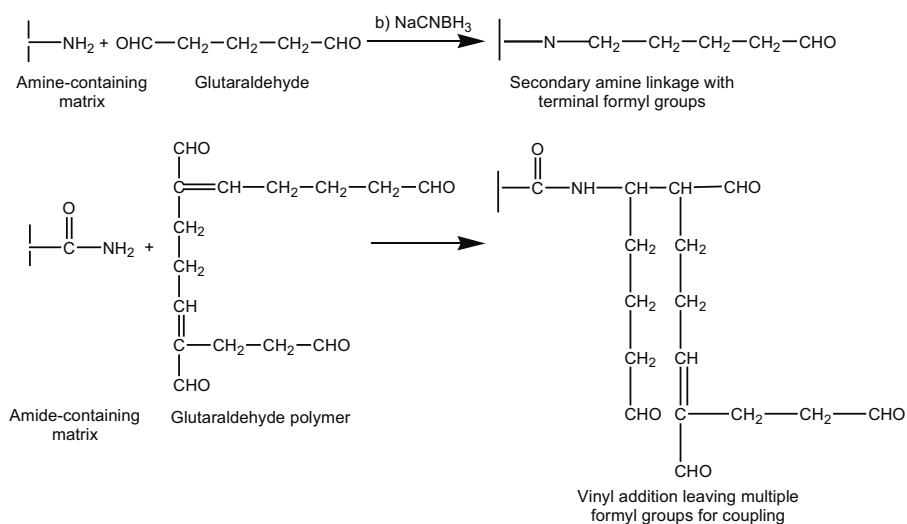


Figure 7. Different routes to a glutaraldehyde-activated matrix.

Table 3. Covalent immobilisation methods of enzymes.

SUPPORT FUNCTION	COUPLING AGENT	ACTIVE INTERMEDIATE	ENZYME REACTING GROUP	RESULTING COVALENT BOND
<i>Amide bond formation (Support—CO—NH—Enzyme)</i>				
—OH —OH	BrCN Cyanogen bromide	$\begin{array}{c} \text{—O—CN} \\ \text{—OH} \end{array}$ Cyanate ester (Very reactive)	ENZ—NH <sub>2</sub>	$\begin{array}{c} \text{NH}_2^+ \\ \parallel \\ \text{—O—C—NH—ENZ} \\   \\ \text{—OH} \end{array}$
		$\begin{array}{c} \text{—O—C=NH} \\   \quad   \\ \text{—O—} \quad \text{—O—} \end{array}$ Cyclic imidocarbonate (Slightly reactive)		$\begin{array}{c} \text{—O—C=N—ENZ} \\   \quad   \\ \text{—O—} \quad \text{—O—} \end{array}$
—NH <sub>2</sub>	$\begin{array}{c} \text{S} \\ \parallel \\ \text{Cl—C—Cl} \\ \text{Thionyl chloride} \end{array}$	—N=C=S	ENZ—NH <sub>2</sub>	$\begin{array}{c} \text{—NH—C—NH—ENZ} \\ \parallel \\ \text{S} \end{array}$
—NH <sub>2</sub>	$\begin{array}{c} \text{O} \\ \parallel \\ \text{Cl—C—Cl} \\ \text{Phosgene} \end{array}$	—N=C=O	ENZ—NH <sub>2</sub>	$\begin{array}{c} \text{—NH—C—NH—ENZ} \\ \parallel \\ \text{O} \end{array}$



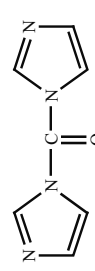
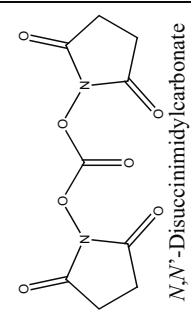
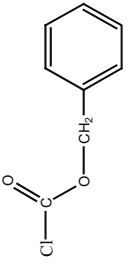
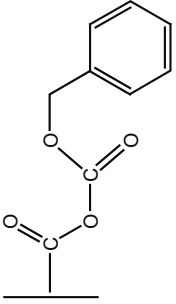
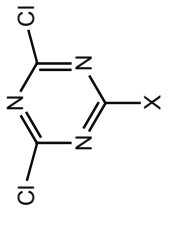
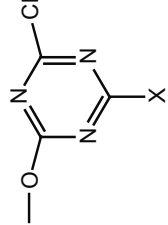
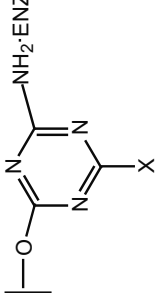
$\text{—COOH}$	$\text{R—N=C=N—R'}$ Carbodiimide	$\text{—C(=O)—O—C(=NR')NHR}$	$\text{ENZ—NH}_2$	$\text{—C(=O)—NH—ENZ}$
$\text{—OH}$	$\text{N}$  Carbonyl diimidazole	 N,N'-Disuccinimidyl carbonate	$\text{ENZ—SH}$	$\text{—C(=O)—S—ENZ}$
$\text{—COOH}$			$\text{—OH}$	$\text{ENZ—NH}_2$
$\text{—OH}$			$\text{ENZ—NH}_2$	$\text{—C(=O)—NH—ENZ}$

Table 3. Continued.

$\text{—NH}_2$	$\text{H}_2\text{N—NH}_2$ $\text{HNO}_2$	$\text{—C(=O)—N}_3^+$	$\text{ENZ—NH}_2$	$\text{—C(=O)—NH—ENZ}$
$\text{—COOH}$			$\text{ENZ—NH}_2$	$\text{—C(=O)—NH—ENZ}$
<i>Alkylation/ Arylation Reactions (Support —CH<sub>2</sub>—NH—Enzyme)</i>				
$\text{—OH}$	 X: Cl, NH <sub>2</sub> , OCH <sub>2</sub> COOH, NHCH <sub>2</sub> COOH		$\text{ENZ—NH}_2$	

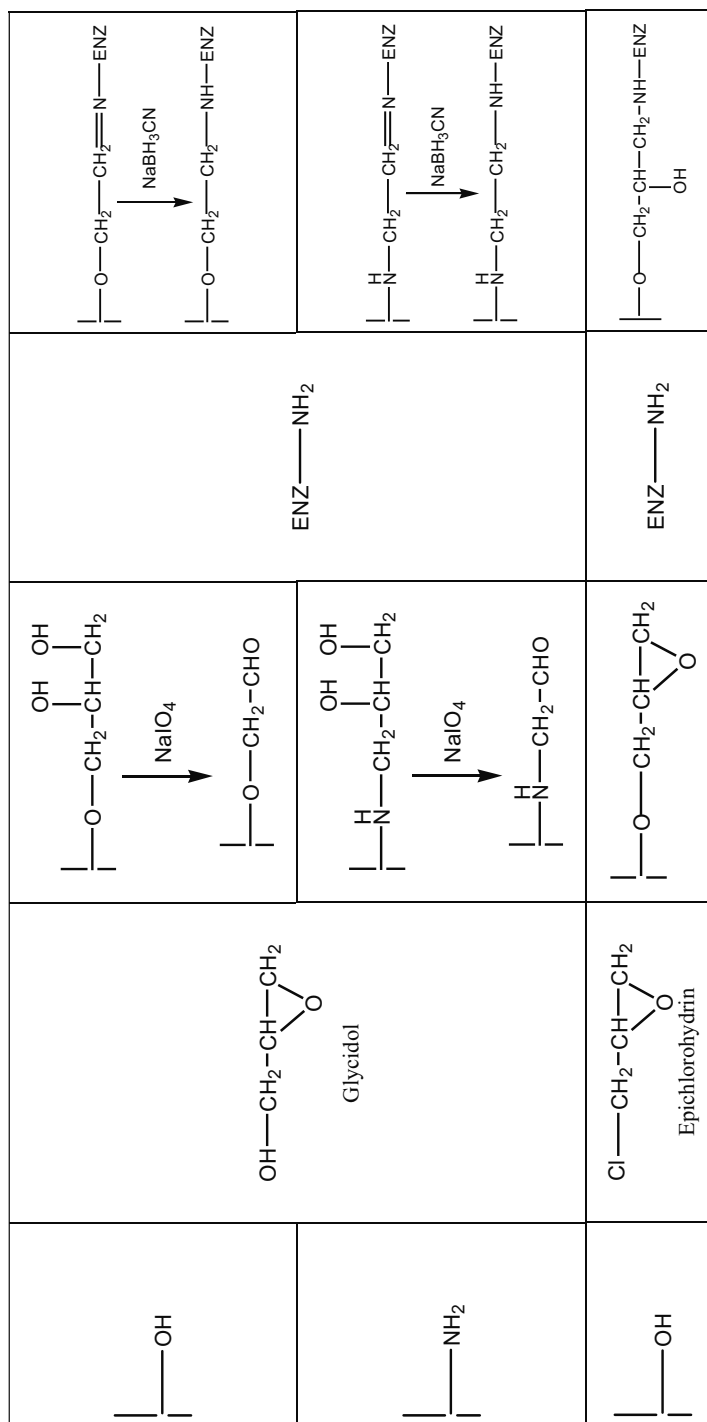


Table 3. Continued.

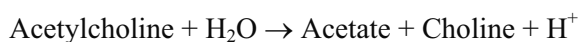
<i>Diazotization (Support —N=N—Enzyme)</i>				
	$\text{NaNO}_2/\text{HCl}$			
	$\text{NaNO}_2/\text{HCl}$		$\text{ENZ}-\text{NH}_2$	
	$\text{NaNO}_2/\text{HCl}$			
<i>Thiol Disulfide Exchange: Support —S—S—Enzyme</i>				

### 3. ENZYME-BASED FIBER OPTIC SENSORS

Optical fiber sensors that use enzymes can operate in the direct or indirect detection mode. In the first case, the optical properties of the reactives, intermediates or products of the biocatalyzed reaction can be monitored using the optical fibers. In the second type, an optochemical transducer generates the optical changes.

As it was indicated above, the main optical interrogation methods include absorbance, reflectance, fluorescence, chemiluminescence (CL), or electrogenerated chemiluminescence (ECL)<sup>9, 41-42</sup>.

Absorbance- and reflectance-based measurements are widespread, as there are many enzymatic reaction products or intermediates that are colored or if not, can react with the appropriate indicator. Sensors using acetylcholinesterase for carbamate pesticides detection are an example of indirect optical fiber biosensors. This enzyme catalyses the hydrolysis of acetylcholine with concomitant decrease in pH<sup>41</sup>:



The pH change can be monitored using a colorimetric pH indicator dye such as chlorophenol red,<sup>22</sup> phenol red or bromothymol blue<sup>41</sup>.

Direct sensors based on fluorescent measurements are less common than the absorbance ones, because there are not many intermediates or products with this optical feature. Some examples have been described using the intrinsic fluorescence of flavin-containing enzymes as the analytical signal<sup>41</sup>. These devices are advantageous since they do not require an optochemical transducer, but their sensitivity is usually very low and their response range is narrow. Alternatively, the enzyme can be coupled to a fluorescent-based optode. Either steady state or time resolved fluorescence measurements can be related to the substrate concentration. Oxygen, pH, NH<sub>3</sub>, or CO<sub>2</sub> optodes have been coupled with the immobilized enzymes for sensing purposes. Some typical designs are depicted in Figure 8.

CL and ECL are characterized by the simplicity of the measuring instrumentation and for their high sensitivity and selectivity. These methods are based on the measurements of the H<sub>2</sub>O<sub>2</sub> originated in an enzymatic reaction using substrates such as luminol or oxalic acid esters to produce light. ECL monitoring requires a potentiostatically-controlled electrochemical cell and a luminometer. The electrode is usually placed opposite to the distal end of the optical fiber to electrochemically trigger CL, and the fiber carries the ECL signal to the detector. This approach has not been exploited to a great extent so far but it yields extremely low detection limits and can be useful in the near future.

As it is shown in Figure 8, the enzyme can be immobilized in the vicinity (membrane, beads, etc) or on the surface of the fiber for optical fiber sensor development. Alternatively, it can be placed in a reactor and use the optode

as a detector<sup>41</sup>. The last approach is very useful in combination with flow injection analysis (FIA).

Enzyme-based optical sensor applications will be further described in this book. They are still the most widespread optical biosensors but work is needed to overcome limitations such as shelf life, long term stability, *in situ* measurements, miniaturization, and the marketing of competitive devices.

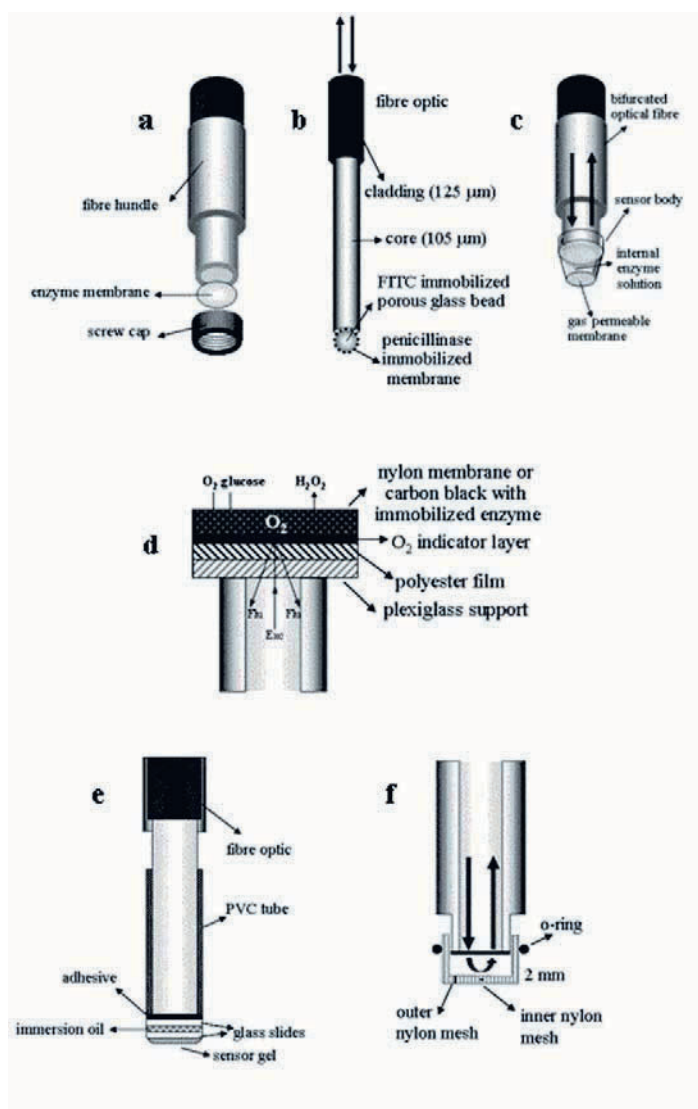


Figure 8. Examples of enzyme-based fiber-optic sensor designs. Adapted from refs. a) 43; b) 44; c) 45; d) 46; e) 47; f) 48.

## REFERENCES

1. Clark Jr. L.C., Mishray G., Fox R.P., Chronically implanted polarographic electrodes, *J. Appl. Physiol.* 1958; 13:85-91.
2. Clark Jr. L.C., Lyons C., Electrode systems for continuous monitoring in cardiovascular surgery, *Ann. N.Y. Acad. Sci.* 1962; 102:29-45.
3. Seitz, W.R., Chemical sensors based on immobilized indicators and fiber optics, *CRC Crit. Revs. Anal. Chem.* 1988; 19: 135-173.
4. Thevenot D.R., Toth K., Durst R.A., Wilson G.S., Electrochemical biosensors: Recommended definitions and classification, *Pure Appl. Chem.* 1999; 71: 2333-2348.
5. Vo-Dinh T., Cullum B., Biosensors and biochips: advances in biological and medical diagnostics, *Fresenius J. Anal. Chem.* 2000; 366:540-551.
6. Arnold M.A., Meyerhoff M.E., Recent advances in the development and analytical applications of biosensing probes, *CRC Crit. Revs. Anal. Chem.* 1988; 20:149-196.
7. <http://www.chem.qmul.ac.uk/iubmb/enzyme/history.html>
8. Lehninger A.L., Nelson D.L., Cox M.M., *Principles of Biochemistry*. 3rd Ed., Worth Publishers, New York (USA) 2000.
9. Marazuela M.D., Moreno-Bondi M.C., Fiber-optic biosensors. An overview, *Anal. Bioanal. Chem.* 2002; 372: 664-682.
10. <http://pigtrail.uark.edu/news/images/enzyme.jpg>. Check also the web page of the RSSB Protein Data Bank (<http://www.rcsb.org/pdb/>)
11. Branden C. And Tooze J., *Introduction to protein sequence*. Garland Publishing Inc., New York (USA) 1991.
12. Koshland D.E., Neet K.E., Catalytic and regulatory properties of enzymes, *Ann. Rev. Biochem.* 1968; 37: 359.
13. *Enzyme Nomenclature*, Academic Press, San Diego, (USA), 1992.
14. *Enzyme Nomenclature*, Supplement 1 (1993), Supplement 2 (1994), Supplement 3 (1995), Supplement 4 (1997) and Supplement 5 (1999) (in *Eur. J. Biochem.* 1994; 223:1-5; *Eur. J. Biochem.* 1995; 232:1-6; *Eur. J. Biochem.* 1996; 237:1-5; *Eur. J. Biochem.* 1997; 250:1-6, and *Eur. J. Biochem.* 1999; 264:610-650, respectively).
15. <http://www.chem.qmw.ac.uk/iubmb/>
16. Rosenweig Z., Kopelman R., Analytical properties of miniaturized oxygen and glucose sensors, *Sensor Actuat B-Chem.* 1996; 35-36: 475-483
17. Tsafack V.C., Marquette C.A., Leca B., Blum L.J., An electrochemiluminescence-based fibre optic biosensor for choline flow injection analysis, *Analyst* 2000; 125:151-155.
18. Zang W., Chang H., Rechnitz A., Dual enzyme fiber-optic biosensor for pyruvate, *Anal. Chim. Acta.* 1997; 350:59-65.
19. Michel P.E., Gautier-Sauvigné S.M., Blum L.J., Luciferin incorporation in the structure of acrylic microspheres with subsequent confinement in a polymeric film: A new method to develop a controlled release-based biosensor for ATP, ADP and AMP, *Talanta*; 1998; 47: 169-181.
20. Hikima S., Kakizaki T., Hasebel K., Enzyme sensor for L-lactate using differential pulse amperometric detection, *Fresen. J. Anal. Chem.* 1995; 351(2-3): 237-240.
21. Müller C., Hitzmann B., Schubert F., Scheper T., Optical chemo- and biosensors for use in clinical applications, *Sensor Actuat B-Chem.* 1997; 40: 71-77
22. Xavier M.P., Vallejo B., Marazuela M.D., Moreno-Bondi M.C., Baldini F., Falai A., Fiber optic monitoring of carbamate pesticides using porous glass with covalently bound chlorophenol red, *Biosens. Bioelectron.*, 2000; 14:895-905.
23. He X.; Rechnitz G.A., Plant tissue-based pyruvate fiberoptic sensor, *Anal. Chim. Acta*; 1995; 316(1): 57-63.
24. Bilitewski U., Jaeger A., Rueger P., Weise W., Enzyme electrodes for the determination of carbohydrates in food, *Sensor Actuat B-Chem.* 1993; 15(1-3): 113-118.

25. Iida T., Kawabe T., Noguchi F., Mitamura T., Nagata K., Tomita K., ISFET-type - glutamate sensor using thermophilic glutamine-synthetase from a thermophile, *Nippon-Kagaku-Kaishi* 1987;10: 1817-1821.
26. Choi J.W., Bae J.Y., Min J., Cho K.S., Lee W.H., Fiber-optic ethanol sensor using alcohol dehydrogenase-immobilized Langmuir-Blodgett film, *Sensor Mater.* 1996; 8:493-504.
27. D'Orazio P., Biosensors in Clinical Chemistry, *Clin. Chim. Acta* 2003; 334:41-69.
28. Cordek J., Wang X., Tan W., Direct immobilization of glutamate dehydrogenase on optical fiber probes for ultrasensitive glutamate detection, *Anal. Chem.* 1999; 71:1529-1533.
29. Marazuela M.D., Cuesta B., Moreno-Bondi M.C., Quejido A., Free cholesterol fiber-optic biosensor for serum samples with samples optimization, *Biosens. Bioelectron.* 1997; 12:233-240.
30. Marquette C.A., Blum L.J., Luminol electrochemiluminescence-based fibre optic biosensors for flow injection analysis of glucose and lactate in natural samples, *Anal. Chim. Acta* 1999; 381:1-10.
31. Copeland R.A., *Enzymes. A Practical Introduction to Structure, Mechanism, and Data Analysis*. 2nd Ed., Wiley-Interscience, New York (USA), 2000.
32. Eggins B.R., *Chemical Sensors and Biosensors*. John Wiley & Sons, West Sussex (UK), 2002.
33. Fersht A., *Enzyme Structure and Mechanism*. 2nd Ed., W.H. Freeman, New York (USA), 1984.
34. Tran Minh C., *Biosensors*. Kluwer Academic Publishers, Dordrecht Hardbound (Netherlands), 1993.
35. Cunningham A.J., *Introduction to Bioanalytical Chemistry*, John Wiley & Sons, New Jersey (USA), 1998.
36. Zaborsky O., *Immobilised Enzymes*, CRC Press, Cleveland (USA) 1972.
37. Carr P.W., Bowers, L.D., *Immobilised Enzymes in Analytical and Clinical Chemistry. Fundamentals and Applications*, Wiley-Interscience, New York (USA), 1980.
38. Hermanson G.T., Krishna Mallia A., Smith P.K., *Immobilized Affinity Ligand Techniques*, Academic Press, Inc. San Diego (USA) 1992.
39. Faber K., *Biotransformations in Organic Chemistry. A textbook*, 3rd Ed. Springer, Berlin (Germany), 1997.
40. Cass T., Ligler F.S. (eds), *Immobilized Biomolecules in Analysis. A Practical Approach*, Oxford University Press, Oxford (Great Britain), 1998.
41. Kuswandi B., Andres R., Narayanaswamy R., Optical fibre biosensors based on immobilized enzymes, *Analyst* 2001; 126:1469-91.
42. Wolfbeis O., *Anal. Chem.* 2002; 74:2663-2677.
43. Blum L.J., Gautier S.M., Coulet P.R., Luminescence fiber optic biosensor, *Anal. Lett.* 1988; 21:717-726.
44. Fuh M.R.S., Burgess L.W., Christian G.D., Single fiber-optic fluorescence enzyme-based sensor, *Anal. Chem.* 1988; 60:433-435.
45. Walters B.S., Nielsen T.J., Arnold M.A., Fiber-optic biosensor for ethanol based on an internal enzyme concept, *Talanta* 1988; 35:151-155.
46. Moreno Bondi M.C., Wolfbeis O.S., Leiner M.J.P., Schaffar B.P.H., Oxygen optrode for use in a fiberoptic glucose biosensor, *Anal. Chem.* 1990; 62:2377-2380.
47. Hobel W., Papperger A., Polster J., Penicillinase optodes-substrate determinations using batch, continuous-flow and flow injection analysis operation conditions, *Biosens. Bioelectron.* 1992; 7:549-557.
48. Arnold M.A., Enzyme-based fiber optic sensor, *Anal. Chem.* 1985; 57:565-566.



## Chapter 17

# SOL-GELS FOR OPTICAL SENSORS

Halina Podbielska, Agnieszka Ulatowska-Jarza, Gerhard Müller, Hans J. Eichler

*Wroclaw University of Technology, Institute of Physics  
Wybrzeze Wyspianskiego 27  
50-370 Wroclaw, Poland*

### 1. INTRODUCTION

Sol-gel process allows for formation of glassy and ceramics materials in temperatures much lower than offered by conventional melting techniques. The first paper on sol-gels was published over 150 years ago by Ebelmen<sup>1</sup>, however, the rapid development of this technology and applications occurred in the last few years. There is a broad range of possible applications of sol-gel derived materials, what marked this technology as one of the most promising fields of contemporary material sciences<sup>2-5</sup>.

Various materials can be produced by sol-gel methods: monoliths, thin films, fibers, powders can. Controlling of the physical and chemical parameters of production process yields materials with precisely tailored parameters such as mechanical strength, transparency, size and distribution of the pores network<sup>7</sup>. The sol-gel derived materials may provide excellent matrices for a variety of organic and inorganic compounds.

### 2. SILICA SOL-GELS

Combination of inorganic and organic networks facilitates the design of new engineering materials with exciting properties for a wide range of applications<sup>8</sup>. The pioneering works on those materials were led by Schmidt<sup>9</sup> and Wilkes<sup>10</sup>. They had investigated the possibilities of changing the properties of sol-gel-derived materials by incorporating the organic components to a silica matrix. The new hybrid materials, so-called ORGANICALLY MODIFIED SILICATEs or ormosils, created new possibilities for metrology and other applications, including biomedical ones. Ormosils are

networks of silicates cross-linked with organic groups<sup>11</sup>. These materials, produced by a sol-gel process, possess a wide range of physical attributes, the nature of which depends on the type and amount of organic component used and other variables (including the preparation conditions like pH, temperature etc.). Ormosils can be transparent and brittle, optically opaque and rubbery or – on the contrary – optically opaque and brittle or transparent and rubbery. Their current applications include optical disks<sup>12</sup>, antireflective coatings<sup>13</sup>, photochromic coatings<sup>14</sup>, optical fibers<sup>15</sup>, Fresnel lenses<sup>16</sup>, durable, heat resistant, pliable materials for use inside cars and aircrafts or super-hard coatings for auto windshields<sup>17</sup>.

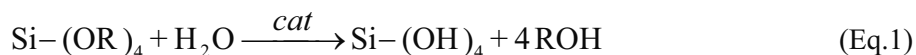
## 2.1 Production of Sol-Gel Materials

There are three methods of preparing organic-inorganic hybrid materials. The first and the simplest one involves organic molecules dissolution in a liquid sol-gel. After gelation these molecules are immobilized in sol-gel matrix<sup>18-23</sup>. In this case no chemical reaction between the two elements is observed. The second way uses impregnation of a porous gel in the organic solution<sup>24</sup>, whereby no chemical reaction between the two phases exists, either. The third type of ormosils can be easily distinguished from the above, because here inorganic precursor either already has an organic group or reactions occur in a liquid solution to form chemical bonds in the hybrid gel.

The sol-gel process itself leads to formation of gels from mixtures of liquid reagents (sols) at ambient temperatures. As its name implies, it involves several steps: the evolution of inorganic networks, formation of colloidal suspension (sol) and gelation of the sol to form a network in a continuous liquid phase (gel). Drying of the obtained gels, even at room temperature, produces glass-like materials called xerogels (xeros – dry). Xerogels are porous, usually transparent and relatively sturdy materials which, when heated at the glass vitrification temperature (ca. 1200 °C), turn into the regular glass, identical with classical glasses obtained by melting.

The sol-gel technology, based on various alkoxides, allows production of classical silica glasses, as well as multicomponent materials, merging silicates with titanates, borates and a variety of other oxides (Zn, La, Al, Li, B, K, etc.). The alkoxide gel method can be also used for production of certain non-silicate oxide glass-like materials (e.g.,  $ZrO_2^-$ , etc.)<sup>25</sup>.

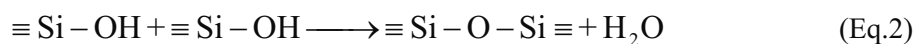
As it was mentioned, the chemistry of the silica based sol-gel process comprises several steps. First, silicate precursor (e.g., tetraethylortosilicate TEOS or tetramethylsilicate TMOS) is mixed with water and catalyst and stirred for a few hours. This process leads to hydrolysis of the Si-O-R bonds. The hydrolysis reaction can be catalyzed by acids (HCl, HF, etc.) or bases (NH<sub>4</sub>OH, NaOH, etc.). The process is schematically described by equation:



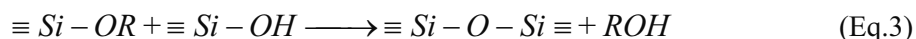
In real process not all of the accessible  $-\text{OR}$  groups have to hydrolyze to the  $-\text{OH}$  form. In fact, the longer the hydrolysis, the larger amount of the  $\text{Si}-\text{OR}$  groups undergoes hydrolysis to the  $\text{Si}-\text{OH}$  form. Thus, the three-dimensional extent of the silicate network is a direct result of the hydrolysis time.

The water-to-silicate molar ratio ( $R$ ) is an another important technological parameter determining the final form of produced material. For example, fibers can be formed from hydrolysates with  $R \sim 1$ , for monodisperse spheres  $R \sim 50$  while bulk samples can be obtained from hydrolysates with  $R$  ranging broadly from 5 to 15. The hydrolysis process is also strongly influenced by such factors as temperature, time and character of the catalyst used.

After the hydrolysis the pH of the obtained homogenous hydrolysate is gradually brought up to ca. 6 by means of, e.g., diluted ammonia solution, in case of acid catalyzed process. This results in quick (approx. 1 min) gelation and formation of the so called "wet" gel. Subsequently, the obtained gel can be aged for a few days in water or ammonia solution. This process reduces the mechanical stress during the drying and prevents, to some extent, the risk of the sample breaking. However, if the solution obtained after acid based hydrolysis remained at low pH (no ammonia addition), much more slower (days) gelation takes place. Generally, this leads to improvement of the mechanical stability of sol-gel bulks. Gelation process is depicted by equations



or



The sol-gel process has a dynamic character. Thus, it is impossible to separate the individual chemical reactions responsible for the formation of the final product. The hydrolysis, gelation and aging/drying processes occur simultaneously. During the "aging" step (after gelation and before drying) the sol-gel derived material expulses the liquid phase (water, alcohol) from the sample. This process is called syneresis and exemplifies the complicated equilibrium involved in the formation of gels via the sol-gel procedure.

Pronounced drying at temperatures not exceeding 100 °C leads to formation of "dry" gels, called xerogels. They are relatively sturdy, typically transparent but porous materials. The pore size depends on such factors as time and temperature of the hydrolysis and the kind of catalyst used. The diameter of the pores is directly related to the shrinkage of the "wet" gels. During the drying process the gel volume decreases even several times

(which is the main reason of cracking). Addition to the hydrolyzate of small amounts of simple organic solvents (e.g., dimethylformamide or dimethylsulfoxide), stabilizes the resultant gels increasing their mechanical strength and improving transparency.

Such organic reagents are called drying control chemical additives (DCCA)<sup>26</sup>. Another method of preventing the samples cracking is the addition of the fine SiO<sub>2</sub> powder (fumed silica, aerosils). This improves significantly the gel stability but causes that the resulting gels became non-transparent due to the light scattering. However, heating at approx. 1200 °C removes the cloudiness. Generally, whilst heating the xerogels at the quartz glass vitrification temperature, the densified glasses almost identical to the conventional ones, can be obtained. The whole process of forming sol-gels is schematically presented in Figure 1.

The technology of preparation of glass-like xerogels offers, in comparison to conventional glasses, some advantages. The whole process can be performed at room temperature and second, the glass is obtained from the liquid precursors. This allows to add to the hydrolyzate various chemical substances (as a solution, suspension or even a solid samples) and, after the gelation step, to entrap them within the gel. Since the whole process (including drying) can be conducted at room temperature, even relatively unstable molecules (e.g., proteins) can be entrapped into the matrix. Since

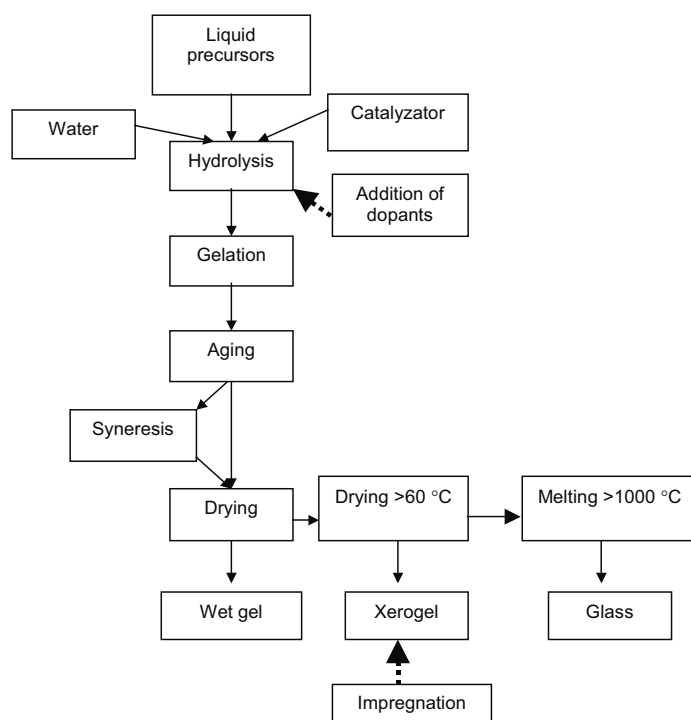


Figure 1. The schematic representation of the sol-gel production process.

xerogels are porous, so thus the entrapped molecules can usually interact with environment through the network of channels and voids. The doped xerogels are very promising materials for various chemical and biological sensors.

## 2.2 Mutual Influences of Sol-Gel Matrices and Dopants

The preparation of sol-gel material enables to add various compounds into the liquid mixture of precursors. This attractive feature of sol-gels can be exploited in number of practical applications. The matrices doped with photosensitive molecules can be used for construction of optical chemical sensors. Entrapment of metals enables the preparation of special antireflection coatings and other optical elements. Immobilization of chemical compounds in the sol gel matrix can also be performed post synthesis by impregnating the prepared matrix. The addition of dopants on optical properties of both, matrix as well as entrapped compound, was studied<sup>27</sup>. Two methods of entrapment were applied. In the first one, the indicators were added to the liquid precursors and the prepared sol-gel bulks were already doped. In the second method, first the sol-gel bulks were produced and then they were placed in the indicator solutions, so thus to impregnate the materials. It was stated that in some cases (e.g. for bromothymol blue) the maximum absorption was observed for the same wavelength, independent whether it was measured in solution or in bulks. Some dyes, however (e.g. Nile red) showed the shift of the absorption peak towards the shorter wavelengths, in case of immobilization during the hydrolysis compare to the case when impregnation was used for doping.

## 2.3 Sol-Gels as Porous Materials

Silica sol-gel glasses are porous materials, which means some kind of solid material that has holes in it. These holes are also called pores. To call a material a porous material, there is usually some kind of implicit assumption of homogenization and length scale. The holes must be smaller enough, compared to the typical size of the piece of material that is considered, so that it is reasonable to consider the material as a mixture of solid framework and pores<sup>28</sup>.

Generally, porous materials have the porosity of 0.2–0.95. The porosity means the fraction of pore volume to the total volume. Let us consider a sample of total volume  $V$ . The volume of the solid phase is  $V_s$ , and the volume of the pore phase (the holes) is  $V_p$ , where  $V=V_s+V_p$ . The volume fraction is normalized variable that is generally more useful. The volume fraction of the pore phase is commonly called the porosity, and is denoted as  $\phi=V_p/V$ . The solid volume fraction is then described as  $1-\phi$ <sup>29</sup>.

Pores are classified into two types: open pores, which connect to the outside of the material, and the closed pores, which are totally within the material. Penetrating pores are kind of open pores; these have at least two openings located on two sides of a porous material. Penetrating pores are permeable for fluid, and therefore are important in applications such as filters. Many porous materials have been used in many applications. They are classified by many different criteria such as pore size, pore shape, materials and production methods. Classification by pore size and by pore shape is useful while considering the applications of porous materials. The classification of porous materials by pore size (according to Schaefer<sup>30</sup>) differentiates between microporous pores (pore diameter < 2 nm), mesoporous pores (2 nm < pore diameter < 50 nm) and macroporous pores (pore diameter > 50 nm).

As described before, the pore size of porous material ranges widely from atomic size to millimeter order. Different pore sizes are required for different applications of porous materials. Most porous materials do not have uniform pores. Pore size distribution is also an important property. Narrow pore size distribution, i.e., uniform pore size, is required for instance for filters and bioreactor beds. Mercury porosimetry and gas adsorption methods are commonly used to measure pores size and pores distribution.

One of the conceptually simplest ways to study porous media is to carry out the small-angle scattering experiments, typically using light, neutrons or X-ray. Small-angle scattering has thus been widely used to investigate the basic morphology of the pore structure and of the internal pore surface. Because of finite instrumental resolution effects, such experiments however, can reveal structural information only up to the length scale of typically a few tenths of nanometers<sup>31-32, 37</sup>.

## **2.4 Sol-Gel Glasses**

### **2.4.1 Gel Formation**

Sol-gel process starts with a solution or a sol that becomes a gel. The solution can be prepared from either inorganic salts or organic components which than are hydrolyzed and condensed to make a sol or a gel. One can stop at the sol stage, which refers to a dispersion of particles of colloidal dimensions in a liquid, or proceed to the gel state which refers to a three-dimensionally-linked solid network with liquid filling the pores. These pores are interconnected in the wet gel state.

The polymerization reaction are affected by the properties of the starting silicate precursors: pH, catalyzator, silica concentration, temperature, presence or absence of salts and additives, aging and drying conditions. Among these various factors, pH and drying conditions are two of the most

important variables that can affect the gel pore structure and polar properties<sup>33</sup>. In case of silica sol-gels the polymerization reaction is based on the condensation of silanol groups. The following steps may be distinguished: (1) formation of dimer and higher molecular species, (2) condensation to form primary particles, (3) growth of the particles, (4) linking of the particles together in chains and then into three-dimensional network.

A nucleation process forms amorphous spheroidal groupings of the dimension about 1 to 2 nm. The smaller particles, which have the higher solubility, dissolve and the silica is redeposited on the larger ones, the total number of particles decreasing. At low pH values, particle growth stops once a size of 2–4 nm is reached. For  $\text{pH} \geq 7$  particles growth continues at room temperature until particles about 5–10 nm in diameter are formed, than it slows down. At higher temperatures particles growth continues, especially for  $\text{pH} > 7$ . For the pH range between 6–10.5 the silica particles are negatively charged and repel one another – growth continues without aggregate, resulting in the formation of stable sols. If, however, salts are present, aggregate and gelling occur. At low pH the particles have little ionic charge; they can collide and form by aggregate continues networks leading to gel. This process may involve primary particles of different size according to the pH level and the presence or absence of salts. Condensation can be controlled and even stopped when the particles reach the required size.

#### **2.4.2 Structure of Dried Sol-Gels (Xerogels)**

The final structure of the dry gel will depends on the structure of the wet gel originally formed in solution; it will be a contracted or a distorted version of the latter. The model comprises (a) aggregates of particles of approximately the same size, essentially massive in nature; (b) aggregates of particles formed by primary particles (with ultrapores); (c) aggregates of more complex nature in which three levels of particles can be distinguished as well as micropores and macropores. The dried amorphous gel differs from a glass by its texture. The gel is essentially agglomerate of elementary particles, the size of which may be of the order of 10 nm, arranged more or less compactly. The porosity may vary considerably, according to the method of preparation.

According to the packing geometry, the systems present different porosity and specific surface. The final characteristics of the dried gel are determined by the physicochemical conditions at every step of the preparation: the size of primary particles at the moment of aggregate, the concentration of particles in solution, the pH, salt concentration, temperature, and time of aging or other treatment in the wet state, mechanical forces present during drying, the temperature, pH, pressure, salt

concentration, and surface tension of the liquid medium during drying, the temperature, time, and atmosphere during drying.

### **3. SILICA SOL-GEL OPTICAL DEVICES**

Applications exploiting porous silica to encapsulate sensor molecules, enzymes and many other compounds are developing rapidly. Nowadays, sol-gel technology is being used in various fields of modern technology, as for example the basis for optodes, integrated systems, fiber optics, lasers, and new materials.

#### **3.1 Sol-Gel Optodes for Fiberoptic Sensors**

Generally, there are two solutions for fiberoptic sensors: direct and indirect sensing techniques. In direct sensing method the changes in the environment (e.g., pH, temperature, pressure or concentration of different compounds) are measured directly, for example by monitoring of the absorption or changes in light polarization. Depending on the analytical method used, the optical sensors can be broadly divided into physical and chemical ones. As an example of direct physical fiberoptic sensors are the sensors exploiting birefringent fibers<sup>34</sup>. The indirect sensing involves the construction of special element, called the optode, which acts as a transducer between environment and fiberoptic guide connected to the photodetector and analyzing unit.

The optode transduces the non-optical signal from the environment to the optical one, readable by the photodetector. Various indirect optical sensors and their applications are described in literature<sup>35</sup>. The optode can work as a chemical sensor that detects certain analytes in aqueous solutions or in air on chemical way. It means that changes in the environment cause the changes in the photosensitive material, which is immobilized in the optode matrix. These chemical changes influence the observed light intensity (for example, due to absorption) or one can analyze the intensity or time decay of luminescence. There are numbers of publications devoted to the family of optical chemical sensors<sup>36</sup>.

Construction of the optode for optical biosensor requires immobilization of sensitive compounds in the host matrix. There are several methods enabling molecules entrapment. One can use gels, polymers, saccharose, various meshes and membranes<sup>78</sup>. In case of fiberoptic indirect sensors optode must be attached to the fiber tip. Nowadays, there are two commonly used optode host materials: sol-gel materials and polymers.

Silica gels seem to be ideal materials for construction of optodes for indirect fiberoptic sensors. Their visible transparency, porosity enabling the



transport of gases or liquids through the material, thermal and chemical stability, and ability to be filled with additional active phases are the key properties that gels bring to sensor applications<sup>37-38</sup>. The sol-gel process, which leads to the silica glass formation, is carried out at room temperature what gives a wide range of potential applications. In addition, it is easy to prepare the sol-gel elements of various shapes.

In order to act as a transducer optode must be attached to the optical fiber. Bulks (>1 mm) of sol-gel matrix can be easily glued to the fiber tip, especially, if the polymer fiber is used<sup>39</sup>. The smaller optodes can be attached to fiber end by dip-coating method or simply by direct painting of the fiber-tip with a liquid gel.

Depending on the optode dimension two constructions are possible: micro- or macrooptodes. If the optode diameter is comparable with the diameter of optical fiber or bigger, it is defined as a macrooptode. If it is smaller, then we have a microoptode construction. Typical sizes of macrooptodes vary from 125  $\mu\text{m}$  up to 2 mm and of microoptodes from 50  $\mu\text{m}$  down to 25  $\mu\text{m}$  or even smaller.

### 3.2 Fiber Tips and Types of Optodes

The most common shape of the sensor fiber tip is the flat one. It is easy to prepare, since only a fiber cutter is needed. However, the bounding of optode is not very robust and it can be destroyed mechanically.

The flat fiber end can be modified, so thus to obtain different shapes, like tapered, beveled, conical ones or even in form of microlenses<sup>40-41</sup>. The thin layer of sol-gel coating may create a microoptode on the distal end of the tapered fiber. Microoptodes offer generally higher resolution of the measurements. However, as in the previous case, such an external optode can be easily scratched and damaged. To avoid the problem of optode damage, the good solution may an internal optode, for example placed in the microchamber inside the fiber tip. This kind of the tip can be made chemically by etching the fiber with the HF acid bath at room temperature. Depending on the etching duration, different depths of microchamber can be achieved to prepare the sensor of this type the liquid sol-gel should be poured into the fiber cavity<sup>42</sup>. It is quite challenging, since the input window diameter is approximately 120  $\mu\text{m}$  and the chamber volume is ca.  $4 \times 10^{-13} \text{m}^3$ .

### 3.3 Integrated Systems

Definition of integrated systems is more complex extension of chemical, biological and physical sensors. We can define integrated systems as optical or electrical (or hybride) measurement devices that exploit physical

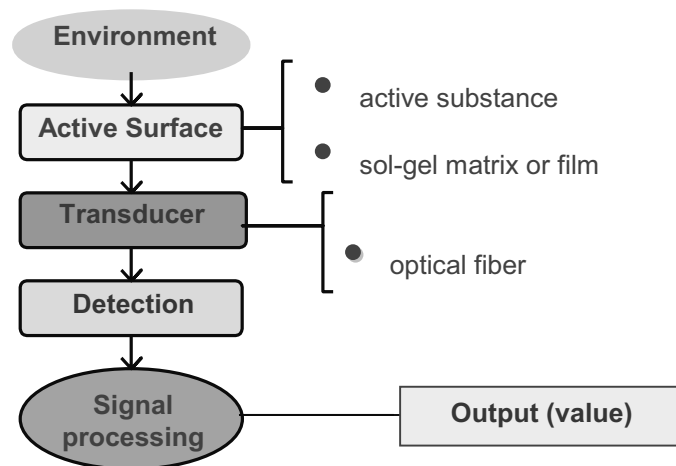


Figure 2. The basic components of an integrated system.

phenomena or chemical and biological reactions to detect and to quantify a specific analyte or event. From this definition, one can define the basic components of an integrated system. Such system includes an active surface, a transducer and an electronic unit with corresponding software, as it is shown in Figure 2.

The active layer contains the detection components, e.g., an immobilized molecule in the matrix (sol-gel glass). Optical fibers are typically used as optical transducer. Photodetectors and ESPC (Electronic Signal Processing and Control) are the last part of the circuitry. Fiber optic chemical and biological sensors represent a relatively new but very rapidly growing research area<sup>43-44</sup>. These kinds of sensors possess a number of potential advantages as immunity to electromagnetic interference, low transmission loss, low cost, small size, geometric flexibility and all dielectric construction being the most obvious. The potential applications of such devices are manifold and diverse. They include remote and distributed sensing for environmental and safety monitoring, biochemical and in vivo sensing and in particular, monitoring of hazardous and explosive environments.

Sol-gel coating technique for optical chemical sensors and biosensors is now in extensive research phase. For example, the side-coating of optical fibers or waveguides in evanescent-wave sensors it is particularly important to control precisely the sensitivity determining parameters, such as the coating thickness and length<sup>45</sup>.

The achievements in optical detection techniques and the interest in the sol-gel process for creation of new materials, are leading to developing of various sensors. The majority of reported sensors developments have concentrated on the use of thin films. There are many reasons for this. The important one is the susceptibility of monoliths to cracking due to internal stresses, particularly when exposed to liquid penetration. More attractive are

the features of sol-gel films. Such films may be applied by dip coating, spin coating or even spray coating methods. These techniques are already established in industrial processes for fabrication antireflection coatings and interference filters. Furthermore, sol-gel films exhibit strong adhesion as well as good mechanical strength. The advantages of sol-gel films may be combined with those of optical fibers or waveguides to produce intrinsic evanescent-wave sensors<sup>46-47</sup>.

Sol-gel technology makes it possible to deposit onto glass substrates two-component coatings that consist of a mixture of silicon dioxide and an indicator (a dye that changes color as a function of the pH)<sup>48</sup>. The spectral and operational characteristics of the resulting coatings are similar to one-component coatings.

### **3.4 Fiber Optics**

A new idea of sol-gel-derived micron scale optical fibers for chemical sensing was first reported in 1996<sup>49</sup>. It was the first preparation of organically-doped room temperature processed sol-gel-derived micron scale optical fibers as platforms for chemical- and bio-sensors. Micron scale optical fibers are drawn from fluorescent dye-doped tetraethoxysilane (TEOS)-derived sol-gel solution processed under ambient conditions. Such a simple methodology to entrap organic and even bioactive species within the optical fiber offers many advantages over more conventional ways of immobilizing organic probes for the development of optical sensors. Specifically, on the photophysical properties of fluorescein (a pH sensitive fluorescent dye) and rhodamine 6G (R6G; laser dye) entrapped within sol-gel-derived optical fibers demonstrate that a fluorescein-doped sol-gel-derived optical fiber responds to ammonia and acid vapors with a response time of 1–2s. Tapered fiber tips with different geometry<sup>50</sup> are fabricated for developing a fiber optic biosensor. Fluorescence experiments were performed to compare the coupling efficiency of light for different fiber tip configurations. When light is generated in a “thick” layer (>1  $\mu\text{m}$ ) around a fiber core, the continuously tapered tip with the steepest taper collects light more efficiently than the longer combination tapered tip. To demonstrate the applicability of the authors' results, they have successfully detected weak chemiluminescent signal collected by a bundle of fibers with the short continuously tapered tips using a cooled CCD array detector. In these case the chemiluminescence reaction was catalyzed by alkaline phosphatase immobilized on the fiber tips by a sol-gel technique.

#### **4. MEDICAL AND ENVIRONMENTAL APPLICATIONS OF SOL-GEL BASED SENSING DEVICES**

The sol-gel process enables the preparation of thin films, fibers and bulk materials for various devices configurations. Applications of this technology include new instrumental methods for clinical chemistry, analytical chemistry, medical diagnosis and therapy, *in vivo* monitoring of metabolites and nutrients, product sensing during fermentation, remote sensing in dangerous environments. The sol-gel technology has created a new way of sensor production. The indicator may be entrapped into a porous sol-gel matrix or can be immobilized on the glass surface. It is possible to integrate a sol-gel element of sensor and optical fiber, thus constructing a simple indicator of analytes concentration in air, blood, serum, urine or other liquids.

##### **4.1 Biosensors**

The group of scientists from University of California, Los Angeles, designed several silicate sol-gels systems, based on encapsulation of enzymes and proteins. These systems can detect biologically relevant analytes like O<sub>2</sub>, CO, NO, glucose and oxalate. For biorecognition of specific compounds, enzymes and metalloproteines may be used.

The recognition of dissolved oxygen is possible with use of hemoglobin and myoglobin. These two heme proteins are capable to bind reversibly the atmospheric oxygen. Myoglobin is mostly chosen because of its higher sensitivity for oxygen. The correlation between the absorption spectra and concentrations of dissolved O<sub>2</sub> was found. The significant differences in absorption maxima of the transition of the deoxy and oxy forms of the protein in the 430 nm region were measured. It is a convenient way to quantitate the protein-oxygen interactions. The linear relationship between the optical response of myoglobin and the concentration of dissolved O<sub>2</sub> was established by monitoring the rate of absorbance change of the 436 nm transition for the deoxy form. The analytical advantages of such biosensing element include linear correlation, short response intervals ( $\cong$  1 min), high specificity, reversibility of the oxy form to the deoxy form, and cost-effectiveness.

Myoglobin can also bind CO, and sol-gel with entrapped myoglobin can be used as the sensor for CO by taking advantages of the changes in the absorption spectrum due to protein-CO interaction.

This same group developed a novel biosensor based on manganese myoglobin to detect nitric oxide. Mn-containing myoglobin was chosen as

the sensor element because of its specificity for NO. The biorecognition of in-situ-generated NO was demonstrated using manganese myoglobin immobilized in sol-gel, as confirmed by the appearance of the characteristic absorption spectrum of MnMbNO.

Glucose biosensor based on sol-gel with entrapped glucose oxidase in combination with horseradish peroxidase and dye precursors (4-aminoantipyrine and p-hydroxybenzene sulfonate) was described. The dye precursors formed a quinoneimine dye with an absorption maximum at 510 nm. Glucose oxidase catalyzed the air oxidation of  $\beta$ -D-glucose to yield gluconic acid and hydrogen peroxide. Hydrogen peroxide triggered the horseradish peroxidase-catalyzed formation of dye from precursors. The rate of formation of colored dye was directly proportional to the concentration of glucose in the sample. By monitoring the absorption maximum of the dye generated, the concentration of glucose could be determined.

For oxalate detection, authors proposed a similar detection approach for recognition of oxalate via an immobilized oxalate oxidase/peroxidase couple and dye precursors MBTH (3-methyl-2-benzothiazolinone hydrazone) and DMAB (3-dimethylaminobenzoic acid). The peroxide generated by oxidation of oxalate to  $\text{CO}_2$  reacted with the dye precursors in a peroxidase-catalyzed reaction to yield an indamine dye with absorption maximum at 590 nm. The concentration of oxalate was correlated with increased absorption from dye.

Reliable measurements of L-lactate are of great interest in clinical chemistry, the dairy and vine industry, biotechnology, or sport medicine. In particular, blood lactate levels are indicative of various pathological states, including shock, respiratory insufficiencies, and heart and liver diseases. Silica sol-gel encapsulation of the lactate dehydrogenase and its cofactor was employed as a disposable sensor for L-lactate<sup>51</sup>. The sensor utilized the changes in absorbance or fluorescence from reduced cofactor nicotinamide adenine dinucleotide (NADH) upon exposure to L-lactate.

#### 4.1.1 Metal Sensors and pH Sensors

Sol-gel materials can show high transparency what is suitable for constructing of optical sensors. Zusman et al.<sup>52</sup> used the transparency of sol-gels in the building of optical chemical sensors. They entrapped various agents sensitive to selected analytes in monolithic (glassy) xerogel blocks. By monitoring of the characteristic color changes in the doped materials, they were able to detect the following: metal cations ( $\text{Fe}^{2+}$ ,  $\text{Al}^{3+}$ ,  $\text{Co}^{2+}$ ,  $\text{Ni}^{2+}$ ,  $\text{Cu}^{2+}$ ,  $\text{Pb}^{2+}$ ), the inorganic anions e.g.  $\text{SO}_4^{2-}$ , the organic analyzates (e.g. orthophenanthroline), pH changes.

British scientists immobilized<sup>53</sup> in a porous sol-gel glass aequorin – the bioluminescent protein found in the jellyfish *Aequorea aequorea*. The luminescence from this protein is specifically triggered by the presence of calcium ions. The intensity of the luminescence, measured at the peak

maximum of 470 nm, for the encapsulated protein has been calibrated against calcium ion concentration. The results suggest that the sol-gel encapsulated aequorin protein offer possibility for the development of an optical biosensor for the determination of calcium ions.

Doped sol-gel films may offer a simple, non-invasive, reusable and fast optical chemical sensing technique<sup>54</sup>. For example, the TMOS based sol-gel films doped with bromophenol blue and eriochrome cyanine RC served for measuring pH (from 3 to 8) and detection of  $\text{Cu}^{2+}$  in solutions. The sol-gel entrapment of xylenol orange (XO) provided optical sensing films selective and sensitive to bismuth(III), with low leaching characteristics, fast response, and long life time<sup>55</sup>. The silica sol-gel thin films (thickness < 1  $\mu\text{m}$ ), doped with bismuth sensitive dye for the determination of Bi(III) in pharmaceutical products., were deposited onto the square glass slides by dip-coating and spin-coating methods.

Heavy metal ions detection with porphyrin in sol-gel is possible, too<sup>56</sup>. The porphyrin, used for detection of heavy metal ions ( $\text{Hg}^{2+}$ ,  $\text{Pb}^{2+}$ ,  $\text{Cd}^{2+}$ ), was 5,10,15,20-tetra(4-N-methylpyridil)porphyrin (TMPyP) preferred to other porphyrins because it was not leaked out of the matrix. The study of metallation of the porphyrin immobilized in sol-gel emphasized the formation of 1:1 complex for each ion with a constant of complexation depending on the nature of the ions. The strongest effects were observed for mercury due to the specific interaction of this metal with the porphyrin.

A dual-transducer approach based on sol-gel optical sensors was recently reported to measure acid and salt concentrations in concentrated aqueous and HCl solutions<sup>57</sup>. The acid sensors containing bromocresol purple, neutral red, and bromocresol green indicators were obtained by the immobilization of indicators in sol-gel derived films. The salt-HCl solution was flowed through the sensor cell<sup>58</sup>.

Multicomponent sol-gels made using polydimethylsiloxane hydroxy-terminated (PDMS) and tetraethoxysilane (TEOS) with the silane coupling reagents, 3-aminopropyltriethoxysilane (APTES) and 3-glycidioxypropyltrimethoxysilane (GPTMS), and a base catalyst are optically transparent, mechanically strong and show little or no shrinkage or cracking<sup>59</sup>. A base-catalyzed sol-gel process proved advantageous over an acid-catalyzed process when amino groups were present, producing optically transparent, homogeneous gels. For that reason, the mentioned base-catalyzed organo-silica sol-gel was applied as the host matrix for immobilization of fluorescein isothiocyanine for fiber-optic pH sensor. Hydrophilic sol-gel films were made by co-polymerizing TEOS and PDMS with APTES and /or GPTMS. These sol-gels were hydrophilic despite the presence of PDMS and were useful for sensor membranes in aqueous solution. Sol solutions could be stored and coated on fibers for up to one month depending on the amounts of APTES and GPTMS used. The pH sensors remain stable over at least two months of storage at pH 6.0-6.5 pH.

American scientists prepared the organo-silica sol-gel membranes<sup>60</sup> and demonstrated in a single layer format for pH measurement and multiple-layer format for both CO<sub>2</sub> and NH<sub>3</sub>. The sensors used a hydroxypyrenetrisulfonic acid (HPTS) as the indicator immobilized in a base-catalyzed sol-gel containing poly(dimethyl)siloxane, aminopropyltriethoxysilane (APTES) and tetraethylorthosilicate (TEOS). This indicator gel was over coated with a hydrophobic sol-gel to reduce cross reactivity to pH when either carbon dioxide or ammonia were examined.

Long lasting and fast response optical sensor for pH determination between 6 and 12 was recently proposed<sup>61</sup>. The sensor was fabricated by spin-coating silica sol in the presence of phenol red. The sol was obtained by acidic hydrolysis of tetraethoxysilane (TEOS) and phenyltriethoxysilane (Ph-TriEOS). The performance of the sensor strongly depended on the ratio of both precursors. Addition of a small amount of organosilane was the key to the sensor's sensitivity, stability and lifetime, due to the increased solubility of the dye in the sol-gel. However, large amount of the organosilane in the hydrolyzate greatly decreased the mobility of the ions in the matrix, therefore, the response time was prolonged. At the optimal composition, the sensor had a response time of less than 20s, the response was completely reversible and its lifetime was over 12 months.

The scientific group from Turkey<sup>62</sup> studied photophysical and photochemical properties and behaviour of an azlactone derivative, 4-(p-N,N-dimethylaminophenylmethylene)-2-phenyl-5-oxazolone in sol-gel matrix. The fluorescent dye doped sol-gels exhibited a pH sensitivity in pH range between 3.0 and 7.0. They discovered that the sol-gel matrix enhanced the fluorescence quantum yield and fluorescence emission lifetime compared to dyes in acetonitrile and tetrahydrofuran solutions.

The fabrication and characterization of a fiber optic pH sensor based on evanescent wave absorption was presented by Lee<sup>63</sup>. The unclad portion of a multi-mode optical fibre was coated with the sol-gel doped with pH sensitive dye. The sensitivity of the device increased when the multiple sol-gel coatings were used in the sensing region. The dynamic range and the temporal response of the sensor were investigated for two different dyes – bromocresol purple and bromocresol green.

Optical pH sensors with linear responses over different pH ranges can be designed by using different groups of indicators. A silica sol-gel glass pH sensor was developed by co-entrapping three indicators (bromocresol green, bromocresol purple, and phenol red)<sup>64</sup>, which produced a linear response over 3.5 pH units from pH 6.3 to 9.8 with a standard deviation of pH equal to 0.03.

The two water-soluble porphyrins, 5,10,15,20-tetra(4-N-methylpyridiniumyl) porphyrin (H<sub>2</sub>TMPyP<sup>4+</sup>) and 5,10,15,20-tetra(4-sulfonato) porphyrin (H<sub>2</sub>TPPS<sup>4-</sup>), were immobilized in the silica sol-gel matrix and served as the pH sensors as well<sup>65</sup>. The sol-gels doped with porphyrin were

placed in a disposable cuvette and stored for 1 week in the dark place. Solid transparent monoliths were obtained with a rectangular parallel-piped shape having a thickness ca 1 cm. They were stored at 3 °C to stop the polymerization reaction. The changes in absorption spectra of porphyrin-doped blocks were observed due to pH changes.

To monitor the brain tissue, the fiber optic sensor based on the immobilization of a pH-sensitive dye, seminaphthorhodamine-1 carboxylate (SNARF-1C), was designed<sup>66</sup>. The dye-doped sol-gel was deposited onto the end of a 12 µm-diameter silica optical fiber and *in vivo* studies were performed.

The fabrication and characterization of pH sensor based on side polished single mode optical fiber was also described<sup>67</sup>. This sensor was prepared by fixing the fiber in a groove made on one of the surfaces of a fused silica block. To make the surface sensitive to pH it was polished up to the core of the fiber and covered with the sol-gel film containing a mixture of three pH sensitive dyes - cresol red, bromophenol blue, and chlorophenol red. These dyes were selected because the mixture of these dyes gives a long pH range. The most important advantage of this sensor based on evanescent wave absorption is that a very small amount of sample (few drops only) is needed to measure its pH.

The introduction of 2-[4-(dimethylamino)phenylazo]benzoic acid into a silica sol allows the preparation of pH-sensitive doped coatings upon glass substrates. The behavior of this system was evaluated as the function of pH changes in liquid and gas media<sup>68</sup>. Optical absorption and sensitivity against pH were monitored by Vis spectroscopy. Chemical and mechanical stability tests carried out with coatings demonstrated that they were resistant enough to be used in sensor devices for pH measurements in laboratories.

Over the last several years, the number of studies on application of artificial neural network for solving modeling problems in analytical chemistry and especially in optical fibre chemical sensor technology, has increased substantially<sup>69</sup>. The constructed sensors (e.g. the optical fibre pH sensor based on bromophenol blue immobilized in silica sol-gel film) are evaluated with respect to prediction of error of the artificial neural network, reproducibility, repeatability, photostability, response time and effect of ionic strength of the buffer solution on the sensor response.

The pH optical fiber sensor without any pH-sensitive dye was also described<sup>70</sup>. Porous silica layer made by the sol-gel method was cladded onto optical fibre core and was exploited as the optical transducer. Acid-base properties of silica surface caused that the surface charge of silica changed with pH of the solution. For example: saturation of the sol-gel layer with cations leads to an increase of the electron density of the film, hence, the refractive index of the film. Since the surface charge of silica depends on pH, the refractive index of silica film varies also with pH. Thus, changes of



the refractive index of the film, which plays role in the fibre cladding, modifies the conditions of light propagation within optical fibre.

An extended range fiber optic pH sensor using evanescent wave absorption of sol-gel entrapped pH indicators is based on evanescent wave absorption using an unclad optical fiber dip-coated in the pH sensitive coating solution<sup>71</sup>. The sol-gel process has been used to entrap pH indicators in porous glass coating for sensor applications. The entrapped pH indicators show a broadening of the pH range with respect to the behavior in solution, giving accurate measurement over three pH units when one indicator is used (bromophenol blue) and over six pH units (pH 3–9) when two indicators are used (bromophenol blue and bromocresol purple). The response of the pH sensor was monitored by measuring absorption at 590 nm referenced against a non absorbing region of the spectrum. This enabled the use of LED sources together with low cost photodiodes. The sensor displayed short response time and good repeatability. Modifying the composition of the starting sol mixture can influence the thickness and stability of the pH sensitive coatings. The evanescent absorption, and hence the sensitivity of the sensor, can be increased by selectively launching higher order modes in the fiber. The operation of the other sensor is based on the pH dependent quenching of fluoresceine dye immobilized in the porous cladding of a PCS (Polymer Clad Silica) optical fiber which has been stripped and re-clad in a sol-gel coating<sup>72</sup>. The analyte distribution is recovered from the OTDR (Optical Time Domain Reflectometer) response of the system to a short excitation pulse.

The same techniques for optical fiber chemical sensor were investigated and a model system for pH measurement was developed. As a result, the discrete signals distributions were obtained<sup>73</sup>. The pH indicator fluorescein sodium was chosen for this work because of its well known properties and high fluorescence intensity. A low temperature sol-gel glass manufacturing process was exploited to immobilize the indicator on the optical fiber core. Robust porous glass thin film (~1  $\mu\text{m}$ ) was grown on the surface of the optical fiber core with indicator molecules entrapped in the matrix. OTDR was employed to obtain the signal at specific positions along the fiber. A dye laser, pumped by a short pulse  $\text{N}_2$  laser, produced blue light pulses at 440 nm which were launched into a 1 $\times$ 2 optical fiber coupler. A fiber with four sensitive sections was spliced to a 50:50. The indicator molecules were excited by the blue light via the evanescent wave. Part of the fluorescent light from the indicator molecules was coupled back into the fiber and transmitted back to the coupler. A fast photomultiplier tube was attached to the other arm of the 1 $\times$ 2 coupler to detect the fluorescent light. Results were obtained for solutions of various pH value. The system appears to have a great potential due to the wide possible applications in chemical, biochemical, environmental and safety monitoring.

The pH measurement can be realized using sol-gel films and evanescent-wave sensors method<sup>74</sup>. To incorporate a near-infrared pH sensitive fluorescent dye, a thin-film coating on the core of a multimode fiber was used. By evanescent wave excitation an absorption or fluorescent based sensor can be realized for use in high pH regions.

## 4.2 Humidity Sensor

The physical and chemical properties of MgO films prepared by the sol-gel technique were the area interest of the examinations presented by Shukla<sup>75</sup>. The aim of mentioned work was to produce films with nano size particles so as to employ them for the sensor applications, as adsorption in such films increases many folds due to the increase of surface area. Infra-red spectroscopic studies indicated the presence of solvent in the precursor, which helped in decomposition to nano-particles during nucleation of the film. The MgO sol-gel films were deposited on the glass rod bend in U-shape for humidity sensor.

## 4.3 Ammonia Sensor

The members of Wolfbeis team constructed an optical sensor for ammonia-based on ion pairing<sup>76</sup>. They immobilized pH-sensitive dye (bromophenol blue) as an ion pair with cetyltrimethylammonium bromide (CTABr) in a silicone polymer matrix. Bromophenol blue, while contact the ammonia (both in water as well as in gaseous form) changes its color reversibly from yellow to blue. The immobilized dye shows long wave absorption with a good photostability.

Lobnik and Wolfbeis used<sup>77</sup> aminofluorescein as a pH indicator in new sol-gel based sensor for ammonia. Ammonia reacts with the aminofluorescein (AF-OH) thus creating the strongly fluorescent anion (AF-O<sup>-</sup>).

## 4.4 Urea Sensor

As the one of the main end products of protein metabolism in living organisms, urea is a primary source of organic nitrogen in soil (from animal urine, fertilizers, etc.). Monitoring the level of urea is important for medicine, as well as for environmental protection. Urease is an enzyme that breaks the carbon-nitrogen bond of amides to form carbon dioxide, ammonia and water. This enzyme is widely used for determination of urea in

biological specimen. As it was mentioned, it catalyses the hydrolysis of urea to  $\text{CO}_2$  and  $\text{NH}_3$ . Hydrolysis of urea in presence of urease as catalyst gives the pH increase proportional to urea concentration. By measuring of pH, urea concentration can be calculated.

Construction of the optode for urea biosensor requires immobilisation of protein (and pH indicator) in the host matrix. There are several methods enabling protein entrapment. One can use gels, polymers, saccharose, various meshes and membranes<sup>78</sup>.

The way of enzyme entrapment has been described<sup>79</sup> proposing the application of sol-gel matrices. The optodes of urea sensor were prepared by the sol-gel method and were stored in a refrigerator. As the pH sensitive dye the bromothymol blue was used. Since it is best acting in pH range 6 to 7.6, the pH of sol-gel bulks obtained in the experiment was chosen as pH 6. Before measurements, the optodes were incubated in the temperature 36.6°C.

#### 4.5 Pesticides, Herbicides, and Insecticides Sensors

There is an urgent demand for water quality monitoring system capable of detecting such species like organophosphates. These neurotoxic compounds irreversibly inhibit the enzyme acetylcholinesterase, which is essential for functioning of the central nervous system of mammals and insects. The organically modified silica sol-gels were applied as recognition layers, combined with mid-infrared evanescent wave sensors, for *in situ* detection of pesticides in aqueous media<sup>80</sup>. The host matrices were prepared by acid-catalyzed co-polymerization of phenyltrimethoxysilane (PTMOS) and tetramethoxysilane (TMOS) and were spin-coated onto ZnSe attenuated total reflection waveguides. It was concluded that sol-gel coated infrared optical sensors enable reproducible detection of organophosphates down to the sub-ppm concentration range.

The design and implementation of a portable fiber-optic cholinesterase biosensor for the detection and determination of pesticides carbaryl and dichlorvos was presented by Andreou<sup>81</sup>. The sensing bioactive material was a three-layer sandwich. The enzyme cholinesterase was immobilized on the outer layer, consisting of hydrophilic modified polyvinylidene fluoride membrane. The membrane was in contact with an intermediate sol-gel layer that incorporated bromocresol purple, deposited on an inner disk. The sensor operated in a static mode at room temperature and the rate of the inhibited reaction served as an analytical signal. This method was successfully applied to the direct analysis of natural water samples (detection and determination of these pesticides), without sample pretreatment, and since the biosensor setup is fully portable (in a small case), it is suitable for in-field use.

Molecularly imprinting sol-gel using a sacrificial spacer was successful in creating a material that could bind DDT<sup>82</sup> with a moderate degree of

selectivity. Use of an environmentally sensitive fluorescent probe (7-nitrobenz-2-oxa-1,3-diazole) can transduce the presence of bound molecule. The imprinted sol-gels, deposited as films on glass microscope slides, were shown to quantitatively detect DDT in water to a limit-of-detection of 50 ppt with a response time of <60s.

The scientists from Hong Kong reported<sup>83</sup> on a sol-gel derived molecular imprinted polymers (MIPs) based luminescent sensing material that made use of a photoinduced electron transfer (PET) mechanism for a sensing of a non-fluorescent herbicide - 2,4-dichlorophenoxyacetic acid. A new organosilane, 3-[*N,N*-bis(9-anthrylmethyl)amino]propyltriethoxysilane, was synthesized and used as the PET sensor monomer. The sensing MIPs material was fabricated by a conventional sol-gel process.

#### 4.6 Gas Sensors

Sol-gel technique is particularly interesting due to possibility of the organic-inorganic composite material production, which porous structure ensures high solid-liquid and solid-gas contact surface.

SnO<sub>2</sub> is a well known and widely studied sensor material for the detection of CO and flammable gases like H<sub>2</sub><sup>84</sup>. The use of porous networks of SnO<sub>2</sub> nanoparticles for an optical detection of gaseous CO was discussed. Nano-sized clusters were prepared by the sol-gel method using an organically modified Sn precursor. After thermal treatment at 550 °C the mean diameters of the primary SnO<sub>2</sub> nanoparticles constructing the network were estimated ~25 nm and ~15 nm, respectively, for particles obtained in acid and base catalysis. The reversible redox behavior of SnO<sub>2</sub> nano-clusters in reducing and oxidizing atmospheres (CO, O<sub>2</sub>) was studied optically by in-situ diffuse reflectance spectroscopy (DR-UV/VIS) spectroscopy.

The detection of chemical species (toxic gases) by using TiO<sub>2</sub> porous films suitably functionalized with metal-phtalocyanine macromolecules (Me-phtalocyanine, where Me = Fe, Pd or Cu) has been successfully carried out<sup>85</sup>. The sol-gel coatings were deposited on the glass slides with a superimposed thin layer of evaporated silver. Vapor sensing behavior of the sol-gel films was tested by a computer-controlled gas-flow system. The monitoring of the response in the optical parameters of the hybrid sol-gel material (refractive index *n* and extinction coefficient *k*) in the presence of NO<sub>2</sub> gas at room temperature and at fixed wavelength (He-Ne laser  $\lambda=633$  nm) was done by means of UV-Vis measurements and SPR sensing tests.

The Japanese scientists tested the fiber optic carbon dioxide sensor<sup>86</sup>, prepared by dip-coating method - the sol-gel film containing indicator dye, thymol blue, was deposited on unclad fiber. The sensitive film had both organic and inorganic parts with good permeability. The differences between attenuation in N<sub>2</sub> gas and in CO<sub>2</sub>/N<sub>2</sub> mixture gas increased with the CO<sub>2</sub>

concentration in the 0.55-0.7  $\mu\text{m}$  range. With the increase of humidity and the ratio of precursors TEOS/MTES, the sensitivity of sensor increased, because of the increase in the solubility of  $\text{CO}_2$  gas in this film.

The miniature fiber optic  $\text{NO}_2$  sensors based upon dye encapsulation in the silica sol-gel can produce linear and reproducible results<sup>87</sup>. The nitrogen dioxide sensor based on immobilization of ruthenium complex  $[\text{Ru}(\text{bpy})_3]\text{Cl}_2$  demonstrated sensitivity in the hundreds parts per million range with reversibility and rapid response time.

Brinkley et al. demonstrated<sup>89</sup> a simple to use, easy to interpret, low cost, and environmentally friendly colorimetric detector of the chemical warfare agent - mustard gas (HD, 1,1-thiobis(2-chloroethane)). An optically transparent xerogel encapsulating Cu(II) acetate was fabricated to detect HD analogues and can serve as the optical sensor based on metal-ligand charge-transfer mechanism.

An optical sensor for the measurement of carbon dioxide in modified atmosphere packaging (MAP) applications was developed<sup>89</sup>. It was based on the fluorescent pH indicator 1-hydroxypyrene-3,6,8-trisulfonate (HPTS) immobilized in a hydrophobic organically modified (ormosil) matrix. The  $\text{CO}_2$  sensor was stable over a period of at least 7 months and its output was in excellent agreement with a standard reference method for carbon dioxide analysis.

The sensor for the measurement of high levels of  $\text{CO}_2$  in gas phase was developed, as well<sup>90</sup>. It was based on fluorescence resonance energy transfer between a long-lifetime ruthenium polypyridyl complex and the pH-active disazo dye Sudan III. The donor luminophore and the acceptor dye were both immobilized in a hydrophobic silica sol-gel/ethyl cellulose hybrid matrix. The sensor exhibited a fast and reversible response to carbon dioxide over a wide range of concentrations.

Optical sensors for oxygen measurement are attractive since they can be fast, do not consume oxygen and are not easily poisoned. The most common method adopted in construction is based on quenching of fluorescence from appropriate chemical species. The variation in fluorescence signal ( $I$ ), or fluorescence decay time ( $\tau$ ) with oxygen concentration  $[\text{O}_2]$  is described by Stern-Volmer equation<sup>91</sup>:

$$\frac{I_0}{I} = 1 + K_{\text{SV}} [\text{O}_2] \quad (\text{Eq.4})$$

$$\frac{\tau_0}{\tau} = 1 + K_{\text{SV}} [\text{O}_2] \quad (\text{Eq.5})$$

$$K_{\text{SV}} = k \tau_0 \quad (\text{Eq.6})$$

where  $I_0$  and  $\tau_0$  are respectively the fluorescence signal and excited-state

lifetime in the absence of oxygen.  $K_{SV}$  is the Stern-Volmer quenching constant and  $k$  is the biomolecular quenching constant. Porous sol-gel was a base for development of a fiber-optic dissolved oxygen sensor<sup>47</sup> based on quenching of a ruthenium complex entrapped in it. Porous sol-gel silica films, dip-coated onto either planar glass substrates or clad optical fibers, were doped with the complex [RuII-tris(4,7-diphenyl-1, 10-phenanthroline)], which fluorescence emission is quenched by oxygen. The sensor was constructed from 10 cm long polymer clad silica (PCS) optical fiber with 600  $\mu\text{m}$  core. The fiber was clad mechanically followed by an etching process. The sensitive complex was entrapped in the cage-like structure of the sol-gel matrix, but it was accessible to oxygen via microporous channels. Sol-gel films of about 50 mm length provided good signal-to-noise ratios under high-intensity blue LED excitation. Described work compares the difference in oxygen quenching response between gas phase and aqueous phase measurements. The sensor response time was very short, less than 5 s, including the filling time of gas chamber and the adjustment time of the mass-flow controllers.

Porous ultrafine tin oxide ethanol gas sensors<sup>92</sup> in the form of a thin film have been prepared from tin alkoxide by the sol-gel process. The microstructural evolution of the tin oxide films, which affected the ethanol gas-sensing properties of the films, was investigated as a function of firing temperature and solution concentration. Theoretically, it was expected that ethanol gas sensitivity would increase monotonically with decreasing film thickness, but experimental results showed a maximum sensitivity at about 70 nm. The sudden decrease of the sensitivity below the thickness of 70 nm seemed to be due to the sudden decrease of film porosity, i.e., the sudden decrease of the number of the available sites for the oxidation reaction of ethanol molecules. Thus, it seemed that below the thickness of 70 nm, the sensitivity was governed by microstructure rather than by film thickness.

New type resistive/capacitive gas sensitive structures were obtained by using a specially prepared substrate-glass, covered by a thin conducting layer, cut into comb teeth-type electrodes with the help of a laser beam<sup>93</sup>. Such, a laser processed gap in the layer of a conducting material, was a prototype of an excellent humidity sensor, especially at high values of relative humidity (RH). Different additional coatings onto a laser processed gap were examined for humidity sensing. Sol-gel, vacuum thermal evaporation and laser evaporation methods were used to obtain thin layers of different materials.

Integrated sensor configurations for gravimetric sensing applications have been demonstrated by employing a sol-gel processed thin piezoelectric lead zirconate titanate (PZT) film<sup>94</sup>. It was coated coaxially on stainless steel tubes and interdigital transducer (IDT) fabricated as the transmitter and receiver on the curved tube surface. The tube waves were observed along both, the axial and circumferential directions between 1 and 6.6 MHz. The

mass sensitivities were analyzed for different modes propagating along the tubes and it was shown that high mass sensitivity can be achieved by keeping the tube thin.

A thin film dissolved oxygen sensor was fabricated by entrapping erythrosin B in a sol-gel matrix<sup>95</sup>. The silica sol-gel doped with the dye was deposited onto the cleaned glass slides by the spin-coating method. The sensor was linear in the most useful range of dissolved oxygen concentrations, up to 9.1 mg·l<sup>-1</sup> concentration obtained in air saturated water at 20 °C.

The line-type sensor that can detect the hydrogen leak along the optical fiber was reported<sup>96</sup>. The silica core of the optical fiber was coated with a thin film of catalyst-supported tungsten trioxide (WO<sub>3</sub>). The part of optical power propagating in the core region leaked to cladding WO<sub>3</sub> region and was susceptible to color change. WO<sub>3</sub> was reduced by hydrogen to form a blue tungsten bronze material with the help of noble metal catalysts (platinum and palladium). This sensor could be operate in the wide temperature range around room temperature. The sensor had a potential for distributed measurement to detect the location of hydrogen leakage points.

A strain of yeast and a strain of bacterium were co-immobilized to fabricate a biochemical oxygen demand (BOD) sensor based on sol-gel derived composite materials<sup>97</sup>. This novel type of biosensor was developed for water monitoring and was used to determine the BOD values of OECD synthetic wastewater, domestic wastewater, and lake waters. The microorganisms *Trichosporon cutaneum* and *Bacillus subtilis* were co-immobilized in the sol-gel composite material, which was composed of silica and the grafting copolymer of poly (vinyl alcohol) and 4-vinylpyridine (PVA-g-P(4-VP)).

The first example of the oxygen sensor based on ruthenium(II) polypyridyl dye covalently incorporated onto a silica glass film was described by Malins<sup>98</sup>. They have successfully functionalised a suitable ruthenium(II) polypyridyl moiety with triethoxysilane groups (using APTES), and utilized the resulting functionalised complex to prepare a glass using a standard sol-gel method.

The O<sub>2</sub>-sensing materials based on spin-coated *n*-octyl-triethoxysilane (Octyl-triEOS) / tetraethylorthosilane (TEOS) composite xerogel films was synthesized and investigated<sup>99</sup>. These sensors were based on the O<sub>2</sub> quenching of tris(4,7-diphenyl-1,10-phenanthroline)ruthenium (II) ([Ru(dpp)<sub>3</sub>]<sup>2+</sup>) sequestered within the xerogels. The results of SEM and luminescence measurements shown that certain ([Ru(dpp)<sub>3</sub>]<sup>2+</sup>) doped Octyl-triEOS/TEOS composites form uniform, crack-free xerogel films that can be used to construct high-sensitivity O<sub>2</sub> sensors that have linear calibration curves and excellent long-term stability (over a period of 11 months).

The oxygen-sensitive TEOS and MTEOS-based films were investigated in order to get knowledge about the influence fabrication parameters (pH,

aging time, R-Value) on the microstructural behavior of Ru(dpp)<sub>3</sub> doped silica sol-gels<sup>100</sup>. The aging time appeared to be a parameter, which had the greatest influence on porosity for TEOS films. Both film types exhibited similar oxygen permeability behavior and had similar optical decay times.

Porphyrin-doped silica sol-gel glass was used as a probe for gaseous oxygen sensing<sup>101</sup>. Inorganic silica glass loaded with platinum octaethylporphyrin (PtOEP), an oxygen-quenchable luminescent dye, was prepared by acidic hydrolysis and condensation of TEOS. The optical properties such as absorption and luminescence spectra were investigated. Using these materials, an optical oxygen sensor was fabricated, based on the phosphorescence quenching of PtOEP, which responded in the range of 0.5-100% O<sub>2</sub>.

It was also demonstrated that thionine dye entrapped in methyltrimethoxysilane (MTMS) film matrix may be used for hydrogen sulfide gas sensing<sup>102</sup>. The films used in this studies were prepared by a dip-coating technique using MTMS as the sol-precursor. This chemical compound poses ability to produce single-layer films of greater than 1 μm thickness without the problem with cracking, which is prevalent in other conventional siloxane-based films such as TEOS and TMOS. These thionine-doped films coated onto transparent substrates shown a remarkable change in optical absorption in the presence of gaseous hydrogen sulfide (H<sub>2</sub>S) diluted in air and in the absence of any buffer gas. The rapid response, sensitivity, reversibility, and durability shown by this material can be exploited in developing absorption-based optical H<sub>2</sub>S sensors in either an integrated optics or all-optical fiber approach using a red diode laser source.

#### 4.7 Toluene Sensor

The physical basis for the design of an optical fiber sensor suited for aqueous medium and gas phase based on the excitation of an evanescent wave at the core/cladding interface was presented<sup>103</sup>. The quantitative toluene detection was based on the refractive index changes (between 1.41 and 1.45) of the silica sol-gel polymer, deposited on the unclad part of the PCS fiber with core diameter 400 μm. Using a xerogel sensing layer (thickness below 500 nm) as optical cladding, toluene detection in water was performed. The observed sensitivity was linear and the detection limit was 1% toluene in water (in volume).

#### 4.8 Amines Sensor

Diffusion of different amines led to changes in the spectra of the silica sol-gel matrix containing the Co(III)porphyrin<sup>104</sup>. This phenomenon was



base of the novel amines sensor production. Grafting of cobalt(II)porphyrins in a sol-gel matrix was realized by using a porphyrin substituted by a triethoxysilyl group and pure tetramethoxysilane as the precursor. The solid blocks of porphyrin-doped material were obtained from the liquid sol-gels dried in the disposable cuvettes. Immobilization done this way lead to the development of optical fiber sensors by using various detection method and different possible applications.

#### **4.9 Sensor Arrays**

The combination of pin printing and sol-gel processing techniques provides a simple method to rapidly fabricate reusable chemical sensor element into arrays that exhibit good analytical figures of merit. This methodology also provides a straightforward means to fabricate reusable sensor arrays for simultaneous multianalyte quantification.

A new approach to rapidly produce micrometer-scale sensor elements into reusable multianalyte chemical sensor array was already described<sup>105</sup>. By using pin printing technology in concert with sol-gel processing methods the discrete silica xerogel-based microsensors on a planar substrate (glass microscope slides) were formed. Simultaneous measurement of oxygen concentration and pH was possible by forming discrete O<sub>2</sub> and pH-responsive sensing elements into arrays that allowed to determine O<sub>2</sub> and pH in aqueous solutions. The pin printing method allows to prepare sensor elements with speed one sensor element per second with a single pin. The sensor element had 100 μm in diameter and 1-2 μm thick.

Integrated optical array sensor platform for oxygen sensing only was demonstrated as well<sup>106</sup>. This sensor scheme was in form of array of 100 discrete O<sub>2</sub>-responsive sensing elements on the face of a single LED. The LED served as the light source to excite chemically responsive luminophores (ruthenium(II) complex) sequestered within the doped silica xerogel microsensors and the analyte-dependent emission from the doped xerogel was detected with a charge couple device (CCD).

#### **4.10 Biorecognition, Bioimprinting**

Quantitative and qualitative analytical techniques are of considerable importance in various aspects of life sciences for the purpose of detection, identification and measurement of concentrations of biologically important molecules, cells, chemical compounds, etc.

Molecularly imprinted polymers (MIPs) are of growing interest for their potential biotechnological applications. Recently, the templating processes with living yeast cells were reported<sup>107</sup> for the preparation of ordered and

porous silica and titanium oxide sol-gels. A versatile procedure to form regular patterns of molded polymer and sol-gel surfaces with yeast as the templates, which results in packed receptor sites directly on the coated transducer surfaces, was described. Compared to polymer sensor coatings, the sol-gel layers appeared more robust. The major difference on sensitivity between imprinted polymer and sol-gel as well as the decreasing sensor response to yeast only in the presence of yeast cell fragments proves the concept of surface imprinting.

Dental caries is a multifunctional, bacterial disease, which is characterized by the demineralization of the organic portion and the destruction of the organic substance of the tooth. The group of scientist from Singapore<sup>108</sup> proposed a fiber optic biosensor for monitor mutants streptococci activity in human saliva. The developed biosensor was based on the selective bacterial growth medium and evanescent wave spectroscopy at the core-cladding interface of a multimode fiber to monitor the bacterial mediated biochemical reaction. In order to achieve this, a short length (10 mm) of the cladding was removed (fiber core diameter  $\phi=100\ \mu\text{m}$ ); the fiber core surface was chemically etched in 40% hydrofluoric acid for approx. 30 minutes and coated with a thin film of porous medium using sol-gel technique. During experiments, the mutants streptococci mediated reaction with sucrose was monitored using a photosensitive indicator bromophenol blue, which was immobilized within the porous silica glass coating. The similar optical set-up was used for monitoring of the bacterial activity by the means of the evanescent wave spectroscopy<sup>109</sup>.

The same scientific group developed above mentioned technique and presented a novel method as well as instrumental system for determination of the total protein concentration in a liquid samples<sup>110</sup>. Their fiber optic total protein sensor (FOPS) applied a dye-immobilized (highly sensitive Coomassie Brilliant Blue) porous glass coating on a multi-mode optical fiber. The evanescent waves at the fiber optic core-cladding interface were used for monitoring of the protein-induced changes in the sensor element. The evanescent waves from the optical fibers excited and sensed the presence of protein (presented the calibration curves of bovine serum albumin, haemoglobin, cytochrome c, and ovalbumin) via colour changes in the dye-doped silica sol-gel film along the cladding denuded section. The FOPS offers a single-step method for quantifying protein concentrations without the sample destruction and with the response time about 10-15 minutes. Moreover, the sensor could be reused by submerging in 40% methanol for about 35 minutes.

Genetically modified bacteria, engineered to generate a quantifiable signal in response to pre-determined sets of environmental conditions, may serve as combined sensing/reporting elements in whole-cell biosensors. Joint project of scientist from Germany and Israel<sup>111</sup> was dedicated to comparison of two of the several available reporter genes in such cells: green fluorescent

proteins (GFPs) (*Aquorea victoria gfp*) and bioluminescence (*Vibrio fischeri luxCDABE*) genes, fused to either SOS (*recA*) or heat shock (*grpE*) promoters. In both cases, bacterial bioluminescence allowed faster and more sensitive detection of the model toxicants; the fluorescent reporter proteins were more stable, and following long-term exposure allowed detection at levels similar to that of the bioluminescent sensors. From the two green fluorescent proteins tested, enhanced GFP displayed a more rapid response and higher signal intensity than GFPuv. To combine the advantages of both reported functions, representatives of both types were jointly encapsulated in a sol-gel matrix and immobilized onto a glass surface, to generate a bioluminescent toxicity and a fluorescent genotoxicity sensor. The dual-function sensor detected both toxic and genotoxic model compounds with no interference from the co-immobilized member.

The development of fiber-optic biosensors requires that a biorecognition element and a fluorescent reporter group be immobilized at the surface or near the surface of an optical element such as planar waveguide or optical fiber. A model biorecognition element-reporter group couple, consisting of human serum albumin (HSA) that was site-selectively labeled at Cys-34 (single free cysteine) with iodoacetoxynitrobenzoxadiazole (NBD), was entrapped into a variety of different sol-gel derived structures<sup>112</sup>. HSA-NBD was immobilized onto the distal end of the fused silica optical fiber *via* entrapment into sol-gel processed beads or thin films, resulting in a prototype of a reagentless fiber-optic biosensor. The entrapped protein was excited using He-Cd laser. Changes in fluorescence intensity were generated by denaturant-induced conformational changes in the protein or by iodide quenching. Both entrapment formats provided good analytical characteristics. However, the entrapment of proteins into beads provided better signal-to-noise and signal-to-background ratios, and required less protein for preparation. Thin films showed faster response times and slightly improved detection limits for a model analyte.

#### 4.11 Immunoassay

The selectivity of antibodies was used for the development of antibody-based biosensors. Wang and team reported on first attempt to encapsulate an antibody in the sol-gel matrix<sup>113</sup>. The antifuorescein antibody has a very high affinity for fluorescein. When fluorescein becomes antibody bound, its fluorescence decreases and the emission spectra red shifts. The decrease in fluorescence and red shift can be used directly to quantify the antifuorescein affinity. The silica sol-gel from TMOS was used to immobilize antifuorescein in glass matrix. The emission spectra of fluorescein without and with antifuorescein in buffer solution and in sol-gel matrix were examined. Both spectra (in solution and in sol-gel glass) are very similar.

Encapsulation of complex antifuorescein–fluorescein did not cause any side effects. Fluorescence of fluorescein decreases when the concentration of antifuorescein in sol-gel matrix increases, and plateaus when the fluorescein becomes antibody bound. If all fluorescein molecules are bound to antifuorescein, the fluorescence intensity is about 10% intensity of free fluorescein. How do sol-gel aging, drying and storage conditions influence the encapsulated antifuorescein antibody affinity? After four-week storage in 4°C temperature all water was removed from sol-gel and the antifuorescein-fluorescein complex was completely disrupted. However, samples placed in water immediately after gelation and stored for 5 weeks gave identical emission spectrum like after 1 week of dry storage.

In France parasitic protozoa were entrapped within sol-gel silica matrices. Specific antigen-antibody reactions were performed within the sol-gel matrix via enzyme-linked immunosorbent assays (ELISA) currently used for the diagnostic of visceral leishmaniasis<sup>14</sup>. Authors measured difference in optical density between positive and negative sera from dogs. Entrapped protozoa antigens were still able to react with specific antibodies through the open porosity of the silica network. These results suggest that sol-gel matrices could be used for the development of immunodiagnostic assays requiring whole cell parasites as antigens.

## REFERENCES

1. Ebelmen M., *Comptes Rendus Acad. Sci. Fr.* 1845; 21: 502.
2. Jorgensen C.K., Reisfeld R., *Structure and Bonding* 1992, 77.
3. Jorgensen C.K., Reisfeld R., *Structure and Bonding* 1996; 92
4. Abramoff B., Klein L.C., PMMA – impregnated silica gels: synthesis and characterization, *SPIE Proc.* 1328, 241–248, (1990).
5. Klein L.C. (ed.): *Sol-Gel Optics: Processing and Applications*, Kluwer Academic Publishers, Boston, 1994.
6. Hench L.L., West J.K., *Chem. Rev.* 1990; 90: 33.
7. Brinker C.J., Scherer G.W., *Sol-Gel Science*, Academic Press, San Diego, 1990.
8. Sakka S., Kozuka H., Sol-gel preparation of coating films containing noble metal colloids, *J. Sol-Gel Sci. Technol.* 1998; 13: 701–705.
9. Schmidt H., *J. Non-Cryst. Solids* 1985; 73: 681.
10. Wilkies G.L., Otter B., Huang H., *Polymer Prep.* 1985; 26: 300.
11. For example, whole issue of *J. Sol-Gel Sci. Technol.* 1998; 13
12. Mitsuhashi Y., Matsuda A., Matsuno Y.: Sol-gel technology for optical disk application, *SPIE Proc.* 1758, 105–112, (1992).
13. Floch H.G., Belleville P.F., Scratch-resistant single-layer antireflective coating by a low-temperature sol-gel route, *SPIE Proc.* 1758, 135–150, (1992).
14. Hou L., Menning M., Schmidt H., Improvement of photofatigue resistance of spirooxazine entrapped in organic-inorganic composite synthesized via sol-gel process, *SPIE Proc.* 2288, 328–339, (1994).
15. Kirkbir F., Chaudhuri R., Optical fibers from sol-gel-derived germania-silica glasses, *SPIE Proc.* 1758, 160–172, (1992).

16. Oliveira P.W., Krug H., Kunstle H., Schmidt H., The production of Fresnel lenses in sol-gel derived ormocers by holography, *SPIE Proc.* 2288, 554–562, (1994).
17. Internet site: <http://www.ea.ucla.edu/~deans/bios/jdm/ormosil.html>.
18. Dave B.C., Dunn B., Selverstone J., Valentine D., Zink J.I., Sol-gel encapsulation methods for biosensors, *Anal. Chem.* 1994; 66: 1120A–1127A.
19. Glezer V. and Lev O., Sol-gel vanadium pentoxide glucose biosensor, *J. Am. Chem. Soc.* 1993; 115: 2533–2534.
20. Zusman R., Rottman C., Ottolenghi M., Avnir D., Doped sol-gel glasses as chemical sensors, *J. Non-Cryst. Solids* 1990; 122: 107–109.
21. Trinkel M., Trettnak W., Reininger F., Benes R., O’Leary P., Wolfbeis O., Study of the performance of an optochemical sensor for ammonia, *Anal. Chim. Acta* 1996; 320: 235–243.
22. Lobnik A., Wolfbeis O., Sol-gel based ammonia optical sensor, in proc.of SOL-GEL’97: 9th International Workshop on Glasses, Ceramics, Hybrids and Nanocomposites from Gels, Sheffield, UK, 1997.
23. Pope E.J.A., Peterson K., Peterson C., Sol-gel bioartificial organs for the treatment of diabetes mellitus, in proc.on SOL-GEL’97: 9th International Workshop on Glasses, Ceramics, Hybrids and Nanocomposites from Gels, Sheffield, UK, 1997.
24. Sieminska L., Zerda T.W., Diffusion of steroids from sol-gel glass, *J. Phys. Chem.* 1996; 100: 4591–4597.
25. Stachs O., Gerber Th., Petkov V., The structure formation of Zirconium oxide gels in alcoholic solutions, *J. Sol-Gel Sci. Technol.* 1999; 15: 23–30.
26. Hensch L.L., Orsel G., Nogues J.L. in *Better Ceramic through Chemistry II*, Brinker C.J., Clark D.E., Ulrich D.R. (eds.), Mat. Res. Soc. Pittsburgh, 1986, p.35.
27. Andrzejewski D., Podbielska H., Mutual influences of sol-gel matrices and dopants on the materials optical properties, *Opt. Appl.* 2001; 31: 223–229.
28. Wong P., *Methods in the Physics of Porous Media*, Academic Press, London, 1999, pp. 17–38.
29. Ishizaki K., Komarneni S., Nanko M., *Porous Materials – Process Technology and Applications*, Kluwer Academic Publishers, London, 1998, pp. 12–27.
30. Schaefer D.W., *MRS Bull.* 1994; 19: 14–17.
31. Lechna-Marczyńska M., Ulatowska A., Podbielska H., Grzegorzewski B., Light scattering measurements in ormosil and PHEMA – possible new materials for contact lenses, *EOS* 23, 33–34, (1999).
32. Kerker M., *The Scattering of Light and Other Electromagnetic Radiation*, Academic Press, 1969, pp.414–486.
33. Uhlmann D.R., Kreidel N.J. (eds.), *Glass Science and Technology*, Vol.2, Academic Press, 1984, pp. 214–217.
34. Bock W.J., Urbańczyk W., Voet M.R.H., Selected applications of fiber-optic sensors based on highly birefringent fibers in engineering mechanics, Proc. Application of Photonic Technology: Sensing, Signal Processing and Communication, G.A. Lamprapoulos (ed.), Plenum Press, 1995, pp. 311–316.
35. Wolfbeis O.S., *Fiber optic chemical sensors and biosensors*, CRC Press, Boca Raton, 1991.
36. Wolfbeis O.S. (ed.), Biochemical and Medical Sensors, *SPIE Proc.* 2085, 1993.
37. Reisfeld R., Jorgensen C.K. (eds.), *Chemistry, Spectroscopy and Applications of Sol-Gel Glasses*, Springer Verlag, Berlin, 1992.
38. Klein L.C. (ed.), *Sol-Gel Optics, Processing and Applications*, Kluwer Academic Publishers, Boston, 1994.
39. Baldini F., Bracci S., Cosi F., Falciai R., Italian Patent: No FI 93 A125, July (1993).
40. Verdaasdonk R.M., Borts C., Ray tracing of optically modified fibertips 1. Spherical probes, *Appl. Opt.* 1991; 30: 2159–2171.

41. Verdaasdonk R.M., Borts C., Ray tracing of optically modified fibertips 2. Laser scalpels, *Appl. Opt.* 1991; 30: 2172–2177.
42. Andrzejewski D., Podbielska H., Examination of various shape of sol-gel optodes for indirect fiberoptic sensors, *OPTIK 112*, 158-162, 2001.
43. Wallace P.A., Yang Y., Campbell M., Towards a distributed optical fibre chemical sensor, *SPIE Proc.* 2360, 465–467, (1994).
44. Taylor R.F., Schultz J.S., *Handbook of Chemical and Biological Sensors*, 1997.
45. MacCraith B.D., McDonagh C.M., O'Keeffe G., McEvoy A.K., Butler T., Sheridan F.R., Sol-gel coatings for optical chemical sensors and biosensors, *Sensors & Actuators B* 1995; 29: 51–57.
46. Montanaro L., Negro A., Pijolat C., Lalauze R., Synthesis and forming of beta alumina to be used as gas sensor, *Annales de Chimie [Science des Matériaux]* 1995; 20: 399–402.
47. McEvoy A.K., McDonagh C.M., MacCraith B.D., Development of a fiber optic dissolved oxygen sensor based on quenching of a ruthenium complex entrapped in a porous sol-gel film, *SPIE Proc.* 2508, 190–198, (1995).
48. Kuleshov A.P., Dmitrieva G.A., Indicator coatings, *J. Opt. Technol.* 1996; 63: 252–259.
49. Narang U., Gvishi R., Bright F.V., Prasad P.N., Sol-gel-derived micron scale optical fibers for chemical sensing, *J. Sol-Gel Sci. Technol.* 1996; 6: 113–119.
50. Gao H.H., Zhongping C., Kumar J., Tripathy S.K., Kaplan D.L., Tapered fiber tips for fiber optic biosensors, *Opt. Eng.* 1995; 34: 3465–3470.
51. Li C., Lin Y., Shih C., Tsaur J., Chau L., Sol-gel encapsulation of lactate dehydrogenase for optical sensing of L-lactate, *Biosens. Bioelectron.* 2002; 17: 323-330.
52. Zusman R., Rottman C., Ottolenghi M., Avnir D., Doped sol-gel glasses as chemical sensors, *J. Non-Cryst. Solids* 1990; 122: 107–109.
53. Blyth D., Poynter S., Russell D., Calcium biosensing with a sol-gel immobilized photoprotein, *Analyst* 1996; 121: 1975–1978.
54. Javaid M., Keay P., A generic technique for coating doped sol-gel films onto the inside of tubes for use as colorimetric sensors, *J. Sol-Gel Sci. Technol.* 2000; 17: 55-59.
55. Jeronimo P., Araujo A., Montenegro M., Satinsky D., Solich P., Colorimetric bismuth determination in pharmaceuticals using a xylenol orange sol-gel sensor coupled to a multicommutated flow system, *Anal. Chim. Acta.* 2004; 504: 235-241.
56. Delmarre D., Meallet R., Bied-Charreton C., Pansu R., Heavy metal ions detection in solution, in sol-gel and with grafted porphyrin monolayers, *J. Photochem. Photobiol. A* 1999; 124: 23-28.
57. Canada T., Allain L., Beach D., Xue Z.: High-acidity determination in salt-containing acids by optical sensors. The scope of a dual-transducer approach and the Hammett acidity function, *Anal. Chem.* 2002; 74: 2535-2540.
58. Allain L., Canada T., Xue Z.: Optical sensors and the salt effect: a dual-transducer approach to acidity determination in a salt-containing concentrated strong acids, *Anal. Chem.* 2001; 73: 4592-4598.
59. Nivens D., Zhang Y., Angel S., A fiber-optic pH sensor prepared using a base-catalyzed organo-silica sol-gel, *Anal. Chim. Acta* 1998; 376: 235-245.
60. Nivens D., Schiza M., Angel S., Multilayer sol-gel membranes for optical sensing applications: single layer pH and dual layer CO<sub>2</sub> and NH<sub>3</sub> sensors, *Talanta* 2002; 58: 543-550.
61. Wang E., Chow K., Kwan V., Chin T., Wong C., Bocarsly A., Fast and long term optical sensor for pH based on sol-gel, *Anal. Chim. Acta* 2003; 495: 45-50.
62. Ertekin K., Karapire C., Alp S., Yenigül B., Icli S., Photophysical and photochemical characteristics of an azlactone dye in sol-gel matrix; a new fluorescent pH indicator, *Dyes and Pigments* 2003; 56: 125-133.

63. Lee S., Gin J., Nampoore V., Vallabhan C., Unnikrishnan N., Radhakrishnan P., A sensitive fibre optic pH sensor using multiple sol-gel coatings, *Journal of Optics A: Pure and Applied Optics* 2003; 3: 355-359.
64. Lin J., Liu D., An optical sensor with a linear response over a broad range, *Anal. Chim. Acta* 2000; 408: 49-55.
65. Delmarre D., Meallet-Renault R., Bied-Charreton C., Pasternack R., Incorporation of water-soluble porphyrins in sol-gel matrices and application to pH sensing, *Anal. Chim. Acta* 1999; 401: 125-128.
66. Grant S.A., Bettencourt K., Krulevitch P., Hamilton J., Glass R., Development of fiber optic and electrochemical pH sensors to monitor brain tissue, *Crit. Rev. Biomed. Eng.* 2000; 28: 159-163.
67. Sharma N.K., Gupta B.D., Fabrication and characterization of pH sensor based on side polished single mode optical fiber, *Opt. Comm.* 2003; 216: 299-303.
68. Villegas M.A., Pascual L., Sol-gel coatings doped with a pH sensitive chromophore, *Thin Solid Films* 1999; 351: 103-108.
69. Suah F.B.M., Ahmad M., Taib M.N., Applications of artificial neural network on signal processing of optical fibre pH sensor based on bromophenol blue doped with sol-gel film, *Sens. Actuat B* 2003; 90: 182-188.
70. Rayss J., Sudolski G., Ion absorption in the porous sol-gel silica layer in the fibre optic pH sensor, *Sens. Actuat B* 2002; 87: 397-405.
71. Butler T.M., MacCraith B.D., McDonagh C.M., Development of an extended range fibre optic pH sensor using evanescent wave absorption of sol-gel entrapped pH indicators, *SPIE Proc. 2508*, 168-178, (1995).
72. Wallace P.A., Yang Y., Campbell M., Towards a distributed optical fibre chemical sensor, *SPIE Proc. 2508*, 36-40 (1995).
73. Yang Y., Wallace P.A., Campbell M., Distributed optical fiber chemical sensor, *SPIE Proc. 2594*, 233-242, (1996).
74. Blue R., Stewart G., Fibre-optic evanescent wave ph sensing with dye doped sol-gel films, *Intern. J. Optoelectron.* 1995; 10: 211-222.
75. Shukla S.K., Parashar G.K., Mishra A.P., Misra P., Yadav B.C., Shukla R.K., Bali L.M., Dubey G.C., Nano-like magnesium oxide films and its significance in optical fiber humidity sensor, *Sens. Actuat B* 2004; 98: 5-11.
76. Trinkel M., Trettnak W., Reiningner F., Benes R., O'Leary P., Wolfbeis O., Study of the performance of an optochemical sensor for ammonia, *Anal. Chim. Acta* 1996; 320: 235-243.
77. Lobnik A., Wolfbeis O., Sol-gel based optical sensor for dissolved ammonia, *Sens. Actuat B* 1998; 51: 203-207.
78. Koncki R., Mohr G., Wolfbeis O.S., Enzyme sensor for urea based on novel pH bulk optode membrane, *Biosens. Bioelectr.* 1995; 10: 653-659.
79. Braun S., Shtelzer S., Rappoport S., Avnir D., Ottolenghi M., Biocatalysis by sol-gel entrapped enzymes, *J. Non-Cryst. Solids* 1992; 147-148: 739-743.
80. Janotta M., Karlowatz M., Vogt F., Mizaikoff B., Sol-gel based mid-infrared evanescent wave sensors for detection of organophosphate pesticides in aqueous solution, *Anal. Chim. Acta* 2003; 496: 339-348.
81. Andreou V., Clonis Y., A portable fiber-optic pesticide biosensor based on immobilized cholinesterase and sol-gel entrapped bromocresol purple for in-field use, *Biosens. Bioelectr.* 2002; 17: 61-69.
82. Graham A., Carlson C., Edmiston P., Development and characterization of molecularly imprinted sol-gel materials for the selective detection of DDT, *Anal. Chem.* 2002; 74: 458-467.
83. Leung M., Chow C., Lam M., A sol-gel derived molecular imprinted luminescent PET sensing material for 2,4-dichlorophenoxyacetic acid, *J. Mater. Chem.* 2001; 11: 2985-2991.

84. Jitianu A., Altindag Y., Zaharescu M., Wark M., New SnO<sub>2</sub> nano-clusters obtained by sol-gel route, structural characterization and their gas sensing applications, *J. Sol-Gel Sci. Technol.* 2003; 26: 483-488.
85. Rella R., Rizzo A., Licciulli A., Siciliano P., Troisi L., Valli L., Tests in controlled atmosphere on new optical gas sensing layers based on TiO<sub>2</sub>/metal-phthalocyanines hybrid system, *Materials Science and Engineering C* 2002; 22: 439-443.
86. Segawa H., Ohnishi E., Arai Y., Yoshida K., Sensitivity of fiber-optic carbon dioxide sensors utilizing indicator dye, *Sens. Actuat B* 2003; 94: 276-281.
87. Grant S.A., Satcher Jr. J.H., Bettencourt K., Development of sol-gel based fiber optic nitrogen dioxide gas sensors, *Sens. Actuat B* 2000; 69: 132-137.
88. Brinkley J.F., Kirkey M.L., Marques A.D.S., Lin C.T., Charge transfer complexes of Cu(II)/HD analogue in sol-gel sensors, *Chemical Physics Letters* 2003; 367: 39-43.
89. von Bültzingslowen C., McEvoy A.K., McDonagh C., MacCraith B.D., Klimant I., Krause C., Wolfbeis O.S., Sol-gel based optical carbon dioxide sensor employing dual luminophore referencing for application in food packaging technology, *Analyst* 2002; 127: 1478-1483.
90. von Bültzingslowen C., McEvoy A.K., McDonagh C., MacCraith B.D., Lifetime-based optical sensor for high-level pCO<sub>2</sub> detection employing fluorescence resonance energy transfer, *Anal. Chim. Acta* 2003; 480: 275-283.
91. Lakowicz J.R., *Principles of Fluorescent Spectroscopy*, Plenum Press, 1983.
92. Park S.S., Mackenzie J.D., Thickness and microstructure effects on alcohol sensing of tin oxide thin films, *Thin Solid Films* 1996; 274: 154-159.
93. Vaivars G., Kleperis J., Zubkans J., Vitins G., Liberts G., Lusis A., Application of sol-gel and laser evaporation methods to obtain thin gas sensitive films, Proc. 8th International Conference on Solid-State Sensors and Actuators and Eurosensors IX, 1995, pp. 870-873.
94. Xing L., Zuoqing W., Cheng J.K., Viens M., Cheeke J.D.N., Ultrasonic thin-walled tube wave structure for sensing devices, *IEEE Transactions on Ultrasonics, Ferroelectrics and Frequency Control* 1996; 43: 331-336.
95. Bailey R.T., Cruickshank F.R., Deans G., Gillanders R.N., Tedford M.C., Characterization of a fluorescent sol-gel encapsulated erythrosine B dissolved oxygen sensor, *Anal. Chim. Acta* 2003; 487: 101-108.
96. Okazaki S., Nakagawa H., Asakura S., Tomiuchi Y., Tsuji N., Murayama H., Washiya M., Sensing characteristics of an optical fiber sensor for hydrogen leak, *Sensors & Actuators B* 2003; 93: 141-147.
97. Jia J., Tang M., Chen X., Qi L., Dong S., Co-immobilized microbial biosensor for BOD estimation based on sol-gel derived composite material, *Biosens. Bioelectr.* 2003; 18: 1023-1029.
98. Malins C., Fanni S., Glever H., Vos J., MacCraith B., The preparation of a sol-gel glass oxygen sensor incorporating a covalently bound fluorescent dye, *Anal. Commun.* 1999; 36: 3-4.
99. Tang Y., Tehan E., Tao Z., Bright F., Sol-gel-derived sensor materials that yield linear calibration plots, high sensitivity, and long-term stability, *Anal. Chem.* 2003; 75: 2407-2413.
100. McDonagh C., Bowe P., Mongey K., MacCraith B., Characterisation of porosity and sensor response times of sol-gel-derived thin films for oxygen sensor applications, *J. Non-Cryst. Solids* 2002; 306: 138-148.
101. Lee S., Okura I., Porphyrin-doped sol-gel glass as a probe for oxygen sensing, *Anal. Chim. Acta* 1997; 342: 181-188.
102. Noor U., Uttamchandani D., Sol-gel derived thin films for hydrogen sulfide gas sensing, *J. Sol-Gel Sci. Technol.* 1998; 11: 177-183.
103. Cherif K., Hleli S., Abdelghani A., Jaffrezic-Renault N., Matejec V., Chemical detection in liquid media with a refractometric sensor based on a multimode optical fibre, *Sensors* 2002; 2: 195-204.



104. Delmarre D., Bied-Charreton C., Grafting of cobalt porphyrins in sol-gel matrices: application to the detection of amines, *Sens. Actuat B* 2000; 62: 136-142.
105. Cho E., Bridht F., Pin-printed chemical sensor arrays for simultaneous multianalyte quantification, *Anal. Chem.* 2002; 74: 1462-1466.
106. Cho E., Bridht F., Integrated chemical sensor array platform based on a light emitting diode, xerogel-derived sensor element, and high-speed pin printing, *Anal. Chim. Acta* 2002; 470: 101-110.
107. Dickert F.L., Hayden O., Bioimprinting of polymers and sol-gel phases. Selective detection of yeast with imprinted polymers, *Anal. Chem.* 2002; 74: 1302-1306.
108. Kishen A., John M.S., Lim C.S., Asundi A., A fiber optic based biosensor to monitor mutants streptococci in saliva, *SPIE Proc.* 5068, 194-201, (2003).
109. Kishen A., John M.S., Lim C.S., Asundi A., A fiber optic biosensor (FOBS) to monitor mutants streptococci in human saliva, *Biosens. Bioelectron.* 2003; 18: 1371-1378.
110. Preejith P.V., Lim C.S., Kishen A., John M.S., A. Asundi: Total protein measurement using a fiber-optic evanescent wave-based biosensor, *Biotechn.Lett.* 2003; 25: 105-110.
111. Sagi E., Hever N., Rosen R., Bartolome A.J., Premkumar J.R., Ulber R., Lev O., Scheper T., Belkin S., Fluorescence and bioluminescence reporter functions in genetically modified bacterial sensor strains, *Sens. Actuat B* 2003; 90: 2-8.
112. Flora K., Brennan J., Comparison of formats for the development of fiber-optic biosensors utilizing sol-gel derived materials entrapping fluorescently-labelled protein, *Analyst* 1999; 124: 1455-1462.
113. Wang R., Narang U., Prasad P.N., Bright F.V., Affinity of anti fluorescein antibodies encapsulated within a transparent sol-gel glass, *Anal. Chem.* 1993; 65: 2671-2675.
114. Barreau J.Y., DaCosta J.M., Desportes I., Livage J., Monjour L., Gentilini M., Fixation and immunological reactivity of parasitic protozoa in sol-gel matrices, *C. R. Acad. Sci. III* 1994; 317: 653-657.

## Chapter 18

# METHODS FOR ATTACHMENT OF ANTIBODIES ONTO OPTICAL BIOSENSORS

Eduard Brynda

*Institute of Macromolecular Chemistry  
Academy of Sciences of the Czech Republic  
162 06 Prague, Czech Republic*

### 1. INTRODUCTION

Biosensors based on the affinity binding of analytes to specific bioreceptors immobilised on the surface of an optical transducer, such as surface plasmon resonance (SPR) sensor<sup>1</sup>, grating coupler<sup>2</sup>, resonant mirror<sup>3</sup>, and various types of interferometers<sup>4, 5</sup>, are of increasing interest for real-time detection of analytes without the use of additional labelled reagents. A sensor consists of an optical transducer on the surface of which a biorecognition layer with immobilized bioreceptors is attached. The transducer optics is modified by changes in optical parameters of an adjacent medium interacting with the evanescent light wave at the transducer surface. An intensity of the evanescent light decays exponentially with a distance from the surface. Thus, the sensor responds to a mass added at its surface due to the analyte binding and is rather insensitive to changes out of a penetration depth of the evanescent wave (Figure 1).

#### 1.1 Antibody

Among various ligands, antibodies pose the most effective and selective receptors for their specific antigens. Antibodies are special kinds of proteins made by cells of the immune system B-lymphocytes. An antibody molecule consists of four polypeptides—two heavy chains and two light chains joined to form a "Y" shaped molecule. The amino acid sequence in the tips of the "Y" varies greatly among different antibodies. This variable region, composed of 110-130 amino acids, give the antibody its specificity for

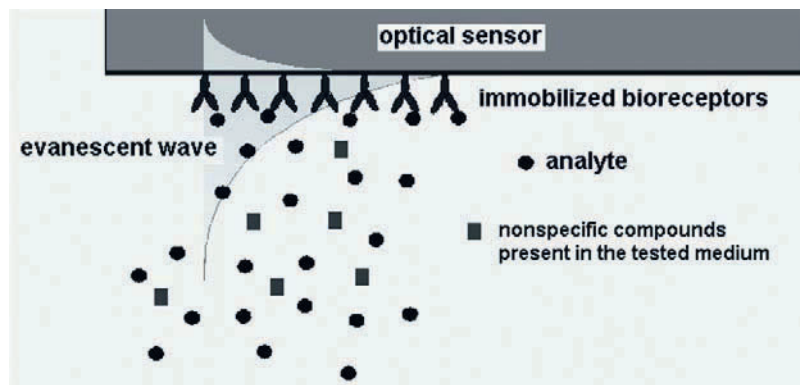


Figure 1. The specific binding of analytes to immobilized receptors induces a response of the optical biosensor due to changes in the evanescent wave at the sensor surface.

binding the antigen. The variable region includes the ends of the light and heavy chains forming a specific folded structure - the antigen binding site.

This site fits a molecular shape (epitope - a molecular structure capable of inducing the production of an antigen by immune cells) present at the matching antigen. The antigen binding is very specific owing to this lock-key mechanism. At the same time, the antibody-antigen affinity is very high due to physical interactions between antigen structural units and antibody amino acid residues mutually oriented in the binding site. The stem of the Y links the antibody to other participants in the immune defences. This area called the constant region is identical in all antibodies of the same class. Antibodies are divided into five major classes, IgM, IgG, IgA, IgD and IgE, according to a structure of their constant region and immune function. Treating with a protease can cleave an antibody into two Fab fragments (fragment antigen binding), that each includes an antigen binding site, and Fc fragment (fragment constant).

Figure 2 shows the most abundant class of antibodies found in blood serum and lymph - immunoglobulin G (IgG). IgG of molecular mass about 156 000, is most frequently used as a receptor in immunosensors. According to X-ray data<sup>6-8</sup>, IgG is a Y-shaped molecule consisting of two identical antigen binding Fab arms of dimensions 6.5 nm by 3.5 nm and an inactive Fc shank of dimensions 5 nm by 3.5 nm.

Antibodies vary in their isoelectric points (pI) within an interval 4.6 – 7.2, most of them in the region 5.4 - 6.7. Thus, all antibodies are negatively charged (above pI) in blood at physiological pH 7.2-7.4 and most of them are positively charged below pH 5. Antibodies are stable in salt containing solutions. They can be stored for months at temperature 2-6 °C in solutions protected against bacteria and fungus, e.g. with addition NaN<sub>3</sub>. Usually, they can endure both acid conditions (pH above 2.5) and basic conditions (pH below 9) and the treatment with nonionogenic detergents, e.g. Tween. The

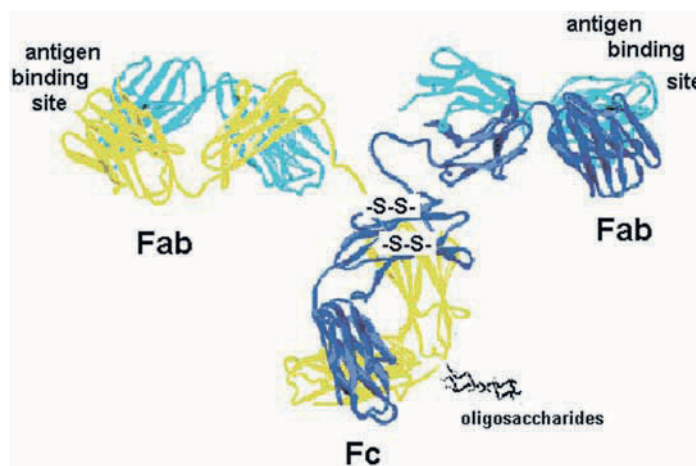


Figure 2. IgG The identical Fab parts are turned one to another.

preservation of the antigen binding sites is a prerequisite for any functional immobilization of antibodies on a sensor surface. Thus, structure of Fab portions should be minimally attacked while Fc part of the molecule can be safely modified.

Antibodies capable of binding an analyte are obtained by immunizing an animal (mouse, rat, rabbit, goat, chicken). The antigen is repeatedly injected in the animal and after the development of the respective antibodies by the immune system, IgG fraction (polyclonal antibodies – a mixture with a high concentration of the antibody against the antigen) is affinity separated from blood serum, ascitic fluid, or eggs. Monoclonal antibodies (pure antibody against a specific epitope of the antigen) can be produced *in vitro* by cells that received the antibody gene from immune cells developed in an immunized animal. Lots of antibodies are available commercially and specialized companies offer the preparation of particular antibodies on a customer's demand.

## 1.2 Nonspecific Adsorption

Biological media, such as, blood, plasma, serum, lymph, yolk, or milk, contain lot of various proteins which are capable of nonspecific adsorption on any solid surface, except of some neutral hydrogels, via physical interactions, mainly the hydrophobic and electrostatic ones. The coating of a surface with water-soluble macromolecules, e.g. dextran or poly (ethylene glycol), can decrease the protein adsorption considerably by preventing a direct contact of the surface with proteins. As most of the proteins are negatively charged above their isoelectric points at physiological pH about

7.4, the presence of negative charges on the surface decreases the nonspecific adsorption while positive charges are undesirable. Positive charges in biorecognition sensor layers increase considerably the nonspecific deposit from blood plasma<sup>9</sup>. However, positively charged proteins, e.g. some complement proteins or interferons, which are present in blood plasma, can adsorb electrostatically on negatively charged surfaces. The adsorption from multicomponent solutions is a complex and dynamic process in which more strongly adsorbing proteins can subsequently replace proteins first adsorbed and other compounds can be attached to adsorbed proteins.

A special nonspecific sensor response might be due to the cross-reactivity of immobilized antibodies. Besides the analyte, an antibody can bind also other entities bearing a similar antigenic epitope, e.g. the detection of some pathogenic bacteria can be interfered by the binding of non-pathogenic bacteria with the same surface antigen.

### 1.3 Immunoanalysis and Optical Immunosensors

#### 1.3.1 Immunoassays

Nowadays, antibodies are utilized in numerous immunoanalytical methods. Those widely used in practice, such as radioimmunoassays, fluoroimmunoassays and enzyme-linked immunosorbent assays (ELISA), require labelled reagents. Millions of ELISA tests for diagnostics of various diseases are daily performed in clinical laboratories. The detection of analytes by two-antibody "sandwich" ELISA, is schematically outlined in Figure 3.

In ELISA, one antibody (the "capture" antibody) is bound to a solid phase. Most frequently, the antibody solution is placed in a multi-well polystyrene plate and the antibodies are attached to the surface by physical adsorption. To improve the adsorption properties, manufacturers modify polystyrene surface by plasma charge or chemical treatment so that antibodies can be attached to the surface by both the hydrophobic and electrostatic interactions. A sample of a tested liquid is added from which the analyte binds to the immobilized antibodies (Figure 3a). Unbound products are then removed with a wash, and a second antibody labelled with an enzyme (the "detection" antibody) is bound to the antigen (Figure 3b). The "capture" and "detection" antibodies have to bind to epitopes that do not overlap on the antigen. This can be accomplished with either two different monoclonal antibodies that recognize discrete sites on the analyte or one batch of affinity-purified polyclonal antibodies. The enzyme, such as, horseradish peroxidase, covalently conjugated with the detection antibody is capable of converting a colourless substrate to a coloured product. After adding the substrate the assay is quantified by colorimetric measurement of the developing product (Figure 3c).

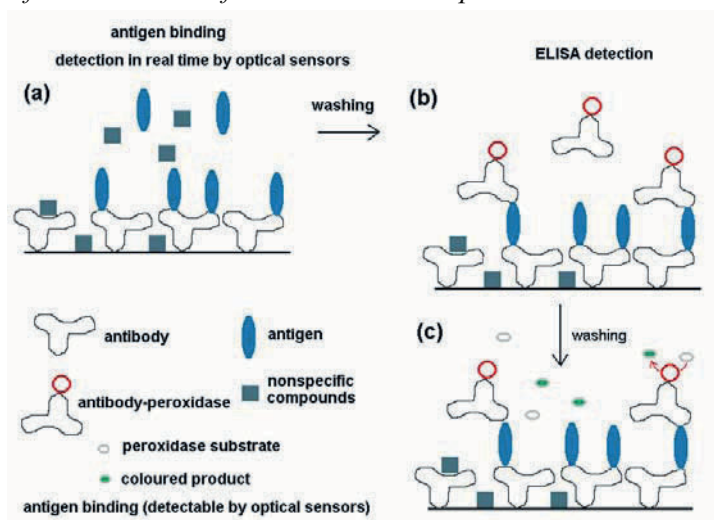


Figure 3. ELISA detection of an analyte in a tested liquid.

Major advantages of ELISA are a high sensitivity provided by the time-unlimited increase in the coloured product concentration produced by the immobilized enzyme and a high specificity provided by the two-antibody sandwich. The specific binding of the antigen to the "capture" antibody is usually accompanied by the nonspecific adsorption of some other compounds present in tested medium. The second "detection" antibody does not bind to these nonspecific compounds captured at the surface. The disadvantage is the time consuming multi-step procedure. There is also no control of the individual steps during the indirect detection. Thus, the troubleshooting is difficult and only rough quantification is possible.

### 1.3.2 Optical Immunosensors

Unlike the immunosorbent assays, optical immunosensors can directly monitor the binding of analytes to the immobilized antibodies (Figure 3a) without any additional reaction step or use of labelled reagents. It makes possible to trace immediately the presence of an analyte in a tested medium and to estimate quickly and quantitatively the analyte concentration from the kinetics of its binding to the immobilized antibodies. Potentially, sensors are capable of continuous monitoring the analyte concentration in situ, e.g. monitoring a patient's state by an implanted sensor or controlling biotechnological processes. For such a monitoring the affinity between the analyte and antibody has not to be too high so that an equilibrium between the association and dissociation can follow changes in the analyte concentration. Unfortunately, the lower is the affinity the lower is the sensor sensitivity. Using only the immobilized "capture" antibody, sensors can

detect also analytes which cannot be detected by sandwich assays because a pair of antibodies for different analyte epitopes is not available.

A major disadvantage is that the direct sensor detection cannot distinguish between the sensor response to the specific analyte binding from the response to a possible nonspecific adsorption of other compounds. The nonspecific fouling from blood or blood serum seems to be one of the main barriers for practical application of immunosensors in medical diagnostics.

The two-antibody sandwich procedure can be used with sensors for increasing the detection sensitivity and selectivity, however, the main advantages of the direct detection in real time would be lost using this approach.

## **2. IMMOBILIZATION OF ANTIBODIES ON SENSOR SURFACES**

### **2.1 General Requirements**

There are various techniques for the immobilization of proteins onto solid supports. To estimate their suitability for preparation of antibody sensing layers one has to consider some general requirements for the sensor function and application.

#### **2.1.1 High Sensor Sensitivity**

The sensitivity is proportional to the analyte binding capacity which increases with increasing number of active antibodies immobilized within the penetration depth of the evanescent wave. An optical response to the analyte binding decreases exponentially with the distance of antibody from the surface. The activity of antigen binding sites must not be destroyed by the immobilization procedure. Only antibody binding sites accessible for the respective analyte epitope can contribute to the sensor response. The sensor sensitivity increases with the increasing facility in which the analyte can approach the immobilized antibody and insert its epitope in the antibody binding site.

#### **2.1.2 Low Nonspecific Sensor Response**

The deposition of nonspecific compounds from tested media on the sensor surface has to be minimized.

### 2.1.3 Durability of Sensor Properties With Respect to the Sensor Application

Noncovalent attachment of antibodies to the sensor surface might be sufficient for one-shot tests in a simple aqueous solution. For repeated measurements, it is usually necessary to regenerate the sensor by releasing the irreversibly captured analytes. Only the immobilization of a sensing layer by covalent bonds is stable at a harsh treatment with acid solutions (pH 2-3) or detergents necessary for the dissociation of analytes from the sensor after each measurement. For detection of analytes in multicomponent biological media the biorecognition layer should be resistant to nonspecific adsorption and the replacement of immobilized antibodies with other proteins. A fouling on the sensor surface, biological degradation, and adverse physiological reactions, such as, blood coagulation or complement activation, should be prevented if sensors were used in vivo.

## 2.2 Immobilization Techniques

### 2.2.1 Transducer Surface

Biorecognition layers are immobilized on surface of inorganic thin layers usually prepared by vacuum deposition of gold on SPR sensors and titanium oxide, tantalum oxide, or silicone nitride on waveguiding structures, such as, grating couplers and interferometers. Metal oxides are often co-deposited as a mixture with silicone oxide ( $\text{Me}(\text{Si})\text{O}_x$ ) to get chemically reactive groups on the surface. Number of reactive groups on these surfaces can be increased by treatment with chrome sulphuric acid just before a covalent immobilization. Contact angles in Table 1 indicate that the character of interfaces between the sensor surfaces and water is closer to hydrophobic polystyrene than to hydrophilic glass.

Metal oxide surfaces become more hydrophilic with time of incubation with aqueous solutions probably due to penetration of water in a porous

Table 1. Air/water/surface contact angles measured using the Wilhelmy plate method on surfaces incubated with deionised water for 10 minutes.

Material	Advancing contact angle (deg)	Receding contact angle (deg)
Polystyrene	86.3	63.0
Au	87.5	60.2
Ti(Si)O <sub>x</sub>	79.5	47.0
glass	51.4	14.5



structure of the films and reactivity of the surface with water and salts. Gold is more stable. Properties of the gold surface are often affected by a storage of the chip after the vacuum deposition of the gold layer, probably, due to deposition of some impurities from the atmosphere. The fresh cleaning of gold surfaces with mixtures of hydrogen peroxide and sulphuric acid is desirable prior any immobilization procedure.

### 2.2.2 Physical Adsorption

Adsorption of IgGs as well as other globular plasma proteins, e.g., albumin, on transducer surfaces is driven mainly by the hydrophobic interaction of their hydrophobic parts. Thus, the protein adsorption depends on previous incubation of  $\text{Me}(\text{Si})\text{O}_x$  in an aqueous solution. Antibodies adsorb at a higher amount on the sensor surfaces if they are positively charged below their pI and they are partly desorbed if their net charge is reverted by increasing pH of the solution above pI. Evidently, negative charges are present on the surfaces, which might be ionic oxide groups on  $\text{Me}(\text{Si})\text{O}_x$  and chemisorbed oxygen anions or some impurities on gold surfaces. The main part of antibodies remain irreversibly adsorbed on the surfaces for days. A rigid attachment of the adsorbed antibodies to the surface restricting their mobility and accompanied with conformation changes as well as unfavourable orientation of many randomly oriented Fab portions decrease the binding capacity of the adsorbed layer. Figure 4 shows atomic force microscopic (AFM) picture of a polystyrene surface coated with a monolayer of antibody molecules adsorbed from a phosphate buffered saline solution. Antibodies were adsorbed for a time corresponded with the adsorption plateau observed by optical methods. Even if the surface was saturated with antibody molecules, i.e., no other antibodies could not be

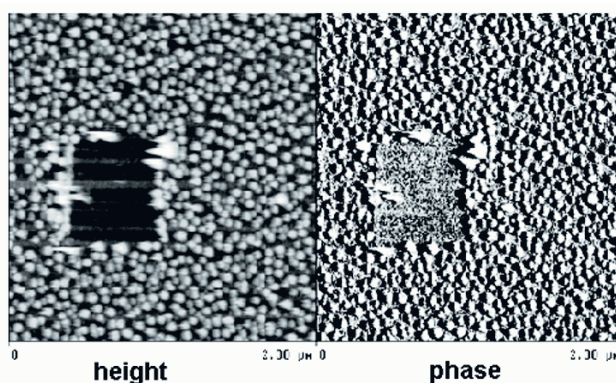


Figure 4. AFM micrograph of a saturated monolayer of antibodies against  $\beta_2$ -microglobulin measured in phosphate buffered saline (PBS) solution using tapping mode. The dark window shows the underlying polystyrene surface obtained by wiping off the antibodies.

adsorbed on the saturated surface, there was still free space among the adsorbed antibodies. To suppress a nonspecific adsorption on these vacancies the free surface should be additionally filled by the adsorption of serum albumin and small nonionogenic detergent Tween. Physical adsorption which is also successfully used for antibody immobilization on ELISA plates may be applied as a fast preparation of a sensing layer in situ in the detecting instrument just before the detection of an analyte in a simple solution. However, the adsorbed layers are not stable enough for the measurement in complex biological media, in which the replacement of antibodies and nonspecific adsorption of other components occur, and for the regeneration of reusable sensors.

### **2.2.3 Covalent Antibody Attachment**

Amino acid residues with reactive chemical groups are distributed at many places of antibody molecule. For covalent binding are suitable mainly  $-\text{NH}_2$  (L-lysine, N-terminus amino group) and  $-\text{COOH}$  (L-aspartate, L-glutamate, C-terminus carboxyl group) which can react with various reagents using techniques developed for conjugation of antibodies and enzymes with other proteins, synthetic polymers, or insoluble matrices<sup>10, 11</sup>. The disadvantage is that the reagents can react also with the amino acid residues located near the antigen binding sites decreasing the antibody activity. Specific reactive groups which are not located at the variable parts of antibody molecule can be prepared by chemical activation of the antibody. Reduction of the disulfide bonds within the hinges region of an IgG molecule ( $-\text{S}-\text{S}-$  in Figure 2) produces half antibody molecules containing thiol ( $-\text{SH}$ ) groups which can react with sulfhydryl-reactive maleimide reagents without a modification of the other parts of antibody. Polyclonal IgGs contain oligosaccharides in the Fc portion of the molecule which is sufficiently far from the antigen binding sites. Activation of these oligosaccharide with sodium periodate forms reactive aldehyde groups which can be used for the further conjugation of the antibody without compromising its activity. However, many monoclonal antibodies are not glycosylated and therefore they can not be activated in this way.

Before the covalent binding transducer surfaces are activated by reagents which contain groups capable of forming covalent bonds with the reactive groups on the antibody and on the other side groups capable of covalent binding to an inorganic transducer surface.

The surface silane chemistry<sup>12</sup>, which was originally developed for the protein binding to glass, silica, or silicone oxide surfaces, can be used for the binding to  $\text{Me}(\text{Si})\text{O}_x$  transducers<sup>13</sup>. A frequently used reagent, 3-aminopropyltriethoxysilane,  $\text{H}_2\text{N}(\text{CH}_2)_3\text{Si}(\text{OC}_2\text{H}_5)_3$ , binds covalently to the surfaces leaving  $-\text{NH}_2$  groups free for further surface reactions. For example,

a bifunctional reagent glutaraldehyde is bound to the activated surface via one of its two aldehyde groups and subsequently antibody is bound to the second aldehyde via its amino groups. It is desirable to finish the procedure by reaction with ethanolamine which converts residual aldehyde groups to inactive  $-(CH_2)_2OH$ .

Thiol chemistry can be used for activation of gold or silver surfaces by reagents containing thiol,  $-SH$ , groups. The self assembling of long n-alkene ( $n = 12-16$ ) thiols containing hydrophilic  $-OH$  or  $-COOH$  end groups is utilized for complete coating the surfaces. Thiol group binds to the metal surface while the dispersion forces between alkene chains organise the molecules into a compact monolayer.

An illustrative protocol for the antibody attachment procedure<sup>14</sup> contains three successive steps: (i) coating a gold SPR sensor surface by soaking it in ethanol solution of a mixture of  $HS-C_{15}COOH$  with  $HS-C_{11}OH$ , (ii) converting  $-COOH$  groups to reactive N-hydroxysuccinimide ester by reaction with N-hydroxysuccinimide and 1-ethyl-3-(3-dimethylamino-propyl)-carbodiimide, and (iii) the attachment of antibody via its amino groups. The dilution of active  $-COOH$  groups on the surface with  $-OH$  groups helps to prevent a multipoint attachment of the antibody molecule and the complete filling of the remaining surface with  $-OH$  decreases the nonspecific adsorption.

The most successful technique has appeared to be the binding of antibodies to a matrix of carboxymethyl dextran macromolecules attached to the surface<sup>15</sup> (Figure 5).

The procedure includes coating gold surface with a  $HS-C_{16}OH$  monolayer, activation of  $-OH$  groups, attachment of dextran from a basic solution, and the formation of carboxymethyl groups on dextran by reaction with bromoacetic acid and sodium hydroxide solution. A fraction of carboxy groups is then activated to N-hydroxysuccinimide esters and antibody is attached via its amino groups. If the attachment is performed at pH below antibody isoelectric point e.g. at pH 5, the positively charged antibodies are attracted into the negatively charged carboxymethyl dextran matrix where



Figure 5. The binding of antibodies to carboxymethyl dextran matrix attached to a sensor surface.

covalent binding occurs. The dextran matrix attached to a transducer surface prevents nonspecific adsorption and lends to the bound antibody molecule a large degree of mobility in all three dimensions. More antibodies can be immobilized in the three-dimensional matrix than in a monolayer configuration limited by the antibody dimensions.

SPR chips coated with a carboxymethyl dextran matrix are supplied commercially by Biacore, a leading manufacturer of SPR instruments. Similar technique can be used for preparation of carboxymethyl dextran matrix on  $\text{Me}(\text{Si})\text{O}_x$  surfaces on which  $-\text{OH}$  groups are generated by reaction with 3-glycidypropyltrimethoxysilane<sup>13</sup>.

### 2.2.4 Multilayer Assemblies

The layer-by-layer deposition technique schematically shown in Figure 6 has been used for immobilization of various antibodies on surfaces of grating coupler<sup>16, 17</sup>, interferometer<sup>9</sup>, and SPR sensors<sup>18, 19</sup>. The first molecular layer is prepared by physical adsorption of antibodies on a transducer surface. At acid pH below pI of the antibody, dextran sulphate polyanions are adsorbed on the positively charged antibody monolayer due to the electrostatic interaction. The second monolayer of positively charged antibodies is adsorbed on the immobilized polyanions and more antibody layers can be successively attached by alternating the electrostatic adsorption of polyanions and antibodies. The antibody assembly is then covalently crosslinked with glutaraldehyde and polyanions are washed out of the antibody network by inverting antibody charge at pH above the antibody pI. In this way a high number of antibodies can be immobilized on a sensor surface. However, only antibodies accessible for the analyte can contribute

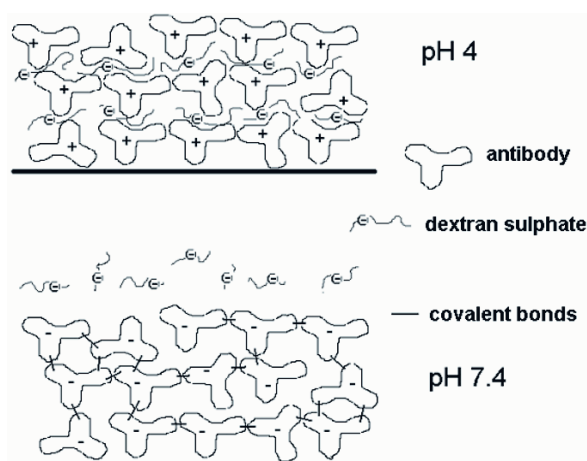


Figure 6. Preparation of antibody multilayer using layer-by-layer deposition technique.

to the binding capacity of the assembly. The analyte penetration into an antibody network depends on the analyte dimensions (Table 2) and on the density and flexibility of the antibody network. A lower crosslinking degree increases the network flexibility and the sensor response<sup>17</sup>. The capability of small analytes (B2M in Table 2) of penetrating inside crosslinked protein assemblies makes possible to increase sensor sensitivity by increasing number of immobilized antibody layers. However, the sensor response is limited by the decay of the evanescent wave with increasing distance of antibodies from the transducer surface. Larger analytes (HCG and HRP in Table 2) can interact only with top layers of an assembly. Even very large analytes, such as bacteria<sup>19</sup>, bind more effectively to a double layer assembly than to an adsorbed antibody monolayer, probably, due to a higher mobility of antibodies immobilized on the top of the assembly. A disadvantage of the method is that the binding activity can be decreased for antibodies in which the glutaraldehyde crosslinking takes place close antigen binding sites.

The glutaraldehyde treatment of antibodies is avoided<sup>19</sup> if a serum albumin layer is first adsorbed on the transducer surface, crosslinked and activated with a high glutaraldehyde concentration. Then a difference between albumin (pI = 4.9) and antibody (pI > 5.5) is utilized for adsorption of positively charged antibody onto negatively charged albumin where the covalent binding occurs between antibody amino groups and residual aldehyde groups on albumin.

The multilayer immobilization does not require any activation of the supporting surface. Thus, it can be performed in the same way on any transducer. Crosslinked multilayers are stable for long time in biological media and prevent significantly the nonspecific adsorption from blood plasma<sup>9</sup>.

*Table 2.* Responses of a grating coupler sensor coated with multilayers of monoclonal antibodies to the respective analytes. The response values are related to that of an adsorbed antibody monolayer (B2M:  $\beta_2$ -microglobulin, HCG: human choriogonadotropin, HRP: horseradish peroxidase).

<i>number of antibody layers</i>	<i>analyte [molecular weight]</i>		
	B2M [12600]	HCG [39000]	HRP [44000]
1	1	1	1
2			1.6
3	2.35	2.35	2.6
5		2.3	2.5
6	4.31		

### **2.2.5 Non Covalent Attachment of Antibodies to a Surface by the Inactive Fc Portion**

In addition to the covalent binding, some methods derived from bioaffinity chromatography can be used for non covalent attachment of antibodies to a surface by the inactive Fc portion. The advantage is that antigen binding sites stay undamaged and accessible for the analytes due to the orientation of antibody with the active Fab portions towards the tested medium.

Protein A and protein G, derived from the cell wall of certain bacteria, bind specifically the Fc region of various antibodies. The proteins can be covalently attached to a sensor surface using any method described above and then antibody is immobilized by simple incubation the surface with the antibody solution. However, differences in the affinity of these proteins for antibodies from different species and for different isotypes within a species must be considered. For example, protein A binds strongly human IgG1, IgG 2, IgG4 and rabbit antibodies and have very low avidity to human IgG3, goat, or chicken antibodies; protein G binds strongly human antibodies and have low avidity to chicken antibodies. Attached antibody can be released if reusable sensors are regenerated by washing the bound analytes. Recombinant protein G in which the albumin binding site has been deleted should be used in sensors for detection in blood serum.

## **2.3 Immunosensor Applications**

So far, optical biosensors have been mostly used in research laboratories for biomolecular interaction analysis in which the binding interactions between a ligand immobilized at the sensor surface and its molecular partner in a solution passed over this surface are studied.

Nonspecific sensor responses to complex biological media should be dealt with for practical application in medical diagnostics or food and environment control. The resistance of biorecognition layers to the nonspecific adsorption and durability of their properties in a biological environment are stressed. Probably, the fouling on artificial surfaces contacted with living entities cannot be entirely prevented. Thus, multichannel sensors are required in which a nonspecific optical response of a biorecognition layer containing the analyte binding antibodies is compared with a response of an analogous layer providing the some nonspecific optical response but insensitive to the analyte.

The continuous monitoring of the analyte concentration is one of the most attractive applications of sensors which cannot be substituted with any other immunoanalytical methods. Biorecognition layers allowing the

equilibrium binding of analytes to the receptors should be developed for these applications.

## ACKNOWLEDGEMENTS

This work was supported by the Grant Agency of the Czech Republic, under Contracts No. 203/02/1326 and 102/03/0633.

## REFERENCES

1. Lundström I., Real-time biospecific interaction analysis, *Biosens. Bioelectron.* 1994; 9: 725-736.
2. Lukosz W., Principles and sensitivities of integrated optical and surface plasmon sensors for direct affinity sensing and immunosensing, *Biosens. Bioelectron.* 1992; 6: 261-289.
3. Cush R., Cronin J.M., Steward W.J., Maule C.H., Molloy J., Goddard N.J., The resonant mirror: a novel optical biosensor for direct sensing of biomolecular interactions, Part 1: Principle of operation and associated instrumentation. *Biosens. Bioelectron.* 1993; 8: 347-353.
4. Heideman R.G., Kooyman R.P.H., Greve J., Performance of a highly optical waveguide Mach-Zehnder interferometer immunosensor, *Sensors Actuators B* 1993; 10: 209-217.
5. Fattinger C., Koller H., Schlatter D., Wehrly P., The difference interferometer: a highly sensitive optical probe for quantification of molecular surface concentration, *Biosens. Bioelectron.* 1993; 8: 99-107.
6. Marquart M., Deisenhofer J., Huber R., Crystallographic refinement and atomic models of the intact immunoglobulin molecule Kol and its antigen binding fragment at 3.0 Å and 1.9 Å resolution, *J. Mol. Biol.*, 1980; 141: 369-391.
7. Harris L.J., Larson S.B., Hasel K.W., Day J., Greenwood A., McPherson A., The three-dimensional structure of an intact monoclonal antibody for canine lymphoma, *Nature*, 1992; 360: 369-372.
8. Harris L. J., Skaletsky E., McPherson A., *Proteins, Struct. Funct. Genet.*, 1995; 23: 285-289.
9. Brynda E., Houska M., Wikerstål A., Brandenburg A., Optical biosensors for real-time measurement of analytes in blood plasma, *Biosens. Bioelectron.* 2002; 17: 665-675.
10. Hermanson G. T., *Bioconjugate Techniques*. San Diego: Academic Press, 1996.
11. Wiesman A., *Handbook of Enzyme Biotechnology, Second Edition.*, West Sussex, England: Ellis Horwood LTD., 1985.
12. Haller, W., *Application of controlled pore glass in solid phase biochemistry*, In W.H. Scouten, ed. *Solid Phase Biochemistry* New York: Wiley, 1983 535-597.
13. Polzius R., Diessel. E., Bier F., Bilitewski U., Real-Time Observation of Affinity Reactions Using Grating Couplers: Determination of the Detection Limit and Calculation of Kinetic Rate Constants, *Analyt. Biochem.* 1997; 249: 269-276.
14. Homola J., Dostalek J., Chen S., Rasooly A., Jiang S., Yee S.S., Spectral Surface Plasmon Resonance Biosensor for detection of Staphylococcal Enterotoxin B (SEB) in milk, *J. Microbiology* 2002; 75: 61-69.
15. Löfås S., Johnsson B., A novel hydrogel matrix on gold surfaces in surface plasmon resonance sensor for fast and efficient covalent immobilisation of ligands, *J.Chem.Soc., Chem.Commun.* 1990; 21: 1526-1528.

16. Brynda E., Houska M., Škvor J., Ramsden J.J., Immobilisation of multilayer bioreceptor assemblies on solid substrates. *Biosens. Bioelectron.* 1998; 13: 165-172.
17. Brynda E., Houska M., Brandenburg A., Wikerstal A., Škvor J., The detection of human  $\beta_2$ -microglobulin by grating coupler immunosensor with three-dimensional antibody networks, *Biosens. Bioelectron.* 1999; 14: 363-368.
18. Brynda E., Homola J., Houska M., Pfeifer P., Škvor J., Antibody networks for surface plasmon resonance immunosensors, *Sensors Actuators B.* 1999; 54: 132-136.
19. Koubová V., Brynda E., Karasová L., Škvor J., Homola J., Dostálek J., Tobiška P., Rošický J., Detection of foodborne pathogens using surface plasmon resonance biosensors, *Sensors Actuators B* 2001; 74: 100-105.



## **APPLICATIONS OF OPTICAL CHEMICAL SENSING**

## Chapter 19

# THE OPTICAL NOSE

David R. Walt and Tamar Sternfeld

*Department of Chemistry*

*Tufts University*

*Medford Massachusetts, 02155*

### 1. INTRODUCTION

“Electronic noses” are vapor detection systems that mimic key principles of biological olfaction<sup>1</sup>. The functioning principles of biological, olfactory systems do not rely upon selective interactions with specific analytes, but rather on cross-reactive receptors<sup>2</sup>. The receptors respond to many odors, generating unique response patterns, which serve as “fingerprints” for each odor.

Using the principles of biological olfaction, electronic nose systems contain arrays of different types of cross-reactive vapor-sensitive sensors. While it is difficult to discriminate analytes entirely by their responses to a single type of sensor, using an array of sensors yields response patterns that can readily distinguish many different vapors. Ideally, the response mechanisms of the sensors are highly varied and encompass both physical and chemical phenomena<sup>1</sup>.

Our electronic nose measures fluorescence intensity responses from an array of polymer sensors over time during exposure to different analyte vapors. The sensors contain solvatochromic dyes that undergo intensity and wavelength shifts depending on changes in microenvironmental polarity. During exposure of the array to vapor-phase analytes, each of the sensor types in the array produces a temporal fluorescence response profile that depends on the sensor-analyte interaction. The combination of different responses from the sensor array to an analyte creates a pattern that characterizes the specific analyte and, therefore, enables identification. Such an array can recognize a variety of volatile organic vapors, and moreover, it can discriminate complex odors that contain multiple components, such as different types of coffees or perfumes. In these complex odors, the electronic nose recognizes the response pattern of the mixture, eliminating the necessity to quantify every single component.

## 2. THE OPTICAL NOSE

The sensor array system is comprised of several important elements. The sensor substrate is an optical imaging fiber bundle, which is a high-density array of micrometer scale optical fibers<sup>3</sup>. The structure of each single fiber comprising this bundle contains a cylindrical “core” material surrounded by an outer “cladding” (Figure 1). The refractive index of the core is slightly higher than the refractive index of the cladding, and as a result, light is transmitted via total internal reflection through the core over long distances. The imaging fiber bundle generally contains thousands to tens of thousands of closely packed individual optical fibers (Figure 2), with each fiber retaining its own isolated optical path, enabling it to transmit a signal from one end to the other. Each individual optical fiber acts as a single pixel, and the assembly of many individual pixels into a fused coherent bundle enables images to be transmitted through the entire length of the bundle (Figure 2)<sup>3c</sup>.

The fiber bundles used for the electronic nose platform are polished and chemically etched with hydrofluoric acid to create an ordered array of micrometer sized wells on the tip of the fiber (Figure 3)<sup>4</sup>. The etching process takes advantage of the difference in reactivity of the core and the

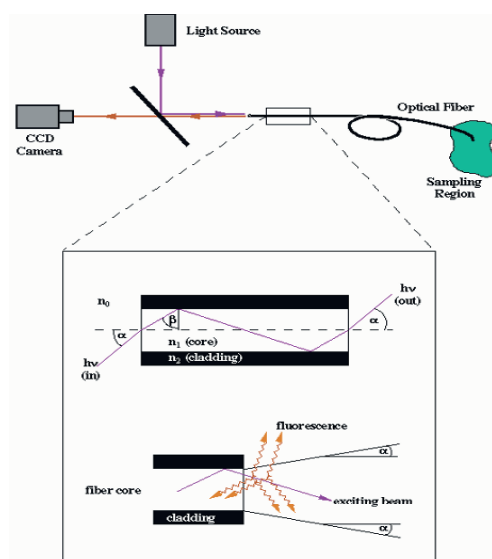


*Figure 1.* Schematic of the optical fiber system. Excitation light is launched into the fiber. Due to the refractive index differences between the fiber core and cladding materials, the light is internally reflected and travels through the fiber with minimal loss (see inset). The emitted light is carried back from the fluorescent sensor located on the tip of the fiber to a CCD camera detector. Reprinted with permission from *Science*, 2000, 287, 451-452. Copyright 2000 AAAS.

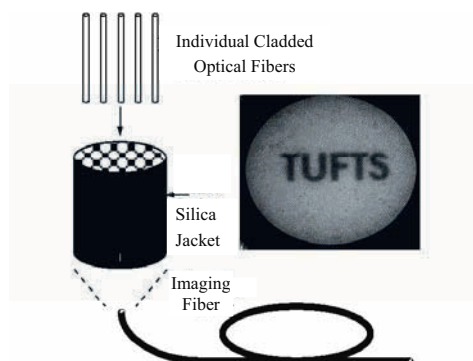


Figure 2. Coherent imaging bundle. The fiber optic imaging bundles are made by fusing many single core fibers<sup>3c</sup>.

cladding materials. All the wells in the array have a depth that is controlled by the etch reaction time. The base of each well in the array is the distal end of an optical fiber, which carries light from the well to the fiber's proximal end attached to a detection system. Thus, the optical fiber well array enables each microwell to be addressed and serves as a useful platform for the sensors on the electronic nose.

The sensors are fabricated by adsorbing or covalently attaching solvatochromic dyes to various microspheres, including differentially modified silica and polymer microspheres (also called beads). The microspheres are slightly smaller than the wells such that the diameter of a microbead sensor is complementary to the diameter of an individual well. A single bead fits inside a well and remains immobilized as a result of complementary binding forces between the glass surface and the functional groups on the microsphere. With tens of thousands of wells in each array, thousands of replicate beads of each sensor type are represented in the array (Figure 3)<sup>3a</sup>. By using a simple procedure for filling the array, 96% of the

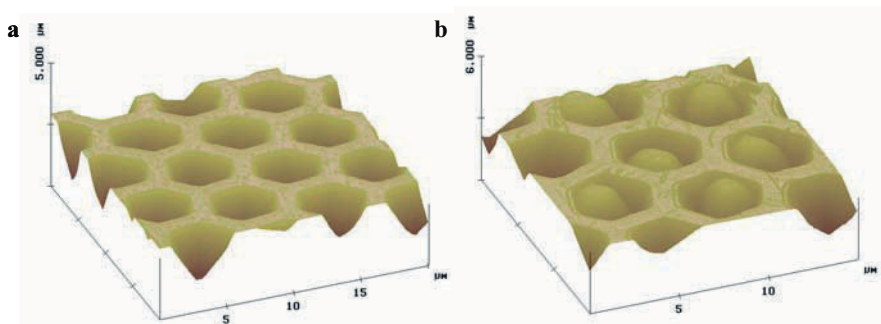


Figure 3. Atomic force microscopy image of an etched fiber bundle (a) before and (b) after microspheres were distributed into the array. Reprinted with permission from ref. 5 Copyright 1998 American Chemical Society.

wells are occupied by the microbeads (Figure 3b)<sup>5</sup>, resulting in a high-density array.

Using the microspheres as a “substrate” for solvatochromic dyes provides many advantages. The silica microspheres have a high surface area and a high affinity for the solvatochromic dye molecule, which ensures adsorption on the surface. These microsphere properties help improve their ability to classify analyte vapors. The loading of dye molecules on microsphere surfaces is adjusted to achieve an optimal concentration, and the dense surface functionality maximizes vapor–dye interaction. As a result, the fluorescent signal-to-noise (S/N) ratio is enhanced. Moreover, by using microspheres that have diverse chemical and material characteristics, such as surface functionality or bead composition, the number of possible different types of sensors is increased. Hence, by adsorbing the same dye to different types of microspheres, multiple sensor types can be generated. Each sensor type interacts differently with different vapors, resulting in a unique fluorescence response profile (to be discussed in detail later)<sup>6</sup>. The solvatochromic dye Nile Red has been used for most of our experiments. This preference is based on the large shifts in the dye’s emission wavelength maximum, and its relatively high photostability<sup>7</sup>.

The silica microspheres provide some diversity but not enough for many complex discrimination tasks. To introduce more sensor variety, hollow polymeric microspheres have been fabricated<sup>8</sup>. The preparation of these hollow microspheres involves coating silica microspheres by living radical polymerization, using the surface as the initiation site. Once the polymer layer forms on the silica microbead surface, the silica core is removed by chemical etching. These hollow spheres can be derivatized with the dye of interest. The main advantage of these polymer microspheres is the variety of monomers that can be employed in their fabrication to produce sensors with many different surface functionalities and polymer compositions.

A fluorescence measurement is performed by directly delivering a vacuum controlled pulse of the analyte vapor diluted with air to the distal end of the optical fiber containing the sensors (Figure 4). The optical instrument includes a fluorescence microscope and a charge coupled device (CCD) camera. The excitation light is launched into the fiber, and the fluorescent light, emitted from the sensors, is carried back along the fiber to the camera (Figure 1). The fluorescence intensity response for each sensor is plotted versus time, which creates a pattern that characterizes the sample.

In analogy to the biological olfactory system that contains a high number of different sensors, the electronic nose can be assembled from many different sensor materials, all of them located on a single fiber bundle to form a heterogeneous array. In such cross-reactive arrays, complex vapor responses are simultaneously collected including changes in intensity, wavelength, and spectral shape.

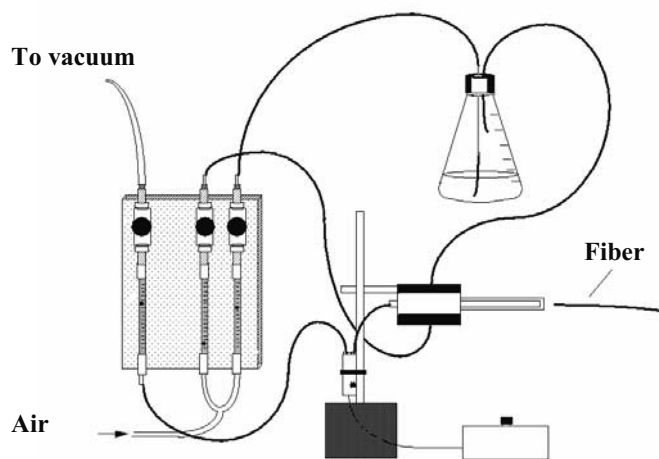
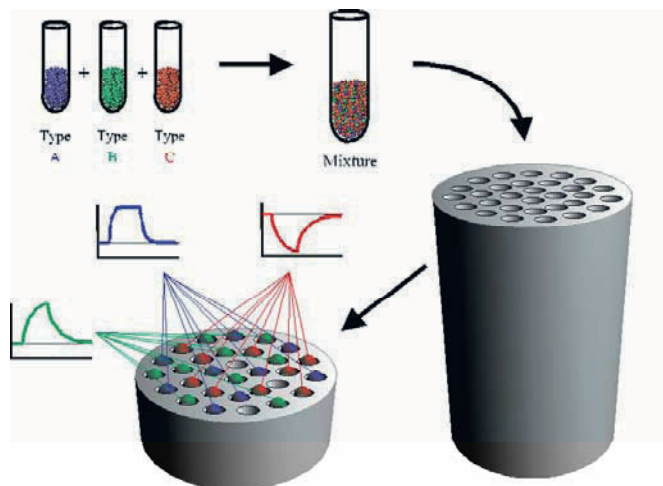


Figure 4. A schematic diagram of the olfactometer system.

The sensors in a heterogeneous array are prepared from different types of microspheres, as well as different dyes. A mixture of sensors is randomly distributed onto the fiber tip, which means that the occupied positions of each type of sensor are different from array to array. Therefore, the first step after array fabrication involves the positional registration of each individual sensor in the array, i.e. decoding of the array<sup>9</sup>. Since each sensor type exhibits a unique response to a given vapor, the decoding is done by exposing the array to known analytes and matching the acquired fluorescence responses to the responses collected separately for each sensor type (Figure 5). We define this method as a “self-encoded bead array” where each bead’s analytical signal can also be used as its encoding signal.

Many advantages arise from a heterogeneous array including the miniaturization of the array, the high density of different sensor types, the presence of many replicates of each sensor type, shorter detection times due to the small sensor sizes, low materials cost, and the ease of preparation.

A critical issue that arises in the development of all electronic noses is array-to-array reproducibility. If arrays cannot be made reproducibly, new training is required for each new array. These microsphere beads show good sensor-to-sensor reproducibility and stability over time<sup>10</sup>. Moreover, these sensors are made in large quantities, which eliminate the issue of batch-to-batch reproducibility. Hence, the main question is whether a sensor response pattern is reproducible from array to array. In one study, arrays of four different microsphere types were exposed to ethanol and 4-nitrotoluene on three different days over a six-month period. The first array was used as the “training array”, while the other two arrays were used as “testing arrays”. Although the responses of each microsphere sensor type to the analytes varied from array to array, the classification was always high (over 93%).



*Figure 5.* Schematic depiction of a self-encoded bead array. A mixture of three sensor types fills the fiber tip wells randomly. The sensors are identified by their characteristic responses to a test vapor pulse. Reprinted with permission from ref. 9b. Copyright 1999 American Chemical Society.

These results demonstrate the ability of the electronic nose to “remember” the odor of different analytes and to recognize them over extended periods of time. Therefore, we are able to create an “odor memory” library that can be maintained from one array to another over time<sup>10</sup>.

Another approach to analyze the multi-sensor array responses is the ensemble approach<sup>11</sup>, which does not require decoding and therefore, speeds up the identification process. The analysis in this approach uses combined response profiles of the entire undecoded array as a single response (Figure 6).

Generally speaking, the higher the number of sensor types in the array, the more likely the array will yield a unique fluorescence response profile for each odor, leading to better classification of odors. For example, a classification of 97% correct was achieved by using a heterogeneous array that contained 18 bead types. In this experiment, 20 different odors, including pure analytes as well as mixtures, were compared using a total of 100 observations (five exposures per odor)<sup>11</sup>.

An important demonstrated application of this artificial nose system is the high-speed detection of low levels of explosives and explosive-like vapors. Several sensors, based on Nile Red attached to silica microspheres, show high sensitivity to nitroaromatic compounds (NAC) within a mixture<sup>12</sup>. Different fluorescence response profiles were observed for several NAC's, such as 1,3,5-trinitrotoluene (TNT) and 1,3-dinitrobenzene (DNB), despite their similar structures. These responses were monitored at low concentrations of the NAC vapors (ca. 5 ppb) and at short vapor exposure

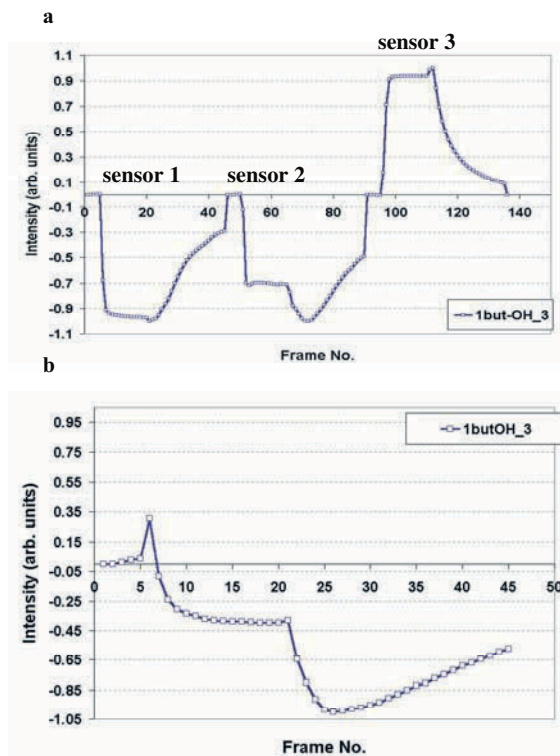


Figure 6. Response profiles from three different sensor types. (a) Concatenated Responses of each of the individual sensor types (decoded array). (b) The collective response (undecoded array). Reprinted with permission from ref. 11. Copyright 2003 American Chemical Society.

times (less than 200 ms). The detection of such low concentrations is possible since we are able to measure simultaneously the responses of a high number of individual sensors and sum their responses, thereby increasing the S/N ratio. Theoretically this ratio increases by  $n^{1/2}$ , where  $n$  is the number of sensors analyzed. Therefore, by combining the responses of a large number of individual beads (1000 beads), the noise is essentially removed and low concentrations of analytes can be detected (Figure 7).

High-speed detection is a necessity for many artificial nose applications. In one study<sup>12a</sup>, it was shown that even at short exposure times (<1 sec), the nose could identify different vapors and the responses were reproducible. Figure 8 demonstrates this quality, when three high-speed exposures (0.38s exposure time) produced reproducible response profiles.

In addition, a linear dependence was found between the concentration of DNB and its fluorescence response profile. All these characteristics demonstrate that this sensor array is suitable for use in detecting explosive vapors.



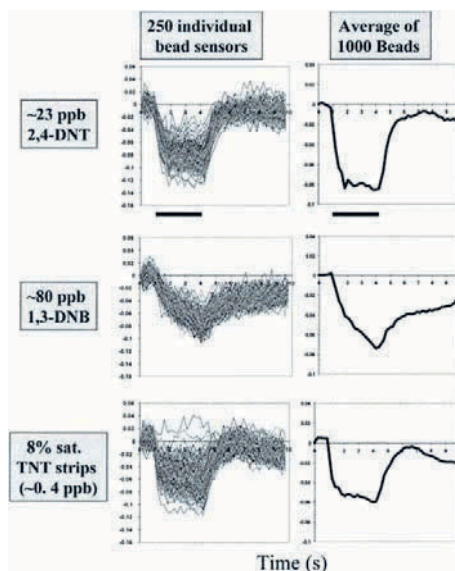


Figure 7. Simultaneously monitoring vapor signatures of 1000 sensors for 2,4-DNT, 1,3-DNB, and TNT vapor strips at 8% saturated vapor levels. The (noisy) responses for 250 individual sensors are compared to the averaged response profile for 1000 individual sensors. Reprinted with permission from ref. 12a. Copyright 2000 American Chemical Society.

The sensor response depends not only on the polarity of the analyte, but also on the flow environment. In the mammalian olfactory system, the nasal cavity structure plays an extremely important role in odor discrimination<sup>13</sup>.

Identical olfactory neurons are located in different places in the cavity, and therefore occupy different positions in the flow path. By using a nasal cavity model, we investigated the influence of the dynamic flow on the sensors' response<sup>14</sup>. The responses from identical fiber optic sensors located

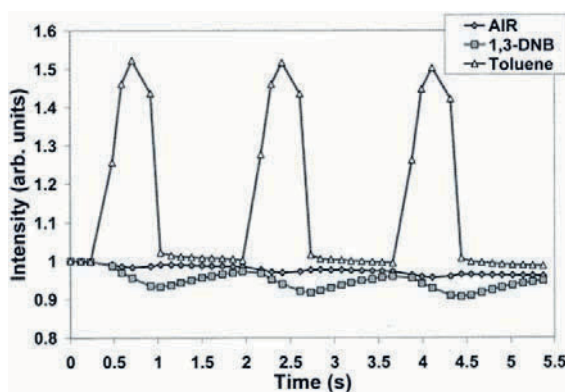


Figure 8. Seventy-six sensor beads (Jupiter C4/Nile Red) monitored to show that the average responses for three consecutive 0.38-s exposures of 50% saturated vapor levels result in reproducible and high-speed response profiles. The sensors are positioned on the distal tip of an optical imaging fiber and relative analyte concentrations are 0.5 and 18700 ppm for 1,3-DNB and toluene, respectively. Reprinted with permission from ref 12a. Copyright 2000 American Chemical Society.

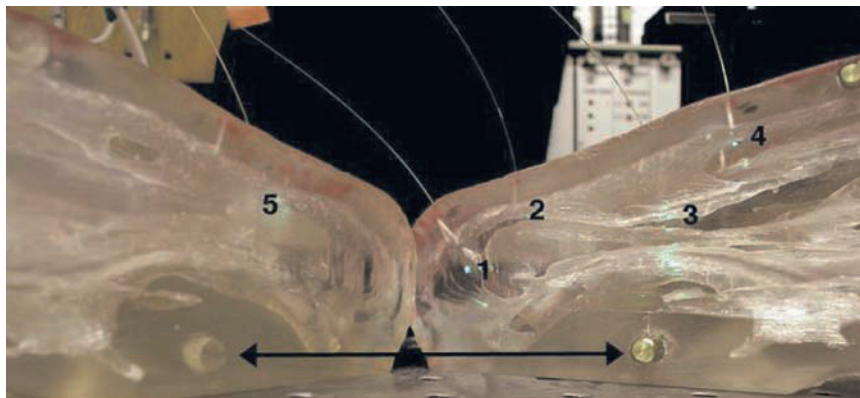


Figure 9. A plastic model of a nasal cavity showing the different positions (numbers 1-5) of the sensors. Reprinted with permission from ref. 14. Copyright 2003 American Chemical Society.

at different positions in a nasal cavity model were measured using different exposure conditions (Figure 9). These identical sensors produced different fluorescence response profiles to the analytes depending on their positions. As a result of the sensors' arrangement, the classification of odors improved. When rums, vodkas, and perfumes were analyzed, the percent classification rates increased by  $8\pm 5\%$ ,  $8\pm 6\%$  and  $7\pm 3\%$ , respectively. Moreover, in some cases, using the nasal cavity model made it possible to distinguish between analytes that could not be distinguished by using the same sensor in a single position.

### 3. CONCLUSIONS

This research demonstrates the ability to employ biological principles using an artificial sensing system. The cross-reactive fluorescence sensor array, which contains a high number of different non-specific sensors, makes it possible to distinguish between a variety of odors. The nasal cavity structure, in which the same type of sensor is placed in different flow environments, further increases the information that can be obtained, as well as improves the ability to classify vapors. The electronic nose system shows high sensitivity, and accordingly, low concentrations of vapors can be detected, which is highly important in the identification of explosive compounds. All of the sensor array's properties described in this chapter, including the reproducible responses of the sensors, provide a means for training the system to "remember" different odors, and for recognizing them in a short measurement time. The use of the system for a variety of applications is the subject of present research.

## ACKNOWLEDGMENTS

This work was funded through generous support of DARPA and the Office of Naval Research.

## REFERENCES

1. Albert K. J., Lewis N. S., Schauer C. L., Sotzing G. A., Stitzel S. E., Vaid T. P., Walt D.R., Cross-reactive chemical sensor arrays, *Chem. Rev.* 2000; 100: 2595-626.
2. Firestein S., How the olfactory system makes sense of scents, *Nature* 2001; 413: 211-18.
3. (a) Walt D. R., Bead-based fiber-optic arrays, *Science* 2000; 287: 451-52.  
(b) Walt D. R., Fiber optic imaging sensors, *Acc. Chem. Res.* 1998; 31: 267-68.  
(c) Epstein J., Walt D. R., Fluorescence-based fibre optic arrays: a universal platform for sensing, *Chem. Soc. Rev.* 2003; 32: 203-14.
4. Pantano P., Walt D. R., Ordered nanowell arrays, *Chem. Mater.* 1996; 8: 2832-835
5. Michael K. L., Taylor L. C., Schultz S. L., Walt D. R., Randomly ordered addressable high-density optical sensor arrays, *Anal. Chem.* 1998; 70: 1242-48.
6. (a) Albert K. J., Gill D. S., Pearce T. C., Walt D. R., Optical multibead arrays for simple and complex odor discrimination, *Anal. Chem.* 2001; 73: 2501-8.  
(b) Johnson S. R., Sutter J. M., Engelhardt H. L., Jurs P. C., White J., Kauer J. S., Dickinson T. A., Walt D. R., Identification of multiple analytes using an optical sensor array and pattern recognition neural networks, *Anal. Chem.* 1997; 69: 4641-8.  
(c) White J., Kauer J. S., Dickinson T. A., Walt D. R., Rapid analyte recognition in a device based on optical sensors and the olfactory system, *Anal. Chem.* 1996; 68: 2191-202.
7. (a) Vauthey E., Picosecond transient grating study of the reorientation dynamics of Nile red in different classes of solvent, *Chem. Phys. Lett.* 1993; 216: 530-6.  
(b) Deye J. F., Berger T. A., Nile Red as a solvatochromic dye for measuring solvent strength in normal liquids and mixtures of normal liquids with supercritical and near critical fluids, *Anal. Chem.* 1990; 63: 615-22.
8. Mandal T. K., Fleming M. S., Walt D. R., Production of hollow polymeric microspheres by surface-confined living radical polymerization on silica templates, *Chem. Mater.* 2000; 12: 3481-7.
9. (a) Dickinson T. A., White J. S., Kauer J. S., Walt D. R., A chemical-detecting system based on cross-reactive optical sensor array, *Nature* 1996; 382: 697-700.  
(b) Dickinson T. A., Michael K. L., Kauer J. S., Walt D. R., Convergent, self-encoded bead sensor arrays in the design of an artificial nose, *Anal. Chem.* 1999; 71: 2192-8.
10. Stitzel S. E., L. Cowen J., Albert K. J., Walt D. R., Array-to-array transfer of an artificial nose classifier, *Anal. Chem.* 2001; 73: 5266-71.
11. Albert K., Walt D. R., Information coding in artificial olfaction multisensor arrays, *Anal. Chem.* 2003; 4161-7.
12. (a) Albert K. J., Walt D. R., High-speed fluorescence detection of explosives-like vapors, *Anal. Chem.* 2000; 72: 1947-55.  
(b) Albert K. J., Myrick M. L., Brown S. B., James D. L., Milanovich F. P., Walt D. R., Field-deployable sniffer for 2,4-dinitrotoluene detection, *Environ. Sci. Technol.* 2001; 35: 3193-200.
13. (a) Keyhani K., Scherer P. W., Mozell M. M., A numerical model of nasal odorant transport for the analysis of human olfaction, *J. Theor. Biol.* 1997; 186: 279-301.

- (b) Kauer J. S., White J., Imaging and coding in the olfactory system, *Annu. Rev. Neurosci.* 2001; 24: 963-79.
14. Stitzel S. E., Stein D. R., Walt D. R., Enhancing vapor sensor discrimination by mimicking a canine nasal cavity flow environment, *J. Am. Chem. Soc.* 2003; 125: 3684-5.

## Chapter 20

# INVASIVE SENSORS IN MEDICINE

Francesco Baldini  
*Institute of Applied Physics*  
*National Council of Research*  
*Via Madonna del Piano 10*  
*50019, Sesto Fiorentino (FI), Italy*

### 1. INTRODUCTION

In biomedicine, an important field of research is the one associated with the development of sensors for the detection of physical and chemical parameters in the human body.

Two classes of sensors can be distinguished:

- non-invasive sensors, in which the probe remains outside of the human body and is placed at a distance from or in contact with the skin;
- invasive sensors, in which the probe must enter the human body through the natural cavities (nostrils, throat, ears).

The general attitude of physicians is to undertake actions which can be easily tolerated by the patient and which introduce a minimum risk for the safety of the patient. From this point of view, non-invasive sensors are definitely preferable to invasive sensors. On the other hand, for several applications, the insertion of optical sensors inside the human body cannot be avoided. In this case, very severe regulations must be satisfied in order to guarantee the safety of patients.

Optics can be an actual solution in many applications. The potential of optical sensors for continuously monitoring physical and chemical parameters is enormous. The absence of electrical contacts or of the passage of electrical current in the transduction mechanism is of paramount importance in an area in which the safety of the patient is a fundamental aspect. In the case of invasive applications, physicians can also take advantage of the fact that optical fibres can guarantee unique performances, thanks to their geometrical versatility, easy handling, and high degree of miniaturisation. Optical catheters with a diameter of the order of dozens of micron and probe heads miniaturised up to 1  $\mu\text{m}$  enable physicians to arrive

at places inside the human body that would be unthinkable with other sensor technologies.

This aspect makes it clear why optical fibre sensors for medical applications have been characterised by a remarkable development after the introduction of optical fibres. The first invasive optical fibre oximeter which was described in 1964<sup>1</sup>, can be considered one of the first optical fibre sensors. Since then, many sensors have been proposed which find application in different biomedical areas, ranging from cardiovascular and intensive care to angiology, gastroenterology and ophthalmology. Some of these are still at the prototype level, whereas others are already available on the market.

Here below some examples of the developed sensors are given.

## 2. BILE SENSOR

Optical fibre sensors play a fundamental role for the detection of enterogastric and non-acid gastro-oesophageal refluxes<sup>2</sup>, which are considered contributing factors to the development of several pathological conditions such as gastric ulcer, "chemical" gastritis, upper dyspeptic syndromes, and severe oesophagitis. Under certain conditions, the enterogastric reflux may also increase the risk of gastric cancer.

Optical detection is based on the optical properties of bile, which is always present in such refluxes<sup>3</sup>. Bilitec 2000 is the commercially available sensor, produced by Cecchi srl<sup>4</sup> and commercialised by Medtronic<sup>5</sup>. Basically, it utilises two light emitting diodes, as sources, at  $\lambda=465$  nm and 570 nm (reference) and an optical fibre bundle to transport the light from the sources to the probe (which is actually a miniaturised spectrophotometric cell, of 3 mm external diameter) and the returning light from the probe to the detector. Figure 1 shows a photo of the optical probe. The instrument evaluates the logarithm of the ratio between the light intensities collected by the detection system. The difference in the logarithms measured in the sample and those measured in a pure water reference is related to the bilirubin concentration. This is related to bile-containing reflux in the

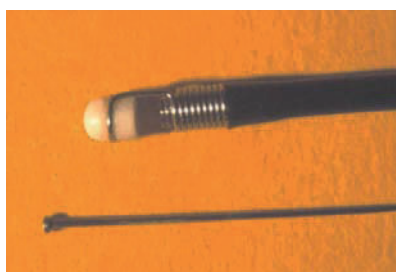


Figure 1. Photo of the optical probe for bile detection.

stomach and/or oesophagus. The sensitivity of the sensor was 2.5  $\mu\text{mol/L}$  (bilirubin concentration) and the working range was 0–100  $\mu\text{mol/L}$ . This range fits well with that encountered in the stomach or oesophagus (although bilirubin concentration in pure bile can be up to 10 mmol/L, it is progressively diluted to its final concentration in the refluxate by pancreatic enzymes, duodenal secretion and, finally, by gastric content). These characteristics clearly refer to *in vitro* tests, whereas, in the case of *in vivo* measurements the nonhomogeneity between the gastric content and the mucus and the solid particles in suspension represents a serious impediment. In such case, although absorbance values could numerically express bilirubin concentration, they can only allow an approximate quantitative assessment of the overall bile-reflux concentration. However the sensor is able to accurately measure the contact time between the refluxate and the gastric and/or oesophageal mucosa. The method was validated on numerous patients, by inserting the optical fibre bundle into the stomach or oesophagus via the nasal cavity<sup>6-9</sup>.

### 3. pH SENSORS

pH is a very important parameter in biomedical applications; its knowledge is strictly related to the diagnosis of good working of many organs and systems in the human body. It is generally detected by a chromophore which changes its optical spectrum as a function of the pH; absorption-based indicators or fluorophores are usually used.

#### 3.1 Blood pH

Real-time monitoring of the blood pH, together with the detection of the blood oxygen ( $\text{pO}_2$ ) and carbon dioxide ( $\text{pCO}_2$ ) partial pressures is of paramount importance in operating rooms and intensive care units in order to determine the quantity of oxygen delivered to the tissues and the quality of the perfusion. All these three parameters are conventionally measured by benchtop blood-gas analysers on hand-drawn blood samples. However significant changes can occur in blood samples after the removal from the body, before the measurements are carried out by the blood gas analyser. Due to their ability to provide continuous monitoring, optical fibre sensors represent a welcome and significant improvement in patient management.

The first pH sensor was developed at NIH (Bethesda, Maryland) and made use of phenol red as acid-base indicator, covalently bound to polyacrylamide microspheres<sup>10</sup>; such microspheres are contained inside a cellulose dialysis tubing (internal diameter 0.3 mm) connected to a 250  $\mu\text{m}$  plastic fibre (Figure 2). The probe was inserted into either the tissue or the

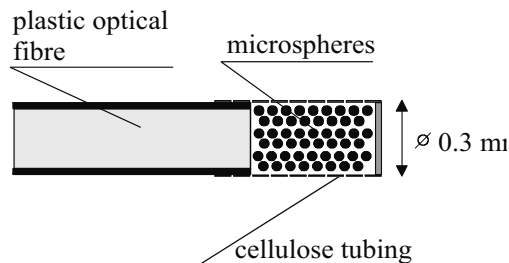


Figure 2. Optode with phenol red bound to polyacrylamide microsphere for blood pH monitoring.

blood vessel through a 22-gauge hypodermic needle. The probe was tested in vivo on animals for the detection of extracellular acidosis during regional ischemia in dog hearts<sup>11</sup>, and for the measurement of transmural pH gradients in canine myocardial ischemia<sup>12</sup>, and of conjunctival pH<sup>13</sup>.

The first intravascular sensor for simultaneous and continuous monitoring of the pH, pO<sub>2</sub>, and pCO<sub>2</sub> was developed by CDI-3M Health Care (Tustin CA)<sup>14</sup> based on a system designed and tested by Gehrich et al.<sup>15</sup>. Three optical fibres (core diameter = 125 µm) are encapsulated in a polymer enclosure, along with a thermocouple embedded for temperature monitoring (Figure 3). pH measurement is carried out by means of a fluorophore, hydroxypyrene trisulfonic acid (HPTS), covalently bonded to a matrix of cellulose, attached to the fibre tip. Both the acidic ( $\lambda_{exc}=410$  nm) and alkaline ( $\lambda_{exc}=460$  nm) excitation bands of the fluorophore are used, since their emission bands are centred on the same wavelength ( $\lambda_{em}=520$  nm). The ratio of the fluorescence intensity for the two excitations is measured, to render the sensor relatively insensitive to fluctuations of optical intensity.

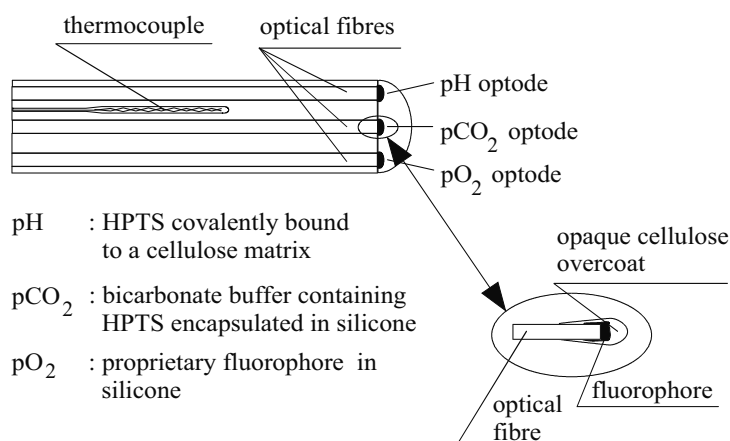


Figure 3. Sketch of the probe for the invasive detection of pH, pO<sub>2</sub>, and pCO<sub>2</sub> in human blood.



Measurements of partial pressure of oxygen ( $pO_2$ ) and of carbon dioxide ( $pCO_2$ ) are described in the following sections.

The probe (OD=0.6 mm) has been tested in-vivo on animals<sup>16-17</sup>, and has shown satisfactory correlation with data obtained ex-vivo from electrochemical blood gas analysers.

Other intravascular-probe systems have been proposed by Abbott (Mountain View, CA)<sup>18</sup> and by Optex Biomedical (Woodlands, TX)<sup>19</sup>, where the structure of the probe is essentially similar to the CDI one previously described: i.e. three different multimode fibres, each of which is associated with the specific chemistry and charged with the detection of a single measurand.

On the other hand some problems regarding the intravascular use of this sensor have emerged during clinical trials on volunteers in critical care and on surgical patients<sup>20</sup>:

- a blood flow decrease due to peripheral vasoconstriction lasting for several hours after surgical operations; this can give rise to a contamination by flush solutions which can seriously affect the measurements;
- the so-called "wall effect" which primarily affects the oxygen count (if the fibre tip is very close to or touches the arterial wall, it measures the tissue oxygen, which is lower than the arterial blood oxygen);
- the formation of a thrombus (clot) around the sensor tip which alters the value of all the analyte values.

Due to the above-mentioned problems, invasive sensors for blood gas measurements remain mainly at the research level.

The intravascular system Paratrend 7<sup>®</sup> was distributed by Diametrics Medical up to 2003 and has been the last one available on the market which assures an intravascular monitoring of pH,  $pO_2$  and  $pCO_2$ , using an optical fibre sensor designed for arterial placement.

One of the last developed version of this system (Neotrend) was developed to monitor blood gases continuously and directly in critically-ill premature babies. The system is equipped with a tiny optical fibre catheter (0.5 mm in diameter) which is inserted into the infant's descending aorta by means of an umbilical artery catheter. A sketch of the probe is shown in Figure 4.

All the problems associated to an invasive application are clearly avoided in a system working in an extracorporeal blood circuit, developed by CDI-3M, which has been commercially available since 1984 (now distributed by Terumo)<sup>21</sup>. A disposable probe which uses the same chemistry as the previously described intravascular optode, is inserted on line in the blood circuit on one side and connected to the fibre bundle on the other (see chapter 2, Figure 5).

A different approach was also described<sup>22</sup>: a fibre optic blood gas and pH monitoring system, capable of performing "paracorporeal" measurements for

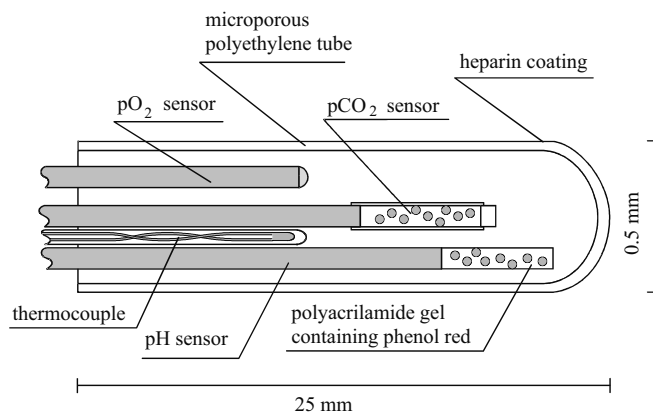


Figure 4. Sketch of the probe used for the detection of blood gases in critically-ill premature babies

use at the patient's bedside, was developed. The developed probe, consisting of three different fluorescent based sensors for pH,  $p\text{CO}_2$  and  $p\text{O}_2$  respectively, is placed in series with a standard arterial line. Measurements were performed on withdrawn samples of arterial blood which return to the patient after the detection.

Though this procedure does not allow continuous monitoring, samples can be withdrawn continuously without any risk of inducing anaemia (which may otherwise occur with the use of benchtop analysers), since no blood loss results from such paracorporeal system.

### 3.2 Gastric pH

Optical fibres sensors have been also proposed for the detection of the acidity in the stomach and in the oesophagus. Monitoring gastric pH for long periods (for example, 24 hours) serves to analyse the physiological pattern of acidity. It provides information regarding changes in the course of the peptic ulcer, and enables assessment of the effect of gastric antisecretory drugs. In the oesophagus, the gastro-oesophageal reflux, which causes a pH decrease in the oesophagus contents from 7 to 2, can determine oesophagitis with possible strictures and Barrett's oesophagus, which is considered a preneoplastic lesion. In addition, in measuring the bile-containing reflux, the bile (generally slightly alkaline) and pH should be measured simultaneously, since, due to a shift in the bilirubin absorption peak to lower wavelengths, the accuracy of the bile measurement decreases by about 20% for values of  $\text{pH} < 3.5^{23}$ .

The current practice is to insert a miniaturised glass electrode mounted in a flexible catheter, in the stomach or oesophagus through the nostrils. This electrical system is, however, impractical, owing to the size and rigidity of

the glass electrode, and has the added drawback of being subject to electromagnetic interference. Optical fibre sensors overcome these problems, although the broad range of interest (from 1 to 8 pH units) generally requires the use of more than one chromophore, thereby complicating the design and construction of the optode. This is probably the reason why almost all the pH sensors developed for biomedical applications have been proposed for blood pH detection.

The first sensor proposed for detecting gastric and oesophageal pH<sup>24</sup>, made use of two fluorophores, fluorescein and eosin, immobilised onto fibrous particles of amino-ethyl cellulose, fixed on polyester foils. Only tested *in vitro*, the sensor reveals a satisfactory response time of around 20 seconds.

Other two sensors have been proposed and in this case, *in vivo* tests have been reported<sup>25-26</sup>, but none of the proposed pH sensors appears completely satisfactory.

The first one, proposed by Peterson et al.<sup>25</sup>, is based on two absorbance dyes, meta-cresol purple and bromophenol blue, bound to polyacrylamide microspheres. The configuration of the probe is similar to that one shown in Figure 2. The laboratory optical system arrangement was composed of a lamp plus filters, a fibre coupled probe, a CCD spectrometer and a personal computer. The sensor was tested on samples of human gastric fluid and was also tested *in vivo* after inserting the optical probe into the stomach of a dog. The accuracy (better than 0.1 pH units) satisfies clinical requirements, but the response time to each pH step was longer than desired, ranging between 1 and 6 minutes. Such a long response time would prevent the detection of fast changes in pH, and makes the sensor useless for the detection of gastro-oesophageal reflux, where pH changes are usually extremely rapid (less than 1 minute).

The other sensor makes use of two dyes, bromophenol blue (BPB) and thymol blue (TB), to cover the range of interest<sup>26</sup>. The chromophores, immobilised on controlled pore glasses, are fixed at the end of plastic optical fibres. The distal end of the fibres is then heated and the CPGs form a very thin pH-sensitive layer on the fibre tips. The probe has four fibres (two for each chromophore) and its sketch is shown in Figure 5. A Teflon diffuse

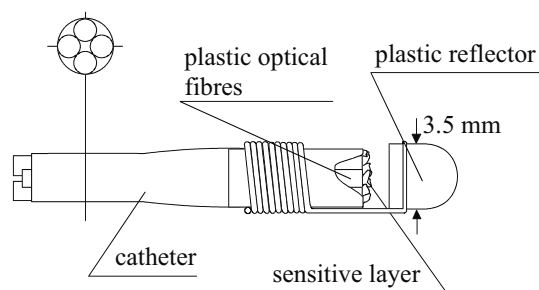


Figure 5. Optical probe for the measurement of gastric pH.

reflector was held in front of the fibres, using a small fine steel wire, in order to improve the return coupling of the modulated light. An optoelectronic unit, similar to that used for bilimetric monitoring, was developed. It consists of two identical channels, separately connected to each of the two fibres carrying TB and BPB, for the detection of pH in the ranges 1 to 3.5 and 3.5 to 7.5, respectively. The use of LEDs as sources, photodetectors and an internal microprocessor make it a truly portable, battery-powered sensor. Response time was less than 1 minute for every pH step. Although the *in vitro* accuracy was 0.05 pH units, satisfactory *in vivo* accuracy has not been attained, since, in some cases, a step of some tenths of pH is present between the response of the optical sensor and of the pH electrode. The reason for this behaviour could be ascribed to colour/turbidity interference, since the optical fibres see not only the colour of CPGs, but also the colour/turbidity existing between the fibres and the reflector. This drawback could be removed by measuring the absorption coming from the sample at the working wavelengths of TB and BPB, by means of other fibres without the immobilised CPGs, but this would imply the manufacture of a very complicated probe and optoelectronic unit.

The use of only one indicator to cover the whole range would simplify the whole system and recent studies indicate methyl red as feasible indicator for gastric pH measurement. The dye, immobilised on CPG was shown to be capable of covering the whole pH range between 1 and 8<sup>27-28</sup>.

### 3.3 pH for Stroke Analysis

An application still at laboratory level, although at an advanced stage, in which the potential miniaturisation of optical fibre sensors plays a fundamental role, is the pH detection of brain tissue after a traumatic brain injury or after a stroke. A stroke is a cerebrovascular incident caused by a decrease in the blood flow: the brain cells are deprived of oxygen, and if the interruption in providing oxygen is long enough, irreversible damage to the brain cells occurs.

Knowledge of the health of the cells after a stroke is fundamental: if the cells are still alive, the use of neuroprotectant drugs can be useful to minimise brain damage; otherwise, their utilisation is useless. A chemical parameter capable of assessing the state of health of tissue cells is pH. In fact, the death of tissue cells is followed by formation of lactic acid, which causes a decrease in blood pH. Normal values are around 7.4: a decrease below this value in the region in which a stroke has taken place is an index of the death of cells.

Although pH optical fibre sensors have been already developed for blood analysis, they were not designed to reach, through a catheter, the vascular system of the brain. A pH sensor was developed for this purpose at the

Center for Healthcare Technologies at Lawrence Livermore National Laboratory in Livermore, potentially capable to measure pH at or near the stroke site<sup>29</sup>. The probe is the distal end of a 125  $\mu\text{m}$  fibre tapered up to a diameter of 50  $\mu\text{m}$ . A fluorescent pH-indicator, seminaphthorhodamine-1-carboxylate, is embedded inside a silica sol-gel matrix which is fixed to the fibre tip. Excitation of the dye takes place at 533 nm and the emission in correspondence of the acid (580 nm) and basic (640 nm) bands are separately detected. The use of this ratiometric technique obviates worrying about source fluctuations, which have the same effects on the two detected signals. The pH sensor developed was first characterised in the laboratory, where it showed fast response time (of the order of tens of seconds) and an accuracy of 0.05 pH units, well below the limit of detection necessary for this clinical application (0.1 pH units). The pH sensor was also tested *in vivo* on rats, by placing the pH sensor in the brain of a Sprague-Dawley rat at a depth of approximately 5 mm<sup>30</sup>.

#### 4. OXYGEN

Together with pH, oxygen is surely the chemical parameter most investigated for biomedical applications, as its knowledge and continuous monitoring are very important in many fields, such as those of circulatory and respiratory gas analysis.

A knowledge of the oxygen content in blood is essential in order to know how the cardiovascular and cardiopulmonary systems work. This measurement can be performed either spectroscopically by exploiting the optical properties of haemoglobin, the oxygen-carrying pigment of erythrocytes, or by using an appropriate fluorophore, the fluorescence of which is quenched by oxygen.

Oxygen saturation, i.e. the amount of oxygen carried by the haemoglobin (Hb) in the erythrocytes in relation to its maximum capacity, was the first quantity measured with optical fibres<sup>1</sup>. This parameter is measured optically by exploiting the different absorption spectra of the Hb and the oxyhemoglobin (OxyHb) in the visible/near infrared region. Numerous artery and vein insertion models are now commercially available. In the simpler version, reflected or absorbed light is collected at two different wavelengths and the oxygen saturation is calculated via the ratio technique on the basis of the isosbestic regions of Hb and OxyHb absorption. On the other hand, the presence of other haemoglobin derivatives, such as carboxyhemoglobin, carbon monoxide haemoglobin, methemoglobin and sulfhemoglobin, makes preferable the use of multiple wavelengths or of the whole spectrum, which allow their discrimination<sup>31</sup>. Noninvasive optical oximeters, which calculate oxygen saturation via the light transmitted through the earlobes, toes, or fingertips have also been developed, primarily

for neonatal care. In this case, particular attention has to be paid to differentiating between the light absorption due to arterial blood and that due to all other tissues and blood in the light path. This implies the use of multiple wavelengths, such as the eight-wavelength Hewlett Packard ear oximeter. The advent of pulse oximetry has made it possible to overcome this problem. This approach is based on the assumption that a change in the light absorbed by tissue during systole will be caused primarily by the passage of arterial blood. By an appropriate choice of two wavelengths, it is possible to measure the oxygen saturation non-invasively by analysing the pulsatile, rather than the absolute level of transmitted or reflected, light intensity<sup>32-34</sup>. The detection of blood absorbance fluctuations that are synchronous with systolic heart contractions is called photoplethysmography.

Just to give an idea of the potentiality of optical fibres, Oxifirst is a pulse oximeter produced by Mallinckrodt<sup>35</sup> (which in 1997 acquired Nellcor Puritan Bennett), and designed for the detection of the status of fetal oxygen. The detection of fetal oxygen saturation can be particularly important in determining how the baby is tolerating labour. If an abnormality in the fetal heart rate is observed (this occurs in 30% of all labours), the reason can be ascribed to a dangerous lack of oxygen in the baby or to a more innocuous situation, such as the baby falling asleep. The particular design of the probe makes possible its location on the fetal cheek in the mother's womb (Figure 6). The continuous monitoring of oxygen saturation offers a tool to obstetrical teams when deciding whether the labour can progress safely or an intervention is necessary (e.g. the use of forceps, or caesarean delivery)<sup>36</sup>.

The development of new oximeters is also in progress, with the application of time- and frequency-domain techniques which are, in principle, capable of discriminating between the absorption and scattering contributions coming from human tissue, thus making possible the detection of tissue oxygenation<sup>37-39</sup>.

The disadvantage of utilising haemoglobin as an indirect indicator for the measurement of oxygen is its full saturation at  $\approx 100$  Torr: this fact prevents,

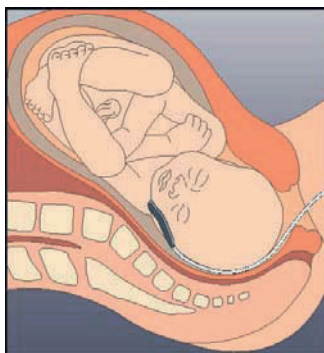


Figure 6. Sketch of the location of the Oxifirst probe on the fetal cheek.

for example, the use of this method in the case of the respiration of gas mixtures with an O<sub>2</sub> content larger than 20% as routinely used in anaesthesia. Therefore the use of a chemical transducer becomes necessary in some cases. The first optode-based oxygen sensor was described by John Peterson, and makes use of a fluorophore, perylene-dibutyrate, the fluorescence of which is efficiently quenched by oxygen<sup>40</sup>. The dye, adsorbed on amberlite resin beads, was fixed at the distal end of two plastic optical fibres with a hydrophobic membrane permeable to oxygen. The probe described was tested in-vivo for the measurement of the arterial pO<sub>2</sub> level in dog eyes<sup>41</sup>.

Other optodes have been developed and tested in-vivo, all of them using a fluorophore, the fluorescence of which is quenched by oxygen. In the intravascular sensor developed by CDI, previously described, a specially synthesised fluorophore, a modified decacyclene ( $\lambda_{\text{exc}}=385$  nm,  $\lambda_{\text{em}}=515$  nm), is combined with a second reference-fluorophore that is insensitive to oxygen, and is incorporated into a hydrophobic silicon membrane that is permeable to oxygen.

## 5. CONTINUOUS MONITORING OF GASTRIC CARBON DIOXIDE

Gastric carbon dioxide monitoring can help physicians in making rapid diagnosis of disturbances in tissue perfusion, since the stomach is one of the first regions of the body to be affected in cases of shock and the last one to be restored<sup>42-43</sup>. Its monitoring in the stomach has been shown to be a convenient method in critically-ill patients and has been proven to be of particular relevance to patient morbidity and mortality<sup>44</sup>.

Currently, gastric CO<sub>2</sub> is measured semi-continuously by means of gastric tonometry, according to which a silicone air-filled balloon is inserted inside the stomach (Tonocap, Tonometrics, Datex Ohmeda) and equilibrium is reached between the contents of the balloon and the gastric environment<sup>45</sup>. A gas sample is taken every ten minutes, and detection of CO<sub>2</sub> takes place outside the patient, by means of an infrared sensor. The main disadvantage of this lies in the equilibrating time necessary until the CO<sub>2</sub> content in the balloon becomes equal to the gastric CO<sub>2</sub>.

An optical fibre sensor for the continuous detection of gastric carbon dioxide partial pressure (pCO<sub>2</sub>) has recently been developed<sup>46</sup>. The sensor is based on the measurement of the pH change induced in the optode following the diffusion of carbon dioxide<sup>47-49</sup>. The CO<sub>2</sub>-sensitive layer consists of an ion pair dissolved in a thin layer of ethylcellulose. A pH indicator (DH) and an organic quaternary hydroxide (Q<sup>+</sup>OH<sup>-</sup>) form the ion pair. The hydrated ion pair (Q<sup>+</sup>D<sup>-</sup>)<sub>x</sub>H<sub>2</sub>O provides the water molecules to dissolve CO<sub>2</sub>, and no wet microenvironment is necessary. In the presence of CO<sub>2</sub>, a new ion pair



Figure 7. Photo of the CO<sub>2</sub>-probe head used in the clinical validation.

( $\text{Q}^+\text{HCO}_3^-$ ) is formed and the indicator is protonated (DH), thus changing its optical properties. The value of  $\text{pCO}_2$  is clearly related to the  $\text{CO}_2$  concentration.

The sensing layer is mounted on a probe head fixed at the end of a catheter that contains an optical fibre connected to an optoelectronic unit. A photo of the probe head is shown in Figure 7.

A laboratory characterisation was carried out, during which the performances of the optical fibre sensor were carefully verified and compared with those of the Tonocap. The results showed the capability of the optical fibre sensor to detect  $\text{CO}_2$  correctly even in the presence of rapid changes of the order of 1 minute.

First clinical results were obtained by using a combined catheter which included both the optical fibre sensor and the Tonocap balloon (Figure 8). A typical result obtained on an intensive care patient, is shown in Figure 9. In the graph the tracing of the end-tidal  $\text{CO}_2$  ( $\text{EtCO}_2$ ), i.e. the  $\text{CO}_2$  concentration in the expiration at the end of the expiratory phase, and the values of the arterial  $\text{CO}_2$  ( $\text{PaCO}_2$ ), obtained from blood samples drawn from the patient, are also shown. As expected, a rapid  $\text{CO}_2$  peak was detected only by the optical fibre sensor, and was not seen by Tonocap (as in the measurements carried out on volunteers). Moreover, the optical fibre sensor seems to follow better the end-tidal  $\text{CO}_2$ .



Figure 8. Photo of the tip of the combined catheter.



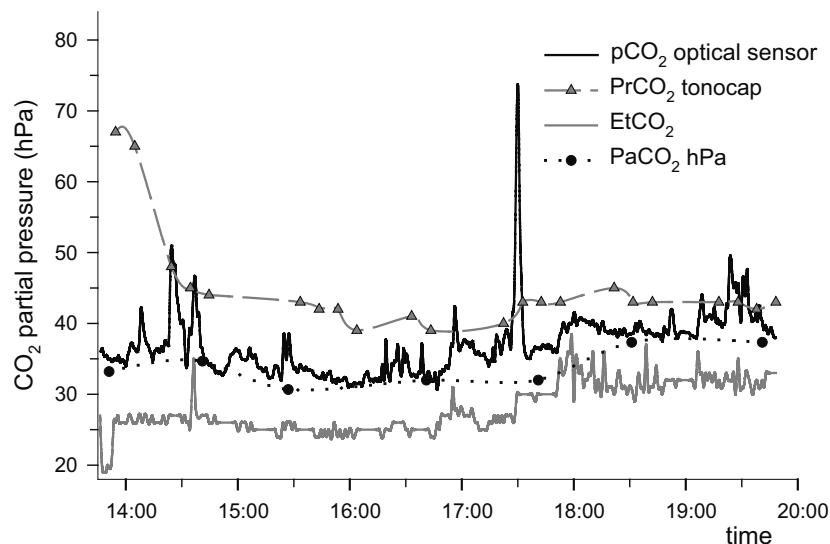


Figure 9. Clinical test on a patient: response curve of the optical fibre sensor and of Tonocap.

An investigation of the rapid changes of gastric CO<sub>2</sub> observed, possibly using the new optical fibre sensor, could lead to a better understanding of gastrointestinal physiology.

## 6. CONTINUOUS MONITORING OF GLUCOSE

The development of a sensor capable of continuously monitoring glucose in diabetic patients is a big challenge which scientists have not still won.

World-wide, about 130 million people are believed to suffer from diabetes, a disease which occurs when the body does not adequately produce the insulin needed to maintain a normal circulating blood glucose (80-120 mg/dl). It is estimated that the disease is in rapid expansion (300 million in 2025). Frequent monitoring of blood glucose is crucial for effective treatment and to reduce the morbidity and mortality of diabetes. Blindness, kidney and heart failure, peripheral neuropathy, pure circulation, gangrene are the severe complications which, over time, are related to diabetes.

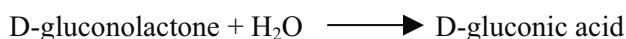
The more diffuse clinical classes of diabetes are two, type 1 and type 2. Patients suffering from type 1 diabetes must use continuously insulin to regulate their blood glucose levels, due to the destruction of their insulin-producing beta cells in the pancreas. People with Type 2 diabetes are not insulin-dependent, but can usually regulate their blood glucose levels by following an individual meal plan, exercising, and by taking certain medicines, including insulin, when needed. Differently from type I diabetes,

which may occur at any age, type II diabetes usually occurs in people 40 years old or older.

It is apparent that monitoring glucose levels in blood is an important element in the treatment of diabetic patients. Currently, the monitoring technique consists of the taking of blood samples 4-7 times a day on a regular basis, by means of a finger prick, and subsequent analysis by means of colorimetric strips coated with glucose oxidase and peroxidase enzymes. In the presence of glucose oxidase, the catalysation of glucose takes place according to the reaction



D-gluconolactone is rapidly converted in gluconic acid according to the following reaction:



Therefore, glucose concentration can be measured by monitoring the oxygen consumption<sup>50</sup> or the change in pH caused by the formation of gluconic acid<sup>51</sup>.

The finger prick technique is invasive, painful, and potentially dangerous, because of the risk of infection. Also, since it is not continuous, it is not possible to predict a blood glucose pattern over the day nor the exact dose of insulin needed. In addition, depending on the training of the individual performing the test, the results are subject to inaccuracy.

Many attempts, based on different technologies, are in progress in order to develop a continuous glucose sensor<sup>52-53</sup>, and optics seems to play a fundamental role, in these.

One interesting approach is based on the measurement of the glucose content in the interstitial fluids (ISF) of the skin. It has been demonstrated that glucose levels in ISF consistently track blood glucose concentrations, although with a delay of 2-5 minutes, due to the physiological transfer of glucose from the blood to the ISF<sup>54-55</sup>.

With this approach, SpectRx (SpectRx Inc, USA)<sup>56</sup> is developing a compact and portable glucose sensor. An array of micropores is created on the external layer of the skin by means of laser microporation (Figure 10 on the left). A patch containing a colorimetric sensor, which is based on the enzymatic reaction mentioned above, is applied in correspondence with the array, and collects the interstitial fluid which flows through the pores (Figure 10 on the right). The signal detected is sent to a meter equipped with a display which shows the glucose concentration. Microporation lasts 1 second, and a few minutes are necessary to collect an amount of interstitial fluid sufficient for measuring glucose. The measurement can then be repeated at intervals of 10-15 minutes. If the measurement is repeated fairly

frequently, the micropores remain viable without the necessity of repeating the microporation process. Clinical tests under way in the United States

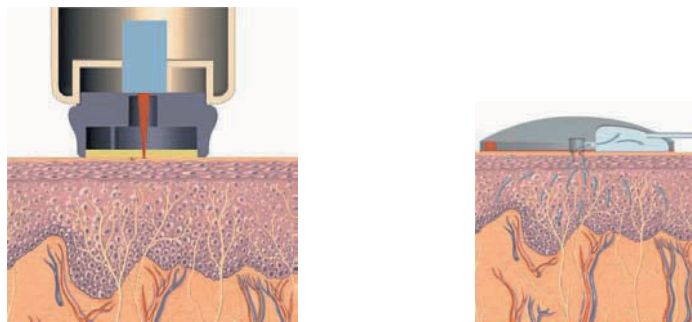


Figure 10. Sketch of the laser microporation of the skin (left) and of the SpectRx path applied to the skin (right).

showed a noticeable correlation between the glucose detected with the SpectRx sensor and fingerstick glucose readings, although there was a delay of about 10 minutes. It should be considered that, in addition to the physiological delay of 2-5 minutes, there is a delay due to the ISF extraction and to the reaction time of the glucose sensor.

The above-mentioned approach cannot be considered noninvasive, although the invasivity is really minimal.

Near-infrared spectroscopy can be used to perform a completely noninvasive detection of glucose<sup>57</sup>. Light in the infrared region (700–2500 nm) illuminates a small area of skin, penetrates through the skin up to a depth of 1-10  $\mu\text{m}$ , and reaches the capillary system below the epidermis. The light scattered back out through the skin is collected, and an infrared spectrum is detected. This spectrum contains information on the complex mixture of constituents tissues and blood, including glucose. It is apparent that special algorithms, based on multivariate mathematical analysis, are necessary in order to extract the information on glucose; it is equally apparent that special calibration is necessary, since the physiological and spectral characteristics of the skin change from subject to subject.

Different approaches based on NIR spectroscopy have led to the development of different optical instrumentation which are almost all at a research level<sup>58</sup>.

The ideal glucose monitoring system should be non invasive, should allow continuous or frequent monitoring over long periods without the need to replace the changeable parts (strip, transdermal patch, etc.), should interfere minimally with daily life, and, last but not least, should be low in cost.

The prototype developed by Lifetrac System (LifeTrac Systems, USA)<sup>59</sup>, also based on NIR spectroscopy, is very interesting and seems to satisfy the above-mentioned requirements. It is shown in Figure 11. In this case, it is not the light scattered back out through the skin that is detected, but rather



Figure 11. Photo of the prototype of the glucose sensor developed by Lifetrac.

the light emitted by an infrared LED that crosses the ear lobe. Appropriate software is still necessary to extract the information on glucose concentration from the detected signal. No interference coming from the skin pigmentation occurs with this approach. In comparison with the Diasensor system, it is portable and very compact and should be less expensive. Clinical trials are in progress to test the accuracy and consistency of LifeTrac Systems.

## 7. CONCLUSIONS

Optical sensors are in continuous development and are offering to the physicians reliable and efficient tools for in-vivo continuous diagnosis. The several instruments already available on the market and the more numerous systems developed at an advanced stage in the labs testifies that optical sensors are one of the primary choice for scientists and for physicians when an in-vivo continuous monitoring should be carried out.

## REFERENCES

1. Kapany N.S., Silbertrust N., Fiber optics spectrophotometer for in-vivo oximetry, *Nature* 1964; 208:138.
2. Falciai R., Scheggi A.M., Baldini F., and Bechi P., U.S.A. Patent 4,976,265 (1990).
3. Falciai R., Baldini F., Cosi F., Bechi P., Pucciani F., Bile enterogastric reflux sensor using plastic optical fibres, *Fiber and Integr. Opt.* 1993; 12: 215.
4. Cecchi srl, Viadotto Indiano 50145, Firenze, Italy.
5. Medtronic Functional Diagnostics, Tonsbakken 16-18, Skovlunde, Denmark, <http://www.mfd.medtronic.com>.
6. Bechi P., Pucciani F., Baldini F., Cosi F., Falciai R., Mazzanti R., Castagnoli A., Passeri A., Boscherini S., Long-term ambulatory enterogastric reflux monitoring. Validation of a new fiberoptic technique, *Digestive Diseases and Sciences* 1993; 38: 1297.
7. Vaezi M.F., Lacamera R.G., Richter J.E., Validation studies of Bilitec 2000: an ambulatory duodenogastric reflux monitoring system., *Am.J.Physiol.* 1994; G1050.

8. Stipa F., Stein H.J., Feussner H., Kraemer S., Siewert J.R., Assessment of non-acid esophageal reflux: comparison between long-term reflux aspiration test and fiberoptic bilirubin monitoring, *Dis. Esophagus* 1997; 10: 1.
9. Barrett M.W., Myers J.C., Watson D.I., Jamieson G.G., Detection of bile reflux; in vivo validation of Bilitec fibreoptic system, *Diseases of the Esophagus* 2000; 13: 44.
10. Peterson J.I., Goldstein S.R., Fitzgerald R.V., Buckhold R.V., Fiber optic pH probe for physiological use, *Anal. Chem.* 1980; 52: 864.
11. Tait G.A., Young R.B., Wilson G.J., Steward D.J., Mac Gregor D.A., Myocardial pH during regional ischemia: evaluation of a fiber-optic photometric probe, *Am. J. Physiol.* 1982; 243:H1027.
12. Watson R.M., Markle D.R., Ro Y.M., Goldstein S.R., McGuire D.A., Peterson J.I., Patterson R.E., Transmural pH gradient in canine myocardial ischemia, *Am. J. Physiol.* 1984; 246:H232.
13. Abraham E., Fink S.E., Markle D.R., Plinholster G., and Tsang M., Continuous monitoring of tissue pH with a fiberoptic conjunctival sensor, *Am. Energ. Med.* 1985; 14:840.
14. CDI-3M Health Care, 1311 Valencia Avenue, Tustin CA 92680.
15. Gehrich J.L., Lübbers D.W., Opitz N., Hansmann D.R., Miller W.W., Tusa K.K., Yafuso M., Optical fluorescence and its application to an intravascular blood gas monitoring system, *IEEE Trans. Biomed. Eng.* 1986; BME-33:117.
16. Miller W.W., Yafuso M., Yan C.F., Hui H.K., Arick S., Performance of an *in-vivo*, continuous blood-gas monitor with disposable probe, *Clin. Chem.* 1987; 33:1358.
17. Hansmann D.R., Gehrich G.L., Practical perspectives on the *in-vitro* and *in-vivo* evaluation of a fiber optic blood gas sensor, *Proc. SPIE* 906:4 (1988).
18. Khalil G., Yim J., Vurek G.G., *In-vivo* blood gases: problems and solutions, *Proc. SPIE* 2131:437 (1994).
19. Schlain L., Spar S., Continuous arterial blood gas monitoring with transmitted light sensors and LED light sources, *Proc. SPIE* 2131:452 (1994).
20. Khalil G., Malin S.F., *In-vivo* blood gases: promises and realities, *Proc. SPIE* 2388:502 (1995).
21. Terumo Cardiovascular Systems Corporation, 6200 Jackson Road, Ann Arbor, MI 48103, <http://www.terumo-cvs.com>.
22. Martin R.C., Malin S.F., Bartnik D.J., Schilling A.M., Furlong S.C., Performance and use of paracorporeal fiber optic blood gas sensors, *Proc. SPIE* 2131:426 (1994).
23. Baldini F., Bechi P., Cianchi F., Falai A., Fiorillo C., Francalanci M., Nassi P., Analysis of the optical properties of the bile, *J. Biomedical Optics* 2000; 5: 321.
24. Posch H.E., Leiner M.J.P., Wolfbeis O.S., Towards a gastric pH-sensor: an optrode for the pH 0-7 range, *Fres. Z. Anal. Chem.* 1989; 334:162.
25. Baldini F., Bechi P., Bracci S., Cosi F., Pucciani F., *In-vivo* optical fibre pH sensor for gastro-oesophageal measurements, *Sensors and Actuat.B* 1995; 29:164.
26. Netto E.J., Peterson J.I., McShane M., Hampshire V., A fiber-optic broad-range pH sensor system for gastric measurements *Sensors and Actuat.B* 1995; 29:157.
27. Baldini F., Falai A., Characterization of an optical fibre pH sensor with methyl red as optical indicator, in "Optical Sensors and Microsystems. New Concepts, Materials and Technologies", S. Martellucci, A.Chester and A.G. Mignani eds, Kluwer Academic, New York, 2000.
28. Baldini F., In vivo monitoring of the gastroesophageal system using optical fibre sensors, *Anal. Bioanal. Chem.* 2003; 375: 732-743.
29. Grant S.A., Glass S.R., A sol-gel based fiber optic sensor for local blood pH measurements, *Sensors and Actuat. B* 1997; 45: 35.
30. Grant S.A., Bettencourt K., Krulevich P., Hamilton J., Glass S.R., *In vitro* and *in vivo* measurements of fiber optic and electrochemical sensors to monitor brain tissue pH, *Sensors and Actuat.B* 2001; 72: 174.

31. Lubbers D.W., Chemical *in vivo* monitoring by optical sensors in medicine, *Sensors and Actuat.B* 1993; 11: 253.
32. Mendelson Y., Ochs B.D., Noninvasive pulse oximetry utilizing skin reflectance photoplethysmography, *IEEE Trans. Biomed. Eng.* 1988; BME-35: 798.
33. Cui W., Ostrander L.E., Lee B.Y., *In vivo* reflectance of blood and tissue as a function of wavelength, *IEEE Trans. Biomed. Eng.* 1990; BME-37: 632.
34. Ugnell H., Oberg P.A., The time variable photoplethysmographic signal. Its dependance on light wavelength and sample volume, *Proc. SPIE* vol.2331: 89 (1994).
35. Mallinckrodt Corporate Communications, Corporate Headquarters, 675 McDonnell Blvd., Hazelwood, 63042 MO, USA, <http://www.mallinckrodt.com>
36. Dildy G., Clark S., Loucks C., Intrapartum fetal pulse oximetry: Past, present, and future, *American Journal of Obstetrics and Gynecology* 1996; 175: 1.
37. Chance B., Yodh A., Spectroscopy and imaging with diffusing light, *Physics Today* 1995; 40: 34.
38. Oda M., Yamashita Y., Nishimura G., Tamura M., A simple and novel algorithm for time-resolved multiwavelength oximetry, *Phys. Med. Biol.* 1996; 41: 551.
39. Cubeddu R., Pifferi A., Taroni P., Torricelli A., Valentini G., Compact tissue oximeter based on dual-wavelength multichannel time-resolved reflectance, *Appl. Opt.* 1999; 38: 3670.
40. Peterson J.I., Fitzgerald R.V., Buckhold D.K., Fiber-optic probe for *in vivo* measurement of oxygen partial pressure, *Anal. Chem.* 1984; 56: 62.
41. Stefansson E., Peterson J.I., Wang Y.H., Intraocular oxygen tension measured with a fiber optic sensor in normal and diabetic dogs, *Am. J. Phys.* 1989; 256: H1127.
42. Ruokonen E., Takala J., Kari A., Saxen H., Mertsola J., Hansen E.J., Regional blood flow and oxygen transport in septic shock, *Crit. Care Med.* 1993; 21: 1296-1303.
43. Tang W., Weil M.H., Sun S., Noc M., Gazmuri R.J., Bisera J., Gastric intramural pCO<sub>2</sub> as a monitor of perfusion failure and anaphylactic shock, *J. Appl. Physiol.* 1994; 76: 572-577.
44. Bams J.L., Mariani M.A., Groeneveld A.B.J., Predicting outcome after cardiac surgery: comparison of global haemodynamic and tonometric variables, *Br.J.Anaesth.* 1999; 82: 33-37.
45. Heinonen P.O., Jousela I. T., Blomqvist K.A., Olkkola K.T., Takkenen O.S., Validation of air tonometric measurement of gastric regional concentrations of CO<sub>2</sub> in critically ill septic patients, *Intens. Care Med.* 1997; 23: 524-529.
46. Baldini F., Falai A., De Gaudio A.R., Landi D., Lueger A., Mencaglia A., Scherr D., Trettnak W., Continuous monitoring of gastric carbon dioxide with optical fibres, *Sensors and Actuators B* 2003; 90: 132-138.
47. Mills A., Chang Q., McMurray N., Equilibrium studies on novel colorimetric plastic film sensors for carbon dioxide, *Anal. Chem.* 64; 1383-1389, 1992.
48. Mills A., Chang Q., Fluorescent plastic thin-film sensor for carbon dioxide, *Analyst* 1993; 118: 839-843.
49. Weigl B.H., Wolfbeis O.S., Sensitivity studies on optical carbon dioxide sensors based on ion-pairing, *Sens. Actuators B* 1995; 28: 151-156.
50. Rosenzweig Z., Kopelman R., Analytical properties and sensor size effects of a micrometer-sized optical fiber glucose biosensors, *Anal. Chem.* 1996; 68: 1408-1413.
51. Trettnak W., Leiner M.J.P., Wolfbeis O.S., Fibre-optic glucose sensor with a pH optrode as the transducer, *Biosensors* 1988; 4: 15-26.
52. Wilkins E., Atamasov P., Glucose monitoring: state of the art and future possibilities, *Med. Eng. Phys* 1996; 18 (4): 273-288.
53. Klonoff D.C., Noninvasive blood glucose monitoring, *Diabetes Care* 1997; 20 (3): 433-437.
54. Service F.J., O'Brien P.C., Wise S.D., Ness S., LeBlanc S.M., Dermal interstitial glucose as an indicator of ambient glycemia, *Diabetes Care* 1997; 20: 1429-1429.

55. Bantle J.P., Thomas W., Glucose measurement in patients with diabetes mellitus with dermal interstitial fluid, *J.Lab. Clin. Med.* 1997; 130: 436-441.
56. SpectRx, Inc., 6025A Unity Drive, Norcross, GA USA 30071, <http://www.spectrx.com>.
57. Heise H.M., Non-invasive monitoring of metabolites using near infrared spectroscopy: state of the art, *Horm. Met. Research* 1996; 28 (10): 527-534.
58. Malin S.F., Ruchti T.L., Blank T.B., Thennadil S.N., Monfre S.L., Noninvasive prediction of glucose by near-infrared diffuse reflectance spectroscopy, *Clin. Chem.* 1999; 45 (9): 1651-1658.
59. LifeTrac Systems, 316 Main Street, Biddeford, Maine, USA, <http://www.sugartrac.com>.

## Chapter 21

# BIOSENSORS FOR DETECTION OF BIOTERRORIST THREATS

Frances S. Ligler, D. Phil., D.Sc.  
*Center for Bio/Molecular Science & Engineering*  
*Naval Research Laboratory*  
*Washington, DC 20375-5348 USA*

### 1. SCENARIOS AND REQUIREMENTS

There is no universal sensor appropriate for the detection of bioterrorist threats in all situations. All biothreats are composed of very similar compounds--molecules composed predominantly of carbon, nitrogen, oxygen, and hydrogen atoms and generally organized into amino acids and nucleotides. These molecules are highly similar when viewed spectroscopically or using other long-range interrogation techniques. Thus specific identification requires direct contact with the threat for further analysis. The most rapid and specific methods for such analyses involve molecular recognition using complementary biomolecules. Such molecules are incorporated into biosensors to provide an optoelectronic signal when the recognition event occurs. Distinct biosensor approaches provide different information and are useful in different scenarios.

In general, methods for determining the presence of a biothreat agent can be divided into three categories: triggers, rapid screening systems, and confirmatory techniques. Each method is useful for different reasons and provides different types of information.

Triggers determine that something has changed from the normal background but do not determine what the new material is. Most frequently employed triggers use light scatter to identify particles (in air) in the respiratory range of 1-10 microns, with the possible addition of ultraviolet analysis to determine that the particles are of biological origin. ATP assays have also been employed to determine that bacteria are present, but do not adequately detect toxins or viruses. In most cases, triggers are used as inexpensive, very rapid (< 1 minute) methods for continuous monitoring of fixed sites and to initialize sample collection and identification procedures.



Spectroscopic standoff or LIDAR approaches are being explored as triggers that can be used at a longer distance from the area to be interrogated (Figure 1<sup>1</sup>).

Rapid screening systems distinguish the biothreat from the background, provide a presumptive identification, and almost exclusively employ biomolecular recognition. The emphasis is on speed first, then sensitivity, and finally specificity. This is the niche for which the biosensors have provided critically needed technology. Response times of 3-15 minutes are typical from sample introduction to warning. Little if any sample preparation is involved other than introducing the sample into an aqueous matrix. Aerosolized agents can be collected into water using various cyclone or electrostatic collectors, ground and drinking water samples can be directly introduced into the sensor, solid materials can be wiped or homogenized and the resulting solution tested. Information obtained includes the likely type of toxin or pathogen present. In some cases, quantitative data can be measured; however, the spatially random nature of the sampling procedures limit the value of exact quantitation. The specificity of the results is a function of the capture molecules used to identify the biothreat. The sensitivity, as measured by the signal over background, is a function of the affinity of the capture biomolecules used, the capability of the biosensor to distinguish true positive responses from signals generated by nonspecific binding of other sample components and/or labeled reagents, optical or electronic background, and the increase in response generated by the use of a target preconcentration step. The speed of the response is usually a function of the sensitivity required, the affinity of the biochemical reagents used, the number of steps in the detection procedure, and the efficiency of the fluidics and data processing procedures. Ideal screening systems would detect toxins and pathogens below the lethal dose in 1-5 minutes with no false positive responses. They would also analyze for all known threat agents



Figure 1. US Army's Long Range Standoff Biological Detection System operates off a Black Hawk Helicopter and uses LIDAR to detect changes in particle concentration<sup>2</sup>.

simultaneously and would be reusable after interrogation of a negative sample. Many idealists would also require the response to be reversible so that reuse after a positive response was possible, but this quality tends to be incompatible with high affinity binding usually required for high sensitivity.

The final category of biothreat analysis is confirmation. Confirmatory tests can take longer than rapid screening methods and must be based on different principles of identification. More complex procedures can be included such as sample preparation steps, separation methods, and extended incubations for culture, capture by probes, or signal amplification. Cell culture has long been the gold standard for confirmation, but it is limited primarily to bacterial identification. Gene analysis is replacing cell culture as the method of choice since it can be used for both bacteria and viruses; however, toxins do not contain identifiable DNA or RNA except as a variable contaminant of the preparation. In addition to confirming the identity of an agent, the analysis of genetic material also has the potential to provide information on the strain of an organism and antibiotic resistance. Trojan horse organisms which are not inherently pathogenic but which have been modified to produce toxins can be identified using gene probes. As biosensors, particularly those employing gene probes, become more capable of simultaneous analysis of multiple targets, the potential for automated biosensors to contribute to confirmation capability increases. One additional technology that is showing significant capacity for confirmatory analysis is mass spectroscopy (MS)<sup>3</sup>. Technology growing out of the proteomics and bioinformatics research communities is expanding MS methods for analysis of large molecules; data bases of peptides and other molecules unique to toxins and pathogens and the combination of MS with other separations techniques can be applied for the identification of biothreat agents.

The remainder of this chapter will focus on biosensors using biological recognition motifs for identification of biothreat agents. Unless otherwise indicated, the primary application is for rapid screening applications. While we have not included a discussion of cell-based biosensors, the potential of such systems for screening for unanticipated threats, based on their capability to cause physiological harm, should not be overlooked<sup>4</sup>.

## **2. BIOMOLECULES FOR BIOTHREAT RECOGNITION**

The most popular biomolecule for the recognition of biothreat agents is, not surprisingly, the antibody. Antibodies have been used for diagnostic applications for over half a century; they are relatively robust and specific for the target, amenable to immobilization on a variety of sensor surfaces, can be stored dry for over a year, and are well characterized in terms of structure and function. Antibodies can be produced by simple antigen injection into animals, by production of monoclonal cell lines<sup>5</sup> and by

recombinant DNA technologies. Recombinant techniques have been used to produce a variety of structural variants including Fab<sup>6</sup> and scAb<sup>7</sup> fragments which retain the antigen combining site but have added advantages in terms of potential for immobilization on sensor surfaces in defined orientations and at high surface density. In addition, the selection of the recombinant antibodies, which is performed entirely *in vitro*, can be automated<sup>7</sup> and production of larger quantities can be performed using bacteria instead of animals or mammalian cell culture.

The next most frequently employed biomolecule for biothreat detection is the oligonucleotide. Currently fielded systems use DNA probes and the polymerase chain reaction (PCR) to recognize specific DNA sequences from threat organisms. If the pathogen is an RNA virus, the RNA must be converted to DNA using a reverse transcriptase prior to the recognition event. A PCR probe first binds to the target DNA and that piece of DNA is replicated using a polymerase. Both fielded systems, the R.A.P.I.D. (Idaho Technologies, Salt Lake City, UT) and Gene Xpert (Cepheid, Sunnyvale, CA), use fluorescent dyes to measure the formation of such replicates by the increase in concentration of double stranded DNA as additional probes continue to bind to the newly formed replicates at appropriate temperature. The number of targets that can be measured simultaneously with this approach is on the order of 3-5. In order to increase the number of oligonucleotides that can be detected, scientists are immobilizing the DNA probes in arrays on surfaces and investigating other methods for improving the signal. These include amplification of all DNA in the sample to provide more material for analysis (Vora *et al.*, 2004), highly sensitive staining techniques geared to eliminate the requirement for amplification, and creation of target DNA-based molecular wires as an ultrasensitive transduction system<sup>8</sup>.

In addition to the use of DNA probes to detect genetic material from pathogens via base pairing and hybridization, oligonucleotides can be used as affinity recognition molecules directly comparable to antibodies<sup>9</sup>. In this case, combinatorially produced oligonucleotides are screened for binding to toxins or pathogens and the binding molecules replicated in bacteria<sup>10</sup>. Using SELEX technology<sup>11</sup>, the entire selection process can be automated. Binding has been demonstrated to both proteins and small molecules. In addition, the photoaptamer technology recently reported covalently attaches the aptamer to the target so that the surface with the immobilized complex can be washed under very harsh conditions to remove any material that would create a background signal, thus enhancing the signal/background ratio and reducing the limit of detection<sup>12</sup>.

Other biomolecules are also being explored for binding to biothreat agents with the potential for recognizing families of agents. A major concern about the use of highly specific recognition elements such as antibodies, DNA probes, and aptamers is that you have to know ahead of time what

threats to look for in order to select the probes. Oligosaccharides (including gangliosides)<sup>13-15</sup>, combinatorial peptides, and siderophores<sup>16</sup> are potential recognition molecules that recognize groups of threat agents and might bind a toxin or pathogen whose presence was not anticipated. The exact identity of the threat could then be determined using a confirmatory method.

### 3. BIOSENSORS FOR A FEW TARGETS

The first commercially available biosensors, glucose monitors and pregnancy tests, were designed to detect a single analyte. The development of biosensors for biothreats also began with one test-one target paradigms. Many of the approaches have been expanded to provide for detection of multiple targets by either including multiple, parallel and independent sensing surfaces or by limited multiplexing of the capture and/or detection reagents. In general, however, the numbers of targets detectable at the same time has proven to be about 8. The detection ranges for these assays are in 0.1 to 200 ppm range in food samples.

One of the first bioagent detection technologies fielded in the early 90's was the immunochromatographic assay (also known as Hand Held Assays, Figure 2). The immunochromatographic assays include a nitrocellulose strip to which a liquid sample is added at one end. As the liquid flows down the

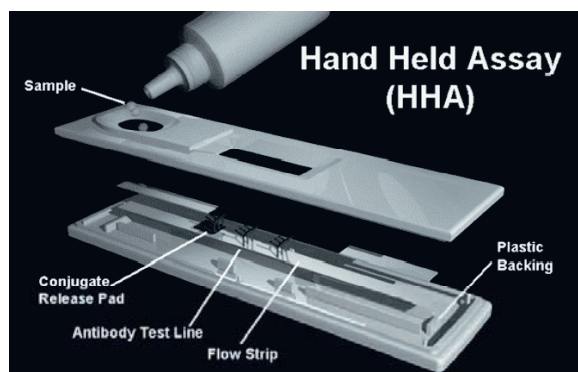


Figure 2. Hand Held Assay<sup>17</sup>.

strip, it contacts a pad impregnated with a colloidal gold labeled antibody which binds any target in the sample. A stripe of antibody further down the chromatographic strip captures the target-gold complex to generate a positive signal. An additional antibody stripe also binds particles and acts as a positive control to show that the assay is working properly. Purple color is visible where the particles bind. Since these assays are easy to operate and stable for over a year in storage, they have been widely disseminated to the first responder community. However, users have reported difficulties due to interferents in some samples (particularly if the samples are highly

particulate or viscous) and to human variation in vision. To compensate for the first problem, users are currently directed not to consider a sample positive until at least two assays register a positive response. To address the vision issue, Alexeter (Wheeling, IL) markets an automated ticket reader, the Guardian, which reproducibly quantifies the amount of target-gold colloid immobilized on the strip. The Guardian is sold in conjunction with immunochromatographic assays from Tetracore (Gaithersburg, MD) with detection capabilities for anthrax, ricin, botulinum toxin, Staphylococcal Enterotoxin B, plague, tularemia, and brucella.

The Portal Shield system, originally developed by the Naval Surface Weapons Center (Dahlgren, VA) and currently marketed by Camber, Corp. (Huntsville, AL) uses immunochromatographic assays to interrogate air samples collected automatically using a cyclone collector (Figure 3)<sup>18</sup>. Fluid flows over 8 tickets testing for different targets and are read using a diode laser system. Tickets are housed in a carousel, which rotates to provide a fresh batch of tickets after each set of assays is completed. Several investigators are developing immunochromatographic assays that test for multiple targets and produce a separate line for each target present; however, no assays using the test strips for more than 5 targets have been reported to date. The immunochromatographic tickets are very convenient to use in terms of storage and technical simplicity and are cost effective when few assays are performed. However, they are very expensive for routine monitoring procedures or for testing a large number of samples for a rare positive event.



Figure 3. Recent version of the Portal Shield system housed in a temperature controlled chamber for long-term monitoring around fixed sites ([www.dcfp.navy.mil/cbrd/ca/actd.htm](http://www.dcfp.navy.mil/cbrd/ca/actd.htm), March 20, 2004).

In addition to the immunochromatographic assays, another system used by the Allies during Desert Storm for the detection of biological warfare agents was the Light Addressable Potentiometric System (LAPS) produced by Molecular Devices (Sunnyvale, CA)<sup>19</sup>. The LAPS detected toxins and

pathogens using a sandwich immunoassay with urease attached to one antibody. If immobilized in a complex with the target, the urease would cause a detectable pH change in the solution. The same readout technology was automated by Environmental Technologies Group (Baltimore, MD) and subsequently marketed as the Bio-Detector (Figure 4)<sup>20</sup>. The biosensor included a collection device to trap particles from air onto a filter tape, automated fluidics, and eight parallel sensor elements for performing eight immunoassays simultaneously. It weighed about 150 pounds and, due to the cost of the reagents, was very expensive to operate.



Figure 4. The Bio-Detector performs 8 immunoassays simultaneously and is currently marketed by Smiths Detection (Edgewood, MD).

Another biodetection system first adapted for the detection of biothreat agents during Desert Storm was the fiber optic biosensor<sup>21</sup>. Capture antibodies are immobilized on the fiber surface and the sample flowed over the fiber. Any target present binds to the capture antibodies and then binds a dye-labeled antibody to form a fluorescent complex. Laser light at the surface of the fiber excites the complex and generates a signal. Subsequent versions of the sensor were fabricated to analyze four fibers simultaneously, miniaturized and automated. A ten-pound system, including a ram-air cyclone for particle collection, was flown on small, unmanned planes (Figure 5) and demonstrated the capability to collect aerosolized bacteria, identify the bacteria five minutes later, and transmit the information to an operator on the ground<sup>22-24</sup>.



Figure 5. The unmanned plane used to collect and identify aerosolized bacteria in field trials at Dugway Proving Ground, UT. The plane carried a ten-pound payload including a cyclone air sampler and 4-probe fiber optic biosensor.

Currently, Research International (Monroe, WA) is marketing a fully automated, man-portable fiber optic biosensor called the RAPTOR (Figure 6). The RAPTOR weighs 12 pounds including batteries, accepts samples added manually or automatically from an air sampler, and has been evaluated by the US Marines for monitoring drinking water loaded on Navy ships. The fiber optic biosensor has also been successfully used for detection of pathogens in food<sup>25-26</sup>, water<sup>27-28</sup>, clinical fluids<sup>25, 29</sup> and environmental samples<sup>30</sup>. It is simple to operate, the fiber probes and fluorescent reagents can be reused after negative samples, and can test for four to eight targets simultaneously<sup>31-32</sup>.

Probably the most sensitive biosensor for rapid screening has been the ORIGIN electrochemiluminescence system (IGEN, Gaithersburg, MD). The primary reason for the ORIGIN's enhanced sensitivity is that it preconcentrates the target prior to the assay. Immunomagnetic beads are



Figure 6. US Marine using the RAPTOR to test for toxins and pathogens in drinking water in Bahrain.

used to recognize and capture the target onto a magnetized anode. Detection is accomplished by addition of a tracer antibody labeled with  $\text{Ru}(\text{bpy})_3^{2+}$ ; excitation of the  $\text{Ru}(\text{bpy})_3^{2+}$  label results in emission of photons by chemiluminescence. Inclusion of an immunomagnetic separation step renders this system particularly suitable for analysis of foods and environmental samples where a target preconcentration step significantly lowers the limit of detection<sup>33-36</sup>. For detection of multiple analytes, parallel analyses are performed, using up to eight separate substrates in parallel. In order to avoid interferences from the sample matrices, conditions may need to be worked out separately for each sample type. Assays are handled sequentially, but the initial steps can be conducted in parallel during the 15-20 minute incubation steps and the ECL signals evaluated at 1-minute intervals. Notwithstanding these issues, sensitivities of 100-1000 cfu/mL for bacteria in have been reported in matrices as complex as food and soils. The electrochemiluminescence devices are being widely used in forward and mobile laboratories for clinical, environmental, and forensic analyses.

Magnetic beads have been used in a completely different way in the Force Differentiation Biosensor in which the fluorescently labeled, antibody-coated beads are used in a sandwich assay on the surface of a transparent filter, and the beads that are not attached to the target are removed using a magnet. This decreases the background from loosely adsorbed fluorescent beads and significantly increases the signal/background ratio to lower the limit of detection. Whitman and colleagues report detection limits of 100 pg/mL for ovalbumin and 10,000 cfu/mL for *Bacillus globigii*<sup>37</sup>.

Several investigators have explored lab-on-a-chip microfluidic approaches for bioagent detection in order to produce smaller, more easily automated systems. The concept is that even if each microchannel is responsible for a single assay, many channels can be operated in parallel for multianalyte sensing. Of the reports to date, the Sandia group has probably come the closest to making a fieldable sensor. They have demonstrated the capability of distinguishing between different toxins based on electrophoretic mobility<sup>38</sup>, but development of the capability for distinguishing between significant numbers of pathogens is still an ongoing process. In addition, as with other very small microfluidic systems, the utility of the device in dirty, complex sample matrices remains to be determined (Figure 7).

As mentioned in the first section, the use of real-time PCR for high sensitivity detection of relatively limited numbers of analytes is well established in the field thanks in particular to the use of the Ruggedized Advanced Pathogen Identification Device (R.A.P.I.D; Idaho Technology, Salt Lake City, UT) by the US military in the last few years. Samples must be manually prepared to separate oligonucleotides from other sample matrix components prior to the analysis, but the amplification of target DNA can be accomplished in 30-60 minutes and the resulting limits of detection are very





Figure 7. MicroChemLab system developed at Sandia National Laboratory<sup>38</sup>.

low (femtomoles). The R.A.P.I.D. and its case weigh 30 pounds with the rest of the required equipment bringing the total weight to 50 pounds (Figure 8).



Figure 8. R.A.P.I.D. automated PCR system.

Cepheid has improved on the automation of the PCR reaction by incorporating a sample preparation unit in their automated device<sup>39-41</sup> which automatically produces purified DNA for amplification (Figure 9). The GeneXpert technology is being used for monitoring post office sorting machines for anthrax contamination in the US ([www.Cepheid.com/pages/press](http://www.Cepheid.com/pages/press); March 22, 2004). It is very specific and very sensitive, and the assay time is shorter than for most PCR systems, but the cost of the reagents makes it expensive to operate on a routine basis.

#### 4. BIOSENSORS FOR MANY TARGETS

With the focus on biological threats shifting from nations to terrorist organizations, the type of potential agents that might be employed has



Figure 9. Cepheid GeneXpert for automated sample preparation and PCR analysis. (www.Cepheid.com; March 18, 2004).

broadened and the targets have shifted from military to civilian. These changes significantly expand the number of biological threats that we need to be able to detect. For this reason, the number of simultaneous assays that should be performed on any sample have grown from numbers like 4-8 to 40-80 or even 400-800, depending on the scenario in mind. DNA array technology demonstrated the capacity to detect thousands of targets simultaneously, and similar approaches are being investigated for biothreat detection and confirmation. The majority of highly multiplexed biosensors described to date rely on an array of biomolecules to capture the target from a solution and then measure a label co-immobilized in a capture molecule-target-label complex. The identity of the target is determined from the position of the complex in the two-dimensional array on the sensor surface. Methods for measurement include fluorescence, light scatter, magnetometry and electrical resistance.

The Array Biosensor developed at the Naval Research Laboratory (NRL) is an automated, portable detection device for simultaneous analysis of up to six samples for multiple analytes with the size of a shoebox (Figure 10)<sup>42-43</sup>.

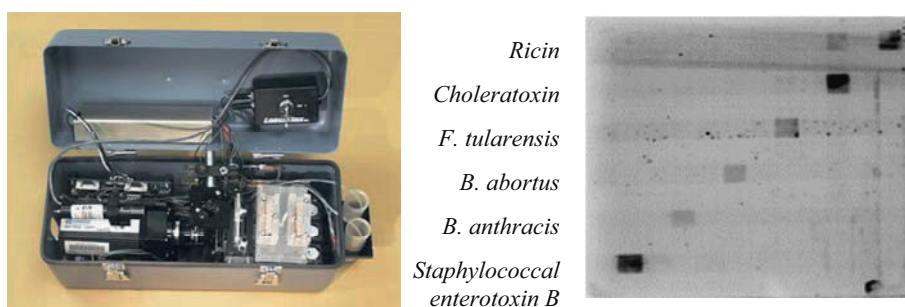


Figure 10. The automated, portable Array Biosensor (Golden et al., 2004) and an image from an array used to detect six samples simultaneously for six biothreat agents in 12 minutes<sup>49</sup>.

The biochemical component of the multi-analyte biosensor consists of a patterned array of biological recognition elements immobilized on the surface of a planar waveguide. A fluorescence assay is performed on the patterned surface, yielding an array of spots excited using evanescent illumination. Signal transduction is accomplished by means of a diode laser for fluorescence excitation and a CCD camera for image capture. Data analysis software has been developed to quantify the fluorescent signals in each spot. The assays are fast, sensitive, and specific, even in the presence of complex sample components<sup>14, 44-46</sup>. Capture molecules used for the detection of toxins and bacteria include antibodies, gangliosides, peptides and siderophores as the recognition elements. Limits of detection using antibodies are typically 0.1-1 ng/mL for toxins<sup>47</sup> and 1000-10,000 cfu/mL for bacteria<sup>48</sup>. Analysis of 144 different spots simultaneously has become routine and both positive and negative controls can be incorporated with every assay. Assays have been demonstrated in clinical fluids, liquid and homogenized foods, and environmental samples. Constellation Technologies and Siemens Corp. have collaborated to produce a modified version of the array biosensor for continuous monitoring of post office sorting machines that produce assays in less than 15 minutes on samples collected every minute; no sample preparation is required and there is no interference from the dust or fluorescent particles derived from mail.

McDevitt and colleagues have created another type of array using silica chips micromachined to include flow-through wells. Beads coated with capture molecules are placed in the wells and the sample flows through the chip. Target is captured and detected using a fluorescently labeled tracer, such as an antibody or aptamer. Called the Electronic Tongue<sup>50</sup>, the sensor has the advantage of efficient exposure of the sample solution to the capture surface, but potential disadvantages of susceptibility to clogging and potential difficulty for mass production (Figure 11).

Fiber optic biosensors have also been incorporated into array formats for detecting hundreds to thousands of targets simultaneously<sup>51-52</sup>. Thousands of fibers are incorporated into bundles and the ends etched to form wells.

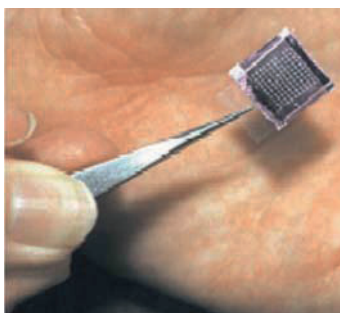


Figure 11. Flow through chip which provides the basis for the Electronic Tongue biosensor ([www.cm.utexas.edu/mcdevitt/tastechip.htm](http://www.cm.utexas.edu/mcdevitt/tastechip.htm), March 22, 2004).

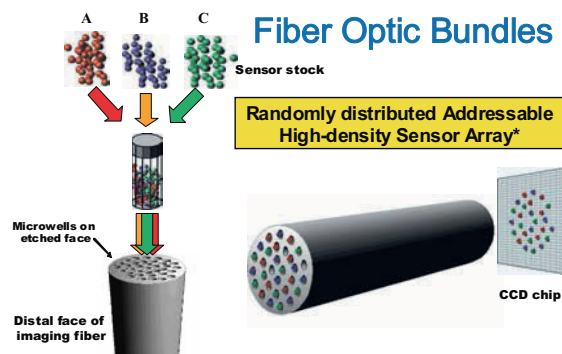


Figure 12. The high density biosensor based on a fiber optic bundle. Figure provided by Dr. David Walt (Tufts University, Boston, MA).

Fluorescent, color-coded beads, coated with capture molecules, are randomly deposited in the wells. Upon binding the target, a fluorescent signal of a third color is generated. The identity of the positive bead can be determined by its color code. Since multiple beads are present for each target, replicate positive signals increase the reliability of the response and lower the limit of detection. Walt and his colleagues have demonstrated that this technology can be used for detection using DNA probes, antibodies, enzymes, aptamers, and genetically engineered bacteria. Illumina, Inc. (San Diego, CA) currently markets systems using this technology for interrogating DNA arrays (Figure 12).

Colton and colleagues<sup>54</sup> (Figure 13) use the magnetic beads as a label in DNA hybridization assays and a 64-target magnetometer array (plus two control regions) to read the signal generated upon binding. Sensitivity limits of  $<1$  fM suggest that this technique might be useable for DNA detection without amplification<sup>53-55</sup>.

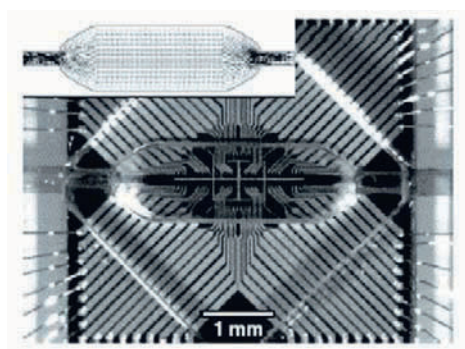


Figure 13. The magnetoresistor chip is covered with a flow cell for the introduction of sample after immobilization of an array of DNA probes. The photo shows a diffuser channel placed over the 65 magnetoresistor sensors on the chip<sup>54</sup>.

Vo-Dinh and colleagues at Oak Ridge National Laboratory have published a series of papers describing an array biosensor built around a CMOS chip<sup>56-59</sup> which currently uses a porous membrane as the sensing surface. In the most recently published version (Stratis-Collum et al., 2003), the system uses a 635 nm laser beam diffracted into 16 separate beams corresponding to the number of elements in a specially configured CMOS chip which includes application-specific signal amplification and filtering circuitry. The individual photosensors in the  $4 \times 4$  array are  $900 \mu\text{m}^2$  in size. The sensitivity of the system for measuring directly labeled IgG was 130 ng/mL<sup>58</sup>, which is not as good as obtained by the groups using CCD cameras; however, the sensitivity was significantly enhanced with the addition of an enzymic amplification method<sup>59</sup>. While the increased number of biochemical steps will complicate automation of the assays, this system has the advantage that the detector is very small.

Flow cytometry is also being used for the detection of biological threat agents. In one system, beads coded with two colors of dye are coated with capture molecules (Figure 14). They are mixed with the sample containing target and fluorescent antibodies to targets of interest. The beads, targets,

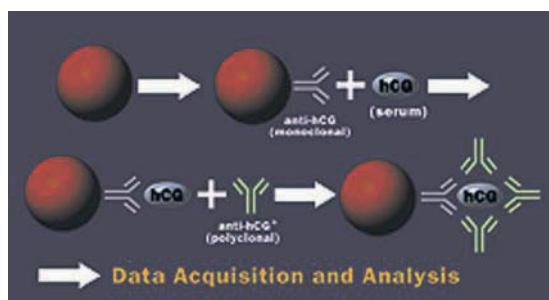


Figure 14. Homogeneous assay used with the FlowMetrix systems<sup>61</sup>.

and fluorescent antibodies form a complex that can be distinguished by the signal from the three colors of fluorescence. The FlowMetrix System (Luminex, The Woodlands, TX) is designed to simultaneously detect 64 different coded beads<sup>60</sup>. To date the Flow Metrix has been primarily used with immunoassays. The system seems to work well with relatively clean samples such as those collected from air, but large particulates may clog the nozzle in applications using more complex sample matrices. Furthermore, since the analyses are homogeneous, they may be susceptible to high dose hook effects.

DNA arrays certainly offer an extremely high degree of multiplex capability for testing for multiple targets simultaneously in confirmatory assays. As the methods for detecting hybrids on the arrays improve, perhaps it will be possible to eliminate the requirement for PCR. PCR does amplify targets of interest to levels where detection is currently possible, but the

number of targets that can be simultaneously amplified is less than 10. Vora et al.<sup>62</sup> have just reported a method for amplifying all genes in a prep and using a microarray to analyze which pathogens are present; this approach could significantly increase the amount of information to be gleaned from a single DNA microarray. Thus automation, miniaturization, and systems integration will increase in importance for producing microarray systems for less technically sophisticated users. A first step in the automation of sample preparation and DNA microarray production has been reported by Affimetrix (Santa Clara, CA)<sup>63</sup>. A single integrated system, embossed in plastic, handles the sample from introduction to microarray formation (Figure 15). Krihak and colleagues have reported a stacked device for BW agents that combines an antibody capture device with elution and DNA analysis<sup>64</sup>, but the actual concentration of bacteria captured in the small volume interrogated was quite high.

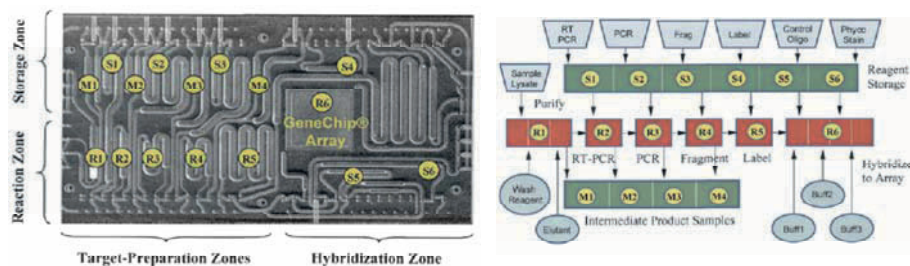


Figure 15. Miniaturized integrated system for DNA extraction and hybridization to a microarray<sup>63</sup>.

## 5. CONCLUSIONS

To address the need for detection of biological threat agents, biosensor need to be commercially produced in formats that are user friendly, fully automated, low cost, and small enough for the particular scenario of use. Obviously, a system engineered for continuous surveillance of a fixed site can be more bulky than a man-portable system and can include larger supplies of reagents. However, the storage and reliability requirements may also be more rigorous for a system designed to operate with no human intervention for extended periods. Reagents for continuous monitoring systems must generally be less expensive or reusable, compared to those in devices intended to be used only on rare occasions. The level of sensitivity required, specificity demanded, and tolerance for false positive responses also vary significantly depending on the intended use. In designing or selecting a biosensor, the operating parameters, logistical burden and life cycle costs must be fully considered.

A feature of biosensors that should be more fully appreciated by the counterterrorism community is their potential for dual use. Not only will commercial production be more sustainable if there is also a civilian application that produces a steady market demand, but users will have more confidence in a system that becomes thoroughly validated in a more predictable application. If the civilian application is one that also employs potential first responders, such as emergency room staff, veterinarians, or water treatment technicians, such individuals will more fully appreciate the value and limits of the technology.

Plenty of biosensor technologies work in the lab. Yet as soon as targets are tested in samples other than laboratory buffers, many of these technologies fall by the wayside due to interferences with the biochemistry, optoelectronics, or fluidics. The second biggest hurdle is the degree to which the technologies can be automated for wider use; multi-step protocols and sensitive reagents are not well adapted for use in continuous monitoring or by civilian populations. New microfluidic technologies may help (Hewish, 1998), but the fact that users frequently need to interrogate relatively large volumes for very low numbers of targets limits the amount of size reduction that is feasible. Array technologies offer perhaps the brightest horizon with the potential to analyze samples for so many different threats simultaneously.

## ACKNOWLEDGEMENTS

This work was supported by NIH RO1 grant EB02-002. Any opinions are those of the author and not the US Navy or Department of Defense.

## REFERENCES

1. Hewish M., Chem-bio warfare, surviving cbw detection and protection: what you don't know, *International Defense Rev* 1997; 30(003): 30-48.
2. Casagrande R. Technology against terror. *Scientific American* 83-87, Oct. 2002.
3. Bryden W.A., Benson R.C., Ko H.W., Donlon M., *Universal agent sensor for counterproliferation applications*, Johns Hopkins APL Technical Digest. 18:302-308, 1997.
4. Pancrazio J.J. (Ed.) Special Issue: Cell-based Biosensors, *Biosens. Bioelectron.* 2001; 16: 427-608.
5. Steichen C., Chen P., Kearney J.F., Turnbough C.L., Identification of the immunodominant protein and other proteins of the *Bacillus anthracis* exosporium, *J. Bacteriol.* 2003; 185:1903-1910.
6. Emanuel P.A., Dang J., Gebhardt J.S., Aldrich J., Garber E.A.E., Kulaga H., Stopa P., Valdes J.J., Dion-Schultz A., Recombinant antibodies: a new reagent for biological agent detection, *Biosens. Bioelectron.* 2000; 14:751-759.

7. Hayhurst A., Happe S., Mabry R., Koch Z., Iverson B.L., Georgiou G., Isolation and expression of recombinant antibody fragments to the biological warfare pathogen *Brucella melitensis*, *J. Immunol. Meth.* 2003; 276:185-196.
8. Park S.-J., Taton T.A., Mirkin C.A., Array-based electrical detection of DNA using nanoparticle probes, *Science* 2002; 295:1503-1506.
9. Brody E.N., Willis M.C., Smith J.D., Jayasena S., Zichi, D. Gold, L., The use of aptamers in large arrays for molecular diagnostics, *Molecular Diagnostics* 1999; 4(4):381-388
10. Bruno J.G., Kiel J.L., In vitro selection of DNA aptamers to anthrax spores with electrochemiluminescence detection, *Biosens. Bioelectron.* 1999; 14:457-464.
11. Golden M.C., Collins B.D., Willis M.C., Koch T.H., Diagnostic potential of PhotoSELEX-evolved ssDNA aptamers, *J. Biotechnol.* 2000; 81:167-178.
12. Zichi D., Koga T., Greef C., Ostroff R., Petach H., Photoaptamer technology: development of multiplexed microarray protein assays, *Clin. Chem.* 2002; 48:1865-1868.
13. Song X., Swanson B.I., Direct, ultrasensitive, and selective optical detection of protein toxins using multivalent interactions, *Anal. Chem.* 1999; 71:2097-2107.
14. Rowe-Taitt C.A., Cras J.J., Patterson C.H., Golden J.P., Ligler F.S., A ganglioside-based assay for cholera toxin using an array biosensor, *Anal. Biochem.* 2000a; 281:123-133.
15. Fang Y., Frutos A.G., Lahiri J., Ganglioside microarrays for toxin detection, *Langmuir* 19:1500-1505, 2003.
16. Mason H.Y., Lloyd C., Dice M., Sinclair R., Ellis W., Powers L., Taxonomic identification of microorganisms by capture and intrinsic fluorescence detection, *Biosens. Bioelectron.* 2003, 18:521-527.
17. Emanuel P.A., Biosecurity and bioterrorism. Biodefense Strategy, Practice, and Science, 2003, 1:131-137.
18. Walt, D.R., Franz, D.R., Biological warfare detection, *Anal. Chem.* 2000; 738:A-746-757.
19. Dill K., Song J.H., Blomdahl J.A., Olson J.D., Rapid, sensitive and specific detection of whole cells and spores using the light-addressable potentiometric sensor, *J. Biochem. Biophys. Meth.* 1997; 3:161-166.
20. Uithoven K.A., Schmidt J.C., Ballman M.E., Rapid identification of biological warfare agents using an instrument employing a light addressable potentiometric sensor and a flow-through immunofiltration-enzyme assay system, *Biosens. Bioelectron.* 2000, 14:761-770.
21. Ogert R.A., Shriver-Lake L.C., Ligler F.S., Toxin detection using a fiber optic-based biosensor, *Proc. SPIE.* 1885:11-17, 1993.
22. Ligler F.S., Anderson G.P., Davidson P.T., Foch R.J., Ives J.T., King K.D., Page G., Stenger D.A., Whelan J.P., Remote sensing using an airborne biosensor, *Environ. Sci. Technol.* 1998a; 32: 2461-2466.
23. Hewish M., On alert against the bioagents, *International Defense Rev.* 31(011), 53 pp., 1998.
24. Anderson G.P., King K.D., Cuttino D.S., Whelan J.P., Ligler F.S., MacKrell J.F., Bovais C.S., Indyke D.K., Foch R.J., Biological agent detection using an airborne biosensor, *FACT* 1999; 3:307-314.
25. Tempelman L.A., King K.D., Anderson G.P., Ligler F.S., Quantitating staphylococcal enterotoxin B in diverse media using a portable fiber optic biosensor, *Anal. Biochem.* 1996; 223: 50-57.
26. Demarco D.R., Lim D.V., Detection of *Escherichia coli* O157 : H7 in 10-and 25-gram ground beef samples with an evanescent-wave biosensor with silica and polystyrene waveguides, *J. Food Protect.* 2002; 65: 596-602.



27. Narang U., Anderson G.P., King K.D., Liss H.S., Ligler F.S., Enhanced biosensor performance using an avidin-biotin bridge for antibody immobilization, *Proc. SPIE*. 2980:187-194, 1997.
28. Anderson G.P., Rowe-Taitt C.A., Water quality monitoring using an automated portable fiber optic biosensor: RAPTOR, *Proc. SPIE* 4206:58-63, 2001.
29. Cao L.K., Anderson G.P., Ligler F.S., Ezzell J., Detection of Yersinia pestis F1 antigen by a fiber optic biosensor, *J. Clin. Micro.* 1995; 33: 336-341.
30. King K.D., Vanniere J.M., LeBlanc J.L., Bullock K.E., Anderson G.P., Automated fiber optic biosensor for multiplexed immunoassays, *Environ. Sci. Technol.* 2000; 34: 2845-2850.
31. Anderson G.P., King K.D., Gaffney K.L., Johnson L.H., Multianalyte interrogation using the fiber optic biosensor, *Biosens. Bioelectron.* 2000; 14: 771-778.
32. Yu H., Bruno J.G., Immunomagnetic-electrochemiluminescent detection of Escherichia coli O157 and Salmonella typhimurium in foods and environmental water samples, *Appl. Environ. Micro.* 1995; 62: 587-592.
33. Anderson G.P., Lingerfelt B.M., Taitt C.R., Eight analyte detection using a four-channel optical biosensor, *Sensor Letters* 2004; 2 (1): 18-24.
34. Bruno J.G., Yu H., Immunomagnetic electrochemiluminescent detection of Bacillus anthracis spores in soil matrices, *Appl. Environ. Micro.* 1996; 62:3474-3476.
35. Crawford C.G., Wijey C., Fratamico P., Tu S.I., Brewster J., Immunomagnetic-electrochemiluminescent detection of E. coli O157:H7 in ground beef, *J. Rapid Meth. Auto. Micro.* 2000; 8: 249-264.
36. Kuczynska E., Boyer D.G., Shelton D.R., Comparison of immunofluorescence assay and immunomagnetic electrochemiluminescence in detection of Cryptosporidium parvum oocysts in karst water samples, *J. Microbiol. Meth.* 2003; 53: 17-26.
37. Lee G.U., Metzger S., Natesan M., Yanavich C., Dufrêne Y.F., Implementation of force differentiation in the immunoassay, *Anal. Biochem.* 2000; 287: 261-271.
38. Linder D., The  $\mu$ ChemLab™ project: micrototal analysis system R&D at Sandia National Laboratories, *Lab on a Chip*. 2001; 1: 15N-19N.
39. Belgrader P., Okuzumi, M., Pourahmadi, F., Borkholder, D., Northrup, M.A., A microfluidic cartridge to prepare spores for PCR analysis, *Biosens. Bioelectron.* 2000; 14: 849-852.
40. Taylor M.T., Belgrader P., Joshi R., Kintz G.A., Northrup M.A., Fully automated sample preparation for pathogen detection performed in a microfluidic cassette. In *Micro Total Analysis Systems 2000*, Berg, A. van den, Olthuis, W., Bergveld, P., eds. Kluwer Academic Publishers, The Netherlands, pp 670-672, 2000.
41. Taylor M.T., Belgrader P., Furman B.J., Pourahmadi F., Kovacs G.T.A., Northrup M.A., Lysing bacterial spores by sonication through a flexible interface in a microfluidic system, *Anal. Chem.* 2001; 73: 492-496.
42. Taitt C.R., Anderson G.P., Lingerfelt B.M., Feldstein M.J., Ligler F.S., Nine-analyte detection using an array-based biosensor, *Anal. Chem.* 2002; 74: 6114-6120.
43. Golden J.P.; Taitt C.R.; Shriver-Lake L.C.; Shubin Y.S.; Ligler F.S., A portable automated multianalyte biosensor, *Talanta*, 2005; 65 (5): 1078-1085.
44. Ligler F.S., Conrad D.W., Golden J.P., Feldstein M.J., MacCraith B.D., Balderson S.D., Czarnaski J., Rowe C.A., Array biosensor for multi-analyte sensing, *Proc. SPIE*. 3258:50-55, 1998b.
45. Rowe C.A., Scruggs S.B., Feldstein M.J., Golden J.P., Ligler F.S., An array immunosensor for simultaneous detection of clinical analytes, *Anal. Chem.* 1999; 71: 433-439.
46. Shriver-Lake L.C., Shubin Y., Ligler F.S., Detection of staphylococcal enterotoxin B in spiked food samples, *J. Food Protect.* 2003; 66: 1851-1856.
47. Ligler F.S., Taitt C.R., Shriver-Lake L.C., Sapsford K.E., Shubin Y., Golden J.P., Array biosensor for detection of toxins, *Anal. Bioanal. Chem.* 2003; 377: 469-477.

48. Taitt C.R., Golden J.P., Shubin Y.S., Shriver-Lake L.C., Sapsford K.E., Rasooly A., Ligler F.S. A portable array biosensor for detecting multiple analytes in complex samples, *J. Microbiol. Ecol.* 2003; Feb 9.
49. Rowe-Taitt C.A., Hazzard J.W., Hoffman K.E., Cras J.J., Golden J.P., Ligler F.S., Simultaneous detection of six biohazardous agents using a planar waveguide array biosensor, *Biosens. Bioelectron.* 2000b; 15: 579-589.
50. Goodey A., Lavigne J.J., Savoy S.M., Rodriguez M., Currey T., Tsao A., Simmons G., Wright J., Yoo S.-J., Sohn Anslyn E.V., Shear J.B., Neikirk D.P., McDevitt J.T., Development of multi-analyte sensor arrays composed of chemically derivatized polymeric microspheres localized in micromachined cavities, *J. Am. Chem. Soc.* 2000b; 123: 2559-2570.
51. Michael K.L., Taylor L.C., Schultz S.L., Walt D.R., Randomly ordered addressable high-density optical sensor arrays, *Anal. Chem.* 1998; 70: 1242-1248.
52. Epstein J.R., Walt D.R., Fluorescence-based fibre optic arrays: a universal platform for sensing, *Chem. Soc. Rev.* 2003; 32: 203-214.
53. Rife J.C., Miller M.M., Sheehan P.E., Tamanaha C.R., Tondra M., Whitman L.J., Design and performance of GMR sensors for the detection of magnetic microbeads in biosensors, *Sensor Actuat A-Phys.* 2003; 107: 209-218.
54. Tamanaha C.R., Whitman L.J., Colton R.J., Hybrid macro-micro fluidics system for a chip-based biosensor, *J. Micromech. Microeng.* 2002; 12: N7.
55. Edelstein R.L., Tamanaha C.R., Sheehan P.E., Miller M.M., Baselt D.R., Whitman L.J., Colton R.J., The BARC biosensor applied to the detection of biological warfare agents, *Biosens. Bioelectron.* 2000; 14: 805-813.
56. Vo-Dinh T., Development of a DNA biochip: Principle and applications, *Sensor Actuat B-Chem.* 1998; 51: 52-59.
57. Vo-Dinh T., Alarie J.P., Isola N., Landis D., Wintenberg A.L., Ericson M.N., DNA biochip using a phototransistor integrated circuit, *Anal. Chem.* 1998; 71: 358-363.
58. Moreno-Bondi M.C., Alarie J.P., Vo-Dinh T., Multianalyte analyses system using an antibody-based biochip, *Anal. Bioanal. Chem.* 2003; 375: 120-124.
59. Stratis-Cullum D.N., Griffin G.D., Mobley J., Vass A.A., Vo-Dinh T., A miniature biochip system for detection of aerosolized *Bacillus globigii* spores, *Anal. Chem.* 2003; 75: 275-280.
60. Fulton R.J., Mc Dade R.L., Smith P.L., Kienker L.J., Kettman J.R.Jr., Advanced multiplexed analysis with the FloMetrix system, *Clin. Chem.* 1997; 43: 1749-1756.
61. McDade R.L., Fulton R.J., True multiplexed analysis by computer-enhanced flow cytometry, *Medical Device and Diagnostic Industry*, 6 pp., April 1977.
62. Vora G.J., Meadors C.E., Stenger D.A., Andreadis J.D., Nucleic acid amplification strategies for DNA microarray-based pathogen detection, *Appl. Environ. Microbiol.* 2004; 70: 3047-3054.
63. Anderson R.C., Xing S., Bogdan G.J., Fenton J., A miniature integrated device for automated multistep genetic assays, *Nucleic Acids Research.* 2000; 28: e60 .
64. Yang J.M., Bell B., Huang Y., Tirado M., Thomas D., Forster A.H., Haigis R.W., Swanson P.D., Wallace B., Martinsons B., Krihak M., An integrated stacked microlaboratory for biological agent detection with DNA and immunoassays, *Biosens. Bioelectron.* 2002; 17: 605-618.

## Chapter 22

### **REVIEW OF METHODS OF OPTICAL GAS**

#### *Detection by Direct Optical Spectroscopy, with Emphasis on Correlation Spectroscopy*

John P. Dakin and Paul Chambers

*Optoelectronics Research Centre*

*University of Southampton*

*SO17 1BJ, Southampton, U.K.*

### **1. INTRODUCTION**

This chapter reviews the development of optical gas sensors, starting with an initial emphasis on optical-fibre remoted techniques and finishing with a particular focus on our own group's work on highly selective methods using correlation spectroscopy. This latter section includes extensive theoretical modelling of a correlation spectroscopy method, and compares theory with practice for a CO<sub>2</sub> sensor.

Gas sensors are of importance for a variety of environmental, industrial, medical, scientific and even domestic applications. The gas may be, for example, hazardous to human health, an atmospheric pollutant, or important, in terms of its concentration, for an industrial or medical process. Apart from systems merely providing an alarm signal, it is frequently required to obtain accurate real-time measurements of the concentration of a particular target gas, often in a mixture of other gases.

Gas detection methods may be split into two groups, (i) direct methods, which monitor a physical parameter of the target gas, and (ii) indirect methods, which use a chemical reaction or indicator to show the concentration of the gas being sensed. This division of methods may be further split into optical sensing techniques and non-optical techniques. This review will predominantly focus on direct optical-spectroscopy fibre sensing techniques.

A list of commonly used direct and indirect methods of gas detection methods is given in Table 1, listing their principal advantages and disadvantages.

Table 1. Advantages and Disadvantages of Gas Detection Method.

<i>Method</i>	<i>Advantages</i>	<i>Disadvantages</i>
	<b>Direct Methods</b>	
Optical spectroscopy: measurement of optical absorption, emission or scattering	Offers a direct and rapid, and often highly selective means, of measuring gas concentration with good sensitivity.	The gas must have a significant and distinct absorption, emission or scattering in a convenient region of the optical spectrum.
Mass spectrometry	Very accurate and highly selective means of detecting concentrations of gas, including isotope abundance, etc.	slowly acting / very bulky / very expensive. Not easy to use on-line, as gas sampling necessary.
Gas chromatography	Very accurate and highly selective means of detecting concentration.	Very expensive Not easy to use on-line, as gas sampling necessary.
	<b>Indirect Methods</b>	
Interaction with a chemical indicator	Can be highly specific, if suitable indicator. Can measure total exposure over time (dosimetry), if a non-reversible reaction is used. Can allow operation at a convenient wavelength, when gas has no convenient absorption in that spectral range.	Poisoning can occur, and is easily fouled. Sensitive to groups of chemicals, e.g. acid gases, rather than to a specific gas. May exhibit non-reversible behaviour, which, in many cases, may be undesirable. May need water vapour present, to act as a catalyst, if "dry" reaction is too slow.
Sensors involving interaction with the surface of a semiconductor, or ceramic layer, e.g. (CHEMFETS and other electrochemical sensors)	Low cost. Can measure total exposure over time, if a non-reversible reaction is used.	Poisoning can occur. May exhibit non-reversible behaviour, which may be undesirable. May consume analyte.
Catalytically induced combustion and measurement of the heat change (Pellistor gas sensors)	Low cost and practical means of detecting presence of flammable gases.	Poisoning can occur. Sensitive to groups of gases, rather than specific gas in a group. If other flammable gas is present, may give reading which is not predictably related to the lower explosive limit (LEL).

Optical methods monitor the optical absorption/emission/scattering of a gas species at defined optical wavelengths. The distribution of this optical absorption/emission with wavelength provides an optical 'fingerprint' for any gas species present, and the magnitude typically shows the concentration.

Direct spectroscopic optical methods provide a fast, accurate and stable measurement of a gas species, provided that it has significant absorption or emission of optical radiation over a suitable wavelength band. The simplest absorption-based methods usually involve probing at one wavelength, where absorption occurs, and also at a wavelength chosen to be essentially free of any absorption of the target gas (also preferably not absorbed by any likely contaminant, or referencing errors will occur). A comparison of the received powers from these wavelengths enables the target gas concentration to be deduced.

The spectroscopic sensing of chemical species is not new. Most analytical chemistry laboratories possess at least one bench-top spectrophotometer for the recognition of a wide range of chemical species, based on their characteristic absorption, fluorescence or Raman-scattering spectra, and normally optical gas sensing methods use more dedicated versions of such spectrometers. However, simple sensor heads can also be addressed using these more complex laboratory spectrometers, using optical fibre extension leads with suitable focussing/collimation optics to first launch the collimated instrument beams into the small-area, wider-angle fibre aperture and then re-collimate the fibre exit beam to match the instrument.

It should be mentioned, in passing that, there are many remote free-space laser methods involving LIDAR. One of the most useful is DIAL (Differential Absorption LIDAR), where a dual-wavelength laser pulse is directed into the atmosphere and the time-varying back-scattered signatures from light at each of the two wavelengths are compared to determine the differential absorption as a function of distance along the path. A non-linear method called CARS (Coherent Anti-Stokes Raman Scattering) has also been used. These methods, and also several other more complex alternatives using multi-photon processes, are unsuitable for use with optical fibres. Also a full description of these would fill a chapter in its own right, so the focus of this review will be restricted to direct absorption methods.

## **2. USE OF OPTICAL FIBRES FOR REMOTE GAS DETECTION APPLICATION**

Optical fibre based optical detection systems offer a number of advantages over bulk optical sensing systems. The principal one is that a robust passive sensing head may be remoted from the monitoring station; a factor giving particular advantages in severe environments. This also allows

multiplexed networked systems to be developed, where a single interrogation unit can monitor many low-cost passive sensing heads via a predictable propagation medium in the optical cable. Conventional silica fibres have the disadvantage that transmission is restricted to the visible and near-infrared region (600 nm to 2000 nm). Fluoride and other fibres may be used to extend the operation of these sensors further into the infra-red, allowing accurate detection of gases with infrared absorption in the mid- and far-infra-red. Unfortunately, however, these fibres are expensive and far less robust. Optical fibre sensors are also generally believed to be safe for use in explosive atmospheres. However, the safety of optical fibre sensors is not unqualified as it has been established that in the case of very high powers, of the order of 100 mW, or greater in multi-mode fibre, explosive risks may present themselves<sup>1, 2</sup>. Optical fibres have a very small acceptance aperture, which severely restricts the amount of light that can be coupled into a fibre. Thus, the power launched into optical fibres from high-radiance near-infrared (NIR, ~700 nm~1.55  $\mu$ m) light emitting diodes (LEDs) is rarely above 1mW, even when large core optical fibres are used, and the spectral radiance of incandescent filament lamps is usually at least an order of magnitude less. Longer wavelength LEDs (>~1.55 $\mu$ m) often have an even lower spectral radiance. As the launched power is relatively low carefully designed light detection systems are required to produce practical sensors. With laser sources, there is no difficulty in achieving launch efficiencies of over 80% into multimode fibres, so higher powers can be launched, and the detection system constraints are eased substantially.

It was realised that narrow-linewidth diode lasers could readily be used in fibre-optic remoted environmental detection systems. Inaba<sup>3</sup> suggested the use of a dual-wavelength laser to realise a differential absorption method that could be used over many kilometres of low-loss optical fibre, provided that suitable gas absorption bands are present. This typically involves the comparison of the received power at two, or more, different wavelengths, each having passed through a remote measurement gas cell, so that the differential absorption of the gas sample could be used to infer the concentration of the target gas. Lasers offer excellent spectral radiance, and couple efficiently into optical fibres, but extreme care has to be taken to avoid problems arising with these highly coherent sources (see discussion later).

A laser-based detection system for NO<sub>2</sub> gas (which is an industrial hazard and common environmental pollutant) was developed by Koybayashi et al.<sup>4</sup>. This was achieved by splitting light, from an Ar-ion multi-line laser, into two paths, one passing through a measurement gas, and the other being transmitted directly to the measurement unit as a reference signal. The detection unit contained two filters to separate the two chosen laser lines, and these were then detected on separate optical receivers. One of these chosen laser lines coincided with a strong absorption line in the NO<sub>2</sub>

absorption spectrum, whilst the other absorption line was somewhat weaker, hence giving a differential absorption method, by which the concentration of  $\text{NO}_2$  in the measurement cell could be found. The system had an estimated detection limit of 17 ppm. The advantage of this dual-wavelength system was that the measurement was not dependent upon the optical power of a single source, which could drift, or the system transmission could be affected by optical alignment, surface contamination, etc. It was realised that the selection of light sources used in this type of detection system was not necessarily limited to lasers, but broad-band sources such as filtered incandescent lamps or LEDs could also be used.

Hordvik et al.<sup>5</sup> developed a fibre-optic system, for the remote detection of methane gas ( $\text{CH}_4$ ), see Figure 1. This system used a halogen lamp light source, which was alternately chopped into two separately filtered paths. One path was passed through a narrow-band interference filter, centred at the same wavelength as a strong absorption band of  $\text{CH}_4$  (Q-branch centred at  $1.666 \mu\text{m}$ ), whilst the other filter covered a broader spectral range, so had lower average absorption. These two complementary-modulated beams were combined by means of a fibre-coupler, with two output ports. Light from one was passed through a measurement cell to an optical detector (the measurement signal), and light from the other was passed directly to an optical detector (reference signal). By comparison of the optical powers in the narrow-band and broadband signal beams, i.e. those that had or had not passed through the measurement cell, it was possible to calculate the methane concentration.

A somewhat similar system, again based on the use of optical fibres and optical fibre couplers, but now using compact LED light sources, was developed by Stueflotten et al.<sup>6</sup> The schematic of the system is shown in Figure 2. Again, two different optical filter wavelengths were used, to give differential attenuation in strong and weak gas absorption regions. This was proposed for remote measurement in hazardous industrial environments, particularly off-shore oil platforms. Both of the systems above, i.e. those

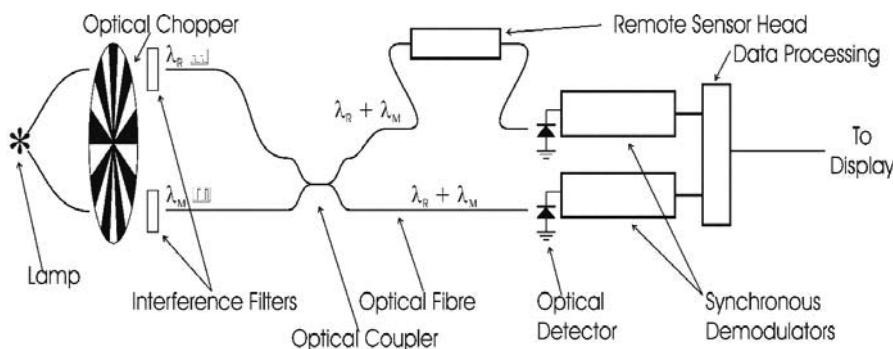


Figure 1. Schematic of a differential fibre-optic detection system (redrawn from diagram in Hordvik et al.).

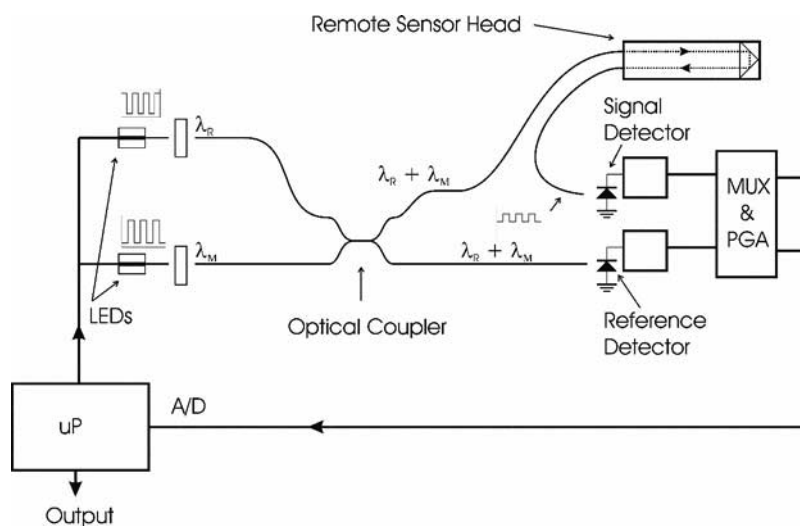


Figure 2. Schematic of the differential fibre-optic detection system (redrawn from diagram of Stueflotten et al.).

developed by Hordvik and Stueflotten, had a reported detection limit of approximately 5000 ppm (0.5% vol/vol).

### 3. SENSING USING INELASTIC PROCESSES

Other forms of spectrophotometric processes rely on Raman scattering. Raman scattering will now be briefly described, before our area of particular research interest, correlation spectroscopy, is discussed in detail.

Raman scattering involves the inelastic scattering of light, i.e. first absorption and then delayed re-emission of light at a different wavelength to that incident on the material. The Raman process represents a form of scattering in which an incident photon may gain energy from (the anti-Stokes Raman process), or donate energy to (the Stokes Raman process) a vibrational or rotational energy level in a material. This produces a re-emitted photon of different energy and, hence, of a different wavelength. A method of detection that exploits Raman spectroscopy was developed by Samson<sup>7</sup>, using the detection system shown in Figure 3. Raman scattering in gases is very weak, but usually occurs in narrow spectral lines.

In this system, the excitation laser excites the gas and a mirror is used to reflect back the incident light through the interaction zone. Another concave mirror reflector doubles the level of Raman light received by the collection lenses. The alternative inelastic scattering process of fluorescence is rare in gases, so is not commonly used for optical gas sensors, but fluorescence cannot be ignored when using Raman sensing, as, without care, it can cause



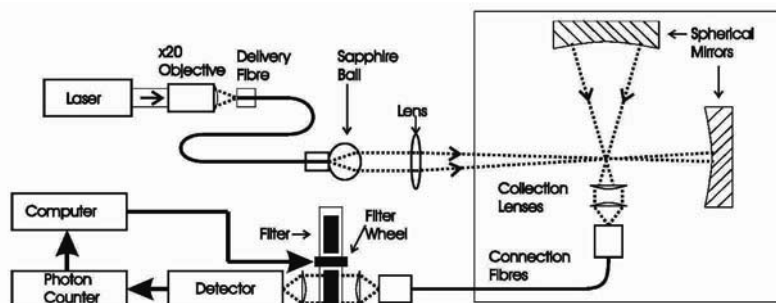


Figure 3. Schematic of gas sensor using Raman Scattering (Redrawn from Samson).

crosstalk if it occurs in optical glass components or at mirror surfaces. Fortunately, Raman lines for simple gases are narrow, whereas fluorescence emission is relatively broadband.

#### 4. COMB FILTER MODULATOR FOR PARTIALLY MATCHING SEVERAL SPECTRAL LINES

Rather than measuring on a single line, or using a broadband source to cover many, there are advantages in using some form of optical “comb” filter, with several periodic narrow transmission windows, to match several spectral lines simultaneously. Such a comb filter can be scanned through a set of gas lines to give an intensity modulation. The method has the advantage of better selectivity, as a synthetic multiple-narrow-line comb-filter spectrum allows simultaneous measurement on several spectral lines. This reduces the severe “speckle- pattern” interference effects, which can cause severe problems with laser sources. A method of doing this, with a scanned Fabry-Perot comb filter, has been demonstrated<sup>8, 9</sup> for methane detection. A sensitivity of 100 ppm methane was found by Dakin et al. The disadvantage of the Fabry-Perot filter is that it has a regular frequency spacing, whereas the gas lines are not normally equally spaced. An improved method is to use true correlation spectroscopy (see below), where a filter more exactly matching the gas lines is used. The area of correlation spectroscopy will be discussed in considerably more detail in the following section.

#### 5. CORRELATION SPECTROSCOPY TECHNIQUES

Optical absorption-based correlation spectroscopy is a means of selectively detecting, or “fingerprinting”, gases, in this work, of industrial importance. Optical correlation spectroscopy methods of gas detection are

ones that compare most or all of the usefully attainable spectral features of a target gas, eg. its absorption or emission spectrum, with a similar reference spectrum. This reference might be a synthetically-designed optical filter, or a sample of the gas itself, or even a stored computer record of the gas spectrum that can be compared to a spectrum measured with a spectrometer. In this way, the concentration of a chosen target gas may be deduced and, in most cases, the gas can be uniquely identified. This forms the basis of many highly selective gas sensors. The Fabry-Perot filter method discussed above clearly goes part-way to achieving this aim.

Although not as fundamentally sensitive as laser-based detection systems, which offer greater spectral intensity from the source and high detection contrast, when centred on a strong absorption line, correlation spectroscopy has many real-world advantages. Firstly, it can readily be arranged to be inherently self-referencing to the various factors that might cause optical intensity changes (e.g. light source variations, bending loss in fibres, etc.). Unlike laser systems, it is relatively immune to the problems that can occur with coherent sources, such as lasers, which can exhibit multi-path interference effects. These can be particularly troublesome in optical-fibre-based systems using laser-sources, due to inter-modal interference (modal noise) in the fibre. Even when using single-mode fibre, laser signals can be significantly affected by Fabry-Perot effects in connectors or lenses, or multi-path interference, for example if any cladding mode coupling occurs.

An early paper, which explored the possibility of selectively detecting a specified target gas by a correlation spectroscopy technique, was published by Goody in 1968<sup>10</sup> (Figure 4). Goody introduced a pressure modulation “cross-correlating spectrometer”, a device which involved the passing of light from an optical source through two sequential gas cells and an optical filter, before impinging on an optical detector. The first gas cell contained the gas volume to be analysed (the measurement cell) and the second (the reference cell) contained only the target gas (i.e. 100% concentration). Modulation of the pressure within the reference cell resulted in a modulation of the detected light power level at the optical detector that was indicative of

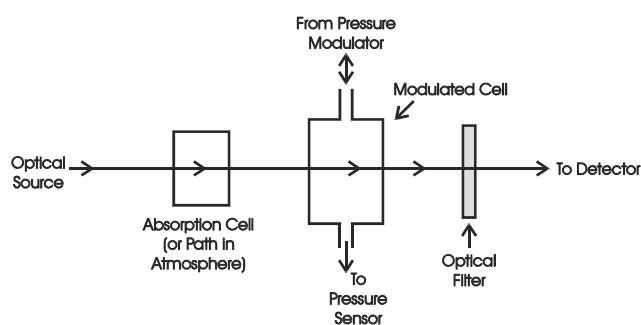


Figure 4. Pressure Modulation Spectroscopy System (Reproduced from Goody, 1968).

the concentration of the target gas present in the sample cell. The method showed excellent rejection of drifts in source power and had high rejection of contaminant gas. For example, a  $\text{NH}_3$  sensor was shown to give a 140 fold smaller signal, with an equivalent concentration of  $\text{N}_2\text{O}$  impurity in the measurement cell, even though the absorption of  $\text{N}_2\text{O}$  was actually significantly stronger in the band of interest.

In 1972, Taylor et al.<sup>11</sup> published details of a similar system, intended to measure remotely, from a satellite, the concentration of  $\text{CO}_2$  in the upper atmosphere. This method utilised the spectral emission of  $\text{CO}_2$  at 15  $\mu\text{m}$ . Herget et al.<sup>12</sup>, also developed a similar system. However, Herget arranged for a null reading by equalising the transmitted intensity of the reference gas cell with an alternately switched-in neutral density filter. As the concentration of the target gas in the measurement cell was changed, a positive modulation was observed. Conversely, as contaminant gas was introduced, a negative modulation was observed.

Another reported method of modulating the transmission of the reference cell was that of Stark modulation. This is the line-splitting effect that results when a high electric field is applied to a gas. It is only effective on molecules having a significant dipole moment, e.g.  $\text{H}_2\text{O}$ ,  $\text{CH}_4$  etc. Edwards and Dakin<sup>13</sup> investigated the use of Stark modulation for the detection of ammonia and water vapour, both of industrial significance, using optical fibre-based systems.

## 6. THE COSM METHOD OF CORRELATION SPECTROSCOPY

The remainder of this text will now focus on the complementary source modulation (CoSM) method of gas detection.

The CoSM technique<sup>14, 15</sup> involves the alternate on/off driving of two light sources in anti-phase, where light from the first source is passed through a reference cell containing the target gas (or gases) of interest. This now-partially-absorbed beam is then combined with a fraction of the direct (unaffected) light from the second source. The optical combination of these beams is made in such a proportion that, after appropriate filtering to match the gas band, there is no net intensity modulation. This combined beam is then used to probe the target gas. As the beam component that has already passed through the reference gas sample now has less optical energy at the wavelengths of the narrow absorption lines of the gas, there is now less energy available to be absorbed in the measurement cell. Thus, an intensity modulation of the combined beam will be re-established when it subsequently passes through the measurement cell, provided that this cell contains a quantity of the target gas of interest. This induced intensity modulation is related to the target gas concentration, because only

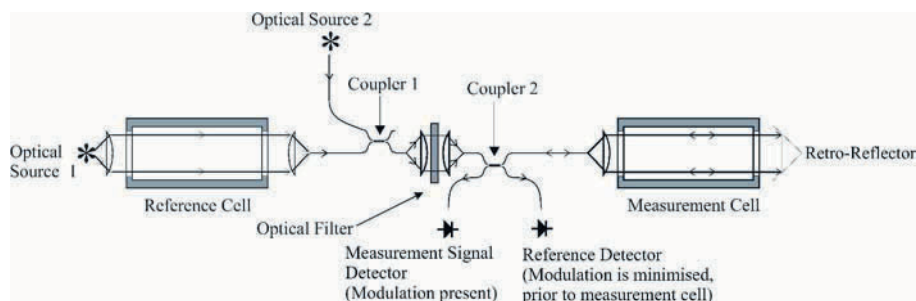


Figure 5. Schematic of a Complementary Source Modulation method of correlation spectroscopy.

differential absorption between the two beam components can give rise to a signal modulation. Other gases will normally have a zero, or greatly reduced, effect.

A fibre optic-based schematic of a CoSM correlation spectroscopy gas sensing system is shown in Figure 5. The reference signal detector receives a fraction of the combined light, ensuring balanced light powers at this point, and the measurement detector is used to evaluate any renewed intensity modulation arising from gas absorption in the measurement cell. The figure shows a retro-reflective arrangement for the measurement cell, which not only eases directional alignment of the collimator when small-area low noise detectors are used, but also causes the light to pass twice through the cell, thereby doubling the effective absorption path.

## 6.1 System Model

It is important to model a correlation spectroscopy system, firstly to predict performance, and also to aid the very important choice of optical filter (or choose the best LED or super-luminescent optical fibre source to give the optimal spectral output), in order to achieve the best detection performance or best selectivity possible. The length of the cells and the pressure of gas (or gas concentration) are also important parameters (although all simulated results described below are based on use of 1m long cells).

The first practically important system parameter to be modelled is the modulation index of the signal seen at the measurement detector. This is effectively a measure of the optical "contrast", and is the fractional intensity change, in the optical signal at this detector. A small fractional change with changing gas concentration (low contrast) would give a high susceptibility to environmental effects, such as dust particles passing through the cells or undesirable mechanical vibration. In addition, the optoelectronic feedback control scheme used to equalise the beams, before passing through the

measurement cell, has to be particularly well balanced to avoid systematic errors. It is therefore clearly highly desirable to achieve a high modulation index.

The modulation index is related to the transmission spectra of the gas-filled reference cell,  $T_{\text{Ref}}(\lambda)$ , the measurement cell, with its unknown gas concentration,  $T_{\text{Meas}}(\lambda)$ , and the optical filter,  $F(\lambda)$ , all of which are shown in Equation 1. If required, the source spectra can also be taken into account, by using additional spectral functions (although this will usually have little spectral variation over the linewidth of the gas band):

$$m = 2 \left( \frac{\int T_{\text{Ref}}(\lambda) T_{\text{Meas}}(\lambda) F(\lambda) d\lambda \int F(\lambda) d\lambda - \int T_{\text{Ref}}(\lambda) F(\lambda) d\lambda \int T_{\text{Meas}}(\lambda) F(\lambda) d\lambda}{\int T_{\text{Ref}}(\lambda) T_{\text{Meas}}(\lambda) F(\lambda) d\lambda \int F(\lambda) d\lambda + \int T_{\text{Ref}}(\lambda) F(\lambda) d\lambda \int T_{\text{Meas}}(\lambda) F(\lambda) d\lambda} \right) \quad (\text{Eq.1})$$

## 6.2 Simulation Results for the Detection of CO<sub>2</sub>

Using the modelling approach above, the predicted response of a CO<sub>2</sub> correlation spectroscopy system will now be shown. This requires knowledge of the transmission spectrum of CO<sub>2</sub> gas, so that predictions from the model can be made, for the expected modulation index, SNR (signal to noise ratio) and cross-sensitivity to a contaminant gas.

### 6.2.1 Description of the Absorption of CO<sub>2</sub> Gas Around 2 $\mu\text{m}$

Carbon dioxide gas (CO<sub>2</sub>) exhibits a set of relatively strong absorption bands at approximately 2  $\mu\text{m}$ , which coincides with the infra-red edge of the transmission band of silica optical fibres (see Figure 6). These absorption

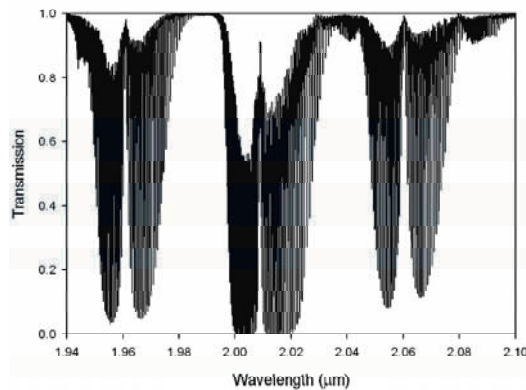


Figure 6. Transmission of 100% CO<sub>2</sub> gas over a 1 m path length at 1 Bar and 20 °C (transmission data obtained from HITRAN database).

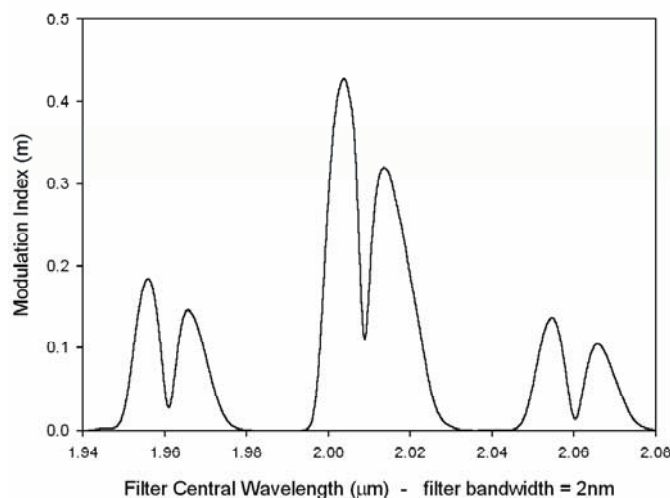


Figure 7. Modulation index ( $m$ ), as a function of filter centre wavelength, assuming the reference and measurement cells contain 100%  $\text{CO}_2$  gas at 1 Bar, 20 °C and are of 1m length. An optical filter with 2 nm FWHM bandwidth is assumed. This shows that, with this filter bandwidth, the maximum modulation index occurs at a filter centre wavelength of 2.004  $\mu\text{m}$ .

bands are composed of the  $3\nu_3$  absorption band and the two bands in the Fermi-tetrad<sup>16</sup>. The spectral data was extracted from the HITRAN gas spectra database<sup>17</sup>.

### 6.2.2 Prediction of Expected Modulation Index ('Optical Contrast')

Initially the variation of modulation index was calculated as the central wavelength of the Gaussian-shaped optical filter was changed, assuming a 2 nm Full Width at Half Maximum (FWHM) bandwidth (see Figure 7). This predicted a clear peak in modulation index at a filter centre wavelength of 2.004  $\mu\text{m}$ , where  $\text{CO}_2$  has a closely-spaced set of absorption lines. The optimum filter bandwidth for operating at this peak central wavelength was determined by plotting the modulation index as a function of filter bandwidth, as shown in Figure 8. This shows the peak in modulation index actually occurs when using as narrow an optical filter bandwidth as possible. However, it will be shown that such a narrow filter bandwidth is not a practical choice for either good SNR, as so little light is transmitted from a broadband source. Also, the use of a very narrow line-width can give poor selectivity and give rise to a high level of "modal noise" in optical fibre systems, as a result of selective mode coupling, that may greatly offset any advantages of the higher modulation index. Such intensity changes, which can occur whenever optical fibres carrying coherent signals are bent or even slightly moved, can be very problematic.

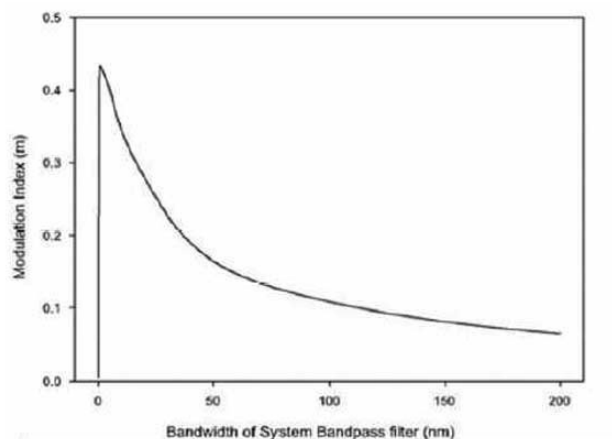


Figure 8. Variation of modulation Index (m) with optical filter bandwidth, assuming the 1m long reference and measurement cells contain 100% CO<sub>2</sub> gas at 1 Bar/20 °C. A filter centre wavelength of 2.004 μm was assumed.

The maxima in the modulation index correspond to the use of an unrealistically narrowband optical filter. Figure 9 is a 3D plot, showing modulation index as a function of optical selection filter bandwidth and centre wavelength. Optical filters with centre wavelengths between 1.9 μm and 2.1 μm, and bandwidths between 0.01 nm and 80 nm were considered.

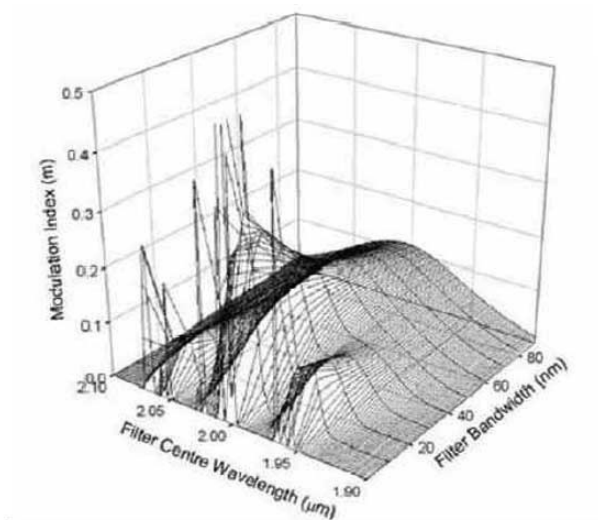


Figure 9. CO<sub>2</sub> Detection: variation of modulation Index (m), with optical filter centre wavelength and bandwidth. The broad range of absorption lines causes a very complex variation of modulation indices when using narrow filters (not all peaks at narrow filter bandwidths are shown, as this would obscure the behaviour with wider filter bandwidths). Reference and measurement cells are assumed to be of 1 m length and contain 100% CO<sub>2</sub> gas at 1 Bar/20 °C.

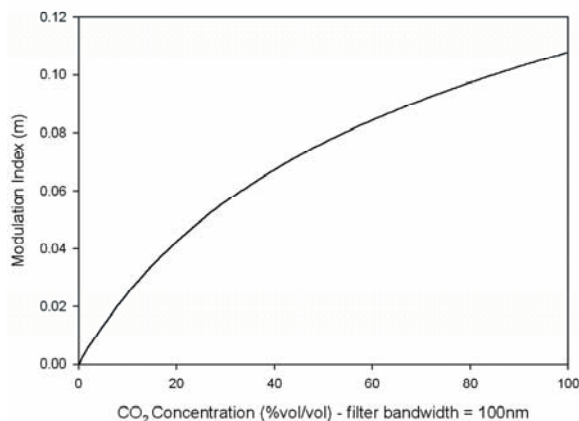


Figure 10. Predicted modulation index ( $m$ ), as a function of  $\text{CO}_2$  gas concentration (%v/v) in the measurement cell. Reference and measurement cells were of 1m length and the reference cell contained 100%  $\text{CO}_2$  gas at 1Bar/20 °C. A choice of optical filter, having a bandwidth of 100 nm and a centre wavelength of 2.004  $\mu\text{m}$ , was assumed.

As can be seen, the modulation index response is highly complex, with several other narrow-bandwidth maxima in the response. As already discussed, and as will be shown by the SNR analysis later, peaks corresponding to the use of a very narrow bandwidth filter (2 nm) are unsuitable, and unfortunately no further clear peaks are seen as the filter bandwidth is increased. To optimize the system, it was therefore necessary to take account of other system parameters, such as SNR in measurements, which will now be considered.

Figure 10 shows the dependency of the modulation index on the measurement gas cell concentration (%v/v), assuming dilution by nitrogen gas, at a pressure of 1 Bar and a temperature of 20 °C. This shows that there is a significant non-linearity in the modulation index response, particularly at higher  $\text{CO}_2$  gas concentrations in the measurement cell. As before, an optical filter bandwidth of 100 nm was assumed.

### 6.2.3 Prediction of Signal to Noise Ratio (SNR) at the Detector

The SNR of the detected signal is defined as the ratio of the signal change (produced as a result of the intensity modulation in the measurement cell) to the noise equivalent power (NEP) of the detection system for a given average received light intensity. In order to derive a figure for the NEP, various assumptions about the optical receiver must first be made. Optical receiver noise can arise partly from fundamental photon noise and partly from thermal noise in the receiver circuit. For  $\text{CO}_2$  detection, it was assumed that the optical receiver was an extended InGaAs detector, followed



by a 10 M $\Omega$  transimpedance amplifier. A combination of photon (shot) noise and Johnson (thermal) noise in the feedback resistor is normally found to be the main source of noise in optical receivers at low frequencies. The shot and Johnson thermal noise sources are expressed in Equation 2 and Equation 3, respectively:

$$I_{Shot\ Noise} = \sqrt{2qI_{Sig} B} \quad (\text{Eq.2})$$

$$I_{Thermal\ Noise} = \sqrt{\frac{4kTB}{R_{Feedback}}} \quad (\text{Eq.3})$$

where  $q$  is electronic charge,  $k$  is the Boltzmann constant,  $T$  is absolute temperature (modelled as 293 °K),  $I_{Sig}$  is the DC output current of the output detector and  $B$  is the post-detection bandwidth (assumed to be 0.1 Hz).

Figure 11 plots the SNR versus filter bandwidth, at 3 levels of received optical intensity. It may be observed that the SNR is not very dependent on filter centre wavelength, but is more strongly related to the bandwidth of the optical filter. Optimum SNR is attained with an optical filter bandwidth of approximately 80-100 nm, i.e. significantly wider than the very narrow bandwidth that was found to maximise the modulation index.

It may also be observed that small variations in the received light intensity at the detector have very little effect on the choice of best filter bandwidth to maximise SNR. Note, in these results, the very poor SNR obtained with narrow filter bandwidths (Figure 12).

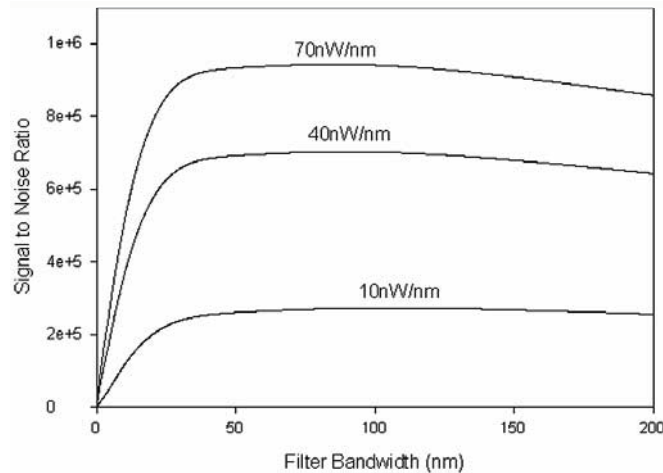


Figure 11. Predicted variation in SNR at different source power intensities, as the bandwidth of the Gaussian-response optical filter (centred at 2.004  $\mu\text{m}$ ) is increased. Reference and measurement gas cells are assumed to be 1 m long and to contain 100% CO<sub>2</sub> gas at 1 Bar/20°C.

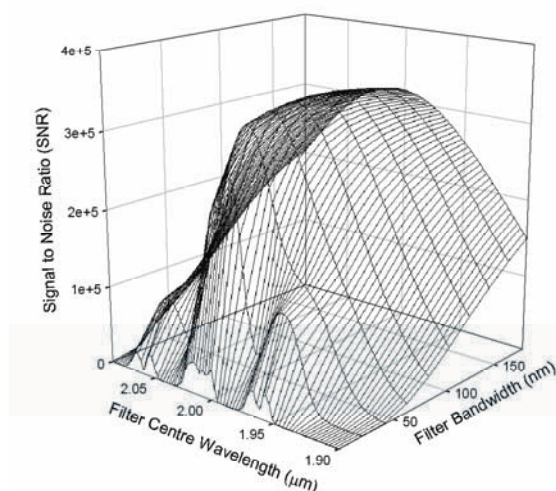


Figure 12. CO<sub>2</sub> Detection: expected variation of SNR as a function of optical filter centre wavelength and bandwidth, assuming a mean optical power incident on the reference detector of 10 nW nm<sup>-1</sup>. Reference and measurement cells were assumed to be 1 m long and to contain 100% CO<sub>2</sub> gas at 1 Bar/20 °C.

#### 6.2.4 Dependence of Modulation Index on Measurement Cell Gas Pressure

The effects of gas pressure on the measurement will now be determined. The first examples that were chosen are relevant to a gas sensing system, where the sealed reference cell would have a fixed gas concentration, whereas the measurement cell would be subject to variations in atmospheric pressure, as might be the case for many practical sensing scenarios. The HITRAN database allows the effects of pressure broadening (collision broadening) to be modelled. The effects have been simulated of changing the measurement cell pressure from 0.8 to 1.2 Bar, keeping the reference cell pressure at 1 Bar, and holding the temperature of both reference and measurement cells constant at 293 °K, with 100% CO<sub>2</sub> in each. Figure 13 shows one result of this simulation, indicating, when compared to results at 1 Bar, that the normal likely range of variation of atmospheric pressure (0.9 Bar-1.1 Bar) could lead to an -6.0%/+5.2% error in absolute measurement if not corrected for.

#### 6.2.5 Dependence of Modulation Index on Measurement Cell Gas Temperature

The effects of changing the temperature of the measurement cell were modelled, over a large range from -20 °C to 80 °C, assuming the

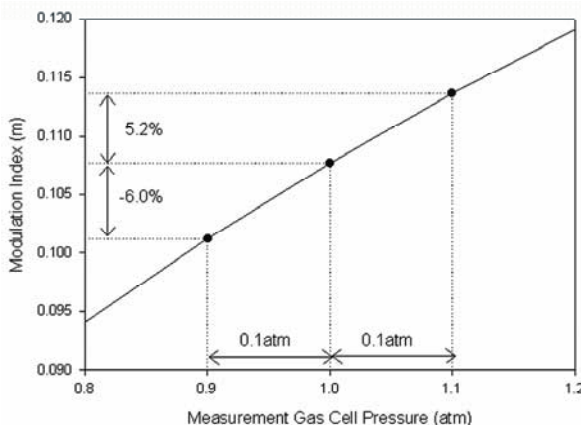


Figure 13. Expected dependence of modulation index on total gas measurement cell pressure, over the likely possible range of variation (0.8 to 1.2 Bar) of terrestrial atmospheric pressure, as calculated at 293 °K. It was assumed that the reference cell contained 100% CO<sub>2</sub> gas at 1 Bar 20°C , and that the optical filter had a centre wavelength of 2.004 μm, with a bandwidth of 100 nm.

concentration and pressure of CO<sub>2</sub> in both gas cells always remained constant, at 100% and 1 Bar, respectively. The temperature of CO<sub>2</sub> in the reference cell was assumed to remain constant at 293 °K. As before, the optical filter was assumed to be centred at 2.004 μm, with a bandwidth of 100 nm. Figure 14 shows the result of this simulation, indicating that a variation of temperature, between 0 °C and 40 °C, would potentially lead to a -3.68% / 3.71% error in the measurement, if not corrected for.

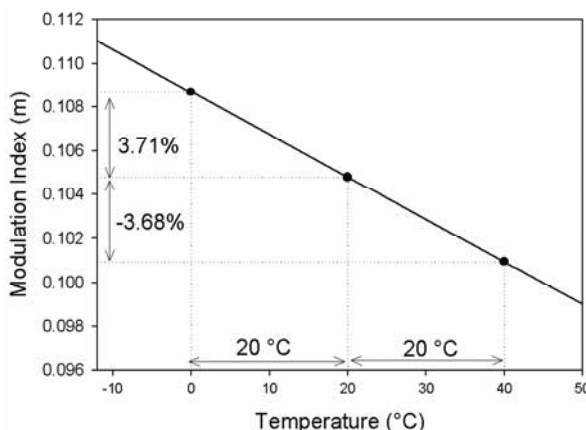


Figure 14. Expected variation of modulation index with temperature of the measurement cell, assuming both cells contained 100% CO<sub>2</sub> at 1 Bar and were 1 m long. The reference cell was held at 20 °C and the optical filter had a centre wavelength of 2.004 μm and a bandwidth of 100 nm.

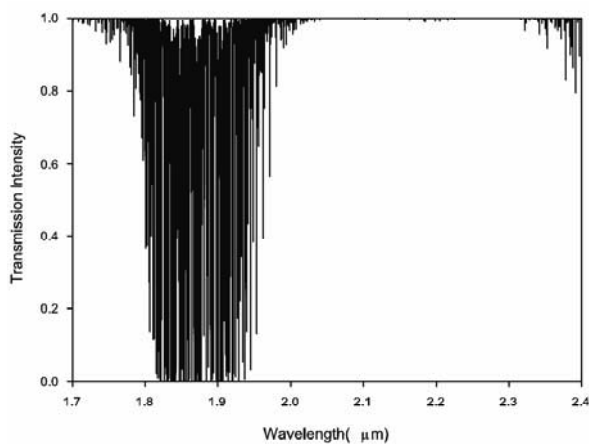


Figure 15. Transmission spectrum of water vapour over a 1 m path length at STP (transmission data obtained from HITRAN database).

### 6.2.6 Cross Sensitivity to Water Vapour

The cross sensitivity of the CO<sub>2</sub> sensor to a contaminant gas will now be analysed, choosing water (H<sub>2</sub>O) vapour, as a likely contaminant species which also has significant absorption overlap with the spectrum of CO<sub>2</sub>. The transmission spectrum of water vapor is plotted in Figure 15. The correlation spectroscopy method, as defined by Equation 1, has the highly attractive property of having high selectivity, even when exposed to a gas having non-coincident optical absorption lines in the same spectral region as that of the target gas.

The cross-sensitivity of the CO<sub>2</sub> sensor to water vapor is shown in Figure 16, where the expected modulation index, with the measurement cell filled

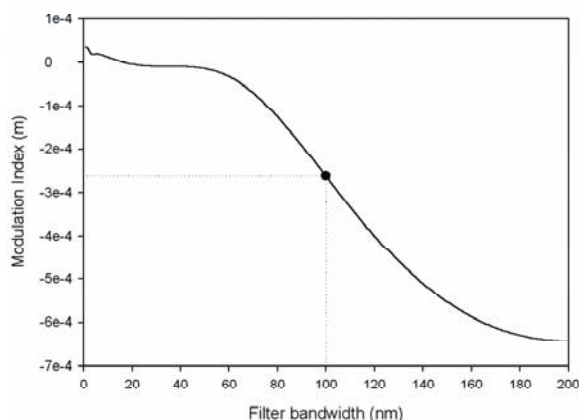


Figure 16. The variation (crosstalk) of modulation index with filter bandwidth, when the measurement cell contains a high concentration (0.05 Bar partial pressure) of H<sub>2</sub>O vapour impurity (both cells are 1 m in length cell at 1 Bar and 20 °C, and the reference cell contains 100% CO<sub>2</sub> gas).

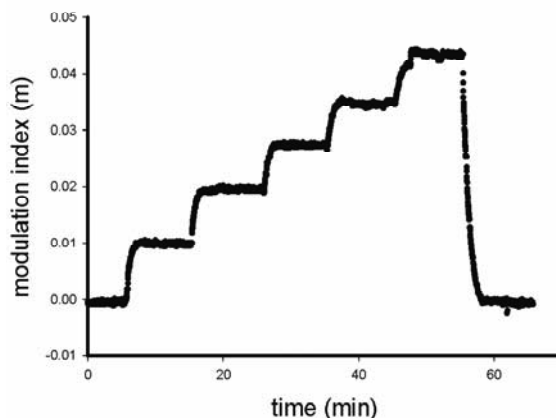


Figure 17. Modulation index as a function of applied CO<sub>2</sub> concentration. 0%, 15.6%, 33.0%, 52.5%, 74.7% and 100% CO<sub>2</sub> concentration was applied to the measurement cell. The 90 cm long reference cell, contained 100% CO<sub>2</sub>, and the 30 cm long measurement gas cell, contained 100% CO<sub>2</sub>, were at 1 Bar and 20 °C. The optical LED emission spectrum was centred at 2.04 μm and had a 150 nm FWHM bandwidth.

with water vapour at 0.05 Bar, partial pressure, is plotted as a function of optical filter bandwidth. Optical filters of varying bandwidth, but having the previously determined optimum centre wavelength of 2.004 μm were assumed. The sensor starts to become sensitive to water vapor when a filter bandwidth above 50 nm is used. However, even though we chose a gas likely to have crosstalk, the cross-sensitivity is very small, 5% water vapor giving a signal equivalent to 0.5% CO<sub>2</sub> when a 100 nm wide optical filter is used.

### 6.2.7 Comparison with Experimental Results

Figure 17 shows recent experimental results for modulation index changes, in response to changing CO<sub>2</sub> gas concentration in the measurement cell<sup>18</sup>.

Figure 18, below, shows a comparison of the experimental results (experimental points) with the theoretical predictions (solid curve) from our model above. It can be seen that there is good agreement.

## 7. CONCLUSIONS

A general review of optical gas sensing techniques, particularly optical fibre-based ones, has been presented to set the scene, before finishing with a more detailed description of our own methods using correlation

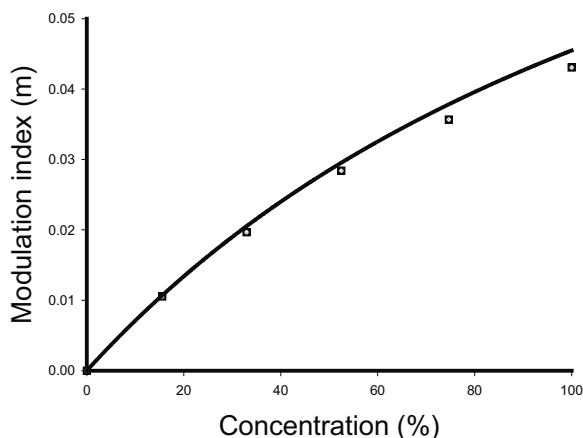


Figure 18. Modulation Index as a function of CO<sub>2</sub> concentration (%vol/vol) in the measurement cell. This shows experiment (points) and the theoretical curve. The 90 cm long reference cell, contained 100% CO<sub>2</sub>, and the 30 cm long measurement gas cell, contained 100% CO<sub>2</sub>, were at 1 Bar and 20 °C. The optical LED emission spectrum was centred at 2.04 μm and had a 150 nm FWHM bandwidth.

spectroscopy. The CoSM method has been analysed in detail, and specific results for CO<sub>2</sub> detection have been presented. The analysis has shown how the method may be optimised. Early experimental results for CO<sub>2</sub> detection have been shown to give good agreement with our model, and show the promise of this selective gas detection method.

## REFERENCES

1. Hills P.C., Samson P.J., Webster I., Optical fibres are intrinsically safe: Reviewing the myth, *J. Electrical and Electronics Eng.* 1993; 10 (3): 207-220.
2. Zhang D.K., Hills P.C., Zheng C., Wall T.F., Samson P., Fibre optic ignition of combustible gas mixtures by the radiative heating of small particles, Proceedings of the 24th international symposium on combustion (code 19626), Pittsburgh, PA, USA, 1992, pp. 1761-1767.
3. Inaba H., Kobayasi T., Hirama M., Hamza M., Optical-fiber network system for air-pollution monitoring over a wide area by optical absorption method, *Electronics Letters* 1979; 15 (23): 749-751.
4. Kobayashi T., Hirana M., Inaba H., Remote monitoring of NO<sub>2</sub> molecules by differential absorption using optical fibre link, *Appl. Opt.* 1981; 20 (5): 3279.
5. Hordvik A., Berg A., Thingbo D., A fibre optic gas detection system, Proc. 9th int. Conf. On opt. Comms., 'ECOC 83', 1983, p. 317.
6. Stueflotten S., Christensen T., Iversen S., Hellvik J. O., Almas K., Wien T., An infrared fibre optic gas detection system, Proc. Ofs-94 int conf, 1986, p. 87.
7. Samson P.J., Fibre optic gas sensing using raman spectrometry, Proc. 14th Australian Conf. on Optical Fibre Technology, Brisbane, 1989, pp. 59-65.
8. Dakin J.P., Wade C.A., Pinchbeck D., Wykes J. S., A novel optical fibre methane system, *Fibre Optics '87*, vol. 734, SPIE, London, 1987.

9. Mohebati A., King T.A., Remote detection of gases by diode laser spectroscopy, *J. Modern Optics* 1988; 35 (3): 319-324.
10. Goody R., Cross-correlating spectrometer, *J. Opt. Soc. Amer.* 1968; 58 (7): 900-908.
11. Taylor F.W., Houghton J.T., Peskett G.D., Rogers C. D., Williamson E. J., Radiometer for remote sounding of the upper atmosphere, *Appl. Opt.* 1972; 11 (1): 135-141.
12. Herget W.F., Jahnke J.A., Burch D.E., Gryvna D.A., Infrared gas-filter correlation instrument for in situ measurement of gaseous pollutant concentrations, *Appl. Opt.* 1976; 15: 1222-1228.
13. Edwards H.O., Dakin J.P., Gas sensors using correlation spectroscopy compatible with fibre-optic operation, *Sens. & Actuators B Chem* 1993; 11: 9.
14. Dakin J.P., Evolution of highly-selective gas sensing methods using correlation spectroscopy, Proc. Advances in optoelectronics for environmental monitoring (Eric), Nov 1998.
15. Chambers P., Austin E.A.D., Dakin J.P., Theoretical analysis of a methane gas detection system using the complementary source modulation of correlation spectroscopy, *Measurement Science and Technology* 2004; 15 (8): 1629-1636.
16. Weirauch G., Campargue A., Spectroscopy and intensity measurements of the  $3\nu_1+3\nu_3$  tetrad of  $^{12}\text{CO}_2$  and  $^{13}\text{CO}_2$ , *J. Mol. Spectr.* 2001; 207: 263-268.
17. Rothman L.S., Barbe A., Benner D.C., Brown L.R., Camy-Peyret C., Carleer M.R., Chance K., Clerbaux C., Dana V., Devi V.M., Fayt A., Flaud J.-M., Gamache R.R., Goldman, Jacquemart D., Jucks K.W., Lafferty W.J., Mandin J.-Y., Massie S.T., Nemtchinov A., Newnham D.A., Perrin A., Rinsland C.P., Schroeder J., Smith K.M., Smith M.A.H., Tang K., Toth R.A., Auwera J.V., Varanasi P., Yoshino K., The hitran molecular spectroscopic database: Edition of 2000 including updates through 2001, *Journal of Quantitative Spectroscopy and Radiative Transfer* 82 (2003).
18. Austin E.A.D., P. Chambers and J. P. Dakin, Theoretical analysis of a  $\text{CO}_2$  gas detection system using correlation spectroscopy, Europtrode VII, 2004.

## Chapter 23

# DNA AND PROTEIN SENSOR ARRAYS

Claudia Preininger  
ARC Seibersdorf research GmbH  
Dept. Biotechnology  
2444 Seibersdorf, Austria

### 1. INTRODUCTION

Biochips ([www.gene-chips.com](http://www.gene-chips.com); [www.functionalgenomics.org.uk](http://www.functionalgenomics.org.uk)) are bioanalytical devices applicable to diagnostics, drug discovery, and life science research. According to Weller<sup>1</sup> "*microarrays can be defined as spatially ordered, miniaturized arrangement of a multitude of immobilized reagents*". In addition to "microarray" other terms, such as chip, microchip and biochip are in use. These terms, however, are often registered trademarks or might be mistaken as an analysis system based on semiconductors ("chip") or as containing living cells ("biochip").

Diagnostics include a range of targets including metabolites, proteins, microbes, toxins, and drugs for medical, veterinary, environmental, and agricultural applications. New modes of drug discovery, applicable to biochips, encompass target identification, lead compound discovery and optimization, and toxicology. Life science research connects to biochips in the areas of gene discovery and functional genomics. Biochip technologies have broad potential, but are especially useful in the areas genomics, high-throughput screening, and infectious disease diagnostics. Biochips incorporate elements of microfluidics, micromachining, synthetic chemistry, separation science, and detection technologies. Key attributes include:

- miniaturization;
- functional integration;
- parallelism;
- virtual automation.

Antibodies have been used extensively as diagnostic tools in many different formats, especially for measurement of protein and cytokine abundances. Applications of antigen arrays can be found in reverse immunoassays for detection of allergens and autoimmune antibodies.



Proteins from cDNA libraries are used for measurement of kinase substrate specificity and identification of phospholipid-binding proteins.

## 2. PRINCIPLE AND APPLICATIONS

A fluorescently labelled target is hybridized to the chip, consisting of a set of regularly arranged spots of biomolecular probes such as oligonucleotides, PCR-amplified cDNA or proteins. At positions on the array where the immobilized probe recognizes a complementary target, binding occurs which is then detected by a fluorescence scanner. The data output consists of a list of binding events, indicating the presence or the relative abundance of specific targets in the sample.

Biochips can be used for either measuring differential expression between two populations or for testing for the presence of a DNA sequence (resequencing). Protein chips have been applied in expression profiling and antibody detection, binding specificities of a protein expression library and protein-protein interactions.

### 2.1 Oligonucleotide Arrays for Diagnostic Applications

e.g. detection of antibiotic resistances (ABR) (for scheme see Figure 1), pathogens ([www.diagnostic-arrays.com](http://www.diagnostic-arrays.com))

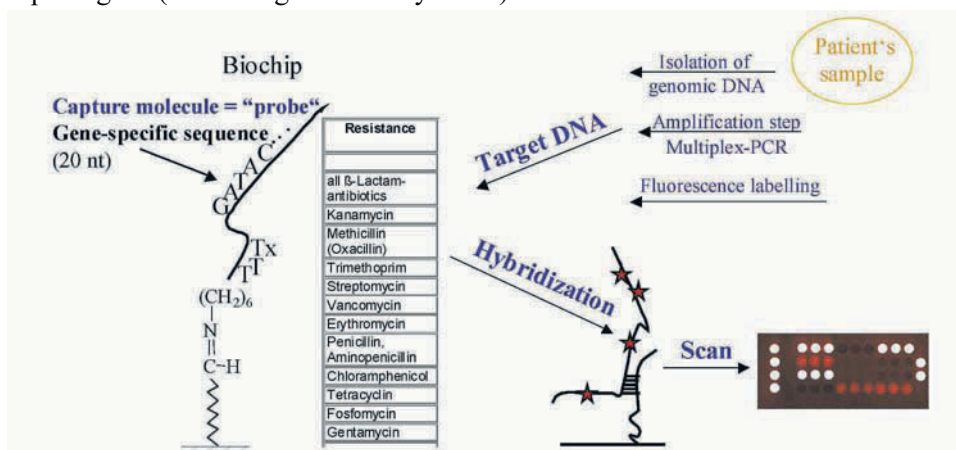


Figure 1. Principle of ABR-ARChip.

## 2.2 cDNA Arrays for Gene Expression Studies

e.g. cancer research (for scheme see Figure 2)

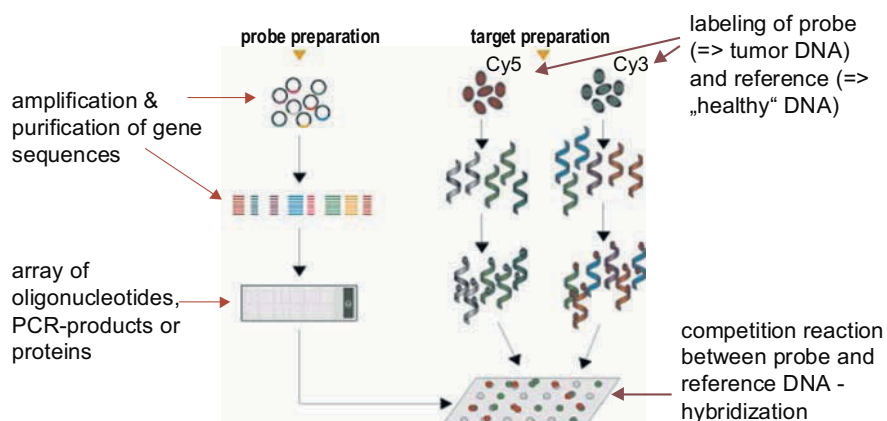


Figure 2. Principle of two-color arrays.

## 2.3 Immunoassay Formats for Protein Arrays

An immunoassay is a ligand binding assay which uses an antibody and the antibody-corresponding antigen as the binder and ligand. The term immunoassay is often expanded to include any procedure in which the quantitation of an analyte depends on the progressive saturation of a specific binder or ligand, either of which may be the analyte, and the subsequent determination of the distribution of the analyte between the bound and free fractions. This includes competitive protein binding assays, where the binder is a naturally occurring binding protein, and receptor assays, where the binder is a naturally occurring cell receptor.

In a direct immunoassay the immobilized antibody binds to the corresponding antigen. The competitive immunoassay relies upon the competition of the analyte with a labelled analyte for antibody binding. These formats are widely used for high throughput affinity arrays. A sandwich immunoassay is based on the trapping or capture of the analyte by another antibody. In ELISA (enzyme linked immunosorbent assays) the second antibody is conjugated with an enzyme. The bound enzyme labelled antibody is detected by its ability to break down its substrate to a colored product.

Antibody arrays are used in detection and expression profiling of e.g. cytokines (Figure 3)<sup>2-4</sup> and allergens ([www.vbc-genomics.com](http://www.vbc-genomics.com)). Microarrays containing antigens are developed for detection of autoantibodies in rheumatoid diseases<sup>5</sup>.

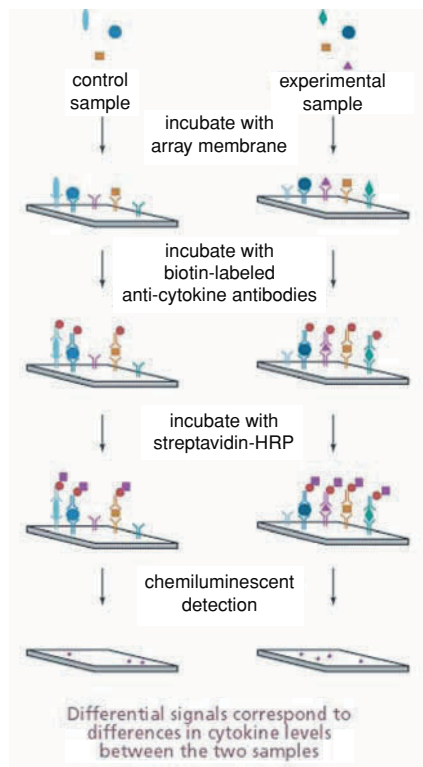


Figure 3. Principle of cytokine array (www.biocat.de).

### 3. ARRAY FORMATION

#### 3.1 *In-situ* Light-Directed Synthesis of Oligonucleotides for High Density Arrays

Light-directed chemical synthesis<sup>6, 7</sup> makes use of photolithographic masks to define the chip exposure sites. In this process, the chip surface containing light-protective groups is selectively illuminated by light passing through a photolithographic mask (Figure 4-step 1). Deprotection of the illuminated sites leads to activation and chemical coupling of nucleosides at

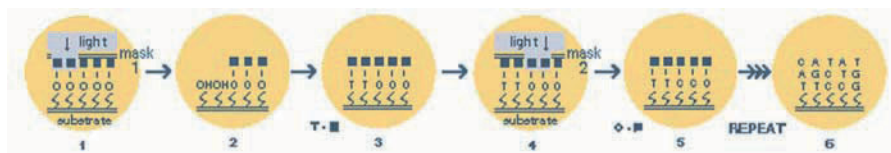


Figure 4. The *in-situ* synthesis process (www.affymetrix.com).

the specific test sites (Figure 4 steps 2-3). The process is repeated several times in order to grow base chains and complete the multiple probe array (Figure 4 steps 4-6). *In situ* light-directed synthesis can produce the highest packing density of all spotting techniques (at least one order of magnitude higher than conventional biochip arrayers). However, errors occurring in the synthesis process cannot be corrected, and, compared to printing techniques, the photolithographic method is rather expensive, since a different photolithographic mask is required for every DNA letter.

### 3.2 Arraying of Pre-synthesized Probes for Low-Density Arrays

In contrast to high density arrays low density arrays are made by deposition of pre-synthesized oligonucleotides or proteins on activated surfaces. There are several printing techniques for fabricating microarrays:

Non-contact biochip arrayers, commonly based on the piezoelectric effect, can apply controlled sub-nanoliter probe volumes to pre-specified locations on the chip surface. Due to the fact that the dispenser does not touch the surface, a non-contact arrayer provides low risk of contamination and is most suitable for printing on soft materials such as hydrogels.

Contact arrayers (Figure 5) make use of pins or capillaries to transfer probes to specific test sites on the chip.

The Pin-and-Ring<sup>TM</sup> technology by Affymetrix consists of a horizontal open ring and a vertical pin (Figure 6). During arraying, the ring is dipped into the probe – the probe is held within the ring by means of surface tension – and moved to the desired position on the chip. In order to make a spot, the pin is driven down through the ring and a portion of the probe is transferred to the pin's end and deposited at the desired position on the surface.



Figure 5. Contact spotter OmniGrid<sup>TM</sup> (GeneMachines).

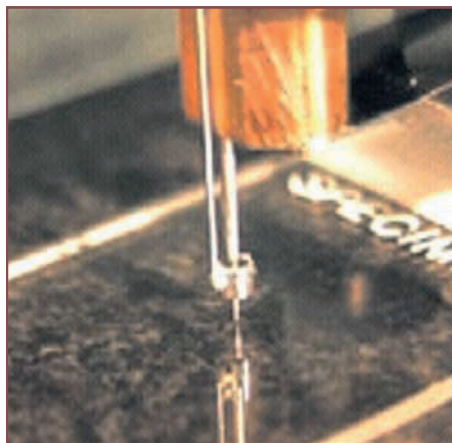


Figure 6. Ring-and-Pin™ system.

Electronic addressing (Figure 7) is the placement of charged molecules at specific test sites. Since DNA has a strong negative charge, it can be electronically moved to an area of positive charge. A test site or a row of test sites on the microchip is electronically activated with a positive charge. A solution of DNA probes is introduced onto the microchip. The negatively charged probes rapidly move to the positively charged sites, where they concentrate and are chemically bound to that site. The microchip is then washed and another solution of distinct DNA probes can be added. Site by site, row by row, an array of specifically bound DNA probes can be assembled or addressed on the microchip. In the electronic addressing illustration, a total of five sets of different capture probes have been electronically addressed to the microchip.

Alternative printing is based on soft lithography technologies like microcontact printing ( $\mu$ CP) which allows the printing of delicate biomolecules together with a tiny hydrogel spot onto surfaces. Electrospray deposition (ESD) of protein solutions on slightly conductive surfaces might be another future possibility to handle delicate proteins.

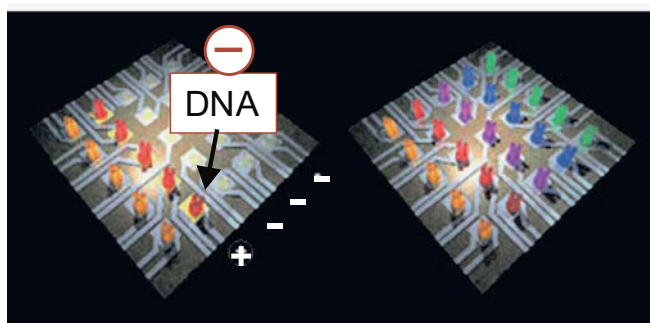


Figure 7. Electronic addressing ([www.nanogen.com](http://www.nanogen.com)).

The choice of print buffer<sup>8-10</sup> is critical for spot homogeneity and signal strength and thus has direct impact on data analysis and data reliability. The choice of print buffer also depends on the biochip surface properties and the coupling chemistry; e.g. for binding amino-modified oligonucleotides to an epoxy surface, a pH of at least 8 is required. Criteria for an optimum print buffer are: strong fluorescence signal; weak fluorescence background; and uniform spot morphology (no doughnut effect). Most print buffers in biochip technology use water as a carrier medium, which provides a naturally high surface tension. However, the surface tension of aqueous print buffers must be lower than the wettability of the substrate in order to attain good printability and adhesion. For reducing the buffer surface tension, salts and surfactants are added to the print buffer. Water-miscible organic solvents, such as alcohol, glycol and DMSO, can assist in lowering the surface tension as well as in controlling wetting and drying characteristics. Increasing the viscosity also leads to a more compact spot. Images of hybridized oligonucleotide probes in Table 1 demonstrate that the effect of print buffer on the spot morphology and spot size is significantly higher when using the piezo spotter. The far larger spots obtained with the piezoelectric spotter are a result of the interaction between print buffer, slide surface and spotter dispensers. Because the spot delay times are far shorter with contact spotters not allowing the probe spreading to an area larger than the pin diameter, the interaction of buffered probe and slide surface and thus the effect of buffer on the spot morphology is smaller. However, smaller spots produce higher signals as was already shown in the microspot theory by Ekins and coworkers in 1989<sup>11</sup>. For protein printing surfactants, such as glycerine, trehalose or poly(ethyleneglycol) are added to the print buffer.

Humidity control guarantees the correct arraying environment and moreover, optimum spot morphology and probe stability. We found the optimum humidity for oligonucleotide arraying to be 60%, the optimum humidity for protein arraying 40%. Depending on the print buffer fluorescence intensity of processed IgG was increased two- to four-fold from 80% to 40% humidity<sup>12</sup>.

The degree of uniformity among printed spots strongly affects the quality of data obtained from chip analysis. The spots must be of the same shape and size throughout a slide and from one slide to another. The uniformity of an array's grid depends to a critical extent on the arrayer's ability to precisely and accurately move to the desired location. Some arrayers are equipped with enclosed filter, source and slide-plate cooling, as well as humidity and temperature control. In deciding what sort of arrayer is most suitable, researchers are recommended to refer to several reviews on different arraying technologies and instruments: [www.biorobotics.com/](http://www.biorobotics.com/); [www.genemachines.com/](http://www.genemachines.com/); [www.lab-on-chip.com/suppliers/comtab.html](http://www.lab-on-chip.com/suppliers/comtab.html); [www.xenopore.com/products.htm](http://www.xenopore.com/products.htm).

Table 1. Spot morphology of oligonucleotides in various print buffers.

<i>print buffer</i>	<i>scan of piezo- / contact spotted probes after hybridization</i>
ArrayIt (Telechem)	
ArrayIt plus (Telechem)	
QTM I (Quantifoil)	
QTM III (Quantifoil)	
0.1 N sodium phosphate, pH 8	
0.1 N sodium carbonate, pH 9	
0.1 N sodium phosphate, pH 8 / 50% DMSO	
0.1 N sodium carbonate, pH 9 / 50% DMSO	
3xSSC, 1.5 M betaine	
0.1 N sodium phosphate, pH 8 / 1.5 M betaine	
0.1 N sodium phosphate, pH 8 / 0.01% SDS	
ArrayLink (GeneScan)	

#### 4. BIOMOLECULE IMMOBILIZATION

Arrays have been produced on filter supports, in microtiter plate wells and on glass slides coated and modified with one-, two- or 3-dimensional surface architectures as shown schematically in Figure 8<sup>13-19</sup>. Glass offers a number of practical advantages, such as mechanical stability and low autofluorescence. Due to the non-porous character of glass chips, the volume of the hybridization solution can be kept to a minimum and probe-target interaction is not limited by diffusion into pores. However, three-

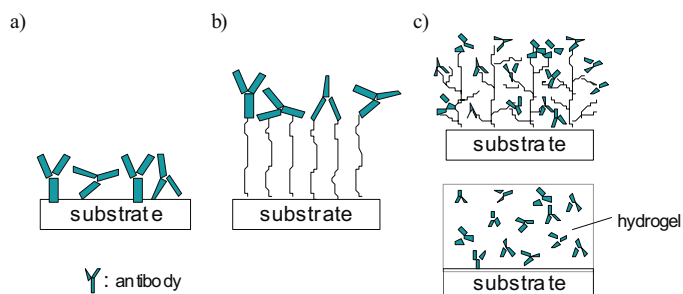


Figure 8. Schematic of a) one-dimensional, b) two-dimensional and c) three-dimensional surface coatings.

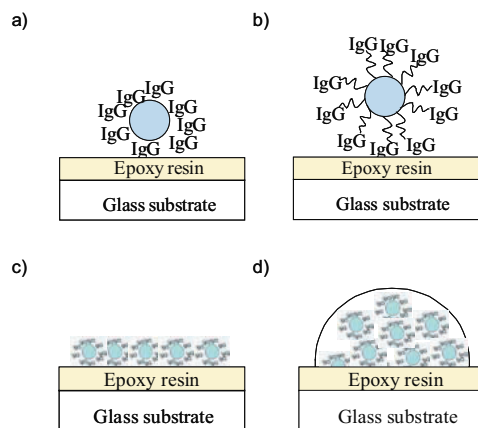


Figure 9. Immobilization of antibodies, a) directly on functional beads, or b) via crosslinkers (e.g. biotin-streptavidin chemistry). Arraying onto the slide in c) print buffer or d) entrapped in hydrogel.

dimensional microporous surfaces such as nitrocellulose or polyacrylamide yield stronger signals and thus more consistent data than do two-dimensional glass surfaces.

Biomolecules are also immobilized on beads on planar surfaces (Figure 9), in microtubes ([www.clondiag.com](http://www.clondiag.com)), and in microtiter plates. Immobilized particle arrays<sup>20</sup> combine the advantages of suspension (e.g. array element is prepared in bulk; variety of surface chemistries) and planar arrays (e.g. high throughput), but are 6 fold superior to suspension and 200 fold superior to planar arrays. Microparticles ( $\varnothing$  0.8  $\mu\text{m}$ ) coated with the same capture reagent are arrayed onto hydrogel-coated slides providing multiple assay replicates. Detection limits of 0.01 ng/mL antibody are easily achievable. As a powerful alternative to planar microarrays, bead-based assays combined with fluorescence-activated cell sorting have been developed to perform multiplexed immunoassays<sup>21</sup>. In each individual immunoassay the capture molecule is coupled to a distinct type of microsphere which is color-coded by a uniform mixture of red and orange fluorescent dyes. After formation of the sandwich immuno-complex, only the fluorophores that are definitely

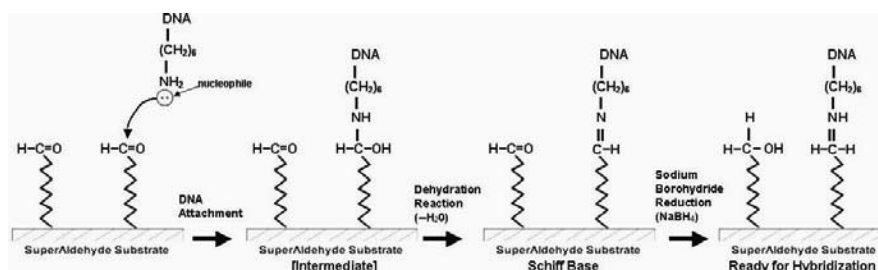


Figure 10. Covalent coupling on aldehyde-slides ([www.arrayit.com](http://www.arrayit.com)).



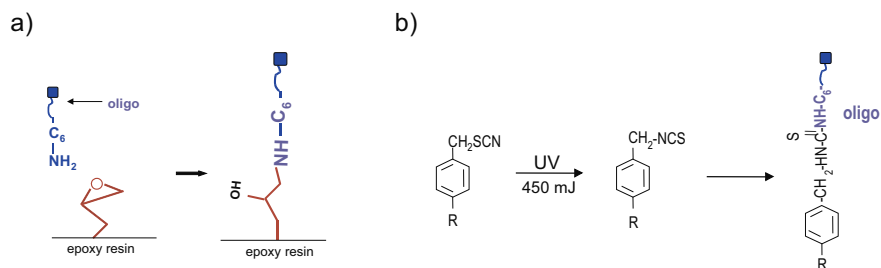


Figure 11. Covalent immobilization of oligonucleotides on a) epoxy- and b) photoactivated isothiocyanate-slides.

bound are counted in the flow cytometer. Flow cytometry is mainly used for analysis of haematological malignancies in routine clinical diagnosis, but more recently also in disease monitoring and in the evaluation of tumor response to therapy.

Important criteria for biomolecule immobilization are:

- high functionality of the chip surface;
- high immobilization capacity;
- optimized density of functional groups;
- stable linkage between the biomolecule and the solid support;
- good accessibility for the interacting molecules;
- low non-specific binding.

Depending on the size of the probe, either covalent (Figures 10 and 11) or electrostatic immobilization (Figure 12) may be preferred. In general, oligonucleotides and DNA fragments of approximately 20 to 70 bases are amino-modified and bound covalently to the chip surface. Complete or partially complementary DNA of up to 5000 nucleotide bases is bound to the chip by electrostatic adsorption.

Commercially available glass chips provide reactive aldehyde-, amino-, mercapto-, isothiocyanate-, active ester- or epoxy-groups for covalent binding of DNA ([www.arrayit.com](http://www.arrayit.com); [www.picorapid.com](http://www.picorapid.com); [www.prolinx.com](http://www.prolinx.com); [www.accelr8.com](http://www.accelr8.com); [www4.amershambiosciences.com](http://www4.amershambiosciences.com); [las.perkinelmer.com](http://las.perkinelmer.com); [www.schleicher-schuell.com](http://www.schleicher-schuell.com); [www.quantifoil.com](http://www.quantifoil.com); [www.xenopore.com](http://www.xenopore.com);

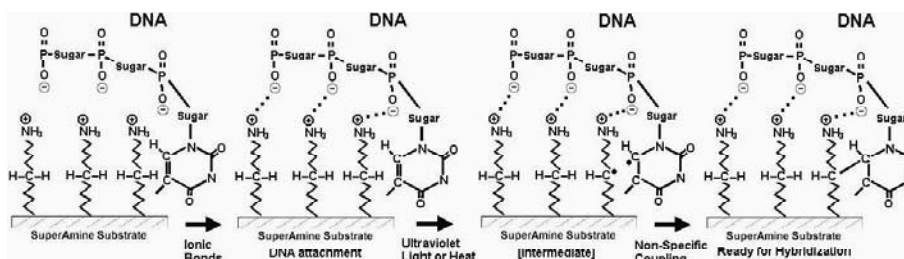


Figure 12. Electrostatic binding on amino-slides.

www.xantec.com; www.exiqon.com; www.noabbiobdiscoveries.com; www.u-vision-biotech.com; www.corning.com; etc.).

Ph. Angenendt et al.<sup>17</sup> compared seven different slides for use in antibody (anti-fibrinogen) and protein microarrays (HSA). The highest signal intensities in both antibody and protein microarrays were achieved on dendrimer epoxy slides (Chimera Biotech). PEG-Epoxy (Microsynth GmbH) and epoxy slides (Telechem) revealed similar signal intensities. Nitrocellulose slides (Schleicher & Schuell) gave especially good results with antibody arrays. Amine (Telechem), silanated (Telechem), poly-L-lysine and polystyrene (Nalge Nunc Int.) surfaces showed only average performance. Interestingly, the surface chemistries relying on the immobilization via epoxy groups revealed the best results. The lowest detection limits – 100 amol antibody and 60 amol protein – were reached using amine and dendrimer slides. Activated polystyrene slides showed the far highest detection limit: 1900 amol antibody, 190 amol protein. In [18] the same authors compared gel-coated and non-gel coated surfaces for antibody and protein arrays: HydroGel (polyacrylamide) (Perkin Elmer); aldehyde (Telechem); Poly-L-lysine; Maxisorb (polystyrene-based) (Nunc A/S); reflective microarray (APTES) (Amersham BioSciences). Highest signals and lowest variations were achieved with non-gel-coated glass and plastic slides. However, there is no universal protein or antibody array coating, for each individual antibody the coating has to be selected based on the experimental requirements.

Modified dextrans, such as carboxymethylated dextran were also coated onto glass slides to serve as matrix for protein immobilization and at the same time reduce non-specific binding<sup>22</sup>.

Michael Schaeferling et al.<sup>23</sup> reviewed a variety of protein microarray surfaces, pointing out current state of glass-based protein arrays, principles of self-assembly techniques, 2D- and 3D-surfaces and lipid layers. In self-assembly techniques thiols and disulfides are mostly used on metal substrates like gold and silver, while silanes are generally used on non-metallic surfaces such as SiO<sub>2</sub> and TiO<sub>2</sub>. Self-assembled monolayers (SAMs) of alkanethiols on gold have been extensively investigated because of the ease of fabrication, the degree of perfection, chemical stability, availability of materials and flexibility in chemical functionalization. SAMs of poly(ethylen)glycol are also widely used.

2D protein arrays based on biotin-streptavidin architectures are likely to be the system of choice due to their ease in handling, excellent signal-to-noise ratio and non-specific interactions. 3D surfaces based on porous gold, sol-gel materials, polymer brushes and dextran surfaces are widely used to mimic the properties of bulk solution and increase the immobilization capacity of proteins.

Filter arrays are superior in their high binding capacity, but suffer from low resolution, considerable background and difficulties in automating the

process. In contrast, glass slides offer a variety of different immobilization chemistries. One-dimensional coatings, such as silanized surfaces providing aldehyde and amino functions are especially used for oligonucleotide immobilization. Proteins, however, often denature on those surfaces, if protective substances, such as glycerol, disaccharides or polyethylene glycol (PEG) are not added to the print buffer. Two-dimensional coatings can be achieved by functional PEGs<sup>24, 25</sup>, biotin-streptavidin chemistry and self-assembled monolayers (SAMs) on gold surfaces. The advantage of PEG-coated surfaces is the extremely low non-specific adsorption and the large spacer preventing steric hindrance and thus allowing for a higher target capture capacity. Actually, functional and non-functional polymers are mixed prior to binding to adjust the density of reactive groups. 3D-coatings are based on hydrogels, such as poly(acryl amide)<sup>26</sup>, dendrimeric structures, (photopolymerized) brushes and porous materials, such as nitrocellulose (FAST<sup>TM</sup>, Schleicher & Schuell). Zyomyx provides biotin-derivatized poly(L-lysine)-g-poly(ethylene glycol)-coated pillars engineered into a silicon wafer. Though these chips resist non-specific adsorption, reaction times are drastically increased due to diffusion limits within the hydrogel.

## 5. CHOICE OF PROBES AND TARGETS

Modified oligonucleotides, cDNA, gene fragments and PCR products are used as probes in DNA chips. To covalently bind oligonucleotides to reactive chip surfaces, the oligonucleotides are modified at their 5' end, most often with a primary amino group. However, thiol- and allyl-modified, silanized and acrylic-labelled, acrylamide-modified, hydrazide and biotinylated oligonucleotides have also been synthesized<sup>14</sup>. Targets come either from genomic DNA, cloned DNA, cDNA or RNA. Fluorescently labelled targets are prepared by appropriate methods, for instance isolated DNA or RNA is amplified by PCR using fluorescent primer pairs. For gene expression studies, the fluorescent probes are usually produced from RNA by incorporating fluorescent nucleotides into complementary DNA (cDNA). 20  $\mu\text{M}$  oligonucleotide probe and 50-250  $\text{ng}/\mu\text{l}$  PCR-product are recommended for chip immobilization. For probe design software programmes, such as the ARB phylogenetic software, developed by Strunk and Ludwig ([www.arb-home.de](http://www.arb-home.de)) are freely available on the net.

Monoclonal and polyclonal antibodies serve as specific affinity ligands in protein chips. Though monoclonal/polyclonal pairs are more readily available than monoclonal/monoclonal pairs, polyclonal antibodies often cause higher background and lower sensitivity and specificity.

Though protein arrays borrow extensively from DNA-arrays, there are fundamental differences:

- nucleic acid arrays are more robust than protein arrays due to the DNA structure and sample preparation in assay designs;

- in contrast to proteins isolated DNA or RNA can be easily amplified at high purity levels;
- dissolved ssDNA or RNA is homogeneously negatively charged and hydrated, and thus can be conveniently immobilized on cationic surfaces (e.g. poly-L-lysine or aminosilane); by contrast, proteins have tremendous structural variability that complicate their interactions with biochip surfaces. Very often proteins unfold or denature;
- in contrast to DNA proteins exhibit strong non-specific surface activity, referred to as non-specific adsorption.

While antibodies display similar structures – in fact, various types of IgGs are commonly used in immunoassays, antigens and proteins show tremendous variations in size, structure and charge strongly effecting the array performance.

Antibodies are usually immobilized via electrostatic adsorption and hydrophobic adhesion on nitrocellulose, poly-L-lysine or polystyrene or covalently coupled via amino-groups. Additionally, antibodies can be bound by means of their thiol groups in the hinge-region or between light and heavy chains or via the carbohydrate residues of the Fc region or coupling with proteins A or G. In contrast to direct immobilization the antibodies need to be modified prior to arraying, which is rather difficult and might lead to loss in antibody yield and activity after modification and purification. Peluso et al.<sup>16</sup> showed that the effect of spacer length was negligible with short spacers on different surfaces, but up to 10 times increased with long spacers.

Proteins can be covalently immobilized by randomly conjugating them to amino-reactive surfaces or in case of recombinant proteins by introducing synthetic tags, such as carboxy-terminal or biotin-tags for specific site orientation. However, it shall be kept in mind that the epitope mapping domains of the proteins are not affected during the surface modification and immobilization step. Table 2 shows coupling chemistries for proteins relying on their chemical functionalities in the side chains or on synthetic tags. RA Vijayendran et al.<sup>27</sup> demonstrated that in contrast to randomly bound antibodies specifically oriented antibodies showed a higher activity and more homogeneous binding to analytes. Antibodies can also be oriented on surfaces, either using Fab' fragments or through protein A or G. For stabilization of protein structure surfactants, such as glycerol, trehalose, or poly(ethylene) glycol are added to the print buffer.

The development of the systematic evolution of ligands by exponential enrichment (SELEX) process<sup>28</sup> ([www.somallogic.com](http://www.somallogic.com)), however, made possible the isolation of oligonucleotide sequences with the capacity to recognize virtually any class of target molecules with high affinity and specificity. These oligonucleotide sequences, referred to as "aptamers", are beginning to emerge as a class of molecules that rival antibodies in both therapeutic and diagnostic applications. Aptamers are different from antibodies, yet they mimic properties of antibodies in a variety of diagnostic

Table 2. Attachment chemistry for proteins.

<i>Functional group protein</i>	<i>Functional group surface</i>	<i>binding</i>
-COOH (asparagine, glutamine)	-NH <sub>2</sub>	Electrostatic Covalent after carboxy activation → amide
-NH <sub>2</sub> (Lysine, arginine)	-COOH active ester epoxy	electrostatic covalent → amide
-SH (cysteine)	maleimide	covalent → thioether
-OH (serine)	epoxy	covalent → ether
His-Tag	Ni-NTA complex	coordination complex
Strep-Tag	streptavidin	Supramolecular complex
Biotin	streptavidin	Supramolecular complex

formats, having the following advantages:

- aptamers are identified through an in vitro process that does not depend on animals, cells, or even in vivo conditions; as a result, the properties of aptamers can be changed on demand;
- because animals or cells are not involved in aptamer identification, toxins as well as molecules that do not elicit a good immune responses can be used to generate high-affinity aptamers;
- aptamers are produced by chemical synthesis with extreme accuracy, reproducibility and purity; therefore, little or no batch-to-batch variation is expected in aptamer production;
- reporter molecules such as fluorescein and biotin, but also functional groups can be attached to aptamers at precise locations during the chemical synthesis;
- aptamers undergo reversible denaturation and can be regenerated easily within minutes; they are stable to long-term storage and can be transported at ambient temperature.

There is a useful public database of functionally active aptamers: [aptamer.icmb.utexas.edu](http://aptamer.icmb.utexas.edu).

## 6. DETECTION

In conventional chip experiments, fluorescence scanners are used for chip read-out. In the case of laser scanners, HeNe lasers are used as excitation sources and photomultiplier tubes as detectors, whereas CCD-based scanners use white light sources. The optical system can be confocal or non-confocal. Standard biochip experiments are performed using two fluorescent labels as

reporter molecules. The most widely used fluorescent labels are Cy3 ( $\lambda_{\text{ex}}=532$  nm) and Cy5 ( $\lambda_{\text{ex}}=635$  nm) (Amersham). Alternative indicators are the Alexa Fluor dyes from Molecular Probes and a series of bridged hemicyanine dyes, e.g. Dy-630-NHS from Dyomics. Multiple laser excitation becomes necessary with simultaneous detection of single nucleotide polymorphisms (SNPs).

The background problem can be further overcome when using a surface-confined fluorescence excitation and detection scheme: at a certain angle of incident light, total internal reflection (TIR) occurs at the interface of a dense (e.g. quartz) and less dense (e.g. water) medium. An evanescent wave is generated which penetrates into the less dense medium and decays exponentially. Optical detection of the binding event is restricted to the penetration depth of the evanescent field and thus to the surface-bound molecules. Fluorescence from unbound molecules in the bulk solution is not detected. In contrast to standard fluorescence scanners, which detect the fluorescence after hybridization, evanescent wave technology allows the measurement of real-time kinetics ([www.zeptosens.com](http://www.zeptosens.com), [www.affinity-sensors.com](http://www.affinity-sensors.com)).

Alternative optical methods that are not requiring any label are based on either surface plasmon resonance (SPR) ([www.biacore.com](http://www.biacore.com)) or reflectometric interference spectroscopy (RifS) ([www.analytik-jena.de](http://www.analytik-jena.de)). Though biochip technology is advancing and gaining increasing importance in life sciences, biochips suffer from insufficient sensitivity at low RNA concentrations and from a sometimes poor signal-to-noise ratio. By applying surface-enhanced fluorescence techniques (SEF) using metal nanofilms and nanoclusters, this problem can be overcome. The principle is based on the enhanced absorption and emission of a fluorophore when bound at a certain distance to a resonant layer of a metal or a semiconductor or both. On excitation the fluorescence of the fluorophore changes due to radiative losses of the molecular field to nonradiating plasmons in the metal. At zero distance from the metal, the fluorescence emission is completely quenched<sup>25</sup>.

In the place of fluorescent indicators, nanoparticles<sup>29</sup> such as latex fluorescent nanospheres (commercially available), luminescent quantum dots and optically active metal nanoparticles<sup>30</sup> are used for labelling DNA and protein probes. Compared to organic fluorophores, nanoparticle probes are more photostable and provide bright and steady fluorescence. However, 20-nm sized nanoparticles are much larger than fluorescent indicators, a fact that could cause problems due to binding kinetics and steric hindrance. DNA probes are attached to gold nanoparticles which bind to the target present in the sample solution. Upon binding the nanoparticle probe changes color. No amplification step is required. Using gold nanoprobe technology<sup>31,32</sup>, the chips can be developed like photographs and thus do not require expensive optical set-ups. The silver in the photographic developing solution reacts with gold and amplifies the probe signal by as much as 100 000 times.

Hybridized spots appear as grey spots in the scan. The darker the spot, the more target DNA is present. Kits based on this technology are currently under development by Eppendorf, Nanosphere and Clontech.

Semiconductor quantum dots (QDs) ([www.qdots.com](http://www.qdots.com); [www.evidentech.com](http://www.evidentech.com))<sup>33, 34</sup> such as ZnS-capped CdSe nanocrystals allow multicolour optical coding of biochips by means of conjugating a biomolecular probe with the surface of a polymer bead containing an identification code in its interior. Quantum dots act as ideal fluorophores because their fluorescence emission wavelength can continuously be tuned by changing the particle size, and a single wavelength can be used for simultaneous excitation of different-sized QDs. In general,  $n$  intensity levels with  $m$  colors generate  $(n^m-1)$  unique codes. Quantum dots are photostable and emit absorbed light in multiple, resolvable colours varying according to size. Thus, the wavelength of both the incident and the emitted light can be tuned by the particle size, producing a whole set of colours ranging from ultraviolet to infrared. In contrast to fluorophores, a number of quantum dots can be excited simultaneously at a single wavelength using only one light source. Suitable light sources are lamps, lasers and light emitting diodes (LEDs).

An increase in sensitivity and reliability of chip analysis can also be achieved by using fluorescence resonance energy transfer (FRET). For this purpose both the probe and the target are labeled with a fluorophore. When the emission spectrum of the donor, e.g. Cy5, overlaps with the absorption spectrum of the acceptor, e.g. Cy5.5, and the donor and the acceptor are at a certain distance from each other, energy is transferred from the donor to the acceptor on excitation of the donor fluorophore.

## 7. DATA COLLECTION AND ANALYSIS

Biochips produce huge data sets. Data collected from microarray experiments are random snapshots with errors, inherently noisy and incomplete. Extracting meaningful information from thousands of data points by means of bioinformatics and statistical analysis is sophisticated and calls for collaboration among researchers from different disciplines. An increasing number of image and data analysis tools, in part freely accessible (\*) to academic researchers and non-profit institutions, is available in the web. Some examples are found in Tables 3 and 4.

Image analysis is a crucial step on the way to meaningful data. There are a lot of software packages available using different algorithms for spot characterization, most of them providing basic data mining tools as well (Table 3). A high quality spot is characterized by a high signal-to-noise ratio, stable spot size and regular shape. Intensity variations within a spot and spot homogeneity can be checked with the standard deviation of the mean pixel intensities and visualized by 3D views showing the intensity values of each

pixel (IconoClust). A regularly spaced mask (grid) is placed over the array and aligned with the features automatically or manually, though the latter method is prone to errors. In order to facilitate finding the position of the grid on the chip, guide dots may be added.

Image analysis is a crucial step on the way to meaningful data. There are a lot of software packages available using different algorithms for spot characterization, most of them providing basic data mining tools as well (Table 3). A high quality spot is characterized by a high signal-to-noise ratio, stable spot size and regular shape. Intensity variations within a spot and spot homogeneity can be checked with the standard deviation of the mean pixel intensities and visualized by 3D views showing the intensity values of each pixel (IconoClust). A regularly spaced mask (grid) is placed over the array and aligned with the features automatically or manually, though the latter method is prone to errors. In order to facilitate finding the position of the grid on the chip, guide dots may be added. The guide dots are located at a certain position and contain labelled material. The algorithms for spot image analysis include matched filtering, hierarchical methods and thresholding (e.g. TIGR\_Spotfinder), seeded region growing, and other methods. These should be robust against outliers and meet the problems of overlapping spots, contamination, strong background and varying spot size. The software

Table 3. Image analysis software.

<i>Product</i>	<i>Source</i>	<i>Web address</i>
Tigr Spotfinder*	The Institute for Genomic Research	<a href="http://www.tigr.org/software/">www.tigr.org/software/</a>
ScanAlyze*	University of California Berkeley, Eisen Lab	<a href="http://rana.lbl.gov/EisenSoftware.html">http://rana.lbl.gov/EisenSoftware.html</a>
F-scan*	National Institutes of Health, Bethesda	<a href="http://abs.cit.nih.gov/fscan/">http://abs.cit.nih.gov/fscan/</a>
P-scan*	National Institutes of Health, Bethesda	<a href="http://abs.cit.nih.gov/pscan/index.html">http://abs.cit.nih.gov/pscan/index.html</a>
UCSF Spot*	UCSF, Jain Lab	<a href="http://jainlab.ucsf.edu/Projects.html">http://jainlab.ucsf.edu/Projects.html</a>
GenePix Pro	Axon Instruments	<a href="http://www.axon.com">www.axon.com</a>
Iconoclust	Clondiag Chip Technologies	<a href="http://www.clondiag.com">www.clondiag.com</a>
ArrayPro	Media Cybernetic	<a href="http://www.mediacy.com">www.mediacy.com</a>
Spot	CSIRO Mathematical & Information Science	<a href="http://www.cmis.csiro.au/iap/spot.htm">www.cmis.csiro.au/iap/spot.htm</a>
QuantArray	Packard Bioscience	<a href="http://www.packardbioscience.com/products/products">www.packardbioscience.com/products/products</a>
ArrayVision	Imaging Research Inc.	<a href="http://www.imagingresearch.com/products/ARV.asp">www.imagingresearch.com/products/ARV.asp</a>
ImaGene	BioDiscovery	<a href="http://www.biodiscovery.com/imagene.asp">www.biodiscovery.com/imagene.asp</a>
Gene Traffic	Iobion Informatics	<a href="http://www.iobion.com/products/products.html">www.iobion.com/products/products.html</a>



Table 4. Data analysis software.

<i>Product</i>	<i>Source</i>	<i>Web address</i>
Cyber T*	University of California, Irvine	<a href="http://genomics.biochem.uci.edu/genex/cybert">http://genomics.biochem.uci.edu/genex/cybert</a>
SNOMAD*	Pevsner Lab, Johns Hopkins University	<a href="http://pevsnerlab.kennedykrieger.org/snomadinput.html">http://pevsnerlab.kennedykrieger.org/snomadinput.html</a>
GeneViz*	Contentsoft AG	<a href="http://www.contentsoft.de/index.htm?geneviz.htm">www.contentsoft.de/index.htm?geneviz.htm</a>
MA-ANOVA*	The Jackson Laboratory	<a href="http://www.jax.org/research/churchill/software/anova/index.html">www.jax.org/research/churchill/software/anova/index.html</a>
BASE *	Lund University	<a href="http://base.thep.lu.se/">http://base.thep.lu.se/</a>
AMIADA*	Hong Kong University	<a href="http://web.hku.hk/~xxia/software/amiada.html">http://web.hku.hk/~xxia/software/amiada.html</a>
DNA-Chip Analyse *	Harvard University, Wong Lab	<a href="http://www.dchip.org/">www.dchip.org/</a>
Genesis*	IBMT Graz University of Technology	<a href="http://genome.tugraz.at/Software/GenesisCenter.html">http://genome.tugraz.at/Software/GenesisCenter.html</a>
Cleaver*	Stanford Biomedical Inform.	<a href="http://classify.stanford.edu/">http://classify.stanford.edu/</a>
DataMachine*	Dept Medicine, Boston Univ.	<a href="http://people.bu.edu/strehlow/">http://people.bu.edu/strehlow/</a>
SOTA*	alma Bioinformatica	<a href="http://www.almabioinfo.com/">www.almabioinfo.com/</a>
CTWC*	Weizmann Institute of Science	<a href="http://ctwc.weizmann.ac.il/">http://ctwc.weizmann.ac.il/</a>
FASTA*	University of Virginia	<a href="ftp://ftp.virginia.edu/pub/fasta">ftp.virginia.edu/pub/fasta</a>
GeneSpring	Silicon Genetics	<a href="http://www.silicongenetics.com/cgi/SiG.cgi/company/index.smf">www.silicongenetics.com/cgi/SiG.cgi/company/index.smf</a>
Spotfire	Spotfire	<a href="http://www.spotfire.com/products/comp.asp">www.spotfire.com/products/comp.asp</a>
Acuity	Axon Instruments	<a href="http://www.axon.com/GN_Acuity.html">www.axon.com/GN_Acuity.html</a>

should check the image automatically with regard to its quality: flagging, that is the marking of spots deemed bad, is a critical step in establishing data reliability. Reasons for flagging may be saturated measurement, dust, scratches, donuts, heavy background, or spots that are not at the expected location. The software has to be able to associate a feature on the array with a probe identity, and possibly with its sequence in a database.

Estimating background intensities is necessary for the purpose of correcting non-specific hybridization. Reactive groups on the slide surface at sites where no probe is immobilized have to be blocked before hybridization. Otherwise, labelled targets and impurities will bind with these regions and result in a strong background. Autofluorescence of the support (nylon or glass) and of the layer has to be considered as well. Low uniform background is important for good signal-to-noise ratios. Several calculation methods are implemented in image analysis software packages for estimating background data.

The analysis tool computes the arithmetic mean or the median of the pixel intensities for each spot in both color channels. Median intensities are less susceptible to extreme values, whereas variability of the data can be estimated from mean intensities. Local sampling of background or spots from only buffer (negative controls) can be used to establish a threshold which a true signal must exceed, e.g. two standard deviations above background. Raw intensities or background-subtracted intensities may be used for further analysis.

To account for differences in labelling and for quantum yield of the fluorescence labels, as well as for differences in the quantities of targets, normalization of the fluorescence intensities in each channel is necessary in dual colour experiments<sup>35</sup>. Furthermore, normalization is needed making comparisons across arrays and experiments. Methods for normalization have to be adapted to experimental designs and issues. At least the majority of systematic and random fluctuation should be eliminated by the normalization procedure. Global normalization is widely used in gene expression experiments, although it comes out to be the weakest method. This strategy assumes that the total mass of RNA labelled with the two dyes is equal, and subsequently the average ratio of an array should be set to one, thereby introducing a normalization factor, or -the median of the distribution of log ratios is set to zero<sup>36</sup>. Alternatively, a subset of genes with constant expression, so-called house-keeping genes, may be used for normalization. In toxicological studies this method is limited due to the lack of genes not somehow regulated by a toxic compound. When employing the spiked controls method, synthetic DNA sequences or DNA sequences from another organism are spotted on the array and included in the two different samples in equal amounts. Thus, they should have equal red and green intensities and can be used for normalization. Another approach uses a function of intensities of added controls in increasing concentrations for normalization.

## 8. GLOSSARY

Antibody: an antibody made by certain white blood cells in response to a foreign substance (antigen) is an immunological protein which binds to a specific antigen (ligand).

Antigen: any substance that stimulates the immune system. Antigens are often foreign substances such as bacteria or viruses that invade the body. An antigen is a ligand that contains a region or epitope which is specifically recognized by an antibody binding site.

cDNA: strong, cloned copies of otherwise fragile mRNA - the essential messenger element of the genes in the DNA which help in the coding of proteins.

DNA: DNA (deoxyribonucleic acid) is a double-stranded helix of nucleotides

which carries the genetic information of a cell. It encodes the information for the proteins and is able self-replicate.

Hybridization: the process of a single-stranded nucleic acid molecule binding with a complementary single strand of nucleic acid to form a stable double-stranded molecule. Hybridization is temperature dependent, so DNA's that hybridize strongly at low temperature can be temporarily separated (denatured) by heating.

Monoclonal antibody: an antibody produced by a single clone of cells (specifically, a single clone of hybridoma cells) and therefore a single pure homogeneous type of antibody that binds to the same target.

Multiplex PCR: a PCR reaction where more than one primer set is included in the reaction pool allowing 2 or more different DNA targets to be amplified by PCR in a single reaction tube.

Nucleotide: a subunit of RNA or DNA containing a base, a phosphate, and a sugar; thousands of nucleotides link up to form a molecule of DNA or RNA. One of the structural components, or building blocks, of DNA and RNA. A nucleotide consists of a base (one of four chemicals: adenine, thymine, guanine, and cytosine) plus a molecule of sugar and one of phosphoric acid.

Oligonucleotide: short segments of DNA ("oligo").

PCR: a technique for making many copies of a specific DNA sequence. The reaction is initiated using a pair of short primer sequences which match the ends of the sequence to be copied. Thereafter, each cycle of the reaction copies the sequence between the primers. Primers can bind to the copies as well as the original sequence, so the total number of copies increases exponentially with time.

Polyclonal antibody: a mixture of a number of antibodies that will treat a problem by attacking a number of different targets

Primer: an oligonucleotide or pair of oligonucleotides used to direct an activity to a region of nucleic acid. With PCR (polymerase chain reaction), a pair of primers defines the area of the genome to be amplified.

Probe: the solution of labeled DNA that is hybridized with the array.

Protein: a complex macromolecule made up of one or more unbranched chains of amino acids. Every function in the living cell depends on proteins.

Recombinant proteins: new proteins, with therapeutic benefits such as insulin or hemoglobin, artificially produced through the manipulation of DNA. A specific series of proteins containing the desired genetic information can be spliced in between two ends of a DNA molecule and the ends of the DNA molecule can be "recombined," producing recombinant DNA. For example, Recombinant Human Insulin was produced using recombinant techniques. Insulin DNA was placed in a bacterial plasmid (as known as a cloning vector). Plasmids contain DNA and can carry the DNA into a bacteria cell. The DNA on the plasmid is understood by the bacteria and the bacteria cell can manufacture the insulin protein.

**RNA:** RNA (ribonucleic acid) is an information encoded strand of nucleotides, similar to DNA, but with a slightly different chemical structure. In RNA, the letter U (uracil) is substituted for T in the genetic code. RNA delivers DNA's genetic message to the cytoplasm of a cell where proteins are made.

## REFERENCES

1. Weller M.G., Classification of protein microarrays and related techniques, *Anal Bioanal Chem.* 2003; 375: 15-17.
2. Du W., Xu Z., Ma X., Song L., Schneider M., Biochip as a potential platform of serological interferon alpha2b antibody assay, *J Biotechnol.* 2003; 106: 87-100.
3. Copeland S., Siddiqui J., Remick D., Direct comparison of traditional ELISAs and membrane protein arrays for detection and quantification of human cytokines, *J Immunol Methods* 2004; 284: 99-106.
4. Lin Y., Huang R., Cao X., Wang S.M., Shi Q., Huang R.P., Detection of multiple cytokines by protein arrays from cell lysate and tissue lysate, *Clin Chem lab Med.* 2003; 41: 139-45.
5. Feng Y., Ke X., Ma R., Chen Y., Hu G., Liu F., Parallel detection of autoantibodies with microarrays in rheumatoid diseases, *Clin. Chem.* 2004; 50: 416-22.
6. Fodor S.P.A., Read J.L., Pirrung M.C., Stryer L., Lu A.T., Solas D., Light-directed, spatially addressable parallel chemical synthesis, *Science* 1991; 251: 767-773.
7. Beier M., Hoheisel J.D., Production by quantitative photolithographic synthesis of individually quality checked DNA microarrays, *Nucl Acid Res.* 2000; 28: e11.
8. Preininger C., Bodrossy L., Sauer U., Pichler R., Weilharter A. AR, Chip Epoxy and ARChip UV for covalent on-chip immobilization of *pmoA* gene specific oligonucleotides, *Anal Biochem.* 2004; 330: 29-36.
9. Rickman D.S., Herbert C.J., Aggerbeck L.P., Optimizing spotting solutions for increased reproducibility of cDNA microarrays, *Nucl Acid Res.* 2003; 31: e109.
10. McQuain M.K., Seale K., Peck J., Levy S., Haselton F.R., Effects of relative humidity and buffer additives on the contact printing of microarrays by quill pins, *Anal Biochem.* 2003; 320: 281-291.
11. Ekins R.P., Multi-analyte immunoassay, *J Pharm Biomed Ana.l* 1989; 7: 155-168.
12. Preininger C., Sauer U., Dayteg J., Pichler R., Optimizing process parameters for signal enhancement of oligonucleotide and protein arrays on ARChip Epoxy, *Electrochim Acta* 2005; 67: 155-162.
13. Kusnezow W., Hoheisel J.D., Antibody microarrays: promises and problems, *Biotechniques* 2002; 33: 14-23.
14. Preininger, Claudia, Sauer, Ursula., Design, quality control and normalization of biosensor chips, In *Optical Sensors for Industrial, Environmental and Diagnostic Applications*, Otto S. Wolfbeis, Rainer Narayanaswamy, ed. Springer, 2003.
15. Kusnezow W., Hoheisel J.D., Solid supports for microarray immunoassays, *J Mol Recogn.* 2003; 16: 165-176.
16. Peluso P., Wilson D.S., Do D., Tran H., Venkatasubbaiah M., Quincy D., Heidecker B., Poindexter K., Tolani N., Phelan M., Witte K., Jung L.S., Wagner P., Nock S., Optimizing antibody immobilization strategies for the construction of protein microarrays, *Anal Biochem.* 2003; 312: 113-124.
17. Angenendt P., Gloekler J., Sobek J., Lehrach H., Cahill D.J., Next generation of protein microarray support materials: evaluation for protein and microarray applications, *J. Chromatography A* 2003; 1009: 97-104.

18. Angenendt P., Gloekler J., Murphy D., Lehrach H., Cahill D.J., Toward optimized antibody microarrays: a comparison of current microarray support materials, *Anal Biochem.* 2002; 309: 253-260.
19. Kusnezow W., Hoheisel, J.D., Solid supports for microarray immunoassays, *J Mol Recognit* 2003; 16: 165-176.
20. Stevens P.W., Wang C.H.J., Kelso D.M., Immobilized particle arrays: coalescence of planar- and suspension-array technologies, *Anal Chem* 2003; 75: 1141-1146.
21. Joos Th.O., Stoll D., Templin M.F., Miniaturized multiplexed immunoassays, *Curr Opin Chem. Biol.* 2001; 6: 76-80.
22. Akkoyun A., Bilitewski U., Optimisation of glass surfaces for optical immunosensors, *Biosens & Bioelectron.* 2002; 17: 655-664.
23. Schaeferling M., Schiller S., Paul H., Kruschina M., Pavlickova P., Meerkamp M., Giammasi C., Kambhampati D., Application of self-assembly techniques in the design of biocompatible protein microarray surfaces, *Electrophoresis* 2002; 23: 3097-3105.
24. Yadavalli V.K., Koh W.-G., Lazur G.L., Pishko M.V., Microfabricated protein-containing poly(ethylene glycol) hydrogel arrays for biosensing, *Sensors & Actuators B* 2004; 97: 290-297.
25. Nakayama Y., Miyamura M., Hirano Y., Goto K., Matsuda T., Preparation of poly(ethylene glycol)-polystyrene block copolymers using photochemistry of dithiocarbamate as a reduced cell-adhesive coating material, *Biomaterials* 1999; 20: 963-970.
26. Rubina A.Y., Dementieva E.I., Stomakhin A.A., Darii E.L., Pan'kov S.V., Barsky V.E., Ivanov S.M., Konovalova E.V., Mirzabekov A.D., Hydrogel-based protein microchips: manufacturing, properties and applications, *Biotechniques* 2003; 34: 1008-1022.
27. Vijayendran R.A., Leckband D.E., A quantitative assessment of heterogeneity for surface-immobilized proteins, *Anal Chem.* 2001; 73: 471-480.
28. Sumedha D. J., Aptamers: An Emerging Class of Molecules That Rival Antibodies in Diagnostics, *Clin Chem.* 1999; 45: 1628-1650.
29. Taylor J.R., Fang M.M., Nie S., Probing specific sequences on single DNA molecules with bioconjugated fluorescent nanoparticles, *Anal Chem.* 2000; 72: 1979-1986.
30. Köhler J.M., Csáki A., Reichert J., Möller R., Straube W., Fritzsche W., Selective labeling of oligonucleotide monolayers by metallic nanobeads for fast optical readout of DNA-chips, *Sens Act B* 2001; 76: 166-172.
31. Taton T.A., Lu G., Mirkin C.A., Two-Color Labeling of Oligonucleotide Arrays via Size-Selective Scattering of Nanoparticle Probes, *J Am Chem Soc.* 2001; 123: 5164-65.
32. Taton T.A., Mirkin C.A., Letsinger R.L., Scanometric DNA array detection with nanoparticle probes, *Science* 2000; 289: 1757-1760.
33. Han M., Gao X., Su J.Z., Nie S., Quantum-dot-tagged microbeads for multiplexed optical coding of biomolecules, *Nature Biotechnol.* 2001; 19: 631-635.
34. Mitchell G.P., Mirkin C.A., Letsinger R.L., Programmed assembly of DNA functionalized quantum dots, *J Am Chem Soc.* 1999; 121: 8122-8123.
35. Hegde P., Qi R., Abernathy K., Gay C., Dharap S., Gaspard R., Earle H.J., Snesrud E., Lee N., Quackenbush J., A Concise Guide to cDNA Microarray Analysis, *Biotechniques* 2000; 29: 548-562.
36. Yang Y.H., Dudoit S., Luu P., Lin D.M., Peng V., Ngai J., Speed T., Normalization for cDNA microarray data: a robust composite method addressing single and multiple slide systematic variation, *Nucl Acid Res.* 2002; 30: e15.

## Chapter 24

# SENSORS FOR FOOD SAFETY AND SECURITY

Dmitri B. Papkovsky

*Biochemistry Department/ABCRF, University College Cork  
Lee Maltings, Prospect Row, Cork, Ireland*

### 1. INTRODUCTION

Active packaging of food products is aimed at extending shelf life, preserving and improving quality, taste characteristics and appearance of a product<sup>1-3</sup>. Modified atmosphere packaging (MAP) have become widely used with oxygen sensitive foods<sup>3</sup>, as it enables to inhibit or delay undesirable processes inside packs such as oxidation of lipids and heme-containing pigments, enzymatic degradation, microbial spoilage, etc. In MAP process, the package container with food is flushed with a mixture of CO<sub>2</sub>, N<sub>2</sub>, and O<sub>2</sub> gases to replace air, and then sealed. The function of CO<sub>2</sub> is to decrease the growth rate of micro-organisms, N<sub>2</sub> displaces O<sub>2</sub> and also prevents the packaging from collapsing when some of the CO<sub>2</sub> is absorbed by moisture in the product<sup>1</sup>. The majority of MAP foods are packed under the atmosphere with considerably reduced oxygen levels, while products such as raw meat, fruit and vegetables require high concentration of oxygen to keep their appearance and/or shelf life<sup>1,2</sup>.

Despite the wide use and automation of MAP process, it is not always 100% efficient. Improper flushing, sealing, accidental damage of packs during their processing, handling and transportation, improper storage conditions and diffusion of air through packaging material, may result in elevated oxygen levels in some packs. This has been reported to affect up to 1-5% of all packs<sup>4-6</sup>. Obviously, improper gas composition in such faulty packs may stimulate rapid deterioration of the food, thus possessing a considerable threat to the safety of food and to the consumer. Besides that, MAP food packs comprise dynamic systems in which gas composition in the headspace is changing over time due to respiration, on-going metabolism, diffusion of gases in and out of packs, other processes<sup>1,2</sup>.

Therefore, the development of methods for monitoring critical components and parameters within food packs is of paramount importance, to ensure high quality and safety of all MAP foods entering the retail chain.

Knowledge of the actual gas composition in packs allows the assessment of quality and integrity of the final food packages, the efficiency of packaging processes, and aids in the identification or anticipated quality changes of the food product within the pack<sup>2,5</sup>.

## 2. METHODS OF ASSESSMENT AND QUALITY CONTROL OF PACKAGED FOODS

Common methods of analysis of headspace gases, such as O<sub>2</sub>, CO<sub>2</sub>, N<sub>2</sub>, flavours and volatile components, include gas chromatography (GC) or gas chromatography/mass spectrometry (GC/MS)<sup>7,8</sup>. Although these techniques are well-established, accurate and can provide information about several components, they are complicated and expensive, provide low sample throughput, and by nature destructive. Portable headspace gas analysers produced by PBI Dansensor have recently been developed, which operate by puncturing packages with a thin needle and aspirating headspace gas. The gas is then analyzed with electrochemical O<sub>2</sub> and infra-red CO<sub>2</sub> sensors which are built into the device and give quantitative readout of these parameters<sup>6,9</sup>. Such instruments are relatively inexpensive, can perform many measurements with little maintenance and utilise almost no consumables. This technique can be considered as “minimally destructive” as the package can be resealed after testing with a rubber patch and put back into storage. However, it is not applicable for on-line control of packaging processes and for mass scale usage. All these methods only allow for random quality control testing.

As opposed to conventional analytical techniques, optical sensors and biosensors, particularly those employing absorption and fluorescence-based sensing materials potentially allow for measurement through transparent or semi-transparent materials in a non-destructive fashion<sup>4,5,9,10</sup>. Chemical sensor technology has developed rapidly over the past years and a number of systems for food applications have been introduced and evaluated with foods.

Thus, color indicators provide qualitative or semi-quantitative information about a particular parameter via color changes detected by visual observation or instrumentally<sup>4,9,11</sup>. Oxygen leak color indicators usually respond to very low levels of oxygen (0.1-0.2%)<sup>4,11</sup>. High sensitivity and irreversible mechanism of sensing are not always advantageous as they complicate the handling and preparation of such sensors<sup>4,10</sup>. The application of headspace CO<sub>2</sub> indicator inserts allows spoilage detection in aseptic packages<sup>12</sup>, as well as other indicators, which react with the by-products of microbial metabolism in the headspace of food packs<sup>4,13</sup>. The use of color indicators in packs, however, has not gained widespread use, due to high

costs and limited applicability of such systems, as well as the resistance from retailers and ethical issues, associated with their use in foods<sup>5, 10</sup>.

### 3. FLUORESCENCE-BASED OXYGEN SENSORS

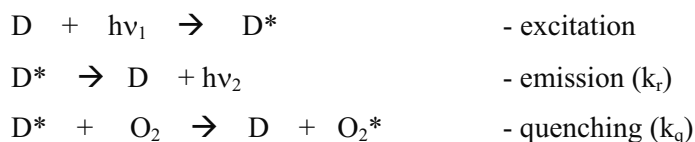
Quenched-fluorescence oxygen sensing provides a simple and efficient means for rapid and non-destructive assessment of packs for residual oxygen<sup>5</sup>. This is achieved by incorporating small solid-state sensors inside packs and monitoring them with an external device interrogating with the sensor through the (semi)transparent packaging material<sup>14-16</sup>. Real-time measurement of oxygen in each pack and at any number of points along the production line and product shelf-life can thus be implemented, to obtain direct information about the integrity and levels of residual oxygen in all packages and possible leaks<sup>17-19</sup>. Optical oxygen sensors have already demonstrated high utility and potential for use on a mass scale in MAP, so they may be regarded as one of the most exciting and successful sensor developments in food-related applications and packaging<sup>5</sup>.

At the same time, many practical issues associated with the use of optical oxygen sensors in food packs still remain. These have to be addressed to adapt the existing sensing materials and prototype systems for real-life applications, achieve the required sensor specifications, operational performance and safety. Considerable technological developments and effort in eliminating current problems and bottlenecks are required, to facilitate widespread use of the oxygen sensors by food and packaging industry.

In the following sections, the principles of oxygen sensing, design strategies and practical requirements for the oxygen-sensitive materials for food packaging, and examples of their use in particular food applications will be described. Some of the existing sensor systems and their uses will be analyzed, highlighting their merits and limitations and avenues of further research and development towards broad practical use. This analysis will be translated to other optical chemical sensor systems for similar applications.

#### 3.1 Principles of Oxygen Sensing

Quenching of a photoluminescent dye (D) by molecular oxygen (O<sub>2</sub>) is a non-chemical collisional process which can be presented as follows:



where  $h\nu_1$ ,  $h\nu_2$  denote photons of excited light and emission. This process is described by the Stern-Volmer equation relating the oxygen concentration



and experimentally measured parameters of fluorescence<sup>20</sup>:

$$I_0/I = \tau_0/\tau = 1 + K_{S-V} \cdot [O_2] \quad (\text{Eq.1})$$

where  $I_0$ ,  $I$ ,  $\tau_0$ ,  $\tau$  are the emission intensities and the lifetimes in the absence and in the presence of oxygen, respectively and  $K_{S-V}$  is Stern-Volmer quenching constant. By measuring the luminescence intensity or lifetime, oxygen concentration in the sample can be quantified<sup>5</sup>:

$$[O_2] = (I_0 - I) / (I \cdot k_Q \cdot \tau_0) = (\tau_0 - \tau) / (\tau \cdot \tau_0 \cdot k_Q) \quad (\text{Eq.2})$$

The majority of industrial applications of optical oxygen sensing, including food applications, operate with solid-state sensing materials. Such sensors typically comprise an oxygen-sensitive photoluminescent dye embedded in a suitable quenching medium such as polymer and applied on a solid support<sup>21, 22</sup>. Oxygen diffuses from the sample into polymer, collides with the dye molecules and quenches them. Solid-state sensors are simple, robust and relatively easy to make, they prevent contamination of sample with sensor components, allow sensor reuse when needed. Oxygen-sensitive materials are optimised to produce a distinct fluorescent response to oxygen concentration within the desired range, and strong overall fluorescence signals detectable by simple means and devices.

Molecular oxygen is a weak quencher, and for sensing in ambient oxygen range 0-21 kPa (0-21%) long-decay fluorescent or phosphorescent dyes are usually employed<sup>5, 20, 22</sup>. Ruthenium(II) complexes (tris-bipyridyl or tris-diphenylphenanthroline and platinum(II)-porphyrins are the dyes most commonly used in oxygen sensors, usually in combination with polystyrene and some other polymers including sol-gels, silicones, etc.

A number of relatively simple, compact and inexpensive instruments (prototypes and commercial devices) have been developed to operate with these materials<sup>14, 17-19, 23</sup>. These instruments usually employ fluorescence lifetime-based sensing performed by phase-modulation techniques (phase measurements).

In phase-fluorimetric oxygen sensors, active elements are excited with periodically modulated light, and changes in fluorescence phase characteristics are measured. The delay or emission (phase shift,  $\phi$ , measured in degrees angle) relates to the lifetime of the dye ( $\tau$ ) and oxygen concentration as follows:

$$\tan(\phi) = 2 \cdot \pi \cdot \nu \cdot \tau, \quad (\text{Eq.3})$$

$\nu$  - frequency of excitation (i.e. device working frequency),  $\pi = 3.14\dots$ , and Stern-Volmer equation has the following form<sup>5</sup>:

$$\frac{\tan(\phi_0)}{\tan(\phi)} = 1 + K_{Sv} \cdot [O_2] \quad (\text{Eq.4})$$

Phase-fluorometric oxygen detection using long-decay oxygen-sensitive dyes requires modulation frequencies of excitation in the kHz range, and can be realised with simple optoelectronic components such as LEDs and photodiodes. Phase measurements enable discrimination of specific (modulated) fluorescent signal from the sensor from background (non-modulated) light by frequency filtering. Phase-fluorometric sensors allow operation under ambient light and work with detached sensors and variable sample geometry<sup>5</sup>.

### 3.2 Oxygen-Sensitive Materials for Packaging Applications

A variety of optical oxygen sensor systems have been developed for applications such as biomedical, environmental and process control<sup>20, 22, 24</sup>. But very few of them have been critically assessed for their suitability for food packaging applications. It has been proven that substantial development, optimization and redesign of the oxygen-sensitive materials and fabrication processes are required for the oxygen sensors to match practical requirements for these applications<sup>5</sup>. In particular, specific requirements of food applications are:

- to optimize and characterize the sensors for operation in broad temperature range (-20 °C - +40 °C), and with various types of foods, packaging materials and packaging processes;
- to make the sensors 'food and consumer-friendly', ensure their safety and minimize potential hazards that might originate from the sensors, when they are placed into packs;
- to validate the sensors with respect to their analytical performance, stability, safety, behavior in various types of foods, and in conditions of direct contact with foods;
- to make the sensors convenient for use by food producers, and integrate the sensors into packaging materials commonly used with MAP foods;
- to substantially reduce the costs of sensors and measurement equipment and make them affordable for use on a large scale by food producers, retailers, end-users; the costs of existing sensors (~1\$) are still prohibitive for use on disposable basis on a mass scale and have to be reduced 10-100-fold;
- to deal with ethical and legislative issues associated with the use of sensors with food products;
- to specialize the sensors and measurement equipment for specific food products and applications

Many of these tasks require extensive and multi-disciplinary R&D efforts supported by considerable investments, as well as active interaction with potential users (food and packaging industries, food research organizations, and with government institutions). This should be followed by extensive validation of such sensors with real foods and conditions of use.

Some examples of common materials developed for oxygen sensing are given in Table 1. The top part of Table 1 describes general purpose sensors, while the bottom part is concerned with specialized PtOEPK-PS based sensors developed for food packaging.

The main results of sensor optimization (modifications to the general purpose formulations) can be summarized as follows:

*Table 1.* Common materials used in quenched-fluorescence oxygen sensing (Ru(dpp)<sub>3</sub>(ClO<sub>4</sub>)<sub>2</sub>: tris(diphenylphenanthroline) ruthenium(II) perchlorate; PtOEPK: platinum(II)-octaethylporphine-ketone; PtPFPP: platinum(II)-tetrakis(pentafluorophenyl)porphine; PS: poly(styrene), PSu: poly(sulfone); PSB: poly(styrene-butadiene) block co-polymer; PVC: poly(vinylchloride); APET: amorphous poly(ethyleneterephthalate); PE: poly(ethylene).

<i>Oxygen-sensitive dye</i>	<i>Encapsulation medium</i>	<i>Support</i>	<i>Fabrication Technique</i>	<i>Solvent</i>	<i>Limitations/improvements</i>
General purpose oxygen sensors					
Ru(dpp) <sub>3</sub> ClO <sub>4</sub> (470/615nm)	PS, PVC	Polyester (Mylar)	Casting, tampon printing	Toluene	General sensing <sup>25</sup> O <sub>2</sub>
Ru(dpp) <sub>3</sub> ClO <sub>4</sub> (470/615nm)	Sol-gel	Glass, fibre, film, etc	Dip-coating, spin-coating (PreSens)	Alcohols	General sensing, curing required <sup>26</sup> O <sub>2</sub>
PtOEPK (590/760nm)	PS, PVC, PSu, plasticized PVC	Polyester (Mylar)	Casting	Chloroform, toluene	Good spectral and sensing properties, <sup>23,27</sup>
PtOEPK (590/760nm)	PS	Microporous membrane	Spotting	Chloroform, toluene	Enhanced signals, ease of fabrication <sup>28</sup>
PtPFPP (520/650nm)	PS, PSu	Polyester (Mylar)	Tampon printing	Toluene	Sterilizable <sup>29</sup>
Sensors optimised for packaging applications					
PtOEPK (590/760nm)	Food grade PS, PSB	Filter paper inserts	Spotting	Ethylacetate	Friendly solvent, optimised support <sup>16,17</sup>
PtOEPK (590/760nm)	Food grade PS	Packaging laminates (APET)	Spotting	Ethylacetate	Interaction with support, changes in calibration <sup>19</sup>
PtOEPK (590/760nm)	Food grade PS	Packaging laminates (PE)	Spotting	Ethylacetate	Poor sensor adhesion
PtOEPK (590/760nm)	Food grade PS	Paper with adhesive	Pre-made (Luxcel)	Ethylacetate	Adhesive sensor stickers <sup>30</sup>

- *oxygen-sensitive dye*: based on the chemical structures (low toxicity, biogenic nature), spectral characteristics and the results of migration studies, we give preference to the phosphorescent Pt-porphyrin dyes<sup>24</sup>; other dyes are also suitable, such as Ru(DPP)<sub>2</sub>, provided that corresponding safety tests and extensive performance evaluation are carried out and supported by solid experimental data;
- *encapsulation media*: polymers commonly used as packaging materials, e.g. food grade PS; plasticized polymers and systems requiring curing (sol-gels) are undesirable;
- *organic solvent*: those used in food industry, e.g. ethylacetate, methylethylketone; toxic solvents such as toluene, chloroform, THF should be avoided;
- *sensor supports*:
  - flat, non-porous, optically inert gas-impermeable supports (e.g. Mylar, polyester) – have excellent working characteristics, inert, but require special techniques for making sensors (casting, printing);
  - porous, gas-permeable optically active supports (e.g. white filter paper, polymer membranes) – provide higher signals, easy to make, robust<sup>28</sup>, but are often heterogeneous and have more complex sensing behavior; some were short-listed based on the results of comparative studies;
  - custom supports, e.g. fibre, packaging film, etc. – determined by the application;
- *ways of sensor incorporation in packs*
  - inserts – technically simple, but sensors can move within packs, dip into food or become difficult to access by the detector for measurement;
  - adhesive stickers – permanent attachment of sensors at a particular place in a pack (e.g. sealing film) facilitate the measurements, allow automation of both sensor incorporation and measurement processes;
  - sensors printed directly on packaging film – in development, performance still problematic.

Other specific issues to be considered when developing oxygen sensor systems for packaging applications include:

- the requirement to work in broad temperature range (-18 - +30 °C or at least +4 - +25 °C) and under ambient light; sensing materials with steeper temperature dependence of calibration (e.g. RuDPP compared to Pt-Por) are less preferred;
- direct contact of sensors with various foods (including fatty and greasy foods) and over prolonged shelf life may result in considerable changes in sensor calibration and migration of sensor components into food;
- the requirement to perform measurements under ambient light and at considerable distance from the sensor (some applications require up to 10 cm) is a major challenge for the external detector;

- variable size of packaged products, softness and irregular shape and variable physical (aqueous, fatty, solid) and optical properties necessitates the use of lifetime-based sensing (phase measurements).

All these factors should have minimal effect on the optical signal and oxygen readout obtained from the oxygen sensor, or they should be compensated for by the instrument or application software, by sensor manufacturer or by the user.

As a matter of fact, another important factor determining sensor performance and suitability for food applications is the degree of leaching of sensor components into food. The sensors which normally contain non-biogenic components (often very toxic ones) must be carefully assessed for the migration of these components into food. Comparative study performed with a number of oxygen sensors have shown detectable levels of migration of the dye in some media such as olive oil and 95% alcohol (both mimic fatty foods), and for RuDPP-based sensors migration was also observed in 3% lactic acid<sup>31</sup>. It is very important to reduce these undesirable processes to an absolute minimum, and this can be achieved by proper selection of the dyes, encapsulation media, support materials, fabrication process, etc.

### 3.3 The Use of Optical Oxygen Sensing in Food Packaging

A typical set-up for measurement of residual oxygen in a closed vessel, such as food packs is shown in Figure 1<sup>5, 24</sup>. The system consists of a benchtop phase-fluorometric detector (Luxcel Biosciences) built on the basis of low-cost optoelectronic components, which operates with a flexible fibre-

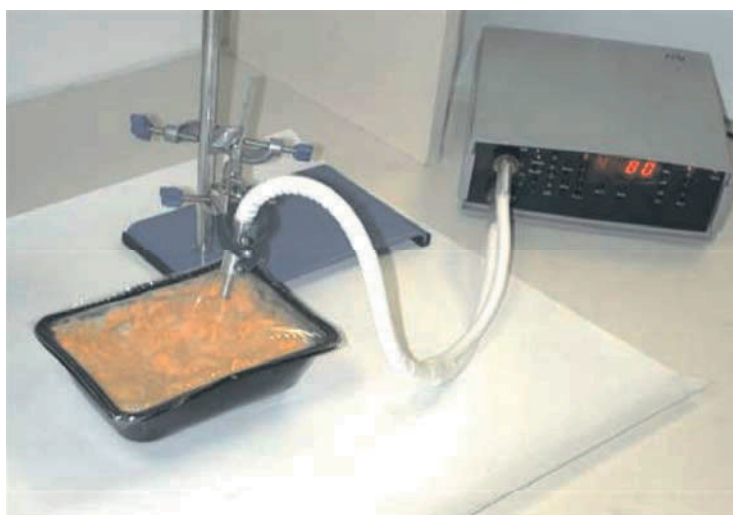


Figure 1. Typical set-up for measurement residual oxygen in food packs.

optic probe (40 cm long, 6 mm in diameter) and performs phosphorescence phase measurements with PtOEPK-PS based oxygen sensors<sup>18</sup>. The sensors are incorporated in samples during packaging (at the MAP packager or at the production line). Sensor stickers (Luxcel) are attached to the inside of packaging film with a labeling device<sup>30</sup>. The packs are subsequently flushed with modified atmosphere gas and sealed by heat-sealer.

This oxygen sensor system has been successfully used by us with a number of different types of packaged foods and packaging processes, being continuously developed and optimized in these real-life conditions and applications. It was validated in several small laboratory scale and medium industrial scale trials<sup>19,30</sup> with the following foods and processes:

- vacuum packaged meats (raw meat, chicken meat, chicken thighs) – lab trials;
- MAP smoked fish (hot and cold smoking) – lab trials;
- MAP bakery, bread – lab trials;
- MAP sliced hams - industrial trial;
- sous vide beef lasagna (convenience food) - industrial;
- MAP cheddar cheese – industrial trial.

These experiments have shown that the oxygen sensors are capable of providing important information about packaged products. They allow quantitative assessment of the quality of packs, their contents and packaging process in a simple, rapid and non-destructive fashion<sup>5</sup>. The sensors can be used to perform the following tasks:

- screening of batches of MAP food packs and detection of improper flushing with modified atmosphere gas in individual packs and variation in oxygen levels between packs;
- testing of integrity of packs and detection of air leaks in damaged or improperly sealed packs;
- detection of deviations from product/process specifications and predicted oxygen levels in batches of convenience food products (sous vide lasagna);
- measurement of residual oxygen profiles in packs over product shelf life;
- assessment of oxygen permeability of packaging materials and whole packages under various storage conditions used with different MAP products;
- prediction of food deterioration, spoilage e.g. due to improper storage conditions, poor quality of raw material – at early stages;
- quantification of microorganisms and their growth in packs (destructively).

Demonstration of some of these applications and practical results obtained with MAP foods are presented on the Figures 2 and 3.

At the same time, there are also limitations for the use of oxygen sensors. For example, their utility in in-line control of MAP process and *in situ*

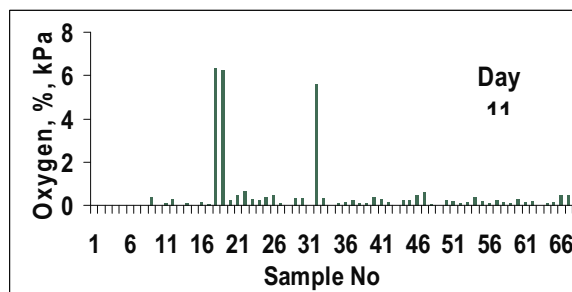


Figure 2. Screening for oxygen leaks in commercial MAP cheese packs using the oxygen sensor system: greatly elevated oxygen levels in packs 18,19, 32 on Day 11 after packaging.

detection of packs with oxygen leaks is problematic, due to the very short time between sealing and oxygen measurement, high throughput and small resident time for the packs on the packaging line. Oxygen sensors were shown to be rather inefficient with respect to monitoring of integrity of vacuum packaged foods, where they have failed to detect minor damages occurring close to the sensor<sup>32</sup>.

#### 4. OTHER OPTICAL SENSORS FOR FOOD APPLICATIONS

A few other optical chemical sensors for food applications are under development. Thus, sensors for carbon dioxide are in high demand, as the

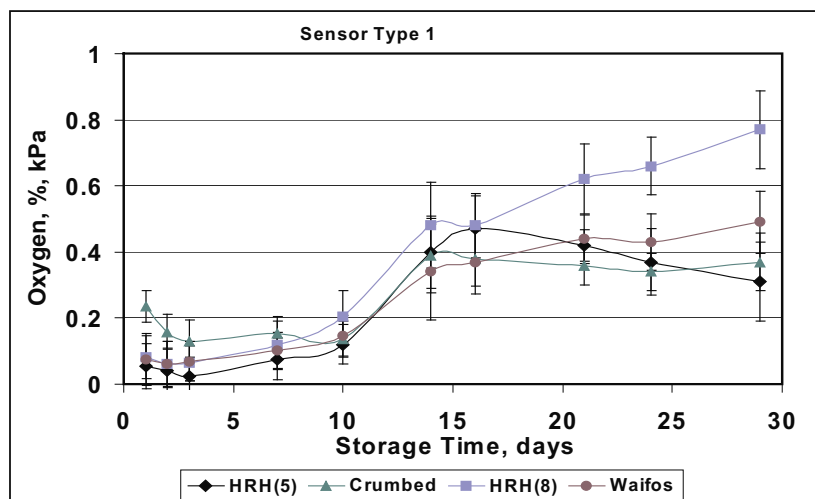


Figure 3. Oxygen profiles in four different types of commercial MAP hams over their shelf life measured with the oxygen sensors system. Changes between Days 10 and 15 and subsequent differentiation are seen.

levels of CO<sub>2</sub> in MAP packs tend to change considerably over shelf life, due to food respiration, absorption by moisture, etc.<sup>1-3</sup>. The possibility of parallel assessment of both oxygen and CO<sub>2</sub> would be highly desirable for quality assessment of MAP foods.

A number of promising CO<sub>2</sub> sensors have been described<sup>13, 33</sup>. The phase-fluorometric system employing dual luminophore referencing, which is rather complex (two dyes, internal buffer system, sol-gel polymer matrix), has demonstrated satisfactory working characteristics<sup>33</sup>. But it still has to prove its safety and cost-effectiveness, and requires extensive validation with real food samples.

A smart method for non-destructive testing of CO<sub>2</sub> content based on infra-red absorption has been described by Nix et al.<sup>34</sup>. Although working reliably with samples containing high levels of CO<sub>2</sub> (bottled carbonated beverages), this method demonstrated limitations in terms of sensitivity and sample optical properties.

Sensor for total volatile basic nitrogen using acidochromic calix[4]arene-based dye systems and reflectance measurements (digital camera or spectrometer) were described and used to monitor the release of volatile amines in the headspace of MA packs containing fish<sup>35, 36</sup>. This approach proved to be viable, although, its broad specificity could be potentially problematic, and other practical issues, such as sensor safety, interaction with package contents, range of compatible products, still have to be addressed in detail.

A novel approach for measurement of relative humidity (water vapour) by luminescence quenching and lifetime-based sensing using a fluorescent ruthenium dye immobilised in polymer membrane was described recently<sup>37</sup>. It allows direct sensing of relative humidity within the whole range 0 – 100%, and is essentially free from interference by molecular oxygen and organic vapours. These features make the system, which was developed for environmental applications, promising for packaging applications, particularly with moisture-sensitive foods (cereals, coffee, etc.).

## **5. CONCLUSIONS**

A number of optical chemical sensor systems have been developed for food and packaging applications and proven their utility. Some sensors, such as phase-fluorimetric oxygen sensor, have already reached high degree of maturity and demonstrated their potential for use on a mass scale. While the others still require extensive research, development and search for new solutions, so as to match basic practical requirements for such sensors. The experience and lessons learned with current optical sensor systems must be



exploited in full to develop improved or new sensors that are viable in food applications and can be used on a large scale.

## ACKNOWLEDGEMENT

This work was supported by the Irish Higher Educational Authority and the Department of Agriculture, Food and Fisheries, which are gratefully acknowledged.

## REFERENCES

1. Robertson G.L., *Food packaging: principles and practice*, Marcel Dekker Inc., New York, 1993.
2. Rooney M.L., Active packaging in polymer films. In M.L Rooney (Ed.) *Active food packaging*, London: Chapman and Hall, 1995; 74-110.
3. Louis P.J., Food packaging in the new millenium, *Packaging Technol. Sci.* 1999, 12: 1-7.
4. Smolander M., Hurme E., and Ahvenainen R., Leak indicators for modified-atmosphere packages, *Trends Food Sci. Technol.* 1997; 8(4): 101-106
5. Kerry J.P., Papkovsky D.B., Development and use of non-destructive, continuous assessment, chemical oxygen sensors in packs containing sensitive foodstuffs. *Res. Adv. Food Sci.* 2002; 3: 121-140.
6. Smiddy M.A., Papkovsky D.B., Kerry J.P., Evaluation of oxygen content in commercial modified atmosphere packs (MAP) of processed cooked meats, *Food Research International* 2002; 35: 571-575.
7. Cook J.M., Karelitz R.L. and Dalsis D.E., Measurement of oxygen, nitrogen, and carbon dioxide in beverage headspace, *J. Chromatogr. Sci.* 1985; 23: 57-63.
8. Johnson B., Headspace analysis and shelf life, *Cereal Foods World* 1997; 42: 752-754.
9. Stephens S.K., Cullen D.C. and Warner P.J., Novel detection systems for rapid assays in the food industry. *European Food and Drink Review, Autumn*, 1997; pp.83-84: 86-88.
10. Kress-Rodgers E., Instrumentation for Food Quality Assurance, in: Kress-Rodgers, E., editor. *Instrumentation and sensors in the food industry*. London: Woodhead Publishing Ltd., 1998, p.1-34.
11. Yoshikawa Y., Nawata T., Goto M. and Fujii Y., US Patent 4,169,811.
12. Gestrelus H., Mattila-Sandholm T. and Ahvenainen R., Methods for non-invasive sterility control in aseptically packaging foods, *Trends Food Sci. Technol.* 1994; 5: 379-383.
13. Mills A., Chang Q., McMurray H.C., Equilibrium study on colourimetric plastic film sensors for carbon dioxide, *Anal. Chem.* 1992, 64: 1383-1389.
14. Reininger F., Kolle C., Trettnak W. and Gruber W., Quality control of gas-packed food by an optical oxygen sensor, In *Proc. Int. Symp. Food Packaging: Ensuring the Safety and Quality of Foods*, 11-13 September, 1996, Budapest, Hungary.
15. Fitzgerald M., Papkovsky D.B., O'Sullivan C.K., Guilbault G.G., Optical oxygen sensing in vacuum packed foods, *Proc. workshop Biosensors for Environmental Monitoring*, Kinsale, Ireland, 12-15 May, 1998, p.89.
16. Papkovsky D.B., Papkovskaia N., Smyth A., Kerry J.P., Ogurtsov V.I., Phosphorescent sensor approach for non-destructive measurement of oxygen in packaged foods: optimisation of disposable oxygen sensors and their characterization over a wide temperature range, *Anal. Lett.* 2000; 33: 1755-1777.

17. Papkovsky D.P., Smiddy M.A., Papkovskaia N.Y., Kerry J.P., Non-destructive measurement of oxygen in modified atmosphere packaged hams using a phase-fluorimetric sensor system, *J. Food Sci.* 2002; 67: 3164-3169.
18. Saini D.P., Desault M., An exciting new non-invasive technology for measuring oxygen in sealed packages the OxySense™ 100, Proc. Worldpack-2002, June 23-28, Michigan.
19. O'Mahony F.C., O'Riordan T.C., Papkovskaia N., Ogurtsov V.I., Kerry J.P., Papkovsky D.B., Assessment of oxygen levels in convenience-style muscle-based sous vide products through optical means and impact on shelf-life stability. *Packaging Technol. Sci.*, 2004; 17 (4): 225-234.
20. Demas J.N., DeGraff B.A. and Coleman P.B., Oxygen sensors based on luminescence quenching. *Anal. Chem.* 1999, 71: 793A-800A.
21. Trettnak W., In: *Fluorescence Spectroscopy. New Methods and Applications*, O.S.Wolfbeis, Ed., Springer-Verlag, Berlin, 1993, p.79.
22. Wolfbeis O.S., Fluorescence-based optical sensors for biomedical applications, In: Scheggi A.M.V., Martelluci, S., Chester, A.N., Pratesi, R. (Eds.), *Biomedical Optical Instrumentation and laser-Assisted Biotechnology*, Kluwer Academic Publishers, 1996, p.327-337.
23. Papkovsky D.B., Ponomarev G.V., Trettnak W., O'Leary P., Phosphorescent complexes of porphyrin-ketones: optical properties and application to oxygen sensing, *Anal. Chem.* 1995; 67: 4112-4117.
24. Papkovsky D.B., Methods in optical oxygen sensing: protocols and critical analyses, *Methods Enzymol.*, Ed., C.K.Sen, G.L.Semenza, 2004, 383, 715-734.
25. Hartmann P., Photochemically induced energy-transfer effects on the decay times of ruthenium complexes in polymers, *Anal. Chem.* 2000, 72(13): 2828-2834.
26. McDonagh C., MacCraith B.D., McEvoy A.K., Tailoring of sol-gel films for optical sensing of oxygen in gas and aqueous phase, *Anal. Chem.* 1998, 70(1): 45-50.
27. Hartmann P., Trettnak W., Effects of polymer matrices on calibration functions of luminescent oxygen sensors based on porphyrin ketone complexes, *Anal. Chem.* 1996; 68(15): 2615-2620.
28. Papkovsky D.B., Ovchinnikov A.N., Ogurtsov V.I., Korpela T., Biosensors on the basis of luminescent oxygen sensor: the use of microporous light-scattering support materials. *Sens. Actuat.B* 1998; 51: 137-145.
29. Voraberger H.S., Kreimaier H., Biebernik K., Kern W., Novel oxygen optrode withstanding autoclavation: technical solutions and performance, *Sens. Actuat. B* 2001; 74 (1-3): 179-185.
30. O'Mahony F.C., O'Riordan T.C., Papkovskaia N., Kerry J.P., Papkovsky D.B., Non-destructive assessment of oxygen levels in industrial modified atmosphere packaged cheddar cheese, *Food Control* Available online 2006 17 (4) 286-292.
31. O'Riordan T.C., Voraberger H., Casey N., Kerry J.P., Papkovsky D.B., Study of migration of active components of phosphorescent oxygen sensors for food packaging applications, *Anal. Chim. Acta* 2005; 350, 135-141.
32. Smiddy M., Fitzgerald M., Kerry J.P., Papkovsky D.B., O'Sullivan C.K., Buckley D.J., Guilbault G.G., Use of oxygen sensors to non-destructively measure the oxygen content in modified atmosphere and vacuum packed beef: impact of oxygen content on lipid oxidation, *Meat Science* 2002; 61: 285-290.
33. von Bultzingslowen C., McEvoy A.K., McDonagh C., MacCraith B.D., Klimant I., Krause C., Wolfbeis O.S., Sol-gel based optical carbon dioxide sensor employing dual luminophore referencing for application in food packaging technology, *Analyst* 2002; 127(11): 1478-1483.
34. Nix J.A., Zagarola S.W., Jolie L. (1995). US Patent 5,473,161.
35. Loughran M., Diamond D., Monitoring of volatile bases in fish sample headspace using an acidochromic dye, *Food Chem.* 2000; 69: 97-103.

36. Byrne L., Lau K.T., Diamond D., Monitoring of headspace total volatile basic nitrogen from selected fish species using reflectance spectroscopic measurements of pH sensitive films, *Analyst* 2002; 127 (10): 1338-1341.
37. Bedoya M., Orellana G., Moreno-Bondi M.C., Fluorescent optosensor for humidity measurements in air, *Helv. Chim. Acta* 2001; 84 (9): 2628-2639.

## Chapter 25

# OPTICAL CHEMICAL SENSORS FOR CULTURAL HERITAGE

Gabriele Cristoforetti, Stefano Legnaioli, Vincenzo Palleschi,  
Azenio Salvetti and Elisabetta Tognoni  
*Applied Laser Spectroscopy Laboratory*  
*Istituto per i Processi Chimico Fisici del CNR*  
*Area di Ricerca di Pisa, Via G. Moruzzi, 1 – 56124 Pisa (ITALY)*

### 1. INTRODUCTION

In recent years, several groups have proposed the use of Laser Induced Breakdown Spectroscopy as a technique capable of giving information on the pigment compositions with minimal damage of the artwork. However, until the development of quantitative methods for accurate elemental analysis, the LIBS technique was hardly competitive with other methods for quantitative analysis of the samples.

A new approach to LIBS spectroscopy, developed by the Applied Laser Spectroscopy Team at IPCF-CNR (Pisa), has re-proposed this technique as a viable technique for the self-calibrated, precise quantitative analysis of pigments used in Cultural Heritage. Moreover, we have also demonstrated the possibility of obtaining micrometric resolutions ( $\mu$ -LIBS) in LIBS analysis of paintings, reducing the surface damages at minimal levels. On the other hand, micro-Raman spectroscopy is a well-assessed technique which gives valuable, although qualitative, information on the structure of the pigments and binders used in the artwork

As an example of the application of joint micro-LIBS and micro-Raman analysis on actual samples, results are reported on the study of a small fragment (less than 1 mm<sup>2</sup>) of the “S. Antonio Abate”, a wooden painted artwork decorating the Arciconfraternita della Misericordia in Siena, attributed to the Renaissance Italian artist Domenico di Pace, also known as “Il Beccafumi” (Montaperti 1486 – Siena 1551). The sample, whose dimensions were relatively small (less than 1 mm<sup>2</sup>), was given by Opificio delle Pietre Dure di Firenze (OPD) to the Department of Chemistry of Pisa University, where it was going to be analysed for the presence of lakes in the

red painting. Before these measurements, a LIBS and Raman analysis was performed for a preliminary characterization of the sample.

## 2. EXPERIMENTAL

The experimental set-up used for the micro-LIBS measurements on the painted sample is sketched in Figure 1.

The laser beam is focussed on the sample surface using a microscope objective, and the signal is taken on axis through the same objective. An optical digital microscope allows for the visual inspection of the sample during the measurement; the sample is mounted on a three-axis motorised stage, controlled by a personal computer, for adjustment of the focusing position.

The laser source is a Nd:YAG pulsed laser, operating at 1064 nm, which delivers about 10 mJ on the sample surface, in 8 ns. The spatial lateral resolution of the LIBS measurements corresponds to the dimensions of the micro-crater left by the laser on the sample surface. The same dimensions are also a measurement of the damage induced on the pigment. A computer-enhanced enlargement of a typical laser crater is shown in Figure 2; its diameter does not exceed 10  $\mu\text{m}$ , which is practically invisible at naked eye. The reduced size of the crater also allows for a high spatial resolution of the LIBS analysis.

The LIBS spectral signal is detected using an Echelle spectrometer + iCCD camera, which provides the whole time-resolved NUV-NIR spectrum in a single laser shot.

A computer controls the whole measurement process; dedicated software allows to perform surface scanning, spectral averages and acquisition of the

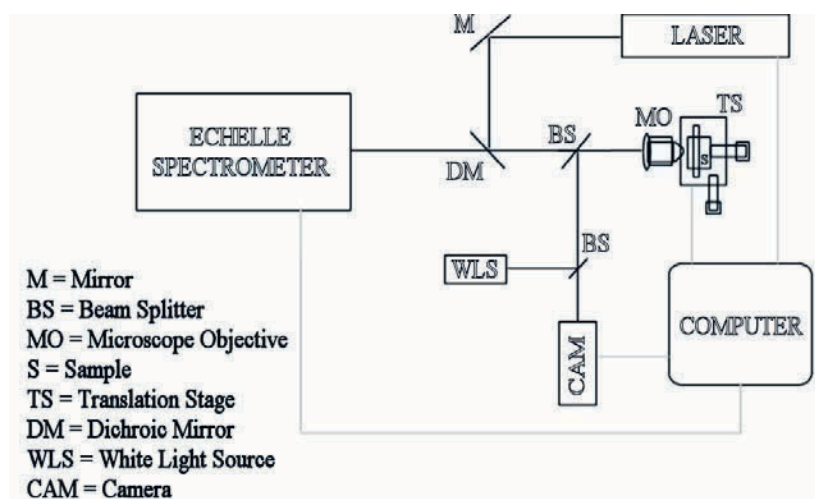


Figure 1.  $\mu$ -LIBS experimental setup.

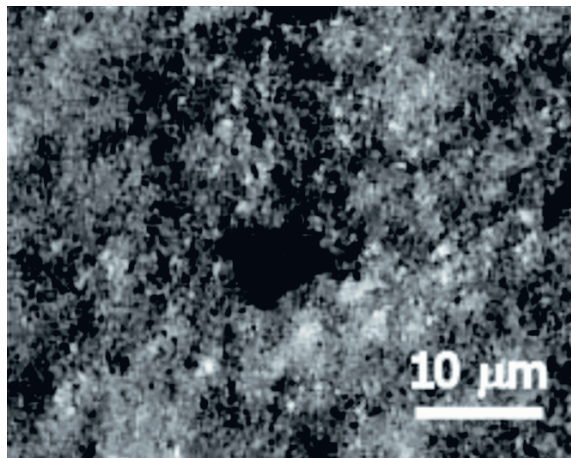


Figure 2. Computer-enhanced enlargement of the crater produced by the laser on the surface.

spectra. In typical experimental conditions, the micro-LIBS spectra are taken in a single laser shot, 300 ns after the laser pulse and using a measuring gate of 200 ns. The LIBS spectra are analysed with proprietary software, developed at IPCF-CNR, which implements the Calibration-Free LIBS procedure (CF-LIBS) and allows the precise quantitative determination of the elemental composition of the material without any reference sample or calibration curve. The software also automatically implements the corrections for plasma self-absorption recently developed by the IPCF-CNR group; a more detailed discussion of the CF-LIBS technique and self-absorption correction has been given in [4]. In typical experimental conditions, the complete characterisation of the material is performed in less than five minutes, with practically no damage of the painted surface.

In Figure 3 is shown the experimental set-up used for micro-Raman measurements.

The experimental set-up used for micro-Raman measurements is essentially identical to the one used for the micro-LIBS analysis. In this case, the laser beam generated by an ion laser  $\text{Ar}^+$  multimode (operating in continuum) goes through a filter, which selects the 514 nm component and excludes the others frequencies; the laser radiation is reflected by the notch filter, which, in a first phase, behaves exactly as a mirror; then is focused on the sample by a 50X microscope objective. The light diffused goes back to the notch filter, which does not transmit the laser wavelength. The light is collected onto the entrance slit of a spectrometer (Jobin Yvon THR1000) with a 600 lines/mm grating, flat field and long focal length (1000 mm), allowing a spectral resolution of about  $1 \text{ cm}^{-1}$ . The spectral signal is detected by a cooled CCD (KAF-1001E, produced by DTA Scientific Instrument) and then analyzed with appropriate software. The sample is mounted on a three-axis motorised stage, controlled by a personal computer, for adjustment of

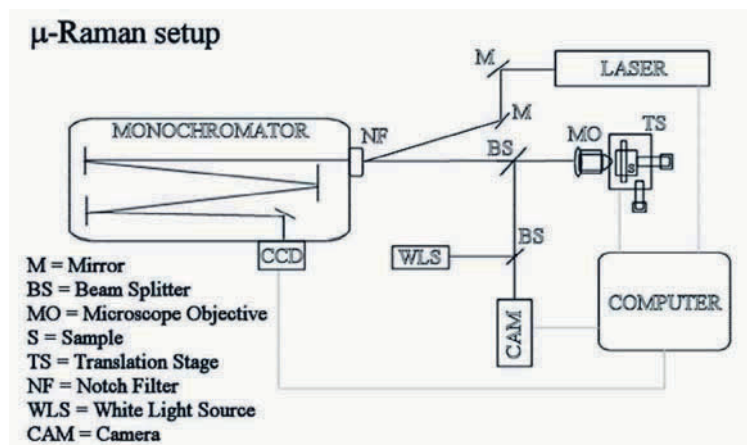


Figure 3. –  $\mu$ -Raman experimental setup.

the focusing position. Moreover, a camera allows the visualization of the examining zone, assuring a perfect focusing of the position.

### 3. RESULTS AND DISCUSSION

The sample analysed was taken from a painted fragment from the “S. Antonio Abate” painting of Domenico Di Pace, called “Il Beccafumi” (Montaperti 1486 – Siena 1551) (see Figure 4). The artwork is a wooden

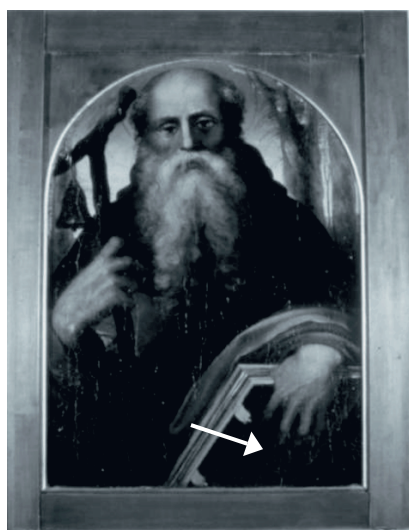


Figure 4. The “S. Antonio Abate” by Beccafumi. The arrow indicates the point from where the fragment was taken.

painting decorating the Arciconfraternita della Misericordia in Siena. The sample, whose dimensions were relatively small (less than  $1 \text{ mm}^2$ ), was given by Opificio delle Pietre Dure di Firenze (OPD) to the Department of Chemistry of Pisa University, where it was going to be analysed for the presence of lakes in the red painting. Before these measurements, a LIBS analysis was performed for a preliminary characterization of the sample. In particular, the presence of aluminium in the red painting could be considered as an indicator of the possible use of organic lakes along with the main red pigment.

The LIBS analysis of the fragment involved a single laser shot focussed on the painted surface; the aluminium concentration detected (about 2% in weight) is compatible with the use of a small quantity of organic lake mixed to the main red pigment. The presence of high concentration of Mercury in the sample revealed the main red pigment as Cinnabar ( $\text{HgS}$ ), probably mixed with white lead ( $2\text{PbCO}_3\text{Pb(OH)}_2$ ) or minium ( $\text{Pb}_3\text{O}_4$ ) (see Figure 5). White lead was often used in conjunction with organic lakes for obtaining a particular shade of red; however, Cennino Cennini in its "Libro dell'Arte" reports that sometimes cinnabar in the red pigments was diluted with minium, for reducing its cost. Therefore, the high concentration of lead detected by LIBS in the red pigment cannot be univocally attributed to the use of white lead or minium, or both.

Since LIBS analysis doesn't give information about the molecular composition of the pigments, a micro-Raman analysis was performed for an exact characterization of the sample.

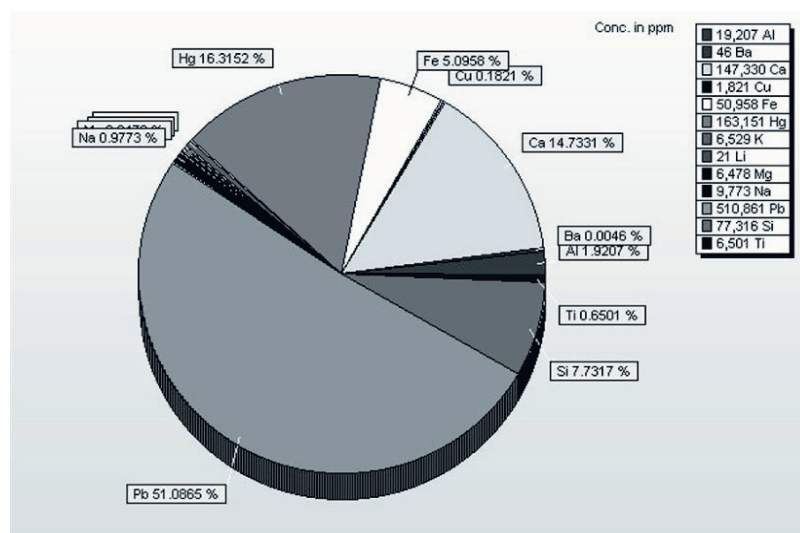


Figure 5. Composition of the red pigment in the Beccafumi fragment.



For Raman measurements, the collected spectra were compared directly with the Raman spectra database of pigments compiled by the Chemical Department of University College of London.

Figure 6 shows the Raman spectra obtained for the red pigment. The Raman signal observed in the first spectrum is very low due to the use of a reduced laser power onto the sample; in fact, Cinnabar is a very delicate pigment and the painted surface can be easily irreparably damaged by the focused laser. Consequently the signal/noise ratio decreased. Nevertheless, in the first Raman spectrum the lines at  $252\text{ cm}^{-1}$  and  $343\text{ cm}^{-1}$ , typical of Cinnabar, are evident, while the line at  $282\text{ cm}^{-1}$  is sketchy. The second spectrum corresponds to the analysis of a close point in the fragment. Here, the line at  $548\text{ cm}^{-1}$  and the line at  $1050\text{ cm}^{-1}$  (the most intense lines of minium and white lead respectively) can be distinguished. This fact confirms

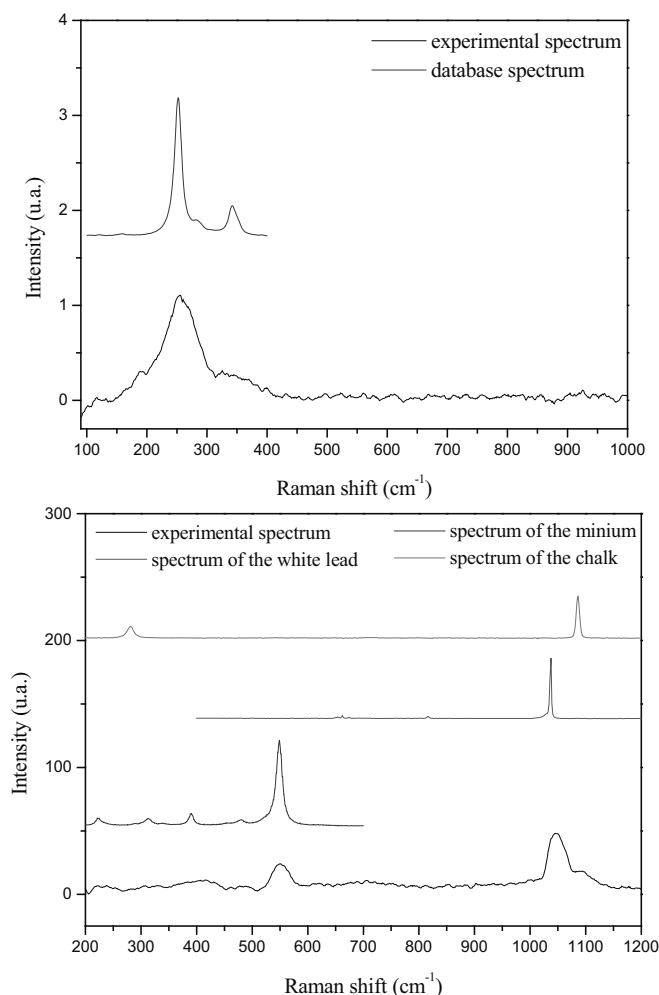


Figure 6. Raman spectra of the red pigment.

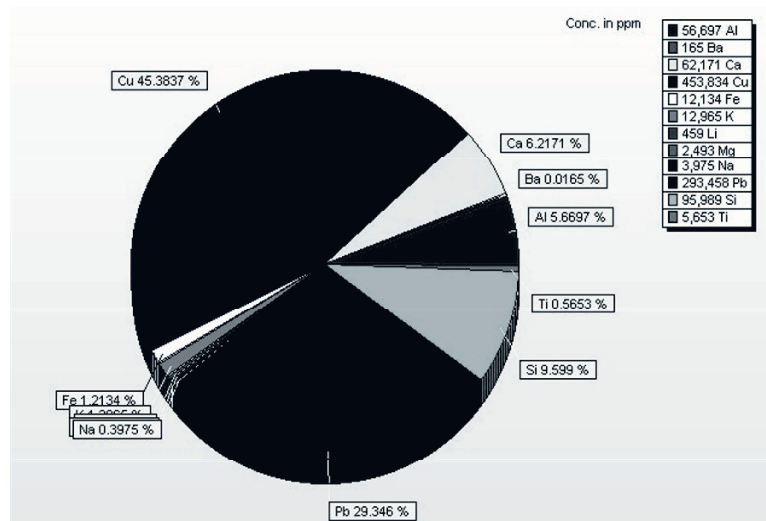


Figure 7. Composition of the blue pigment in the Beccafumi fragment.

the hypothesis of the use of both Cinnabar and minium in the red pigment, mixed with white lead. In the Raman spectrum is also visible the chalk line at  $1088\text{ cm}^{-1}$ ; in fact, according to Cennini<sup>7</sup>, for the realization of a painting on wood, a canvas was stuck on the board and was coated with a mixture of glue and chalk, constituting the basis for the priming and creating a waterproof layer on the wood.

An accurate observation of the first crater produced during the LIBS measurement with a camera revealed the presence of a blue substrate under the upper red layer of painting. The LIBS analysis demonstrated that the underlying blue substrate is composed by azurite (a copper based pigment) mixed with white lead (Figure 7).

The Raman analysis confirmed this identification. In Figure 8 are reported the Raman spectrum of the blue pigment obtained and the one provided by the UCL database: the superimposition of the two spectra is, in this case, about perfect.

It's interesting to note that a Cinnabar+white lead layer over azurite+white lead substrate was used in the "Maria Maddalena" painting by Giacomo Cozzarelli (1453-1515), an artist contemporary to Beccafumi.

#### 4. MULTI-SPECTRAL SENSOR

The method of multispectral imaging exploits the characteristics of CCD cameras for obtaining information on the wavelength dependence of the reflectivity of the objects of interest. Different approaches are possible for reaching this goal:

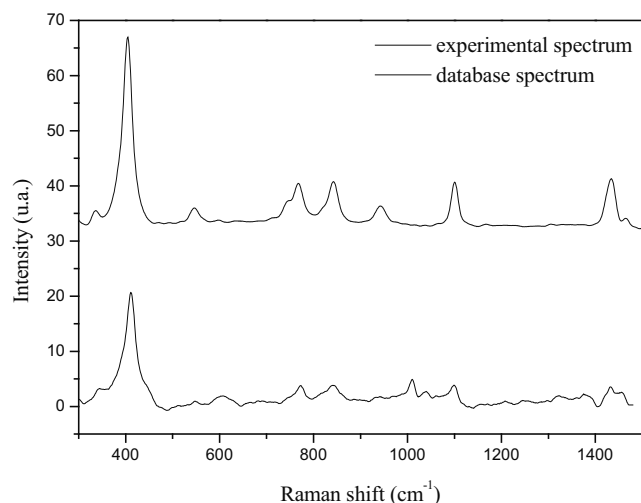


Figure 8. Raman spectrum of the blue pigment.

1. Extraction of the Red, Green and Blue (RGB) components from a standard digital image. This approach does not require the use of specialized hardware, and most commercial software are capable of performing RGB splitting on color images in various formats (GIF, JPG, BMP, TIF, ecc.). The main drawback of this method is the sensitivity to compression or acquisition artifacts affecting the original image; in fact, the color reconstruction on the CCD is obtained through interpolation of the original image obtained using a pattern of micro red, green and blue filters placed over each pixel. As previously discussed the ratio of green filters to that of red and blue is two to one. The true color is made by averaging the light intensity of the pixels around it - a process known as color interpolation; this method reduces the resolution of the final image, producing a kind of 'color blurring' of the resulting decomposed images.
2. A series of gray-scale, full resolution pictures are taken, either filtering the reflected light before the digital camera objective, or filtering the light which illuminates the object. Both these approaches give the same result, i.e. an image proportional to the reflectivity of the object at the wavelength selected by the filter.

The advantages of this latter method are evident, since the image is taken at its full resolution (full scan) and the bandpass of the filter(s) can be appropriately chosen in order to optimize the image quality. Several wavelengths bands can be acquired and the color image can be easily reconstructed combining the Red, Green and Blue bands, if available. Moreover, non-visible regions of the spectrum can also be sampled (namely infrared and ultra-violet reflection) exploiting the extended sensitivity of the

CCD sensor which, in these regions, is usually higher than the sensitivity of the human eye. For comparison, the wavelength dependence of the response of human eye and the CCD camera used at IPCF is shown in figure 9.

As a further advantage of the full scan approach to multispectral imaging is that the individual parameters of the acquisition - namely focus, diaphragm aperture and acquisition time - can be separately optimized in order to have perfect images in all the spectral bands considered. The drawback of this approach, with respect to standard color decomposition, is the need of taking separate exposures at all the spectral bands of interest and the need of 'balancing white' at the beginning of the acquisition in order to have a faithful color reconstruction of the image.

The IPCF camera can be used in UV reflectivity and UV fluorescence mode, illuminating the object with UV light and choosing the proper acquisition mode by software. The light source used for UV reflectivity and fluorescence measurements was a 150 W Wood lamp illuminating the sample at a distance of 50 cm from the surface.

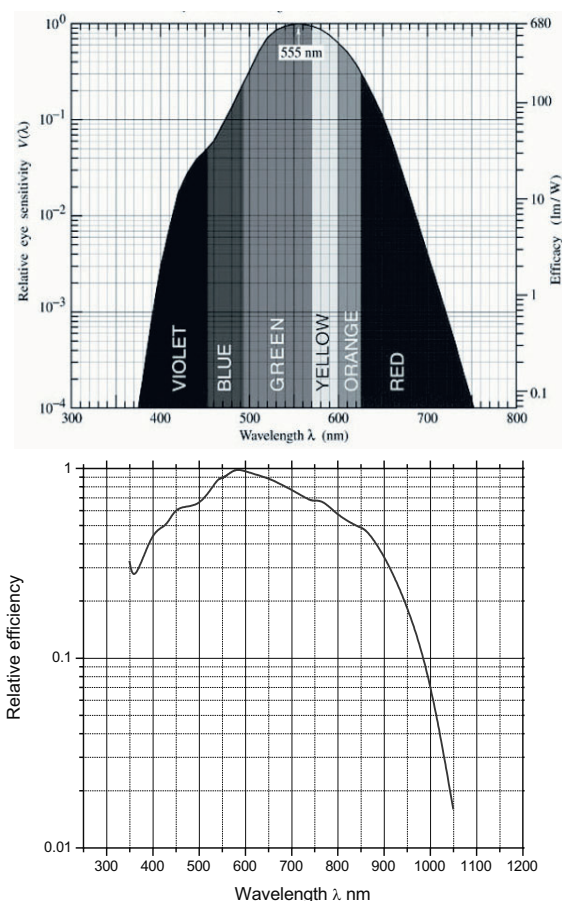


Figure 9. Spectral sensitivity of human eye (at the top) vs. IPCF CCD sensor (at the bottom).

The near UV spectral range is divided in three bands: the short wave band or UV-C emission runs from 180 to 280 nm with a peak at 254 nm. The medium wave band or UV-B runs from 280 to 320 nm with a peak at 312 nm, while the UV-A long wave band runs from 320 to 380 nm with a peak at 365 nm. The long wave emission is commonly called "Black light" or "Wood's light". Only the UV-A portion of the lamp spectrum is useful for UV reflectivity measurements, since wavelengths under 400 nm are cut off by the glass optics of the objective. However, the full power of the lamp is used for UV fluorescence measurements.

Measures in UV reflectivity mode are thus possible, using a 400 nm peaked narrowband filter. However, because of the glass optics absorption below 400 nm and the low sensor sensitivity in the UV, the quality of the images in UV reflection mode is not particularly good, because of the long exposure time need for compensating the low illumination on the sensor.

On the contrary, since spectral incandescent lamps have their maximum emission in the IR band, good quality images can be obtained - taking also into account the spectral sensitivity of the CCD sensor - in the band comprised between 700 and 1100 nm.

The long wavelength of the infrared illumination allows penetration of the light below the surface layers of the painting, often revealing details of the underdrawing or giving evidence of damages not visible at the naked eye (see figure 10).

The difference in reflectivity of various materials in visible and IR band can also be useful exploited for identification of the materials in a fully non-invasive way.



Figure 10. IR image (at the left) of a XVII century Russian icon, evidencing sub-surface damages not visible in the RGB image at the right.

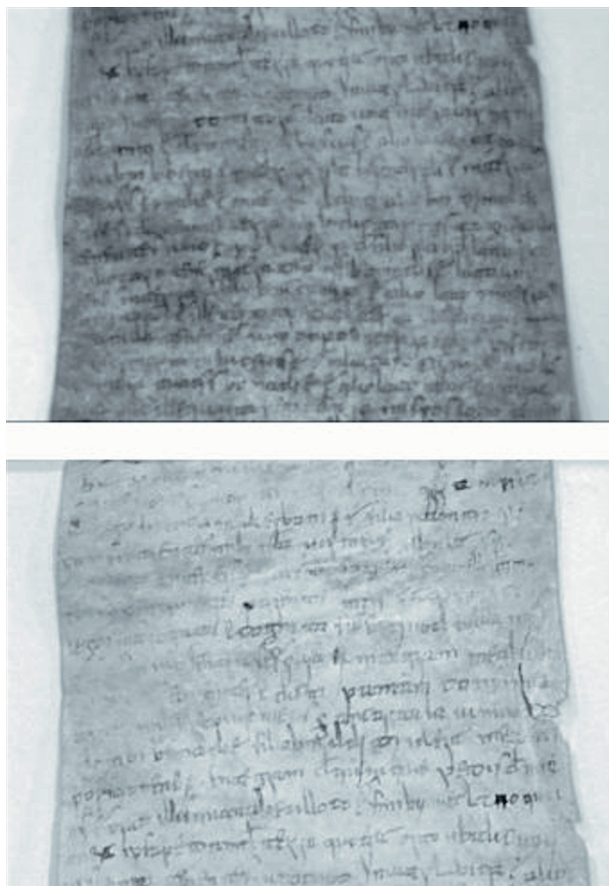


*Figure 11.* The increased readability of the text in the IR image (at the bottom) with respect to the visible image (at the top) in a XI century manuscript evidences that carbon nature of the ink used.

An interesting example of this possibility is the identification of different kinds of inks in ancient manuscripts. It is well known that Iron gall, the most used ink in manuscripts since Middle Age, is highly corrosive for the substrate. Many efforts have been devoted in recent past to the restoring of damaged texts and drawings; however, proper identification of the ink is crucial for determining the best conservative and restoring procedures.

For identification of the iron gall inks, one must consider that the visibility of iron gall texts and drawings dramatically decreases in the IR band. On the other hand, carbon based inks absorb IR light, thus giving enhanced readability in the IR image (see figure 11).

These findings therefore suggest the possibility of using the information on the different absorption in the visible and the IR for a very quick, cheap and non-invasive determination of the ink composition using this optical sensor.

## 5. CONCLUSIONS

The results reported show that the joint use of different spectroscopic techniques allows the complete characterization, both structural and elemental, of the materials under study. The measurements performed with these techniques are fast, reliable and virtually non-destructive. The results obtained are, therefore, encouraging for the use of optical chemical sensors in the field of Cultural Heritage.

## REFERENCES

1. Palleschi V., Arca G., Rastelli S., Ciucci A., Tognoni E., Verso il laser intelligente: applicazione alla pulitura di monumenti, Internal Report IFAM B01LS/96 (1996).
2. Anglos D., Couris S., Fotakis C., Laser Diagnostics of Painted Artworks: Laser-Induced Breakdown Spectroscopy in Pigment Identification, *Appl. Spectrosc.* 1997; 51(7): 1025.
3. Ciucci A., Palleschi V., Rastelli S., Salvetti A., Tognoni E., New procedure for quantitative elemental analysis by Laser Induced Plasma Spectroscopy, *Appl. Spectrosc.*, 1999; 53 (8): 960.
4. Bulajic D., Corsi M., Cristoforetti G., Legnaioli S., Palleschi V., Salvetti A., Tognoni E., A procedure for correcting self-absorption in calibration-free Laser Induced Breakdown Spectroscopy, *Spectrochimica Acta B* 2002; 57: 339-357.
5. Bicchieri M., Nardone M., Russo P.A., Sodo A., Corsi M., Cristoforetti G., Palleschi V., Salvetti A., Tognoni E., Characterization of azurite and lazurite based pigments by LIBS and micro-Raman spectroscopy, *Spectrochim. Acta B* 2001; 56: 915-922.
6. Bussotti L., Castellucci E., Matteini M., The Micro-Raman Technique in the Studies for the Conservation of Art Works: Identification of Lakes in Paints, *Science and Technology for Cultural Heritage* 1996; 5 (1): 13.
7. Cennini C., *Il Libro dell'Arte* (XIV sec.), cured by R. Simi, R. Carabba Editore, Lanciano 1932.
8. Raman spectral database available on-line at address: <http://www.chem.ucl.ac.uk/resources/raman/speclib.html>.
9. Hain M., Bartl J., Jacko V., Multispectral analysis of Cultural Heritage artefacts, *Measurement Science Review*, Volume 3, Section 3 (2003).
10. Poger S., Angelopoulou E., Selecting Components for Building Multispectral Sensors, IEEE CVPR Technical Sketches 2001, IEEE Computer Society Press (2001).
11. Hechts E., *Optics*, 3rd ed. Addison Wesley Longman, (1998).

## INDEX

- $\alpha$ -helix, 327
- $\beta$ -sheet, 327
- 1,2-dioxetanedione, 159
- 1,3,5-trinitrotoluene, 410
- 1,3-dinitrobenzene, 410
- 2,4-dichlorophenoxyacetic acid, 372
- 2-[4-(dimethylamino)phenylazo] benzoic acid, 368
- 2-cyanophenyl octyl ether, 299
- 2-nitrophenyl octyl ether, 299
- 3-methylcrotonyl-coenzyme-A carboxylase, 332
- 4-(p-N,N-dimethylaminophenylmethylene)-2-phenyl-5-oxazolone, 367
- 4-nitrotoluene, 409
- 8-hydroxypyrene-1,3,6-trisulfonyl chloride, 306
- 9,10-diphenylanthracene, 23, 160
- absorbance, 81
- absorption, 77, 79, 89, 99, 100, 150, 197, 201, 213, 466
  - charge-transfer, 81
  - coefficient, 101
- acetic acid, 316
- acetylcholine, 349
- acetylcholinesterase, 349, 371
- acetyl-coenzyme A carboxylase, 332
- acrylamide, 89
- activator, 326
- adenosine triphosphate, 33, 160, 161, 162, 167, 168
- ADP, 167, 168
- adsorption, 338
- Aequorea*, 160
- aerogel, 302
- affinity biosensor, 184
- affinity sensor, 33
- alcohol, 316
- alcohol dehydrogenase, 332
- alcohol oxidase, 164
- aldehyde, 316
- alkali ion, 29
- alkaline phosphatase, 31, 33
- alkane, 21
- allergen, 481
- amberlite, 24, 29, 427
- amine, 316, 377
- aminoethyl cellulose, 306
- ammonia, 26, 31, 89, 204, 317, 349, 367, 370, 465
- ammonium ion, 31
- AMP, 167, 168
- anion, 31, 310
- anthrax, 446
- antibody, 387, 439, 497
  - immobilization, 491
  - isoelectric point, 388
  - monoclonal, 389
  - polyclonal, 389
  - polyclonal, 498
- antibody immobilization
  - covalent attachment, 395
  - multilayer assemblies, 397
  - physical adsorption, 394
- antigen, 388, 497
- anti-Stokes line, 126
- aptamer, 491
- aryl-aldehyde dehydrogenase, 332
- ATP. *See* adenosine triphosphate
- ATR. *See* attenuated total reflection
- attenuated total reflection, 123, 129, 130, 132, 139, 146
- attenuation, 48, 61
- azo dyes, 18, 84, 85
- azurite, 521
- Bacillus abortus*, 447
- Bacillus anthracis*, 447
- Bacillus globigii*, 445
- bacterial artificial chromosome, 250
- bacterial artificial chromosomes, 250
- Barrett's oesophagus, 422
- Beer-Lambert law, 81
- benzoyl-coenzyme A reductase, 332
- bile, 418
- bilirubin, 22, 418
- Bilitec 2000, 418
- bioaffinity sensor, 324
- biocatalytic sensor, 324
- biochemical oxygen demand, 112, 375
- biochip, 157, 171, 172, 173, 174, 479



- biomolecule immobilization, 486
  - printing technique, 483
- bioluminescence, 157, 160
  - bacterial, 161
  - firefly, 161
- bis(2-ethylhexyl) phthalate, 299
- bis(2-ethylhexyl) sebacate, 299
- bismuth, 366
- BOD. *See* biochemical oxygen demand
- Botulinum toxin*, 190
- bovine serum albumin, 378
- brilliant blue, 378
- bromocresol green, 86, 366, 367
- bromocresol purple, 86, 204, 366, 367, 369, 371
- bromophenol blue, 89, 304, 316, 366, 368, 369, 370, 378, 423
- bromothymol blue, 88, 349, 371
- butane, 146
- calcium, 94, 161, 309
- carbamate, 349
- carbon dioxide, 23, 24, 26, 31, 106, 146, 316, 349, 365, 367, 372, 373, 465, 467, 470, 474, 511
  - blood, 35, 419
  - end-tidal, 428
  - gastric, 427
  - vibrational modes, 127
- carbon dioxide partial pressure, 419, 421, 422
- carbon monoxide, 364
- carbon monoxide haemoglobin, 425
- carbonic anhydrase, 332
- carboxyhemoglobin, 425
- carboxymethyl cellulose, 306
- carboxypeptidases, 332
- carboxy-poly(vinyl chloride), 306
- cation, 29, 92, 308
- CCD, 56, 172, 273
- cDNA, 497
- cDNA array, 480
- cellulose, 314
- cetyltrimethylammonium bromide, 370
- chalcogenide, 138
- chelators, 91
- chemiluminescence, 99, 101, 157, 158, 159, 163, 169, 171, 349
- chloride, 23, 31
- chlorophenol red, 349
- cholera toxin, 447
- cholesterol, 171
- choline, 111, 164, 169, 171
- choline oxidase, 171
- cholinesterase, 371
- chorismate synthase, 332
- chromogenic indicators, 313
- chromophoric group, 92
- cinnabar, 519, 520
- cis-polybutadiene, 300
- CO<sub>2</sub>. *See* carbon dioxide
- cobalt chloride, 23
- comb filter, 463
- combination vibration, 123
- complementary source modulation, 465
- concanavalin, 20, 33
- connectors, 49
- copper, 21, 34, 92, 93, 314, 315
- correlation spectroscopy, 463, 466
- cresol red, 88, 368
- critical angle, 219
- crown ether, 29
- Cu(II). *See* copper
- cytochrome c, 247, 378
- cytochrome oxidase, 332
- cytokines, 481
- dabcyl-N-succinimidyl ester, 306
- DDT, 371
- DEAE-Sepharose, 171
- decacyclene, 427
- decanal, 162
- decay time, 24, 37
- deformation vibration, 119
- deuterium, 152
- deuterium lamp, 51, 83
- diabetes, 429
- dibutyl sebacate, 299
- difference interferometer, 274
- diffuse reflection, 131
- dimethylamino methacrylate, 303
- direct optical fibre chemical sensor, 20
- DLR. *See* dual lifetime referencing
- DNA, 171, 172, 174, 200, 233, 247, 249, 252, 440, 447, 450, 497
- DNA chip, 490

- dual lifetime referencing, 109
- earth alkali ion, 29
- ECL. *See* electrochemiluminescence
- effective refractive index, 264, 268
- effector, 326
- electrochemiluminescence, 157, 169, 170, 171, 172, 173, 349
- electronic transition, 79
- ELISA test, 390, 481
- enantio-selective, 31
- energy transfer, 24, 88, 89, 102, 126
- enzyme, 325
  - activity, 333
  - classification, 329
  - cofactor, 332
  - covalent attachment, 342
  - immobilisation, 338
  - intermolecular cross-linking, 341
  - kinetics, 334
  - microencapsulation, 340
- enzyme-based sensor, 31, 174, 324, 349
- eosin, 89, 423
- epitope, 388
- epitope mapping, 233
- erythrosine, 29
- Escherichia coli*, 190
- Escherichia coli enterotoxin*, 190
- ETH 1001, 309
- ETH 2439, 310, 311
- ethanol, 163, 164, 168, 169, 286, 409
- ethyl cellulose, 92, 315, 423
- ethylene, 85, 146
- europium (III)-complex, 88
- evanescent field, 194, 197, 198, 219, 266
- evanescent wave, 197
- evanescent wave spectroscopy, 134
- Fab fragment, 388
- Fabry-Perot filter, 463, 464
- FAD. *See* flavin adenine dinucleotide
- Fc fragment, 388
- FIA. *See* flow injection analysis
- finesse, 284
- FITC. *See* fluorescein:isothiocyanate
- flavin adenine dinucleotide, 33, 332
- flavine mononucleotide, 162, 167, 168, 332
- flow injection analysis, 165, 169, 171, 350
- fluorescein, 18, 33, 363, 369, 379, 423, 492
  - 2,5,1',3',7',9'-hexachloro-6-carboxy, 252
  - amino, 306, 370
  - isothiocyanate, 33
  - isothiocyanine, 366
  - succinimidyl ester, 305
- fluorescence, 99, 100, 150, 213, 315, 450
  - decay time, 373
  - enhancement, 205, 207
  - lifetime, 107
  - surface-enhanced, 493
- fluorescence resonance energy transfer, 110, 111, 494
- fluorescence scanner, 492
- fluoride, 138
- fluorogenic indicator, 313
- FMN. *See* flavine mononucleotide
- food packaging, 501, 505
- Francisella tularensis*, 447
- free spectral range, 284
- FRET. *See* fluorescence resonance energy transfer
- fumaric hydrogenase, 332
- fusion splice, 50
- gel entrapment, 339
- gene probe, 249
- gene sensor, 33
- gG3
  - human, 399
- glass transition temperature, 320
- glassy carbon electrode, 169, 170, 171, 172
- gluconic acid, 430
- glucose, 20, 28, 31, 33, 169, 170, 286, 287, 365, 430
  - blood, 429
- glucose oxidase, 33, 164, 170, 365, 430
- glutamate, 164, 169, 333
- glutamate dehydrogenase, 332
- glutamate oxidase, 164
- glutaminase, 164
- glutamine, 164, 169
- glycine oxidase, 332

- GOx. *See* glucose oxidase  
 grating coupler, 187, 275  
 H<sub>2</sub>O<sub>2</sub>. *See* hydrogen peroxide  
 haemoglobin, 378, 425  
 halide, 31, 110, 315  
 halogenide ion, 315  
 halothane, 26  
 heavy metal, 29, 30, 366  
 Henderson Hasselbach equation, 84  
 hexadecyltrimethylammonium  
   chloride, 304  
 hollow waveguide, 139  
 horseradish peroxidase, 158, 164,  
   165, 170, 172, 259, 365  
 HPTS. *See* hydroxypyrene trisulfonic  
   acid  
 human serum albumin, 379  
 humidity, 23, 24, 370, 373, 374, 485,  
   511  
 hybridization, 498  
 hydrocarbons, 20, 67, 106  
   aromatic, 21  
   chlorinated, 26, 29  
   halogenated, 70  
 hydrochloric acid, 316  
 hydrogen, 22, 26, 152, 375  
 hydrogen lamp, 83  
 hydrogen peroxide, 31, 90, 162, 163,  
   164, 169, 170, 171, 349, 365  
 hydrogen sulfide, 376  
 hydroxypyrene trisulfonic acid, 106,  
   367, 373, 420  
 hypoxanthine, 164, 169  
 IgA, 388  
 IgD, 388  
 IgE, 388  
 IgG, 172, 174, 388, 394, 450, 485,  
   491  
   anti-mouse, 248  
   human, 33, 172, 399  
   polyclonal, 395  
 IgG2, 399  
 IgG4, 399  
 IgM, 388  
 imaging sensor, 135  
 immunoassay, 248, 379, 390, 481  
 immunoglobulin-G, 248  
 immunosensor, 33, 391  
 indamine dye, 365  
 indirect optical fibre chemical sensor,  
   22  
 indocyanine green, 288  
 infrared selection rule, 122  
 infrared sensors, 128  
 infrared spectroscopy, 142  
 inhibitor, 325  
 integrated optical sensor, 266  
 integrated optics, 263  
 interaction length, 198, 269  
 interstitial fluid, 430  
 intramolecular charge transfer, 102  
 iodoacetoxynitrobenzoxadiazole, 379  
 ion exchange, 29, 92  
 ion pair, 26, 92, 93, 304, 305, 311,  
   312, 314, 315, 427  
 ionic strength, 27  
 ionophore, 29, 30, 91, 112, 299, 304,  
   308, 310, 311  
   calcium-selective, 94, 309  
   chromogenic, 91  
   nitrite-selective, 310  
 iron gall, 525  
 L 109, 309  
 lactate, 163, 164, 168, 169, 170, 365  
 lactate dehydrogenase, 168  
 lactate mono-oxygenase, 33  
 lactate oxidase, 164, 332  
 laser induced breakdown  
   spectroscopy, 515  
 LDH. *See* lactate dehydrogenase  
 lead salt laser, 136  
 leaky guide, 139  
 LED. *See* light emitting diode  
 LIBS. *See* laser induced breakdown  
   spectroscopy  
 light emitting diode, 51, 52, 57, 136  
 light source, 51  
 Lineweaver-Burke equation, 337  
 lipophilicity, 310, 318  
*Listeria monocytogenes*, 190  
 luciferase  
   bacterial, 162  
   firefly, 160, 161, 167, 168  
 luciferin, 160, 161, 167, 168  
*Luciola mingrelica*, 160  
 luminescence, 60, 99, 100, 105, 157,  
   166, 167  
 lifetime, 107

- polarization, 111
- luminol, 158, 159, 162, 163, 164, 169, 171, 172, 173, 349
- lysine, 164, 169
- lysine oxidase, 164
- Mach-Zehnder interferometer, 22, 220, 227, 228, 269
- MAP. *See* modified atmosphere
  - packaging
- mercury, 519
- metacresol purple, 423
- metal cation, 365
- metal island films, 244
- methacrylic acid, 303
- methane, 20, 21, 146, 461, 463
  - absorption, 80
- methemoglobin, 425
- methionine synthase reductase, 332
- methyltrimethoxysilane, 88, 90
- Michaelis-Menten constant, 336
- Michaelis-Menten equation, 334, 336
- Michelson interferometer, 273
- microporation, 430
- microsphere, 407
- minium, 519
- MIP. *See* molecularly imprinted
  - polymer
- modified atmosphere packaging, 501, 509
- modifier, 326
- modulation index, 466, 467, 468
- molar absorptivity coefficient, 81
- molecular imprinted polymer, 372
- molecular vibrations, 119
- molecularly imprinted polymer, 112, 140, 302, 377
- monoclonal antibody, 498
- monomer, 303
- MTMOS. *See* methyltrimethoxy-silane
- mustard gas, 373
- NADH. *See* nicotinamide adenine dinucleotide
- nafion, 300
- nanofilm, 493
- nanoisland, 210
- nanoparticle, 111, 209, 243, 249, 318, 493
  - gold, 248, 251
  - metal-coated, 246
  - silver, 246, 251, 252
- nanoshell, 249
- nanosphere
  - metal-coated, 245
- near-field scanning optical microscopy, 250
- NI 1, 310
- nickel, 93, 94
- nicotinamide adenine dinucleotide, 31, 33, 160, 162, 163, 168, 332, 333, 365
- nile blue, 29, 304
- nile red, 410
- nitrate, 31
- nitric oxide, 27, 364
- nitroaromatic compound, 410
- nitrogen dioxide, 22, 146, 372, 373, 460
- NO<sub>2</sub>. *See* nitrogen dioxide
- nonspecific adsorption, 389
- nucleotide, 498
- numerical aperture, 61
- octadecyl nile blue, 304
- oligonucleotide, 174, 440, 480, 498
- optical fibre
  - silica, 138
- optical fibre, 48, 61, 63, 138
  - chalcogenide, 138
  - D-shaped, 67
  - fluoride, 65, 460
  - hollow, 69, 138
  - inverted graded index, 67
  - plastic, 65
  - polymer-clad-silica, 66
  - sapphire, 138
  - sectorial fibre, 68
  - silica, 64
  - silicate, 64
  - silver halide, 139
  - single-mode, 67
  - sol-gel derived, 363
  - step-index, 65
- optical fibre coating, 70
- optical fibre connector, 72
- optical fibre coupler, 50
- optical fibre grating, 74
  - Bragg, 74
  - long period, 74

- optical loss, 49, 61
- optical microresonator, 283, 286
- optical nose, 406
- optode, 42, 94, 100
- ormosil, 302, 353
- ovalbumin, 378, 445
- overtone vibration, 123
- oxalate, 365
- oxalate ester, 158
- oxalic acid ester, 349
- oxaloacetate, 163
- oximeter, 418
  - pulse, 426
- oxygen, 18, 19, 23, 26, 31, 33, 36, 53, 109, 316, 318, 349, 364, 373, 375, 425, 430, 503, 505, 508
  - blood, 35, 419
- oxygen partial pressure, 19, 23, 421, 422, 427
- oxygen saturation
  - fetal, 426
- oxyhemoglobin, 425
- oxyluciferin, 161
- palladium, 22, 26
- Paratrend 7, 421
- pCO<sub>2</sub>. *See* carbon dioxide partial pressure
- PCR. *See* polymerase chain reaction
- Pd. *see* palladium
- PDMS. *See* poly(dimethylsiloxane)
- penetration depth, 197
- penicillinate, 31
- peroxidase, 249, 430
- perylene, 160
- perylene dibutyrate, 24, 427
- PET. *See* photoinduced electron transfer
- pH, 18, 23, 24, 26, 27, 30, 84, 106, 308, 310, 316, 317, 349, 365, 430
  - blood, 35, 419, 424
  - gastric, 422
- phase shift, 108, 504
- phenol red, 27, 86, 89, 349, 367, 419
- phosphate, 164, 169
- phosphorescence, 99, 109
- Photinus pyralis*, 160
- Photobacterium leiognathi*, 161
- Photobacterium phosphoreum*, 161
- photodiode, 55, 56
  - infrared, 144
- photoinduced electron transfer, 110, 372
- photomultiplier tube, 54
- photonic bandgap, 282
- photonic crystal, 288
- photoplethysmography, 426
- pK, 27, 84, 86
  - bromophenol blue, 304
  - hydroxypyrene trisulfonic acid, 106
  - nile blue, 304
  - vinylsulfonyl dye, 307
  - Zincon, 315
- planar waveguide, 196
- plasticizer, 298
  - lipophilic, 299
- polar, 299
- platinum(II)
  - octaethyl-porphine-ketone, 506
  - tetrakis(pentafluorophenyl)porphine, 506
- pO<sub>2</sub>. *See* oxygen partial pressure
- polarity, 310
- polarity-sensitive dye, 310, 312
- poly(2-hydroxyethyl methacrylate), 300
- poly(dimethylsiloxane), 23, 172, 173, 175, 300
- poly(ethylene vinyl acetate), 300
- poly(ethyleneterephthalate), 506
- poly(hexyl methacrylate), 300
- poly(methyl methacrylate), 298, 299
- poly(vinyl acetate), 92, 298, 299, 315
- poly(vinyl chloride), 23, 29, 87, 93, 173, 298, 299, 305, 308, 309, 311, 312, 313, 319, 506
- polyacrylamide, 24, 27, 165, 300, 339, 343, 419, 423
- polyaniline, 300
- polyelectrolyte, 300
- polymer
  - dielectric constant, 318
  - hydrophilic, 300
  - ionic, 300
  - lipophilic, 298
  - unpolar, 300
- polymerase chain reaction, 250, 440, 498

- polystyrene, 27, 210, 298, 299, 506
- polystyrene sulfonate, 300
- polyurethane, 92, 300, 315, 339
- polyvinyl alcohol, 87, 171, 172, 339
- polyvinylidene fluoride, 371
- porous glass, 23
- porphyrin, 366, 367
  - 5,10,15,20-tetra(4-N-methylpyridil), 366
  - 5,10,15,20-tetra(4-N-methylpyridiniumyl), 367
  - 5,10,15,20-tetra(4-sulfonato), 367
- Co(III), 376
- cobalt(II), 377
- platinum, 316
- platinum octaethyl, 376
- platinum(II):, 504
- post
  - metal-coated quartz, 246
- potassium, 29, 308, 311, 314, 318
- primer, 498
- prism coupler, 186, 187
- propane, 21
- protein, 498
  - immobilization, 491
  - primary structure, 327
  - secondary structure, 327
  - tertiary structure, 328
- PSD. *See* polarity-sensitive dye
- PVA. *See* polyvinyl alcohol
- PVC. *See* poly(vinyl chloride)
- pyrenebutyric acid, 23
- pyrocatechol violet, 93
- pyruvate kinase, 332
- quality factor, 284
- quantum cascade laser, 137
- quantum detector, 143
- quantum dots, 111, 493, 494
- quantum efficiency, 210
- quantum yield, 101
  - bacterial bioluminescence, 168
  - firefly luciferase, 161
  - luciferase firefly, 168
  - luminol, 168
- quenching, 26, 102, 109, 111, 210, 315, 503
  - dynamic, 103
  - energy transfer, 103, 109
  - rate constant, 104
  - static, 103, 104
- radiating dipole, 205
- Raman scattering, 125, 126, 128, 148, 150, 241, 462
  - surface enhanced resonance, 250, 252
  - surface-enhanced, 128, 148, 152, 241
    - active substrate, 243
    - gene probe, 249
    - immunoassay, 248
    - instrumentation, 242
    - intracellular analysis, 252
    - optical microscopy, 250
    - overcoatings, 247
    - single molecule detection, 251
- Raman spectroscopy, 118, 125, 149, 239, 462, 515
- Rayleigh scattering, 126
- recombinant proteins, 498
- redox indicators, 89
- reflectometric interference
  - spectroscopy, *See* spectroscopy: reflectometric interference
- reflux
  - enterogastric, 418
  - gastro-oesophageal, 418
- refractive index, 22, 61, 184, 186, 201, 219, 263
- refractive sensor, 267, 276
- refractometry, 22
- resonance wavelength, 211
- resonator, 282
- resonators, 274
- RGB components, 521
- rhodamine 6G, 363
- rhodamine B octadecylester
  - perchlorate, 312
- ribonucleic acid, 252, 440, 490, 498
- ricin, 447
- RifS. *See* spectroscopy: reflectometric interference
- RNA. *See* ribonucleic acid
- rotational level, 121
- rubrene, 160
- ruthenium
  - complex, 24, 208, 373, 374, 504, 506
  - phenanthroline derivative, 316

- tris(bipyridyl), 24
- ruthenium (II)
  - tris(diphenylphenantroline) perchlorate, 506
- ruthenium(II)
  - polypyridyl, 375
  - tris(4,7-diphenyl-1,10-phenanthroline), 375
- saccharide, 316
- salicylate, 31
- salinity, 22
- Salmonella enteritidis*, 190
- sapphire, 138
- SEIRA. *See* surface enhanced infrared absorption spectroscopy
- SELEX, 440, 491
- self-assembled monolayer, 247
- self-encoded bead array, 409
- seminaphthorhodamine-1
  - carboxylate, 368
- seminaphthorhodamine-1-carboxylate, 425
- SERG. *See* surface-enhanced Raman gene
- serrodyne modulation, 271
- SERRS. *See* Raman scattering:surface-enhanced resonance
- SERS. *See* Raman scattering:surface-enhanced
- silver halide, 138
- simazine, 229
- slabguide. *See* waveguide:slab
- Snellius law, 219
- sodium, 29, 110, 318
- sol, 301
- sol-gel
  - condensation, 301
  - gelation, 355
  - hydrolysis, 301, 354
  - process, 301, 356, 358
- sorbitol, 163
- spectroscopy
  - far infrared, 123
  - infrared, 122
  - infrared emission, 124
  - mid-infrared, 122
  - near-infrared, 123
  - reflectometric interference, 219, 221, 227, 231, 493
  - vibrational, 118
- staphylococcal enterotoxin B, 190, 447
- Stark modulation, 465
- Stern-Volmer
  - constant, 104, 504
  - equation, 103, 105, 373, 503, 504
- Stokes line, 126, 241
- streptococci activity, 378
- stroke, 424
- sulfhemoglobin, 425
- sulfur dioxide, 26, 316
- sulphite, 164, 169
- sulphonophthalein indicator, 86
- surface plasmon, 182
- surface plasmon resonanc, 493
- surface plasmon resonance, 185, 275
- surface-enhanced infrared absorption spectroscopy, 128
- surface-enhanced Raman gene, 247
- surface-enhanced Raman spectroscopy. *See* Raman scattering:surface-enhanced
- TCPO, 159
- TE mode, 181, 264
- tellurium halide, 138
- TEOS. *See* tetraethoxysilane
- tetraethoxysilane, 88, 354
- tetralkylammonium salt, 31
- tetramethoxysilane, 90, 301, 354, 371
- tetraoctylammonium, 93, 315
- Texas red, 306
- thermal detector, 143
- thermal source, 136
- thermoluminescence, 23
- thionine, 376
- thymol blue, 86, 423
- TM mode, 181, 264
- TMOS. *See* tetramethoxysilane
- toluene, 21, 376
- tonometry, 427
- toxin, 442, 448
- transflection, 131
- transmittance, 82
- triazine, 231
- triethylammonium-methylcellulose, 300

- tris(2-ethylhexyl) phosphate, 299
- tris(2-ethylhexyl) trimellitate, 299
- tryptaflavine, 18
- tungsten halogen lamp, 51
- tungsten lamp, 83
- uranium, 18, 26
- urea, 370
- urease, 332, 370
- uric acid, 172
- valence vibration, 119
- valinomycin, 29, 308, 311
- vibrational spectroscopy, 118
- vibrational state, 120
- vibrational transition, 121
- Vibrio fischeri*, 161
- Vibrio harveyi*, 161
- vinylpyridine, 303
- vinylsulfonyl dye, 306
- wall effect, 421
- waveguide
  - capillary, 26
  - channel, 282
  - cylindrical. *See* optical fibre
  - enhanced platform, 203
  - planar, 179
  - slab, 263, 282
- whispering gallery mode, 282, 286
- white lead, 519
- whole-cell biosensor, 378
- XAD 4, 24
- xanthine, 164, 169
- xanthine oxidase, 164, 332
- xenon arc lamp, 51
- xerogel, 302, 355, 359
- xylene, 21
- xylene orange, 366
- Young interferometer, 273
- zinc, 53, 92, 314, 315
- zincon, 314